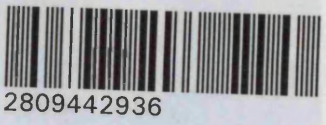

UNIVERSITY OF LONDON THESIS

Degree PhD Year 2007 Name of Author ANDREW JON LOVE

Interpolation of SIF Weight Functions in Fracture Mechanics Analyses

Andrew Jon Love

Submitted for the Degree of
Doctor of Philosophy

Department of Mechanical Engineering
University College London

August 2005

ProQuest LLC
789 East Eisenhower Parkway
P.O. Box 1346
Ann Arbor, MI 48106-1346

Abstract

Engineers are commonly confronted by complex, linear elastic crack problems, typically cracks situated at notches, for which relevant and readily available SIF solutions are sparse. The difficulty in accurately determining such solutions for rapid engineering defect assessment without resorting to specialist analyses, e.g. numerical or experimental methods, is well known and longstanding. The thesis documents the development of a novel methodology for the calculation of SIF solutions for cracks in complex geometries subject to non-simple loading arrangements.

A methodology, termed an 'interpolation of base geometry weight functions' was designed to empower the engineer with a tool to generate broad ranging solutions accurately and rapidly in a manner that is robust and requires minimal specialist insight. The methodology utilises constituent geometry SIF solutions, of more simple form, to isolate the geometric influence of the notch upon SIF. Expressed as an interpolation factor the geometric influence is used to interpolate two extreme, plane geometry (or 'base' geometry) weight functions to determine a weight function for the notched geometry. Once determined the notched geometry weight function is used with crack-line stress distributions to efficiently calculate new SIF solutions for a number of loading arrangements. The interpolation methodology allows large numbers of new SIF solutions to be readily generated from a relatively small, 'library' of constituent geometry solutions.

The primary body of work details development and validation of the methodology, applied to a wide range of two-dimensional notch geometry types, both symmetric and asymmetric. Generation of constituent geometry SIF solutions, using FEA; their subsequent manipulation, dictated by the interpolation scheme and formulation of base geometry weight functions, using a contemporary methodology are presented. New SIF solutions obtained are rigorously validated against those developed from finite element and experimental methods and compared to existing, closely related weight function methodologies. The interpolation scheme was shown to display excellent performance, economy and versatility and universal applicability to all notch types.

Application of the interpolation methodology was extended to determine deepest point SIF solutions for surface cracks in complex three-dimensional bodies. Weight function formulation utilises two-dimensional constituent geometry solutions together with three-dimensional 'base' geometry weight functions. Though presently restricted by a number of approximations, results achieved for surface cracks in notched flat plates compared well to those determined via full three-dimensional FEA. The broad ranging scope for applications and future developments of the interpolation scheme are identified and cited.

Acknowledgements

The excellent supervision and inspiration provided by Dr Feargal Brennan and Professor Bill Dover is hereby acknowledged. My thanks go to Feargal for providing the opportunity to pursue this study, his comprehensive guidance and advice throughout its duration, and patience to see its conclusion.

I would like to thank my parents for their continued love, support and encouragement throughout my years of study.

I would also like to thank the numerous colleagues, with whom I've had the pleasure of working alongside in the NDE Centre and Department of Mechanical Engineering.

Table of Contents

List of Tables

List of Figures

Nomenclature

a	Crack depth
a_I	Initial Crack Size/Depth
a_C	Critical Crack Size/Depth
b	Notch Depth
B	Fatigue Specimen Width
c	Crack half-width
C	Paris Law Constant
C_x, $C(a)$	MRS Weight Function Coefficient
$C_N^F(a)$	MRS WF Coefficient (Notched, Finite Thickness Geometry)
$C_N^S(a)$	MRS WF Coefficient (Notched, Semi-Finite Thickness Geometry)
$C_S^F(a)$	MRS WF Coefficient (Stiffened, Finite Thickness Geometry)
$C_S^S(a)$	MRS WF Coefficient (Stiffened, Semi-Finite Thickness Geometry)
$C_U^F(a)$	MRS WF Coefficient (Unstiffened, Finite Thickness Geometry)
$C_U^S(a)$	MRS WF Coefficient (Unstiffened, Semi-Finite Thickness Geometry
COD	Crack Opening Displacement
D_x	Interpolation Factor Curve Fit Coefficient
E	Elastic Modulus for Plane Stress
E'	Elastic Modulus for Plane Strain
F	Point Load
F_{max}	Maximum Load
F_{min}	Minimum Load
$f(a)$	Interpolation Factor
FE	Finite Element
FEA	Finite Element Analysis
G	Energy Release Rate
$g(a)$	Normalised SIF Distribution (Semi-Finite Thickness Geometry)
H	Generalised Elastic Modulus
J	J-Integral
K	Stress intensity factor
K_{IC}	Fracture Toughness
K_{max}	Maximum SIF
K_{min}	Minimum SIF
L	Fatigue Specimen Length
L_I	Intrusion Notch Width
L_P	Protrusion Notch Width
m	Paris law exponent
M	Bending Moment
M_x	SIF Distribution Curve Fit Coefficient (Semi-Finite Thickness Geometry)
M'_x	SIF Distribution Curve Fit Coefficient (Semi-Finite Thickness Geometry)
$m(a,x)$	SIF Weight Function
$m_N^F(a,x)$	Weight Function (Notched, Finite Thickness Geometry)
$m_N^S(a,x)$	Weight Function (Notched, Semi-Finite Thickness Geometry)
$m_S^F(a,x)$	Weight Function (Stiffened, Finite Thickness Geometry)
$m_S^S(a,x)$	Weight Function (Stiffened, Semi-Finite Thickness Geometry)
$m_U^F(a,x)$	Weight Function (Unstiffened, Finite Thickness Geometry)

$m_U^S(a,x)$	Weight Function (Unstiffened, Semi-Finite Thickness Geometry)
MRS	Multiple Reference State
N	Number of Stress Cycles
N_x	Crack-line Stress Distribution Curve Fit Coefficient (Semi-Finite Thickness Geometry)
P	Axial Load
P_x	Crack-line Stress Distribution Curve Fit Coefficient (Finite Thickness Geometry)
PB	Pure Bending
PT	Pure Tension
Q	Shear Force
R	Stress Ratio
R_x	SIF Distribution Curve Fit Coefficient (Finite Thickness Geometry)
R^2	Coefficient of Determination
RMS	Root Mean Square
r_P	Plastic Zone Size
SCF	Stress Concentration Factor
SIF	Stress Intensity Factor
t	Minimum section thickness
T	Maximum section thickness
UT	Uniform Tension
W	Plate width
WF	Weight Function
Y, $Y(a)$	Normalised SIF
$Y_N^F(a)$	Normalised SIF (Notched, Finite Thickness Geometry)
$Y_N^S(a)$	Normalised SIF (Notched, Semi-Finite Thickness Geometry)
$Y_S^F(a)$	Normalised SIF (Stiffened, Finite Thickness Geometry)
$Y_S^S(a)$	Normalised SIF (Stiffened, Semi-Finite Thickness Geometry)
$Y_U^F(a)$	Normalised SIF (Unstiffened, Finite Thickness Geometry)
$Y_U^S(a)$	Normalised SIF (Unstiffened, Semi-Finite Thickness Geometry
α	Flank angle
β	Interpolation Factor for Weight Functions
ΔK	SIF Range
$\Delta\sigma$	Stress Range
ϕ	Surface Crack Characteristic Angle
γ	Non-Dimensional Crack Depth
φ	Interpolation Factor for SIFs
λ	Non-Dimensional Crack Depth
ρ	Notch root radius
σ_f	Flow Stress $(\sigma_Y + \sigma_{UTS})/2$
σ_{max}	Maximum Stress
σ_{min}	Minimum Stress
σ_o	Nominal stress
σ_{UTS}	Ultimate Tensile Strength
σ_Y	Yield Stress
$\sigma_{yy}(x)$	Crack line direct stress
τ_o	Nominal Shear Stress
$\tau_{xy}(x)$	Crack line Shear stress

Chapter 1 – Introduction and Background

Throughout history mankind has sought to build structures to achieve comfort, mobility and convenience that meet his economic benefit. Rational analysis applied to engineering design has afforded the modern world a host of impressive structures, which would astonish the designer of even the more recent past generations. Common throughout history is a structure's susceptibility to failure by fracture. Though much progress has been made to understand these phenomena the increased technical complexity of today's world causes it to remain a considerable detriment to society both in terms of financial cost and loss of life. It is the concern of those practising fracture mechanics to assess cracked structures and to ensure a state of safe operation prevails without catastrophic failure.

The demand to design evermore efficient, economic and safer structures continues and is set to only increase throughout the twenty-first century and beyond. Thus, challenges confronting the engineer concerned with ensuring a state of structural integrity prevails grow evermore demanding. Realisation of these demands requires application of novel and increasingly sophisticated analysis tools to accurately model new designs or materials.

1.1 – Defect Assessment and Linear Elastic Fracture Mechanics (LEFM)

Many engineering structures contain flaws or crack-like defects arising from rigorous manufacturing and fabrication techniques or initiation during service. Manufacturing flaws exist as imperfections in the materials' microstructure such as sites of porosity, second phase particles and impurities. Flaws created during fabrication are often associated with harsh processing procedures such as welding and drilling. The initial size of flaws may be small, even microscopic, but have a propensity to grow, or new cracks develop, due to the action of a variable service load (fatigue) or attack from the environment (corrosion). The presence and size of cracks in a component have a profound adverse affect upon its static (residual) strength. If the residual strength depreciates sufficiently then loss of structural integrity occurs under normal operating conditions. Assessment of defects or components containing defects may involve determination of one or more of the following.

- Residual strength as a function of crack size
- The critical crack size tolerated by a structure
- Crack growth rates from an initial flaw size to a critical size
- Appropriate inspection schedules for cracked components
- The size of pre-existing flaws in the as manufactured state

Fracture mechanics is an engineering discipline that assesses the state of cracks or cracked structures to quantitatively evaluate phenomena listed above. A quantitative assessment allows engineering optimisation of many areas of structural and component management including those given below.

- Design
- Material selection
- Inspection schedules
- Maintenance procedures
- Decisions regarding remedial action

Engineering metals, such as high strength steels, are of relatively low fracture toughness, a material property gauging the resistance to brittle fracture. Structures, containing cracks, composed of such materials ultimately fail by a rapid severance mechanism termed brittle fracture as opposed to plastic collapse, or rupture. LEFM assumes that linear elastic theory can be applied to describe the stress field in the region of a crack embedded in a loaded body. Though plasticity occurs at the crack tip, the principles of LEFM remain valid if the plasticity is confined to a zone small in size compared to the overall dimensions of the crack and cracked body.

Initial attempts to characterise fracture of materials were based on an energy-balance theory formulated by Griffith[1.1]. Irwin[1.2] subsequently proposed an energy approach for crack systems defining a term for the elastic energy release rate, 'G' quantifying the energy available for an increment of crack extension.

$$G = -\frac{d\Pi}{dA} \qquad \text{- (1.1)}$$

'G' is the rate of change of potential energy, 'Π' with crack area, 'A'. This crack driving force was used to characterise stable and unstable crack growth. In situations where crack tip plasticity is appreciable, Rice's[1.3] J-Integral, 'J' provides a more representative crack characterising parameter. It may be viewed as an equivalent energy release rate for cracks obeying non-linear elastic material behaviour. The J-Integral lends itself well to calculation via numerical means and hence is useful in LEFM analyses if a linear elastic material response is specified. Though energy approaches provided great advancement of the theory of LEFM, subsequent development focused on a more practicable and tangible stress-field approach. With the exception of ideally brittle materials and those of relatively high toughness, characterisation of cracks in linear elastic

materials through the crack-tip stress-field theory of fracture has gained precedence, and is currently preferred by most researchers.

Cracks embedded in brittle materials can be characterised by a single parameter, the stress intensity factor (SIF), describing the crack tip stress field. It is a function of loading on the cracked configuration, crack size and shape and other geometrical boundaries. The SIF is employed in many aspects of fracture mechanics such as to quantify critical flaw size, fatigue and stress corrosion cracking. The application of such analyses to practical problems requires knowledge of the SIF solution for the given geometrical configuration under the specified loading. Solutions for many configurations are available from various sources these are typically confined to simple, idealised geometries under simple load cases and are mostly restricted to two-dimensional geometries as three-dimensional solutions are more difficult to calculate.

Many practical engineering problems are concerned with complex geometries under complex loading arrangements. The available SIF solutions are often inappropriate, as their usage invariably constitutes an approximation to the physical problem, which may incur unacceptable errors in fracture mechanics models. Contrary to the judgement of many, that there are sufficient SIF solutions applicable to the vast range of physical problems, design engineers continually strive to generate new reliable and accurate SIF solutions. Furthermore, engineering optimisation and defect assessment requires SIF solutions that have broad limits of validity that can be rapidly calculated. The difficulty in calculating SIF solutions that meet the criteria stated above is widely recognised and constitutes a longstanding limitation common to many fracture mechanics analyses.

1.2 – The Stress Intensity Factor (SIF)

LEFM applies to cracks in linear elastic materials and defines the stress field in the region of the crack, characterising crack propagation, in terms of global parameters of load and geometry. Representing the crack as a perfectly thin slit embedded in an isotropic linear elastic material it is possible to derive closed form analytical expressions for the stress field in the body, for simple cracked geometries. Williams[1.4] was amongst the first to develop a general stress function approach to solve elasticity equations of compatibility and equilibrium for this geometric configuration under various boundary conditions. Thorough description and derivations were detailed and stress fields in the crack tip region expressed in the following form, described by the polar co-ordinate system defined in fig. 1.1.

$$\sigma_{ij}(r,\theta) = \frac{K}{\sqrt{2\pi r}} f_{ij}(\theta) + \textit{higher order terms in 'r'} \qquad \text{- (1.2)}$$

Eq. 1.2 predicts a singular stress solution approaching the crack tip ($r \rightarrow 0$) higher order terms, depend on geometry and loading, are either constant or tend to zero. The stress solution for a crack subject to any set of boundary conditions are expressed in this form sharing the same leading term. The stress intensity factor (SIF), 'K' defines the amplitude of the stress singularity at the crack tip. There exists a region ahead of the crack tip, known as the singularity dominated zone, within which the single parameter of SIF provides a complete measure of the stress field.

The stress field is governed by distance from the crack tip and trigonometric functions of the angular co-ordinate, which are dependent upon the mode of crack deformation. Mode I deformation, denoted by the subscript 'I' is produced by a pure crack opening loading and is identified as being the most damaging mode in the majority of practical situations. The trigonometric functions completely describing the crack tip stress field for mode I opening and associated displacement field are given as eq. 1.3 and 1.4. Stress and displacement fields, near any crack tip are governed by the constant factor 'K' that depends on component loading and geometry.

$$\begin{Bmatrix} \sigma_{xx} \\ \sigma_{yy} \\ \tau_{xy} \end{Bmatrix} = \frac{K_I}{\sqrt{2\pi r}} \begin{Bmatrix} \cos\left(\frac{\theta}{2}\right)\left[1-\sin\left(\frac{\theta}{2}\right)\sin\left(\frac{3\theta}{2}\right)\right] \\ \cos\left(\frac{\theta}{2}\right)\left[1+\sin\left(\frac{\theta}{2}\right)\sin\left(\frac{3\theta}{2}\right)\right] \\ \cos\left(\frac{\theta}{2}\right)\sin\left(\frac{\theta}{2}\right)\cos\left(\frac{3\theta}{2}\right) \end{Bmatrix} \quad \text{- (1.3)}$$

$$\begin{Bmatrix} u_x \\ u_y \end{Bmatrix} = \frac{K_I}{2\mu}\sqrt{\frac{r}{2\pi}} \begin{Bmatrix} \cos\left(\frac{\theta}{2}\right)\left[\kappa-1+2\sin^2\left(\frac{\theta}{2}\right)\right] \\ \cos\left(\frac{\theta}{2}\right)\left[\kappa-1+2\sin^2\left(\frac{\theta}{2}\right)\right] \end{Bmatrix} \quad \text{- (1.4)}$$

where: $\kappa = (3\text{-}4\nu)$ for plane stress and $\kappa = (3\text{-}\nu)/(1+\nu)$ for plane strain

ν = Poisson's ratio μ = shear modulus

The near tip stress solution given in eq. 1.3 is based upon a perfectly sharp crack and predicts a stress singularity approaching infinity at the crack tip, which physically cannot occur due to material plasticity in this region. If this plastic region is small compared to that over which the $1/\sqrt{r}$ term dominates, then the stress intensity factor concept holds and is sufficient for characterisation of the crack tip stress field. This single parameter, completely describing a crack tip stress field is

a fundamental concept in linear elastic fracture mechanics, providing a measure of the driving force for crack extension, and central to numerous analytical models.

1.2.1 – Normalisation of the SIF

The SIF is a function of the crack size and shape; other geometrical boundaries and the loading arrangement to which it is subject. Inspection of eq. 1.3 indicates the SIF as having the units of $N\sqrt{m}$. The crack tip stresses in linear elastic materials are proportional to the remotely applied loading and the only length dimension common to all cracked geometries is a crack size parameter. A relationship between SIF, 'K' and global conditions can therefore be written in the following form.

$$K = f\left(\sigma, \sqrt{a}\right) \quad \text{- (1.5)}$$

The actual SIF solution for a Griffith crack (fig. 1.2) is presented below.

$$K = \sigma\sqrt{\pi a} \quad \text{- (1.6)}$$

For all other crack configurations, geometrical boundaries and alternative loading arrangements exert an influence upon the SIF. A factor, 'Y' accounts for different boundary conditions and corrects the SIF as predicted by eq. 1.6. The SIF for any crack configuration and loading can be written in the form of eq. 1.7 or in a non-dimensional form by eq. 1.8. For two-dimensional geometries crack depth, 'a' for edge cracks and crack half width, 'a' for through cracks are utilised as the crack size parameter.

$$K = Y\sigma_o\sqrt{\pi a} \quad \text{- (1.7)} \qquad Y = \frac{K}{\sigma_o\sqrt{\pi a}} \quad \text{- (1.8)}$$

Description of stress intensity factor, or in its non-dimensional form 'Y', is achieved by normalisation to terms describing a characteristic stress, 'σ_o' usually taken as a nominal stress, and a crack size parameter, 'a'. Though numerous possible relations exist to normalise the SIF, the most concise and frequently used is the form of that given by eqs. 1.7 and 1.8, and is the form preferred throughout this text.

Presenting the SIF, for a Griffith crack, in the form of eq. 1.6 allows a simple relationship between the SIF and energy release rate, 'G' (or 'J', if a linear elastic material response is specified) to be written.

$$G = J = \frac{K^2}{E'} \quad \text{- (1.9a)} \qquad Y = \frac{1}{\sigma_o}\sqrt{\frac{JE'}{\pi a}} \quad \text{- (1.9b)}$$

Eq. 1.9a relates the net change in potential energy of the cracked body to the local stresses and strains at the crack tip. It is applicable to all cracked geometries and, by the definition given in eq. 1.7, allows simple calculation of the normalised SIF from a J-Integral value quantified through numerical means by eq. 1.9b.

1.2.2 – SIF as a Crack Characterising Parameter

Fracture of a structure occurs when the crack tip stress increases above a level which can be borne by the material. The foregoing discussion introduced the stress intensity factor, 'K' as a crack tip stress field parameter and therefore brittle fracture occurs when its value increases above a critical level. LEFM defines a limiting material property, termed the fracture toughness or critical stress intensity factor, 'K_{IC}' for mode I loading. It is a material property, independent of size and geometry of the cracked component and is measure of a material's resistance to brittle fracture. A test, comprising monitoring of the monotonic loading of pre-cracked specimens that adheres to guidelines presented in BS 7448-1[1.5] must be implemented to determine the material property. Once determined the critical flaw size, 'a_c' for a cracked component can be expressed by eq. 1.10.

$$a_c = \frac{K_{IC}^2}{Y^2 \sigma_o^2 \pi} \quad \text{- (1.10)}$$

Eq. 1.10 assumes that the failure mechanism is entirely fracture driven. The SIF and fracture toughness are central to numerous alternative integrity assessment methodologies such as the 'FAD' approach incorporated into BS 7910:1999[1.6] which accounts for an alternative extreme failure mechanism of plastic collapse.

The action of fatigue is a common mechanism of sub-critical crack growth arising due to cyclic stressing of either constant or variable amplitude. The stressing under constant amplitude loading may be fully defined by the minimum stress, 'σ_{min}', maximum stress, 'σ_{max}' or alternatively by the stress range, '$\Delta\sigma$' (σ_{max} - σ_{min}) and stress ratio, 'R' (σ_{min} / σ_{max}). Application of a number of stress cycles, 'N' causes cracks of length, 'a' to propagate. A number of empirical relations exist to model the crack growth rate, 'da/dN' as a function of SIF range, 'ΔK'. The simplest and most widely utilised expression is given as eq. 1.11

$$\frac{da}{dN} = C\Delta K^m \quad \text{- (1.11)} \qquad \Delta K = Y\Delta\sigma\sqrt{\pi a} \quad \text{- (1.12)}$$

The crack growth rate is described as a function of SIF range and dependent upon the material constants, 'C' and 'm', which are determined experimentally as described in BS 6835-1[1.7]. Paris and Erdogan[1.8] were the first to propose an empirical power law relationship of eq. 1.11, widely referred to as the Paris Law. It is applicable to the majority of situations however, crack growth rates at low SIF ranges due to the threshold value, 'ΔK_{th}' and situations where 'K_{max}' approaches 'K_{IC}' require description by alternative empirical relations based upon the SIF range, 'K_{IC}' and 'ΔK_{th}'. An integrated form of the Paris Law permits the modelling of crack growth rates or the estimation of the number of load cycles of a crack to grow from an initial size, 'a_i' to the critical size, 'a_c' (eq. 1.13).

$$N = \int_{a_i}^{a_c} \frac{da}{C\Delta K^m} \quad \text{- (1.13)}$$

Calculation of a critical flaw size and implementation of the Paris Law forms the basis of a commonly used design methodology for fatigue prone components, termed defect tolerance, summarised in fig. 1.3. The component is designed to have a period of service life free from significant fatigue damage. A prolonged service life is justified by regular inspection to size the crack and monitor sub-critical growth, thus avoiding catastrophic fatigue damage. In the case of notched components the proportion of service life for crack initiation is short compared to that for fatigue propagation. Schematic crack growth curves depicted in fig. 1.3 indicate that SIF data, particularly for short cracks as this is where the majority of service life is spent, is crucial to the development of a reliable and optimised inspection schedule and also to the estimation of critical flaw size. SIF data is fundamental to a defect tolerant approach to crack management or any integrity assessment of cracked structures. Accurate and reliable SIF data is essential for the optimisation of a fracture control plan in the design and service life of components and structures.

1.2.3 – SIF Solutions

Practical application of LEFM analyses requires knowledge of the SIF for the specified geometry under the given loading conditions. SIF data, presented in its non-dimensional form, for a variety of geometries and loading arrangements are available in published literature, derived using various means. These are commonly presented in the concise format of handbooks and compendia, Rooke and Cartwright[1.9]; Tada, Paris, and Irwin[1.10]; Sih[1.11] and Murakami[1.12, 1.13] are among the more established and expansive sources. SIF solutions contained in such sources

are often limited to simple idealised geometries subject to the simplest load cases (typically remotely applied uniform tension and pure bending) applicable to linear elastic, isotropic and homogeneous materials. The majority of solutions are also limited to edge or embedded cracks in two-dimensional geometries due to the greatly increased analytical complexity associated with surface or penny cracks in three-dimensional geometries.

The magnitude of SIF for cracks situated in plane geometries of finite dimensions are influenced by remote boundaries. Fig. 1.4 displays the SIF solution for an embedded crack located centrally in a finite width strip subject to a remotely applied tensile loading arrangement. Solutions shown are provided by Isida[1.14] and Benthem and Koiter[1.15] both indicate the boundary influence increasing the magnitude of SIF with increasing crack size.

A structural discontinuity or notch in a component is known to increase the magnitude of the local stress field above the nominal stress, the stress at a position far from the notch. Maximum stress occurs at the notch root, characterised by the stress concentration factor (SCF). The elevated local stress at the notch root causes such sites to be susceptible to rapid crack initiation and growth when subject to fatigue loading. Analysis of cracks at notches is commonly identified as critical to the assessment of the integrity of components and structures. Fig. 1.5 shows the SIF solutions of Nisitani and Isida[1.16] for cracks emanating from various elliptical holes, of differing acuity, embedded in a semi-finite plane subject remotely applied uniform tensile loading. The influence of the notch as a stress raiser is evident from the elevated SIF solutions with respect to the equivalent un-unotched geometry (Y=1). The magnitude of the normalised SIF decreases as crack length increases, as the influence of the notch becomes less influential upon the solution. SIF solutions for such geometries are only valid as approximations to situations involving geometries of finite dimensions if the notch is remote from other boundaries.

SIF solutions presented in compendia, quoted with an associated accuracy, are invariably presented in the form of tables, charts or fitted to closed-form parametric equations for ready incorporation into fracture mechanics analyses. The two cases described above are typical of the majority of SIF data contained in compendia. Such solutions are useful; however their relevance to real engineering components and structures often represents an unsatisfactory approximation. SIF solutions for cracks situated in complex geometries, those influenced by the presence of both notches and other remote boundaries, are more useful but far less common. Fig. 1.6 shows a number of representative examples of complex geometries for which SIF solutions are commonly desired but largely unavailable. The number of possible geometric configurations is considerable and furthermore, accounting for alternative loading arrangements, complex geometries constitute an almost limitless number of possible crack, geometry and loading configurations. A parametric

numerical or analytical study of each geometry would constitute a considerable number of analysis runs. Furthermore, effective presentation of individual SIF solutions in tables and charts is prohibitively large and expressed as parametric equations yield cumbersome relations comprising many terms, which invariably degrade accuracy of original data.

Numerous methods have been developed to approximate SIF solutions for complex geometries and/or complex loading arrangements. The simple methodolgies presented in section 1.4 utilise existing SIF solutions for simple geometry configurations or loading arrangements to make them relevant to a more complex situation.

1.2.4 – Superposition of SIFs

A useful feature of the SIF for the characterisation of cracks is that a SIF for a complex loading arrangement can be considered a combination of SIF solutions of a number of simpler loading arrangements. The principle of superposition states that components of stress, strain and displacement are additive for linear elastic materials. If two or more different loadings are applied to a system, the combined effect of the loads is the sum of their individual effects. In fracture mechanics, the SIFs for simpler loading arrangements are superposed through an algebraic summation to obtain a total solution often of a more complex loading arrangement. A useful result of application of the principle applied to cracked bodies is that stresses acting on remote boundaries (tractions) can be replaced by the crack face tractions present in the uncracked body to yield the same SIF. Consider an uncracked body under a general remotely applied loading arrangement, shown in fig. 1.7a. Tractions '$T(x)$' give rise to a purely normal stress distribution, '$\sigma(x)$' in the plane of potential crack propagation, or crack-line stress. Figs. 1.7b-d and eq. 1.14 indicate that through the principle of superposition removal of tractions, '$T(x)$' and addition of tractions, '$\sigma(x)$' results in an unchanged SIF.

$$K^{(b)} = K^{(c)} + K^{(d)} = K^{(c)} \qquad \text{- (1.14)} \qquad \text{since: } K^{(d)} = 0$$

1.3 – Calculation of SIF

Numerous methods exist for the calculation of SIF solutions for cracked geometries containing boundaries and subject to various loading arrangements. These are grouped below as the three general classes of numerical, experimental and analytical. While each methodology has been employed to develop useful SIF data a short description of each is designed to highlight the limitations of each approach for application to defect assessment.

1.3.1 – Numerical Methods

Recent years have seen the advent of readily available and greatly enhanced computer processing ability leading to exciting developments in finite element and boundary element approaches to complex fracture problems. There are indeed few crack situations, which cannot be modelled to a good degree of accuracy, given enough time and resources. A multitude of commercial software packages exist, often incorporating 'user-friendly' model pre and post-processing, promoting the techniques to one of the most powerful stress analysis tools available to the analyst.

Their implementation requires considerable skill and insight from the operator and are, therefore, likely to remain the preserve of specialists working in a research context. Moreover, implementation by a non-specialist could yield dangerously erroneous solutions. Further to these limitations, solutions gained through numerical techniques are often developed for specific applications and are generally applicable within restrictive limits of validity. Engineering optimisation and defect assessment of components in service however, often require broad ranging solutions, which can be rapidly calculated. The versatility of the approaches, however, makes them extremely useful. Chapters 3 and 9 contain a more in-depth description of their application to cracked geometries.

1.3.2 – Analytical Methods

A great number of analytical methods have been used to calculate the SIF for cracked structures. In general, they involve the application of complex stress analysis tools that are beyond the scope of many engineers outside the research community. Many of the approaches can be applied to simple and idealised geometries to formulate closed-form expressions for crack tip SIFs and make up the majority of those contained in compendia. Generally, these approaches do not lend themselves well to the analyses of geometries containing more than one boundary or to cracks embedded in three-dimensional geometries, unless applied numerically. If applied numerically the approaches suffer similar limitations to those described in the preceding section.

Conformal mapping (transformation) as implemented by Hasebe and Iida[1.17] to cracks at triangular notches in semi-finite planes, body force methods by Nisitani and Isida[1.16] to cracks at semi-elliptical notches in infinite and semi-finite planes are two salient examples of such techniques applied to notched components. In both instances, the influence of the notch upon SIF was the focus of study. As previously stated SIF solutions for cracks influenced by both notches and other remote boundaries are far more useful for the modelling of complex geometries.

1.3.3 – Experimental Methods

Numerous experimental methods exist for the determination of SIF solutions for complex crack situations. The more prominent include optical and crack growth methods. Optical methods are an example of the relation of a measurable quantity to the crack tip stress, strain and displacement fields. An epoxy representation of the component contains a machined thin slit or 'crack'. The phase of polarised light passing through the specimen is altered by the magnitude of stress in the loaded component. A resulting interference fringe pattern is used to evaluate the shear stress field in the region of the crack tip, which relates to the SIF as given by eq. 1.15.

$$K_I = \frac{\tau_{xy}}{f(\theta)}\sqrt{2\pi r} \qquad \text{- (1.15)}$$

Procedures exist for the determination of SIFs in three-dimensional bodies and has been implemented by Smith and Smith[1.18] for mixed-mode problems through usage of eqs. 1.16 and 1.17.

$$(K_I + K_{II})^2_{\theta=\pi/2} = 8\pi r\tau^2_{xy} \qquad \text{- (1.16)} \qquad K_{II\theta=0} = \tau_{xy}\sqrt{2\pi r} \qquad \text{- (1.17)}$$

Conducting a simple fatigue test upon a specimen of interest while measuring simultaneous crack size and the number of applied stress cycles allows the extraction of SIF data from an integrated form of the Paris Law. The approach requires knowledge of material properties pertaining to crack growth.

Both experimental methods introduced above suffer obvious and acute limitations with respect to the defect assessment criteria. Great care and attention is required to derive SIF solutions of good quality and are time-consuming, even when apparatus is pre-existing. Experimental methods are, however, useful for the validation of SIF solutions gained through a numerical or analytical model. An experimental method based on fatigue crack growth rates as described above is applied in chapter 7 for the validation of SIF solutions.

1.4 – Approximate SIF Solutions

The difficulty associated with the calculation of SIFs for engineering components was stated in the preceding section. The methodologies highlighted in section 1.3 indicate that no one approach can be used to generate SIF solutions that satisfy the defect assessment criteria. A number of procedures are presented here that modify known simple solutions to approximate situations that are more complex.

Among the more simple methods for obtaining SIF solutions is that offered by the superposition technique. Complex loading arrangements can be considered a combination of several more simple (or known) arrangements with differing boundary conditions and known SIFs. For the simple case of a finite strip subject to an arbitrary linear stress distribution, the required crack-line stress distribution is modelled as a superposition of known tension and bending solutions crack via eq. 1.18. In the case of a finite width strip, relevant SIF solutions are provided by Brown and Srawley[1.19] for an edge crack or Newman and Raju[1.20] for a surface crack.

$$K = \left(\sigma_t Y_t + \sigma_b Y_b\right)\sqrt{\pi a} \qquad \text{- (1.18)}$$

A number of alternative approximate methods for the computation of SIFs from stress distributions are reviewed by Rooke *et al.*[1.21]. The methods are based on the familiar and firmly established SIF solution for an edge crack in a semi-finite plane, subject to a remotely applied uniform tensile stress. For a crack of depth '*a*', a SIF solution, referred to as the free surface correction, is given below.

$$K = 1.1215\sigma_o\sqrt{\pi a} \qquad \text{- (1.19)}$$

Approximate SIF solutions are possible for cracks situated at notches provided the crack is small compared to the radius of curvature of the notch root. SIF solutions are obtained by the replacement of the term 'σ_o' with a stress characteristic to the local un-cracked geometry's crack-line stress distribution, '$\sigma(x)$'. Three methods are used to approximate SIF solutions:

Maximum stress $\qquad \sigma_o = \sigma_{\max} = \sigma(0) \qquad$ - (1.20a)

Mean stress $\qquad \sigma_o = \sigma_{mean} = \frac{1}{a}\int_0^a \sigma(x)dx \qquad$ - (1.20b)

Tip stress $\qquad \sigma_o = \sigma_{tip} = \sigma(a) \qquad$ - (1.20c)

The maximum stress method applied (eq. 1.20a) to notched geometries provides a simple approximation, as SCF data for numerous notch types are readily available[1.22]. Estimations are conservative, but do accurately represent an extreme situation ($a \ll \rho$). This can be used with the alternative extreme situation ($a \gg \rho$) where the SIF solution is given by eq. 1.21 to provide useful limiting information for an approximate SIF distribution.

$$K = 1.1215\sigma_o\sqrt{\pi(a+b)} \quad \text{- (1.21)}$$

Usage of eqs. 1.20b and 1.20c involve more calculations and require knowledge of the stress distribution ahead of the notch in the un-cracked body. Smith and Miller[1.23] proposed an approximate design rule for evaluating SIFs for cracks at elliptical notches, which encorporates the influences of both notch depth, '*b*' and size defined by root radius, 'ρ'. An approximate measure of the extent of the notch stress field was developed. For elliptical notches cracks within the notch stress field are treated as 'short' and characterised by an approximate SIF expression given as 1.22a. Long cracks are treated as inclusive of the notch depth acted upon by the nominal stress (1.22b).

'short' crack $a < 0.13\sqrt{b\rho}$ $K = \left(1+7.69\sqrt{b/\rho}\right)^{1/2}\sigma_o\sqrt{\pi a}$ - (1.22a)

'long' crack $a > 0.13\sqrt{b\rho}$ $K = \sigma_o\sqrt{\pi(a+b)}$ - (1.22b)

Lukas[1.24] noted that SIFs for cracks ahead of notches given by analytical formulae, given above are often not sufficiently accurate and was amongst the first to propose an empirical expression based upon the notch S.C.F and notch root radius. Eq. 1.23 was developed from the analytical solutions of Newman[1.25] for notches in infinite or semi-finite sheets and was shown to be applicable to notches in finite sheets albeit with a more restricted limit of validity.

$$K = \frac{QK_T}{\sqrt{1+4.5(a/\rho)}}\sigma\sqrt{\pi a} \quad \text{- (1.23)}$$

The similarity of stress fields ahead of many notch forms lead Kujawski[1.26] to adapt a generic expression for the stress field with eq. 1.20c to develop closed form equations for SIF distributions ahead of notches. Eq. 1.24 is reported valid only for short cracks (a/ρ < 3), and compared to published solutions, for cracks at double edge notched and embedded edge notched geometries under uniform tension, gives an approximation with errors reported less than 5%.

$$K = \frac{QfK_t\sigma}{2}\left[\left(1+2\frac{a}{\rho}\right)^{-\frac{1}{2}} + \left(1+2\frac{a}{\rho}\right)^{-\frac{3}{2}}\right]\sqrt{\pi a} \quad \text{- (1.24)}$$

where:

$$f = 1 + \frac{\tan(\pi / 2K_t)}{2.8}\left(\frac{a}{\rho} - 0.2\right) \quad \text{for} \quad \frac{a}{\rho} \geq 0.2; \quad \text{else} \quad f = 1$$

'Q' is a crack shape factor equal to 1.12 for an edge crack and 0.65 for a semi-circular surface crack.

A principle allowing the combination of geometric influences upon SIFs of simpler and known ancillary SIF solutions is described by Rooke[1.27, 1.21, 1.28] and referred to as a compounding technique. Each ancillary solution describes the geometric influence of a single boundary upon the crack, which when compounded with other similar solutions can be used to estimate SIFs for cracks influenced by multiple boundaries. Eq. 1.25 describes the compounding principle where 'K_T' is the SIF for a complex geometry containing multiple boundaries, 'K_n' is the SIF with only the nth boundary present and 'K_o' is the SIF with no boundaries present. 'K_e' represents a term for the influence of boundary-boundary interaction on the SIF solution.

$$K_T = K_o + \sum_n (K_n - K_o) + K_e \qquad \text{- (1.25)}$$

The method was used to formulate cracks emanating from holes in finite width sheets, as shown in fig. 1.8 together with appropriate ancillary configurations. An equivalent crack length, 'a" and section, 'b" for ancillary solutions is calculated to be representative of the crack length, 'a' and section, 'b' for the object solution. A number of alternative geometric situations, common to the aerospace industry such as cracks at fasteners, were solved using the approach. In each case, the remote stress fields were similar for object and ancillary geometries. Performance of the methodology is unclear, when applied to non-similar loading arrangements e.g. bending.

The usefulness of SIF solutions for short cracks at notches, such as those described above does suffer practical limitations. The LEFM assumption of small-scale plasticity at the crack tip is often does not always hold, due to the formation of a plastic zone at the notch root caused by the notch stress concentration. Nevertheless, approximate relations, such as those presented above, have and continue to be, widely employed in design calculations.

In many situations the more prominent methods for determining SIFs for cracks in complex geometric configurations or subject to complex loading arrangements, reviewed here, give approximations that are acceptable for practical cases. As Rooke[1.21] states, errors are often no greater than those due to uncertainties in other parameters such as crack sizing, material characterisation, service loads, etc. There will be, however, cases where the methodologies will

give an unrealistic approximation. Furthermore, it is likely that no methodology, used in isolation, will give a satisfactory result for more demanding situations and will therefore require their combination. Errors introduced into calculations are increased, and with no strict guidance, regarding their limits of applicability renders their validity and accuracy largely unknown.

The preceding sections highlight the difficulty in calculation of SIF solutions, particularly when the crack is situated in a complex geometry and subject to a non-simple stress state. At present no versatile methodology exists that allows the formulation of rapid and reliable SIF solutions universally applicable to determine accurate SIF solutions for a wide range of complex crack problems.

1.5 – The SIF Weight Function

Calculation of the SIF for a cracked body through application of the methods listed in sections 1.3 and 1.4 yields a result specific to a single set of boundary conditions. An alternative set of boundary conditions applied to the same body requires a repeat analysis to determine a new SIF and constitutes a further limitation to those described. Knowledge of a single SIF solution and associated loading condition, however contains sufficient information such that the SIF for that body can be computed subject to an arbitrary loading condition. Recognition that the crack opening displacement (COD) field, '$u(a,x)$' and associated SIF of a cracked linear elastic body for any symmetrical load system is sufficient for the determination of the stress intensity factor for the same body under any other symmetrical load system was made in the seminal works of Rice[1.29] and Bueckner[1.30]. They independently derived the weight function, '$m(a,x)$' expressed as eq. 1.26 in which the known SIF and associated COD are denoted by the subscript 'r'.

$$m(a,x) = \frac{H}{K_r}\frac{\partial u_r(a,x)}{\partial a} \qquad \text{- (1.26)}$$

Once determined, new SIFs for the cracked body subject to arbitrary loading are calculated by integrating the product of the weight function and the crack-line stress distribution, '$\sigma(x)$' present in the crack plane over the crack length (eq.1.27).

$$K = \int_0^a \sigma(x)m(a,x)dx \qquad \text{- (1.27)}$$

The weight function offers a method by which SIF solutions can be accurately and rapidly calculated for cracks subject to complex loading arrangements. In terms of the defect assessment criteria once calculated for a specific geometry, it provides a potentially efficient and powerful tool

for SIF computation. Further discussion of the weight function in this section is restricted to mode I crack opening of one-dimensional edge cracks, however weight function theory is applicable to two-dimensional cracks and mixed mode crack systems.

1.5.1 – Weight Functions for One-Dimensional Cracks

Rice[1.29] showed the SIFs, 'K_1' and 'K_2' of a cracked isotropic elastic body resulting from loading arrangements, denoted by subscipts, '1' and '2', respectively are related as follows.

$$K_2 = \frac{E}{2K_1}\left[\int_\Gamma T_{i2}\frac{\partial u_{i1}}{\partial a}d\Gamma + \int_A F_{i2}\frac{\partial u_{i1}}{\partial a}dA\right] \qquad \text{- (1.28)}$$

where 'T_i' and 'F_i' are boundary tractions and body forces respectively; 'Γ' and 'A' are the perimeter and area of the body respectively and 'u_i' are displacements in the 'x' and 'y' directions (fig. 1.9). As loading systems '1' and '2' are arbitrarily selected it follows the 'K_2' cannot depend upon 'K_1' and 'u_{i1}' and therefore the weight function, '$m_i(x_i)$' is independent of load system '1'. Thus a weight function is defined as eq. 1.29

$$m_i(x_i) = \frac{E}{2K_1}\frac{\partial u_{i1}}{\partial a} \qquad \text{- (1.29)}$$

From the principle of superposition, any loading system can be represented by tractions applied to the crack face. Description of the weight function can be simplified by eqs. 1.30a,b,c and written in the commonly presented form (without subscript 'y') for a one-dimensional crack subject to pure mode I loading (fig. 1.10), as given in eq. 1.26.

$$m_i(x_i) \rightarrow m_y(a,x), \qquad T_i \rightarrow \sigma_y, \qquad u_i(x_i) \rightarrow u_y(a,x) \qquad \text{- (1.30a,b,c)}$$

An alternative derivation of the weight function considers the purely mode I opening of an edge crack subject to an arbitrary remotely applied loading arrangement, 'T' (fig. 1.10a). A known function describes the corresponding normal stress, '$\sigma(x)$' along the crack-line of the uncracked body. Application of the known normal stress or traction directly to the crack faces causes a displacement, 'u', a function of crack size, 'a' and crack ordinate, 'x' in the 'y' direction (fig. 1.10b). An equation for the associated strain energy, 'U' is presented as eq. 1.31.

$$U = \frac{1}{2}\int_0^a \sigma(x)u(a,x)dx \qquad \text{- (1.31)}$$

Differentiating with respect to crack size gives:

$$\frac{\partial U}{\partial a} = \frac{1}{2}\int_0^a \sigma(x)\frac{\partial u(a,x)}{\partial a}dx \qquad \text{- (1.32)}$$

A fracture mechanics expression (eq. 1.33) relates the elastic strain energy release rate, '∂U/∂a' to the SIF.

$$\frac{\partial U}{\partial a} = G = \frac{K_I^2}{H} \qquad \text{- (1.33)}$$

where: $H = E$ for plane stress $\qquad H = \frac{E}{(1-\upsilon^2)}$ for plane strain

Substitution of eq. 1.33 into 1.32 yields the elementary weight function equations given as eq. 1.26.

Fett *et al.*[1.31] provide a similar derivation of the weight function and demonstrate its independence of loading using Betti's reciprocal theorem. They considered a crack subject to two different loading arrangements resulting in crack-line stress distributions, '$\sigma_1(x)$' and '$\sigma_2(x)$', two mode I crack opening displacements, '$u_1(a,x)$' and '$u_2(a,x)$' and crack tip SIFs, 'K_1' and 'K_2' respectively. Two energy balance equations for the two situations can be written (eq. 1.34a,b)

$$\frac{K_1^2}{H} = \frac{1}{2}\frac{\partial}{\partial a}\int_0^a \sigma_1(x)u_1(a,x)dx \qquad \frac{K_2^2}{H} = \frac{1}{2}\frac{\partial}{\partial a}\int_0^a \sigma_2(x)u_2(a,x)dx \qquad \text{- (1.34a,b)}$$

Superposition of the two loading arrangements yields the following.

$$\frac{(K_1+K_2)^2}{H} = \frac{1}{2}\frac{\partial}{\partial a}\int_0^a (\sigma_1(x)+\sigma_2(x))(u_1(a,x)+u_2(a,x))dx \qquad \text{- (1.35)}$$

This expands to.

$$\frac{(K_1+K_2)^2}{H}=\frac{1}{2}\frac{\partial}{\partial a}\left[\int_0^a \sigma_1(x)u_1(a,x)dx+\int_0^a \sigma_1(x)u_2(a,x)dx+\int_0^a \sigma_2(x)u_1(a,x)dx+\int_0^a \sigma_2(x)u_2(a,x)dx\right] \quad \text{- (1.36)}$$

Invoking Betti's reciprocal theorem, which considers two equilibrium conditions '1' and '2' of an elastic body subject to boundary tractions, 'σ_1' and 'σ_2' resulting in associated displacements 'u_1' and 'u_2' respectively. The theorem states that the work done by boundary tractions 'σ_1' moving through displacements 'u_2' is equal to boundary tractions 'σ_2' moving through displacements 'u_1'. Application to the crack problem concerning crack face loading and crack face displacements yields the following relation.

$$\int_0^a \sigma_1(x)u_2(a,x)=\int_0^a \sigma_2(x)u_1(a,x) \quad \text{- (1.37)}$$

Substitution gives.

$$\frac{K_1^{\,2}}{H}+\frac{K_2^{\,2}}{H}+2\frac{K_1K_2}{H}=\frac{1}{2}\frac{\partial}{\partial a}\left[\int_0^a \sigma_1(x)u_1(a,x)dx+2\int_0^a \sigma_1(x)u_2(a,x)dx+\int_0^a \sigma_2(x)u_2(a,x)dx\right] \quad \text{- (1.38)}$$

Further substitutions of eqs. 1.34a,b and subsequent re-arrangement gives the form of the weight function given by eq. 1.26.

$$K_1=\frac{H}{2K_2}\frac{\partial}{\partial a}\int_0^a \sigma_1(x)u_2(a,x)dx \quad \text{- (1.39)}$$

Interpreting loading state '2' as a reference state denoted by a subscript, 'r' results in the fundamental weight function equations for one-dimensional cracks subject to purely mode I opening. Loading states '1' and '2' may be arbitrarily selected, indicating the weight function's independence of loading. A weight function description of SIF, as given by eq. 1.26, is useful as it allows the influence of loading, represented by the crack-line stress, to be separated from the influence of geometry. The weight function represents the Green's function for SIF calculation. The weight function is equal to the SIF resulting from a pair of unit loads, 'F' acting normally to, and opening the crack faces at the point, 'x'' (fig. 1.11) such that:

$$m(a,x')=K \quad \text{- (1.40)}$$

The weight function for an edge crack in a semi-finite plane is shown in fig. 1.12 as the SIF solution for a unit point load applied to an edge crack in a semi-finite plane as described above and published by Hartranft and Sih[1.32]. The singular form of the weight function is evident as 'x' approaches 'a' indicating that stresses near the crack tip strongly influence the SIF. The weight function depends only on the geometry of the crack and component and has units of '$m^{-1/2}$'. The weight function is therefore presented in a non-dimensional form normalised to a characteristic dimension such as crack depth in the case of fig. 1.12.

Once determined, the weight function can be used without limitation to rapidly calculate new SIF solutions for an arbitrary loading arrangement through knowledge of only the crack-line stress distribution. It should be remembered that the term 'crack-line stress distribution' refers to the stress distribution present in the plane of the uncracked geometry. A required stress distribution, '$\sigma(x)$' in many instances, may be calculated by application of standard analytical or numerical stress analysis techniques. Only a single calculation needs to be performed to solve for '$\sigma(x)$', since crack length is not a parameter. For numerical and analytical methods for the determination of SIF, numerous calculations for varying crack size are required.

A weight function approach offers the analyst a versatile tool for the rapid calculation of SIFs for cracks in components subject to complex loading arrangements. Its computational efficiency, compared to alternative means, without compromising accuracy and the simple form of eq. 1.27 makes the weight function approach a powerful and efficient analysis tool for the engineer concerned with the calculation of SIFs. These conducive characteristics can only be realised, however if the same is true of the calculation of the weight function. The success of the methodology depends upon accurate and reliable calculation of the weight function, which has been the focus of much research activity since the weight function was identified.

1.5.2 – Calculation of the Weight Function

Though first presented in the early 1970s, advantages offered by application of the weight function method remained largely unrealised due to the problematic description of the COD field. Though reference SIF data for a range of cracked geometries is widely available from handbooks and compendia[1.9-1.13], accompanying information regarding the associated COD field is only presented for a limited number of simple cases. Petroski and Achanbach[1.33] defined COD as a function of stress intensity factor and corresponding crack-line stress distribution heralding a breakthrough in the practical usefulness of the weight function. An approximate crack face displacement function for edge cracks was proposed (eq. 1.41) requiring a single reference SIF solution and the associated crack-line stress distribution. The principle of self-consistency is applied to yield information concerning the only unknown parameter, '$G(a/t)$'.

$$u(a,x) = \frac{\sigma_o}{H\sqrt{2}}\left[4Y(a,t)\sqrt{a(a-x)} + \frac{G(a,t)(a-x)^{3/2}}{\sqrt{a}}\right] \quad \text{- (1.41)}$$

where:

$$G(a,t) = \frac{\left[\frac{\sqrt{2}}{\sigma_o} I_1 - 4Y(a/t)\sqrt{a} I_2\right]\sqrt{a}}{I_3} \quad \text{- (1.42)}$$

$$I_1 = \int_0^a [K(a)]^2 da \qquad I_2 = \int_0^a \sigma(x)(a-x)^{1/2} dx \qquad I_3 = \int_0^a \sigma(x)(a-x)^{3/2} dx \quad \text{- (1.43a,b,c)}$$

The universal crack face displacement function proposed was based upon three criteria. The displacement must display the appropriate limiting behaviour near the crack tip (eq. 1.44), consistent behaviour for small cracks and simple enough such that unknown parameters can be easily determined from knowledge of the SIF and associated crack-line stress distribution.

$$u_{r(x\to a)} = \left(\frac{8}{\pi}\right)^{\frac{1}{2}} \frac{K_r}{H}\sqrt{a-x} \quad \text{- (1.44)}$$

The approximate crack opening profile proposed by Petroski and Achenbach was implemented to formulate weight functions to solve for edge cracks in semi-finite planes, finite strips and radial cracked rings. Numerous authors,[1.34-1.38] however questioned the methodology's dependence upon the reference stress field and whether applicability is restricted to moderately changing stress fields. Their findings concluded that usage of discontinuous, high gradient, non-uniform and partial crack loading gave discrepancies in the calculated crack opening displacement and subsequent inaccurate weight functions and SIFs. While the Petroski-Achenbach methodology was shown adequate for a range of practical engineering problems involving uniform, small gradient and monotonically varying loading, it has been shown inadequate for complex loading configurations. Fett[1.36] suggests the reason for increasing deviations in COD calculations with increasing non-homogeneity of reference stress field stems from the approximate nature of the assumed form of Petroski-Achenbach's COD. The Petroski-Achenbach COD represents the first two terms of the series representation of COD developed analytically by Wigglesworth[1.39] given in eq. 1.45.

$$u_r(a,x) = \sum_{i=0}^{\infty} C_v \left(1 - \frac{x}{a}\right)^{i+\frac{1}{2}} \quad \text{- (1.45)}$$

Errors introduced by usage of the approximate COD are difficult to estimate and furthermore the process suffers further loss in accuracy due to the cumbersome computational processes involved with differentiation of the approximate COD function.

It was shown by Niu and Glinka[1.40] that usage of the Petroski-Achenbach COD, its subsequent differentiation and substitution into eq. 1.26 results in the form of a 'Bueckner' weight function given below.

$$m(a,x) = \frac{2}{\sqrt{2\pi(a-x)}}\left[1 + M_1\left(1 - \frac{x}{a}\right) + M_2\left(1 - \frac{x}{a}\right)^2\right] \quad \text{- (1.46)}$$

where:

$$M_1 = \frac{4\dfrac{d[Y(a/t)]}{d(a/t)} + 2Y(a/t) + \dfrac{3}{2}G(a/t)}{2Y(a/t)} \quad \text{and} \quad M_2 = \frac{\dfrac{d[G(a/t)]}{d(a/t)} - \dfrac{1}{2}G(a/t)}{2Y(a/t)}$$

The above expression of the Petroski-Achenbach approach as a weight function is a convenient representation, however determination of weight function coefficients 'M_1' and 'M_2' remains computationally involved. To this end coefficients are expressed in a parametric form by Niu and Glinka for a given crack geometry and reference load case. Widespread implementation of the procedure for more general usage remains problematic requiring special attention devoted to differentiation processes. Brennan[1.41] notes that numerical differentiation required for general reference cases is a source of considerable numerical instability resulting in additional sources of error in calculation of the weight function.

Fett[1.42] showed that an arithmetic series representation of COD given by eq. 1.47 and '$C_o = 1$' could be used with additional reference cases (multiple reference states) and geometric observations of the COD to formulate weight functions of higher accuracy for situations involving partial and steep stress gradients. The series representation foregoes the attempt to describe the complete COD field and constitutes an arithmetic power series based upon the near crack tip COD field condition given by eq. 1.44. The first two terms in the series represent the Petroski-Achenbach approximation.

$$u = \sqrt{8}\frac{\sigma_0}{H} aY(a)\sum_{i=0}^{\infty} C_i\left(1-\frac{x}{a}\right)^{i+\frac{1}{2}} \qquad \text{- (1.47)}$$

A number of 'Buckner type' weight functions were subsequently developed, each of the same form and sharing a common leading singular term. Glinka and Shen[1.43] compared the general weight function proposed by Fett[1.42] (eq. 1.48) to a variety of known analytical and numerical weight functions.

$$m(a,x) = \frac{2}{\sqrt{2\pi(a-x)}}\left[1 + C_1\left(1-\frac{x}{a}\right) + C_2\left(1-\frac{x}{a}\right)^2 + C_3\left(1-\frac{x}{a}\right)^3 + ... + C_n\left(1-\frac{x}{a}\right)^n\right] \qquad \text{- (1.48)}$$

The above weight function expression truncated to three terms was shown to approximate known weight functions for a range of edge cracks and through cracks subject to symmetric loading to within 1% for cracks less than half through thickness. A fourth term was needed to satisfactorily approximate deeper cracks, however the form of weight function was reported to be less satisfactory for penny cracks subject to symmetric loading. The same study showed that a more universal form of weight function, requiring four terms, was that proposed by Sha and Yang[1.44] reproduced below as eq. 1.49. This weight function was shown to provide a superior approximation to all available weight functions including that for the penny crack.

$$m(a,x) = \frac{2}{\sqrt{2\pi(a-x)}}\left[1 + C_1\left(1-\frac{x}{a}\right)^{\frac{1}{2}} + C_2\left(1-\frac{x}{a}\right) + C_3\left(1-\frac{x}{a}\right)^{\frac{3}{2}} + ... + C_n\left(1-\frac{x}{a}\right)^{\frac{n}{2}}\right] \qquad \text{- (1.49)}$$

Glinka and Shen[1.43] presented a multiple reference state (MRS) methodology requiring a number of linearly independent reference states. For the calculation of a four term weight function three stress intensity factors, 'K_{r1}', 'K_{r2}' and 'K_{r3}' and their associated crack-line stress fields, 'σ_{r1}', 'σ_{r2}' and 'σ_{r3}' are required. Integration of the right hand side of eq. 1.50 results in a system of linear equations from which weight function coefficients, 'C_1', 'C_2' and 'C_3' may be determined.

The availability of three linearly independent SIF solutions is restricted for widespread implementation of the methodology to encompass geometries that are more complex. Where feasible, reliability of the methodology due to the quality of reference solutions is a further possible source of error.

$$\left.\begin{aligned} K_{r1} &= \int_0^a \sigma_{r1}(x)\frac{2}{\sqrt{2\pi(a-x)}}\left[1+C_1\left(1-\frac{x}{a}\right)^{\frac{1}{2}}+C_2\left(1-\frac{x}{a}\right)+C_3\left(1-\frac{x}{a}\right)^{\frac{3}{2}}\right]dx \\ K_{r2} &= \int_0^a \sigma_{r2}(x)\frac{2}{\sqrt{2\pi(a-x)}}\left[1+C_1\left(1-\frac{x}{a}\right)^{\frac{1}{2}}+C_2\left(1-\frac{x}{a}\right)+C_3\left(1-\frac{x}{a}\right)^{\frac{3}{2}}\right]dx \\ K_{r3} &= \int_0^a \sigma_{r3}(x)\frac{2}{\sqrt{2\pi(a-x)}}\left[1+C_1\left(1-\frac{x}{a}\right)^{\frac{1}{2}}+C_2\left(1-\frac{x}{a}\right)+C_3\left(1-\frac{x}{a}\right)^{\frac{3}{2}}\right]dx \end{aligned}\right\} \quad \text{- (1.50)}$$

In an attempt to reduce the number of reference solutions required Shen and Glinka[1.45] implemented a number of geometrical observations concerning the COD profile first reported by Fett[1.42]. The gradient of the COD for through cracks subject to symmetric loading is zero at '$x = 0$' and hence the first derivative of the weight function with respect to 'x' is zero. A similar condition holds for an edge crack, though due to rotation of the cracked section, the second derivative, or curvature of the COD profile is zero at '$x = 0$' at the crack mouth. The two geometric observations are summarised below.

For through cracks: $$\left.\frac{\partial u(a,x)}{\partial x}\right|_{x=0} = 0 \quad \rightarrow \quad \left.\frac{\partial m(a,x)}{\partial x}\right|_{x=0} = 0 \qquad \text{- (1.51)}$$

For edge cracks: $$\left.\frac{\partial^2 u(a,x)}{\partial x^2}\right|_{x=0} = 0 \quad \rightarrow \quad \left.\frac{\partial^2 m(a,x)}{\partial x^2}\right|_{x=0} = 0 \qquad \text{- (1.52)}$$

Therefore, the system of equations for a through crack is given by eq. 1.53, requiring two independent reference solutions.

$$\left.\begin{aligned} K_{r1} &= \int_0^a \sigma_{r1}(x)\frac{2}{\sqrt{2\pi(a-x)}}\left[1+C_1\left(1-\frac{x}{a}\right)^{\frac{1}{2}}+C_2\left(1-\frac{x}{a}\right)+C_3\left(1-\frac{x}{a}\right)^{\frac{3}{2}}\right]dx \\ K_{r2} &= \int_0^a \sigma_{r2}(x)\frac{2}{\sqrt{2\pi(a-x)}}\left[1+C_1\left(1-\frac{x}{a}\right)^{\frac{1}{2}}+C_2\left(1-\frac{x}{a}\right)+C_3\left(1-\frac{x}{a}\right)^{\frac{3}{2}}\right]dx \\ &\frac{\partial}{\partial x}\left\{\frac{2}{\sqrt{2\pi(a-x)}}\left[1+C_1\left(1-\frac{x}{a}\right)^{\frac{1}{2}}+C_2\left(1-\frac{x}{a}\right)+C_3\left(1-\frac{x}{a}\right)^{\frac{3}{2}}\right]\right\}\Bigg|_{x=0} = 0 \end{aligned}\right\} \quad \text{- (1.53)}$$

1.5.3 – A Contemporary MRS Approach

A contemporary weight function methodology presented by Ojdrovic and Petroski[1.46] and reproduced here employs the derivative of crack opening displacement and application of multiple reference states to yield a process, which is of both reduced computational effort and increased accuracy. The weight function is dependent upon the derivative of COD as opposed to the COD field itself. Direct description of the derivative of COD avoids the need to conduct problematic numerical differentiation of the COD field. Their proposed derivative of COD, given by eq. 1.54 is a differentiated form of Fett's arithmetic power series representation of COD presented as eq. 1.47.

$$\frac{\partial u(a,x)}{\partial a} = \frac{4\sigma_o}{H}\sqrt{2}\sum_{j=0}^{m} C_j \left(1-\frac{x}{a}\right)^{j-1/2} \qquad \text{- (1.54)} \qquad \text{where: } C_0 = \frac{Y_1(a)}{2}$$

A procedure for the determination of weight function coefficients was presented by Brennan[1.41] and is reproduced in full below. For each reference case a self-consistency, or energy balance equation exists and is given as eq. 1.55, in which the subscripts '1' and 'i' refer to the first and ith reference cases respectively.

$$K_i(a)K_1(a) = \int_0^a \frac{H}{2}\sigma_i(x)\frac{\partial u(a,x)}{\partial a}dx \qquad \text{- (1.55)}$$

Substituting for the derivative of crack opening displacement, eq. 1.54, yields the following

$$K_i(a)K_1(a) = 2\sqrt{2}\sigma_0 \int_0^a \sigma_i(x)\sum_{j=0}^{M} C_j \left(1-\frac{a}{x}\right)^{j-1/2} dx \qquad \text{- (1.56)}$$

Introducing a new parameter 'W_{ij}' defined by eq. 1.57.

$$W_{ij} = \int_0^a \sigma_i(x)\left(1-\frac{x}{a}\right)^{j-1/2} dx \qquad \text{- (1.57)}$$

Substituting into eq. 1.56 reduces the expression to the following form.

$$\sum_{j=0}^{m} W_{ij}C_j = K_i(a)\frac{Y_1(a)}{2}\sqrt{\frac{\pi a}{2}} \qquad \text{- (1.58)}$$

Knowledge of the first coefficient 'C_0' gives:

$$\sum_{j=1}^{m} W_{ij} C_j = \frac{Y_1(a)}{2}\left[K_i(a)\sqrt{\frac{\pi a}{2}} - W_{i0} \right] \quad \text{- (1.59)}$$

Replacing the right hand side of eq. 1.59 by the term 'Q' yields a set of 'm' linear equations with 'm' unknowns. In matrix notation the system of equations can be expressed as.

$$\boldsymbol{WC = Q} \quad \text{- (1.60)}$$

For the case of two reference states (m=2) the linear equations are:

$$W_{11}C_1 + W_{12}C_2 = Q_1 \quad \text{- (1.61a)}$$

$$W_{21}C_1 + W_{22}C_2 = Q_2 \quad \text{- (1.61b)}$$

Expressions for the unknown coefficients are

$$C_1 = \frac{Q_1 W_{22} - Q_2 W_{12}}{(W_{11}W_{22} - W_{21}W_{12})} \quad \text{- (1.62a)}$$

$$C_2 = \frac{Q_2 W_{11} - Q_1 W_{21}}{(W_{11}W_{22} - W_{21}W_{12})} \quad \text{- (1.62b)}$$

Knowledge of the coefficients allow computation of the weight function from the expression

$$m(a,x) = \frac{H}{2K_r}\frac{\partial u_r(a,x)}{\partial a} = \frac{2\sigma_0}{K_1(a)}\sqrt{2}\sum_{j=0}^{m} C_j\left(1-\frac{x}{a}\right)^{j-1/2} \quad \text{- (1.63)}$$

An alternative representation gives the non-dimensional SIF directly.

$$Y(a) = \frac{1}{a}\sum_{j=0}^{m} C'_j \int_0^a \frac{\sigma_0}{\sigma}\left(1-\frac{x}{a}\right)^{j-1/2} dx \quad \text{- (1.64)} \qquad \text{where : } C'_j = \frac{2\sqrt{2}}{\pi Y_1(a)} C_j$$

1.6 – Weight Functions for Complex Geometries

Calculation of the weight function for a specific geometry via the contemporary MRS methodology requires a number of reference SIF solutions and associated crack-line stress distributions. In circumstances concerning the calculation of a weight function for idealised geometries, reference SIF solutions are contained in compendia (e.g. for tension and bending), however this is not the general case for complex geometries. For instances concerning the calculation of a complex geometry weight function, even a single reference SIF solution may be unavailable or difficult to obtain as described in preceding sections. Chapter 2 includes a discussion of a number of methodologies employed to modify plane geometry weight functions to account for additional geometric features, such as notches. The distinct advantages offered by a weight function description of crack problems was recognised, however each approach described is flawed in some respect, resulting in limitations that do not realise the full potential of a weight function approach.

1.7 – The Composition of Weight Functions

A recent publication by Brennan and Teh[1.47] offers the most promising methodology for the calculation of complex geometry weight functions. Their approach respects the fact that purely geometric influences can be most effectively combined as weight functions. Complex geometry weight functions are, therefore, 'built' from the combination of more simple, or constituent, geometry weight functions. A methodology, termed 'a composition of constituent geometry weight functions' states that the geometric influence of an edge notch in an edge cracked finite width strip can be represented as three more simple geometry weight functions. The form of the 'composition scheme' is presented diagrammatically in figure 1.13.

With reference to fig. 1.13, the required constituent geometries are those that are plane (containing no geometric discontinuity) with and without a remote boundary and a notched geometry containing no remote boundaries. Reference SIF solutions, required for weight function calculation, are in many cases, likely to appear in published literature as discussed in section 1.2.3. Formulation of a weight function for the complex geometry allows new SIF solutions to be readily and rapidly calculated for a geometric configuration containing both a notch and remote boundary, a situation for which published SIF data is sparse. The economy of the composition approach can be appreciated from recognition that a reference solution for single specific geometric notch can be used to solve for the case of that notch, in a finite strip of arbitrary thickness.

The composition of weight functions approach has been widely applied to a variety of edge cracks at edge notches in finite strips[1.48, 1.49]. The solutions are designed to provide new SIF

solutions for geometries that can be used to model a wide range of structural details and components commonly occurring across all engineering industries. In each case, the composition scheme yielded new SIF solutions in a manner compliant with defect assessment criteria. New SIF solutions were demonstrated to be accurate, reliable, and calculated in a manner that may be readily and rapidly implemented by design and maintenance engineers.

Teh[1.50] highlighted the broad ranging scope for development of the composition principle, citing tailoring of the composition scheme to alternative geometry types including asymmetrically edge notched components. Successful development of a composition scheme sharing the conducive qualities achieved for symmetrically edge notched geometries, was identified as a similarly useful analysis tool for a wide range of commonly occurring fatigue/fracture prone components. Since the majority of cracks in engineering components initiate and develop as surface cracks, extension of the composition principle to permit determination of SIFs for surface cracks located at notches, was also highlighted as a desirable objective of future work.

1.8 – Scope of Thesis

This chapter has highlighted the scarcity of high quality SIF data available to engineers concerned with the design and optimisation of fatigue/fracture prone components. An ability to rapidly and reliably calculate SIF data for such components, particularly those of complex form (containing notches) and subject to non-simple stress states (including residual stress) remains beyond the reach of many designers and engineers implementing LEFM analyses.

The SIF weight function was identified as a potentially powerful and efficient means of calculating SIF data for cracks subject to an arbitrary loading arrangement, in a manner that satisfy the required defect assessment criteria. A key property of the weight function, its sole dependence upon crack and component geometry is unique to the weight function, and permits geometric influences to be combined independently of crack loading.

A weight function composition developed by Brennan and Teh utilises known SIF solutions to formulate constituent geometry weight functions, which are subsequently combined. Their approach allows complex geometry weight functions to be formulated from a number of more simple geometry weight functions. Constituent geometries are of the form of those contained in published literature (cracks at notches with no remote boundaries, cracks in plane geometries with no remote boundaries and cracks in plane geometries with remote boundaries). Teh developed and validated the composition approach applying it to a range of symmetric notch types subject to various loading modes.

The scope of this thesis aims at further development of the composition approach, through application to asymmetric and three-dimensional geometries as described in the preceding section. Chapter 2 discusses the performance of the contemporary MRS weight function approach, reviews previous attempts to affect a weight function solution to complex crack problems including a more in-depth presentation of the composition approach and details the scope of work to be undertaken. Generation of reference solutions via application of FEA is fundamental to a weight function approach and is described in chapter 3 for two-dimensional geometries and chapter 9 for three-dimensional geometries. Chapter 4 proposes a novel weight function approach, closely related to the existing composition scheme, for complex geometries termed an interpolation scheme. The composition scheme is shown to suffer limitations, which when applied to asymmetric geometries are acute. The proposed interpolation scheme overcomes these limitations and is universally applicable to edge cracks at edge notched components. Chapter 5 includes a rigorous investigation of the interpolation scheme, applied to edge cracks at two-dimensional symmetric notches, enhanced performance of the novel scheme over the composition scheme, for notches of extreme geometric form is demonstrated. Chapter 6 demonstrates the enhanced economy of the interpolation scheme through a similar study of step notched components. Chapter 7 describes an experimental programme to determine edge crack SIF solutions for cracks at symmetric and step notch geometries via fatigue testing of representative specimens providing additional validation of analytical and numerical solutions. Chapters 8 and 10 concern application of the interpolation scheme to more general two-dimensional asymmetric geometries and to the deepest point of surface cracks at complex three-dimensional geometries. Chapter 11 reviews and evaluates the interpolation scheme, proposes numerous areas for further development and highlights its conducive nature in terms of a number of more advanced fracture mechanic models.

1.9 – References

[1.1] Griffith, A. A., The Phenomena of Rupture and Flow in Solids, *Philosophical Transactions*, Series A, Vol. 221, 1920, pp. 163 – 198.

[1.2] Irwin, G. R., Onset of Fast Crack Propagation in High Strength Steel and Aluminium Alloys, *Sagamore Research Conference Proceedings*, Vol. 2, 1956, pp. 289 – 305.

[1.3] Rice, J. R., A Path Independent Integral and the Approximate Analysis of Strain Concentration by Notches and Cracks, *Journal of Applied Mechanics*, Vol. 35, 1968, pp. 379 – 386.

[1.4] Williams, M. L., On the Stress Distribution at the Base of a Stationary Crack, *Journal of Applied Mechanics*, Vol. 24, 1957, pp. 109 – 114.

[1.5] BS7448-1: 1991, *Fracture Mechanics Toughness Tests – Part 1: Method for the determination of K_{IC}, critical CTOD and critical J values of metallic materials*, British Standards Institute, 1991

[1.6] BS 7910: 1999, *Guidance on Methods for Assessing the Acceptability of Flaws in Fusion Welded Structures.* British Standards Institute, 1991

[1.7] BS 6835-1: 1998, *Method for the Determination of the Rate of Fatigue Crack Growth in Metallic Materials – Part 1; Fatigue crack growth rates above 10^{-8}m per cycle*, British Standards Institute, 1998

[1.8] Paris, P.C. and Erdogan, F, A Critical Analysis of Crack Propagation Laws, *Journal of Basic Engineering*, Vol. 85, 1960, pp. 528 – 534

[1.9] Rooke, D.P. and Cartwright, D.J., *Compendium of Stress Intensity Factors*, Her Majesty's Stationary Office, London, 1976

[1.10] Tada, H., Paris, P.C. and Irwin, G.R., *The Stress Analysis of Cracks Handbook*, Del Research Corporation, Hellertown, Pennsylvania, 1973

[1.11] Sih, G.C., *Handbook of Stress Intensity Factors*, Institute of Fracture and Solid Mechanics, Leigh University, Bethlehem, Pennsylvania, 1973

[1.12] Murakami, Y. (Editor-in-chief) et al., *Stress Intensity Factors Handbook*, Vol. I-II, Pergamon Press, Oxford, 1987. ISBN: 0-08-034809-2

[1.13] Murakami, Y. (Editor-in-chief) et al., *Stress Intensity Factors Handbook*, Vol. III, Pergamon Press, Oxford, 1991. ISBN: 0-08-034809-2

[1.14] Isida, M., Effect of Width and Length on Stress Intensity factors of Internally Cracked Plates Under Various Boundary Conditions, *International Journal of Fracture*, Vol. 7, No. 3 (1971), pp. 301 – 316

[1.15] Benthem, J.P. and Koiter, W.T., *Asymptotic Approximations to Crack Problems, Methods of Analysis of Crack Problems* (edited by G.C. Sih), Vol. 3 (1972), pp. 131 – 178, Noordhoff Int. Pub.

[1.16] H. Nisitani and M. Isida, Simple Procedure for Calculating K_I of a Notch with a Crack of Arbitrary Size and Its Application to Non-propagating Fatigue Crack, *Proc. Joint JSME-SESA Conf. On Experimental Mechanics* (1982), Part I, pp. 150 – 155

[1.17] N. Hasebe and J. Iida, - A Crack Originating from a Triangular Notch on a Rim of a Semi-infinite Plate, *Engineering Fracture Mechanics*, 10 (1978), pp. 773 – 782

[1.18] Smith, D.G. and Smith, C.W., Photoelastic determination of mixed mode stress intensity factors, *Eng. Fract. Mech.*, 4 (1972), pp. 357 – 366

[1.19] Brown Jr., W.F. and Srawley, J.E., Plain Strain Crack Toughness Testing of High Strength Metallic Materials, *ASTM STP 410* (1966), p. 12.

[1.20] Newman Jr., J.C. and Raju, I.S., An Empirical Stress Intensity Factor Equation for the Surface Crack, *Engineering Fracture mechanics*, Vol. 15, No.1-2, pp. 185 – 192, 1981

[1.21] Rooke, D.P., Baratta, F.I. & Cartwright, D.J., Simple Methods of Determining Stress Intensity Factors, *Engineering Fracture Mechanics*, Vol. 14, pp 397 – 426, 1981

[1.22] Peterson, R.E., *Stress Concentration Factor: charts and relations useful in making strength calculations for machine parts and structural elements*, Wiley-Interscience, London, 1974. ISBN: 0-47168-329-9

[1.23] Smith, R.A. and Miller, K.A., Fatigue Cracks at Notches. *Int J. Mech. Sci.* 19, pp. 11-22 (1977)

[1.24] Lukas, P., Stress Intensity Factors for Small Notch-Emanated Cracks. Engineering Fracture Mechanics Vol. 26, No. 3, pp. 471-473, 1987

[1.25] Newman, Jr, J.C., An Improved Method of Collocation for the Stress Analysis of Cracked Plates with Various Shaped Boundaries, *NASA TN D-6376* (1971)

[1.26] Kujawski, D., Estimation of Stress Intensity Factors for Small Cracks at Notches, *Fatigue and Fracture of Engineering Materials and Structures*, 14 (10) pp 953 – 965, 1991

[1.27] Rooke, D.P., *Compounding Stress Intensity Factors Applications to Engineering Structures*, Research Reports in Materials Science – Series One, Editor: Evans, P.E., The Parthenon Press, United Kingdom. ISBN: 1-85070-110-5

[1.28] Rooke, D.P., An Improved Compounding Method for Calculating Stress-Intensity Factors. *Engineering Fracture Mechanics*, Vol. 23, No. 5, pp 783 – 792, 1986

[1.29] Rice, J.R., Some Remarks on Elastic Crack-Tip Stress Fields. *International Journal of Solids and Structures*, Vol. 8, 1972, pp. 751 - 758

[1.30] Bueckner, H.F, A Novel Principle for the Computation of Stress Intensity Factors. *Zeitschrift für Angewandte Mathematik und Mechanik*, Vol. 50, 1970, pp. 529 – 545

[1.31] Fett, T., Caspers, M., Munz, D. and Stamm, H., Determination of Approximative Weight Functions for Straight Through Cracks, International Journal of Fracture, Vol. 43, 1990, pp. 195 – 211.

[1.32] Hartranft, J.R. and Sih, G.C., Methods of Analysis and Solutions of Crack Problems, G.C. Sih ed. Noordhoff, Holland, 1973

[1.33] Petroski, H.J. and Achenbach, J.D., Computation of the Weight Function From a Stress Intensity Factor, *Engineering Fracture Mechanics*, 1978, Vol. 10, pp. 257 - 266

[1.34] Görner, F. et al., Limitations of the Petroski-Achenbach Crack Opening Displacement Approximation for the Calculation of Weight Functions, *Engineering Fracture Mechanics*, 1985, 22, pp. 269 – 277

[1.35] Niu, X. and Glinka, G., On the Limitations of Petroski-Achenbach Crack Opening Displacement Approximation for the Calculation of Weight Functions – Do They Really Exist? *Engineering Fracture Mechanics*, 1987, 26, pp. 701 – 706

[1.36] Fett, T., Limitations of the Petroski-Achenbach Procedure Demonstrated for a Simple Load Case. *Engineering Fracture Mechanics*, 1988, 29, pp. 713 – 716

[1.37] Niu, X., Some Requirements on the Reference Loading with Large Stress Gradient for the Calculation of Weight Functions Using the Petroski-Achenbach Method. *Engineering Fracture Mechanics*, 1990, 36, pp. 167 – 172

[1.38] Wu, X.R., On the Influence of Reference Load Case on the Crack Face Weight Functions. *International Journal of Fracture* 48, pp. 179 – 192, 1991

[1.39] Wigglesworth, L.A., Stress Distribution in a Notched Plate. *Mathematica* 4, pp. 76 – 96 (1957)

[1.40] Niu, X. and Glinka, G., The Weld Profile Effect on the Stress Intensity Factor. *Int. J. Fracture* 35, pp. 3 – 20 (1987)

[1.41] Brennan, F.P., Evaluation of Stress Intensity Factors by M.R.S. Weight Function Approach, *Theoretical and Applied Fracture Mechanics* 20, pp 249 - 256, 1994

[1.42] Fett, T., Mattheck, C. and Munz, D., On the Calculation of Crack Opening Displacement from the Stress Intensity Factor. *Engineering Fracture Mechanics*, 1987, Vol. 27,No. 6, pp. 697 – 715

[1.43] Glinka, G. and Shen, G., Universal Features of Weight Functions for Cracks in Mode I. *Engineering Fracture Mechanics*, 1991, 40, pp. 1135 – 1146

[1.44] Sha, G.T. and Yang, C.T., Weight Functions for Radial Cracks Emanating from a Circular Hole in a Plate. *Fracture Mechanics: Seventeenth Volume*. Editors: Underwood et al., ASTM STP 905, 1986, pp. 573 – 600

[1.45] Shen, G. and Glinka, G., Determination of Weight Functions from Reference Stress Intensity Factors. *Theoretical and Applied Fracture Mechanics*, 1991, 15, pp 237 – 245

[1.46] Ojdrovic, P.R. and Petroski, H.J., Weight Functions from Multiple Reference States and Crack Profile Derivatives. *Engineering Fracture Mechanics*, 1991, 39, pp. 105 – 111

[1.47] Brennan, F.P. and Teh, L.S., Determination of Crack-Tip Stress Intensity Factors in Complex Geometries by the Composition of Constituent Weight Function Solutions. *Fatigue Fract Engng Mater Struct* 27, pp. 1 – 7, 2004

[1.48] Teh, L.S. and Brennan, F.P., Stress Intensity Factors for Cracks Emanating from Two-Dimensional Semi-Circular Notches Using the Composition of SIF Weight Functions. *Fatigue Fract Engng Mater Struct* 28, pp. 423 – 435, 2005

[1.49] Teh, L.S., Love, A.J. and Brennan, F.P., Mode I Stress Intensity Factors for Edge Cracks Emanating from 2-D U-notches Using Composition of SIF Weight Functions. Accepted for publication in the *International Journal of Fatigue* July 2005.

[1.50] Teh, L.S., *Library of Geometric Influences for Stress Intensity Factor Weight Functions*, Ph.D. Thesis, University College London, 2002

1.10 – Figures

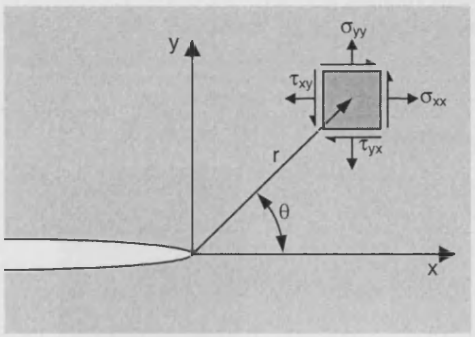

Fig. 1.1 – Definition of Co-ordinate Axis Ahead of a Crack Tip

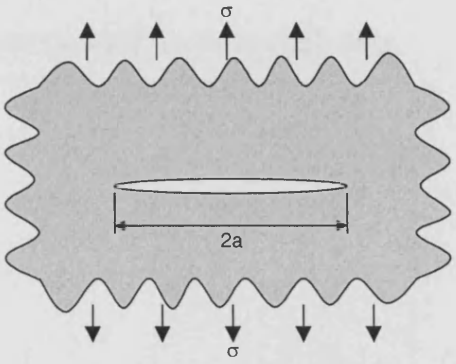

Fig. 1.2 – Griffith Crack

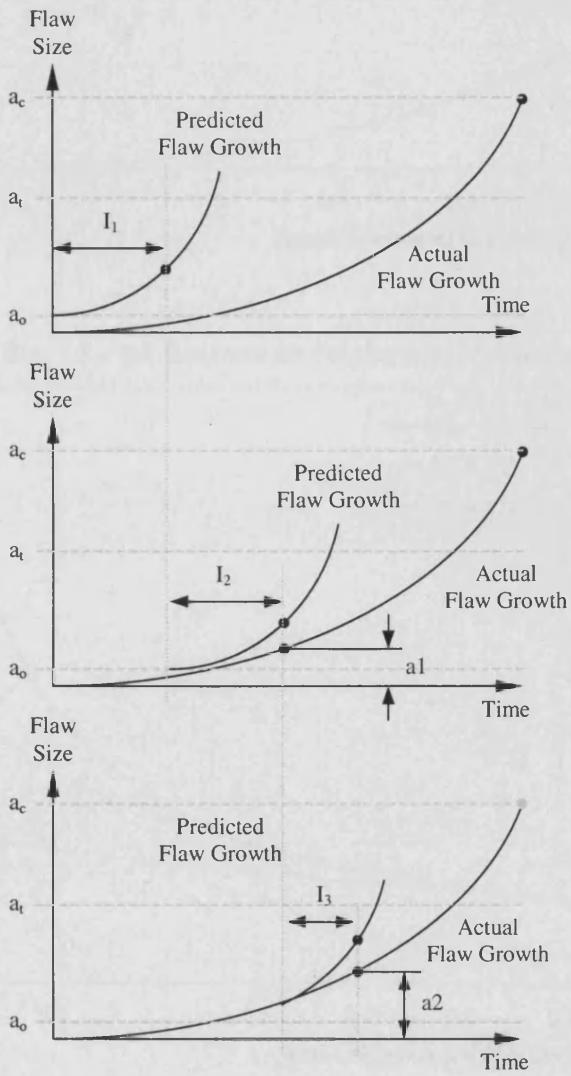

Determination of the first inspection interval I_1. A time calculated to be less than the time taken for the crack to develop from an initial size, a_o to the tolerable flaw size a_t. The tolerable flaw size a_c is determined from the critical flaw size and a factor of safety. NDE techniques are employed for the determination of the initial flaw size.

If no flaws greater than a_o are detected by the first inspection then a second inspection in scheduled at I_2. In general the inspection intervals I_1 and I_2 are of equal length. The second inspection, in the example presented reveals a flaw of size a1, which is greater than a_o

A crack growth analysis is performed to determine the time taken for the flaw to grow from a_1 to a_t. The next inspection interval, I_3 is therefore shorter than those implemented previously. The same process is repeated with inspection intervals decreasing to a point where the crack reaches the tolerable size or the inspection frequency becomes impractical

Fig. 1.3 – Defect Tolerant Design Philosophy

Fig. 1.4 – SIF Solutions for a Through Crack Positioned Centrally in a Finite Width Strip

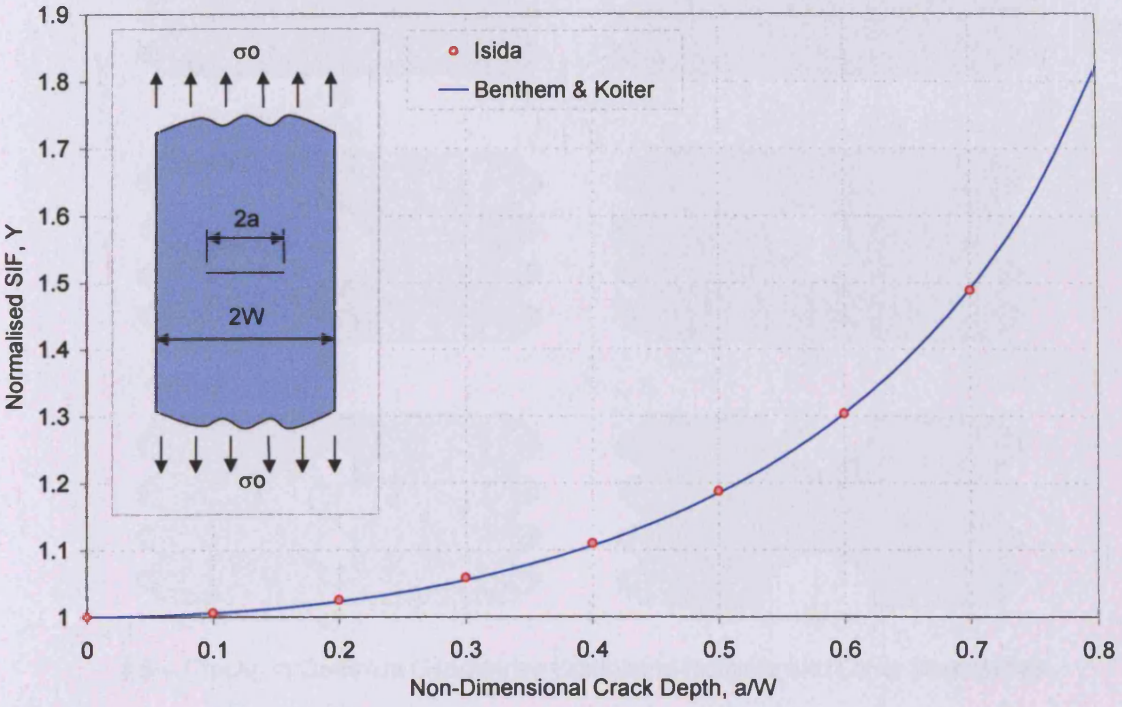

Fig. 1.5 – SIF Solutions for Cracks from an Elliptical Notch in a Semi-finite Plane

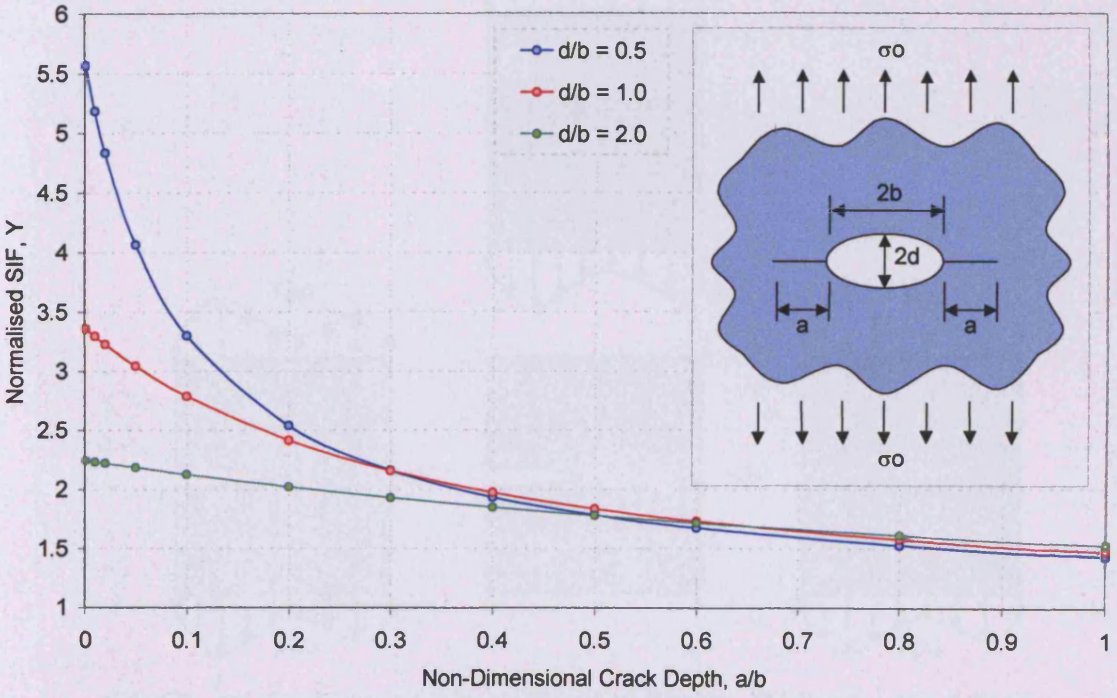

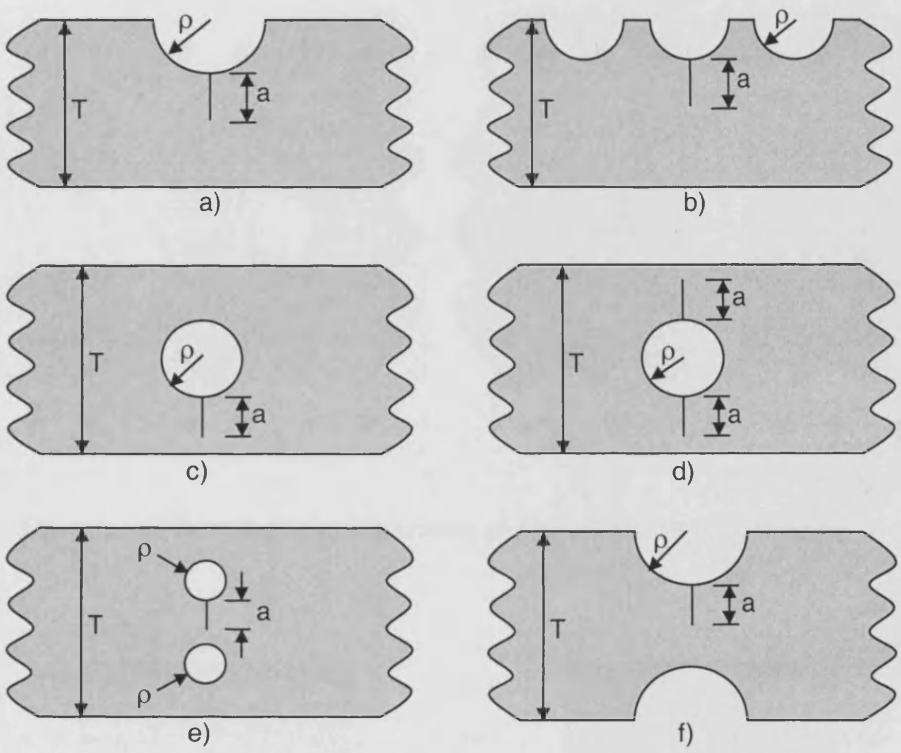

1.6 – Cracks in Complex Geometries Containing Notches and Other Boundaries

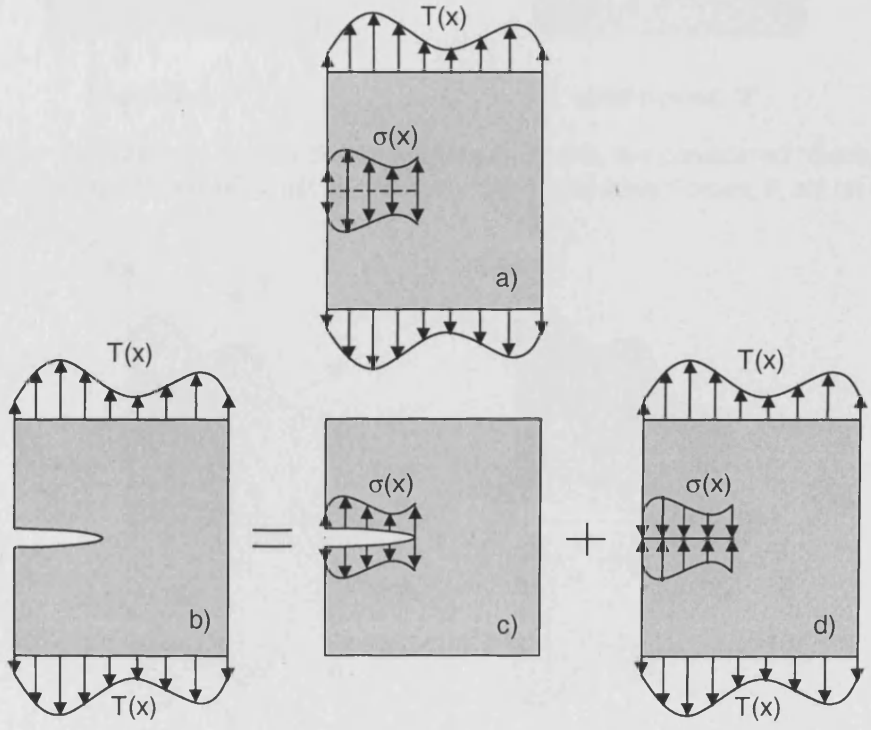

Fig. 1.7 – Replacement of a Remote Boundary Traction, 'T(x)' with a Crack Face Traction, 'σ(x)' Results in an Equal SIF

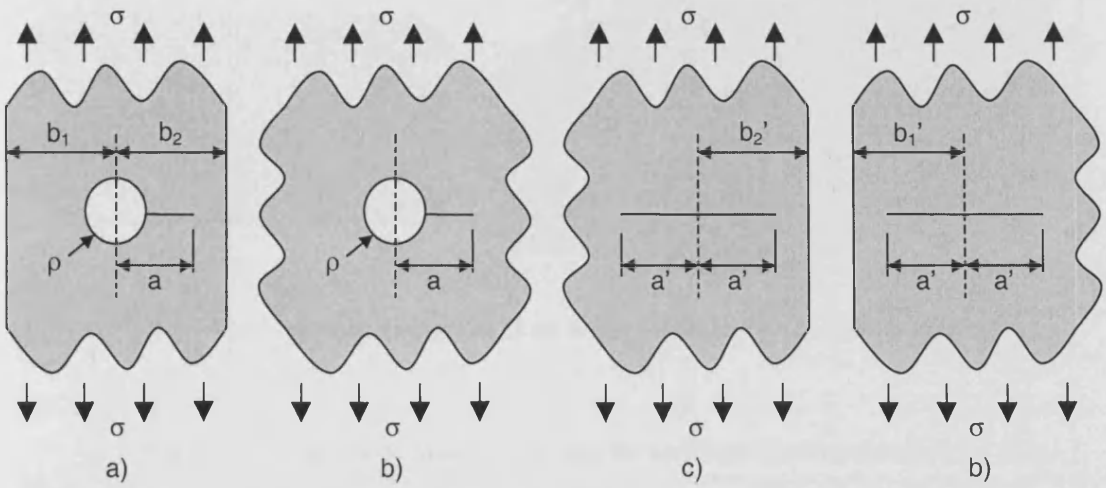

Fig. 1.8 – a) Complex Object Geometry and b,c,d) Ancillary Geomerties

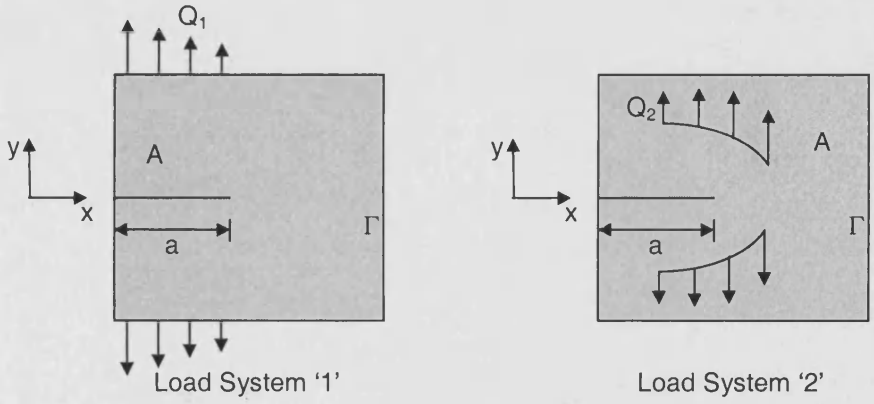

Fig. 1.9 – Two Distinct Loading Systems where Q_1 and Q_2 are considered "Generalised Forces" such that Stresses, T_i act on the Boundary, Γ and Body Forces, F_i act on Area, A

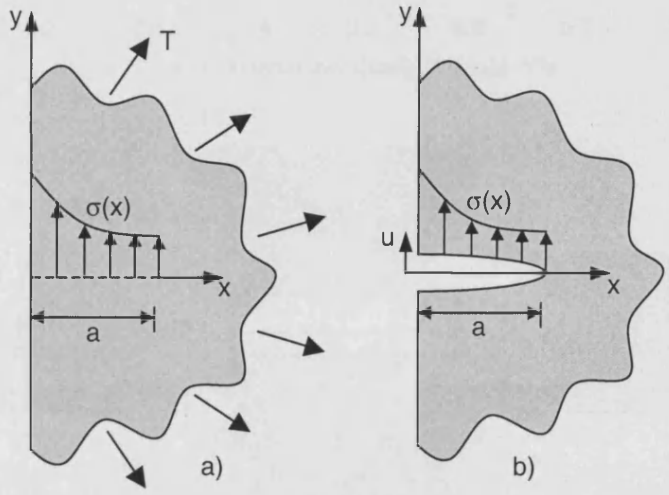

Fig. 1.10 – a) Stress Systems Applied to Uncracked Geometry and b) Resulting Opening Displacement of Crack Faces

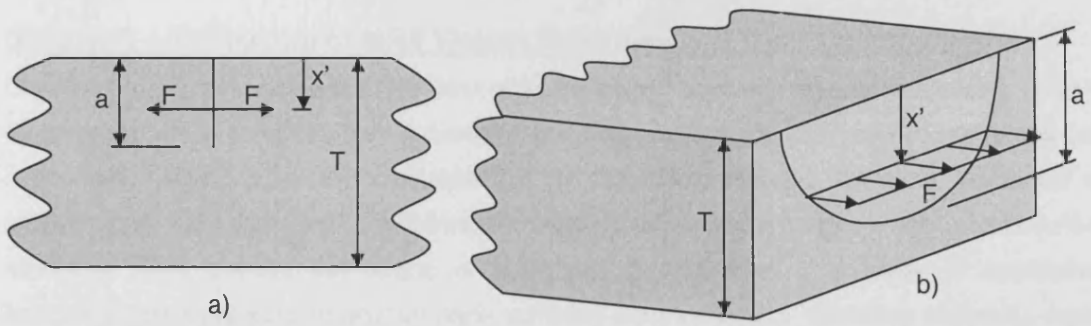

1.11 – Point Loading Applied to a) an Edge Crack and b) a Surface Crack

Fig. 1.12 – Normalised Weight Function for an Edge Cracked Semi-Finite Strip

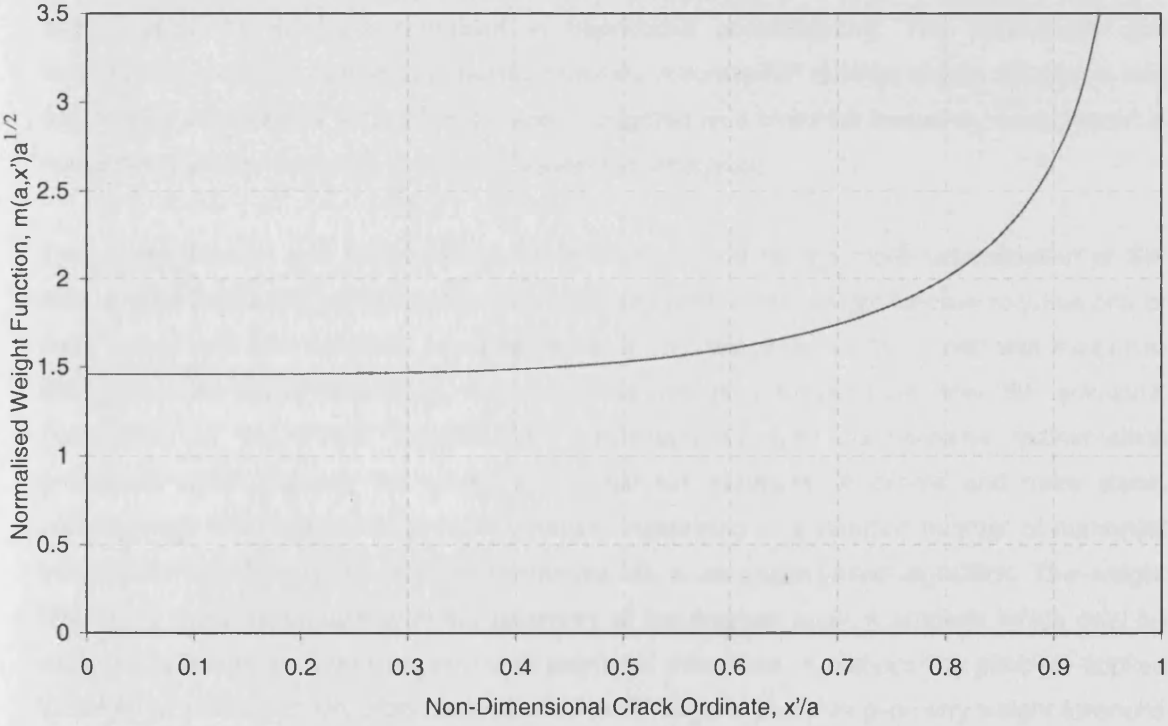

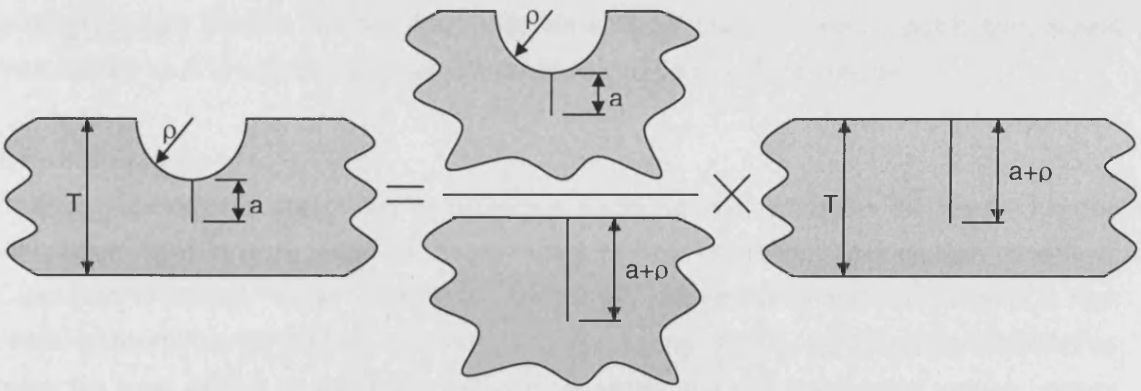

Fig. 1.13 – Diagrammatic Representation of a Composition Scheme

Chapter 2 – The Nature of MRS Weight Functions and Their Composition

Chapter 1 gave an overview of the field of linear elastic fracture mechanics focusing upon the fundamental crack tip stress field parameter, the SIF, employed to characterise numerous crack phenomena. Methods for the calculation of SIF solutions, classed analytical, numerical and experimental, were identified as requiring a considerable level of specialist insight and knowledge rendering them beyond the scope of most design engineers. A number of approximate methodologies were also introduced each suffering from limitations restricting accuracy, rapidity and versatility. Numerous SIF solutions are compiled in the form of handbooks covering a wide range of geometries. These, however are typically confined to idealised geometries subject to the simplest load cases. Engineering optimisation and defect assessment commonly requires SIF solutions for complex geometries subject to complex loading arrangements rendering their approximation by solutions contained in handbooks unsatisfactory. The problematic and longstanding inability to simply and rapidly calculate accurate SIF data for cracks situated in real engineering components and structures was highlighted as a limitation frequently encountered in numerous fracture mechanics and defect assesment analyses.

The weight function was introduced as an efficient method for the rapid determination of SIF solutions for cracks subject to arbitrary loading. Calculation of the weight function requires one or more known reference solutions. However, once determined, it can be integrated with the crack-line stress distribution present in the uncracked geometry to generate new SIF solutions. Formulation of the weight function has traditionally involved cumbersome mathematical processes, which degrade the quality of derived SIF solutions. A simple and more stable contemporary MRS methodology was presented comprising of a reduced number of numerical integrations, which maybe readily implemented via a computer-based algorithm. The weight function is soley dependant upon the geometry of the cracked body, a property which may be exploited to isolate and combine individual geometric influences. A composition principle applied to weight functions was described that allows a wide range of complex geometry weight functions to be 'built' from a relatively small library of constituent geometries. Once formulated the complex geometry weight function can be utilised with an arbitrary crack-line stress distribution, arising from applied loading and residual stress, to rapidly calculate new SIF solutions.

2.1 – Introduction

Chapter 1 included a description of numerous traditional methodologies for weight function formulation from one or more reference solutions and additional geometrical conditions. Calculation of accurate object SIF solutions for partially loaded cracks and those subject to high stress gradients (partial loading, increasing and decreasing tension, fig. 2.1) were identified as being the most difficult to achieve from the most widely available moderately varying uniform

tension and pure bending reference cases. Decisions regarding which, how many and accuracy of reference solutions directly influence the success of a weight function approach and accuracy of object SIF solutions ultimately calculated. The following sections evaluate and discuss the performance of a weight function for an edge cracked strip formulated from various reference load cases using the contemporary MRS approach. The chapter also reviews a number of previously applied schemes to combine geometric influences upon SIF solutions. These are based on the modification of plane geometry weight functions to incorporate additional geometric features, such as notches. The most promising and recent of these is the composition of constituent geometry weight functions proposed by Brennan and Teh[2.1], which is presented in more detail together with an illustration of its excellent performance when applied to a semi-circular notched strip.

2.2 – The Nature of Weight Functions Derived using the Contemporary Methodology

A breakthrough in weight function calculation was made by Petroski and Odjrovic[2.2] who, rather than assume a crack opening displacement field, assumed the form of the derivative of crack opening displacement. Assuming the form of the derivative of crack opening displacement, which is required for weight function formulation, overcomes the requirement to conduct problematic numerical differentiation of the crack opening displacement field. Brennan[2.3] demonstrated the enhanced effectiveness of the contemporary methodology applied to edge cracked geometries and presented a concise MRS approach for weight function calculation.

The contemporary weight function methodology presented in chapter 1 and reviewed above outlines a procedure to overcome the awkward mathematical processes which have hindered previous weight function methodologies and their subsequent wider useage beyond the research community. An ability to simply and acurately calculate weight functions via the implementation of a contemporary MRS approach has been stated. A dedicated study to address the performance of weight functions formulated from various numbers and combinations of reference solutions and their influence upon subsequent new SIF solutions is presented below. This section contains an assessment of weight functions for an edge cracked strip, the plane geometry weight function commonly modified to include additional geometric influences.

2.2.1 - Multiple Reference States

Chapter 1 outlined a procedure by which weight functions may be calculated using the principle of self consistency to a number, 'm' of linearly independent reference load cases allowing expansion of the series representation of the derivative of crack opening displacement to '$m+1$' terms. The number of reference cases available is limited even for the simplest geometries, however the

ability to calculate weight functions of a desired accuracy from *m=1,2* or *3* reference cases was reported.

The present study aims to quantify and verify the number of reference solutions required to formulate weight functions for a simple geometry of a edge cracked finite strip. Brown and Srawley[2.4] obtained mode I SIF solutions for an edge cracked, plane finite width strip by application of the boundary collocation method under uniform tension and pure bending and are reproduced as equations 2.1 and 2.2 respectively. Description of geometry and numerous loading modes are defined in fig. 2.1.

$$Y_{UT} = 1.12 - 0.231\left(\frac{a}{T}\right) + 10.55\left(\frac{a}{T}\right)^2 - 21.72\left(\frac{a}{T}\right)^3 + 30.39\left(\frac{a}{T}\right)^4 \quad \text{- (2.1)}$$

$$Y_{PB} = 1.122 - 1.40\left(\frac{a}{T}\right) + 7.33\left(\frac{a}{T}\right)^2 - 13.08\left(\frac{a}{T}\right)^3 + 14.0\left(\frac{a}{T}\right)^4 \quad \text{- (2.2)}$$

The equations quoted above are an established set of solutions of good accuracy, given as ±0.5% for uniform tension and 0.2% for pure bending over the crack range a/T ≤ 0.6. The associated crack-line stress distributions for the two loading modes are expressed mathematically below.

$$\sigma_{UT}(x) = \sigma_o \quad \text{- (2.3)}$$

$$\sigma_{PB}(x) = \sigma_o\left(1 - \frac{2x}{T}\right) \quad \text{- (2.4)}$$

A third solution for the same geometry subject to linearly decreasing tensile stress over the crack depth applied to the crack faces was calculated via the finite element method, discussion of which and presentation of results is deferred until the following chapter. A curve fit of this SIF solution, to a fourth order polynomial is presented as eq. 2.5 and associated crack-line stress distribution by eq. 2.6

$$Y_{DT} = 0.4397 - 0.196\left(\frac{a}{T}\right) + 6.806\left(\frac{a}{T}\right)^2 - 14.389\left(\frac{a}{T}\right)^3 + 20.035\left(\frac{a}{T}\right)^4 \quad \text{- (2.5)}$$

$$\sigma_{DT}(x) = \sigma_o\left(1 - \frac{x}{a}\right) \quad \text{- (2.6)}$$

Due to the simplistic form of the crack line stress distributions considered above the elements of matrix 'W' and 'Q' maybe determined via closed form integration using eq. 1.55 and 1.57 respectively. These elements are summarised in table 2.1. Similarly matrix inversion and the subsequent determination of weight function coefficients 'C' may be conducted by hand calculation and are produced in table 2.2.

The coefficients presented in table 2.2 are consistent with a weight function of the form given by eq. 1.62. Fig. 2.2 shows the weight functions plotted for a number of crack sizes using one reference case of uniform tension and two refence solutions of uniform tension and pure bending. Also plotted are weight functions calculated via application of the FEA simulating a pair of crack opening point loads as descibed in section 1.5.1. The significant improvement in the accuracy of weight functions calculated with two reference solutions measured with respect to the FE data over those calculated with one reference solution is clearly apparent. This is most evident at larger crack depths where the single reference state weight function gives increasingly worsening solutions whereas accuracy is maintained using two reference states over the crack depth range investigated.

A single reference state weight function maybe applied to derive new SIF solutions in situations where the object loading mode is similar to, or the same as the reference case. In such instances the applied principle of self consistency maintains satisfactory accuracy of derived SIF solutions. If the object loading is markedly different from that of the reference load then derived SIF solutions are less reliable. The two reference state weight function, shown to be of superior accuracy, yields more accurate object SIF solutions irrespective of the forms of object and reference load case. SIF solutions corresponding to an applied uniform tension load case are those that most commonly appear in published in literature. Using this as in a single reference state weight function to derive solutions for partial loading or loading of high gradients can lead to inaccurate SIF solutions. An illustrative example is shown in fig. 2.3 for which new SIF solutions for a partially loaded crack are sought as the object load case (fig. 2.1). The single reference state weight function results in decreasing accuracy compared to those obtained via FEA with increasing crack length. The two reference state weight function solutions show a much improved correlation to the FE data over the range investigated.

Usage of two reference states and the contemporary weight function was shown above, to give solutions of sufficient accuracy for the proposed study. It should be noted, however that the accuracy of derived SIF solutions using an MRS approach are subject to the accuracy of the reference solutions used. Application of a further reference solutions is hindered by the restricted availability of established, high-quality SIF solutions, even when considering the simplest

geometries. A third reference case is judged unnecessary, in this instance, as satisfactory results were shown to be attained using two reference load cases.

2.2.2 - Reference States

Calculation of weight functions by application of multiple reference states requires that reference states are linearly independent such that the determinant of 'W' (eq. 1.58) is non-zero. Considering, once more the formulation of a weight function for an edge cracked finite thickness strip using the two reference states of uniform tension and pure bending, good accuracy is achieved since the two solutions are independent. If, however, the crack depth is shortened, the degree to which the two solutions display independence decreases. At the limit where '$a/T \rightarrow 0$' independence is lost as the two SIF solutions (eqs. 2.1 and 2.2) and crack-line stress distributions (eqs. 2.3 and 2.4) become equal. Matrix 'W' is singular, and therefore no solutions for coefficents 'C' are possible.

The weight function formulated from the reference states of uniform tension and pure bending was used to derive new SIF solutions for the object load case of increasing tension over the crack length (fig. 2.1). The object SIF solutions are plotted in fig. 2.4. The weight function is known to give reliable solutions for long cracks as proven by analysis of the two reference state weight function in the preceding section. For shorter cracks however, the solutions display erronous behaviour, deviating from a known SIF solution for this loading configuration at '$a/T=0$' (an edge crack in a semi-finite plane) given by Ojdrovic and Petroski[2.2] as '$Y=0.6825$'. A plot of the normalised weight function for a range of crack lengths is shown in fig. 2.5 including the 'exact' weight function for '$a/T=0$' obtained from the point loading applied to the edge cracked semi-finite geometry presented by Hartranft and Sih[2.5]. As crack length decreases the weight function for the finite thickness strip would be expected to converge upon that of the semi-finite plane. Fig. 2.5 shows, however that as crack length decreases and the singular condition approaches the weight function displays unstable behaviour. When integrated with a stress distribution of high gradient, such as the increasing tension condition considered here, the generated object solutions are unreliable and of poor accuracy.

Table 2.2 shows the weight function coefficients obtained via the contemporary methodology from the elements listed in table 2.1. The coefficients for the reference cases of uniform tension and pure bending include a troublesome 'T/a' term, which augments errors present in the two reference SIF solutions. The numerical instability of this combination of reference solutions for short cracks limits the accuracy of new SIF solutions. Calculation of new SIF solutions for object load cases with high stress gradients such as those at the root of a sharp notch or as a result of

the presence of a surface residual stress will be subject to a degradation in accuracy similar to that shown here.

A third reference solution corresponding to a decreasing tension over the crack length (fig. 2.1) was generated using FE methods as described and presented in the following chapter. Data was fitted to a polynomial given by eq. 2.5. Utilising this reference state with that of pure bending to formulate a weight function yields a singular matrix 'W' for a crack length equal to '$a/T=0.5$'. No solution is possible at this crack length as shown in fig. 2.4.

The sole two state combination remaining is that of uniform tension and decreasing tension, for which 'W' is non-singular for all crack sizes. Calculation of new SIF solutions for the object load case of increasing tension via the formulation of a weight function from these reference states are shown in fig. 2.6. The form of object SIF solutions are much improved with respect to those calculated using alternative reference case combinations. Thus, utilisation of the less well established reference state solution of decreasing tension, is preferable to that of the published bending solution reference state.

2.2.3 – The Contemporary MRS Weight Function Methodology

The preceding sections have demonstrated the relative ease with which the contemporary methodology can be implemented via a simple algorithm coded into a computer program (section 2.5). Although the contemporary MRS methodology offers a more effective approach for the calculation of weight functions of high accuracy than more traditional approaches detailed in chapter 1, it is not without regard to the number and form of references cases utilised. Decisions regarding the number and type of reference load cases were demonstrated to influence the accuracy of weight function ultimately calculated, particularly where reference and object load cases differ significantly. The most satisfactory SIF solutions for an edge cracked plane strip was obtained utilising a weight function formulated from the two reference load cases of uniform tension and decreasing tension. New SIF solutions calculated via the weight function were shown to be in good agreement with published solutions and those determined from FEA where available.

2.3 – Modification of Plane Geometry Weight Functions for Complex Geometries

The conducive nature of a weight function description of crack problems in terms of the economy and rapidity at which new SIF solutions can be calculated was demonstrated for a simple plane geometry in the preceding section. Reference SIF and associated stress solutions are pre-requisite for weight function formulation, which for situations involving complex geometries, are in most cases, sparse or non-existant. A number of previous attempts to modify plane geometry

weight functions to account for additional geometric influences of a complex geometry were reviewed by Brennan and Teh[2.1]. This section briefly describes a number of these studies, outlining limitations where present and culminates in a more in depth presentation of the most recent and promising development termed a composition of constituent weight functions principle proposed by Brennan and Teh[2.1].

2.3.1 – Previous Attempts to Modify Plane Geometry Weight Functions

An initial attempt to modify a plane geometry weight function was conducted by Impellizeri and Rich[2.6] who sought weight function SIF solutions for cracks emanating from embedded circular notches to approximate those present in lug holes. The procedure involves the correction of an edge crack weight function by modification factors calculated from the ratio of SIF solutions to describe the geometric influence arising from the presence of the notch. Further correction factors based on similar SIF ratios were described to include the geometric influence of finite width and of multiple cracks.

$$m_A(a,x) = m_B(a,x)\frac{Y_C(a)}{Y_D(a)} \quad \text{- (2.7)}$$

Fig 2.7 depicts a diagammatic representation of the simplest methodology to calculate a weight function for an edge crack at a notch embedded in a semi-finite plane. Inclusion of correction factors for finite width indicate the beginings of a composition approach, from the use of more simple constituent geometry SIF solutions to build a weight function for a more complex geometry. In its simplest form shown in fig. 2.7 the methodology uses the exact weight function for an edge crack in a semi-finite plane modified by ratios of SIF solutions describing the geometric influence of the notch. The authors concede, however that their methodology remains an approximation and state that, while the weight function may be used to generate SIF solutions of good accuracy for some loading conditions, it is not the case for all loading conditions. The authors claim that as correction factors are formulated from SIFs for a particular loading condition, uniform pressure on the crack faces, that the resulting weight function may not necessarily be accurate for other loading conditions. Since correction factors are determined from the ratio of SIFs subject to the same crack face loading, it is suggested here that they will be independent of the influence of loading. Measured errors are therefore thought to stem from the precise form of the combination of constituent geometry influences.

Niu and Glinka[2.7, 2.8] sought a weight function solution for welded joints approximated by a step notch geometry. They assumed that the geometric influence of weld angle upon the SIF solution could be manipulated as described by the equation below. The equation states that the ratio of

SIFs for differing weld angles (denoted by superscripts, 'θ and 'α') for similar cracked bodies is equal for both the finite and semi-infinte cases (denoted by subscipts 'f' and 's' respectively).

$$K_f^\theta = \frac{K_s^\theta}{K_s^\alpha} K_f^\alpha \quad \text{- (2.8)}$$

If SIF solutions are for identical loading modes, the following may be written:

$$K_f^\theta = \frac{Y_s^\theta}{Y_s^\alpha} K_f^\alpha \quad \text{- (2.9)}$$

The above equation expressed in the form of weight functions becomes:

$$\int_0^a \sigma^\theta(x) m_f^\theta(a,x) = \frac{Y_s^\theta}{Y_s^\alpha} \int_0^a \sigma^\alpha(x) m_f^\alpha(a,x) \quad \text{- (2.10)}$$

The authors suggest that subsequently the following equation holds:

$$m_f^\theta(a,x) = \frac{Y_s^\theta}{Y_s^\alpha} m_f^\alpha(a,x) \quad \text{- (2.11)}$$

Eq. 2.11, shown diagrammatically as fig. 2.8, can only hold provided that '$\sigma^\theta(x) = \sigma^\alpha(x)$' which is not the case as steps with differing flank angles will have differing local crack-line stress distributions. The modification factor is determined from the ratio of SIF solutions. However unlike Impellizeri and Rich, who utilised SIF solutions for identical crack-line stress distributions, as previously stated the local stress distribution is different for differing notch flank angles. Weight function modifiers, determined from the ratio of SIFs under different crack face loading, will be loading specific. The resulting 'weight function' is dependant upon both loading and geometry, and hence will impair performance of the technique and accuracy of new SIF solutions obtained from it.

Brennan and Dover[2.9] tailored a weight function solution to derive new SIF solutions for surface cracks in threaded connections. A composition of constituent geometry SIF solutions was conducted to evaluate the deepest point SIF solutions for semi-elliptically cracked bars and internally and externally surface cracked threaded connections. SIF solutions for three-

dimensional geometries was achieved utilising a method suggested by Mattheck et al[2.10] by representing a two-dimensional weight function as a one-dimensional weight function.

The composition of SIF solutions (eq. 2.12, fig. 2.9) is similar to that conducted by Niu and Glinka, however the authors recognised both the convenience and significance of using semi-infinite geometries in this process. The semi-infinite geometry is the only situation for which the SIF solutions are identical irrespective of the remotely applied loading (hence the solution is independent of loading mode). Parity of crack-line stress distributions, however is still not achieved and is therefore not independent of loading, subsequently their solution remains an approximation.

$$K_{FS}^{\theta} = \frac{K_{SF}^{\theta} K_{FS}^{0}}{K_{SF}^{0}} \quad \text{- (2.12)}$$

The composition of SIF solutions, described by eq. 2.12 and represented diagrammatically in fig. 2.9 were used as reference solutions for input into a multiple reference state weight function. The authors implemented the weight function methodology developed by Petroski and Odjrovic relieving their proposed weight function solution of the problematic mathematical processes stemming from the Petroski and Achenbach method utilised by Niu and Glinka.

2.3.2 – A Composition Approach

Brennan and Teh[2.1] recognised the crucial fact that purely geometric influences are most effectively described by the SIF weight function. The weight function is solely a property of geometry and therefore, unlike combinations based upon the SIF, a weight function provides a more generalised approach for the calculation of modification factors that are independent of loading. A composition based upon the weight function represented a significant advancement beyond previous approaches, overcoming many of the limitations and approximations of all preceding composition schemes, presented above, to yield a mathematically exact solution.

A weight function composition scheme defined by Brennan and Teh[2.1] for symmetrically notched components is reproduced from chapter 1 as fig. 2.10. It simply states that the ratio of weight functions for the notched geometry to the plane geometry is equal for both finite and semi-finite cases. Upon re-arrangement and expressed mathematically the finite thickness notched geometry weight function can be determined from a combination, or composition, of three more simple geometry weight functions (eq. 2.13)

$$m_D(a,x) = \frac{m_A(a,x)}{m_B(a,x)} m_C(a,x) \quad \text{- (2.13)}$$

Traditionally, a parametric SIF solution for a given notch in a finite strip would necessitate tedious numerical modellling of a number of geometries with differing notch size to strip thickness ratios. The real power and economy of the approach becomes apparent when it is considered that a single specific weight function, that of the notched semi-finite geometry is the sole information required to allow formulation of a weight function for that notch embedded in a strip of arbitrary thickness. The ability to rapidly calculate new SIF solutions from weight functions formulated by the efficient and versatile composition approach indicated that a large number of such solutions could be rapidly generated from a far smaller number of specific solutions.

Teh[2.11] conducted a rigorous study on a weight function composition principle for edge cracked symmetrically notched geometries. A detailed procedure for the determination of Mode I SIF solutions for edge cracks at two-dimensional notched geometries was presented and demonstrated to be accurate and stable across the range of notch sizes and shapes tested and all applied loading modes investigated.

The study utilised the contemporary MRS weight function methodology to formulate constituent geometry weight functions for composition in a manner shown diagrammatically in fig. 2.10 or as the expression given by eq. 2.13. In common with previous investigators a normalisation process using semi-infinite geometries constitues the correction factor which modifies the finite strip geometry, each geometric influence being expressed as a weight function. Further to the pictorial representation of the composition principle a complete mathematical representation of the composition scheme was presented by Teh and reproduced as eq. 2.14.

$$m_D(a,x) = \frac{2\sqrt{\frac{2}{\pi a}}}{Y_{map}} \frac{\left[C_{0A} + C_{1A}\left(1 - \frac{x}{a}\right)\right]}{\left[C_{0B} + C_{1B}\left(1 - \left[\frac{x}{a}\right]_p\right)\right]} \left[C_{0C} + C_{1C}\left(1 - \left[\frac{x}{a}\right]_p\right) + C_{2C}\left(1 - \left[\frac{x}{a}\right]_p\right)^2\right]\left(1 - \frac{x}{a}\right)^{-\frac{1}{2}} \quad \text{- (2.14)}$$

Where: $Y_{map} = \frac{Y_{IA}(a)}{Y_{IB}(a+\rho)} Y_{IC}(a+\rho)$ and $\left[\frac{x}{a}\right]_p = \frac{(x+\rho)}{(a+\rho)}$

The methodology incorporated a single reference state weight function to formulate the semi-finite geometry weight functions since, as Brennan and Dover observed, mode I opening SIF

solutions are identical irrespective of the applied loading mode. A two reference state weight function was used to describe the geometric influence of the finite strip formulated from uniform tension and pure bending loading modes. The premise of the composition scheme was proven by application to a semi-circular notch by Brennan and Teh[2.1]. Excellent performance of the scheme was reported from comparison of new SIF solutions with those published by Wu and Carlsson[2.12]. The composition scheme was demonstrated to yield SIF solutions of high accuracy and reliability in a manner that is rapid and mathematically stable. Once verified, a programme of work was identified to broaden application of the composition scheme to a wide range of symmetric notch types.

2.3.3 – A Library of Geometric Influences for SIF Weight Functions

Once the premise of the composition technique had been verified a programme of work set out to systematically calculate reference stress and SIF solutions for a wide range of notch types. The study incorporated semi-finite, 'U' and 'V' notch types and provided a generic set of reference solutions for input to the weight function composition scheme. A considerable number of finite element models of cracked and uncracked notched semi-finite geometries were created and solved. Ultimately reference solutions were presented, more concisely, as weight function coefficients and in this form were referred to as a 'library' of geometric influences[2.11,2.13]. Validation of a wide range of SIF solutions for cracks at notches in finite width strips were calculated using the composition principle and compared to those derived from in-house finite element studies and those in the published literature, where available. New SIF solutions and constituent geometry weight function coefficients, for numerous symmetrically notched geometries have been presented in recent publications[2.1, 2.14, 2.15]

For all notch configurations investigated, the weight function composition scheme in its presented form was demonstrated to be suitable for deriving new SIF solutions for symmetric bodies under arbitrary symmetric loading conditions. Rigorous validation was achieved through comparison of new SIF solutions to those obtained via numerical means. Several areas of further work were identified by Teh including the broadening of the existing 'Library' of constituent solutions to incorporate asymmetric geometries and weight function composition schemes for surface cracks using one-dimensional weight functions as described by Mattheck et al.[2.10] and employed by Brennan and Dover.

2.4 – Implementation of the Composition of SIF Weight Functions

The following section describes features implemented by Teh to formulate weight functions and derive solutions from them. The scope of work contained in this thesis builds upon that conducted by Brennan and Teh and therefore some of these features are to be used and warrant brief

description here as opposed to subsequent chapters. The composition scheme, applied to a semi-circular notched, finite width strip defined in fig. 2.10, was selected as a demonstrative example of the formulation and composition of constituent geometry weight functions. Implementation of the scheme requires reference SIF and associated stress fields for the three constituent geometries to formulate constituent geometry weight functions.

Numerous existing SIF solutions, under simple loading conditions, for a variety of plane geometries, including the edge cracked finite strip and edge cracked semi-finite strip are available as established fracture mechanics results and can each be described by continuous closed-form equations. As demonstrated in preceding sections these can be used in conjunction with a contemporary methodology to formulate closed-form expressions for weight function coefficients. Reference solutions for the semi-finite notched geometry are non-linear and once determined require to be curve fitted to obtain continuous distributions and integrated numerically as dictated by the comtemporary weight function approach to calculate weight function coefficients. This section describes the calculation of weight function coefficients for the notched semi-finite constituent geometry. The composition scheme, requiring this and plane geometry weight functions, is then applied to generate a new weight function for the notch embedded in a finite strip. New SIF solutions are obtained through integration of the new weight function with crack-line stress distributions corresponding to various loading modes.

2.4.1 – Curve Fitting Reference Solutions

Formulation of weight functions for each constituent geometry requires knowledge of one or more references state SIF and stress solutions. In the case of the two plane geometries, these are readily available from the published literature, many of them presented in preceding sections of this chapter. The form of these SIF solutions and their corresponding stress solutions are of simple linear form and are described mathematically as concise expressions suitable for coding in a computer algorithm. SIF and stress solutions for the notched components are more complex in form and necessitate consideration of the accuracy and limits of validity of the fitted expressions.

The reference SIF solution for the notched semi-finite geometry is influenced by the SCF arising at the notch root under remotely applied loading. This influence decreases as crack depth increases asymptotically to the plane edge crack geometry solution '$Y=1.1215$'. Chen, Nisitani and Mori[2.16] presented discrete SIF data for this configuration depicted in fig. 2.11 subject to a remotely applied uniform stress field. A continuous description of the SIF distribution in terms of the non-dimensional distance from the notch root 'x/ρ' as a polynomial, requires an expression of high order to achieve satisfactory accuracy and limits of validity (eq. 2.15).

$$Y = M_0 + M_1\left(\frac{a}{\rho}\right) + M_2\left(\frac{a}{\rho}\right)^2 + M_3\left(\frac{a}{\rho}\right)^3 + M_4\left(\frac{a}{\rho}\right)^4 + \ldots . M_n\left(\frac{a}{\rho}\right)^n \qquad \text{- (2.15)}$$

Teh[2.11] showed that the SIF distribution can be more concisely and accurately expressed by an equation of the form of eq. 2.16.

$$Y = M_0 + M_1\lambda^1 + M_2\lambda^2 + M_3\lambda^3 + M_4\lambda^4 \qquad \text{- (2.16)}$$

where : $\lambda = \dfrac{1}{1 + a/\rho}$

In a similar manner, the associated crack-line stress distribution for the notched, semi-finite and finite geometries can be more effectively approximated by fourth order polynomials as eqs. 2.17 and 2.18 respectively.

$$\frac{\sigma_{yy}(x)}{\sigma_o} = N_0 + N_1\gamma^1 + N_2\gamma^2 + N_3\gamma^3 + N_4\gamma^4 \qquad \text{- (2.17)}$$

$$\frac{\sigma_{yy}(x)}{\sigma_o} = P_0 + P_1\gamma^1 + P_2\gamma^2 + P_3\gamma^3 + P_4\gamma^4 \qquad \text{- (2.18)}$$

where : $\gamma = \dfrac{1}{1 + x/\rho}$

Teh[2.11] utilised the finite element method to determine SIF solutions and associated crack-line stress distributions for semi-finite geometries, where not available from published literature. For the specific case of the semi-circular notch in a semi-finite strip, solutions published by Chen, Nisitani and Mori[2.16] fit the general form of eq. 2.16 to a high degree of accuracy as illustrated by fig. 2.11. A description of the application of the finite element method to such geometries is deferred to the following chapter, however semi-finite crack-line stress distributions for semi-finite and finite thickness geometries were curve fitted as according to eqs. 2.17 and 2.18. Fig. 2.11 also shows the high degree of correlation achieved for the fitted semi-finite stress distribution.

Coefficients obtained from the curve fitting process, a polynomial regression conducted by Microsoft Excel™ software[2.17] are displayed in tab. 2.3. The terms 'λ' and 'γ' appearing in eqs.

2.12 – 2.14 vary between 1 and 0 and provide a complete description of the SIF and stress distributions whereas the term 'x/ρ' and 'a/ρ' vary between 0 and ∞. The convenience of this representation of both reference solutions allows both the influence of the notch SCF and the nominal stress to which the reference solutions decay, to be modelled without restriction by a concise polynomial expression. Reference solutions for the finite thickness stress distributions are restricted to be valid for the range '$0 < x/t < 0.5$'.

A quantitative assessment of the quality of curve fit (the strength of correlation between fitted curve and discrete data points) can be achieved by quantifying the coefficient of determination termed an *R-squared* value, 'R^2'. The total variation of the discrete data and the variation of that predicted by the curve fit about its arithmetic mean is calculated by the regression analysis conducted by *Microsoft Excel*™ using eqs. 2.19a and 2.19b respectively.

$$\textit{Total Variance in } Y = \sum \left(Y - \overline{Y}\right)^2 \qquad \text{- (2.19a)}$$

$$\textit{Variance in Y Explained by the Curve Fit} = \sum \left(Y' - \overline{Y}\right)^2 \qquad \text{- (2.19b)}$$

The remaining variance is that which cannot be explained by the curve fit giving eqs. 2.19c and 2.20.

$$\textit{Variance in Y Not Explained by the Curve Fit} = \sum \left(Y - Y'\right)^2 \qquad \text{- (2.19c)}$$

$$\sum \left(Y - \overline{Y}\right)^2 = \sum \left(Y' - \overline{Y}\right)^2 + \sum \left(Y - Y'\right)^2 \qquad \text{- (2.20)}$$

The 'R^2 *value*' is calculated as the explained variance divided by the total variance as in eq. 2.21 expressed as a percentage

$$R^2 = \frac{\sum \left(Y' - \overline{Y}\right)^2}{\sum \left(Y - \overline{Y}\right)^2} \qquad \text{- (2.21)}$$

Where Y = Measured discrete data points

$\overline{Y}$ = Arithmetic mean of measured discrete data points

Y' = Data points predicted by fitted equation

'R^2' may take any value between '*0*', indicating no correlation and '*1*', indicating a perfect correlation. With reference to tab. 2.3 the coefficients calculated by the regression analysis allow the discrete reference data to be modelled to a high degree of accuracy. A qualitative assessment of the curve fitting process can be made with reference to fig. 2.11, showing discrete SIF and stress data for the semi-circular notch in a semi-finite plane. 'R^2' values detailed in tab. 2.3, indicate an almost perfect correlation.

2.4.2 – Determination of Weight Function Coefficients

Calculation of weight function coefficients for geometries containing notches is more involved than for plane geometries, as the non-linear reference solutions presented in a format given in the preceding section do not lend themselves well to closed-form integration. For the semi-finite plane containing a notch, numerical integration techniques, conducted by a computer algorithm, are employed for the determination of weight function coefficients. A single reference case is known and therefore a weight function comprising two coefficients may be formed following the methodology outlined in section 1.5.3.

$$W_{01} = \int_0^a \left[N_1\gamma^4 + N_2\gamma^3 + N_3\gamma^2 + N_4\gamma^1 + N_5\right]\left(1-\frac{x}{a}\right)^{-\frac{1}{2}} dx \qquad \text{- (2.22)}$$

$$W_{11} = \int_0^a \left[N_1\gamma^4 + N_2\gamma^3 + N_3\gamma^2 + N_4\gamma^1 + N_5\right]\left(1-\frac{x}{a}\right)^{\frac{1}{2}} dx \qquad \text{- (2.23)}$$

$$C_A = \frac{\sqrt{2}}{\pi} \qquad \text{- (2.24)}$$

$$C_B = \frac{\sqrt{2}}{\pi W_{11}}\left[\frac{Y_t\pi}{\sqrt{2}} - W_{01}\right] \qquad \text{- (2.25)}$$

Weight function coefficients given by eqs. 2.24 and 2.25, are presented in a form compliant with the form of weight function given by eq. 1.62. Complex geometry weight functions are evaluated by the composition of constituent geometry weight functions as dictated diagrammatically by fig. 2.10 and mathematically by eq. 2.13 and subsequently integrated with an object crack-line stress distribution (eq. 2.18) to obtain new SIF solutions.

2.4.3 – A Weight Function Composition Algorithm

The numerical processes required to derive constituent geometry weight function coefficients and new SIF solutions adopting the proposed methodology are most efficiently achieved by computational means. Weight function expressions contain endpoint singularities and therefore caution was exercised to ensure integration procedures produced sufficiently accurate solutions.

Numerous programming languages exist providing powerful tools for the analysis. Digital Fortran™ [2.18] possesses several features conducive for the present study. The outstanding feature offered by the Digital Fortran software package, of special relevance to the proposed algorithm is the inclusion of the ISML (Internal Statistical and Mathematical Libraries) allowing various intrinsic numerical procedures to be called via the subroutine statement. The ISML contains a number of integration routines of which the '*QDAG*' scheme was judged most suitable. The '*QDAG*' scheme is a general-purpose integration routine comprising a 21 point Gauss-Kronrod rule to estimate the integral over a desired subinterval. The routine possesses the capability to estimate the integral of functions containing endpoint singularities to a high degree of accuracy.

The composition algorithm included coding of reference SIF and stress solutions to formulate the constituent weight function coefficients. This was carried out, in the case of the plane geometries, by the usage of the closed-form weight function coefficients, derived in tab. 2.2. In the case of the semi-finite complex geometry the formative parameters of 'W_{ij}' and weight function coefficients were calculated as detailed by eqs. 2.22 – 2.25. Upon calculation of the constituent geometry weight function coefficients, the complex geometry weight function was developed as described by eq. 2.13. New SIF solutions were obtained by integration of the complex geometry weight function with the complex geometry crack-line stress distribution.

2.4.4 – Results

A weight function composition algorithm was constructed to accept reference SIF and associated crack-line stress distributions as described above to formulate constituent geometry weight functions for a semi-circular notch. A composed weight function for the complex geometry of a semi-circular notch in a finite thickness strip was used to determine new SIF solutions from crack-line stress distributions. The performance of the composition technique was evaluated for a range of notch sizes and subject to a variety of applied loading conditions. Validation was sought through the comparison of new SIF solutions obtained from the composition algorithm with those in published literature by Wu and Carlsson[2.12] and those determined from in-house finite element analysis (discussed in chapter 3).

Fig. 2.12 shows two sets of SIF solutions for cracks emanating from the root of a semi-circular notch embedded in a finite thickness strip subject to a remotely applied uniform tension loading condition. For the two notch sizes considered, the results achieved through the composition of weight functions is shown to give an excellent correlation to those calculated by the finite element method. Fig. 2.13 shows a similar plot of SIF solutions for a given notch size and various applied loading modes. Once more, the composed weight function solution is shown to very closely model published and numerical SIF solutions.

The simplicity with which new high quality SIF solutions can be attained via the composition of weight functions is illustrated by this example. The requirement of a notch-specific reference SIF solution and associated crack-line stress distribution was the sole information required by the methodology to formulate the complex geometry weight function. Other information, reference solutions for planar geometries were pre-existing and readily available.

The composition of weight functions methodology was shown to offer a solution for the calculation of complex geometry SIFs. The manner in which this was achieved was demonstrated to be compliant with the defect assessment requirements. The key features of the technique of accuracy, versatility and simplicity were demonstrated and therefore it represents a viable solution for the calculation of complex geometry SIFs.

2.5 – A Programme of Work

The composition of SIF weight functions has been demonstrated to be a convienient method for the determination of SIF solutions for geometries of complex form and subject to complex loading arrangements. At present the composition technique has been comprehensively investigated by Teh[2.11] for a wide range of symmetric notch types and was shown to yield SIF solutions of high accuracy for all notch configurations investigated. The published methodology presents weight function coefficients in the form of a library of constituent geometries allowing the rapid formulation of complex geometry weight functions for finite thickness complex geometries containing edge cracks. The approach is recognised as having great potential for the development of SIF solutions for a great number of alternative geometry types. Those identified by Teh[2.11] include complex geometries which are asymmetric about the crack-line and an extension in application to surface cracks in similar complex geometries.

Asymmetric notches for consideration are those defined as step, intrusion and protrusion notches as displayed and defined in fig. 2.14. The requirement of a weight function approach for these notch configurations is desirable as they may be used to approximate a wide range of engineering components and structural details common throughout engineering industries.

Notches depicted in fig. 2.14 can be used to approximate the thread form of a threaded connection as suggested by Brennan and Dover[2.9] or as welded joints in a manner similar to that of Niu and Glinka[2.7, 2.8] in addition to many more. Both cited fatigue prone applications concern complex stress fields (including residual stress) for which a weight function description is ideally suited.

Application of the composition technique described in this chapter to asymmetric geometries has yet to be verified, however the composition scheme presented by Brennan and Dover[2.9] is reproduced as fig. 2.9 and provides a starting point for investigation. Common to the existing solutions available for symmetric notches, a programme of work is envisaged to systematically describe a library of constituent solutions for notches, defined in fig. 2.14, embedded in semi-finite strips. Extension of the composition principle for the evaluation of SIFs at the deepest point of surface cracks located at notches is presented diagrammatically as fig. 2.15. Both Niu and Glinka[2.7, 2.8] and Brennan and Dover[2.9] have sought similar solutions for three-dimensional geometries however their approaches contained limitations as previously described. A composition of weight functions approach potentially offers a more 'complete' solution and if verified, represents a methodology for the calculation of SIFs for complex three-dimensional situations where very few published solutions exist.

2.6 – References

[2.1] Brennan, F.P. and Teh, L.S., Determination of Crack-Tip Stress Intensity Factors in Complex Geometries by the Composition of Constituent Weight Function Solutions. *Fatigue Fract Engng Mater Struct* 27, pp. 1 – 7, 2004

[2.2] Ojdrovic, R.P. and Petroski, H.J., Weight Functions From Multiple Reference States and Crack Profile Derivatives. *Engineering Fracture Mechanics*, 1991, 39, pp.105 – 111

[2.3] Brennan, F.P., Evaluation of Stress Intensity Factors by Multiple Reference State Weight Function Approach, *Theoretical and Applied Fracture Mechanics*, 1994, 20, pp.249 – 256

[2.4] Brown Jr., W.F. and Srawley, J.E., Plane Strain Crack Toughness Testing of High Strength Metallic Materials, *ASTM STP 410* (1966), p. 12

[2.5] Hartranft, J.R. and Sih, G.C., Methods of Analysis and Solutions of Crack Problems, G.C. Sih ed. Noordhoff, Holland, 1973

[2.6] Impellizzeri, L.F. and Rich, D.L., Spectrum Fatigue Crack Growth in Lugs. *ASTM STP 595*, 1976, pp 320 - 336

[2.7] Niu, X. and Glinka, G., The Weld Profile Effect on Stress Intensity Factors in Weldments. *International Journal of Fracture*, 1987, 35, pp 3 –20

[2.8] Niu, X. and Glinka, G., Stress Intensity Factors for Semi-Elliptical Surface Cracks in Welded Joints. *International Journal of Fracture*, 1989, 40, pp 255 – 270

[2.9] Brennan, F.P. and Dover, W.D., Stress Intensity Factors for Threaded Connections. *Engineering Fracture Mechanics*, 1995, 50, No. 4, pp 545 – 567

[2.10] Mattheck, C., Munz, D. and Stamm, H., Stress Intensity factor for Semi-Elliptical Surface Cracks Loaded by Stress Gradients. *Engineering Fracture Mechanics*, 1983, 18, pp 633 – 641

[2.11] Teh, L.S., *Library of Geometric Influences for Stress Intensity Factor Weight Functions*, Ph.D. Thesis, University College London, 2002

[2.12] Wu, X.R. and Carlsson, A.J., *Weight Functions and Stress Intensity Factors*, Pergamon Press, Oxford, 1991. ISBN: 0-08-041702-7

[2.13] Brennan, F. P. Teh, L. S. and Love, A. J., Library of Geometric Influences for SIF Weight Functions. *Procedings 11th International Conference On Fracture*, Turin 2005

[2.14] Teh, L.S. and Brennan, F.P., Stress Intensity Factors for Cracks Emanating from Two-Dimensional Semi-Circular Notches Using the Composition of SIF Weight Functions. *Fatigue Fract Engng Mater Struct* 28, pp. 423 – 435, 2005

[2.15] Teh, L.S., Love, A.J. and Brennan, F.P., Mode I Stress Intensity Factors for Edge Cracks Emanating from 2-D U-notches Using Composition of SIF Weight Functions. Accepted for publication in the *International Journal of Fatigue* July 2005.

[2.16] Chen, D. Nisitani, H. and Mori, K., Stress Intensity Factors for a Semi-Infinite Plate Having a Semi-Elliptical Notch with a Crack Under Tension. *Transactions of the Japan Society of Mechanical Engineers*, 1989, 55, No. 512, pp 948 – 952.

[2.17] Microsoft Excel, version 97, Microsoft Corporation

[2.18] Digital™ Visual Fortran, Professional Edition Version 5.0.A for Windows NT and Windows 95, Digital Equipment Corporation (now Compaq), 1997

2.7 – Tables

Tab. 2.1 – Elements 'W_j' and 'Q' for the Formulation of Weight Functions for a Crack Subject to Various Loading Conditions.

Loading Mode	Uniform Tension (UT)	Pure Bending (PB)	Decreasing Tension (DT)
Stress Case	σ_o	$\sigma_o\left(1-\frac{2x}{T}\right)$	$\sigma_o\left(1-\frac{x}{a}\right)$
W_0	$2a\sigma_o$	$2a\sigma_o\left(1-\frac{4a}{3T}\right)$	$\frac{2}{3}a\sigma_o$
W_1	$\frac{2}{3}a\sigma_o$	$\frac{2}{3}a\sigma_o\left(1-\frac{4a}{5T}\right)$	$\frac{2}{5}a\sigma_o$
W_2	$\frac{2}{5}a\sigma_o$	$\frac{2}{5}a\sigma_o\left(1-\frac{4a}{7T}\right)$	$\frac{2}{7}a\sigma_o$
W_3	$\frac{2}{7}a\sigma_o$	$\frac{2}{7}a\sigma_o\left(1-\frac{4a}{9T}\right)$	$\frac{2}{9}a\sigma_o$
Q	$\frac{Y_1 a\sigma_o}{2}\left[\frac{Y_{UT}\pi}{\sqrt{2}}-2\right]$	$\frac{Y_1 a\sigma_o}{2}\left[\frac{Y_{PB}\pi}{\sqrt{2}}-2\left(1-\frac{4a}{3T}\right)\right]$	$\frac{Y_1 a\sigma_o}{2}\left[\frac{Y_{DT}\pi}{\sqrt{2}}-\frac{2}{3}\right]$

Tab. 2.2 – Weight Function Coefficients Obtained Using Various Combinations of Loading Conditions

Load Case(s)	C_o	C_1	C_2
UT	$\frac{\sqrt{2}}{\pi}$	$\frac{3\sqrt{2}}{2\pi}\left[\frac{Y_{UT}\pi}{\sqrt{2}}-2\right]$	0
PB	$\frac{\sqrt{2}}{\pi}$	$\frac{\sqrt{2}}{2\pi}\left[\frac{Y_{PB}\pi}{\sqrt{2}}-2+\frac{8a}{3T}\right]\left[1-\frac{4a}{3T}\right]^{-1}$	0
DT	$\frac{\sqrt{2}}{\pi}$	$\frac{5\sqrt{2}}{2\pi}\left[\frac{Y_{DT}\pi}{\sqrt{2}}-\frac{2}{3}\right]$	0
UT & PB	$\frac{\sqrt{2}}{\pi}$	$\frac{525\sqrt{2}}{32\pi}\left(\frac{T}{a}\right)\left[\frac{2\pi}{5\sqrt{2}}(Y_{UT}-Y_{PB})-\frac{8\pi Y_{UT}a}{35\sqrt{2}T}-\frac{64a}{105T}\right]$	$\frac{525\sqrt{2}}{32\pi}\left(\frac{T}{a}\right)\left[\frac{2\pi}{3\sqrt{2}}(Y_{PB}-Y_{UT})+\frac{8\pi Y_{UT}a}{15\sqrt{2}T}+\frac{32a}{45T}\right]$
PB & DT	$\frac{\sqrt{2}}{\pi}$	$\frac{525\sqrt{2}}{32\pi}\left[\frac{1}{2}-\frac{a}{T}\right]^{-1}\left[\frac{2\pi}{\sqrt{2}}\left(\frac{Y_{PB}}{7}-\frac{Y_{DT}}{5}\left(1+\frac{4a}{7T}\right)\right)+\frac{16a}{35T}-\frac{44}{105}\right]$	$\frac{525\sqrt{2}}{32\pi}\left[\frac{1}{2}-\frac{a}{T}\right]^{-1}\left[\frac{2\pi}{\sqrt{2}}\left(\frac{Y_{DT}}{3}\left(1+\frac{4a}{5T}\right)-\frac{Y_{PB}}{5}\right)+\frac{16a}{45T}+\frac{64}{45}\right]$
UT & DT	$\frac{\sqrt{2}}{\pi}$	$\frac{525\sqrt{2}}{8\pi}\left[\frac{\pi}{35\sqrt{2}}(5Y_{UT}-7Y_{DT})-\frac{16}{105}\right]$	$\frac{525\sqrt{2}}{8\pi}\left[\frac{\pi}{15\sqrt{2}}(5Y_{DT}-3Y_{UT})+\frac{8}{45}\right]$

Tab. 2.3 – Curve Fitted SIF and Stress Distributions for a Semi-Circular Notch

Semi-Finite SIF Distribution Coefficients (Eq. 2.16)						
ρ/T	M_0	M_1	M_2	M_3	M_4	R^2 (%)
0	1.1215	0.5187	0.844	-1.0245	1.9671	100.0
Semi-Finite Stress Distribution Coefficients (Eq. 2.17)						
ρ/T	N_0	N_1	N_2	N_3	N_4	R^2 (%)
0	1.003	0.002	0.397	0.677	1.004	100.0
Finite Stress Distribution Coefficients for Uniform Tension (Eq. 2.18)						
ρ/T	P_0	P_1	P_2	P_3	P_4	R^2 (%)
0.0625	0.9846	0.132	0.39	0.4877	1.1822	100.0
0.125	0.8252	1.0363	-1.0806	1.7535	0.8907	100.0
0.250	-0.7849	7.738	-11.129	9.3926	-0.8347	100.0
0.375	-8.7373	37.389	-53.916	38.964	-7.4659	100.0
Finite Stress Distribution Coefficients for Pure Tension (Eq. 2.18)						
ρ/T	P_0	P_1	P_2	P_3	P_4	R^2 (%)
0.25	0.9846	0.132	0.39	0.4877	1.1822	100.0
Finite Stress Distribution Coefficients for Pure Bending (Eq. 2.18)						
ρ/T	P_0	P_1	P_2	P_3	P_4	R^2 (%)
0.25	-4.4012	18.594	-28.131	22.629	-5.7219	100.0

2.8 – Figures

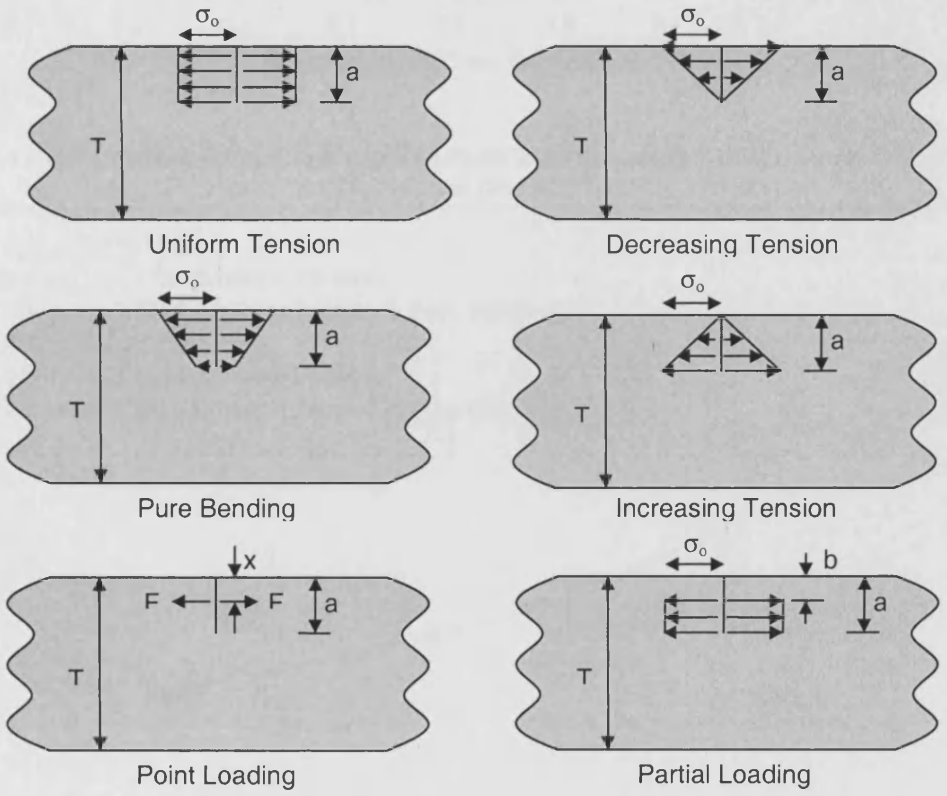

Fig. 2.1 – Definition of Various Loading Conditions Applied to a Finite Strip

Fig. 2.2 – Weight Functions for an Edge Cracked Finite Strip Formulated from One and Two Reference Load Cases

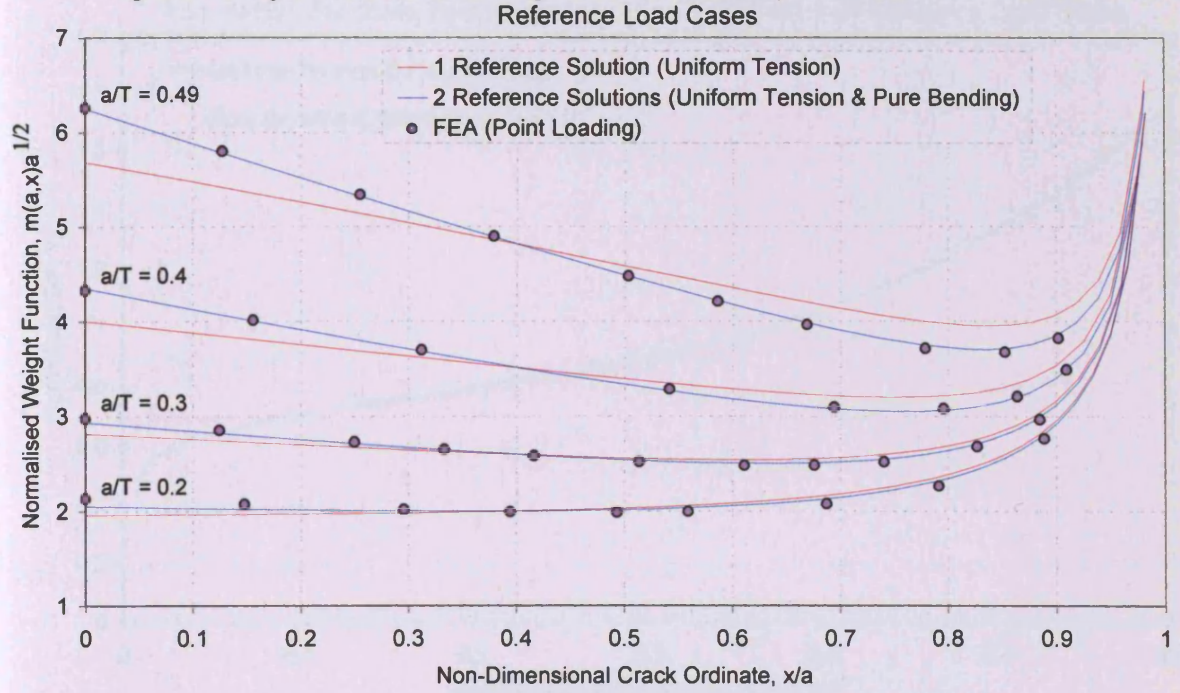

Fig.2.3 – SIF Solutions for an Edge Cracked Finite Strip Subject to Partial Loading Obtained from Weight Functions Formulated from One and Two Reference Load Cases

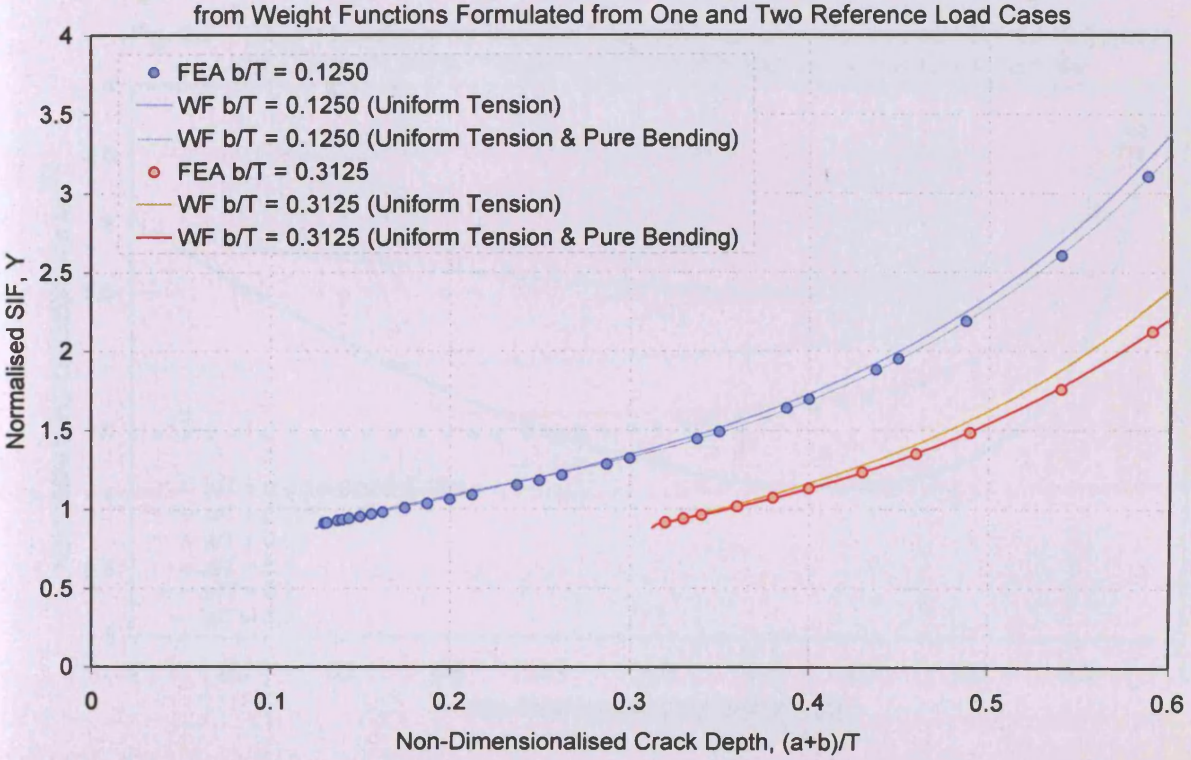

Fig.2.4 – SIF Solutions for an Edge Cracked Finite Strip Subject to Increasing Tension Obtained from Weight Functions Formulated from Two Combinations of Reference Load Cases

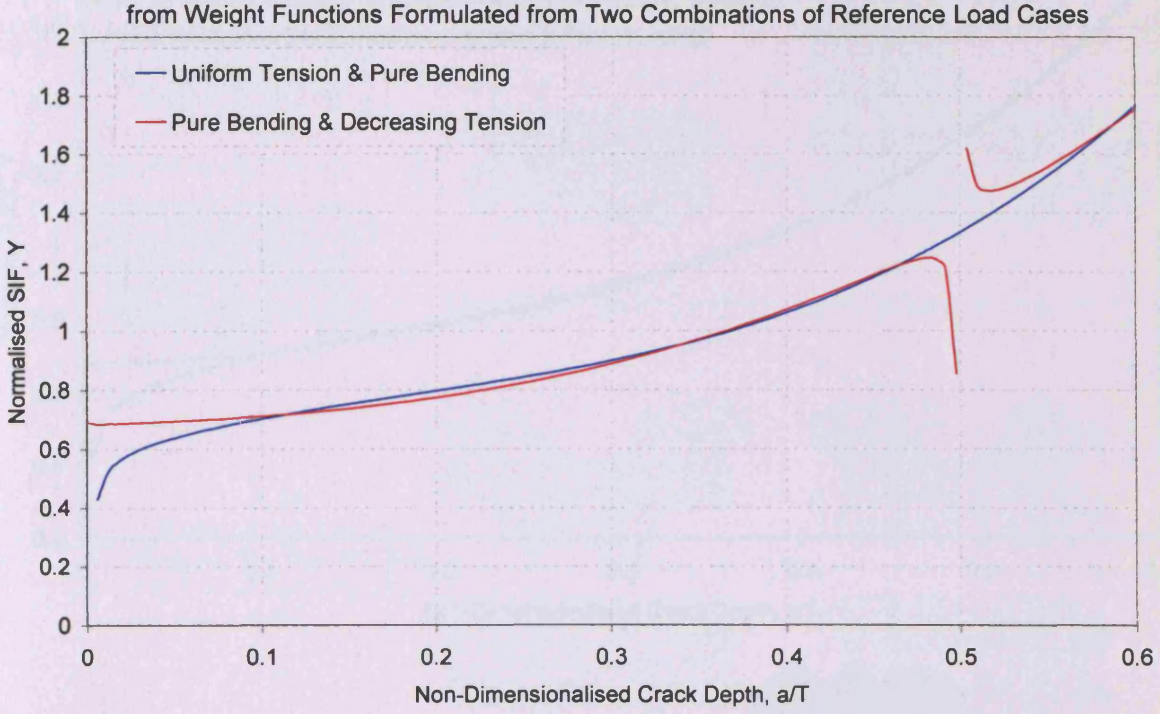

Fig. 2.5 – Weight Functions for an Edge Cracked Finite Strip Formulated from the Reference Load Cases of Uniform Tension and Pure Bending for Various Crack Lengths

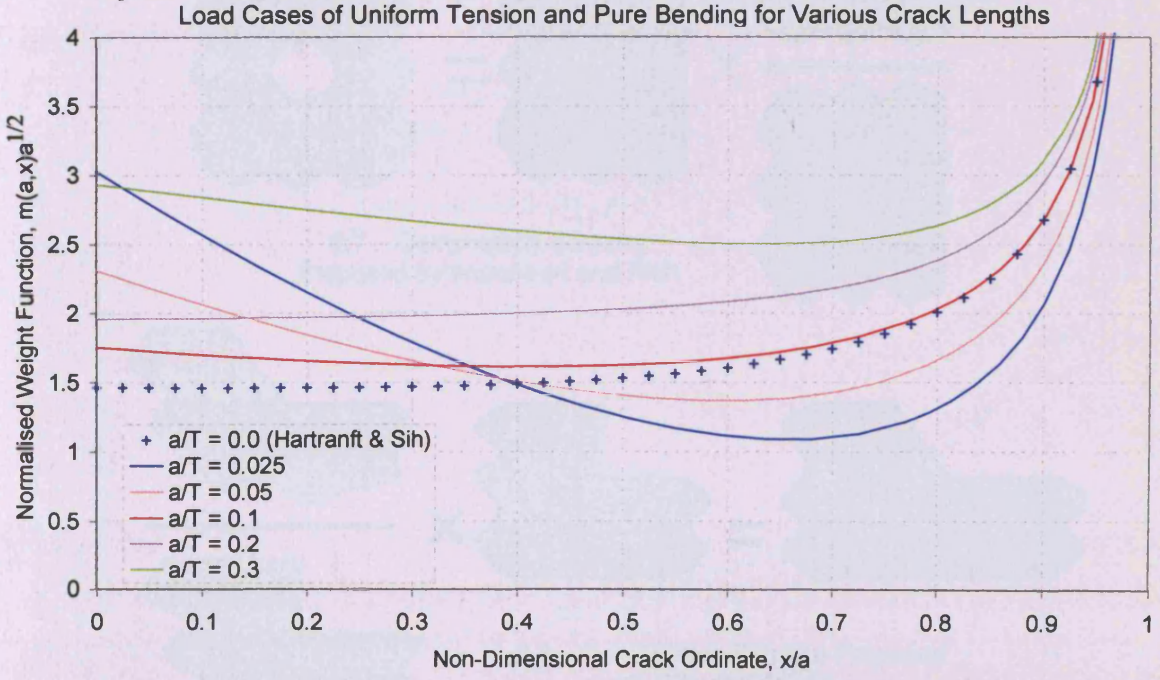

Fig.2.6 – SIF Solutions for an Edge Cracked Finite Strip Subject to Increasing Tension Obtained from Weight Functions Formulated from Two Combinations of Reference Load Cases

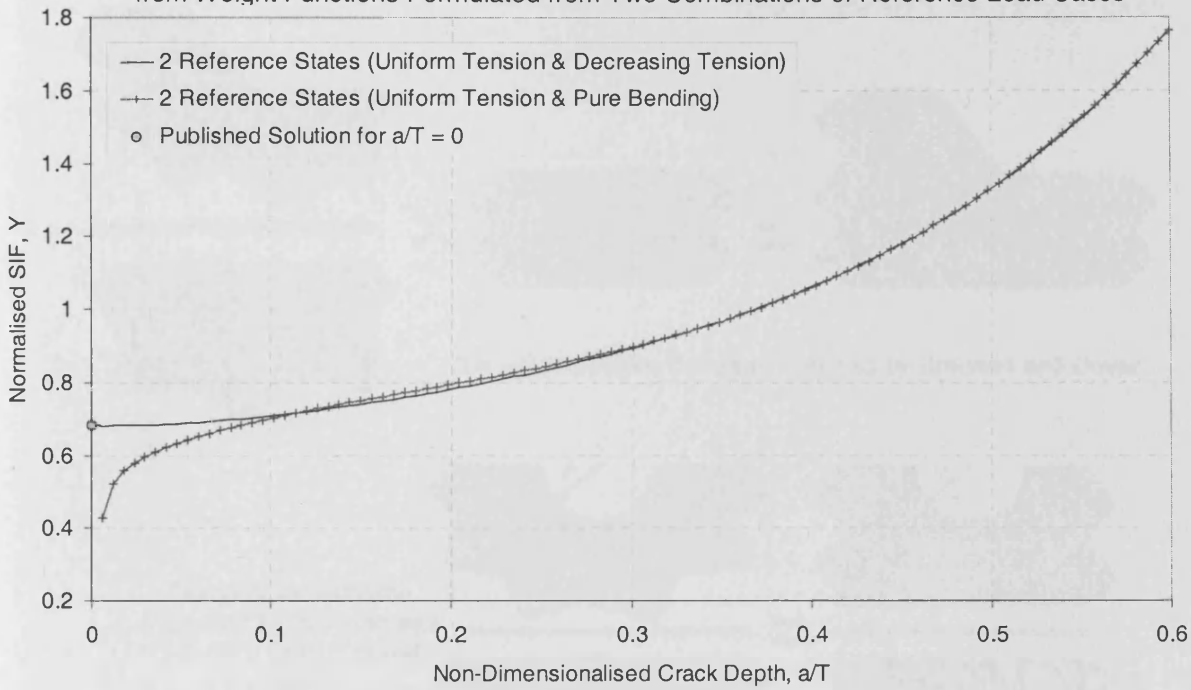

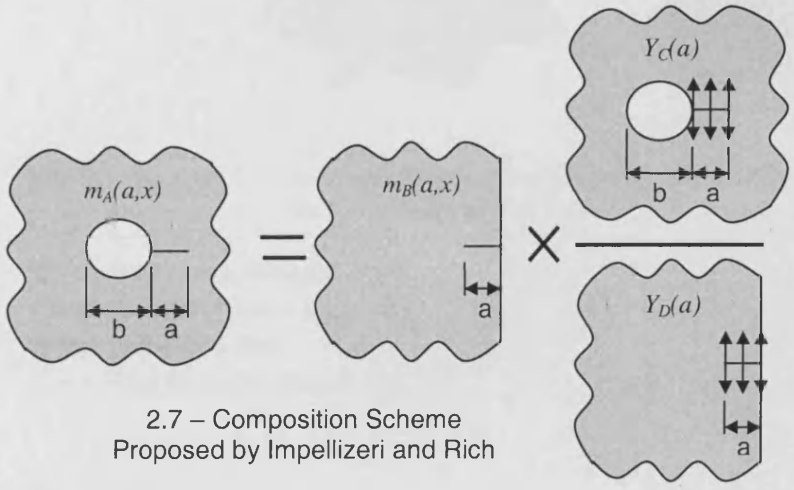

2.7 – Composition Scheme Proposed by Impellizeri and Rich

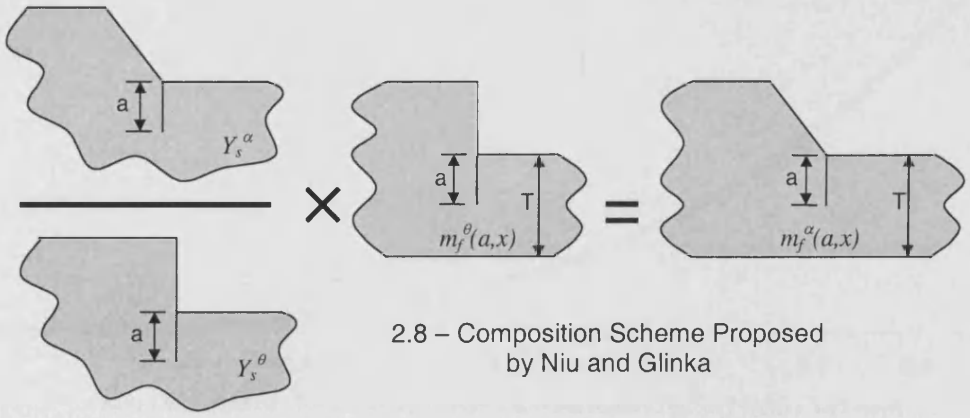

2.8 – Composition Scheme Proposed by Niu and Glinka

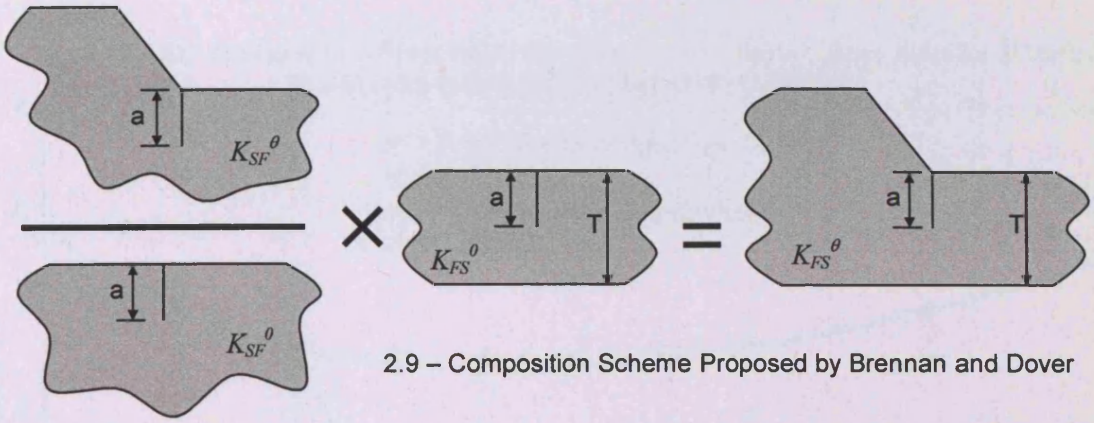

2.9 – Composition Scheme Proposed by Brennan and Dover

2.10 Composition Scheme Proposed by Brennan and Teh for a Semi-Circular Notch

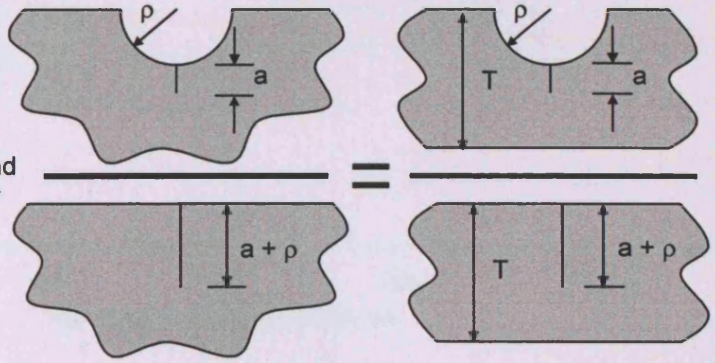

Fig. 2.11 – Curve Fitted SIF and Stress Distributions for a Semi-Circular Notch in a Semi-Finite Plane

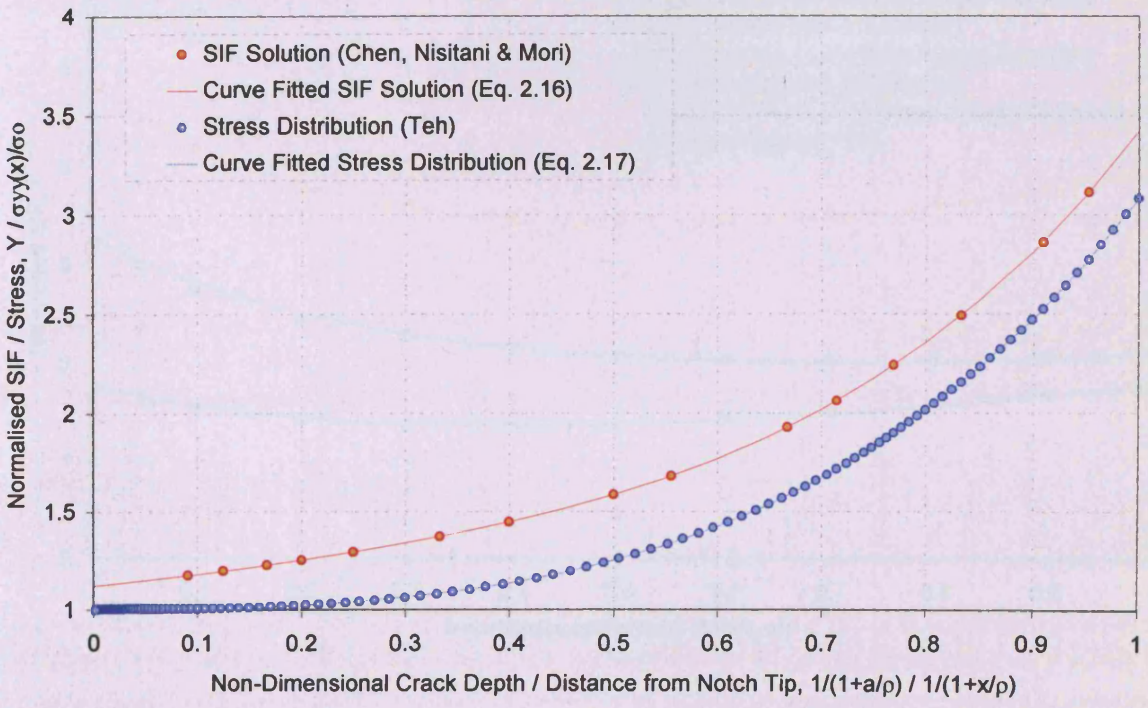

Fig. 2.12 – SIF Solutions for a Finite Width Strip Containing a Semi-Circular Notches of Various Size Subject to Remotely Applied Uniform Tension

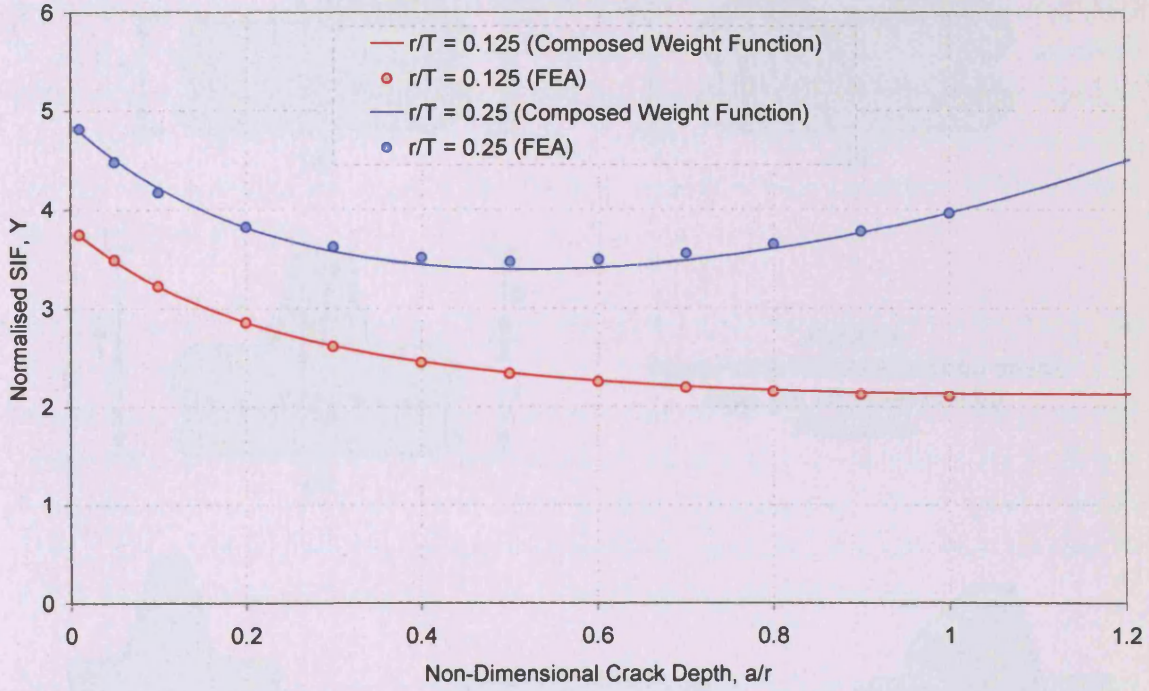

Fig. 2.13 – SIF Solutions for a Finite Width Strip Containing a Semi-Circular Notch (r/T = 0.25) Subject to a Variety of Remotely Applied Load Cases

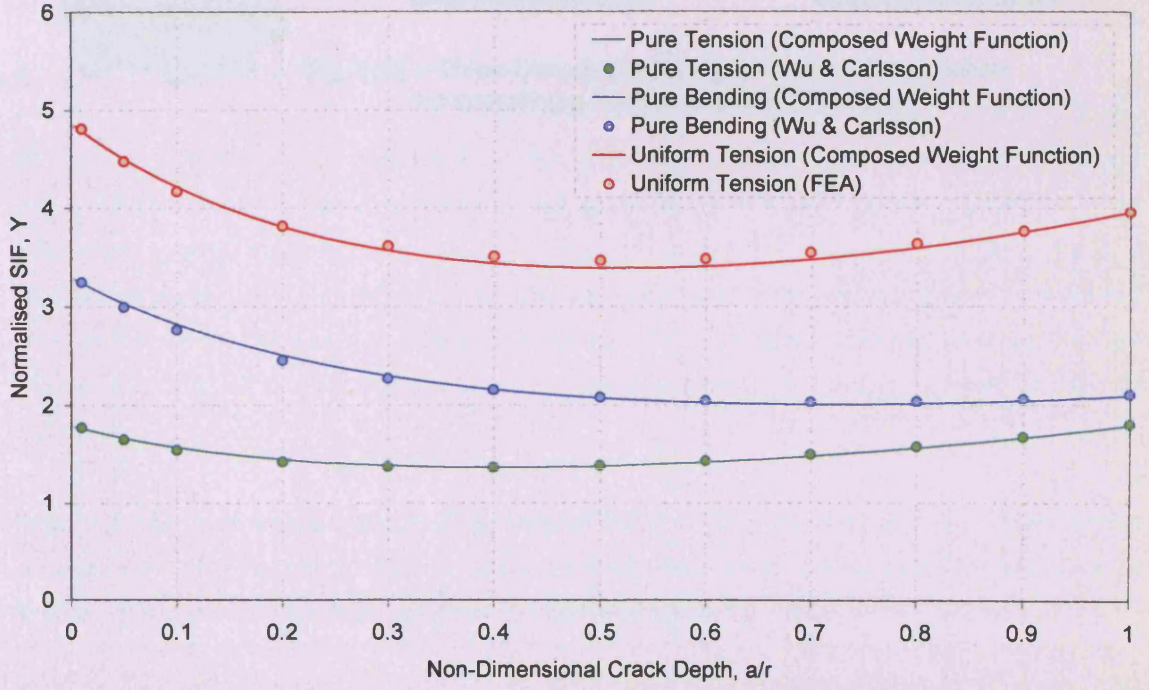

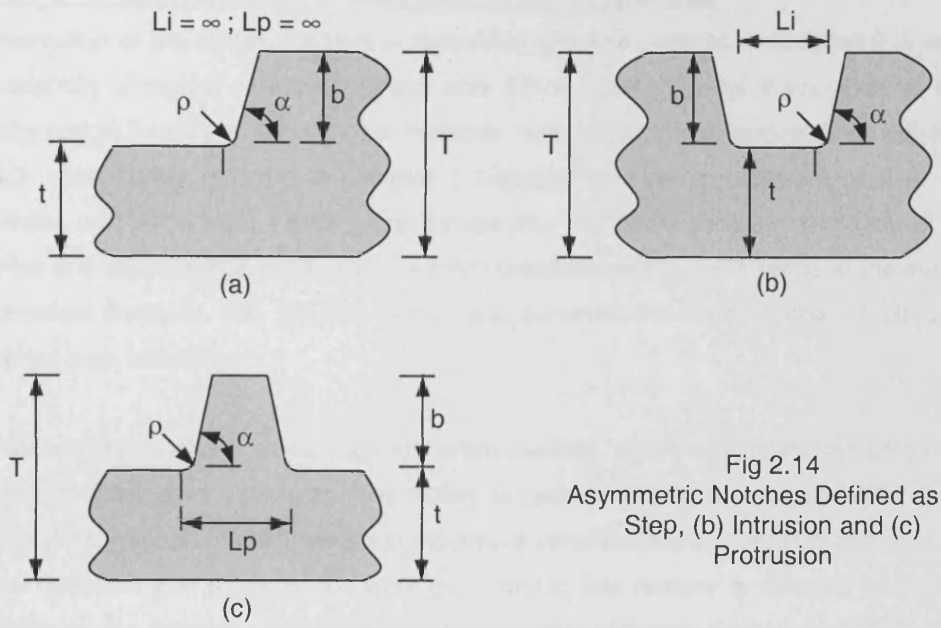

Fig 2.14
Asymmetric Notches Defined as (a) Step, (b) Intrusion and (c) Protrusion

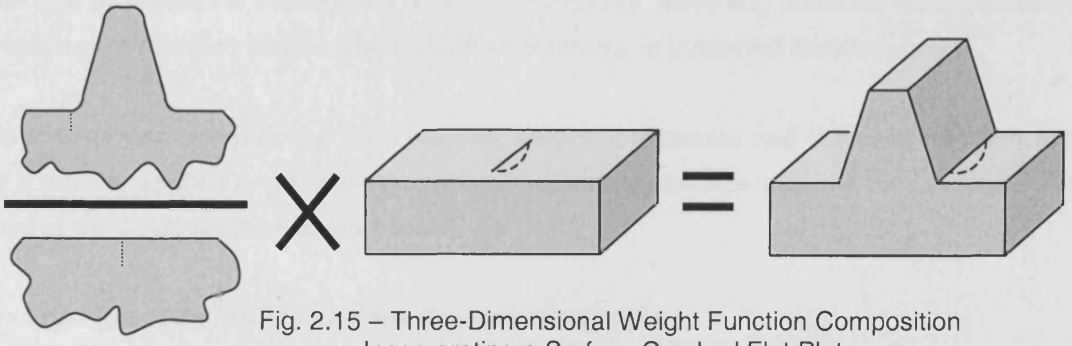

Fig. 2.15 – Three-Dimensional Weight Function Composition Incorporating a Surface Cracked Flat Plate

Chapter 3 - Modelling Edge Cracks Using Finite Elements

Implementation of the weight function composition principle outlined in Chapter 2 is reliant upon the availability of known reference stress and SIF solutions for the formulation of constituent geometry weight functions. A number of methods may be used to determine such solutions, some of which were briefly outlined in Chapter 1 together with an assessment of their respective advantages and limitations. These were divided into the three general categories of analytical, numerical and experimental methods. The most practicable of these in terms of the current study, are numerical methods, with which is possible to generate the large number of SIF solutions of the desired high accuracy.

The finite element analysis is one such numerical method, which may be implemented via the use of commercial software packages. The ability to create models representative of the physical body and derive SIF solutions from them requires a considerable level of skill and comprehension from the operator. The scope of the work contained in this chapter is devoted to the building of such proficiencies through a rigorous series of studies addressing mesh convergence, element types and application of loading and boundary conditions. Modelling practices were validated by comparison of solutions obtained against those contained in published literature.

This chapter demonstrates the finite element method's versatility and accuracy and concludes that it may be applied to generate the relevant reference solutions required for execution of the scope of work outlined in chapters 1 and 2.

3.1 - The Finite Element Method and Fracture Mechanics

Chapter 1 gave a brief outline of the finite element method for stress analysis. A more in-depth discussion of its underlying principles is unwarranted here as many texts devoted to this subject are available, however its application to the analysis of cracked systems deserves some description. Numerical modelling of cracks has become an indispensable tool in fracture mechanics due to the complexity of most crack problems, and the shortcomings of both analytical and experimental approaches. Many commercial FE software packages include fracture mechanics capabilities affording the analyst a versatile tool for the stress analysis of cracked bodies.

Early attempts to evaluate fracture parameters applied a direct method termed a stress and/or displacement matching technique. The stress intensity factor for a body subject to mode I loading is given by the equations below using the notation adopted in fig. 1.1.

$$K_I = \lim_{r \to 0} \left[\sigma_{yy} \sqrt{2\pi r} \right] \qquad (\theta = 0) \qquad \text{- (3.1)}$$

$$K_I = \frac{2\mu}{\kappa+1}\lim_{r\to 0}\left[u_y\sqrt{\frac{2\pi}{r}}\right] \qquad (\theta = \pi) \qquad \text{- (3.2)}$$

The SIF can be determined by plotting either stress or displacement values obtained from a finite element model against crack co-ordinate, '*r*' and extrapolating the resulting line of constant slope to '*r = 0*'. Extrapolation is required since even very fine crack tip meshes of regular elements cannot model the singular stress present at the crack tip. Chan *et al.*[3.1] applied the matching technique to a Griffith crack in an infinite plane subject to remotely applied uniform loading. Mesh convergence studies were reported and the most accurate estimates of stress intensity, obtained via eqs. 3.1 and 3.2 were reported to be within approximately 5% of closed form analytical solutions.

A more sophisticated, accurate and widely applied technique utilised by most modern commercial FE packages is termed an energy domain integral method. Singular elements overcome the need for a fine mesh of regular elements used for the direct methods described above and permit the modelling of the singular stress field in the region of the crack tip with a relatively coarse mesh. In essence, the domain integral method provides an efficient and robust numerical calculation of Rice's path independent J-integral using the divergence theorem to convert the contour integral to an area integral or volume integral for two or three-dimensional problems respectively.

A domain integral formulation is preferred over a line integral since the solution is less sensitive to errors in the local solution and is better suited to situations involving path dependence (problems involving appreciable plasticity). The domain is a finite area (or volume for three-dimensional crack problems) comprising elements surrounding the crack tip (front). Upon completion of the stress analysis of a crack sufficient information exists in the solution to inexpensively compute the J-integral from which SIF data can be extracted. A full description of the domain integral method is provided by Sih *et al*[3.2]

The scope of work contained in this chapter describes implementation of the domain integral method via use of the commercial software package ABAQUS™ [3.3].

3.1.1 - ABAQUS™ Software

The ABAQUS™ Software comprises a suite of engineering simulation programs based on the finite element method. It offers the capability and versatility to solve problems, involving a wide range of physical phenomena, from the very simple to the more complex. The versatility derives from the extensive element library allowing the close approximation to most physical systems.

The elastic analyses conducted in this study were conducted using ABAQUS software operating on a desktop personal computer.

A typical analysis of a finite element problem comprises the three stages of pre-processing, simulation and post-processing. The pre-processing stage involves the modelling of the physical problem to create an input file, which contains all information pertaining to meshing, loading, materials, etc. ABAQUS/Standard is a general-purpose analysis module, which solves the numerical problem defined in the input file. A number of output files result from the execution of a problem by the analysis module including a file giving the requested outputs in a listed format and a file storing outputs in a binary file ready for post-processing. The post-processing stage offers a graphical representation of the model and its solution. A more tangible representation of results in the form of graphs, colour contour plots and deformed meshes providing the analyst with a valuable aid for comprehension of results.

ABAQUS/CAE provides a 'user friendly' graphical to quickly create, view or modify input files in the pre-processing stage. Tools available allow the analyst to create meshes, apply loads and boundary conditions and define material properties. The module can also be used for viewing of results at the post-processing stage. Numerous images in this and following chapters contain images produced by ABAQUS/CAE. The body of work considered in this study requires the formulation of a large number of models, which cannot be conducted efficiently using ABAQUS/CAE. It was also found to suffer acute limitations when defining models containing cracks. Continual modelling and remodelling of similar geometries is both tedious and time consuming and therefore a more efficient alternative method for constructing the input files was sought.

3.1.2 - Mesh Generation

The nature of the study proposed requires the calculation of SIF solutions and stress distributions for a range of geometries of similar form. The geometries are generic in shape and are related to one another by variations in geometric parameters. To avoid the need for repeated modelling of related geometries, mesh generation programs were developed to automate the process of defining model nodal co-ordinates, elements, boundary conditions, loading arrangements, etc.

Mesh generator programs were coded in the flexible scientific programming language VISUAL FORTRAN™ [3.4] and require only the geometric parameters and loading mode as inputs. A data file containing all model information is produced in a format compatible with an input file required by the ABAQUS/standard FE solver.

The two-dimensional models were partitioned into a number of quadrilateral areas each meshed by bi-quadratic elements. Each partition was meshed by a generic subroutine, requiring only the number of elements on two adjacent sides together with the biasing allowing the mesh to become increasingly coarse with distance from the crack tip. Elements are defined by the nodes at the four element corners and at each of the element mid sides. Again a generic subroutine was written, which requires only the number of elements on adjacent sides to be known as inputs to obtain the element definition for the whole partition. The co-ordinates of the partition vertices are described in terms of the geometric parameters of the modelled geometry and therefore, by repeated calling of these subroutines a complete model can be automatically constructed. Other information regarding the model concerning element type, material data, loads and boundary conditions, analysis type and output requests are all included in the mesh generator program.

The VISUAL FORTRAN programming language contains a number of facets, which are conducive for the mesh generation process. A graphics capability exists such that meshes may be viewed on screen prior to their submission to the ABAQUS/Standard module. Thus problems pertaining to model dimensions and meshing (excessive element distortion) can be easily identified. Dialog boxes were used as a 'front end' to interact with the program to provide an interface though which input data were defined upon program initiation.

3.2 - Crack Tip Mesh Convergence Studies

Special consideration is given to the elements surrounding the crack tip. These are formed from the same bi-quadratic elements used throughout the model but are collapsed as shown in fig. 3.1. The 'rosette' of elements is formulated by the collapsing of one vertex of the element to a single point with elements on adjacent sides moved to their quarter points. This causes the element shape function to model the $1/\sqrt{r}$ singularity, which dominates the stress field close to the crack tip to be closely approximated with a relatively coarse mesh.

ABAQUS employs a domain integral method to evaluate the non-linear energy release parameter, J-integral as described in section 3.1. Several evaluations of which may be requested for a single crack. Each estimate concerns the analysis of the virtual motion of a ring of elements, constituting a contour, surrounding the crack tip. Thus the number of contours available for request is equal to the number of element rings surrounding the crack tip. The variation in J-integral estimates between contours is due to numerical approximations known as domain dependence, or contour dependence. Strong variations between J-integral estimates indicate a need for mesh refinement. Typically the innermost J-integral estimate suffers from domain dependence, however, stability is achieved in subsequent J-Integrals evaluated further from the

crack tip. The J-Integral, a measure of the strain energy release rate in the region of a crack, may be converted to the stress intensity factor if the material response is linear elastic.

Initial studies sought to identify an appropriate mesh density in the crack tip region. An inappropriate number of elements could give rise to either spurious results or cause the finite element problem to be larger than required and hence inefficient. The mesh density in this region was altered by the variation in the number of elements that make up the 'rosette' surrounding the crack tip and their size.

An investigation of the appropriate radius for the first row of elements, 'm' (fig. 3.2a) around the crack tip was conducted. Results obtained showed that the radius does not greatly effect the SIF results, over the range tested. Comparison with published solutions indicated that satisfactory convergence was reached for '$m/a < 0.1$'. The number of elements surrounding the half crack tip, 'n' (fig. 3.2b) was also investigated. Of the three 'n' values used (4, 8 and 12), 8 was found to yield the most accurate solutions. All future FE work adheres to these findings.

3.3 - Validation of FE Method

Validation of the SIF solutions obtained via the finite element method was sought by comparing FE solutions for a series of simple geometries to those established solutions which exist in published literature. The solutions selected for this purpose were those of Brown and Srawley[3.5] for a finite width cracked plane under pure tensile and pure bending loading. These solutions were obtained by a boundary collocation technique and are presented in the form of fitted equations for both uniform tension and pure bending and are reproduced below.

$$Y_t = 1.12 - 0.231\left(\frac{a}{T}\right) + 10.55\left(\frac{a}{T}\right)^2 - 21.72\left(\frac{a}{T}\right)^3 + 30.39\left(\frac{a}{T}\right)^4 \qquad \text{- (3.3)}$$

$$Y_b = 1.122 - 1.40\left(\frac{a}{T}\right) + 7.33\left(\frac{a}{T}\right)^2 - 13.08\left(\frac{a}{T}\right)^3 + 14.0\left(\frac{a}{T}\right)^4 \qquad \text{- (3.4)}$$

Eqs. 3.3 and 3.4 have a quoted accuracy of ± 0.5% for a/T ≤ 0.6.

A mesh generator program was constructed to automatically generate models for solution by the ABAQUS/Standard simulation module. A succession of models of varying crack depth were created by alteration of the non-dimensional crack depth, 'a/T'. Other geometric parameters of

strip thickness, '*T*' and half-strip width, '*W*' were also inputs to the program (fig. 3.3a). Examples of the crack tip and global meshes are presented in figs. 3.2 and 3.4 respectively.

Loading was applied either as uniform pressure applied to remote boundaries for the pure tension mode or as concentrated nodal loads shown in fig. 3.5 for both pure tension and pure bending modes. A number of additional loading options and modes were also investigated. Uniform pressure was applied directly to the elements on the crack face to simulate the pure tension loading mode. Point and decreasing pressure loading modes, defined in fig. 2.1 and utilised in section 2.2, were simulated though application of a concentrated load applied to nodes on the crack face and hydrostatic pressure applied to the elements on the crack face respectively.

The model presented in fig. 3.3a shows uniform tensile loading applied to remote boundaries. Application of boundary conditions fixes some of the solution nodal variables to some known value (displacements are set to zero for the cases considered in this study). A more efficient solution may be achieved by recognising that, in this instance, the crack lies on a plane of symmetry. Application of symmetrical boundary conditions on this plane of a half model was used to simulate the whole model. The symmetrical boundary conditions applied to the model depicted in fig. 3.3b 'mirrors' the model about a plane 'x = *constant*' and is achieved by fixing certain degrees of freedom on this plane to zero ($u_x = \phi_y = \phi_z = 0$).

Two-dimensional isoparametric continuum elements were used throughout the mesh. These comprised eight nodes: the mid-side nodes are required for crack tip meshing. They are termed bi-quadratic or second order elements and are denoted by '*CPE8R*' and '*CPS8R*' for plane strain and plane stress respectively. Meshes were constructed so as to conform to guidance offered by Cooke[3.6] and ABAQUS literature[3.7] to ensure that element performance was not impaired. Thus element distortion, size and aspect ratio were maintained within recommended limits.

Investigations were conducted on the finite strip model described above, to assess the accuracy that could be achieved using the finite element method and to validate the processes and modelling techniques presented in this section.

3.3.1 - Critique of Results

A number of models of varying crack size subject to a variety of loading modes and boundary conditions similar to those shown in figs. 3.4 and 3.5 were created and solved. Fig. 3.6 depicts renderings of stress contours and mesh displacement in the region of the crack obtained from a typical analysis. SIF solutions obtained from the finite element analyses are presented in both a graphical and tabular form in fig. 3.7 and tab. 3.1. It can be seen with reference to these figures

that the results show a near perfect correlation to the solutions produced by Brown and Srawley with a maximum percentage difference of 0.6%. They demonstrate the finite elements' ability to yield results of great accuracy and validate the work undertaken to ensure an appropriate mesh density is used.

Also validated are the various methods of applying loading. Concentrated loads and distributed loads applied to remote boundaries produced results for pure tension equal to those obtained for distributed loading applied to the crack face.

Tab. 3.1 shows the variation in J-integral estimates obtained from successive rings of elements surrounding the crack tip. Stability is achieved on and after the third contour. Values of stress intensity factor were determined from an average of the fourth, fifth and sixth J-integral estimates. Future calculations are based solely on the value of the fourth contour, 'J_4'.

Additional loading modes of point and decreasing tension, defined in fig. 2.1 and utilised in section 2.2, were also investigated. No comparative solutions are available in the published literature, however derived solutions, shown in tab. 3.2, were judged to be of a similar high accuracy to those obtained for pure tension and pure bending.

3.4 - Modelling of Cracks at Notches

The cracks modelled in section 3.3 indicate that the finite element method and modelling practices employed are suitable for the analysis of cracks in plane geometries. An additional level of modelling complexity is added by the introduction of a notch, which causes a concentration of stress to be present at the notch root. Common to the work conducted in the preceding section, validation of SIF solutions obtained by the finite element technique was sought through their comparison to those in published literature.

3.4.1 - Symmetric Notches

The symmetric notch type selected for investigation was semi-circular in form embedded in a finite width strip, similar to that considered previously, with a vertical crack at the notch root. The geometry is defined by the geometric parameters as shown in fig. 3.8a. The solutions obtained from a finite element analysis may be compared to those published by Wu and Carlsson[3.8] who produced solutions for a number of notch sizes characterised by the non-dimensional parameter, 'ρ/T'.

A mesh generator program was constructed to automate the process of model generation. The adaptive nature of the mesh generator program produced is shown by the two meshing regimes

shown in fig. 3.9 produced for both short cracks and long cracks, governed by the ratio, 'a/ρ'. Symmetry exists about the crack line and is exploited to allow the half model to be representative of the whole model with appropriate boundary conditions and loading applied. The three loading modes of uniform tension, pure tension and pure bending as defined in fig. 3.8b were investigated. The uniform tension loading mode gives rise to net bending in the plane containing the crack whereas the pure tension loading mode produces none.

SIF solutions obtained are shown in tab. 3.3 for a range of notch sizes subject to uniform tension and a single notch size for pure tension and pure bending loading modes. A graphical comparison is drawn in fig. 3.10 with the solutions of Wu and Carlsson. The profound influence of the notch is readily apparent by comparison to the plane strip solutions of Brown and Srawley. The stress concentration elevates the SIF in the region close to the notch root. The influence of the stress concentration decays with increasing crack depth. An excellent correlation between the two sets of solutions is apparent in fig. 3.10. Discrepancies are negligible with errors evaluated as being less than 0.6% for all cases investigated. Once more the finite element method and applied modelling practices are shown to be sufficient for the accurate determination of SIF solutions.

3.4.2 – Cracks in a Semi-Finite Plane

The weight function composition regime outlined in chapters 1 and 2 comprises a normalisation process to isolate the geometric influence of the notch. Semi-finite geometries were identified as convenient for this purpose. It is of considerable value to ascertain a notch depth to plate thickness ratio, 'ρ/T' at which solely the effect of the notch upon SIF is captured, without any distant boundary influence, to approximate the geometry depicted in fig. 3.11. Using the semi-circular notch geometry and the mesh generator program described in the preceding section solutions for cracks at the roots of semi-circular notches in semi-finite planes were sought. These were compared to the solutions provided in the published literature by Chen, Nisitani and Mori[3.9] who employed a body force method to determine SIF solutions for this geometry quoting an error better than 0.1%.

Tabular SIF data for this geometry, obtained from both the finite element analyses and published literature, is presented in tab. 3.4 and graphically in fig. 3.12. The figure shows SIF solutions produced by FEA for a range of semi-circular notch sizes loaded under uniform tension. For large notches the distant boundary's influence upon the SIF solution is evident. As the notch size decreases, (or plate thickness increases) the influence of the remote boundary effect is reduced over the range of notch influence. The solution provided Chen, Nisitani and Mori represents the semi-infinite plane ($\rho/T = 0$). Teh[3.10] conducted a convergence study to show that the stress analysis of semi-finite geometries can be approximated by a finite element model with a low notch

depth to plate thickness ratio. A similar convergence investigation in this study revealed that SIF solutions corresponding to a 'ρ/T' ratio equal to 0.002 gives a good approximation to the published solutions for semi-finite geometries. Selected results from the convergence study are shown in fig. 3.12 and tab. 3.4. Measured errors between the two solutions in table 3.4 are less than 1%. This value of notch depth to plate thickness ratio was employed for all subsequent analyses of semi-finite geometries.

3.4.3 – Asymmetric Notches

The determination of SIF solutions, using the finite element method, for cracks in bodies where the crack lies on a plane of symmetry has successfully been carried out in preceding sections. Cracks in symmetric geometries subject to a symmetric loading arrangement give rise to a purely mode I crack opening displacement and thus a purely mode I SIF. To advance the current weight function theory beyond this geometry type requires the analysis of SIF solutions for asymmetric geometries. Geometric asymmetry about the plane of the crack gives rise to a mode II component of SIF. This section describes the application of FE methods to asymmetric geometries to verify that modal components of SIF could be reliably and accurately determined.

ABAQUS literature[3.11] gives guidance on the treatment of cracks subject to mixed-mode loading. The J-integral does not distinguish between different modes of loading, however, in an elastic analysis such as that considered here, the following procedure for the evaluation of modal SIF components is recommended. Quantification of the relative displacements of the crack faces, close to the crack tip, in the respective modal directions may be used to evaluate a factor, 'R_m', defined, for an edge crack, with the aid of fig. 3.13, by eq. 3.5.

$$R_m = \frac{|\Delta x|}{|\Delta y|} \qquad \text{- (3.5)}$$

Mode I and II stress intensity factors become:

$$K_I = \sqrt{\frac{JE'}{\left(1+R_m{}^2\right)}} \qquad K_{II} = R_m K_I \qquad \text{- (3.6 a,b)}$$

Once again validation of this process was achieved by comparing solutions derived by the finite element method to those in the published literature. Hasebe and Ueda[3.12] implemented a conformal mapping technique to yield SIF solutions for a sharp step notch embedded in a semi-finite plane subject to a remotely applied uniform stress field. This geometric configuration

described by the parameters shown in fig. 3.14, is closely related to the geometry types to be analysed in subsequent chapters. They form a useful set of solutions with a quoted accuracy of less the 1%.

Although this recommended prodedure was adopted for this study, more recent releases of the ABAQUS software utilise an interaction integral method. This method superimposes an auxiliary pure modal stress fields, of known SIF and J-integral values, upon the actual stress field. The procedure is implemented to decouple the the modal SIF values from the J-integral estimate by a process described in full in ABAQUS documentation[3.13].

Tab. 3.5 shows the finite element data obtained and fig. 3.15 shows displacement of the finite element mesh. Displacements of nodes on the crack face close to the crack tip, 'Δx' and 'Δy' listed in the results file of the analysis were used to ascertain the parameter, 'R_m'. Modal SIF solutions were calculated using eqs 3.6a,b and solutions obtained are compared to those published by Hasebe and Ueda in fig. 3.16. Once more, the two sets of solutions display an excellent correlation, validating the modelling practices employed.

3.5 – Stress Analysis of Uncracked Geometries

Much of the work contained in this chapter has concentrated on the validation of modelling practices applied to cracked geometries. In addition to these, the weight function methodology outlined in chapter 2 requires associated reference stress distributions in the plane of crack propagation corresponding to the same loading mode as the reference SIF solution.

Numerous authors have reported upon the normalised stress distributions arising from the presence of a notch or geometric discontinuity. Newport and Glinka[3.14], Kujawski[3.15], and Xu *et. al.*[3.16] are among the more prominent. The stress concentration is a local phenomenon influencing the region of the notch root, the influence decreasing with distance from the notch tip. The form of the stress distribution ahead of a notch is largely dependent upon the stress concentration factor, 'K_t' and the notch root radius, 'ρ' and is only marginally dependent upon the global notch geometry. The normalised elastic stress distribution ahead of notches can therefore be approximated by two-parameter generic expressions of 'K_t' and 'ρ'. The equations determined from numerical and experimental studies are between them applicable to a wide range of sharp and blunt notches in finite and semi-finite geometries.

The generic stress distribution solutions for notched components described above all claim a high level of accuracy, albeit with generally restrictive limits of validity. Their usage in the present study is judged inappropriate as this document is intended to highlight the accuracy of contemporary

weight function theory and the composition scheme. They do suffer acute limitations with respect to their accuracy and especially, narrow limits of validity, notch geometry types and in some cases are restricted to the simplest loading modes. Furthermore, though numerous sources of stress concentration data for a wide range of notch types are available, such as Peterson's Handbook[3.17], these are not exhaustive and suffer similar shortcomings.

Stress distributions were obtained from FE models created by mesh generator programs written for the fracture mechanics analysis. The focused mesh around the crack tip was replaced by a regular arrangement of quadrilateral elements. Fig. 3.17 shows the mesh and stress contours obtained for a semi-circular notch in a finite width strip subject to uniform tension. The stress in the crack plane is shown graphically in fig. 3.18, for three loading modes, as a plot of non-dimensional stress ('$\sigma_{yy}(x)$' normalised to the notch tip nominal stress, 'σ_{No}') against non-dimensional distance from the notch tip alongside the nominal stress in the net section, '$\sigma_{o(Net)}$' (fig.3.19).

An appropriate mesh density in the region of the notch root was ascertained via analysis of the stress concentration factors determined. An excellent correlation is apparent in fig. 3.20, depicting a graphical comparison between SCFs obtained from the current FEA with those tabulated by Noda and Nisitani[3.18]. The calculated SCF for the same notch in a semi-finite plane approximated by a model with 'ρ/T' equal to 0.002 as described in section 3.4.2 yields a value of 3.084, which is within 0.7% error of the value (3.065) presented by Peterson[3.17].

3.6 – Conclusions

This chapter has sought to validate the modelling practices and demonstrate acquisition of proficiencies required to implement the finite element analysis for the stress analysis of edge cracks in various geometries. In all cases, results achieved were verified against those contained in published literature. All investigations produced results that display an excellent correlation to the established solutions, in many cases being within the quoted accuracy range accompanying the published data. The body of work in this chapter indicates that the FE method, as implemented above, is quite sufficient for the study intended.

3.7 – References

[3.1] Chan, S.K., Tuba, I.S. and Wilson, W.K., On the Finite Element Method in Linear Fracture Mechanics. *Engineering Fracture Mechanics*, Vol. 2, 1970, pp. 1 – 17.

[3.2] Shih, C.F., Moran, B. and Nakamura, T., Energy Release Rate Along a Three-Dimensional Crack Front in a Thermally Stressed Body. *International Journal of Fracture*, Vol. 30, 1986, pp. 79-102

[3.3] ABAQUS, version 5.7, Hibbet,Karlson amd Sorenson Inc., 1997.

[3.4] DIGITAL™ Visual Fortran, Professional Edition Version 5.0 for Windows NT and Windows 95, Digital Equipment Corporation (now COMPAQ), 1997

[3.5] Brown Jr., W.F. and Srawley, J.E., Plain Strain Crack Toughness Testing of High Strength Metallic Materials, *ASTM STP 410* (1966), p. 12

[3.6] Cook, R.D., Finite Element Modelling for Stress Analysis, John Wiley & Sons Inc. 1995

[3.7] Hibbet,Karlson and Sorenson Inc. *ABAQUS user guide manual*, v.5.6 1996

[3.8] Wu, X.R. and Carlsson, A.J., *Weight Functions and Stress Intensity Factors.* Permagon Press, Oxford, 1991

[3.9] Chen, D. Nisitani, H. and Mori, K., Stress Intensity Factors for a Semi-Infinite Plate Having a Semi-Elliptical Notch with a Crack Under Tension. *Transactions of the Japan Society of Mechanical Engineers*, 1989, 55, No. 512, pp 948 – 952.

[3.10] Teh, L.S., *Library of Geometric Influences for Stress Intensity Factor Weight Functions*, Ph.D. Thesis, University College London, 2002

[3.11] Hibbet,Karlson and Sorenson Inc., *ABAQUS Fracture Mechanics Training Course Notes,* 1996

[3.12] Hasebe, N. and Udea, M., Crack Originating from an Angular Corner of a Semi-Infinite Plate with a Step. *Bulletin of the JSME* Vol. 24, No. 184, pp 483 - 488, 1981.

[3.13] ABAQUS version 6.5. Theory Manual. Hibbert, Karlsson and Sorrenson Inc., 2004.

[3.14] Glinka, G. & Newport, A., Universal Features of Elastic-Notch tip Stress Fields. *Int. J. Fatigue* **9** No. 3 pp 143 – 150, 1987

[3.15] Kujawski, D., Estimations of Stress Intensity Factors for Small Crack at Notches. *Fatigue Fract. Engng. Mater. Struct.* Vol. 14 No.10 pp 953 – 965, 1991

[3.16] Xu, R.C., Thompson, J.C. and Topper, T.H., Practical Expressions for Stress Concentration Regions. *Fatigue Fract. Engng. Mater. Struct.* Vol. 18, No. 7/8, pp. 885 – 895, 1995

[3.17] Peterson, R.E., Stress Concentration Factor: charts and relations useful in making strength calculations for machine parts and structural elements, Wiley-Interscience, London, 1974. ISBN: 0-47168-329-9

[3.18] Noda, N.A. ans Nisitani, H., Stress Concentration of a Strip with a Single Edge Notch. *Engineering Fracture Mechanics*, 1987, 28, No.2, pp 223 – 238.

3.8 – Tables

Tab. 3.1 – SIF Solutions Obtained from the Analysis of a Finite Strip Containing an Edge Crack

Plane Strain Element CPE8R UNIFORM TENSION										
a/T	J_1x10^7	J_2x10^7	J_3x10^7	J_4x10^7	J_5x10^7	J_6x10^7	$J_{ave\ (4-6)}$	$Y_{It\ (FEA)}$	$Y_{It\ (B+S)}$	%diff
0.025	0.948	0.950	0.951	0.951	0.951	0.951	9.51E-08	1.125	1.120	0.408
0.05	1.943	1.947	1.950	1.950	1.950	1.950	1.95E-07	1.139	1.132	0.605
0.10	4.233	4.240	4.246	4.246	4.246	4.246	4.25E-07	1.189	1.184	0.416
0.15	7.189	7.200	7.210	7.210	7.210	7.209	7.21E-07	1.265	1.265	-0.009
0.20	11.193	11.213	11.228	11.228	11.228	11.227	1.12E-06	1.367	1.371	-0.283
0.25	16.788	16.812	16.833	16.834	16.834	16.833	1.68E-06	1.497	1.501	-0.271
0.30	24.742	24.787	24.819	24.820	24.819	24.818	2.48E-06	1.659	1.660	-0.042
0.35	36.301	36.358	36.404	36.406	36.404	36.403	3.64E-06	1.860	1.856	0.222
0.40	53.266	53.471	53.543	53.543	53.543	53.540	5.35E-06	2.111	2.104	0.333
0.45	79.224	79.370	79.473	79.476	79.473	79.470	7.95E-06	2.424	2.419	0.201
Plane Stress Element CPS8R UNIFORM TENSION										
a/T	J_1x10^7	J_2x10^7	J_3x10^7	J_4x10^7	J_5x10^7	J_6x10^7	$J_{ave\ (4-6)}$	$Y_{It\ (FEA)}$	$Y_{It\ (B+S)}$	%diff
0.025	1.042	1.044	1.045	1.045	1.045	1.045	1.045E-07	1.125	1.120	0.410
0.05	2.136	2.140	2.143	2.143	2.143	2.143	2.143E-07	1.139	1.132	0.605
0.10	4.654	4.660	4.666	4.666	4.666	4.666	4.666E-07	1.189	1.184	0.416
0.15	7.904	7.913	7.923	7.923	7.923	7.922	7.923E-07	1.265	1.265	-0.010
0.20	12.306	12.323	12.338	12.339	12.338	12.338	1.234E-06	1.367	1.371	-0.282
0.25	18.456	18.477	18.499	18.499	18.499	18.498	1.850E-06	1.497	1.501	-0.271
0.30	27.202	27.241	27.274	27.275	27.274	27.273	2.727E-06	1.659	1.660	-0.042
0.35	39.910	39.958	40.005	40.006	40.005	40.003	4.000E-06	1.860	1.856	0.221
0.40	58.673	58.765	58.839	58.841	58.839	58.836	5.884E-06	2.111	2.104	0.334
0.45	87.102	87.228	87.334	87.337	87.334	87.330	8.733E-06	2.424	2.419	0.201
Plane Strain Element CPE8R PURE BENDING										
a/T	J_1x10^7	J_2x10^7	J_3x10^7	J_4x10^7	J_5x10^7	J_6x10^7	$J_{ave\ (4-6)}$	$Y_{Ib\ (FEA)}$	$Y_{Ib\ (B+S)}$	%diff
0.025	0.125	0.126	0.126	0.126	0.126	0.126	1.257E-08	1.091	1.091	-0.029
0.05	0.241	0.242	0.242	0.242	0.242	0.242	2.420E-08	1.070	1.069	0.147
0.10	0.462	0.462	0.463	0.463	0.463	0.463	4.630E-08	1.047	1.044	0.313
0.15	0.687	0.688	0.689	0.689	0.689	0.689	6.893E-08	1.043	1.040	0.292
0.20	0.938	0.939	0.941	0.941	0.941	0.941	9.405E-08	1.055	1.053	0.198
0.25	1.233	1.235	1.236	1.236	1.236	1.236	1.236E-07	1.082	1.080	0.138
0.30	1.596	1.599	1.601	1.601	1.601	1.601	1.601E-07	1.124	1.122	0.170
0.35	2.061	2.064	2.067	2.067	2.067	2.067	2.067E-07	1.182	1.179	0.263
0.40	2.675	2.681	2.684	2.684	2.684	2.684	2.684E-07	1.260	1.256	0.336
0.45	3.519	3.526	3.530	3.530	3.530	3.530	3.530E-07	1.363	1.358	0.305
Plane Stress Element CPS8R PURE BENDING										
a/T	J_1x10^7	J_2x10^7	J_3x10^7	J_4x10^7	J_5x10^7	J_6x10^7	$J_{ave\ (4-6)}$	$Y_{Ib\ (FEA)}$	$Y_{Ib\ (B+S)}$	%diff
0.025	0.138	0.138	0.138	0.138	0.138	0.138	1.382E-08	1.091	1.091	-0.026
0.05	0.265	0.266	0.266	0.266	0.266	0.266	2.660E-08	1.070	1.069	0.148
0.10	0.508	0.508	0.509	0.509	0.509	0.509	5.088E-08	1.047	1.044	0.313
0.15	0.756	0.757	0.757	0.758	0.757	0.758	7.575E-08	1.043	1.040	0.296
0.20	1.031	1.032	1.034	1.034	1.034	1.034	1.034E-07	1.055	1.053	0.199
0.25	1.356	1.357	1.359	1.359	1.359	1.359	1.359E-07	1.082	1.080	0.137
0.30	1.755	1.757	1.759	1.759	1.759	1.759	1.759E-07	1.124	1.122	0.170
0.35	2.266	2.269	2.271	2.272	2.271	2.271	2.271E-07	1.182	1.179	0.262
0.40	2.941	2.946	2.950	2.950	2.950	2.950	2.950E-07	1.260	1.256	0.335
0.45	3.869	3.875	3.879	3.879	3.879	3.879	3.879E-07	1.363	1.358	0.305

Tab. 3.2 – SIF Solutions for a Finite Strip Subject to Decreasing Tension and Point Loading

Decreasing Tension		Point Loading							
		a/T = 0.2		a/T = 0.3		a/T = 0.4		a/T = 0.49	
a/T	Y	x/a	Y	x/a	Y	x/a	Y	x/a	Y
0.05	0.449	0.000	0.0547	0.000	0.0509	0.000	0.0555	0.000	0.0655
0.1	0.479	0.148	0.0533	0.125	0.0488	0.156	0.0514	0.128	0.0607
0.15	0.524	0.296	0.0518	0.250	0.0467	0.313	0.0474	0.255	0.0559
0.2	0.586	0.395	0.0511	0.333	0.0453	0.542	0.0421	0.379	0.0513
0.25	0.666	0.493	0.0509	0.417	0.0442	0.694	0.0397	0.503	0.0468
0.3	0.766	0.559	0.0512	0.514	0.0431	0.796	0.0395	0.586	0.0440
0.35	0.890	0.688	0.0533	0.611	0.0424	0.864	0.0411	0.669	0.0415
0.4	1.046	0.792	0.0581	0.676	0.0425	0.909	0.0448	0.779	0.0389
0.45	1.243	0.889	0.0709	0.741	0.0431	-	-	0.853	0.0385
0.525	1.649	-	-	0.827	0.0459	-	-	0.902	0.0400
0.55	1.824	-	-	0.885	0.0507	-	-	-	-
0.6	2.265	-	-	-	-	-	-	-	-

Tab. 3.3 –SIF Solutions Obtained from the Analysis of a Semi-Circular Notched Finite Strip Containing an Edge Crack

a/ρ	Y_{Iut}				Y_{Ipt}	Y_{Ipb}
	ρ/T = 0.375	ρ/T = 0.250	ρ/T = 0.125	ρ/T = 0.0625	ρ/T = 0.0625	ρ/T = 0.0625
0.01	-	4.826	3.748	3.479	2.361	3.072
0.025	6.630	-	-	-	-	-
0.05	6.350	4.464	3.486	3.225	2.202	2.846
0.1	5.940	4.140	3.210	2.964	2.059	2.617
0.15	5.689	-	3.000	-	1.967	2.434
0.2	5.558	3.745	2.836	2.594	1.894	2.287
0.25	5.496	-	2.699	-	1.850	2.168
0.3	5.502	3.531	2.589	2.341	1.826	2.066
0.35	5.567	-	-	-	1.814	1.976
0.4	5.671	3.432	2.424	2.167	1.815	1.909
0.45	5.825	-	-	-	-	-
0.5	6.016	3.400	2.307	2.038	1.845	1.796
0.6	-	-	-	-	1.910	1.707
0.7	-	3.524	2.189	1.870	1.993	1.643
0.8	-	-	2.151	-	2.111	1.598
0.9	-	3.792	2.112	1.769	2.248	1.560
1.0	-	-	-	-	-	1.529
1.1	-	4.235	2.126	1.709	-	-

Y_{Iut} – Uniform Tension, Y_{Ipt} – Pure Tension, Y_{Ipb} – Pure Bending

Tab. 3.4 – SIF Solutions Obtained from the Analysis of a Semi-Circular Notched Semi-Finite Strip Containing an Edge Crack

Chen Nisitani & Mori		FEA	
a/ρ	Y_{It}	a/ρ	Y_{It}
0.05	3.116	0.05	3.130
0.1	2.863	0.1	2.880
0.2	2.494	0.2	2.511
0.3	2.242	0.3	2.259
0.4	2.062	0.4	2.078
0.5	1.929	0.5	1.941
0.8	1.683	0.8	1.694
1	1.587	1	1.599
1.5	1.448	1.5	1.458
2	1.373	2	1.384
3	1.295	3	1.305
4	1.254	4	1.263
5	1.229	5	1.240
7	1.199	-	-
10	1.176	-	-

Tab. 3.5 – SIF Solutions Obtained from the Analysis of a Sharp Step Notched Semi-Finite Strip (α = 90 Deg.) Containing an Edge Crack

a/b	R	Y_{It}	Y_{IIt}
0.031	0.217	3.254	0.739
0.066	0.190	2.539	0.500
0.105	0.160	2.206	0.362
0.202	0.125	1.840	0.234
0.401	0.089	1.568	0.141
0.606	0.070	1.448	0.102
0.794	0.059	1.385	0.082
1.001	0.050	1.339	0.067
1.247	0.043	1.302	0.056
1.653	0.034	1.262	0.043
2.421	0.025	1.221	0.031
5.102	0.013	1.170	0.015

3.9 – Figures

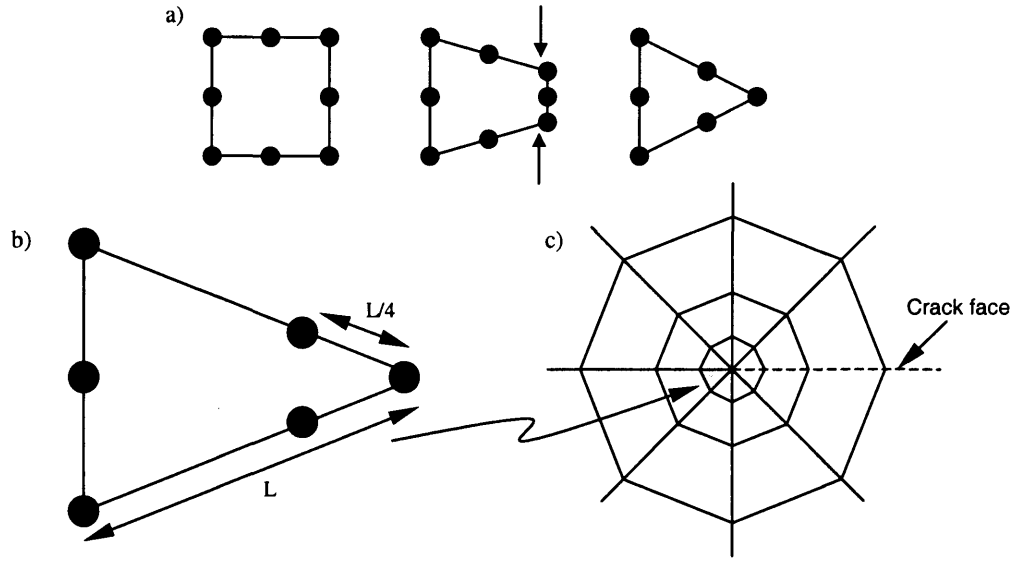

Fig. 3.1 – a) Collapsing of 8 Node Element to Form Singular Element. b) Mid-side Nodes Positioned at Quarter Points. c) Its Position in the 'Rosette' of Elements around the Crack Tip

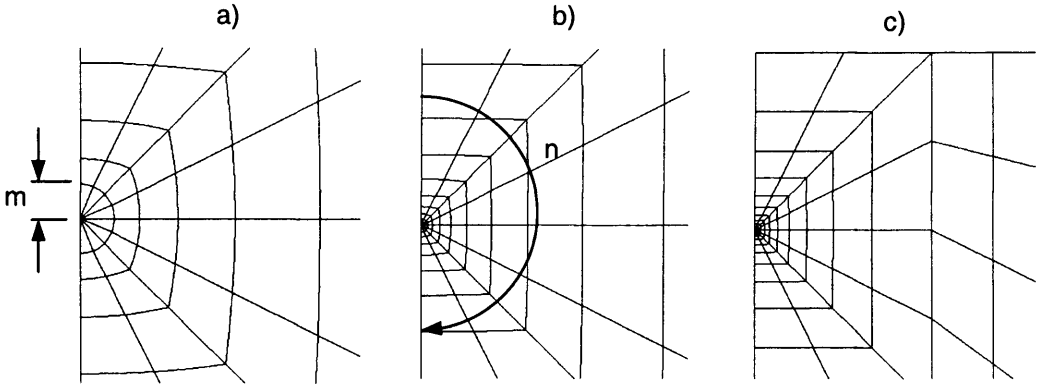

Fig. 3.2 – Crack Tip Detail (Half Model in which n = 8)

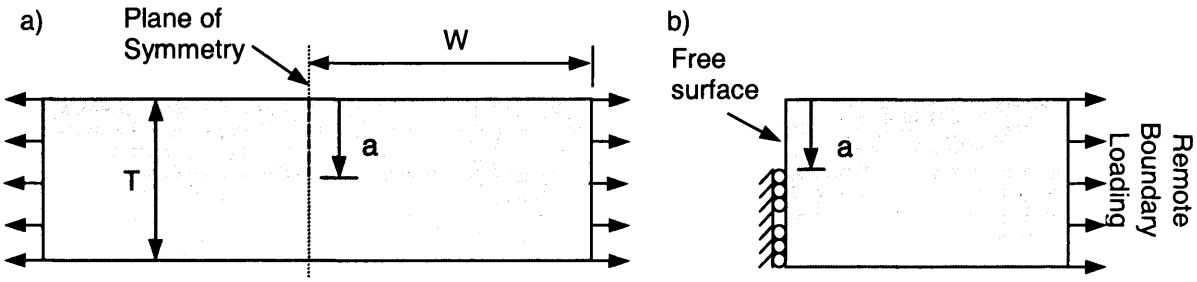

Fig. 3.3 – Geometric Definition of the Finite Strip Geometry. a) Whole Model b) Half Model

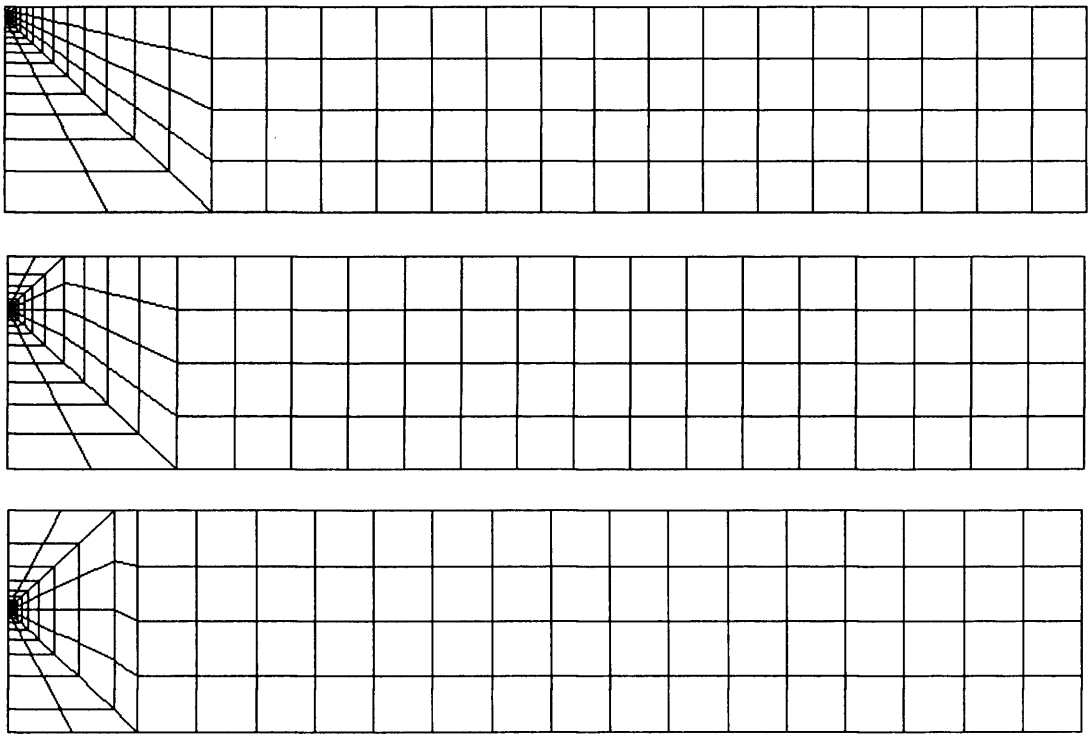

Fig. 3.4 - FE Meshes Produced for a Finite Strip Containing Edge Cracks of Varying Lengths (a/T = 0.05, a/T = 0.25 & a/T = 0.45)

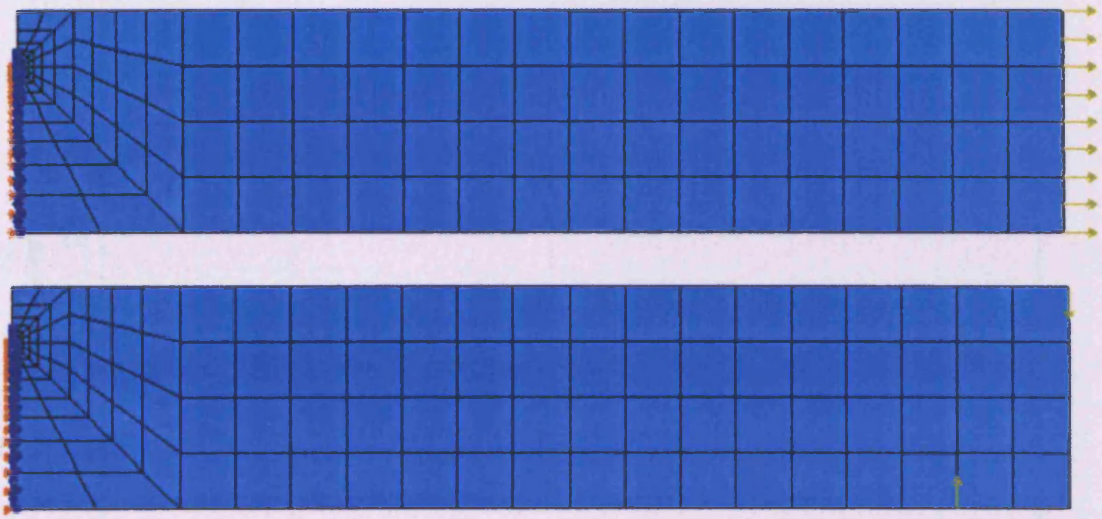

Fig. 3.5 - FE Meshes Displaying Applied Loading and Constraints for Uniform Tension and Pure Bending

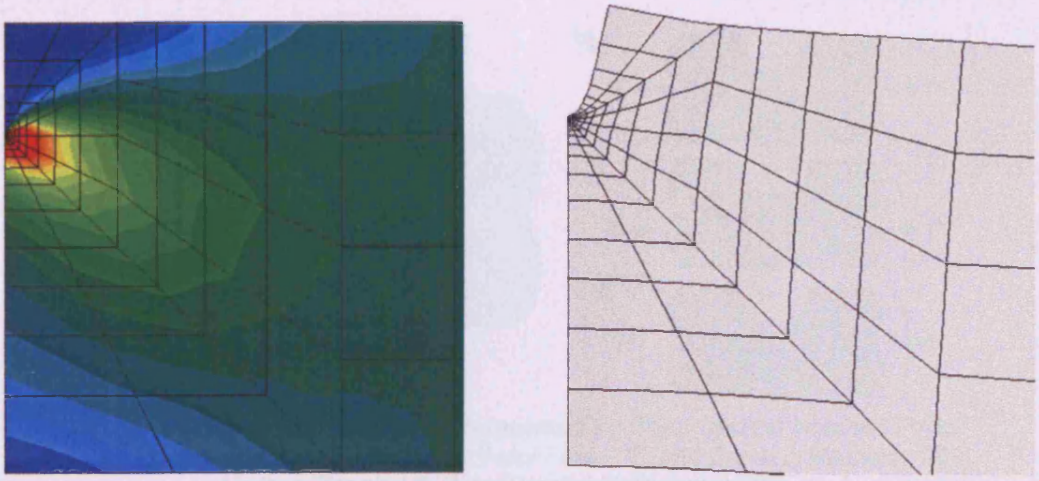

Fig. 3.6 – Images Taken from AQBAQUS/CAE Post-Processing Software Showing Stress Contours and Mesh Deformation

Fig. 3.7 – SIF Solutions Published by Brown & Srawley and Obtained from FEA for a Finite Thickness Strip

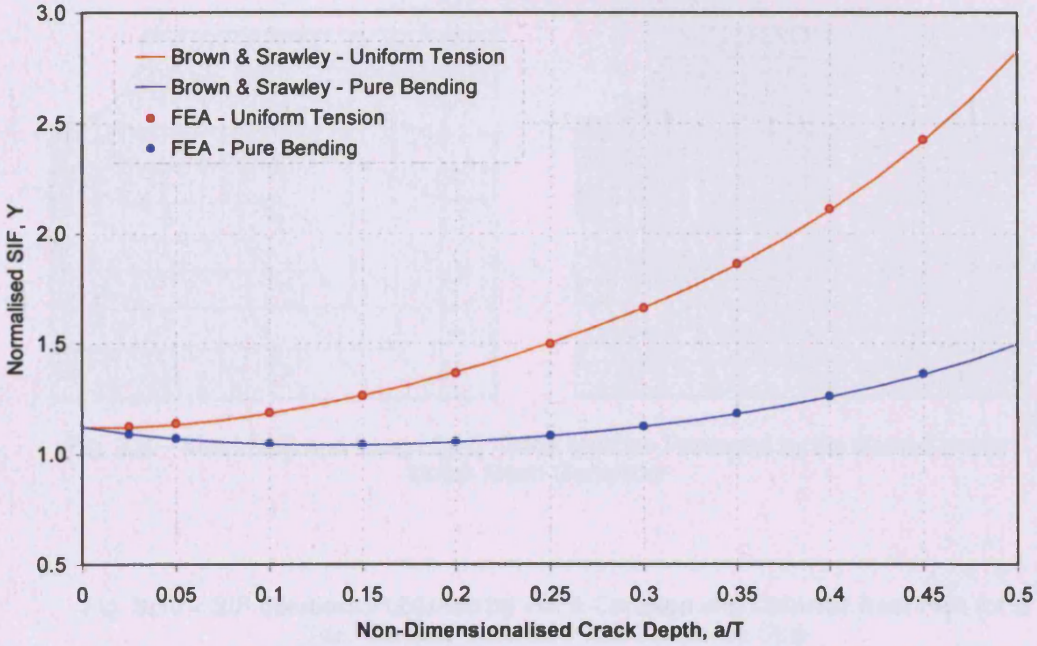

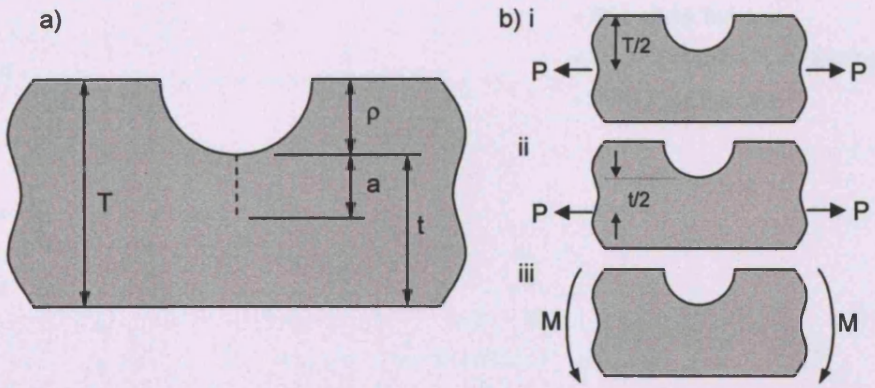

Fig. 3.8 – a) Description Geometric Parameters for Semi-Circular Notched Finite Strip. b) Loading Conditions Subject to Axial Force, 'P' and Bending Moment, 'M' i) Uniform Tension ii) Pure Tension iii) Pure Bending

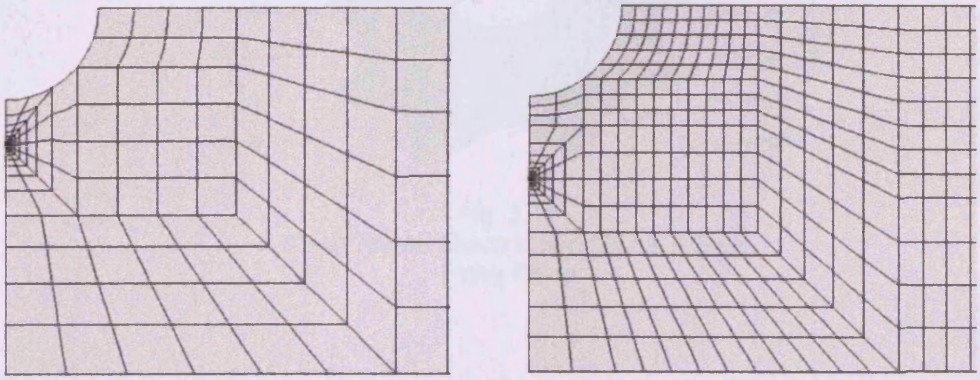

Fig. 3.9 – Short (left) and Long (right) Crack Meshes Produced by the Semi-Circular Notch Mesh Generator

Fig. 3.10 – SIF Solutions Published by Wu & Carlsson and Obtained from FEA for a Semi-Circular Notched Finite Thickness Strip

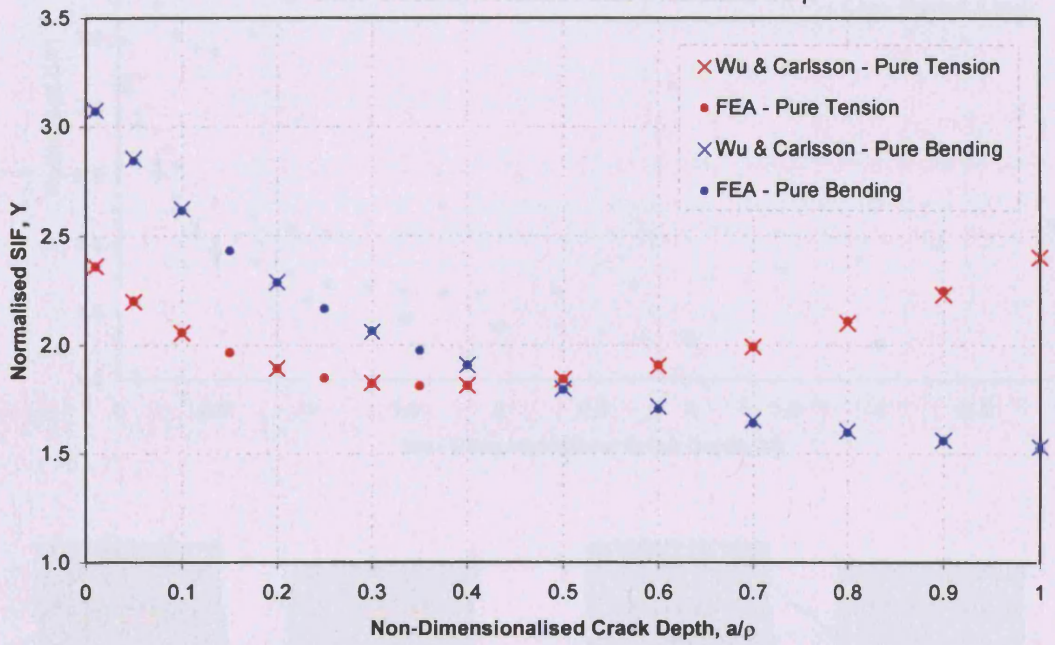

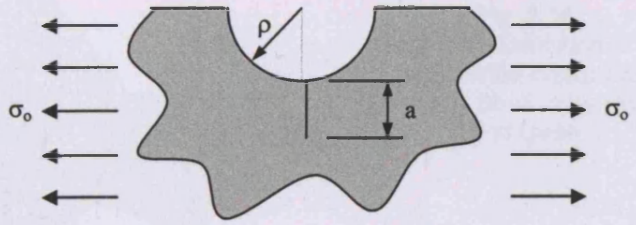

Fig. 3.11
A Semi-Circular Notch Embedded in a Semi-Finite Plane

Fig. 3.12 – SIF Solutions Published by Chen, Nisitani & Mori and those Obtained from FEA for a Semi-Circular Notched Semi-Infinite Thickness Strip

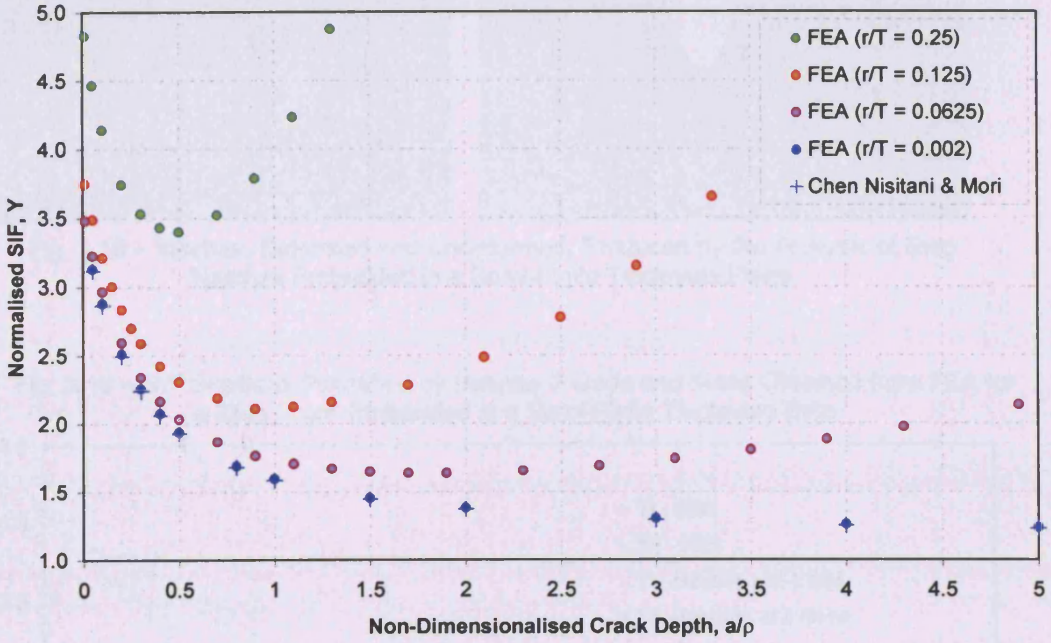

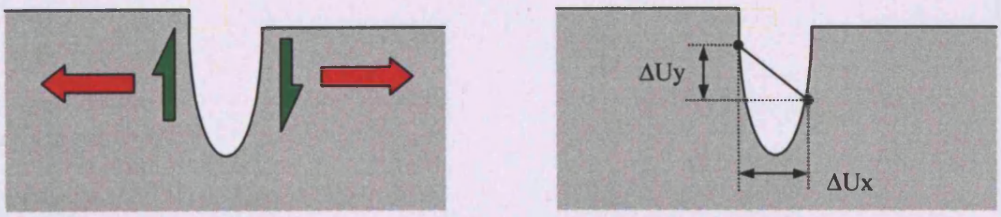

Fig. 3.13 – Relative Displacement of Crack Faces Subject to Mixed Mode Loading Mode 1 Crack Opening K_I (red arrows) and Mode 2 Crack Opening K_{II} (green arrows)

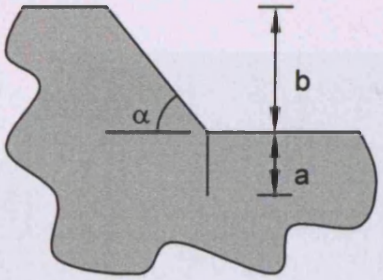

Fig. 3.14
Geometric Definition of the Semi-Finite Sharp Step Geometry Studied by Hasebe and Udea

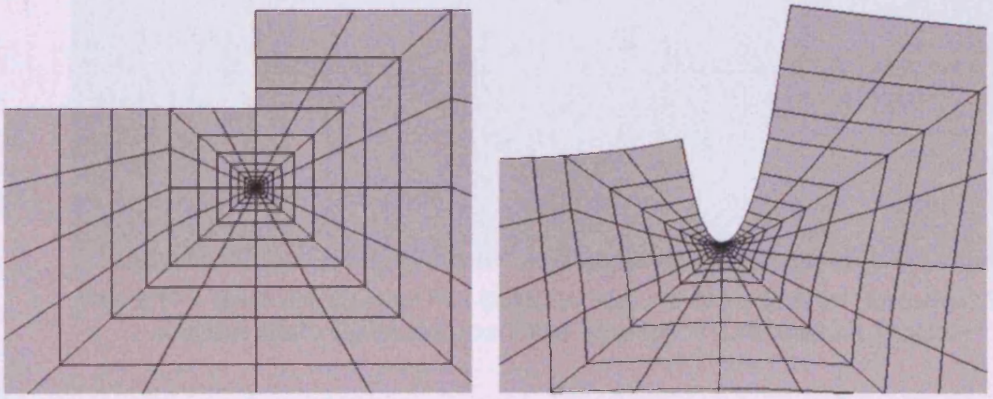

Fig. 3.15 – Meshes, Deformed and Undeformed, Produced by the Analysis of Step Notches Embedded in a Semi-Finite Thickness Plane

Fig. 3.16 – SIF Solutions Published by Hasebe & Ueda and those Obtained from FEA for a Step Notch Embedded in a Semi-Finite Thickness Strip

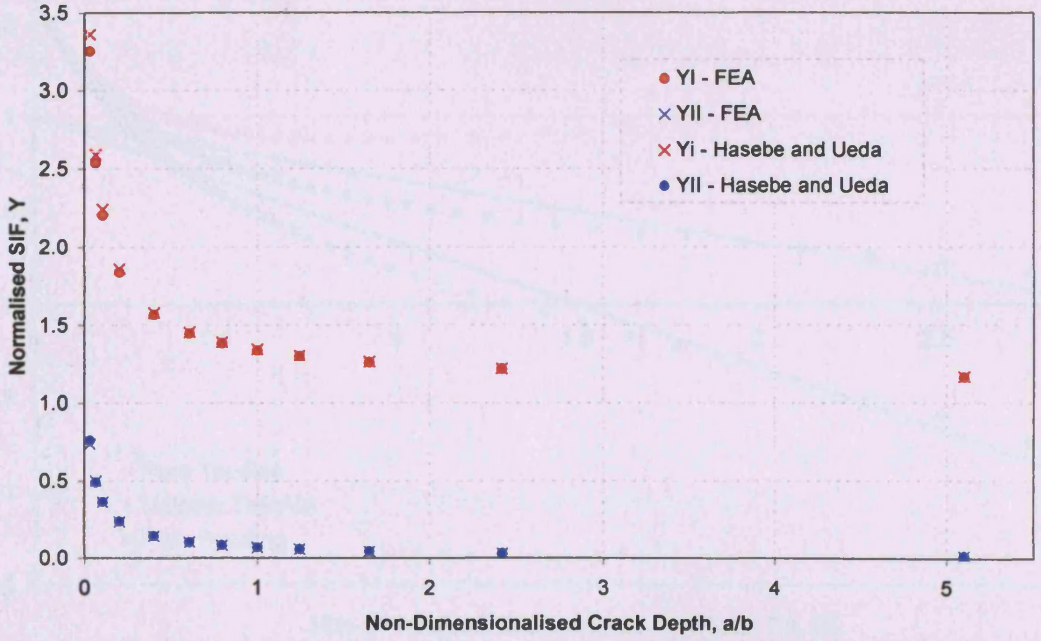

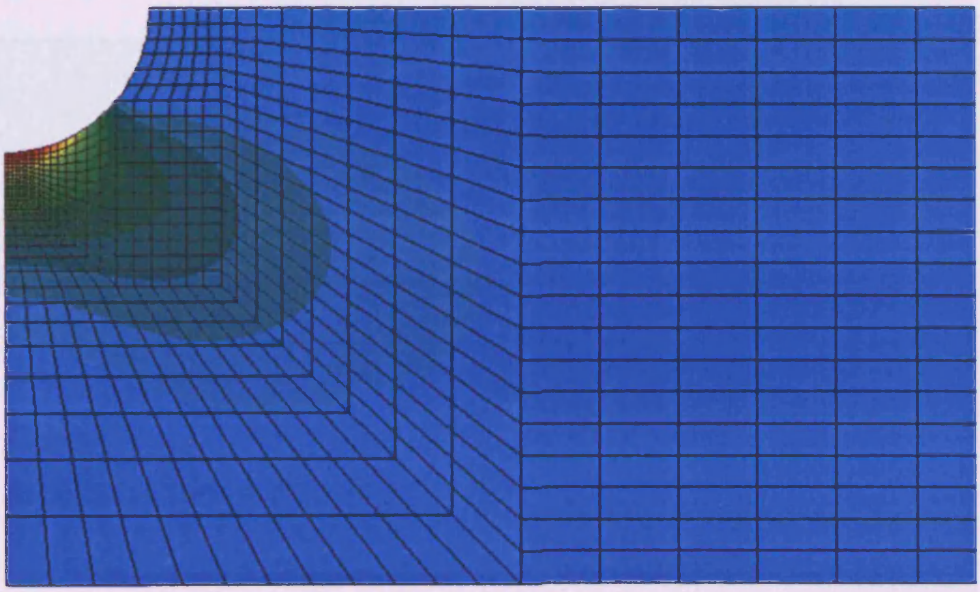

Fig. 3.17 – Mesh and Contour Plot Obtained from the Analysis of an Uncracked Semi-Circular Notch Embedded in a Finite Strip ($\rho/T = 0.25$, Uniform Tension)

Fig. 3.18 – Normalised Stress Distributions Obtained from the Analysis of an Uncracked Semi-Circular Notch Embedded in a Finite Strip ($\rho/T = 0.25$)

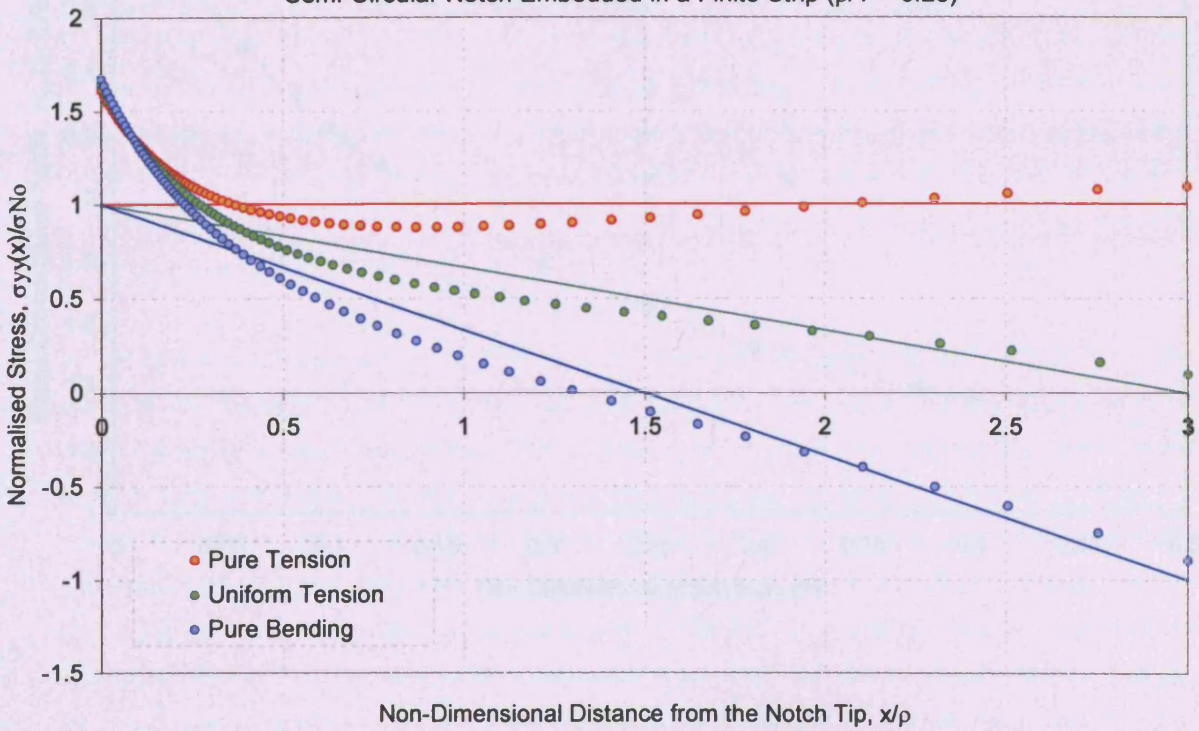

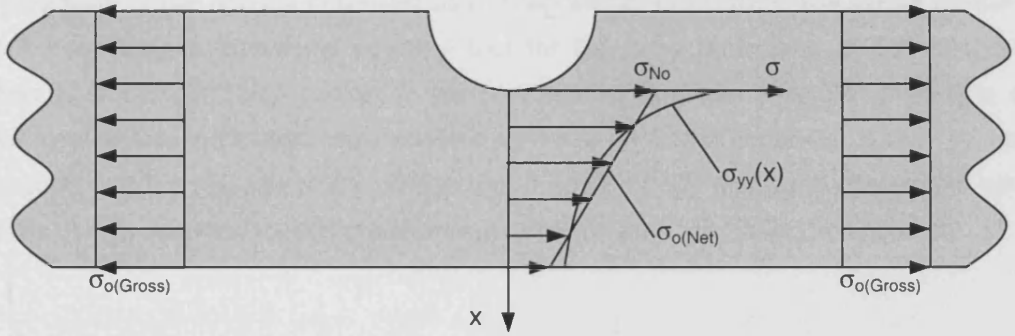

Fig. 3.19 – Definition of Stress Distributions and Concentrations arising ahead of a Semi-Circular Notched, Finite Width Strip.

Fig. 3.20 – Stress Concentration Factors Present at Semi-Circular Notches in Finite Width Strips Subject to Uniform Tension

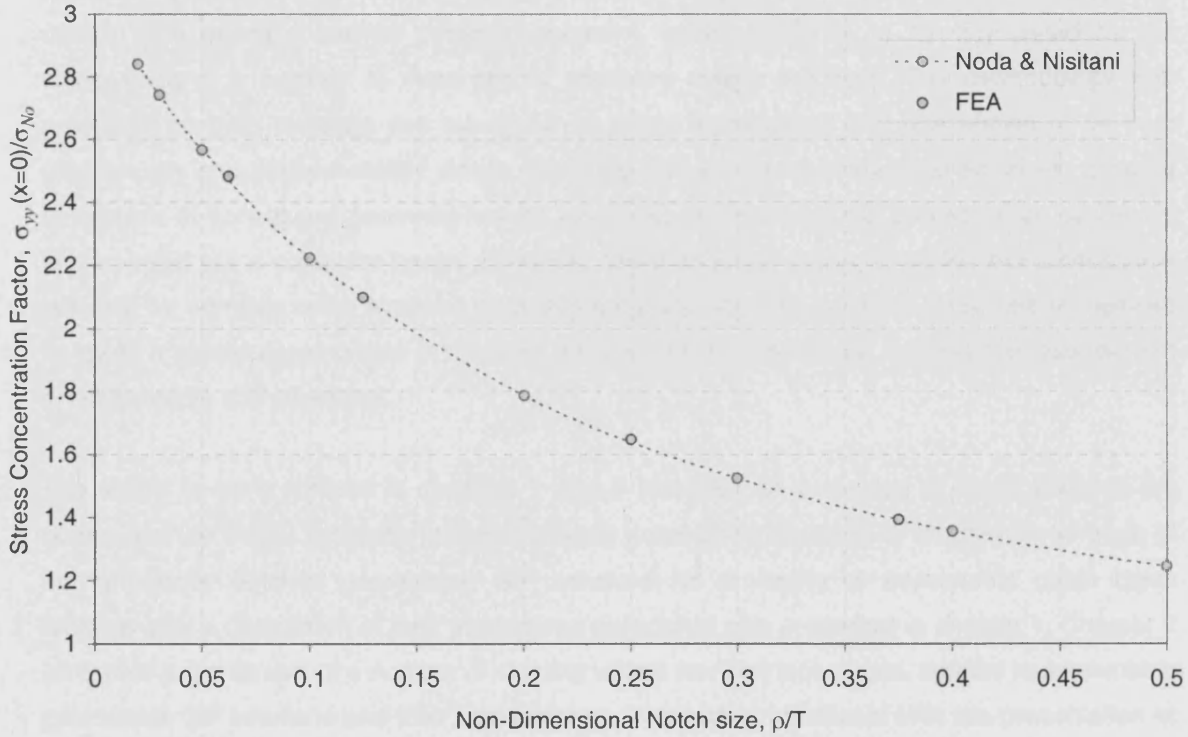

Chapter 4 – Composition and Interpolation of SIF Weight Functions

Chapter 1 gave an overview of the field of fracture mechanics focusing on the crack tip stress field parameter of SIF and the difficulties associated with its calculation. The weight function was identified as being a potentially powerful tool for the rapid generation of SIF solutions for geometries of complex form subject to complex loading arrangements. The properties of the weight function are such that, once determined for a particular geometry, it may be used in conjunction with a crack line stress distribution to economically and rapidly determine new SIF solutions of high accuracy for that geometry subject to an arbitrary loading arrangement.

$$K = \int_0^a \sigma_{yy}(x) m(a,x) dx \qquad \text{- (4.1)}$$

Chapter 2 contained a review of methods used by numerous investigators to modify plane geometry weight functions to account for additional geometric influences such as notches. The most salient of these was that proposed by Brennan and Teh[4.1] termed the composition of constituent geometry weight functions. Development of this principle by Teh *et al.*[4.2-4.5] generated numerous SIF solutions for two-dimensional, symmetrically notched components containing edge cracks. The principle permits complex geometry weight functions to be formulated by the composition of a number of more simple geometry weight functions. The methodology was proven to be both accurate and robust for all cases investigated and was shown to be both conceptually and mathematically simple. Provided that appropriate reference solutions, allowing calculation of constituent geometry weight functions, are available the process may be readily implemented via a computer-based algorithm. Great potential exists to exploit the composition principle for complex crack systems to rapidly generate new SIF solutions. This was recognised as being a crucial development in terms of the initial design and future, rapid defect assessment of components and structures.

The scope of work outlined in chapters 1 and 2 identified an extension to Teh's work on the composition of weight functions for symmetrically notched components to incorporate a range of asymmetrically notched geometries. SIF solutions for a variety of asymmetric notch types together with a description of their widespread application was presented in chapter 1. Chapter 2 contained a discussion of a number of existing weight function techniques, applied to asymmetric geometries SIF solutions and their shortcomings. The review concluded with the presentation of the significant advancements to be gained by application of a weight function composition approach. Presently, the composition approach has been validated for symmetric notches, however three asymmetric types were highlighted for investigation termed step, intrusion and protrusion notches as defined in fig. 4.1. This study intends to verify that a weight function

composition principle similar to that developed by Teh may be applied to these geometries to derive new SIF solutions of high accuracy in a concise and mathematically undemanding manner.

4.1 – Introduction

A generic study, comprising the generation of SIF solutions for a wide range of asymmetrically notched geometries was desired. Brennan and Teh[4.1] envisaged a 'library' of constituent geometry reference solutions, conducive for incorporation in design standards and codes. The development of a weight function composition scheme yielding results of high accuracy over such a geometry range highlights the methodology's versatility, stability and robustness. Such qualities have been absent from traditional weight function procedures confining their usage to a select group of specialists with expert insight. A primary objective of this study is to apply the contemporary MRS weight function methodology, presented in section 1.5.3, to allow implementation of weight function techniques by a broader range of non-specialist engineers. Publication of generic reference SIF and stress solutions is intended to provide design engineers and researchers with a close approximation to any notch adhering to a given generic form. To examine the suitability of the proposed weight function composition scheme, a single step notch geometry was initially selected for investigation, prior to development of generic solutions.

The weight function composition scheme applied by Brennan and Dover[4.6] depicted diagrammatically in fig. 4.2 isolates the geometric influence of the notch upon the SIF via a normalisation process involving semi-finite geometries. This geometric influence is composed via a finite thickness, plane geometry weight function. A weight function for the notched finite thickness geometry results. The composed weight function may be integrated with the crack-line stress distribution in the uncracked finite thickness geometry to yield new SIF solutions as described by eq. 4.2, in which subscripts refer to geometries indicated in fig. 4.2. The crack-line stress distribution can be that arising from any applied loading but is restricted in the present study to the modes of pure tension and pure bending.

$$K_C = \int_0^a \sigma_{yy}(x) \frac{m_A(a,x)}{m_B(a,x)} m_D(a,x) dx \quad \text{- (4.2)}$$

For asymmetric geometries, pure tension refers to a remotely applied tensile loading condition, which gives rise to no net bending in the plane of the crack. This definition is designed to be consistent with that adopted by Wu and Carlsson[4.7] and distinguishes it from uniform tension, which results in the presence of a net bending stress in the plane of the crack as indicated in fig. 4.3.

4.2 – An Initial Weight Function Composition Scheme for Step Notches

The weight function composition scheme defined in fig. 4.2 was initially applied to the step notch geometry. A composition algorithm, modified from that discussed in chapter 2 required reference SIF solutions and associated stress distributions from which constituent geometry weight functions are formed. These were then combined in the required manner, according to eq. 4.2, and integrated over the crack depth with the finite thickness stress distribution to yield new SIF solutions for the finite width step notched geometry. Reference solutions to formulate the weight function for the semi-finite notched geometry were unknown and were required to be determined. Finite element modelling has been shown to be a suitable method for deriving SIF solutions and the associated stress field for geometries of the required type in chapter 3. A mesh generator program was constructed to automate the development of finite element models of cracked and uncracked step notch models to be analysed using the ABAQUS^{TM} finite element solver. Similar solutions for the plane geometries are readily available from the published literature and constitute familiar and firmly established results. Reference solutions for the constituent plane geometries are identical to those utilised in chapter 2 (eqs. 2.1 and 2.2).

The step notch geometry identified for analysis prior to the generation of generic solutions was defined by the non-dimensional geometric parameters of $b/\rho = 6$, $\alpha = 45°$ and $b/T = 0.2727$.

Tabular and graphical representations of the reference SIF solutions and stress distributions are given in tabs. 4.1 and 4.2 and figs. 4.4 and 4.5 respectively. The reference solutions collected are of similar form to those derived by Teh for symmetric notches. The SIF distribution for the semi-finite geometry is shown in fig. 4.4 showing the profound influence of the notch upon the SIF in the stress concentration region, which decays to the known edge crack in a semi-finite plane solution of '$Y=1.1215$' as crack depth increases. Similarly the normalised stress distribution in the crack plane shows the decay of the notch influence to unity as crack depth increases (fig. 4.5).

Also collected are the corresponding finite width geometry's SIF solutions and crack line stress distributions for both pure tension and pure bending loading arrangements. Tabulated crack line stress distribution data is presented in tab. 4.3. Fig. 4.6 displays the normalised stress distribution in the plane of crack propagation showing again the stress concentration effect of the notch and the equilibrium of tensile and bending loads across the section for both loading arrangements.

Reference SIF solutions and associated stress distributions for the notched semi-finite geometry were fitted to a polynomial expression in the convenient form of eqs. 2.16 and 2.17 respectively, as described in chapter 2. Continuous SIF and stress solutions were formulated from the discrete FE data to a high degree of accuracy ($R^2 = 1$) The coefficients 'M_x' and 'N_x' of eqs. 2.16 and 2.17

are summarised in tab. 4.4. A similar quality of curve fit was achieved for the finite thickness stress distributions for both pure tension and pure bending in the form of eq 2.18. Coefficients 'P_x' are also shown in tab. 4.4. These solutions were coded into a composition algorithm.

Weight functions for the semi-finite geometries were formulated from a single reference solution of remotely applied tension. Weight functions for the plane finite thickness strip were also formulated from the single reference solution of tension. This formulation of constituent geometry weight functions was identical to that used by Teh and applied to a semi-circular notch in chapter 2. The sole difference to the composition scheme is the definition of crack length, which for the case considered here is defined as being equal for each constituent geometry.

Fig. 4.7 shows the SIF solutions obtained via the composition of constituent geometry weight functions for a step notch in a finite thickness plane. Solutions presented correspond to both pure tension and bending loading modes and depict the stress concentration effect, which decays to the level of the plane strip solution with increasing crack depth. The solution obtained for both pure tension and pure bending via the composition of constituent geometry weight functions is shown to give a poor correlation to the finite width FE data, also shown on fig. 4.7 and contained in tab. 4.5. The weight function solution gives a good approximation for short cracks, however the correlation decreases rapidly with increasing crack depth to give an unconservative 'undershoot' for deeper cracks. The results obtained do not complement the high degree of accuracy achieved for symmetric notches by Teh[4.2] nor do they reflect the potential advantages, in terms of accuracy, of a weight function methodology. Since confidence associated with the derivation of reference solutions, curve fitting of reference solutions and composition algorithm was not in question, as each had been independently verified, an error was thought to exist in the form of composition scheme applied. The remainder of this chapter discusses various composition schemes and presents a novel methodology applicable to all externally notched geometry types.

4.3 – An Alternative Weight Function Composition Scheme for Symmetric Notches

The symmetric and asymmetric geometries are arranged in fig. 4.8 to highlight the geometric inter-relationship existing between them. The symmetric and step notches are special cases of the more general intrusion notch. A 'complete' solution, applicable to all notches of fig. 4.8 is sought, however the composition scheme applied in the preceding section demonstrated the requirement for a greater appreciation of the composition principle. To achieve this, the finite element method was applied to develop new SIF solutions for symmetric and step notch components subject to a considered loading condition.

Fig. 4.9 shows SIF solutions for a symmetric notch and its asymmetric step notch equivalent (b/ρ = 6, α = 45°) both embedded in semi-finite planes with a uniformly distributed load applied directly to the crack face (fig. 4.10). Differences between SIF solutions for notched and plane geometries subject to this loading configuration are solely due to the geometry of the cracked bodies. A direct comparison between SIF solutions free from the influence of loading mode is therefore possible.

The form of solutions shown in fig. 4.9 for both geometries show the SIF decreasing rapidly from the uniformly loaded plane edge crack solution of '$Y=1.1215$' before increasing asymptotically towards this value as crack depth increases. At very short crack lengths the radius of the notch root becomes increasingly large with respect to crack depth and the other notch parameters are sufficiently distant and do not influence the solution. Therefore, as crack depth decreases the solution tends to that of the plane edge crack due to the free surface provided by the finite radius of the notch. As crack length increases the influence of the notch acts to stiffen the crack faces decreasing the SIF below that of the plane edge crack solution. As crack depth increases further with respect to notch depth the effective stiffness provided by the notch decreases giving the asymptotic increase of the solution to '$Y=1.1215$'. Two effects dominate the solution: that of the notch root radius termed the near surface effect and that of notch stiffness termed the global notch effect.

SIF solutions for symmetrically and asymmetrically notched semi-finite geometries subject to a uniformly distributed crack loading configuration are subject to the same geometric influences described above. With reference to fig. 4.9, the magnitude of these influences is shown to differ for the two notch types and is identified as the major source of error observed in section 4.2. This section describes an alternative composition scheme, utilising differing constituent geometries to replicate the results of Teh. The analysis is initially confined to symmetric notches to demonstrate a more complete appreciation of the process prior to its modification for application to step notches.

4.3.1 – A Stiffened Edge Crack in a Semi-Finite Plane

Hartranft and Sih[4.8] provide a reference solution, which accounts solely for the global notch effect. SIF solutions were derived by the application of an alternating method to a geometry they termed a partially loaded edge crack in a semi-infinite plane defined in fig 4.11a. This solution is superimposed upon the FE solutions obtained for crack face loading applied to the semi-finite, notched geometries in fig. 4.9. The comparison is made using this solution with a crack length, 'a' equal to '$(a_s - b)$' and a value of 'b' equal to the notch depth.

Hartranft and Sih's solution shows the stiffening effect of the unloaded crack face material becoming less influential as crack depth increases. Similar to the description of the form of fig. 4.9, the stiffening effect resists crack opening and manifests itself as a decrease in SIF with respect to the fully loaded edge crack solution. As crack length increases the effective stiffness offered by the unloaded material decreases causing the SIF solution, in the absence of any other geometric influences, to increase in magnitude asymptotically to the fully loaded edge crack solution.

Thus the solution normalised in the manner shown in fig. 4.9 may alternatively be described as a stiffened edge crack. The unloaded material on the crack face may be thought of as an additional stiffness acting to resist crack opening. Hereafter this geometry type is referred to as a stiffened edge crack solution and a fully loaded edge crack as an unstiffened edge crack.

Fig. 4.9 shows the near surface effect of the symmetrically notched geometry decreasing rapidly as crack length increases such that at greater notch depths only the global notch influence contributes significantly to the SIF solution. It is thought that this solution and its finite width equivalent maybe used in a composition scheme for symmetric notches as shown in fig. 4.12. In this manner it is the near surface effect of the notch upon the SIF solution, which is isolated by the normalisation process involving semi-finite geometry solutions and composed upon a finite width geometry solution.

The weight function composition scheme given in fig. 4.12 is similar to that used by Teh shown in fig. 2.1. The only difference is the definition of crack depth for constituent plane geometries. It is a subtle difference but crucially furthers appreciation of the physical significance of constituent geometries utilised in the composition scheme for symmetric notches applied by Teh and hence may yield a solution for asymmetric notches. The definition of crack depth used for the constituent plane geometries adopted above views a crack of depth 'a' at the root of an infinitely thin slot of depth 'b' as opposed to a partially loaded crack of depth '$a+b$'.

Irrespective of the manner in which the crack is viewed, although the loading arrangement differs, the geometries are the same and hence have equal weight functions. Teh managed to effect a stiffened crack by defining plane geometry cracks of length '$a+b$' and deferring integration of the plane geometry weight functions by a distance equal to the notch depth 'b'. The procedure is essentially that applied in section 2.2.1 to determine SIF solutions for partially loaded cracks. Thus, application of the SIF solution by Hartranft and Sih and the definition of crack depth utilised in fig. 4.12 will yield the same weight function as that derived by Teh using a fully loaded edge

crack solution and deferred integration. As opposed to the composition scheme of fig. 2.1, the proposed alternative scheme defines crack length as being equal for all constituent geometries.

For the cases considered here, which are edge cracked geometries, the matter of what constitutes a crack and what does not is an arbitrary one, however this is not the case for surface cracked geometries. A potential composition scheme for surface cracks in three-dimensional geometries with differing crack depths is complicated by the problematic definition of a consistent crack shape for constituent geometries. Since the methodologies presented here are to be ultimately extended to incorporate surface cracked geometries the weight function composition scheme defined in fig. 4.12 is, at present preferred.

4.3.2 – Stiffened Edge Crack SIF Solutions

A composition scheme utilising stiffened, edge cracked geometries was discussed and defined in the preceding section. Realisation of the modified scheme requires additional reference solutions for the stiffened geometries. The SIF solution provided by Hartranft and Sih was used for the semi-finite stiffened edge crack. The full solution is given by eq. 4.3 where the parameter '$F(b/as)$' is fitted to a continuous third order polynomial (eq. 4.3a) from the discrete data displayed in Tab. 4.6 and is valid for the full range of possible crack depths ($1 > b/a_s > 0$).

$$Y_S(a_S) = \frac{2}{\pi} ACOS\left(\frac{b}{a_S}\right)\left[1 + F(b/a_S)\right] \qquad \text{- (4.3)}$$

$$a_S = a + b$$

$$F(b/a_S) = 0.0175\left(\frac{b}{a_S}\right)^3 - 0.0162\left(\frac{b}{a_S}\right)^2 - 0.1221\left(\frac{b}{a_S}\right) + 1.1219 \qquad \text{- (4.3a)}$$

No similar SIF solutions for stiffened finite width geometries exist in the published literature. A finite element analysis was conducted on this geometry type defined by geometric parameters described in fig 4.11b in Chapter 3. The results are presented in tab 3.3 and fitted to a fourth order polynomial of the form given by eq. 4.4 which is valid for '$0.75 > (a+b)/T > 0$. Coefficients 'R_x' obtained by the curve fitting process are given in Table 4.7.

$$Y_S = R_0 + R_1\left(\frac{a}{T}\right) + R_2\left(\frac{a}{T}\right)^2 + R_3\left(\frac{a}{T}\right)^3 + R_4\left(\frac{a}{T}\right)^4 \qquad \text{- (4.4)}$$

4.3.3 - Curve Fitting of Notched Semi-Finite SIF Solutions

The reference SIF solutions obtained from uniform loading applied to the crack face (fig. 4.9) are of a more complex form than those derived for remote loading. The advantages of the form of equation developed by Teh is maintained by utilising the solution of Harthanft and Sih to isolate the influence of the near surface and notch flank angle, which may be approximated by an equation of the form of eq. 4.5. The curve fitting is achieved via the set of equations given below.

$$Y(a) = Y_S(a) g_{\alpha,\rho}(a) \quad \text{- (4.5)}$$

Where:

$$g_{\alpha,\rho}(a) = \left[M'_4 \left[\frac{1}{(1+a/\rho)} \right]^4 + M'_3 \left[\frac{1}{(1+a/\rho)} \right]^3 + M'_2 \left[\frac{1}{(1+a/\rho)} \right]^2 + M'_1 \left[\frac{1}{(1+a/\rho)} \right]^1 + M'_0 \right] \quad \text{- (4.5a)}$$

The term '$g_{\alpha,\rho}(a_S)$' describes the geometric influence of the near surface effect and the notch flank angle as a function of non-dimensional crack depth 'a/ρ' as a fourth order polynomial. The coefficients 'M'_x' of Eq 4.5a are summarised for a number of notches in tab. 4.8. '$Y_S(a)$' is the stiffened edge cracked semi-finite plane solution as described by Hartranft and Sih. Application of uniform loading to the crack face simplifies the crack line stress distribution to the form given below.

$$\sigma(x) = \sigma_o \quad \text{- (4.6)}$$

4.3.4 – Equivalent Weight Function Composition Schemes for Symmetrical Notches

The equivalence of weight function compositions based upon the use of schemes determined by Teh and that discussed in this section has already been drawn. A demonstration of this equivalence is provided by the determination of SIF solutions for a semi-circular notched strip via the two schemes. This was achieved in chapter 2 utilising the composition scheme described by Teh and reference solutions determined under a remotely applied tensile load. A composition scheme based on that given by fig. 4.12 utilising reference solutions obtained as described in sections 4.3.2 and 4.3.3 was constructed.

The requirement to publish an associated crack line stress distribution is not required for the crack face loading arrangement, as it is simply given by eq. 4.6. Since the reference solutions for the stiffened geometries are determined for the load case of uniform loading applied to the crack face the weight function coefficients may be determined by closed form expressions as described in chapter 2.

The SIF solutions shown in fig. 4.18 are those obtained via the composition scheme defined in fig. 4.12 for uniform tensile loading. They are equal to those obtained by Teh's methodology shown in fig. 2.12.

4.3.5 – An Improved Weight Function Composition Scheme for Step Notches

Re-inspection of the SIF solutions for the symmetric and step notched geometries subject to crack face loading shows that the additional stiffness of the symmetrically notched geometry with respect to the edge crack solution is halved for the step notched geometry. This observation can be readily appreciated when it is considered that only a single flank acts to stiffen the crack for a step notch as opposed to two flanks for the equivalent symmetric notch. A sharp step notch is defined in fig. 4.13. SIF solutions for this geometry subject to crack face loading may be determined from the average of the stiffened and unstiffened geometries subject to crack face loading and is termed a partially stiffened crack. Plotting the partially stiffened SIF solution upon the notched component solutions in fig. 4.14 shows that it may be used to isolate the near surface effect for step notched geometries in the same manner as a stiffened geometry was used for symmetric notches. The average of the stiffened and unstiffened geometry represents an SIF solution equal to a sharp step notch of 90° as shown in eq. 4.7a where subscripts refer to the geometries given in fig. 4.13

$$Y(a)_{A,D} = \frac{Y(a)_{B,E} + Y(a)_{C,F}}{2} \quad \text{- (4.7a)}$$

The SIF solutions for cracks of varying stiffness may be manipulated by eq. 4.7a. It only applies for cases where the crack line loading arrangement is the same for each geometry as is the case here with uniform loading applied to the crack faces. With reference to the weight function formulation procedure outlined in Chapter 1, section 1.5.3, The same manipulation can be applied to weight function coefficients, 'C' determined for the stiffened and unstiffened crack. Eq. 4.7b is a more general form of eq. 4.7a as the weight function coefficients are independent of the loading condition.

$$C_{A,D} = \frac{C_{B,E} + C_{C,F}}{2} \quad \text{- (4.7b)}$$

As a consequence of eq. 4.7b the manipulation may also be applied to the weight function. Fig. 4.15 depicts weight functions for a stiffened, unstiffened and partially stiffened crack in a semi-finite plane. With reference to this figure it can be observed that eq. 4.7c is independent of 'x'.

$$m_{A,D}(a,x) = \frac{m_{B,E}(a,x) + m_{C,F}(a,x)}{2} \quad \text{- (4.7c)}$$

A weight function composition scheme for step notches is defined in fig. 4.16 based upon the observation made in this section. It makes use of both stiffened and unstiffened geometries, which are given a equal weighting of 0.5 to effect their average. Replacement of the unstiffened crack geometries utilised in the initial composition scheme depicted in fig. 4.2 with the step geometries defined in figs. 4.13a and 4.13b gives a composition scheme shown diagrammatically in fig. 4.16. The reference solutions were unchanged from those utilised for the analysis conducted in section 4.2. The sole difference was the inclusion of the partially stiffened geometry solutions, calculated from stiffened and unstiffened geometry solutions, as proposed in this section.

Application of this composition scheme yields solutions of greatly enhanced accuracy when compared to those obtained initially as shown in fig. 4.17. As before the finite thickness SIF solutions and the finite thickness plane geometry solutions are included alongside the weight function solution. The solutions display an excellent correlation to the finite thickness SIF data in the stress concentration region and also show the decay of the stress concentration effect on SIF to the level of the plane, finite thickness geometry solution. The SIF solutions for both pure tension and pure bending obtained by the weight function composition scheme are shown to be stable and accurate over the range of crack depths investigated. The slight 'drift' of the weight function solution for deeper cracks, particularly evident for the pure bending solution, is due to the use of a single reference solution when formulating constituent geometry weight functions. It may be corrected by application of an additional reference case as described in chapter 2, section 2.2.2.

An alternative weight function composition scheme utilising stiffened edge crack geometries as constituent solutions has been successfully applied to both symmetric and step notched components to yield solutions of high accuracy.

4.4 – Limitations of Composition Schemes

Teh conducted an extensive investigation on a broad range of symmetrically notched geometries and showed that application of the composition of constituent geometry weight functions gave SIF solutions of good accuracy for all cases considered. If, however, the principle is applied to notches of extreme geometric form the composition scheme yields solutions of reduced accuracy. Considering, once more the semi-circular notched, finite width plane geometry solutions derived

by the composition principle in Chapter 2, section 2.4. The solutions show a good correlation to those obtained through finite element means, however, as notch size is increased the correlation decreases. Fig. 4.18 shows SIF solutions for this geometry for a number of notch sizes defined by 'ρ/T' and includes a notch size of '$\rho/T=0.375$' together with finite element data. The loss of accuracy for larger notch sizes is evident and is expected to deteriorate further as notch size increases.

Fig. 4.19a shows a notched geometry, for which the notch is large with respect to strip thickness. SIF solutions for externally notched geometeries comprise the two influences due to the presence of a free surface and the global notch geometry. The extent to which these two influences are affected by a remote boundary differs. The near surface influence is subject to a remote boundary effect at a distance 't' from the notch root. The free surface effect shows characteristics of the plane geometry shown in fig. 4.19b. The global notch influence is subject to a remote boundary given by dimension 'T' and hence shares characteristics with the geometry depicted in fig. 4.19c. The composition scheme, in its present form contains no means by which these differing remote boundary effects can be modelled.

For instances where the notch size is small or the notch is acute the free surface influence is small or does not extend a great distance ahead of the notch. Therefore, the remote boundary influence upon the free surface effect is also small. Many of the notches investigated by Teh were of this form and the composition principle may be applied to them to give SIF solutions of good accuracy. For instances where the notches is large and/or blunt the approximation offered by the composition scheme becomes increasingly invalid.

A complete solution applicable to all notch forms including those of extreme geometric form has yet to be formulated. Additional insight offered by inspection of results under crack face loading permits an improved weight function solution for all types of externally notched geometries to be suggested and is described below.

4.5 – Interpolation of SIF Weight Functions

Consider an edge crack at the root of a semi-elliptical notch in a finite plane. Fig.4.20 shows two possible composition schemes based on the unstiffened (scheme 'A') and stiffened (scheme 'B') plane geometry weight functions described in the preceding sections. As the semi-elliptical notch dimension, 'd' increases the weight function composition scheme 'A' becomes more appropriate. At the limit where '$d = \infty$' the scheme is obviously true and will give an exact result. Conversely if the notch dimension 'd' is decreased, weight function composition scheme 'B' becomes more appropriate. Again at the limit where '$d = 0$' the scheme is true and will give an exact answer. For

each interstitial value of 'd' neither scheme will offer an exact solution, however it will comprise characteristics of both.

A parameter '$f_{\rho,\alpha}(a)$' describes the degree to which the crack obeys composition scheme 'A' (fig. 4.20) and thus '$1 - f_{\rho,\alpha}(a)$' describes the degree to which the crack obeys composition scheme 'B'. Examination of the crack face loading SIF solutions of the semi-finite geometries is used to determine the value of '$f_{\rho,\alpha}(a)$', which is defined by the expression below and diagrammatically as fig. 4.21.

$$f_{\rho,\alpha}(a) = \frac{Y_N(a) - Y_S(a)}{Y_U(a) - Y_S(a)} \qquad \text{- (4.8a)}$$

The parameter '$f_{\rho,\alpha}(a)$' may be viewed as an interpolation factor, which describes the notch influence upon SIF as being that of either a stiffened or unstiffened plane geometry SIF. Terms to the right of eq. 4.8 are arranged in the form of a linear interpolation equation in which the notched geometry SIF is weighted according to its behaviour as either crack type. The manipulation of SIF solutions in this manner is similar to that used in eq. 4.7 to determine SIF solutions for a partially stiffened crack and therefore, maybe expressed in terms of weight function coefficients or weight functions. The interpolation factor defined by eq. 4.8 can therefore be said to be only a property of the notch geometry and may be applied to any stiffened and unstiffened geometries.

Implementation of a weight function scheme composition scheme based upon the interpolation factor as defined here is presented diagrammatically in fig. 4.22. By virtue of the definition of the interpolation factor '$f(a)$' the quotient to the left of the equation involving semi-finite geometries reduces to a value equal to unity. Thus the quotient term may be neglected simplifying the scheme to the form defined in fig. 4.23. The interpolation of weight function approach permits the two geometric influences to be composed via their respective relevant geometry types and therefore may be viewed as a more complete composition approach. Although closely related, the interpolation scheme presented in fig. 4.23 is of a considerably different form to the composition schemes presented previously. At this point the term composition of weight functions is replaced in favour of interpolation of weight functions to distinguish between the two differing approaches.

The interpolation factor '$f(a)$' applies to the fully loaded edge crack geometry of thickness 't', which is used to compose the near surface effect. Thus the weighting '$1-f(a)$' must apply to the stiffened edge crack solution to compose the global notch influence. The interpolation factor defined by eq. 4.8a is valid when the loading applied to the crack faces is equal for each geometry. A similar, more general expression may be written, involving weight function coefficients or weight functions

derived for each geometry relieving the interpolation factor of the requirement for this special loading condition.

$$f(a) = \frac{C_N(a) - C_S(a)}{C_U(a) - C_S(a)} \quad \text{- (4.8b)}$$

$$f(a) = \frac{m_N(a,x) - m_S(a,x)}{m_U(a,x) - m_S(a,x)} \quad \text{- (4.8c)}$$

Fett and Munz[4.9] proposed weight function solutions for notched components using two extreme geometry weight functions in a similar manner to that proposed here. They referred to the two constituent geometries as limiting cases, between which all notch geometry solutions must fall when subject to equal crack face loading. The discussion given above supports the two expressions presented by Fett and Munz, who described externally notched geometry SIF and weight function solutions by Eq. 4.9a and 4.9b.

$$Y_N = \varphi Y_U + (1-\varphi) Y_S \quad \text{- (4.9a)}$$

$$m_N(a,x) = \beta m_U(a,x) + (1-\beta) m_S(a,x) \quad \text{- (4.9b)}$$

Fett and Munz noted the apparent equivalence of interpolation factors 'φ' and 'β', however stated that when applied to the weight function, 'β' must be dependant on both 'a' and 'x'. It is suggested here, however that application of the interpolation factor to a weight function is independent of 'x' such that the following eq. 4.10 holds. Fett and Munz reported weight functions formulated via eq. 4.9 as being accurate to within approximately 3% for internal elliptical notches applying what they perceived to be an approximate condition 'φ = β'. A significant portion of this error is thought to be due to the approximate methodology utilised for the formulation of 'φ' as described below.

$$\varphi = \beta = f(a) \quad \text{- (4.10)}$$

Characterisation of the notch interpolation factor was achieved by Fett and Munz by the description of a view angle, 'ω' (fig. 4.24). The view angle was calculated from geometric considerations for a range of semi-elliptical notches. In the case of a semi-circular externally notched strip the view angle may be written as given by eq. 4.11. An approximate relation between view angle and interpolation factor was developed as a simple expression given below

as eq. 4.12. The performance of this methodology, when applied to V-notches characterised by both 'ρ' and 'α', i.e. where description of 'ω' is impeded by additional notch geometry parameters is unclear.

$$\omega = ASIN\left(\frac{1}{1+a/\rho}\right) \quad \text{- (4.11)}$$

$$\varphi = \beta \approx SIN^{7/2}\omega \quad \text{- (4.12)}$$

Having firstly considered a number of weight function composition schemes with a clearly defined end product in mind has promoted the use of constituent geometry solutions for the calculation of interpolation factors. Unlike geometric methods such as that proposed by Fett and Munz the use of constituent geometries is readily ascertained and unambiguous for all notch geometry types provided that a constituent geometry reference SIF solution and stress distribution is known. The proposed methodology for calculation of the interpolation factor described by eq. 4.8 remains stable, unambiguous and accurate for all notch profiles considered in this study.

A comparison between interpolation factors obtained via the analysis of constituent geometries and the approximate procedure described by eqs. 4.11 and 4.12 is made for the case of a semi-circular notch in fig. 4.25. Both show a good general correlation, however the approximate procedure dictates that the near surface influence will only decay to zero at an infinite distance from the notch root. The analysis of constituent geometry SIF solutions predicts that the effective influence will decay to zero at a finite distance from the notch root.

4.6 – Interpolation of SIF Weight Functions for a Symmetric Notches

To demonstrate the enhanced accuracy of the interpolation of weight functions technique outlined in section 4.5, new SIF solutions were determined using this method for the semi-circular notched finite strip. A clear step by step procedure indicating the interpolation method used to obtain final SIF solutions is provided in Appendix B. An expression for the interpolation is given by eq. 4.13.

$$K_I = \int_0^a \sigma_{yy}(x)\left[f_\rho(a)m_U(a,x) + \left(1 - f_\rho(a)\right)m_S(a,x)\right] \quad \text{- (4.13)}$$

Where: $m_U(a,x)$ is the equivalent unstiffened plane geometry weight function

$m_S(a,x)$ is the equivalent stiffened plane geometry weight function

$f(a)$ is the interpolation factor for the symmetric notch

The weight function methodology developed in section 4.5 was implemented for a semi-circular notched finite strip. The derived SIF solutions for remotely applied uniform tension are shown in fig. 4.26 for a range of notch sizes against those obtained via the existing composition principle and the finite element solutions contained in tab. 3.3. A high degree of accuracy is maintained for the smaller notch sizes and a good correlation between the three solutions is apparent. As notch size increases the composition of constituent geometry weight functions gives progressively worsening solutions compared to the finite element data. The weight function interpolation scheme developed in this chapter gives solutions of high accuracy for all notch sizes investigated.

The solutions determined via the weight function interpolation method give good agreement with the finite element data over the geometry range and loading modes tested. The term '$f_{\rho,\alpha}(a)$' is shown to be insensitive to loading mode as predicted in section 4.5. The limited investigation described in this section is expanded in chapter 5 to incorporate a greater range of symmetrically notched geometries. The body of work contained in chapter 5 aims to demonstrate the robust and stable nature of this weight function method and highlight the relative ease with which new SIF solutions of high accuracy may be determined for a wide range of geometric configurations and loading modes.

4.7 – Interpolation of SIF Weight Functions for Step Notches

The findings discussed in this chapter can be compiled to formulate a weight function interpolation technique, for use in determining SIF solutions for asymmetric geometries. An appropriate interpolation scheme comprises both stiffened and unstiffened geometries as recommended in section 4.5. Drawing also upon the weight function composition scheme described and implemented in section 4.3.5 gives rise to the suggested weight function interpolation scheme given as eq. 4.14.

$$K_I = \int_0^a \sigma_{yy}(x)\left[\frac{1}{2}[f(a)m_U(a,x)+(1-f(a))m_S(a,x)]+\frac{1}{2}m_U(a,x)\right] \quad \text{- (4.14)}$$

Where: $m_U(a,x)$ is the equivalent unstiffened plane geometry weight function

$m_S(a,x)$ is the equivalent stiffened plane geometry weight function

$f(a)$ is the interpolation factor for the equivalent symmetric notch

The scheme expressed by eq. 4.14 indicates that a weight function comprised of both stiffened and unstiffened finite thickness, edge crack solutions can be compiled to yield a solution for the step notch geometry. The scheme comprises an interpolation factor for the equivalent symmetrically notched geometry solution with a weighting of 0.5 as applied in section 4.3. The remaining influence is provided solely by the unstiffened geometry solution. In this manner the step notch system may be said to be comprised of equally weighted characteristics of both the equivalent symmetrically notched geometry and the equivalent unstiffened geometry.

The step notch represents a special case for which the application of a weighting of 0.5 to the equivalent symmetrical notch interpolation factor yields a correct solution. An interpolation factor for the step notch can be ascertained from eq 4.8 provided that reference SIF and associated stress distributions for the step geometry are known and finite width step notch solutions obtained via eq. 4.14.

$$K_I = \int_0^a \sigma_{yy}(x)\left[f_\rho(a)m_U(a,x) + \left(1 - f_\rho(a)\right)m_S(a,x)\right] \quad \text{- (4.15)}$$

Where: $m_U(a,x)$ is the equivalent unstiffened plane geometry weight function

$m_S(a,x)$ is the equivalent stiffened plane geometry weight function

$f(a)$ is the interpolation factor for the step notch

Chapter 6 contains an extensive appraisal of the performance of the interpolation scheme in the form of eq. 4.14 and presents solutions for a broad range of step notch geometries. The ability to manipulate the interpolation factor in the manner given in eq 4.14 suggests a procedure for the calculation of SIF solution for notches of more intricate form from interpolation factors of more basic notch types. This theme is not expanded upon in this text, however a discussion of the geometry types for which this is valid and recommended weight function interpolation schemes are identified for validation in future work contained in chapter 11.

4.8 – Interpolation of SIF Weight Functions for Asymmetric Notches

The weight function schemes defined in sections 4.6 and 4.7 apply to symmetrically notched and step notched components respectively. Both notch types are special cases of a more general termed an intrusion notch. Eq. 4.16 is recommended as a suitable weight function interpolation scheme and is of the same form of eqs. 4.13 and 4.15. Provided that at least a single reference SIF solution and associated crack line stress distribution are available for the notched, semi-finite geometry an interpolation factor can be determined and applied as recommended.

$$K_I = \int_0^a \sigma_{yy}(x)\left[f_\rho(a)m_U(a,x) + \left(1 - f_\rho(a)\right)m_S(a,x)\right] \quad \text{- (4.16)}$$

Where: $m_U(a,x)$ is the equivalent unstiffened plane geometry weight function

$m_S(a,x)$ is the equivalent stiffened plane geometry weight function

$f(a)$ is the interpolation factor for the asymmetric notch (eq. 4.8)

The form of interpolation scheme defined by eq. 4.13 and 4.14 are rigorously validated in chapters 5 and 6 respectively whereas chapter 8 contains a more limited appraisal of interpolation schemes applied to general asymmetric notches.

4.9 - Conclusions

This chapter sought to derive SIF solutions for asymmetric geometries via a weight function composition scheme similar to that implemented by Teh for symmetric geometries. Initial solutions were disappointing in terms of their accuracy with respect to those achieved by Teh and indicated that a re-evaluation of initial concepts outlined in chapter 2 was required. A number of observations on the geometric influences present in notched components stemming from the application of uniform loading to their crack faces were made. An improvement to the initial composition scheme, regarding the form of the composition, was applied to yield more satisfactory solutions for the step notch geometries. Also noted however, were limitations present in the composition scheme.

A weight function methodology closely related to the composition principle was developed and termed the interpolation of weight functions. It was shown to give more accurate solutions for notches of extreme geometric form for which the approximation offered by a composition principle becomes invalid. The interpolation scheme was suggested as a 'complete' solution allowing rapid and accurate determination of SIF solutions for complex geometries. The mathematical simplicity of the composition scheme was maintained and was shown to provide excellent solutions for a semi-circular notched finite strip.

The following chapters aim to demonstrate the improved accuracy of the interpolation scheme. Chapter 5 applies the principle to a range of symmetrically notched components, chapter 6 to step notches and chapter 8 to general asymmetric notches. Desired generic solutions are not published, although numerous useful solutions are presented, each chapter aims to validate the interpolation procedure against finite element data.

Chapter 10 extends the study on two-dimensional geometries outlined above to three-dimensional geometries containing surface cracks. The interpolation of weight function scheme may be applied to generate approximate SIF solutions for the deepest point of flaws present at notch roots of three-dimensional equivalents of the geometries considered here.

The scope of work outlined in chapters 1 and 2 is restricted to the notch types discussed in this section. The same principles may, however be applied to numerous other notch types to generate an almost limitless range of new SIF solutions. The possibility to extend the current study to incorporate these notch types is discussed in chapter 11.

4.10 – References

[4.1] Brennan, F. P. Teh, L. S., Determination of Crack-Tip Stress Intensity Factors in Complex Geometries by the Composition of Constituent Weight Function Solutions, *Fatigue Fract Engng Mater Struct*, 2003

[4.2] Teh, L.S., *Library of Geometric Influences for Stress Intensity Factor Weight Functions.* PhD Thesis, 2002, UCL.

[4.3] Teh, L.S. and Brennan, F.P., Stress Intensity Factors for Cracks Emanating from Two-Dimensional Semi-Circular Notches Using the Composition of SIF Weight Functions. *Fatigue Fract Engng Mater Struct* 28, pp. 423 – 435, 2005

[4.4] Teh, L.S., Love, A.J. and Brennan, F.P., Mode I Stress Intensity Factors for Edge Cracks Emanating from 2-D U-notches Using Composition of SIF Weight Functions. Accepted for publication in the *International Journal of Fatigue* July 2005.

[4.5] Brennan, F. P. Teh, L. S. and Love, A. J., "Library of Geometric Influences for SIF Weight Functions" 11th International Conference On Fracture, Turin 2005

[4.6] Brennan, F.P. and Dover, W.D., Stress Intensity Factors for Threaded Connections, *Engineering Fracture Mechanics*, 1995, **50**, No.4, 545-567.

[4.7] Wu, X.R. and Carlsson, A.J., *Weight Functions and Stress Intensity Factors*, Permagon Press, Oxford, 1991. ISBN: 0-08-041702-7

[4.8] Hartranft, R.J. and Sih, G.C., *Methods of Analysis and Solutions of Crack Problems*, G.C.Sih ed. Noordhoff, Holland, 1973.

[4.9] Fett, T. and Munz, D., *Stress Intensity Factors and Weight Functions*, Computational Mechanics Publications, Southampton, UK, 1997. ISBN: 1-85312-497-4

4.11 - Tables

Tab. 4.1 – SIF Solutions for Semi-Finite Step Notch (b/ρ = 6; α = 45°)

a/ρ	Y_I	a/ρ	Y_I
0.05	3.058	1.6	1.733
0.1	2.931	1.9	1.665
0.15	2.816	2.2	1.611
0.2	2.714	2.5	1.568
0.25	2.623	3	1.511
0.3	2.542	3.5	1.467
0.4	2.404	4	1.432
0.5	2.291	5	1.380
0.7	2.118	6	1.343
0.9	1.993	7	1.315
1.1	1.897	8	1.294
1.3	1.821	10	1.263

Tab. 4.2 – Stress Distributions for Semi-Finite Step Notch Under Tension (b/ρ = 6; α = 45°)

x/ρ	$\sigma_{yy}(x)$	x/ρ	$\sigma_{yy}(x)$	x/ρ	$\sigma_{yy}(x)$
0.000	2.865	0.288	2.178	1.992	1.317
0.012	2.827	0.326	2.120	2.221	1.288
0.025	2.790	0.364	2.062	2.451	1.259
0.038	2.753	0.413	2.001	2.738	1.234
0.050	2.717	0.463	1.940	3.025	1.208
0.062	2.681	0.527	1.878	3.383	1.186
0.075	2.645	0.591	1.816	3.742	1.164
0.088	2.611	0.674	1.755	4.190	1.145
0.100	2.577	0.757	1.696	4.639	1.127
0.111	2.550	0.833	1.654	5.199	1.111
0.121	2.522	0.908	1.612	5.759	1.095
0.135	2.489	1.002	1.571	6.484	1.082
0.148	2.456	1.096	1.530	7.208	1.069
0.166	2.416	1.213	1.492	8.113	1.059
0.183	2.376	1.331	1.453	9.018	1.049
0.206	2.330	1.478	1.418	10.150	1.041
0.229	2.283	1.625	1.382	11.281	1.034
0.258	2.231	1.808	1.350	12.696	1.028

Tab. 4.3 – Stress Distribution for Finite Thickness Step Notch (b/ρ = 6; α = 45°; b/T = 0.2727)

x/t	$\sigma_{yy}(x)$ PT	$\sigma_{yy}(x)$ PB	x/t	$\sigma_{yy}(x)$ PT	$\sigma_{yy}(x)$ PB	x/t	$\sigma_{yy}(x)$ PT	$\sigma_{yy}(x)$ PB
0.0000	1.840	1.957	0.0204	1.376	1.419	0.1531	0.933	0.615
0.0008	1.816	1.932	0.0227	1.342	1.376	0.1711	0.926	0.570
0.0016	1.793	1.907	0.0258	1.307	1.329	0.1890	0.920	0.524
0.0023	1.769	1.881	0.0289	1.271	1.282	0.2114	0.917	0.474
0.0031	1.745	1.855	0.0329	1.236	1.233	0.2338	0.914	0.425
0.0039	1.722	1.829	0.0369	1.201	1.183	0.2618	0.914	0.369
0.0047	1.699	1.803	0.0421	1.167	1.133	0.2898	0.915	0.313
0.0055	1.677	1.779	0.0473	1.135	1.084	0.3248	0.920	0.248
0.0062	1.655	1.754	0.0520	1.113	1.047	0.3598	0.925	0.184
0.0069	1.638	1.735	0.0567	1.090	1.011	0.3988	0.932	0.115
0.0076	1.621	1.715	0.0626	1.069	0.973	0.4378	0.940	0.047
0.0084	1.601	1.691	0.0685	1.048	0.936	0.4866	0.952	-0.035
0.0092	1.580	1.667	0.0758	1.030	0.897	0.5353	0.964	-0.118
0.0103	1.555	1.638	0.0831	1.011	0.859	0.5963	0.979	-0.220
0.0114	1.531	1.609	0.0923	0.995	0.820	0.6572	0.994	-0.321
0.0129	1.503	1.575	0.1015	0.979	0.781	0.7334	1.013	-0.450
0.0143	1.474	1.541	0.1130	0.966	0.740	0.8096	1.031	-0.579
0.0161	1.442	1.502	0.1244	0.953	0.700	0.9048	1.047	-0.751
0.0180	1.411	1.463	0.1388	0.943	0.657	1.0000	1.061	-0.925

Tab. 4.4 – Reference Solutions for Step Notch Geometry

SIF Solution Coeff. eq. 2.16 Semi-Finite Step Notch b/ρ = 6, α = 45°, Remotely Applied Tension					
M_0	M_1	M_2	M_3	M_4	R^2
1.1202	1.6131	-0.5226	1.3325	-0.3317	1.00
Stress Distribution Coeff. Eq. 2.17 Semi-Finite Step Notch b/ρ = 6, α = 45°, Remotely Applied Tension					
N_0	N_1	N_2	N_3	N_4	R^2
0.9788	0.6916	0.7963	0.3419	0.0712	1.00
Stress Distribution Coeff. eq. 2.18 - Finite Step Notch b/ρ = 6, α = 45°, b/T = 0.2727, Pure Tension					
P_0	P_1	P_2	P_3	P_4	R^2
1.0449	-1.279	3.8351	-3.0039	1.2541	1.00
Stress Distribution Coeff. eq. 2.18 - Finite Step Notch b/ρ = 6, α = 45°, b/T = 0.2727, Pure Bending					
P_0	P_1	P_2	P_3	P_4	R^2
-0.831	9.222	-20.137	21.941	-8.2494	1.00

Tab. 4.5 – SIF Solutions for Finite Thickness Step Notch (b/ρ = 6; α = 45°; b/T = 0.2727)

Pure Tension		Pure Bending	
a/t	Y_I	a/t	Y_I
0.002	2.013	0.002	2.139
0.003	1.969	0.003	2.090
0.005	1.926	0.005	2.045
0.006	1.886	0.006	2.002
0.009	1.814	0.009	1.923
0.012	1.752	0.012	1.852
0.016	1.700	0.016	1.790
0.019	1.650	0.019	1.735
0.025	1.572	0.025	1.641
0.031	1.512	0.031	1.565
0.044	1.426	0.044	1.450
0.056	1.372	0.056	1.368
0.069	1.337	0.069	1.307
0.081	1.316	0.081	1.261
0.100	1.301	0.100	1.209
0.119	1.301	0.119	1.173
0.137	1.311	0.137	1.148
0.156	1.330	0.156	1.130
0.187	1.377	0.187	1.114
0.219	1.439	0.219	1.110
0.250	1.517	0.250	1.117
0.312	1.716	0.312	1.157
0.375	1.985	0.375	1.229
0.437	2.342	0.437	1.340
0.500	2.826	0.500	1.499

Tab. 4.6 – SIF Solution Coefficients (eq. 4.3) by Hartranft & Sih

b/a	f(b/a)
0	0.12147
0.1	0.10984
0.2	0.09733
0.3	0.08443
0.4	0.07150
0.5	0.05874
0.6	0.04624
0.7	0.03408
0.8	0.02244
0.9	0.01383
1.0	0.00

Tab. 4.7 – Reference Solutions for Stiffened, Plane Finite Thickness Geometry (eq. 4.4)

b/T	R_4	R_3	R_2	R_1	R_0	R^2
0.0625	83.58	-93.14	40.59	-4.73	1.13	0.999
0.125	91.70	-113.85	55.59	-9.13	1.41	1.000
0.1875	112.33	-159.22	88.16	-18.87	2.27	1.000
0.25	133.40	-211.78	131.25	-33.68	3.93	1.000
0.2727	52.79	-68.42	38.34	-7.91	1.30	1.000
0.3125	153.21	-265.11	178.64	-51.51	6.20	1.000
0.375	182.26	-339.00	244.29	-76.82	9.63	1.000
0.4375	229.78	-478.58	385.97	-138.31	19.22	1.000
0.50	267.20	-584.96	492.37	-184.52	26.49	1.000

Tab. 4.8 – Reference Solutions for Symmetric Semi-Finite Notches

SIF Solution Coeff. Eq. 4.5a Semi-Finite Semi-Circular Notch Crack Face Loading					
M'_0	M'_1	M'_2	M'_3	M'_4	R^2
1.000	0.0075	-0.0287	-0.1268	0.3907	1.00
SIF Solution Coeff. eq. 4.5a Semi-finite Symmetric Notch $b/\rho = 6$, $\alpha = 45°$, Crack Face Loading					
M'_0	M'_1	M'_2	M'_3	M'_4	R^2
1.003	-0.1096	0.7141	-1.1526	0.8382	1.00

4.12 – Figures

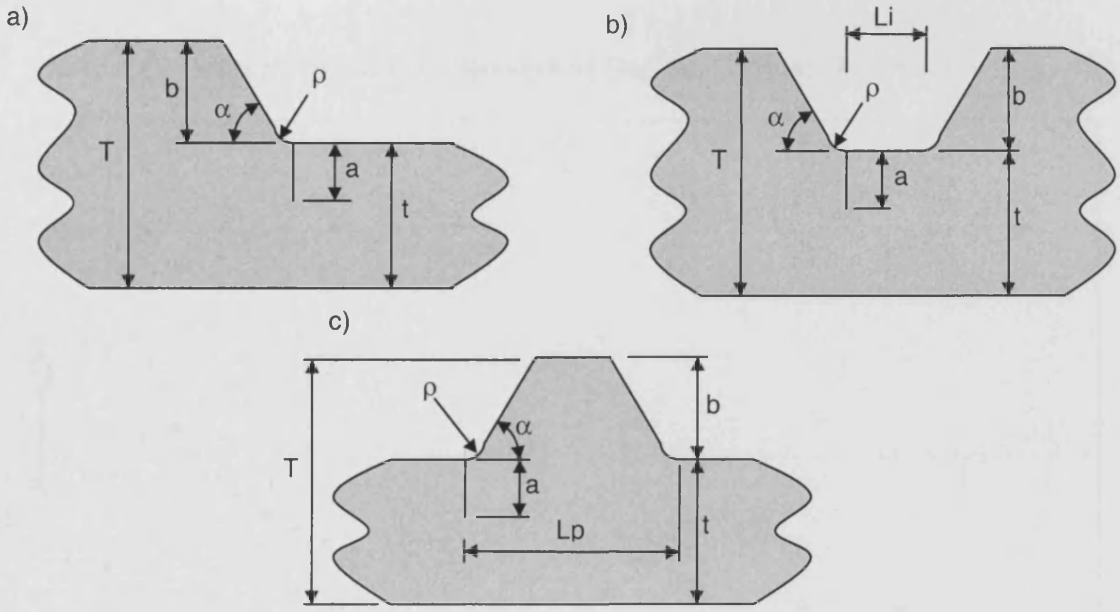

Fig. 4.1 – a) Step, b) Intrusion and c) Protrusion Notches

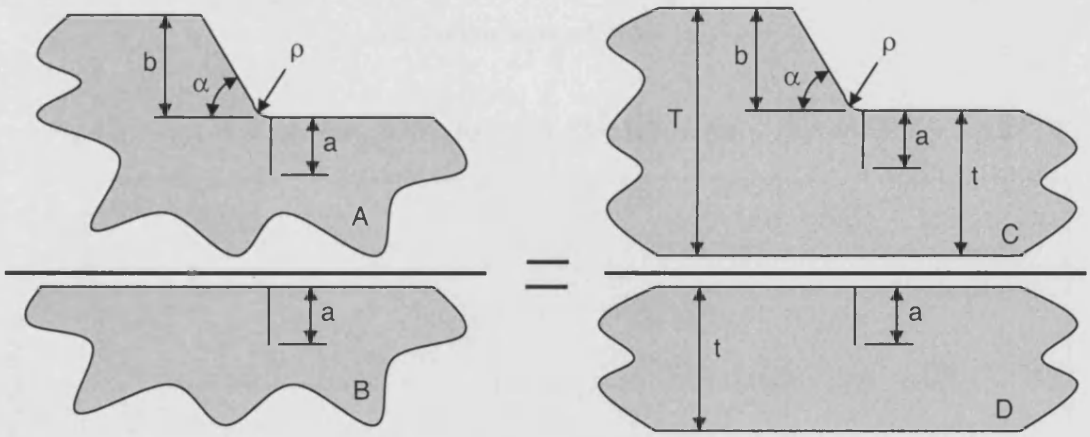

Fig. 4.2 – A Weight Function Composition Scheme for Step Notched Components

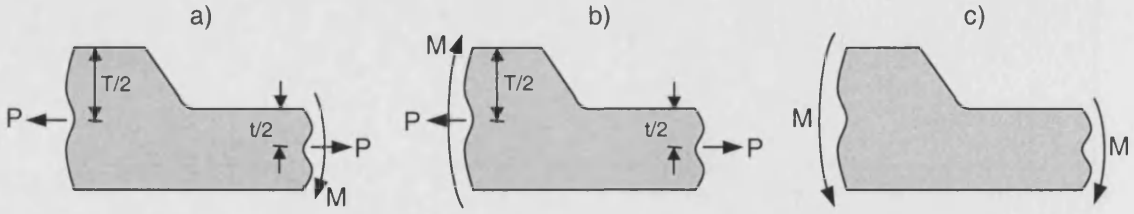

Fig. 4.3 – The Three Loading Modes Applied to the Step Geometry Subject to Axial Loads, P and Bending Moments, M. a) Uniform Tension b) Pure Tension c) Pure Bending

Fig 4.4 – Plot of SIF Solution for Semi-Infinite Step Notch Under Tension (b/ρ = 6; α = 45°)

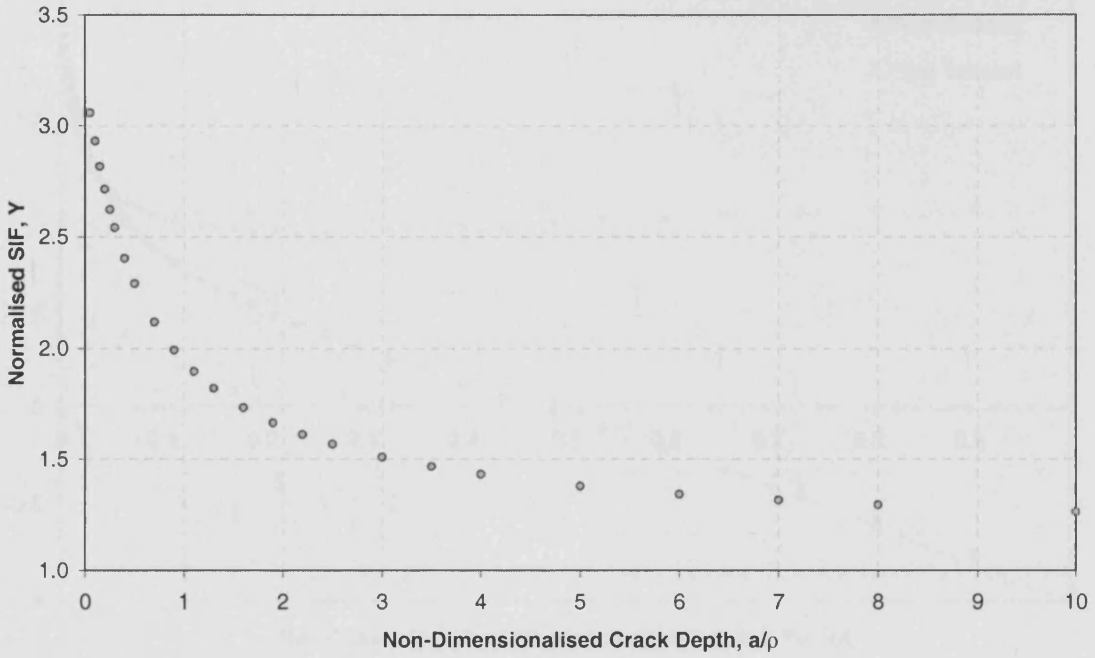

Fig 4.5 – Plot of Stress Distribution for Finite Step Notch (b/ρ = 6; α = 45°; b/T = 0.2727)

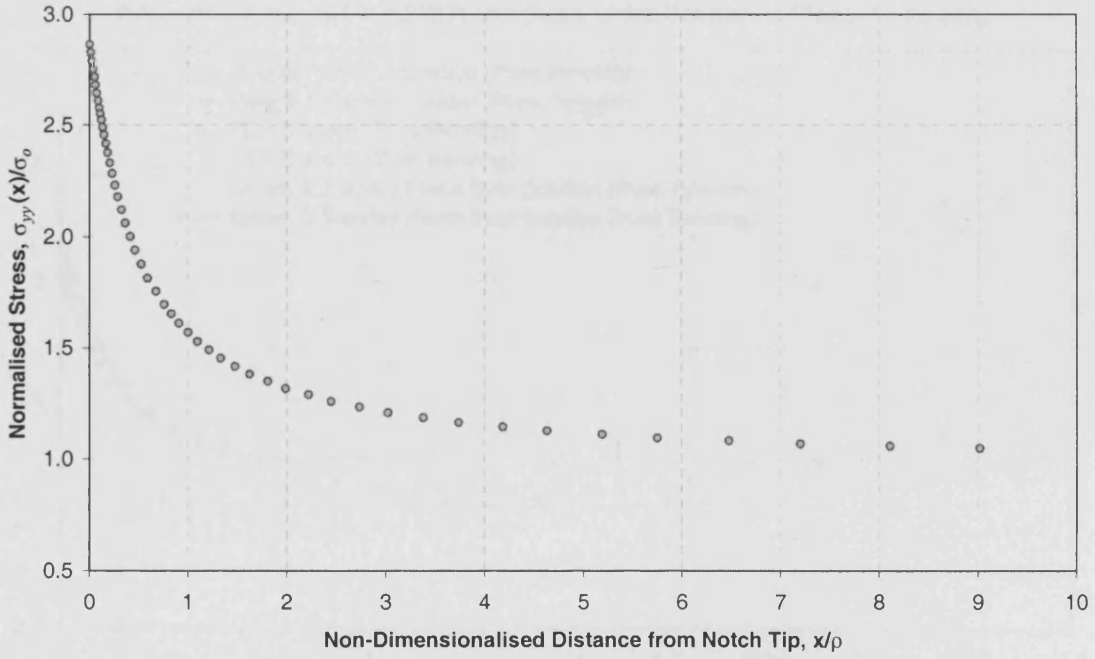

Fig 4.6 – Plot of Crack Line Stress Distributions for Finite Step Notch
($b/\rho = 6$; $\alpha = 45°$; $b/T = 0.2727$) and those of the Equivalent Planar Finite Strip

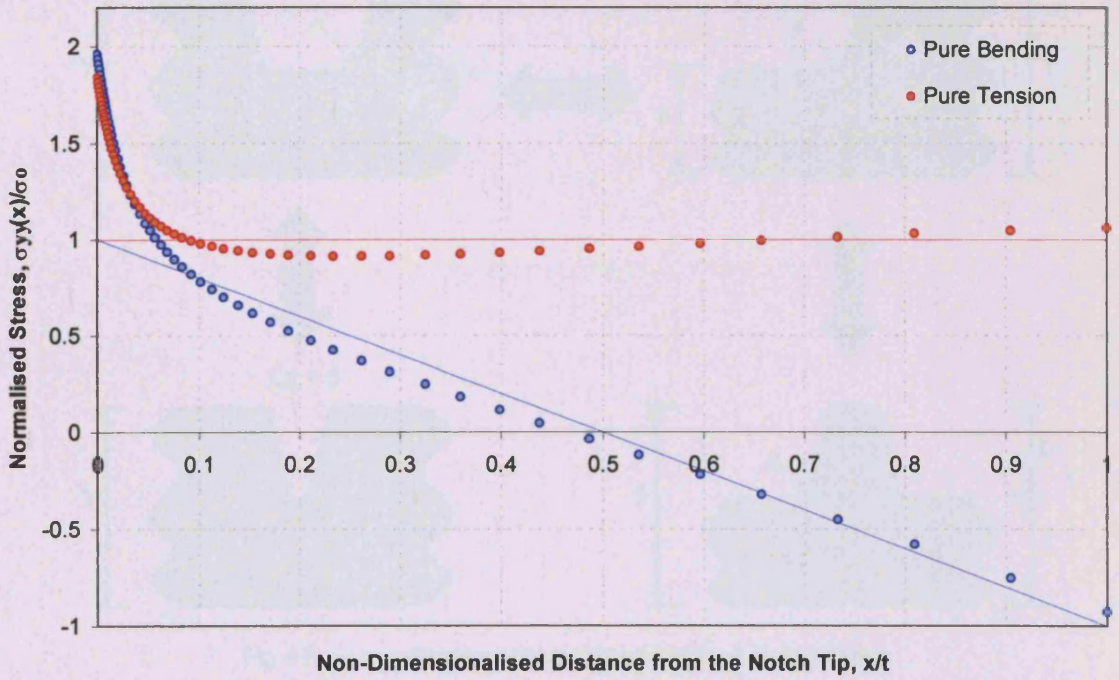

Fig 4.7 – Plot of SIF Solutions for Finite Step Notch
($b/\rho = 6$; $\alpha = 45°$; $b/T = 0.2727$) and those of the Equivalent Planar Finite Strip

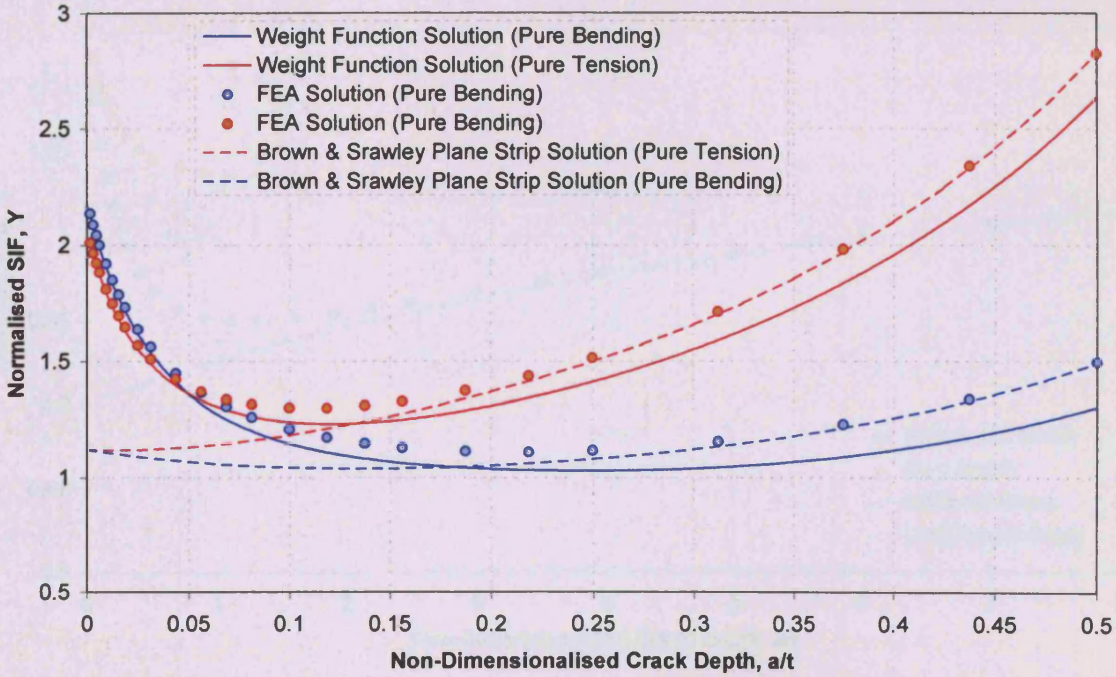

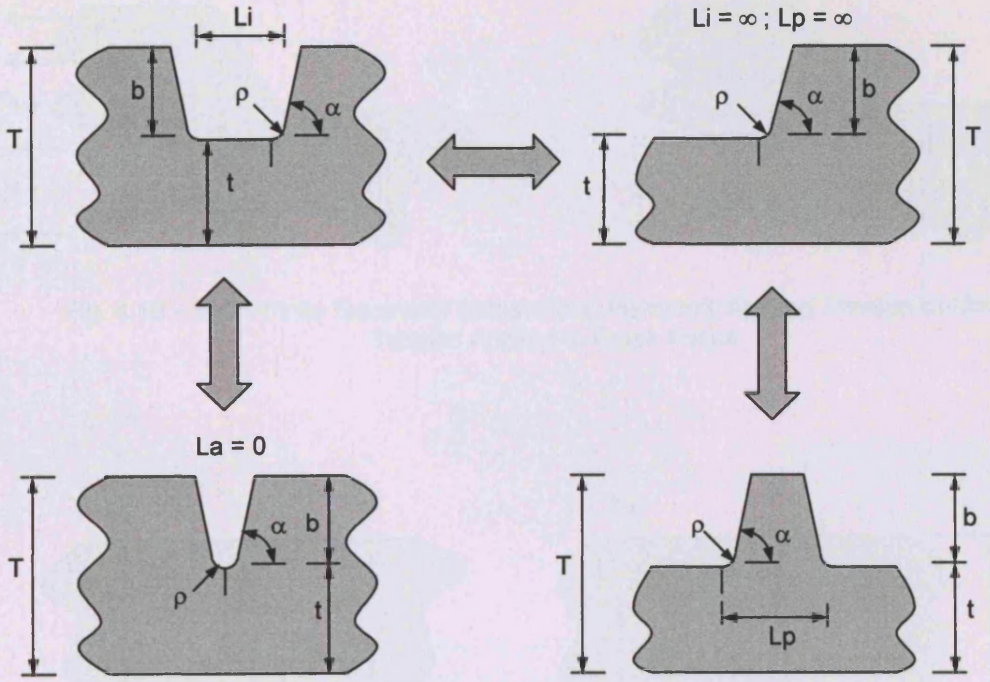

Fig 4.8 – Inter-Relationship between Various Notch Types

Fig 4.9 – Plot of SIF Solutions for the Step Notch and Equivalent Symmetric Notch Subject to Uniform Crack Face Loading

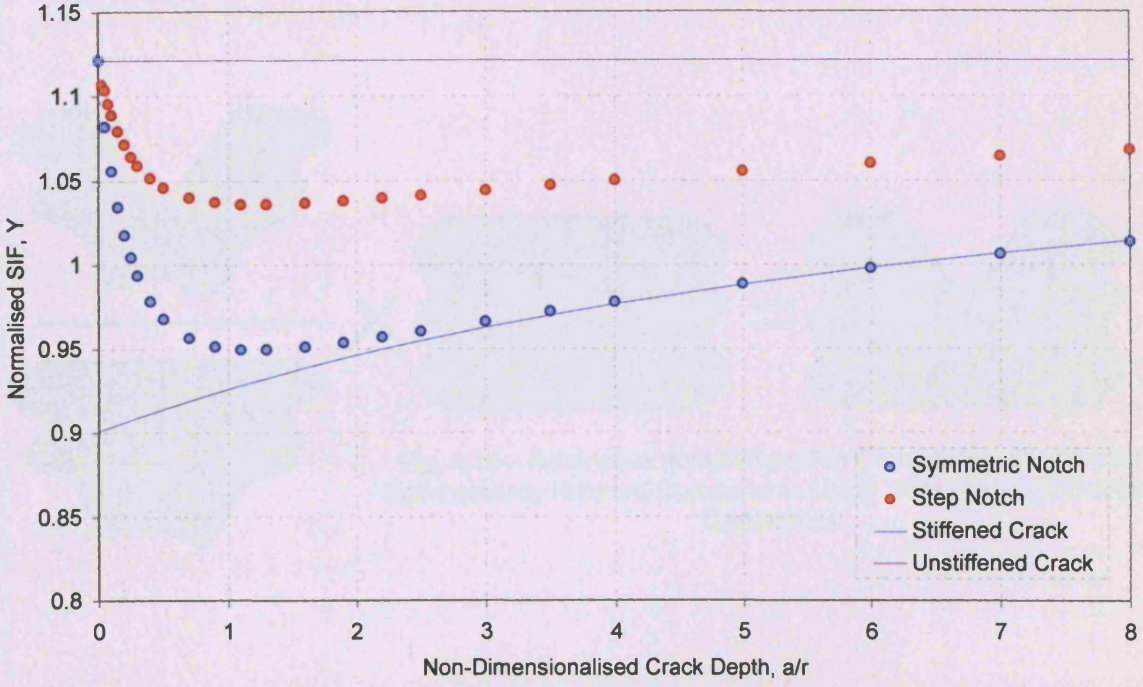

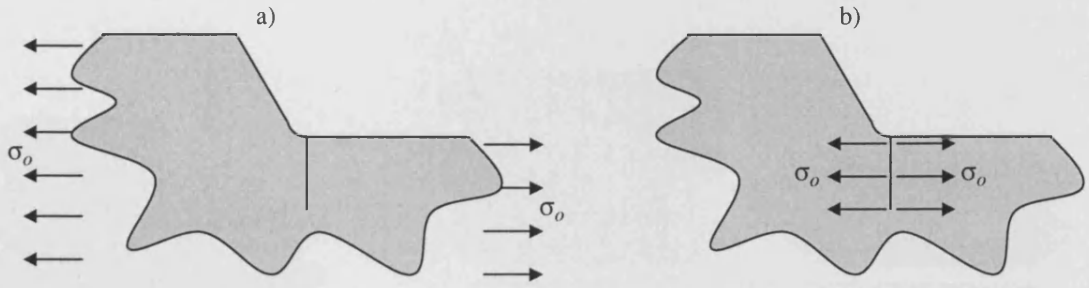

Fig. 4.10 – Semi-Finite Geometry Subject to a) Remotely Applied Tension b) Uniform Tension Applied to Crack Faces

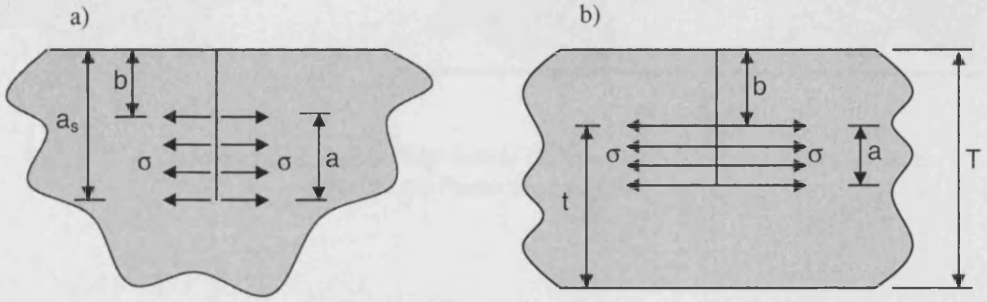

Fig. 4.11 – Definition of Stiffened a) Semi-Finite and b) Finite Thickness Geometry

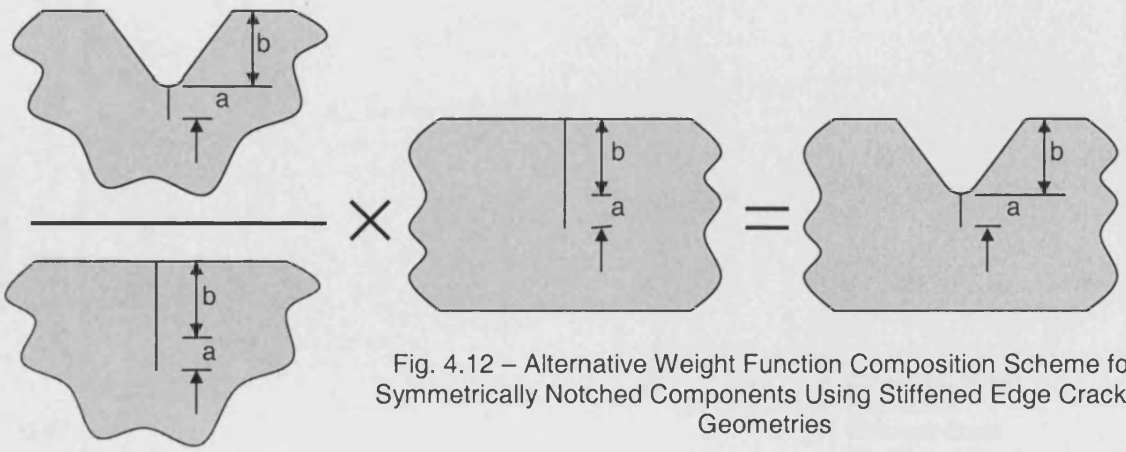

Fig. 4.12 – Alternative Weight Function Composition Scheme for Symmetrically Notched Components Using Stiffened Edge Cracked Geometries

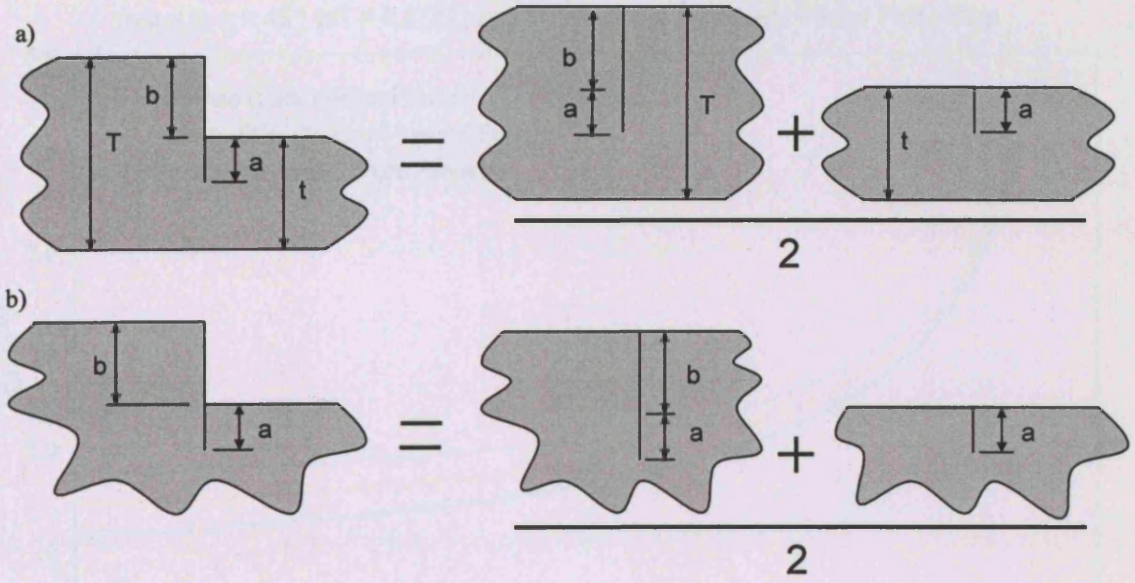

Fig. 4.13 – Definition of a Sharp Step Notch Geometry in Terms of Stiffened and Unsiffened Plane Geometries

Fig 4.14 – Plot of SIF Solutions for Finite Step Notch
(b/ρ = 6; α = 45°; b/T = 0.2727) and Those of the Equivalent Planar Finite Strip

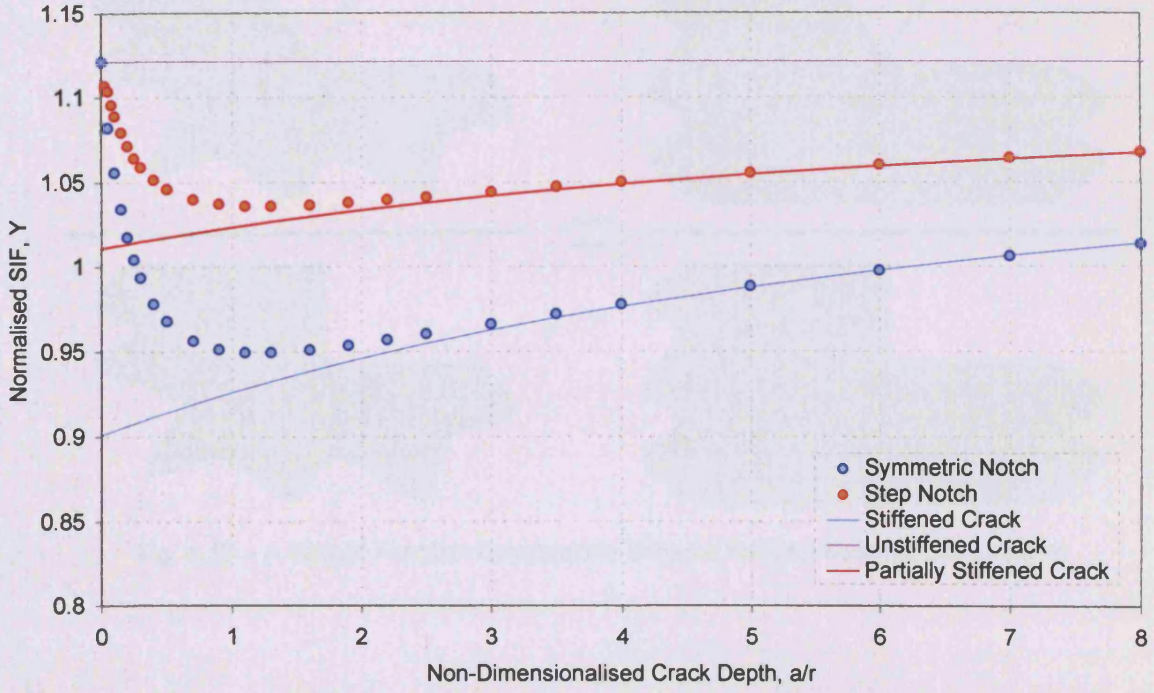

Fig 4.15 – Plot of SIF Solutions for Finite Step Notch
($b/\rho = 6$; $\alpha = 45°$; $b/T = 0.2727$) and Those of the Equivalent Planar Finite Strip

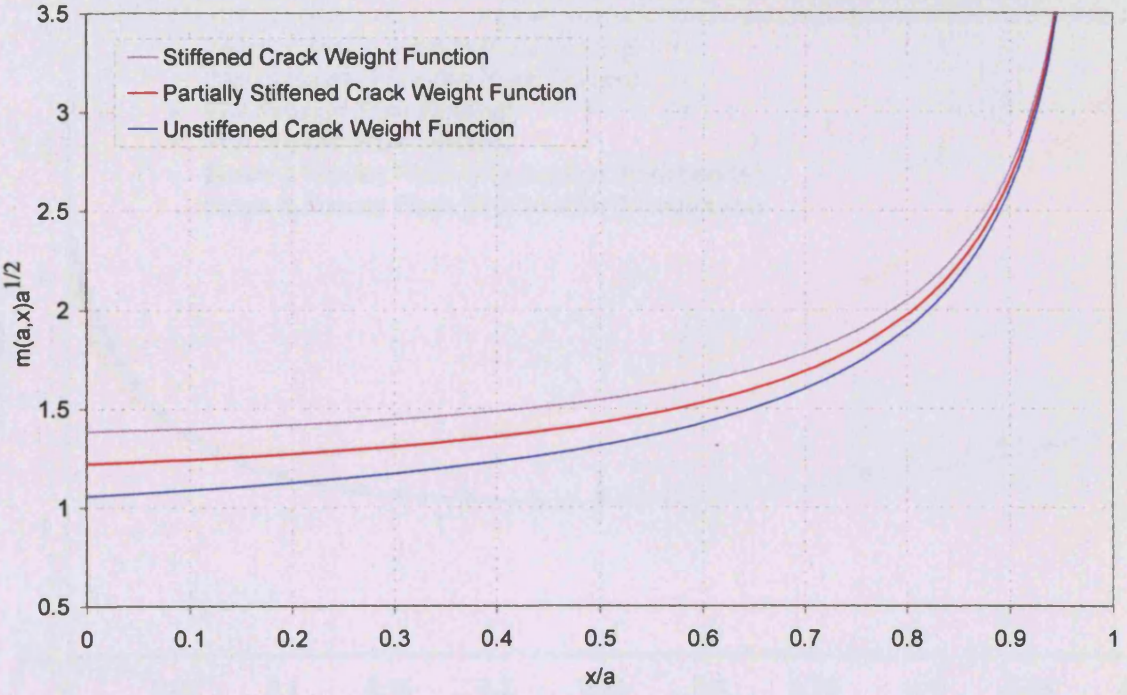

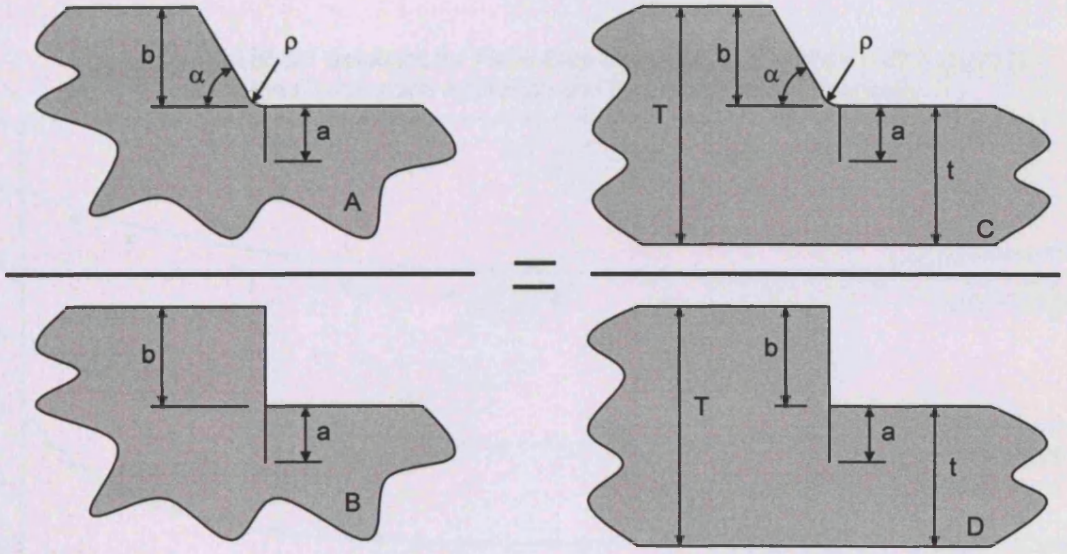

Fig. 4.16 – A Weight Function Composition Scheme for Step Notched Components

Fig 4.17 – Plot of SIF Solutions for Finite Step Notch
($b/\rho = 6$; $\alpha = 45°$; $b/T = 0.2727$) and Those of the Equivalent Planar Finite Strip

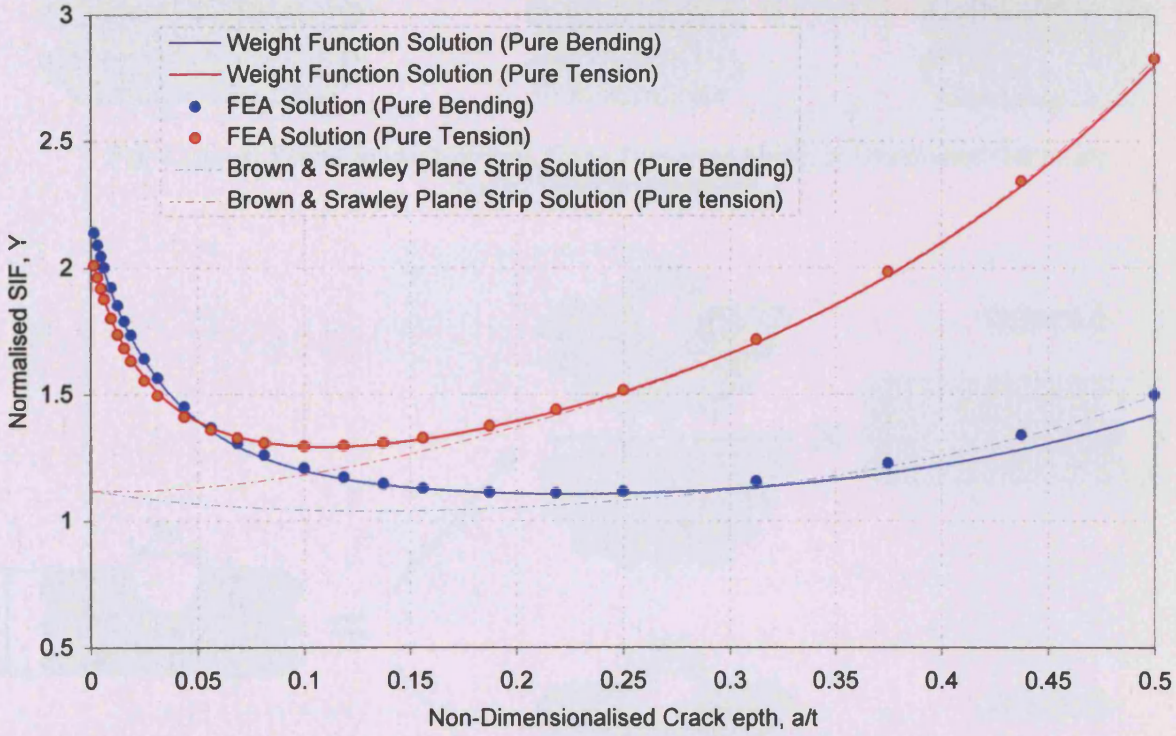

Fig 4.18 – Plot of SIF Solutions for Finite Step Notch ($b/\rho = 6$; $\alpha = 45°$; $b/T = 0.2727$)
using the Composition Approach and those Obtained Numerically

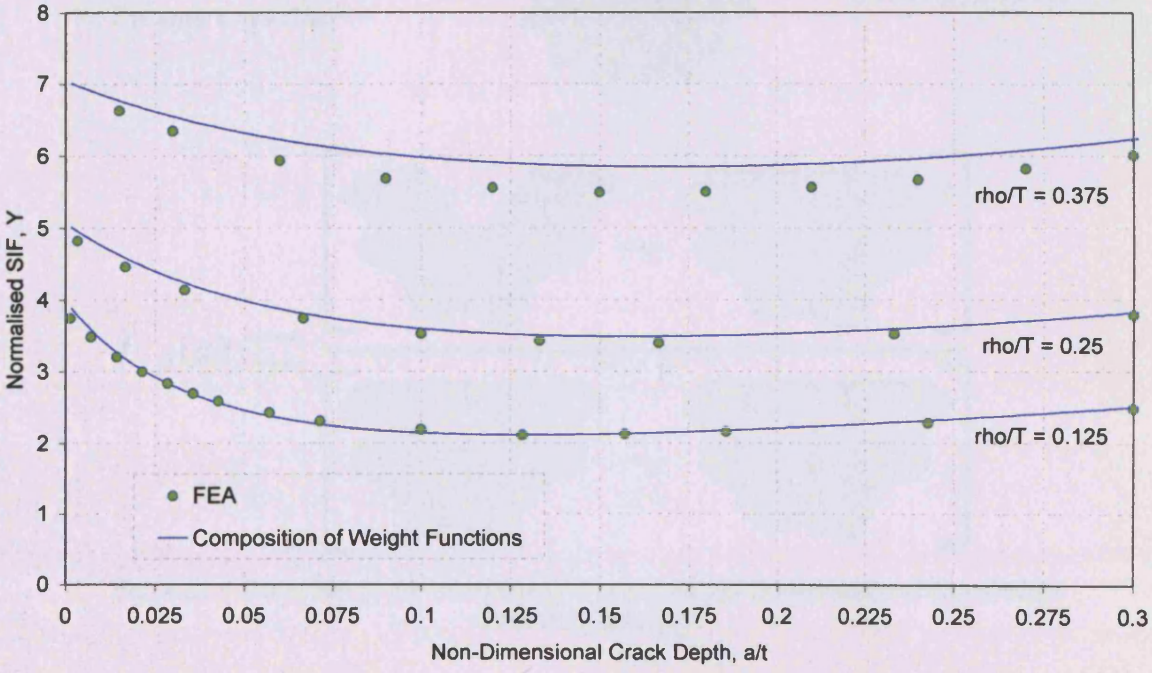

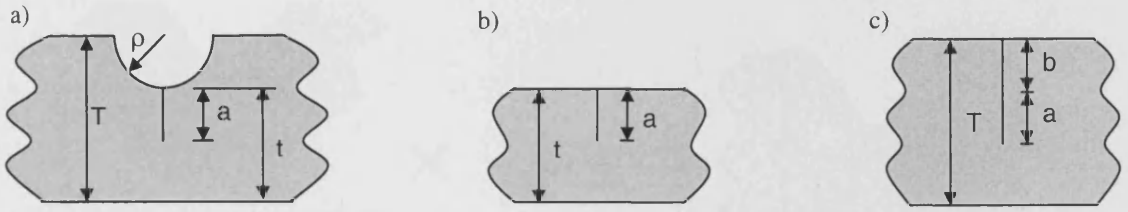

Fig. 4.19 – a) Semi-Circular Notched, Finite Thickness Plane, b) Unstiffened Geometry and c) Stiffened Geometry

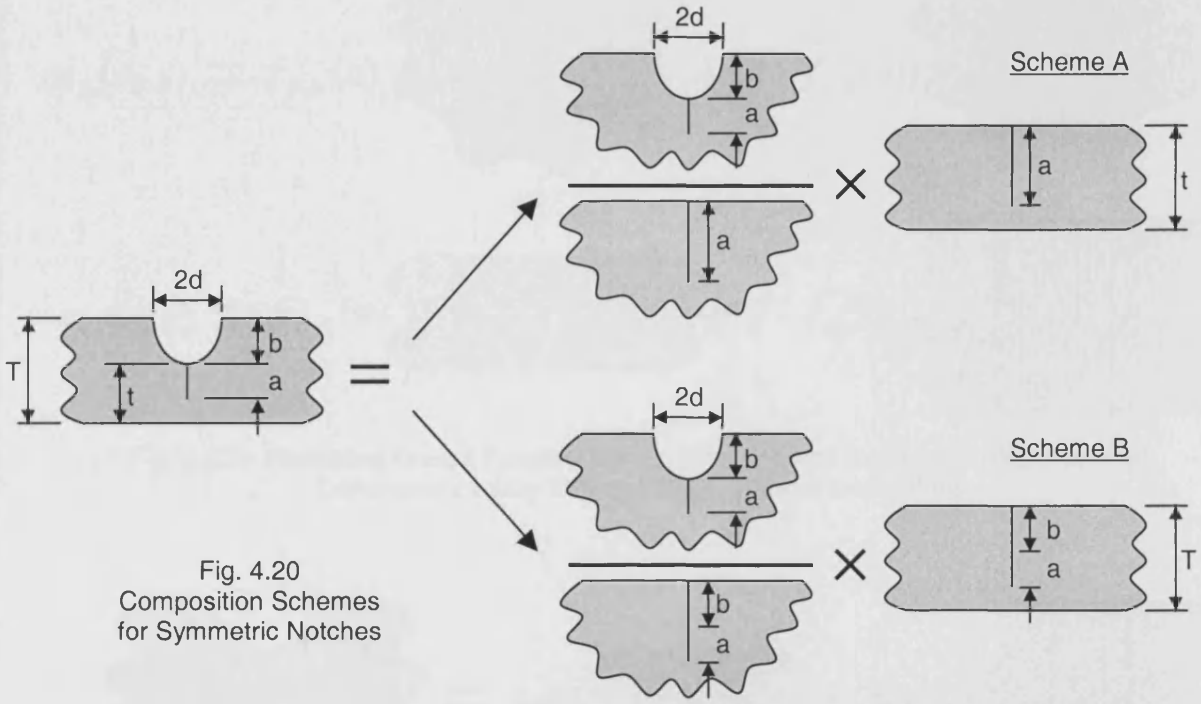

Fig. 4.20
Composition Schemes
for Symmetric Notches

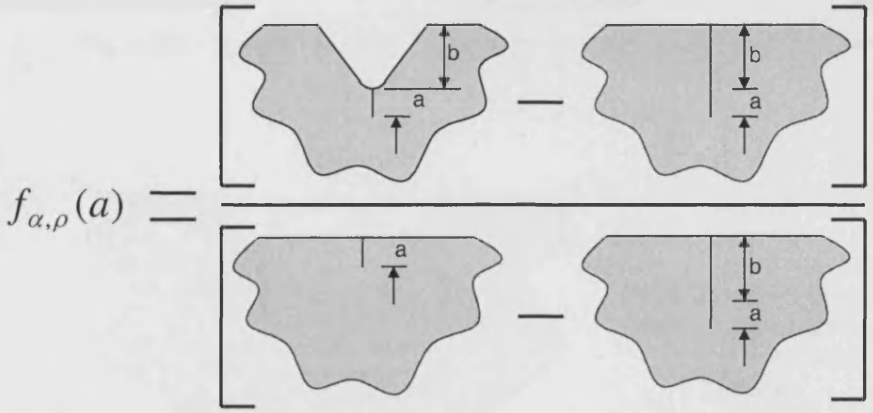

Fig. 4.21 – Definition of the Interpolation Factor via the Combination of Constituent Geometry Solutions

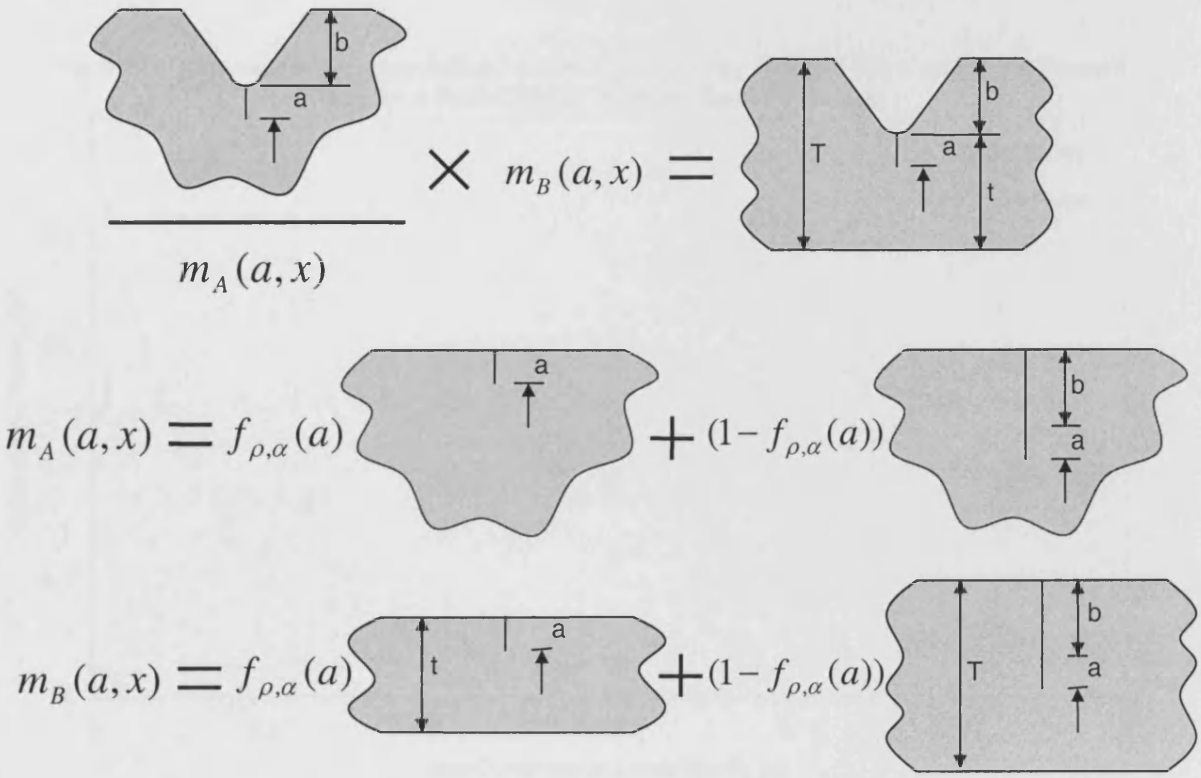

Fig. 4.22 – Alternative Weight Function Composition Scheme for Symmetrically Notched Components Using Stiffened Edge Cracked Geometries

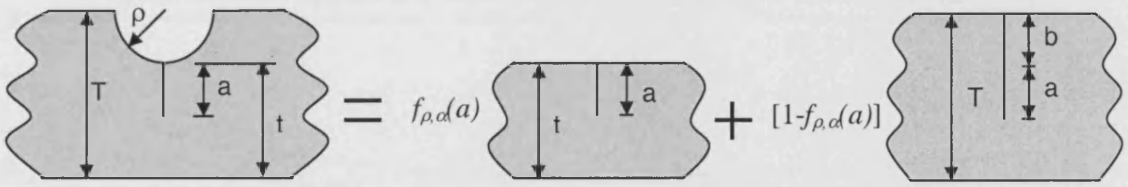

Fig. 4.23 – Weight Function Scheme for Symmetrically Notched Components

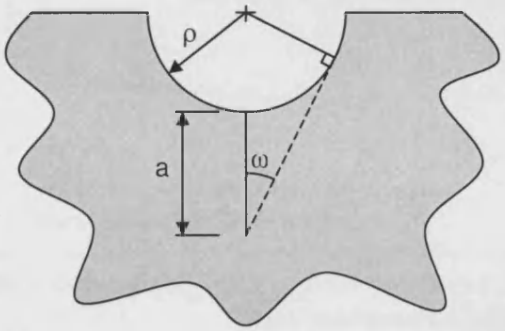

Fig. 4.24 – Definition of View Angle for Semi-Elliptical Symmetric Notches

Fig 4.25 – Comparison of Interpolation Factors Calculated by Fett and Munz and in the Present Study for a Semi-Circular Notched Semi-Finite Strip

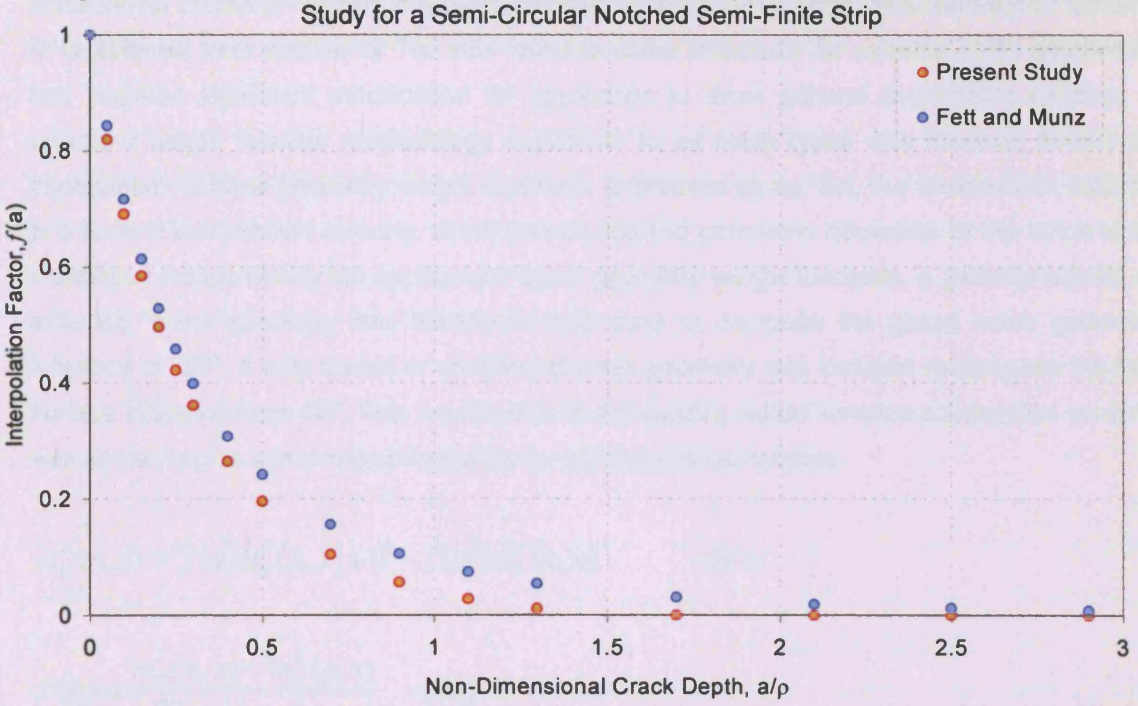

Fig 4.26 – Comparison Between SIF Solutions Obtained Via the Two Weight Function Schemes When Applied to a Semi-Circular Notch Subject to Uniform Tension

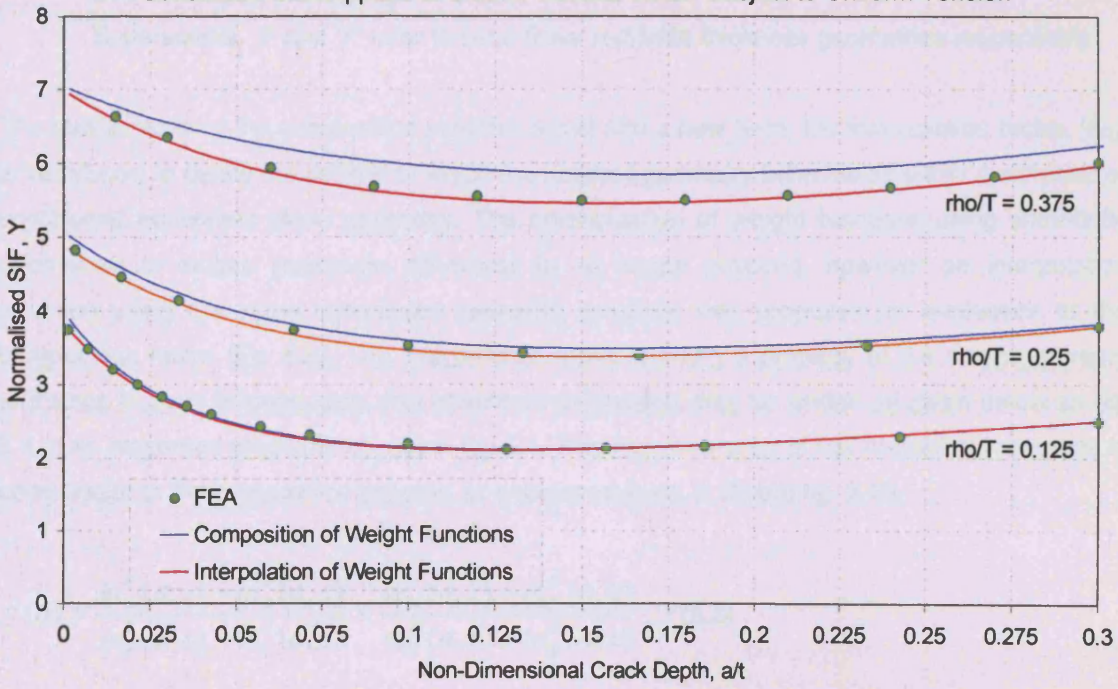

Chapter 5 – Interpolation of Weight Functions for Symmetric Notches

The preceding chapter discussed weight function composition techniques to determine new SIF solutions for cracks at notches in two-dimensional finite thickness strips. The composition scheme in its simplest form applied by Teh was found to suffer limitations for extreme notch geometries and required significant modification for application to more general asymmetric notches. A universal weight function methodology applicable to all notch types was devised, termed an interpolation of base geometry weight functions. Expressed as eq. 5.1, the interpolation scheme is a form of composition scheme, which permits the two geometric influences of the notch to be composed independently via appropriate 'base' geometry weight functions. A partially loaded, or stiffened, crack geometry was introduced and used to compose the global notch geometry influence on SIF. A fully loaded or unstiffened crack geometry was included to compose the free surface influence upon SIF. This modification to the existing weight function composition scheme was shown to give enhanced performance for blunt and deep notches.

$$m_N^F(a,x) = f(a)m_U^F(a,x) + (1 - f(a))m_S^F(a,x) \qquad \text{- (5.1)}$$

$$f(a) = \frac{m_N^S(a,x) - m_S^S(a,x)}{m_U^S(a,x) - m_S^S(a,x)} \qquad \text{- (5.2)}$$

Where: Subscripts, '*N*', '*S*' and '*U*' refer to the notched geometry and stiffened and unstiffened equivalent geometries respectively.
Superscripts, '*S*' and '*F*' refer to semi-finite and finite thickness geometries respectively.

The familiar form of the composition scheme is lost and a new term, the interpolation factor, '*f(a)*' is introduced to define the degree to which the notched geometry behaves as either a stiffened or unstiffened equivalent plane geometry. The normalisation of weight functions using semi-finite geometries to isolate geometric influences is no longer required, however an interpolation equation using the same constituent geometry solutions was proposed for evaluation of the interpolation factor (Eq. 5.2). The interpolation factor is solely a property of the notch geometry and since it is not influenced by size effects an expression may be written as given below as eq. 5.3 or as presented diagrammatically in fig. 5.1. This representation of the interpolation scheme is comparable to the composition scheme as expressed in eq. 2.13 and fig. 2.10.

$$f(a) = \frac{m_N^S(a,x) - m_S^S(a,x)}{m_U^S(a,x) - m_S^S(a,x)} = \frac{m_N^F(a,x) - m_S^F(a,x)}{m_U^F(a,x) - m_S^F(a,x)} \qquad \text{- (5.3)}$$

Simple re-arrangement of eq. 5.3 results in eq. 5.1, which is also represented diagrammatically as fig. 5.2. Initial observations from application of the interpolation scheme to formulate weight functions for semi-circular notches indicated that it represents a significant improvement over the composition scheme for certain extreme notch geometry configurations.

Further validation of the interpolation of weight functions technique can be gained, and an assessment of any limitations present, by the analysis of a range of symmetric notch shapes and sizes. This chapter presents the calculation of new SIF solutions for a number of 'V' notches embedded in a finite thickness strip. These new solutions are compared to finite thickness SIF solutions determined from finite element methods.

5.1 – Introduction

The geometry under investigation is shown diagrammatically in fig. 5.3. Fig. 5.3a shows a V-notch embedded in a semi-finite strip and fig. 5.3b shows the same notch in a finite thickness strip. The semi-finite notched geometry is completely defined by the notch root radius 'ρ', notch depth, 'b', and flank angle 'α' or, more concisely, by the non-dimensional geometric parameter 'b/ρ', and angle, 'α'. Parameters 't' and 'T' are included to describe the notched finite thickness equivalent geometry and to aid normalisation and presentation of results by the additional non-dimensional parameter, 'b/T'. Thickness 't' describes the minimum plane thickness from the notch root to the remote boundary and 'T' defines the maximum plane thickness as depicted in fig. 5.3b. SIF solutions are sought for an edge crack emanating from the root of the notch defined by its depth, 'a', or non-dimensionally as 'a/ρ' or 'a/t'.

An interpolation factor '$f(a)$' characterises the relative geometric influence of the notch as either an unstiffened geometry or a stiffened geometry. It is equal for both finite and semi finite geometries and for convenience is derived by the analysis of semi-finite notched geometries. This condition is not essential but advantageous, as SIF solutions and associated stress distributions are described more concisely by fewer non-dimensional parameters. Calculation of SIF solutions for this geometry subject to uniform crack face loading allows the direct comparison and manipulation with the plane, stiffened and unstiffened semi-finite equivalent geometry SIF solutions when subject to uniform loading, fig. 5.4c,d. The present study generates a number of SIF solutions for semi-finite notched geometries subject to this special loading configuration. Once more, this condition is not essential but convenient, as the accompanying crack-line stress distribution requires no additional analysis and can be simply defined as given below.

$$\sigma_{yy}^{S}(x) = \sigma_o \quad \text{- (5.4)}$$

Subsequently, the interpolation factor is deduced from, in this case either form of the linear interpolation equations presented below.

$$f(a)=\frac{Y_N^S(a)-Y_S^S(a)}{Y_U^S(a)-Y_S^S(a)}=\frac{C_N^S(a)-C_S^S(a)}{C_U^S(a)-C_S^S(a)}=\frac{m_N^S(a,x)-m_S^S(a,x)}{m_U^S(a,x)-m_S^S(a,x)} \quad \text{- (5.5a,b,c)}$$

For the more common case, where constituent notched geometry SIF solutions are only available for a more generalised loading condition, usually that of remotely applied uniform tension, only eq. 5.4b and 5.4c are applicable for determination of the interpolation factor. Calculation of weight functions or weight function coefficients requires knowledge of the uncracked geometry's crack-line stress distribution when subject to the same loading condition. The present study allows usage of eq. 5.5a for calculation of the interpolation factor.

Once determined, the interpolation factor is applied to the equivalent finite thickness plane geometry weight functions (or base geometry weight functions) in the manner dictated by eq. 5.1 and depicted diagrammatically in fig. 5.2. A weight function for the notched finite thickness geometry is subsequently obtained. The base geometry solutions required are those for the stiffened and unstiffened finite thickness plane geometries, which were presented in chapter 4 allowing weight functions for these geometries to be formulated.

The resulting weight function is used with the uncracked, finite thickness geometry crack-line stress distribution present when subject to any loading mode to yield new SIF solutions for the geometry subject to that specific loading mode (eq 5.6). New SIF solutions are restricted for illustrative purposes in the present study to the commonly sought applied load cases of uniform tension and pure bending as defined in chapter 4.

$$K_N^F(a)=\int_0^a \sigma_{yy}^F(x)m_N^F(a,x)dx \quad \text{- (5.6)}$$

This chapter describes the collection of required constituent geometry reference SIF solutions for notched, semi-finite geometries allowing weight functions for finite thickness equivalent geometries to be formulated. These are used in conjunction with calculated finite thickness stress distributions arising from the applied loading modes of uniform tension and pure bending to calculate new SIF solutions. New solutions, presented in their non-dimensional form, are compared to those obtained via FEA to assess the performance of the interpolation scheme.

Investigation of a range of notch shapes and sizes is undertaken to gauge the stability and robustness of the proposed weight function interpolation scheme, rather than for the formulation of a generic set of constituent geometry reference SIF solutions. Numerous, although not exhaustive, appropriate SIF solutions exist in the published literature for this purpose, notably those determined by Teh[5.1], who also details associated crack-line stress distributions. Fig. 5.5 depicts a matrix of notched geometries considered for the present study. The matrix is not complete, however variation of each non-dimensional parameter (notch size 'b/T', notch acuity 'b/ρ' and flank angle 'α') is undertaken to assess any limitations present and qualify recommendations for implementation of the interpolation scheme. The remainder of this chapter documents the generation of required constituent geometry reference SIF solutions and required finite thickness, crack-line stress distributions. A description of the implementation of the weight function interpolation scheme and a discussion and comparison of results obtained is also presented.

5.2 - Generation of Semi-Finite Notched Geometry SIF Solutions

The finite element method was used to model the semi-finite plane containing the notch and crack. Since a plane of symmetry exists about the crack plane, symmetrical boundary conditions were applied to this plane allowing the half geometry to be modelled. A uniformly distributed load was applied to the crack face and boundary conditions simulating symmetry in the plane of the crack were applied to constrained nodes on this plane.

A mesh generator program was written to automate formulation of the mesh and define the model as described above. A thorough discussion of implementation of the FEM to determine SIF solutions and associated crack-line stress solutions was given in chapter 3. Further description of similar themes is not presented here, however this section focuses on the nature of results obtained and the curve fitting process applied to yield continuous solutions.

5.2.1 – Semi-Finite Notched Geometry SIF Solutions

Tab. 5.1 displays the SIF solutions obtained for a notched, semi-finite geometry subject to uniform crack face loading. Results for a number of notch root radii 'b/ρ' are shown and are presented graphically as fig. 5.6. The equivalent stiffened semi finite plane geometry solution subject to the same loading, provided by Hartranft and Sih[5.2] presented in chapter 4, is also plotted. The familiar fracture mechanics result '$Y=1.1215$' is the equivalent unstiffened semi-finite plane geometry solution.

The form of the SIF solutions shown is similar to those discussed in chapter 4. The free surface influence and global notch influence are apparent in all solutions. Blunt notches (high 'b/ρ')

display a near surface influence, which affects the SIF solution to a greater degree for deeper cracks than sharper notches. In all cases the near surface effect is shown to dominate the solution for very short cracks. As crack depth tends to zero, the solutions converge on the unstiffened, semi-finite, plane geometry solution. As crack depth increases the free surface influence diminishes to zero and the solutions are equal to that of a stiffened, semi-finite, plane geometry. Thus, at greater crack depths the global notch influence dominates the solution.

Tab. 5.2 shows SIF solutions for a semi-finite geometry containing notches of various flank angles subject to uniform crack face loading. Fig. 5.7 is a graphical display of this data together with the equivalent stiffened and unstiffened, semi finite, plane geometry solutions. Also shown are solutions for sharp notches ('b/ρ' = 0) for a number of flank angles investigated (tab. 5.3). In addition to sharpness, notch flank angle is shown to influence the form of solution. Perfectly sharp notches have no radius and therefore no accompanying free surface influence, however flank angle does influence the global stiffness of the notch. The SIF solutions show the notch to be comparatively insensitive to variations in flank angle between 90° and 45° with respect to lower flank angles in the region between 45° and 0°.

5.2.2 – Curve Fitting of Semi-Finite Notched Geometry SIF Solutions

SIF solutions for semi-finite geometries containing notches of varying dimensions at a number of discrete crack depths have been determined. The formulation of a weight function solution for notched finite thickness geometries requires continuous SIF solutions obtained from a curve fitting process to formulate closed form expressions modelling the discrete SIF data. Chapter 2 introduced a form of equation convenient for this purpose, and usage in weight function methodologies, in which the non-dimensional crack depth is represented by the term 'λ' as defined below. Whereas 'a/ρ' may take any value between zero and infinity, 'λ' varies between unity and zero, allowing data to be represented more conveniently and concisely by a polynomial of low order.

Further normalisation of the SIF data, to the semi-finite stiffened geometry solution of Hantraft and Sih, isolates the near surface influence upon the solution, as described in chapter 4. The resulting ratio termed '$g(a)$' maybe fitted to a polynomial of fifth order to a high degree of accuracy. Figs. 5.8 and 5.9 depict variation of '$g(a)$' with non-dimensional crack depth along with the fitted polynomial curves. Tab 5.4 displays the coefficients 'M'_x' of the fitted fifth order polynomial. The expressions used for curve fitting of solutions are reproduced below.

$$Y_N^S(a) = Y_S^S(a)g(a) \quad \text{- (5.7)}$$

$$g(a) = \left[M'_5\lambda^5 + M'_4\lambda^4 + M'_3\lambda^3 + M'_2\lambda^2 + M'_1\lambda + M'_0\right]$$

$$\lambda = \left[\frac{1}{(1+a/\rho)}\right] \qquad \text{Validity:} \qquad 0 < \lambda < 1$$

5.3 – Finite Thickness SIF Solutions

Similar FE methods were employed to generate SIF solutions for notched, finite thickness geometries to validate the new solutions obtained via the weight function method. Solutions for notch sizes given by the matrix in fig. 5.5 were generated subject to uniform tension and pure bending loading arrangements. The solutions are presented in a tabular format in appendix A.

5.4 – Finite Thickness Stress Distributions

Implementation of a weight function scheme to determine new SIF solutions for the notched, finite thickness geometries subject to a given loading mode requires the crack-line stress distribution arising in the uncracked geometry when subject to that loading mode. The weight function scheme described here is to be tested under loading modes of uniform tension and pure bending. Application of the finite element method, validated in chapter 3 and utilised in chapter 4, was used for this purpose.

The stress component normal to the crack face '$\sigma_{yy}(x)$' creates a pure mode I opening crack opening displacement and thus, this component is used in conjunction with the mode I weight function. The stress distribution is normalised to a characteristic or nominal stress present in the body at a position far from the notch influence (axial stress in the case of uniform tension and extreme fibre stress for pure bending). Again employing a useful normalisation of distance from the notch tip similar to that used to normalise crack depth described previously allows a fifth order polynomial to model the stress distribution to a high degree of accuracy (eq. 5.8).

$$\frac{\sigma_{yy}(x)}{\sigma_o} = P_5\left[\frac{1}{(1+x/\rho)}\right]^5 + P_4\left[\frac{1}{(1+x/\rho)}\right]^4 + P_3\left[\frac{1}{(1+x/\rho)}\right]^3 + P_2\left[\frac{1}{(1+x/\rho)}\right]^2 + P_1\left[\frac{1}{(1+x/\rho)}\right] + P_0 \quad \text{- (5.8)}$$

Validity: $0 < x/t < 0.5$

The large amount of discrete data produced from the stress analyses are not presented, however coefficients 'P_x' determined from the curve fitting process are presented in tab. 5.5 and 5.6 for uniform tension and pure bending respectively.

5.5 – An Interpolated Weight Function Solution for Symmetrically Notched Components

A weight function methodology presented in preceding sections of this chapter constitutes a process, which offers reduced mathematical processes and improved accuracy for the determination of SIF solutions for symmetric notches in finite thickness planes. The methodology, derived from the composition of constituent geometry weight functions as described by Brennan and Teh[5.3], utilises stiffened and unstiffened plane geometry weight functions. A weight function for a notched component displays characteristics of both stiffened and unstiffened plane geometry weight functions. The degree to which the notched geometry weight function acts as an unstiffened plane geometry weight function is expressed as an interpolation factor '$f(a)$'.

The weighting coefficient is determined via an analysis of the semi-finite equivalent geometry '$Y(a)$' solutions. The convenience of using semi-finite geometries is maintained from the composition principle as no geometric influences, other than that of the notch influence the SIF solution. For a generalised V-notch form in a semi-finite plane depicted in fig. 5.1, the interpolation factor is only a function of the notch root radius 'ρ' and notch flank angle, 'α' as shown in figs, 5.6 and 5.7.

Once determined, the interpolation factor is applied to base geometry weight functions as described in chapter 4 and by Eq. 5.2. The constituent weight functions '$m_U^F(a,x)$' and '$m_S^F(a,x)$' are those corresponding to unstiffened and stiffened finite thickness plane geometries. Reference SIF solutions for these geometries were documented in chapter 4 under uniform loading applied to the crack faces. Under this loading mode weight function coefficients may be determined via closed form expressions, a process summarised in chapter 2. The number and mode of applied reference cases was considered and their bearing upon the final solution discussed. Thus a weight function for the notched, finite thickness geometry '$m_N^F(a,x)$' is formulated as described.

The weight function for the notched, finite thickness geometry is integrated in conjunction with a finite thickness, crack-line stress distribution to yield new SIF solutions. The loading modes of uniform tension and pure bending were analysed. New SIF solutions for notches embedded in finite strips under these modes are sought via eq 5.3.

SIF solutions derived from the weight function interpolation scheme are presented in the commonly quoted normalised form of the compliance factor, '$Y_N^F(a)$' as detailed by eq. 5.9. These solutions are compared to those obtained from FEA.

$$Y_N^F(a) = \frac{K_N^F(a)}{\sigma_o\sqrt{\pi a}} \qquad \text{- (5.9)}$$

Equations 5.1, 5.3 and 5.6 can be combined to form the equation quoted below.

$$Y_N^F(a) = f(a)\int_0^a \frac{\sigma_{yy}^F}{\sigma_o} m_U^F(a,x)dx + (1-f(a))\int_0^a \frac{\sigma_{yy}^F}{\sigma_o} m_S^F(a,x)dx \qquad \text{- (5.10)}$$

$$Y_N^F(a) = f(a)Y_U^F(a) + (1-f(a))Y_S^F(a) \qquad \text{- (5.11)}$$

where: $Y_U^F(a) = \int_0^a \frac{\sigma_{yy}^F}{\sigma_o} m_U^F(a,x)dx$ and $Y_S^F(a) = \int_0^a \frac{\sigma_{yy}^F}{\sigma_o} m_S^F(a,x)dx$

Eq. 5.10 calculates the normalised SIF, '$Y_U^F(a)$' and '$Y_S^F(a)$' for the unstiffened and stiffened base geometries subject to the crack-line stress field present in the notched component using a weight function methodology. These two solutions represent the extreme SIF solutions to which the notch interpolation factor is applied to give the notched component compliance factor, '$Y_N^F(a)$' (Eq. 5.11).

5.5.1 – Determination and Application of Interpolation Factors

The interpolation factor for a notched component is defined by eq. 5.5 detailing the required combination of constituent geometry solutions. The manipulation can be achieved via the normalised SIF, eq. 5.4a provided that the crack-line stress fields are equal for all geometries. Eqs. 5.4b and 5.4c, for which this special loading requirement is not necessary, provides a more generalised form of the interpolation equation. The semi-finite, notched constituent geometry SIF solutions collected, as described in section 5.3, are subject to uniform crack face loading in common with the available stiffened and unstiffened equivalent geometry solutions. Determination of the interpolation factor is therefore achieved via the combination of normalised SIF. The base geometry SIF solutions for this loading condition are available and therefore the interpolation equation can be expressed in terms of the normalised SIF alone as given in eq. 5.12.

$$Y_N^F(a) = f(a)Y_U^F(a) + (1-f(a))Y_S^F(a) \qquad \text{- (5.12)}$$

The resulting compliance factor, 'Y_N^F' for the finite thickness notched geometry will be that for uniform tension applied to the crack faces. It may be used in conjunction with the crack-line stress distribution '$\sigma_{yy}^F(x) = \sigma_o$' as a reference solution to formulate a weight function for the finite thickness, notched geometry. The process can be repeated to build more reference solutions provided that the condition of parity of crack-line stress distributions is satisfied. Once formulated the weight function can be used with any crack-line stress distribution to formulate new SIF solutions. While a number of alternative SIF solutions exist for the unstiffened geometry including those under pure bending provided by Brown and Srawley[5.4], no additional SIF solutions for the stiffened geometry are available. Weight functions for the finite thickness notched geometry can therefore only be determined from a single reference state using this technique, and will subsequently yield SIF solutions of reduced accuracy as described in chapter 2.

An alternative, more general form of the interpolation equation is applicable to weight function coefficients. Stiffened and unstiffered geometry weight function coefficients can be operated upon by the interpolation factor to give coefficients for usage in the notched geometry weight function (eq. 5.13).

$$C_N^F(a) = f(a)C_U^F(a) + (1 - f(a))C_S^F(a) \qquad \text{- (5.13)}$$

The study conducted in this chapter utilises constituent geometry normalised SIF for the determination of the interpolation factor, however the more generalised form of interpolation equation expressed in terms of weight functions (eq. 5.1) is preferred. A greater degree of simplicity and flexibility is offered by describing the interpolation in terms of weight functions (or their coefficients).

5.5.2 – Formulation of Base Geometry Weight Functions

Formulation of a finite thickness, notched geometry weight function requires determination of weight functions for equivalent finite thickness, plane stiffened and unstiffened geometries as demanded by eq. 5.1. The contemporary methodology, for the formulation of weight function coefficients presented in chapter 1 and applied in chapters 2 and 4, permit calculation of closed form expressions for the coefficients. Two reference solutions provided by Brown and Srawley for uniform tension and pure bending are available for the unstiffened geometry (fig. 5.4a). However only a single reference solution determined in chapter 3 for uniform tension applied to the crack face is available for the stiffened geometry (fig. 5.4b).

Chapter 2 contained an analysis and discussion of the accuracy of weight functions formulated from a single reference solution. It concluded that they, and SIF solutions derived from them,

degrade in accuracy as crack depth increases. Addition of a second reference load case was recommended, where possible to enhance accuracy for problems concerning deep cracks.

5.5.3 – Application of a Second Reference Load Case to Base Geometry Weight Functions

Initial solutions shown in fig. 5.10 show that SIFs obtained from the interpolation scheme, utilising weight functions formulated from a single reference case, are subject to 'drift' at greater crack depths. Application of a second reference solution is desirable for the formulation of more coefficients in the series expansion definition of crack opening displacement and hence a more accurate weight function. Chapter 2 contained a discussion of the enhanced and satisfactory accuracy gained from the use of two, independent reference loading states to calculate weight functions for two-dimensional edge cracks. It was shown that a similar 'drift' in SIF solutions obtained from weight functions formulated from a single reference state could be largely corrected by application of an additional reference state.

A weight function for the unstiffened base geometry is currently formulated from a single reference state provided by Brown and Srawley[5.4] for this geometry subject to uniform tension. A second may simply be applied by utilisation of their solution for pure bending and the methodology first presented in section 1.5.3.

Chapter 4 discussed the duality of the two-dimensional stiffened geometry as being either that of a partially loaded crack of depth '(a+b)' or a fully loaded crack of depth 'a' at the root of an infinitely thin slot. Chapter 4 highlighted the equivalence of weight functions determined irrespective of the geometrical viewpoint adopted but stated a preference for the latter, more universal of the two definitions given above. Only a single reference state is available for this configuration and therefore addition of a second reference state necessitates the former definition to be adopted.

Fig. 5.10 displays the SIF solutions obtained from interpolation schemes based on one (uniform tension) and two (uniform tension and pure bending) reference loading cases. The improvement in the SIF solutions obtained for two reference cases is clear as the 'drift' obtained from application of a single reference case is greatly diminished.

The account given in section 2.2.2 described the loss of independence between the reference solutions of uniform tension and pure bending for short crack lengths. The resulting weight function is subject to a degraded accuracy for high stress gradient load cases. The unstable behaviour of the weight function manifests itself as a degradation in accuracy of derived SIF solutions, the degree of which is dependant upon the gradient of the stress distribution integrated

with the weight function. The effect described in chapter 2 is most prevalent for the interpolation schemes' unstiffened base geometry. In most cases, where the notch is sufficiently large, the stiffened geometry weight function does not require SIF solutions for such short crack lengths. The composition scheme, as applied by Teh[5.1], utilised only stiffened geometries and therefore the effects described here were not apparent.

The overall loss in accuracy of derived SIF solutions due to the instability of the unstiffened geometry weight function calculated from uniform tension and pure bending is dependent upon the notch acuity. The effect of notch acuity is predicted to be two-fold. The stress gradient ahead of a sharp notch is greater than that of a blunt notch. Utilisation of a stress distribution of high gradient with an unstable weight function yields worse SIF solutions than that of a blunt notch. The relative influence of the unstiffened geometry weight function, dictated by the interpolation factor is reduced for sharp notches, with respect to blunt notches, causing its unstable nature on derived SIF solutions to be obscured. Rather than attempt to describe where, and quantify how much, these effects influence notch geometry SIF solutions, a universally applicable modification to the choice of reference solutions is recommended below.

Chapter 2 applied reference cases of uniform tension and decreasing tension for calculation of an edge cracked weight function. This combination was found to give weight functions of improved stability and good accuracy for all crack depths and was applied to yield SIF solutions with similar qualities including those for short cracks under high stress gradients. An interpolated weight function solution was implemented using pure tension and decreasing tension reference cases for both stiffened and unstiffened base geometries. Fig. 5.11 shows SIF solutions presented in a manner similar to that described by eq. 5.11, plotting SIF components obtained via the composition of the stiffened and unstiffened geometries utilising pure tension/pure bending and pure tension/decreasing tension reference cases. SIF solutions for an intermediate notch geometry ($b/\rho = 6$, $\alpha = 45°$ and $b/T = 0.2727$) subject to the applied load case of uniform tension, indicate that for this configuration the influence of the two applied reference state combinations is marginal. This statement, however cannot at present, be stated to be the case for other notch geometries and applied load cases, and therefore the recommendations outlined here are adopted throughout this and following chapters.

5.5.4 – A Composed Weight Function Solution

The composition of weight functions was shown to give poor SIF solutions for finite thickness geometries containing large and/or blunt notches. Application of this scheme to symmetric notches of extreme geometric forms investigated in this study is intended to highlight the limitations of the composition scheme and verify the improved solution offered by an interpolation

scheme. The extreme geometric forms are blunt notches described by low 'b/ρ', large notches by large 'b/T' and additionally notches of low flank angle by low 'α'. The precise geometric forms of notches investigated are listed and titled below.

- Blunt notch: $b/\rho = 1$, $b/T = 0.2727$, $\alpha = 45$
- Large notch: $b/\rho = 6$, $b/T = 0.4375$, $\alpha = 45$
- Low flank angle notch: $b/\rho = 6$, $b/T = 0.2727$, $\alpha = 15$

The composition scheme, described in chapter 2, assumes isolation of the notch geometry influence on SIF via a normalisation involving semi-finite geometries and composition upon a finite thickness geometry reproduced as eq. 5.14.

$$m_N^F(a,x) = \frac{m_N^S(a,x)}{m_S^S(a,x)} m_S^F(a,x) \qquad \text{- (5.14)}$$

The use of weight functions to compose geometric influences was promoted in Teh's study to ensure that a purely geometric influence was composed. For the common case where crack loading differs for each geometry, this condition is essential as composition of the stress intensity factor composes the additional influence of loading. A similar weight function approach can be adopted, similar to that applied to the interpolation scheme in section 5.10, which ensures that parity of crack loading is achieved for each constituent geometry. The crack-line stress distribution present in the finite thickness, notched geometry is applied to each of the constituent geometry weight functions as described by eq. 5.15.

$$\int_0^a \sigma_{yy}^F m_N^F(a,x) = \frac{\int_0^a \sigma_{yy}^F m_N^S(a,x)}{\int_0^a \sigma_{yy}^F m_S^S(a,x)} \int_0^a \sigma_{yy}^F m_S^F(a,x) \qquad \text{- (5.15)}$$

The resulting SIF solution for each constituent geometry are subject to the same crack-line loading condition and can subsequently be composed.

$$Y_N^F(a) = \frac{Y_N^S(a)}{Y_S^S(a)} Y_S^F(a) \qquad \text{- (5.16)}$$

5.6 - Discussion of Results

This chapter has sought to derive SIF solutions for cracks at the root of a range of symmetrical notches embedded in two-dimensional finite thickness strips. An interpolation of base geometry weight functions scheme was implemented as described in chapter 4 and above to calculate SIF solutions for the notched geometry subject to the loading modes of uniform tension and pure bending. The interpolation scheme was shown to give solutions of enhanced accuracy compared to those determined via the related composition scheme.

A comparison between SIF solutions calculated from the two schemes was conducted for a number of extreme notch geometry configurations. Blunt notches, notches of low flank angle and deep notches (as described by the geometric parameters detail in section 5.5.4) were the configurations investigated and those for which the interpolation scheme was thought to give results of superior accuracy. Solutions are presented in figs. 5.12 – 5.17 against solutions obtained from finite element analysis presented in appendix A.

Fig. 5.12 depicts the extreme SIF solutions 'Y_U^F' and 'Y_S^F' obtained as described by eq. 5.11 in which the crack-line stress distribution, present in the notched finite thickness geometry subject to remote uniform tension, is applied to base geometry weight functions. Finite element data for the notched finite thickness geometry lie between these extreme SIF solutions. The interpolation factor derived from eq. 5.5a using semi-finite geometry normalised SIF solutions is also shown. As described in section 5.1 parity of crack-line stress distributions between base geometry SIFs exists allowing the interpolation to be conducted as defined by eq. 5.12. Fig. 5.13 shows the excellent correlation achieved between SIF solutions obtained via the interpolation scheme and finite element method for the symmetric blunt notch defined in section 5.5.4. The relative influence, of the two base geometries upon the final interpolated SIF solution are clearly visible.

A similar procedure presented in section 5.5.4 allows the relative influence of the constituent geometries of the composition scheme to be viewed via direct manipulation of SIF data through application of eq. 5.10. Parity of the crack-line stress distributions is essential for this equation to hold. Applied to the same blunt notch subject to remote uniform tension, the composition is shown to give a worse correlation to the finite element data (fig. 5.14) than that achieved from the interpolation scheme.

The limitations of the composition scheme are exposed in figs. 5.15 – 5.17, which display direct comparison between SIF solutions obtained by both interpolation and composition schemes under uniform tension and pure bending for all extreme notch geometries defined in section 5.5.4. Though solutions obtained via application of the composition scheme remain conservative with

respect to the finite element data, the solutions derived from the interpolation scheme are shown to be of consistently high accuracy over the wide range of notch profiles investigated.

Figs. 5.18 – 5.23 display SIF solutions obtained for the range of symmetric notches detailed in fig. 5.5 under loading modes of uniform tension and pure bending. Solutions are arranged in each figure to show variation of a single notch parameter alongside selected finite element data. Figs. 5.18 and 5.19 show the localised influence of notch acuity at the notch root, figs. 5.20 and 5.21, the marginal influence of flank angle between 30 and 90° (selected solutions are presented to aid clarity) and figs. 5.22 and 5.23, the influence of notch size. The weight function solutions in figs. 5.22 and 5.23 are truncated at a point where the Brown and Srawley solutions become invalid at '$(a+b)/T=0.6$'.

For all geometry configurations investigated, the SIF solutions derived through the weight function interpolation scheme display an excellent correlation with the finite element data.

5.7 - Conclusions

The interpolation of base geometry weight functions has been rigorously examined by application to a number of symmetric notches in two-dimensional geometries containing edge cracks. SIF solutions of high accuracy were obtained by application of the two considered reference load cases of uniform tension and decreasing tension for the formulation of base geometry weight functions. Derived SIF solutions obtained, by implementation of these observations, have been shown to be stable and robust for the broad range notch configurations considered. The limitations of the composition scheme when applied to notches of extreme geometric form and improvements to be gained by an interpolation scheme were highlighted.

The body of work contained in this chapter has successfully sought to demonstrate the simplicity and versatility with which new SIF solutions, for notched components subject to an arbitrary loading condition, can be derived via a weight function technique. The ability to formulate rapid and accurate SIF solutions via implementation of an interpolation scheme coded into a simple computer-based algorithm has been successfully demonstrated.

5.8 – References

[5.1] Teh, L.S., *Library of Geometric Influences for Stress Intensity Factor Weight Functions*, Ph.D. Thesis, University College London, 2002

[5.2] Hartranft, J.R. and Sih, G.C., Methods of Analysis and Solutions of Crcak Problems, G.C. Sih ed. Noordhoff, Holland, 1973

[5.3] Brennan, F.P. and Teh, L.S., Determination of Crack-Tip Stress Intensity Factors in Complex Geometries by the Composition of Constituent Weight Function Solutions. *Fatigue Fract Engng Mater Struct* 27, pp. 1 – 7, 2004

[5.4] Brown Jr., W.F. and Srawley, J.E., Plane Strain Crack Toughness Testing of High Strength Metallic Materials, *ASTM STP 410* (1966), p. 12.

5.9 – Tables

Tab. 5.1 – SIF Solutions for Symmetrical Notches in a Semi-Finite Strip
(α = 45 Deg, Uniform Crack Face Loading)

b/ρ = 1		b/ρ = 3		b/ρ = 6		b/ρ = 10		b/ρ = 15	
a / ρ	Y_I	a / ρ	Y_I	a / ρ	Y_I	a / ρ	Y_I	a / ρ	Y_I
0.05	1.083	0.05	1.083	0.05	1.082	0.05	1.081	0.05	1.082
0.10	1.058	0.10	1.056	0.10	1.056	0.10	1.055	0.10	1.056
0.15	1.039	0.15	1.036	0.15	1.035	0.15	1.034	0.15	1.034
0.20	1.025	0.20	1.020	0.20	1.018	0.20	1.017	0.20	1.017
0.25	1.015	0.25	1.007	0.25	1.005	0.25	1.004	0.25	1.003
0.30	1.008	0.30	0.997	0.30	0.994	0.30	0.993	0.30	0.992
0.40	0.998	0.40	0.983	0.40	0.979	0.40	0.977	0.40	0.976
0.50	0.995	0.50	0.974	0.50	0.968	0.50	0.966	0.50	0.965
0.70	0.995	0.70	0.966	0.70	0.957	0.70	0.953	0.65	0.954
0.90	1.000	0.90	0.964	0.90	0.952	0.90	0.947	0.90	0.944
1.10	1.007	1.10	0.965	1.10	0.950	1.10	0.944	1.10	0.941
1.30	1.014	1.30	0.967	1.30	0.950	1.30	0.942	1.30	0.939
1.60	1.025	1.60	0.972	1.60	0.951	1.60	0.942	1.60	0.937
1.90	1.033	1.90	0.978	1.90	0.954	1.90	0.943	1.90	0.937
2.20	1.041	2.20	0.984	2.20	0.957	2.20	0.945	2.20	0.938
2.50	1.048	2.50	0.990	2.50	0.961	2.50	0.946	2.50	0.939
-	-	3.00	0.999	3.00	0.967	3.00	0.950	3.00	0.941
-	-	3.50	1.007	3.50	0.973	3.50	0.954	3.50	0.944
-	-	4.00	1.014	4.00	0.978	4.00	0.958	4.00	0.946
-	-	5.00	1.026	5.00	0.989	5.00	0.966	5.00	0.952
-	-	6.00	1.036	6.00	0.998	6.00	0.973	6.00	0.957
-	-	7.00	1.045	7.00	1.007	7.00	0.980	7.00	0.963
-	-	8.00	1.051	8.00	1.014	8.00	0.987	8.00	0.968
-	-	10.00	1.062	10.00	1.027	10.00	0.998	10.00	0.978
-	-	12.00	1.070	12.00	1.037	12.00	1.008	12.00	0.986
-	-	14.00	1.076	14.00	1.045	14.00	1.017	14.00	0.994

Tab. 5.2 – SIF Solutions for Symmetrical Notches in a Semi-Finite Strip
(b/ρ = 6, Uniform Crack Face Loading)

α = 15°		α = 30°		α = 45°		α = 60°		α = 90°	
a / ρ	Y_I	a / ρ	Y_I	a / ρ	Y_I	a / ρ	Y_I	a / ρ	Y_I
0.05	1.085	0.05	1.083	0.05	1.082	0.05	1.082	0.05	1.082
0.10	1.064	0.10	1.057	0.10	1.056	0.10	1.055	0.10	1.055
0.15	1.051	0.15	1.038	0.15	1.035	0.15	1.034	0.15	1.034
0.20	1.042	0.20	1.023	0.20	1.018	0.20	1.017	0.20	1.017
0.25	1.036	0.25	1.011	0.25	1.005	0.25	1.003	0.25	1.003
0.30	1.031	0.30	1.003	0.30	0.994	0.30	0.992	0.30	0.992
0.40	1.027	0.40	0.990	0.40	0.979	0.40	0.976	0.40	0.975
0.55	1.024	0.55	0.980	0.50	0.968	0.50	0.965	0.50	0.964
0.70	1.021	0.70	0.974	0.70	0.957	0.70	0.952	0.70	0.951
0.90	1.020	0.90	0.971	0.90	0.952	0.90	0.946	0.90	0.945
1.10	1.019	1.10	0.969	1.10	0.950	1.10	0.944	1.10	0.943
1.30	1.019	1.30	0.969	1.30	0.950	1.30	0.944	1.30	0.943
1.60	1.018	1.60	0.969	1.60	0.951	1.60	0.946	1.60	0.945
1.90	1.018	1.90	0.971	1.90	0.954	1.90	0.950	1.90	0.948
2.20	1.019	2.20	0.973	2.20	0.957	2.20	0.953	2.20	0.952
2.50	1.019	2.50	0.975	2.50	0.961	2.50	0.957	2.50	0.956
3.00	1.020	3.00	0.978	3.00	0.967	3.00	0.964	3.00	0.963
3.50	1.021	3.50	0.982	3.50	0.973	3.50	0.971	3.50	0.970
4.00	1.022	4.00	0.986	4.00	0.978	4.00	0.977	4.00	0.976
5.00	1.024	5.00	0.994	5.00	0.989	5.00	0.988	5.00	0.988
6.00	1.027	6.00	1.002	6.00	0.998	6.00	0.998	6.00	0.998
7.00	1.030	7.00	1.009	7.00	1.007	7.00	1.007	7.00	1.007
8.00	1.032	8.00	1.015	8.00	1.014	8.00	1.014	8.00	1.014
10.00	1.038	10.00	1.027	10.00	1.027	10.00	1.027	10.00	1.027
12.00	1.044	12.00	1.037	12.00	1.037	12.00	1.037	12.00	1.037
14.00	1.049	14.00	1.045	14.00	1.045	14.00	1.045	14.00	1.045

Tab. 5.3 – SIF Solutions for Symmetrical Notches in a Semi-Finite Strip
($b/\rho = 0$, Uniform Crack Face Loading)

$\alpha = 15°$		$\alpha = 30°$		$\alpha = 45°$	
a/b	Y_I	a/b	Y_I	a/b	Y_I
0.025	1.010	0.025	0.949	0.025	0.918
0.050	1.012	0.050	0.951	0.050	0.922
0.075	1.013	0.075	0.953	0.075	0.924
0.100	1.013	0.100	0.954	0.100	0.927
0.150	1.014	0.150	0.957	0.150	0.932
0.200	1.014	0.200	0.959	0.200	0.937
0.250	1.015	0.250	0.962	0.250	0.942
0.300	1.015	0.300	0.965	0.300	0.947
0.400	1.017	0.400	0.970	0.400	0.956
0.500	1.018	0.500	0.976	0.500	0.964
0.700	1.021	0.650	0.984	0.650	0.976
0.900	1.024	0.900	0.996	-	-
1.100	1.028	1.100	1.006	-	-
1.500	1.035	1.400	1.018	-	-
1.800	1.040	1.800	1.031	-	-
2.100	1.045	-	-	-	-
2.450	1.051	-	-	-	-
2.800	1.056	-	-	-	-
3.200	1.061	-	-	-	-
3.700	1.067	-	-	-	-
4.200	1.072	-	-	-	-
5.200	1.080	-	-	-	-

Tab. 5.4 – SIF Solution Curve Fit Coefficients (eq. 5.7) for Semi-Finite Symmetric Notches

α	b/ρ	M'_5	M'_4	M'_3	M'_2	M'_1	M'_0
15	6	-0.1777	1.6136	-2.2007	0.8718	0.1381	0.9957
30	6	-0.0261	0.9343	-1.3558	0.7446	-0.0539	1.0000
45	6	0.2856	-0.2391	0.0985	0.1177	-0.0194	1.0003
60	6	0.3826	-0.6340	0.6129	-0.1223	0.0042	1.0000
90	6	0.4247	-0.7763	0.7773	-0.1942	0.0119	0.9999
45	1	0.1709	-0.0104	0.1906	-0.1251	0.0174	0.9997
45	3	0.5647	-1.0482	0.9599	-0.2494	0.0165	1.0003
45	10	0.0421	0.3992	-0.4774	0.3005	-0.0211	0.9997
45	15	-0.0936	0.7023	-0.6803	0.3169	-0.0017	0.9992

Tab. 5.5 – Normalised Stress Solution, '$\sigma_{yy}(x)/\sigma_o$' Coefficients for Usage in eq. 5.8 (Uniform Tension)

α	b/ρ	b/T	P_5	P_4	P_3	P_2	P_1	P_0
15	6	0.2727	28.824	-74.195	81.749	-45.903	16.332	0.154
30	6	0.2727	2.228	-6.274	16.784	-13.656	9.024	0.251
45	6	0.2727	-0.166	-1.321	11.407	-8.636	7.220	0.378
60	6	0.2727	1.984	-7.877	17.901	-10.779	7.399	0.369
90	6	0.2727	1.106	-5.368	14.985	-9.054	6.934	0.408
45	1	0.2727	2.046	-7.638	19.263	-18.874	11.417	-1.587
45	3	0.2727	-5.412	13.612	-5.374	-1.169	4.890	0.182
45	10	0.2727	2.463	-8.562	20.21	-12.763	9.161	0.515
45	15	0.2727	5.288	-16.474	30.028	-17.687	11.380	0.607
45	6	0.0625	-3.266	11.723	-10.501	6.729	0.760	0.982
45	6	0.1875	2.904	-6.436	10.649	-4.504	4.180	0.759
45	6	0.3125	15.806	-47.155	62.181	-35.257	14.526	-0.354
45	6	0.4375	56.287	-179.98	235.34	-143.98	51.06	-5.055

Tab. 5.6 – Normalised Stress Solution, '$\sigma_{yy}(x)/\sigma_o$' Coefficients for Usage in eq. 5.8 (Pure Bending)

α	b/ρ	b/T	P_5	P_4	P_3	P_2	P_1	P_0
15	6	0.2727	37.082	-106.97	126.32	-74.618	24.617	-2.0709
30	6	0.2727	21.392	-67.090	88.077	-55.135	20.175	-1.8499
45	6	0.2727	17.512	-57.080	76.848	-47.551	17.945	-1.6906
60	6	0.2727	16.436	-54.025	72.720	-44.383	16.940	-1.6057
90	6	0.2727	18.292	-59.467	78.413	-46.951	17.452	-1.6459
45	1	0.2727	6.7035	-29.768	57.287	-53.498	28.456	-6.1474
45	3	0.2727	8.1808	-32.314	53.493	-40.411	18.131	-2.5908
45	10	0.2727	24.866	-76.000	94.581	-53.336	18.577	-1.2191
45	15	0.2727	31.583	-93.214	111.01	-59.212	19.691	-0.9232
45	6	0.0625	29.003	-80.563	87.414	-41.188	11.293	-0.0387
45	6	0.1875	27.893	-83.016	98.589	-53.480	16.881	-1.1015
45	6	0.3125	23.187	-73.927	96.721	-59.328	21.850	-2.2879
45	6	0.4375	23.881	-82.248	118.26	-81.258	33.499	-4.7056

5.10 – Figures

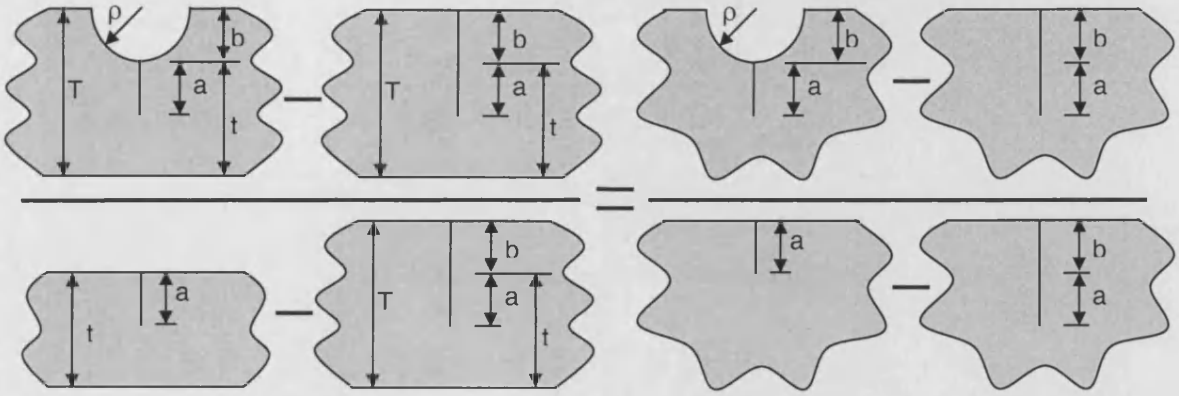

Fig. 5.1 – The Weight Function Interpolation Scheme

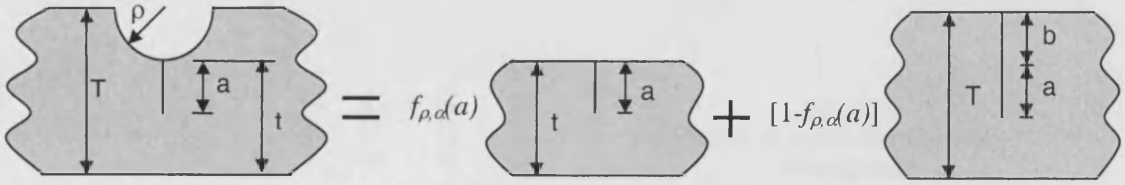

Fig. 5.2 – Weight Function Scheme for Symmetrically Notched Components

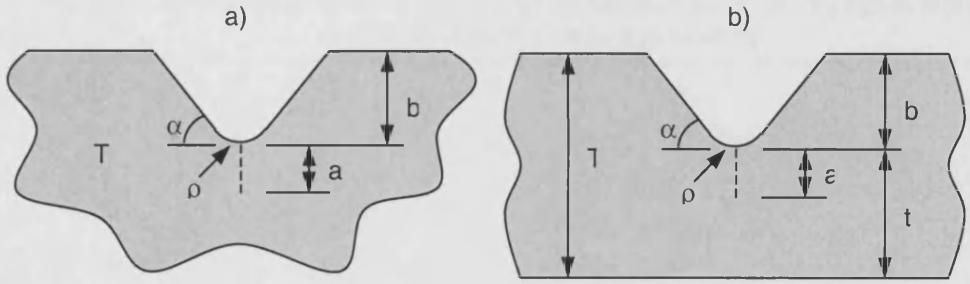

Fig. 5.3 – Geometric Definition of Symmetrically Notched Semi-Finite Plane (a) and Finite Plane (b)

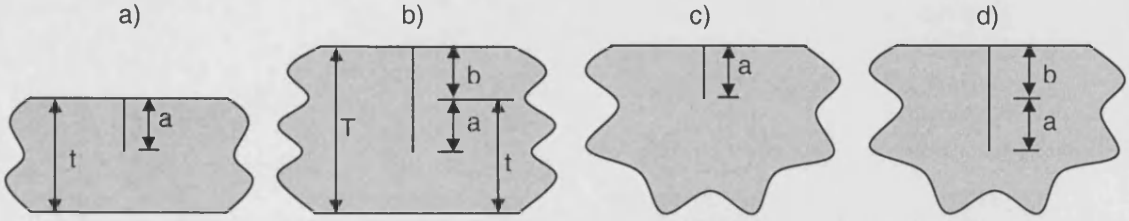

Fig. 5.4 – Geometric Definition of Plane Geometries
(a) Finite, Unsiffened (b) Finite, Stiffened (c) Semi-Finite, Unstiffened (d) Semi-Finite, Stiffened

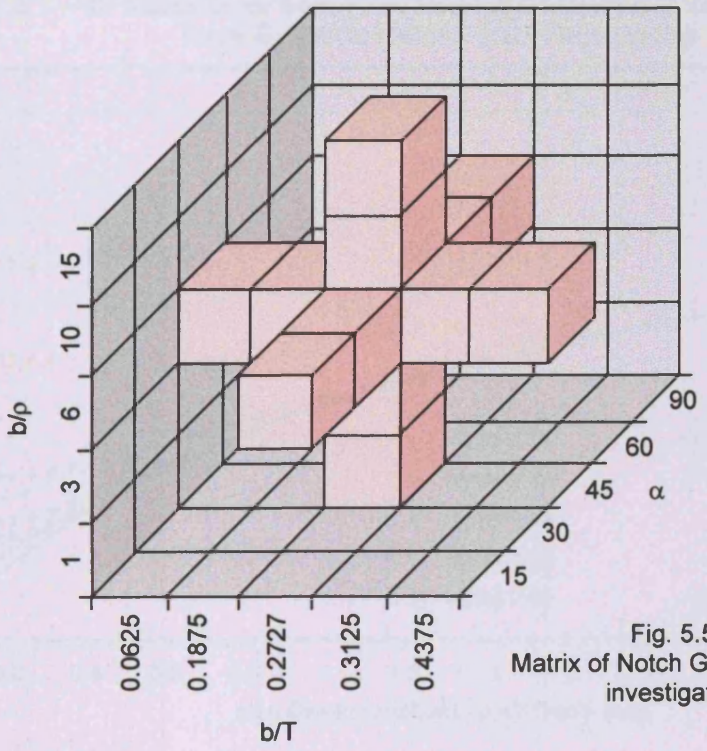

Fig. 5.5
Matrix of Notch Geometeries investigated

Fig. 5.6 – SIF Solutions for Semi-Finite Notched Geometries of Varying Notch Root Radii Subject to Uniform Crack Face Loading

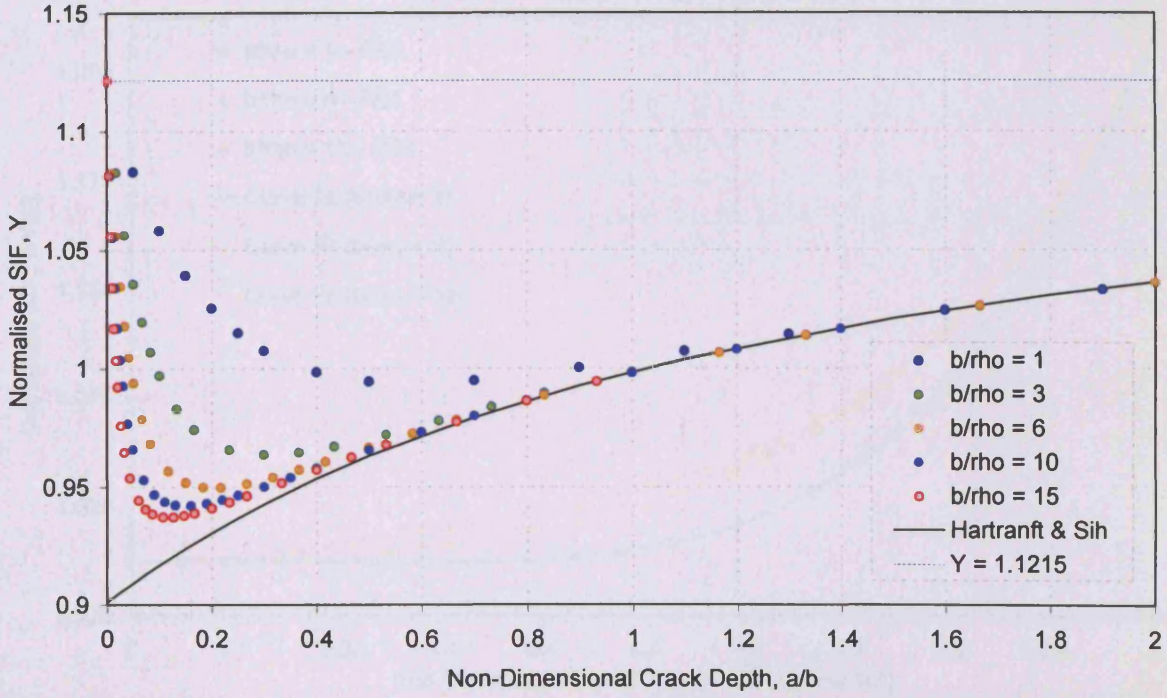

Fig. 5.7 – SIF Solutions for Semi-Finite Notched Geometries of Varying Notch Flank Angle Subject to Uniform Crack Face Loading

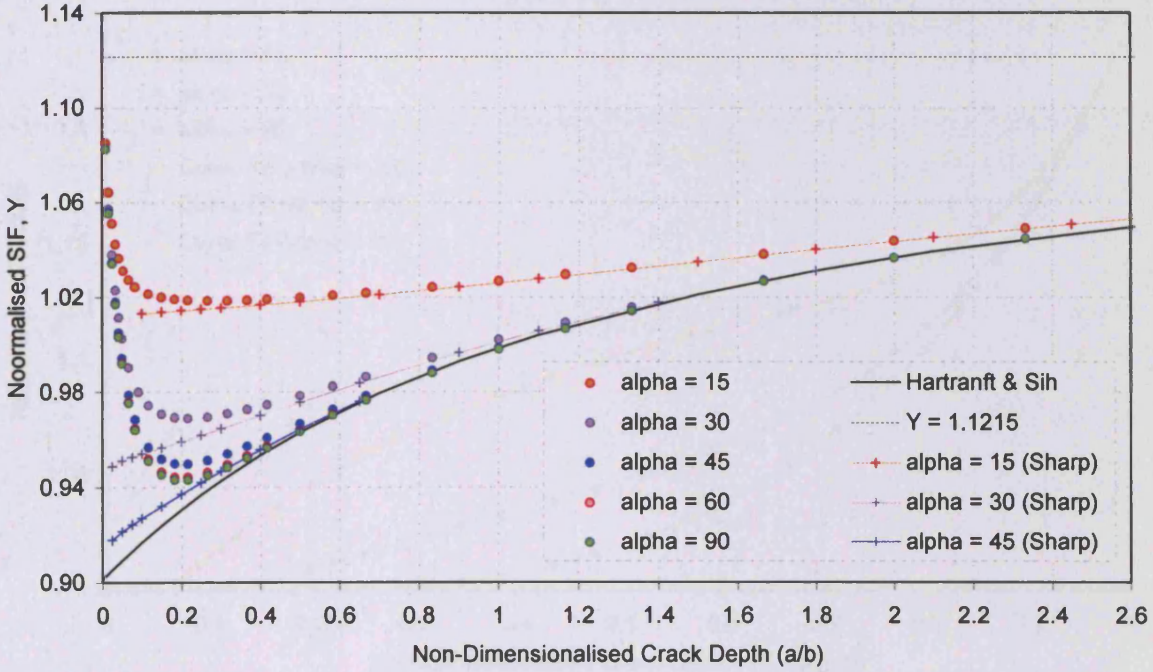

Fig. 5.8 – Discrete FE Data (Tab. 5.1) and Continuous Curve Fitted Polynomial Equations for Notches of Varying Root Radius

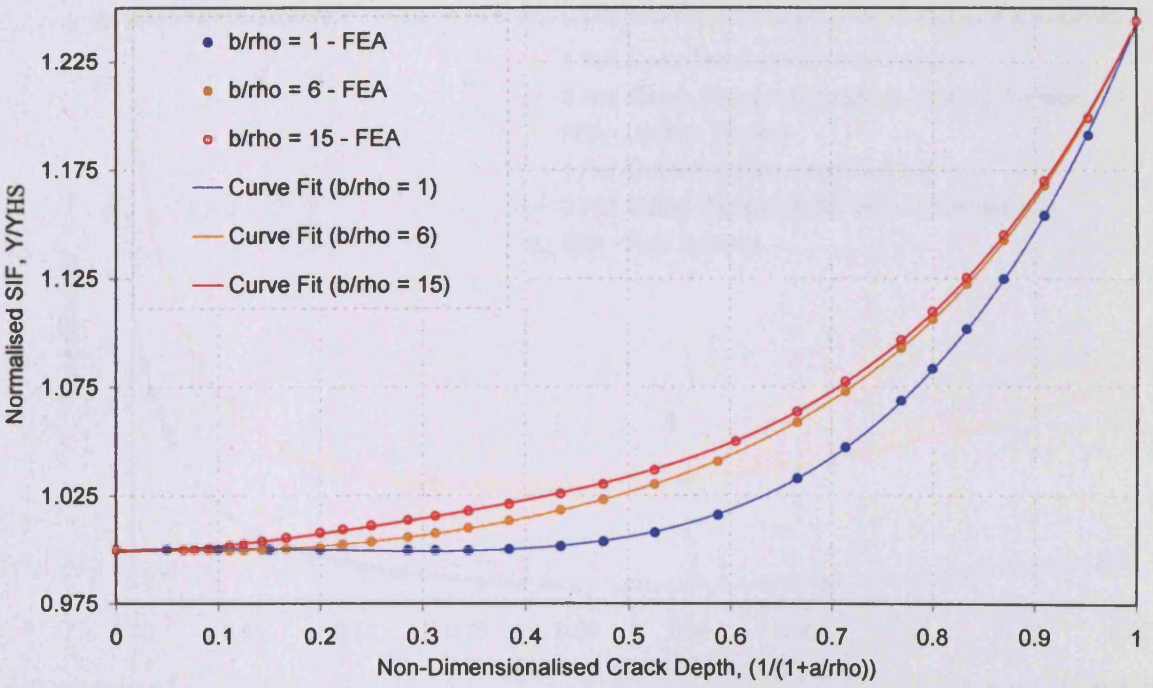

Fig. 5.9 – Discrete FE Data (Tab. 5.2) and Continuous Curve Fitted Polynomial Equations for Notches of Varying Flank Angle

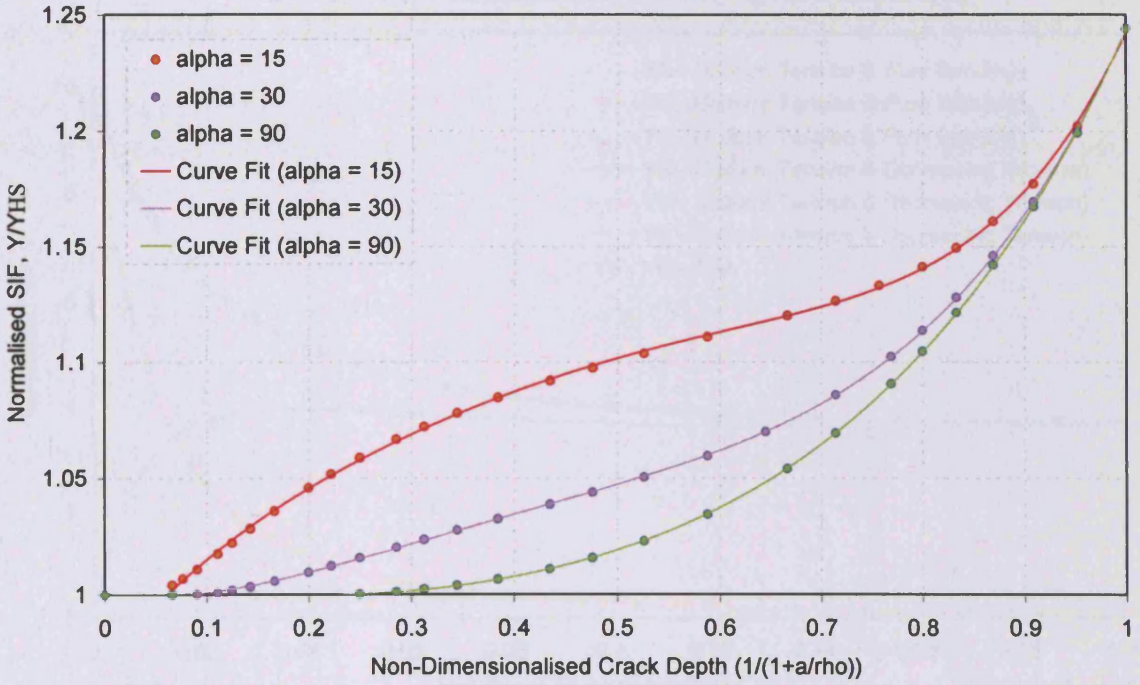

Fig. 5.10 – SIF Solutions Obtained Via an Interpolation Scheme Utilising Base Geometry Weight Functions Formulated from A Single and Two Reference States

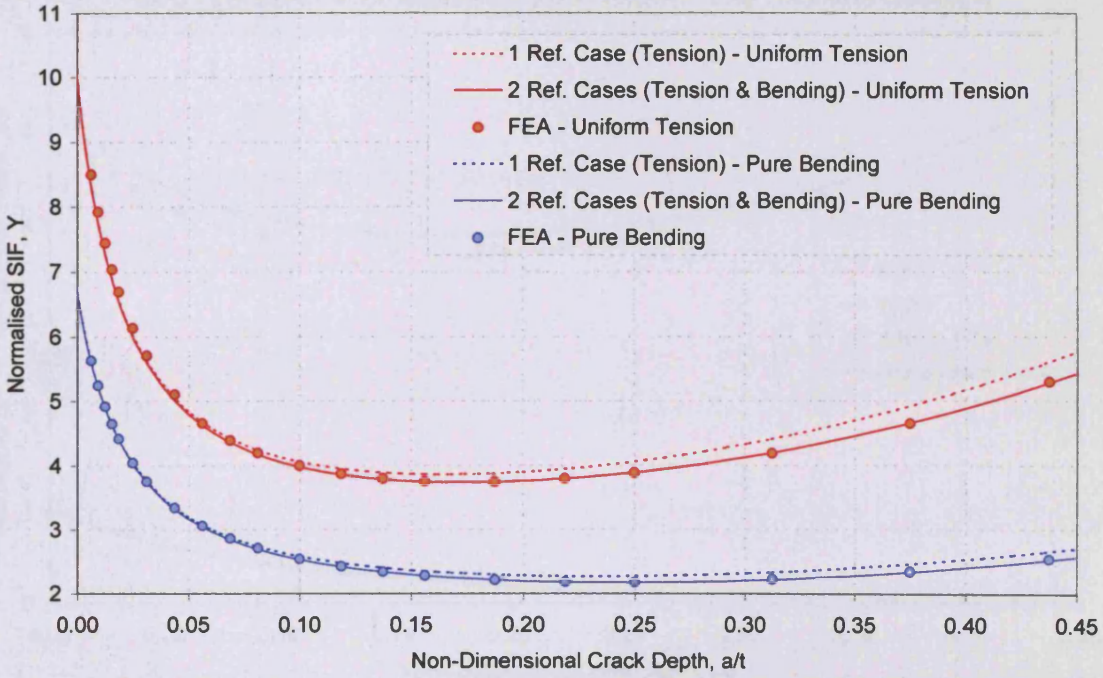

Fig. 5.11 – SIF Solutions Obtained Via an Interpolation Scheme Utilising Base Geometry Weight Functions Formulated from Two Varying Reference States

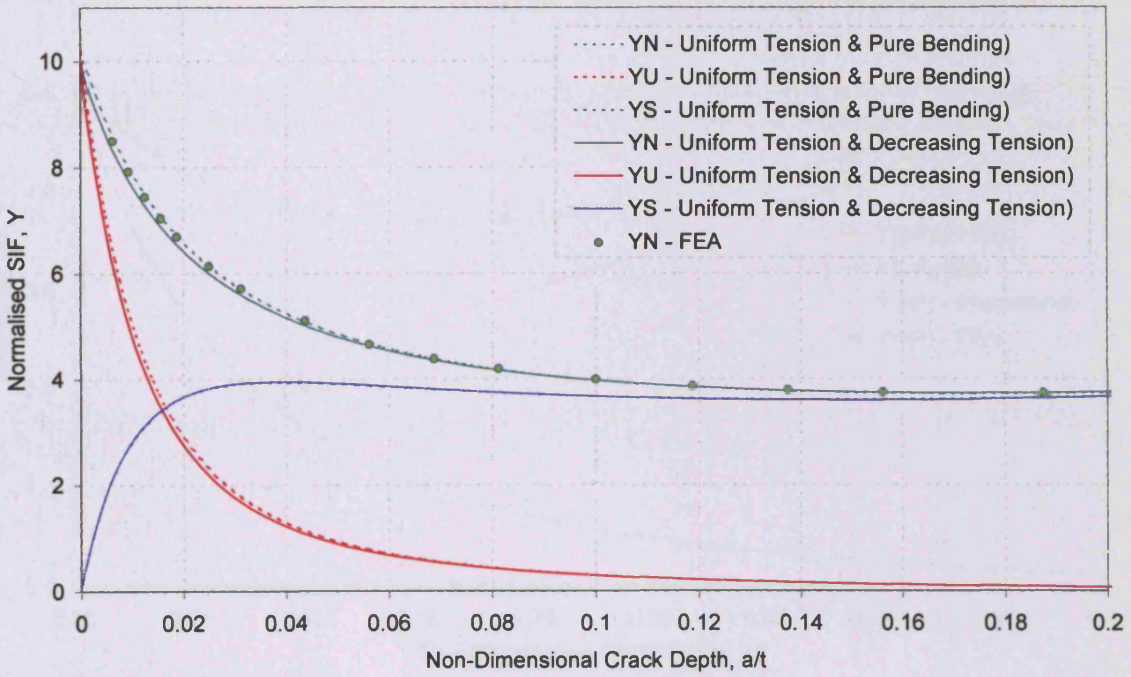

Fig. 5.12 – Extreme SIF Solutions for the Notched Finite Thickness Geometry

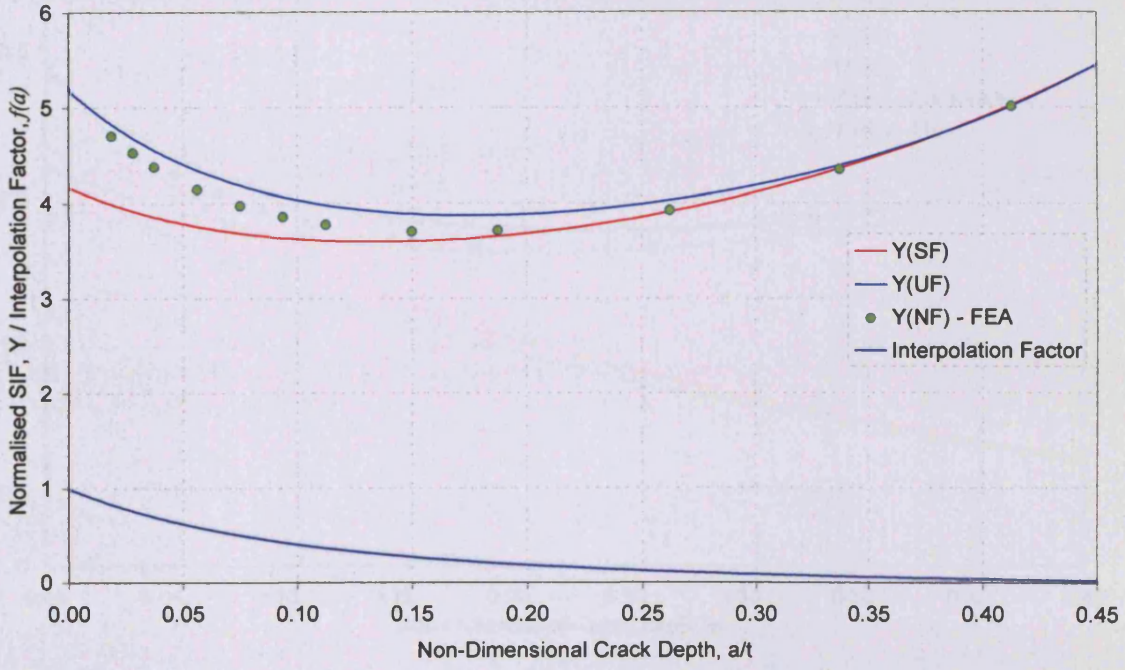

Fig. 5.13 – Influence of the Two Interpolation Scheme Base Geometry Solutions Upon the Notched, Finite Thickness Geometry Solution

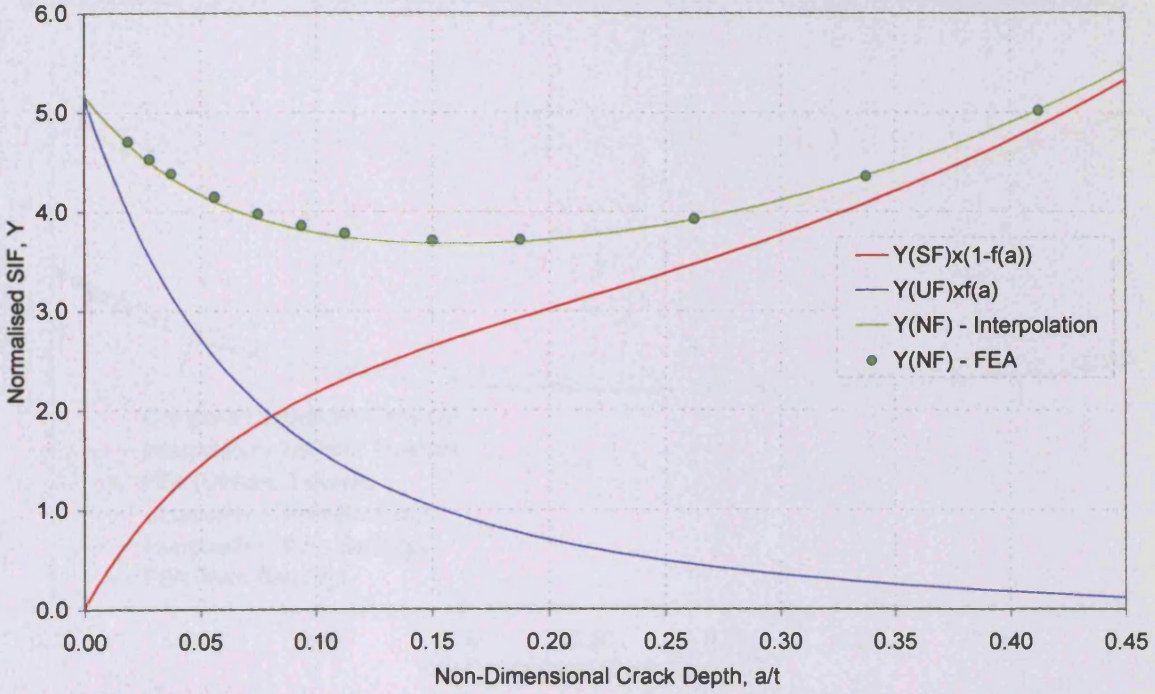

Fig. 5.14 – Influence of the Three Composition Scheme Constituent Geometry Solutions Upon the Notched, Finite Thickness Geometry Solution

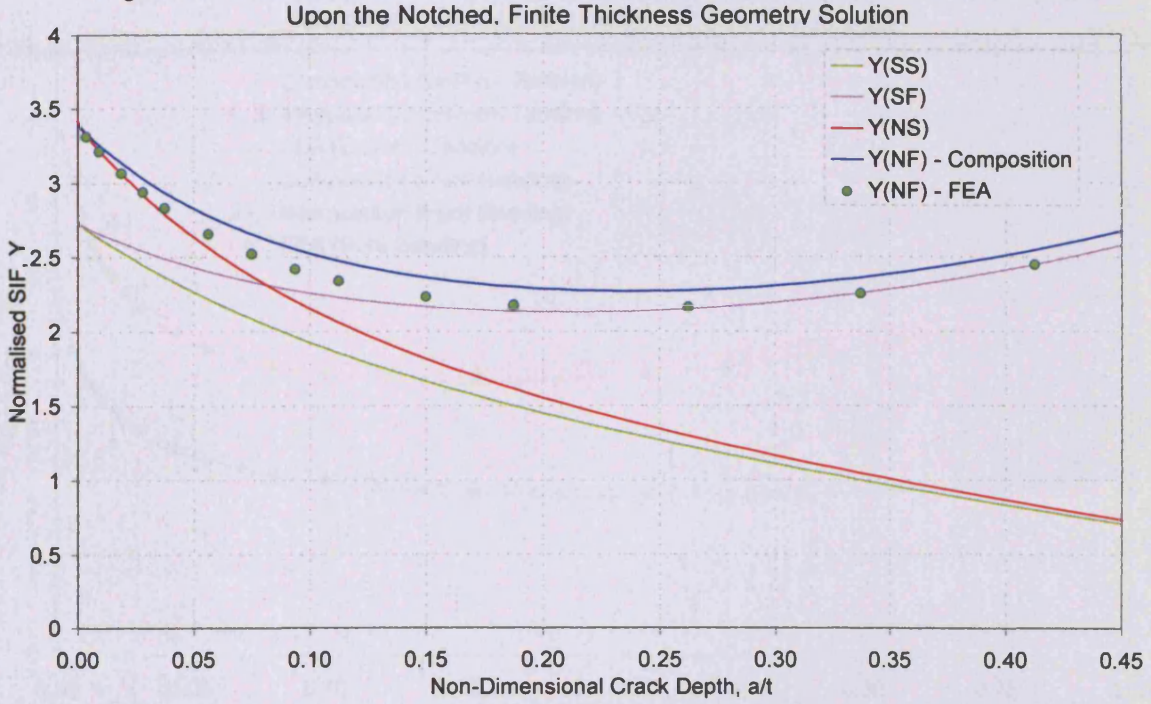

Fig. 5.15 – Composition and Interpolation Scheme SIF Solutions Finite Thickness Geometries Containing a Blunt Notch

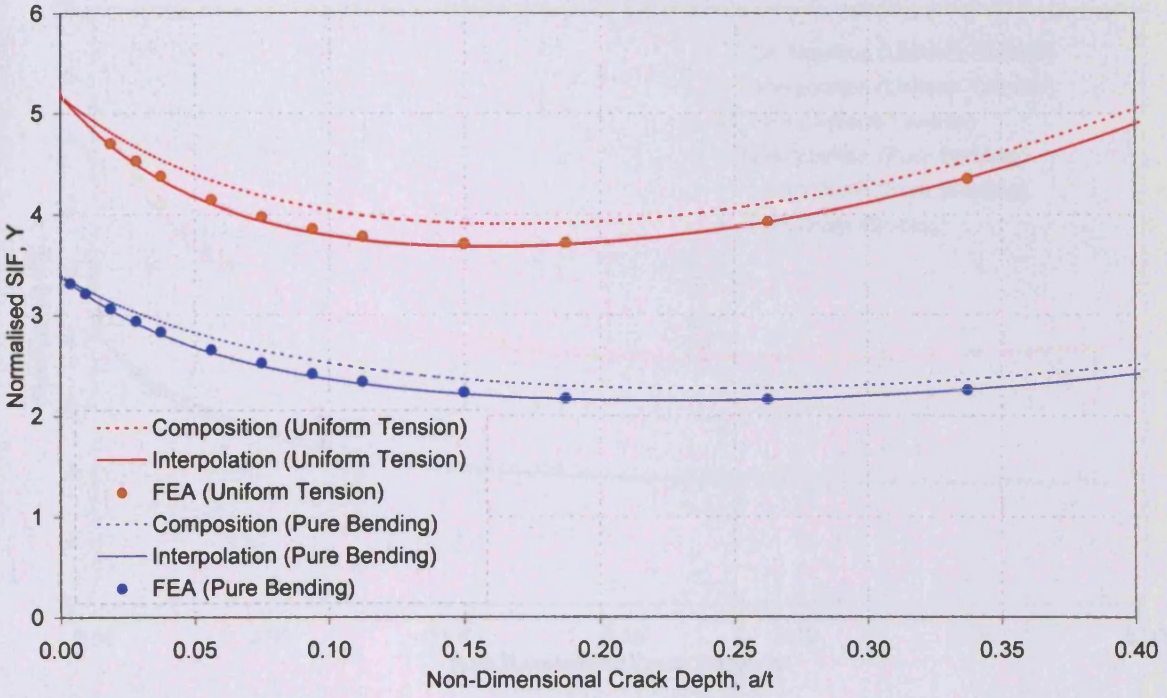

Fig. 5.16 – Composition and Interpolation Scheme SIF Solutions for Finite Thickness Geometries Containing a Notch with Low Flank Angle

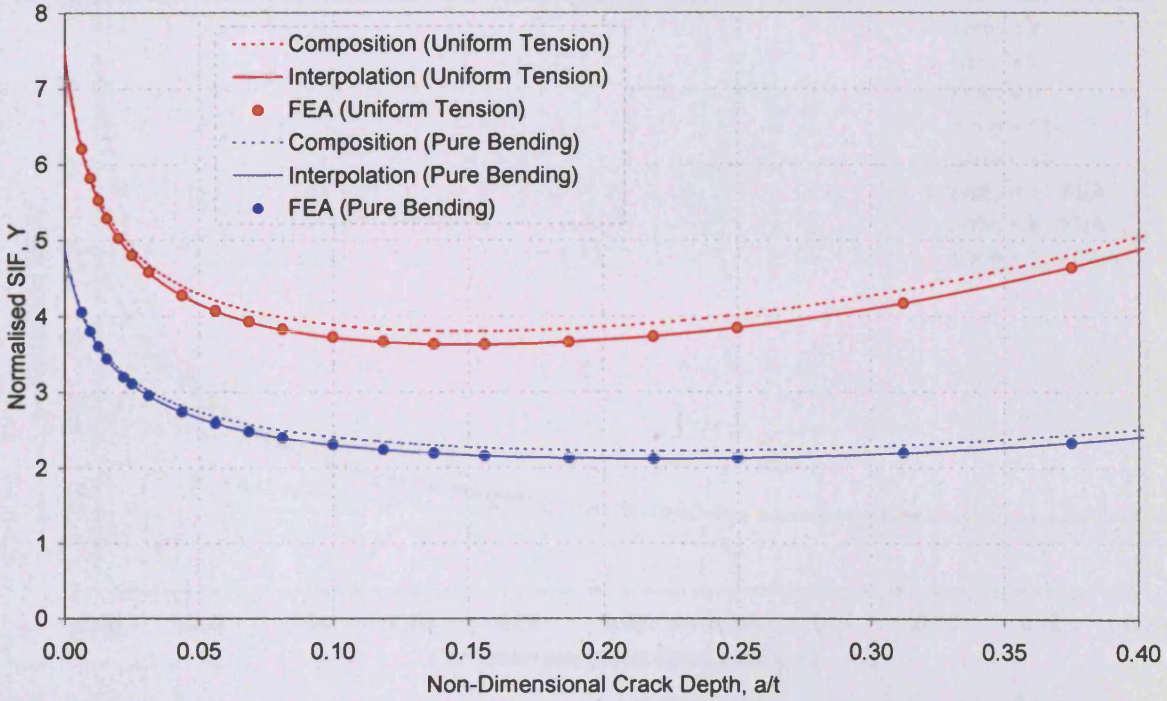

Fig. 5.17 – Composition and Interpolation Scheme SIF Solutions for Finite Thickness Geometries Containing a Deep Notch

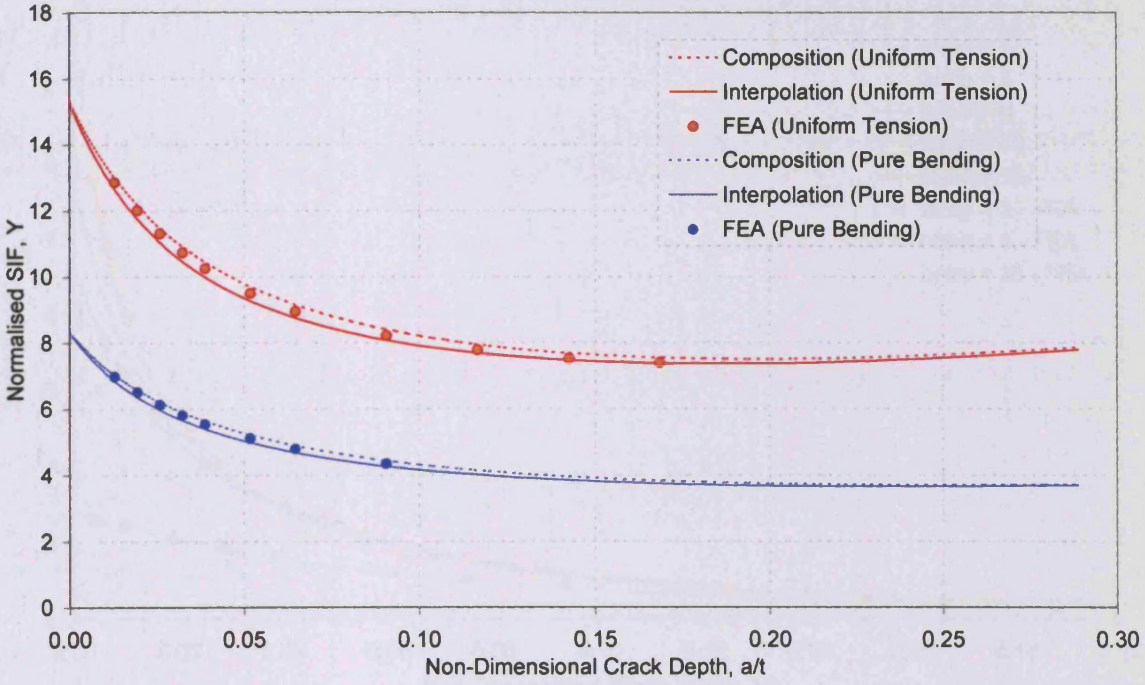

Fig. 5.18 – SIF Solutions Obtained From the Interpolation Scheme for Finite Thickness, Notched Geometries (b/T = 0.2727, α = 45° Uniform Tension)

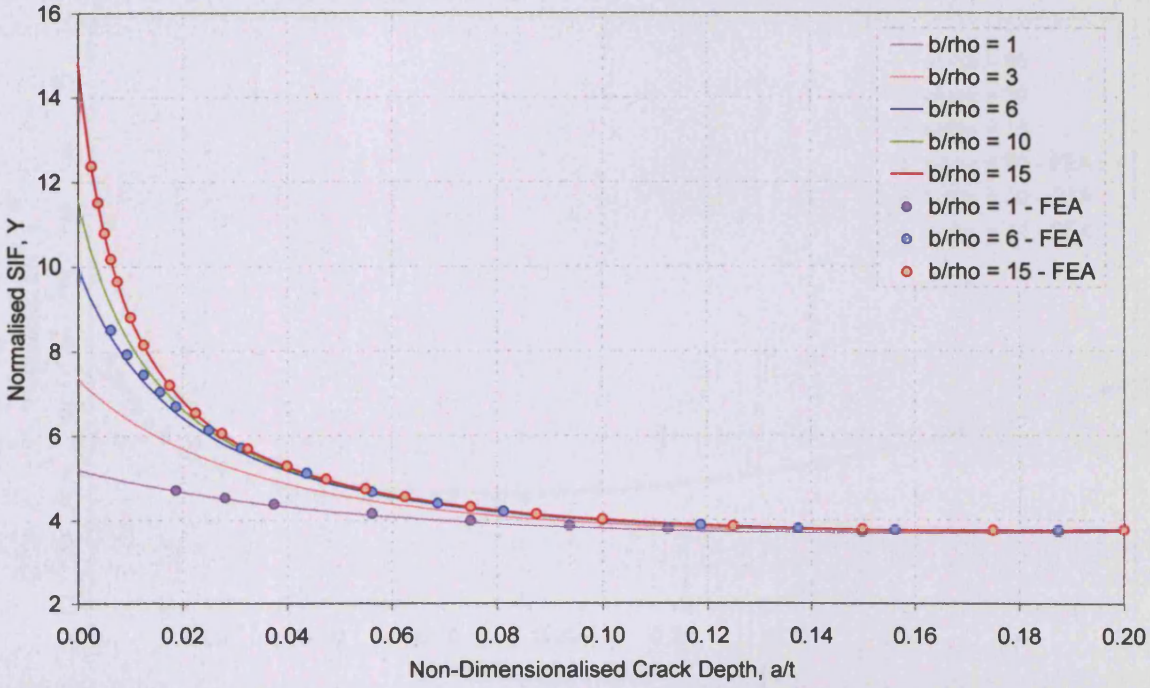

Fig. 5.19 – SIF Solutions Obtained From the Interpolation Scheme for Finite Thickness, Notched Geometries (b/T = 0.2727, α = 45° Pure Bending)

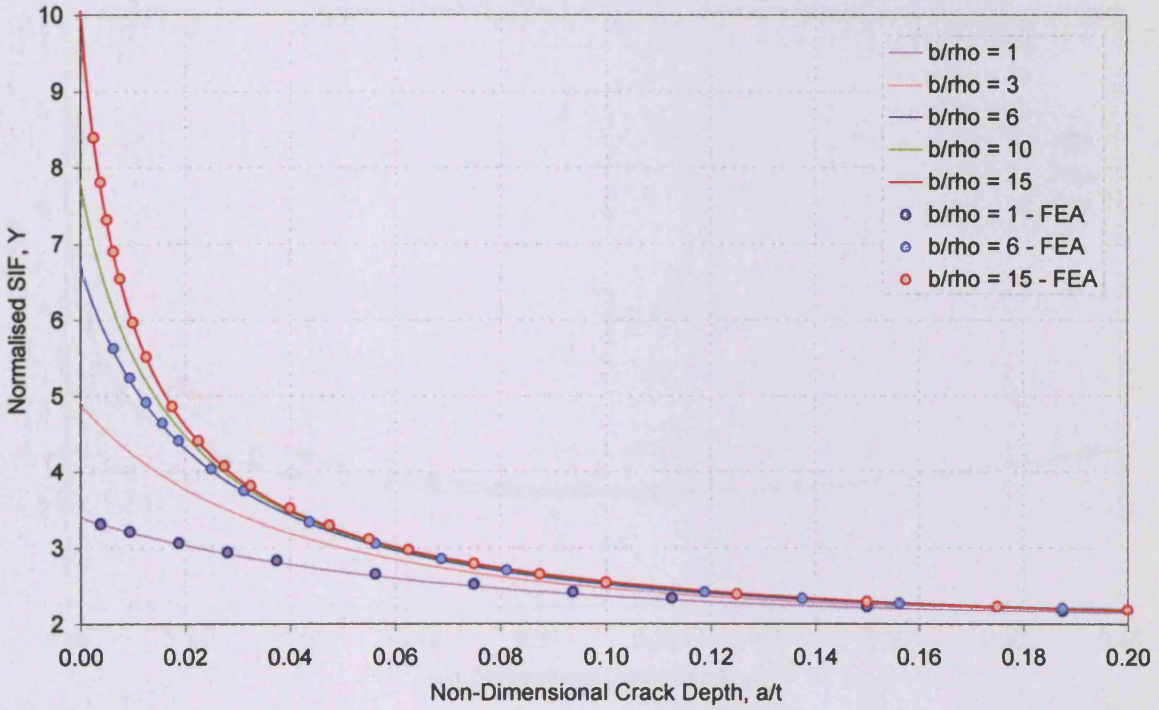

Fig. 5.20 – SIF Solutions Obtained From the Interpolation Scheme for Finite Thickness, Notched Geometries (b/T = 0.2727, b/ρ = 6, Uniform Tension)

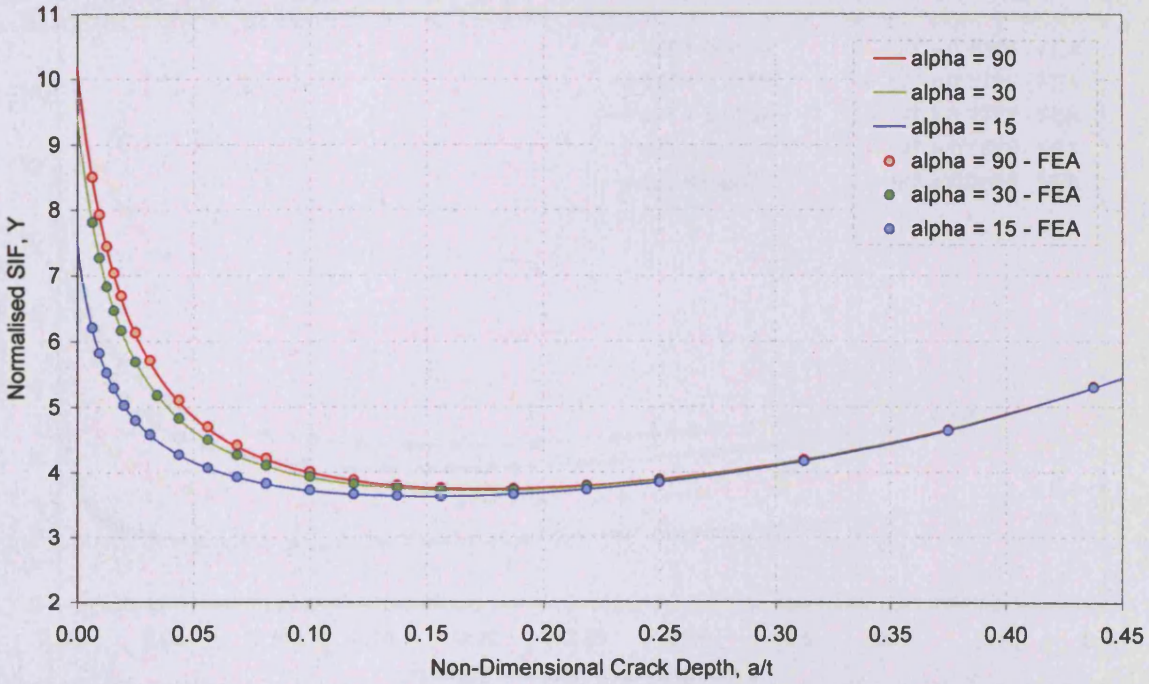

Fig. 5.21 – SIF Solutions Obtained From the Interpolation Scheme for Finite Thickness, Notched Geometries (b/T = 0.2727, b/ρ = 6, Pure Bending)

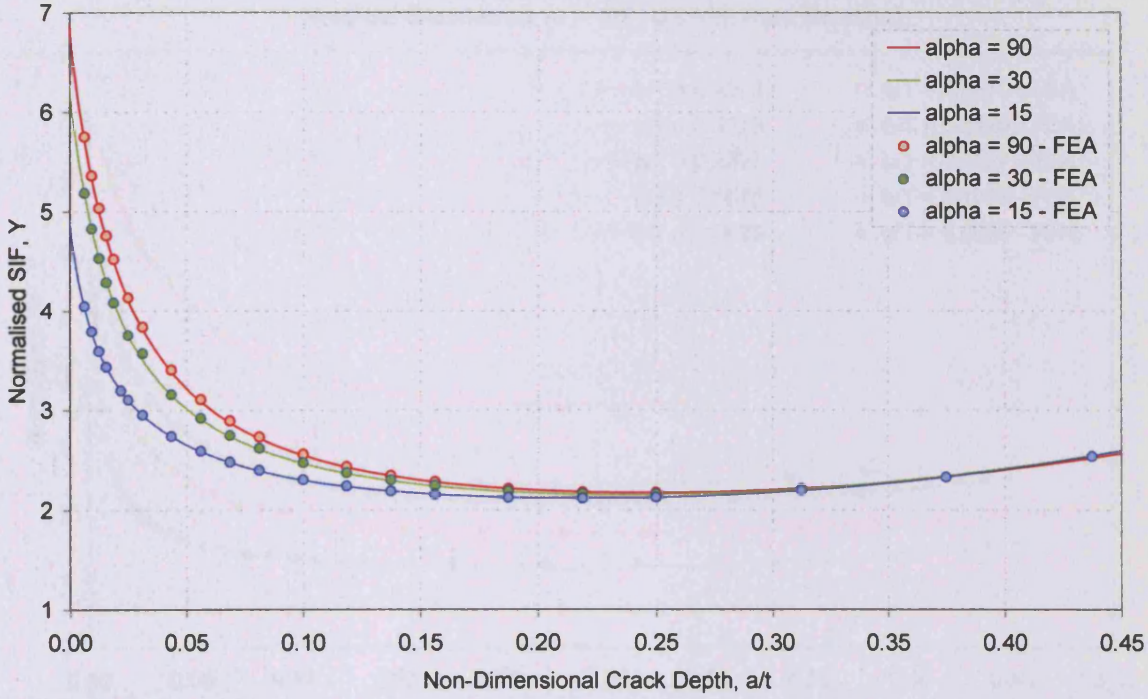

Fig. 5.22 – SIF Solutions Obtained From the Interpolation Scheme for Finite Thickness, Notched Geometries (α = 45°, b/ρ = 6, Uniform Tension)

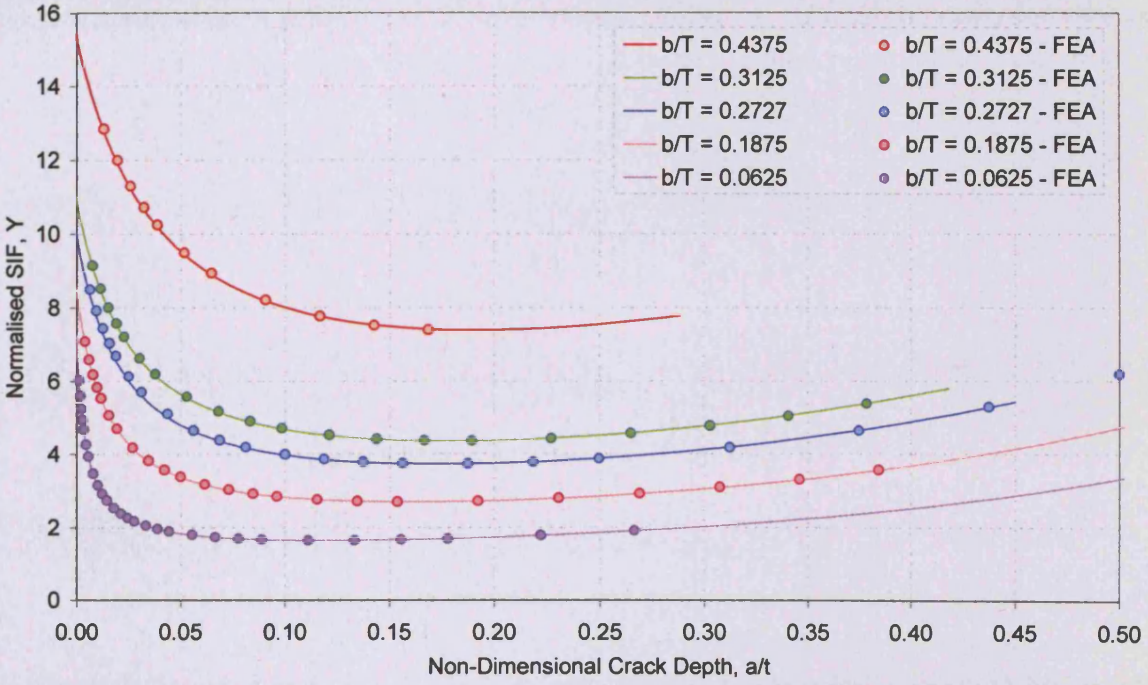

Fig. 5.23 – SIF Solutions Obtained From the Interpolation Scheme for Finite Thickness, Notched Geometries (α = 45°, b/ρ = 6, Pure Bending)

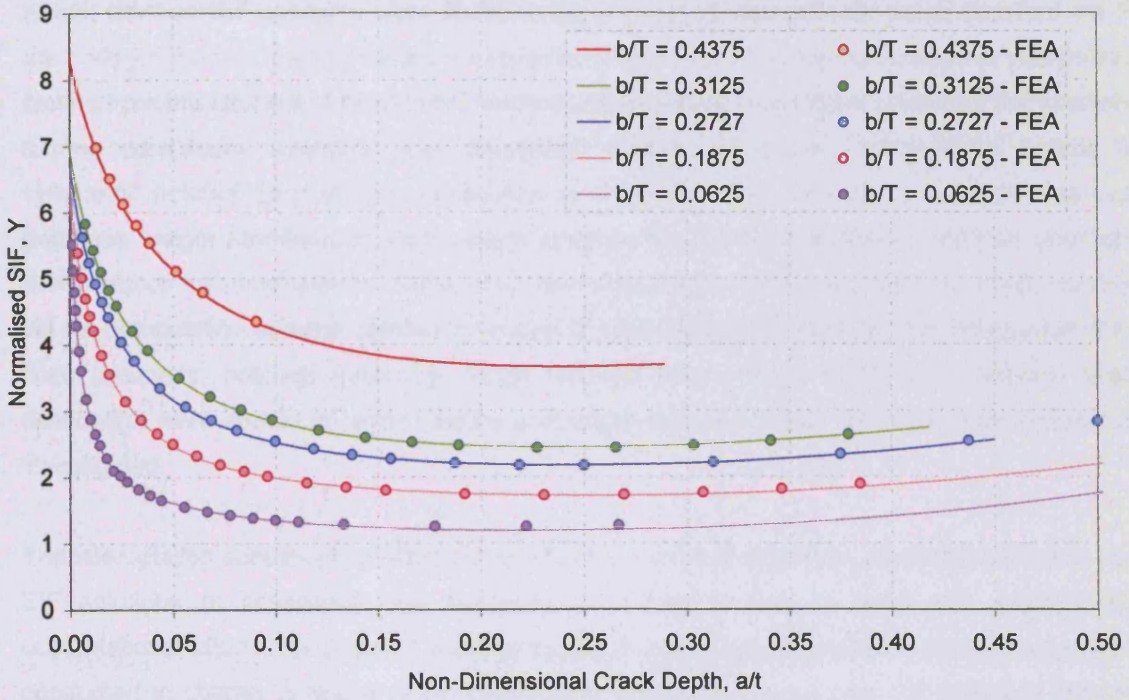

Chapter 6 – Interpolation of Weight Functions for Step Notches

Chapter 5 detailed the implementation of an interpolated weight function scheme to determine new SIF solutions for cracks at symmetric notches in finite thickness geometries. Resulting weight function SIF solutions were found to be in good agreement with those obtained via FE methods for the two loading modes investigated. A procedure for the calculation of interpolation factors from the analysis of semi-finite; notched, stiffened and unstiffened geometry SIF solutions, termed constituent solutions, was presented. Chapter 5 derived interpolation factors for symmetric notches prior to their application to finite thickness stiffened and unstiffened base geometry weight functions, to yield weight functions for the finite thickness notched geometry. Weight functions formulated in this manner were found to be more accurate than those obtained via the composition scheme detailed in chapter 2. Calculated SIF solutions from integration of the finite thickness, notched geometry weight function with a finite thickness, crack-line stress distribution were shown to remain stable and robust over the broad range of notch geometries investigated.

The interpolation scheme, implemented by a computer-based algorithm, has been shown to yield SIF solutions of consistent high accuracy in a manner that is rapid and requires little computational effort. The scope of work contained in this chapter concerns a similar study to that conducted in chapter 5 applying an interpolation scheme to derive new SIF solutions for step notched geometeries.

6.1 – Introduction

Definition of the step notch geometry under consideration is reproduced as fig. 6.1a, in which geometric parameters are allocated the same notation as employed for the symmetric notch. The interpolation of base geometry weight functions scheme developed in chapter 4 is applicable to all notch geometry types and is presented in the preferred form of eq. 6.1.

$$m_N^F(a,x) = f(a)m_U^F(a,x) + (1-f(a))m_S^F(a,x) \qquad \text{- (6.1)}$$

$$f(a) = \frac{Y_N^S(a) - Y_S^S(a)}{Y_U^S(a) - Y_S^S(a)} \qquad \text{- (6.2)}$$

'$Y_N^S(a)$' is an SIF solution for the semi-finite step notch geometry, fig. 6.1b.

Eq. 6.1 requires an interpolation factor to be determined from the semi-finite step notch geometry as defined in fig. 6.1b. Comparison of SIF solutions for this geometry with those of equivalent

semi-finite, stiffened and unstiffened plane geometry solutions ('$Y_S^S(a)$' and '$Y_U^S(a)$' respectively) in the form of eq. 6.2 allows calculation of the notch interpolation factor. Eq 6.2 is an interpolation equation expressed in the form of normalised SIFs, which is applicable when parity of crack-line stress distributions is available for all geometries. A more general case applicable for instances where this condition is not met necessitates usage of an interpolation equation, of the same form, based upon constituent geometry weight functions or weight function coefficients. A rigorous study of step notches utilising this approach requires analysis of the semi-finite step notch geometry using finite element methods similar to that conducted in chapter 5.

The step notch like the symmetric V-notch is a special case of a more generalised intrusion notch. Notch width, 'L_I' is equal to infinity for the step notch and zero for the symmetric notch. Chapter 4 contained a discussion of a relationship between the two extreme intrusion notch types. It stated that since a single flank contributes to the stiffening effect of the notch upon the crack for a step notch, as opposed to two flanks for the equivalent symmetric notch the stiffening effect of a step notch is half that of an equivalent symmetric notch. An interpolation equation based upon this observation was suggested and is of the form given below.

$$m_N^F(a,x) = \frac{1}{2}\left[f(a)m_U^F(a,x) + (1-f(a))m_S^F(a,x)\right] + \frac{1}{2}m_U^F(a,x) \qquad \text{- (6.3)}$$

$$f(a) = \frac{Y_N^S(a) - Y_S^S(a)}{Y_U^S(a) - Y_S^S(a)} \qquad \text{- (6.4)}$$

'$Y_N^S(a)$' is an SIF solution for an equivalent semi-finite symmetric notch geometry, fig. 6.1c.

Eq. 6.3 indicates additional versatility within the interpolation scheme permitting the generation of SIF solutions for a wider range of notch profiles from the relatively small 'library' of symmetric geometry types. Full application of this principle is not included here however, implementation of the procedure in this section, for step notches, constitutes a demonstration of the concept. SIF solutions for asymmetric notches composed of two symmetric notches, as shown in fig. 6.2 may be calculated by application of a factor equal to one half to each crack stiffness, expressed as a weight function interpolation scheme (eq. 6.5a). Asymmetric notches, which are comprised of two symmetric notches, are termed compound notches. This gives rise to the form of expression presented as eq. 6.5b, in which subscripts '1' apply to a general symmetric notch, '2' to a V-Notch and '3' to a compound asymmetric notch composed of '1' and '2'.

$$m_{N3}^{F}(a,x)=\frac{1}{2}m_{N1}^{F}(a,x)+\frac{1}{2}m_{N2}^{F}(a,x) \qquad \text{- (6.5a)}$$

$$m_{N3}^{F}(a,x)=\frac{1}{2}\left[f_1(a)m_U^F(a,x)+(1-f_1(a))m_S^F(a,x)\right]+\frac{1}{2}\left[f_2(a)m_U^F(a,x)+(1-f_2(a))m_S^F(a,x)\right] \qquad \text{- (6.5b)}$$

An extension to this theme, which views an asymmetric or compound notch as being comprised of two symmetric notches is also described, however not implemented. It may be applied to a group of compound notches comprised of two symmetric notches of differing global stiffness. Two representative examples of compound notches, which adhere to this description, are given in fig. 6.3. As previously stated an appropriate interpolation scheme applies an equal weighting of one half to an interpolation equation written for each symmetric geometry.

$$m_{N3}^{F}(a,x)=\frac{1}{2}\left[f_1(a)m_U^F(a,x)+(1-f_1(a))m_{S1}^F(a,x)\right]+\frac{1}{2}\left[f_2(a)m_U^F(a,x)+(1-f_2(a))m_{S2}^F(a,x)\right] \qquad \text{- (6.6)}$$

The two interpolation equations, which make up eq. 6.6, utilise the unstiffened base geometry weight function '$m_U{}^F(a,x)$', and geometry weight functions of differing stiffness '$m_{S1}{}^F(a,x)$' and '$m_{S2}{}^F(a,x)$'. Fig. 6.4 depicts the three base geometry solutions required for implementation of the interpolation scheme given by eq. 6.6 and applicable to the notches shown in fig. 6.3. Fig. 6.3 shows only two examples of this notch type, however, the ability exists to exploit this procedure to yield useful SIF solutions for a large number of notch profiles from a small 'library' of symmetric notch constituent geometry solutions.

6.2 – An Interpolated Weight Function Solution for Step Notched Components

The interpolated weight function scheme applied in this chapter seeks to take advantage of a procedure utilising the equivalent symmetric notch constituent geometry solutions determined in chapter 5. Interpolation factors defined as '$f_1(a)$' for the general symmetric notch and '$f_2(a)$' for the V-notch are applied in an interpolation of base geometry weight functions given by eq. 6.7

$$m_{N3}^{F}(a,x)=\frac{f_1(a)+f_2(a)}{2}m_U^F(a,x)+\left(1-\frac{(f_1(a)+f_2(a))}{2}\right)m_S^F(a,x) \qquad \text{- (6.7)}$$

$$f_1(a)=\frac{m_{N1}^S(a,x)-m_S^S(a,x)}{m_U^S(a,x)-m_S^S(a,x)} \qquad f_2(a)=\frac{m_{N2}^S(a,x)-m_S^S(a,x)}{m_U^S(a,x)-m_S^S(a,x)} \qquad \text{- (6.7a,b)}$$

The step notch geometry is a compound notch shown in fig. 6.2a) to comprise a V-notch, for which interpolation factors '$f_2(a)$' were ascertained via constituent geometry solutions in chapter 5, and an unstiffened geometry, for which '$f_1(a)$' is equal to unity. Eq. 6.7 reduces to the form of interpolation equation expressed as eq. 6.3.

An analysis of a number of step notches of geometric forms equivalent to the symmetric notches defined in fig. 5.5 requires no new constituent geometry solutions. Derivation of new SIF solutions via eq. 6.5 is economic, as only knowledge of the finite thickness geometry's crack-line stress distribution is required. Interpolation factors are determined by comparison of constituent geometry normalised SIFs.

$$f_1(a) = \frac{Y_{N1}^S(a) - Y_S^S(a)}{Y_U^S(a) - Y_S^S(a)} = \frac{Y_U^S(a) - Y_S^S(a)}{Y_U^S(a) - Y_S^S(a)} = 1 \qquad \text{- (6.8a)}$$

$$f_2(a) = \frac{Y_{N2}^S(a) - Y_S^S(a)}{Y_U^S(a) - Y_S^S(a)} \qquad \text{- (6.8b)}$$

Application of interpolation factors to the two base geometry weight functions, as dictated by eq. 6.7, yields a weight function for the finite thickness notched geometry. Integration with a finite thickness, crack-line stress distribution permits new SIF solutions, for this geometry, to be determined.

$$Y_{N3}^F(a) = \int_0^a \frac{\sigma_{yy}^F}{\sigma_o} m_{N3}^F(a,x)dx \qquad \text{- (6.9)}$$

6.3 – Loading Considerations

Common to the analysis conducted on symmetrically notched components the weight function methodology is to be verified by the application of remote boundary loading simulating modes of bending and tension. Application of tensile loads to remote boundaries of the step notch configuration requires an additional bending moment to be present to ensure equilibrium requirements are satisfied.

Chapter 4 described two tensile loading arrangements: one termed pure tension, which results in no net bending stress component in the plane of the crack and another termed uniform tension, which gives rise to a net bending in the plane of the crack. These two loading arrangements are different loading modes and the definition adopted in chapter 4 is consistent with that utilised in

this and other chapters of this thesis. Fig. 6.6 shows the nominal stress, or characteristic stress, present when subjected to pure tension, 'σ_{to}' or uniform tension, 'σ_{To}'.

Application of the pure bending loading mode results in a different magnitude of nominal stress in the two remote sections of thickness 'T' and 't'. A constant bending moment is present in both thick and thin remote sections of the step notch geometry. SIF solutions and stress distributions are identical, but normalised to a different characteristic stress. One may be simply converted to the other by application of the fundamental beam bending equation below to give a relation between characteristic (extreme fibre) stress in the thicker section, 'σ_{To}' and the thinner section, 'σ_{to}' as shown below.

$$\frac{M}{I} = \frac{\sigma_o}{y} \qquad \text{- (6.10)} \qquad\qquad \sigma_{To} = \frac{t^2}{T^2}\sigma_{to} \qquad \text{- (6.11)}$$

6.4 – Finite Thickness SIF Solutions

The finite element method was employed to generate SIF solutions for step notched, finite thickness geometries to validate the new solutions obtained via the weight function method. Finite thickness SIF solutions were generated for the range of notch shapes and sizes depicted in fig. 6.5 subject to the three loading modes described above. The step notch represents a mixed mode crack problem and thus the mode I SIF was ascertained as described in chapter 3, section 3.4.3. The solutions are presented in a tabular format confined to appendix A. Pure bending stress distributions are normalised to the nominal stress, 'σ_{To}'.

6.5 – Finite Thickness Stress Distributions

Implementation of a weight function scheme to determine new SIF solutions for the notched, finite thickness geometries subject to a given loading mode requires the crack-line stress distribution arising in the uncracked geometry when subject to that loading mode. The weight function interpolation scheme described here is to be tested under loading modes of uniform tension, pure tension and pure bending.

Stress distributions arising in the plane of the crack when subject to each loading mode can be accurately modelled by the form of equation utilised in previous chapters of this thesis

$$\frac{\sigma_{yy}(x)}{\sigma_o} = P_5\left[\frac{1}{(1+x/t)}\right]^5 + P_4\left[\frac{1}{(1+x/t)}\right]^4 + P_3\left[\frac{1}{(1+x/t)}\right]^3 + P_2\left[\frac{1}{(1+x/t)}\right]^2 + P_1\left[\frac{1}{(1+x/t)}\right] + P_0 \qquad \text{- (6.12)}$$

Validity: $0 < x/t < 0.5$

Coefficients 'P_x' are presented in tabs. 6.1 – 6.3 for the loading modes of pure tension, pure bending and uniform tension respectively.

6.6 – A Weight Function Solution

This chapter has described a methodology of enhanced economy, for the determination of new SIF solutions for step notches, via an interpolation technique. Inspection of eqs. 6.1 and 6.7, which may both be applied to the notches depicted in fig. 6.2, indicates that the interpolation factor for the more intricate compound notch, given subscript '3' maybe ascertained from the two symmetric notch interpolation factors, given subscripts '1' and '2' as defined below.

$$f_3(a) = \frac{f_1(a) + f_2(a)}{2} \quad \text{- (6.13)}$$

For a step notch this equation can be combined with eqs. 6.8a and 6.8b to give the following expression.

$$f_3(a) = \frac{1}{2} + \frac{Y_{N2}^S(a) + Y_S^S(a)}{2(Y_U^S(a) + Y_S^S(a))} \quad \text{- (6.14)}$$

A comparison of the interpolation factor for a step notch (b/ρ = 6, α = 45°, b/T = 0.2727) obtained using eq. 6.14 and from the finite element solutions first presented in fig. 4.9 is presented as fig. 6.7. Interpolation factors obtained from both methodologies show a close correlation, indicating that the observations utilising symmetric notch constituent geometry SIF solutions, first made in chapter 4, for step notches is valid. It suggests that the broader application, to compound notches, developed in this chapter is also valid.

The influence of application of an interpolation factor can be made by integration of the finite thickness, notched geometry stress distribution with each base geometry weight function in a manner similar to that described in section 5.5.

$$Y_{N3}^F(a) = f_3(a)\int_0^a \sigma_{yy}^F(x) m_U^F(a,x)dx + (1 - f_3(a))\int_0^a \sigma_{yy}^F(x) m_S^F(a,x)dx \quad \text{- (6.15)}$$

$$Y_{N3}^F(a) = f_3(a)Y_U^F + (1 - f_3(a))Y_S^F \quad \text{- (6.16)}$$

Extreme geometry SIF solutions are shown in fig 6.8 for a remotely applied uniform tension loading condition together with the interpolation factor for the intermediate step notch geometry defined by: $b/\rho = 6$, $\alpha = 45°$, $b/T = 0.2727$. Application of the interpolation factor to the extreme solutions and their subsequent summation is depicted in fig. 6.9. Also presented on each figure are SIF solutions for a remotely applied uniform tension loading condition determined from finite element analysis. The solutions derived through application of an interpolation scheme as defined in this chapter show an excellent correlation to those obtained from finite element methods.

New step notch geometry SIF solutions were simply calculated for each geometry defined in the matrix depicted in fig. 6.5 subject to the three loading modes described in section 6.3. Their comparison with finite element solutions provides a further validation of the interpolation scheme and the observations made in this chapter.

6.7 – Discussion of Results

The scope of work contained in this chapter concerns the application of an interpolated weight function scheme to determine mode I SIF solutions for step notched, finite thickness, two-dimensional geometries. The weight function interpolation scheme described, using notched constituent geometry solutions determined in chapter 5 for equivalent symmetric notches was applied to determine SIF solutions for step notches in finite thickness geometries. The scheme constitutes a process of enhanced economy, with respect to the interpolation scheme using semi-finite, step notch constituent geometries, as the only additional information required to formulate new SIF solutions is that of the crack-line stress distribution in the notched, finite thickness geometry.

A matrix of symmetric notch constituent geometry solutions covering a wide range of geometric parameters determined in chapter 5 was available allowing a similar broad ranging study to be undertaken for the step notch. Finite thickness crack-line stress distributions for the applied loading modes of pure and uniform tension and pure bending were calculated permitting new SIF solutions for the notched finite thickness geometry under these modes to be derived.

Figs. 6.10 – 6.16 show the new SIF solutions obtained from the interpolation scheme alongside those obtained from the finite element method. Each figure shows a series of SIF solutions, for a given loading mode, depicting variation of a single geometric parameter. Each weight function SIF solution displays an excellent correlation to the finite element data indicating once more the robust and versatile nature of the interpolation scheme. The weight function methodology has been shown to remain stable over the entire, broad range of notch geometries investigated.

The step notch geometry may be used to approximate a number of frequently encountered structural details such as welded joints, threaded connections and general shoulders and fillets. The methodology presented here provides design engineers with a powerful analysis tool enabling design engineers, and those concerned with the structural integrity of such components, to calculate new SIF solutions. Advantages of the interpolated weight function technique stem from the capability to produce solutions that are accurate and determined rapidly by a process, which is versatile, stable and readily implemented by a simple computer-based algorithm.

6.8 – Conclusions

New SIF solutions for step notched geometries have been determined by application of an interpolated weight function approach. The solutions obtained correlate well to those derived from finite element methods and offer a further validation of the methodology. The universal applicability of the interpolation scheme to external notches of any profile in two-dimensional components has been confirmed and therefore constitutes a more 'complete' solution than that offered by the composition scheme. An additional versatility of interpolation scheme has been demonstrated, that allows certain asymmetric notch types, termed compound notches, to be modelled using constituent geometry solutions of symmetric notches. This chapter has only applied this scheme of increased economy to the step notch, which was identified as a compound notch comprising a V-notch and an unstiffened notch. Scope exists to apply the same technique to analyse numerous commonly sought notch profiles and generate, rapidly and simply, a large number of useful SIF solutions from a small 'library' of constituent geometry solutions.

6.9 – Tables

Tab. 6.1 – Normalised Stress Distribution, '$\sigma_{yy}(x)/\sigma_o$' Coefficients for Usage in eq. 6.12 (Pure Tension)

α	b/ρ	b/T	P_5	P_4	P_3	P_2	P_1	P_0
15	6	0.2727	-1.8949	7.8524	-10.467	6.557	-1.565	1.071
30	6	0.2727	-5.1298	15.896	-18.114	10.507	-2.510	1.126
45	6	0.2727	15.122	-52.929	72.573	-45.505	16.434	-0.1128
90	6	0.2727	-5.6202	16.654	-18.651	11.086	-2.759	1.145
45	1	0.2727	-3.6637	13.373	-18.653	14.004	-5.689	1.898
45	3	0.2727	-4.1006	13.143	-16.062	10.665	-3.400	1.319
45	10	0.2727	-7.2282	20.686	-21.883	11.752	-2.282	1.056
45	15	0.2727	-8.4299	23.395	-23.670	11.893	-1.814	1.003
45	6	0.0625	-0.2977	-0.6977	3.2897	-1.6967	1.659	1.029
45	6	0.1875	6.4732	-23.203	32.401	-19.366	7.3792	0.740
45	6	0.3125	17.827	-63.907	90.059	-58.814	21.867	-0.757
45	6	0.4375	29.358	-113.88	175.31	-128.94	52.979	-5.313

Tab. 6.2 – Normalised Stress Distribution, '$\sigma_{yy}(x)/\sigma_{To}$' Coefficients for Usage in eq. 6.12 (Pure Bending)

α	b/ρ	b/T	P_5	P_4	P_3	P_2	P_1	P_0
15	6	0.2727	13.252	-42.194	54.21	-34.775	12.043	-0.953
30	6	0.2727	14.073	-46.456	60.555	-38.152	12.913	-1.070
45	6	0.2727	23.055	-78.339	103.96	-65.714	22.649	-1.888
60	6	0.2727	26.045	-87.615	114.25	-70.605	23.678	-1.974
90	6	0.2727	15.147	-50.413	64.878	-39.535	13.011	-1.084
45	1	0.2727	3.3982	-18.194	37.550	-37.398	20.132	-4.197
45	3	0.2727	8.8689	-33.136	49.136	-35.535	14.096	-1.793
45	10	0.2727	20.106	-63.272	76.419	-43.087	12.854	-0.735
45	15	0.2727	24.619	-75.029	86.923	-46.335	12.918	-0.516
45	6	0.0625	33.214	-96.555	105.21	-51.354	12.516	-0.004
45	6	0.1875	29.614	-93.318	113.05	-64.014	19.105	-1.085
45	6	0.3125	27.068	-92.673	124.21	-79.867	27.877	-2.646
45	6	0.4375	46.955	-165.07	228.99	-155.31	56.747	-7.041

Tab. 6.3 – Normalised Stress Distribution, '$\sigma_{yy}(x)/\sigma_o$' Coefficients for Usage in eq. 6.12 (Uniform Tension)

α	b/ρ	b/T	P_5	P_4	P_3	P_2	P_1	P_0
45	6	0.0625	-6.5393	17.482	-16.582	7.9579	0.7414	0.971
45	6	0.1875	-6.5190	18.708	-19.848	10.820	-2.149	1.054
45	6	0.2727	-5.6831	16.982	-19.053	11.204	-2.754	1.144
45	6	0.3125	-5.1939	15.804	-18.151	11.046	-2.935	1.186
45	6	0.4375	-4.0684	13.087	-16.052	10.703	-3.448	1.331

6.10 – Figures

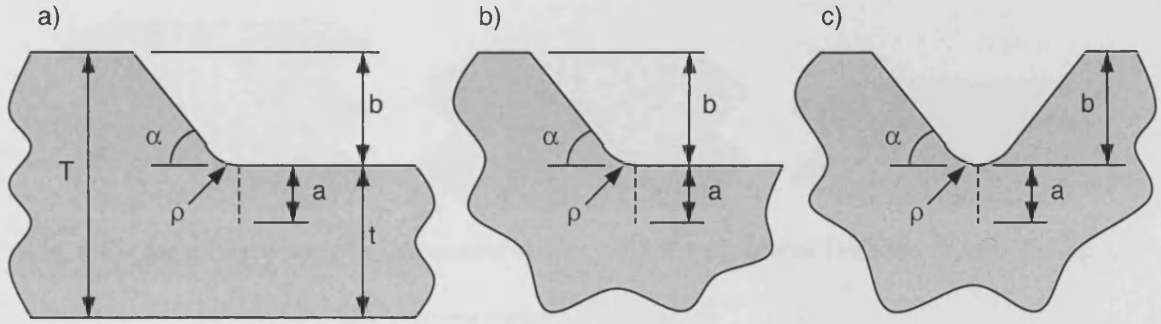

Fig. 6.1 – Geometric Definition of a) Finite Thickness Step Notch b) Semi-Finite Thickness Step Notch and c) Equivalent Semi-Finite Thickness Symmetric Notch

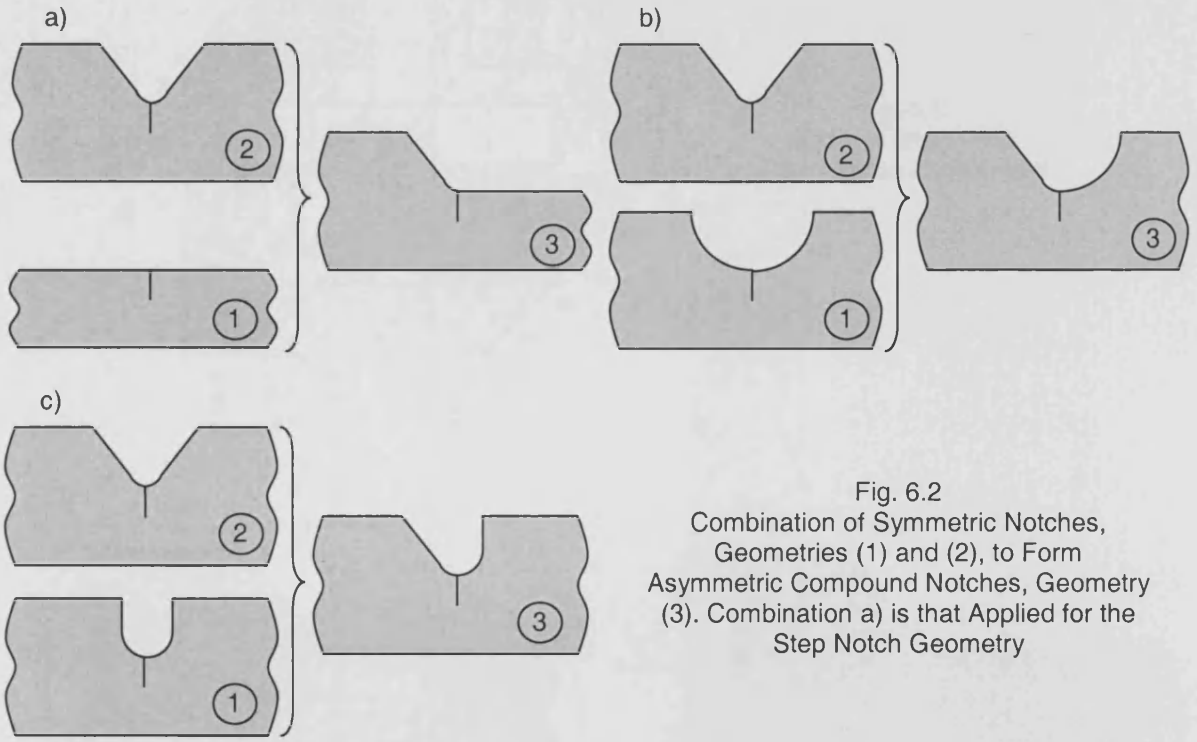

Fig. 6.2
Combination of Symmetric Notches, Geometries (1) and (2), to Form Asymmetric Compound Notches, Geometry (3). Combination a) is that Applied for the Step Notch Geometry

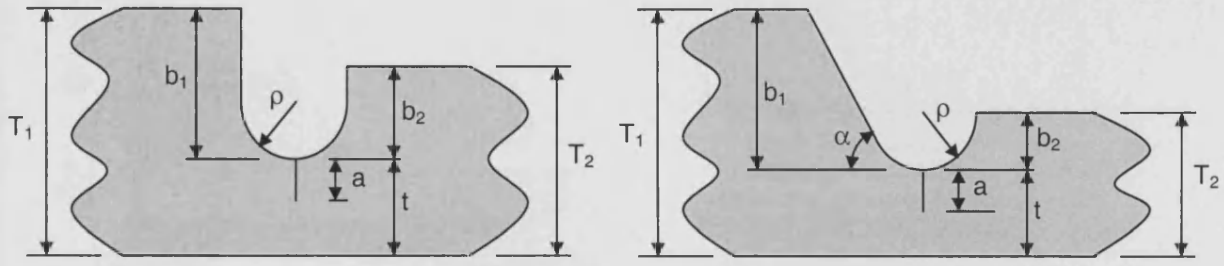

Fig. 6.3 – Asymmetric Compound Notches Formulated from Two Symmetric Notches of Differing Global Stiffness

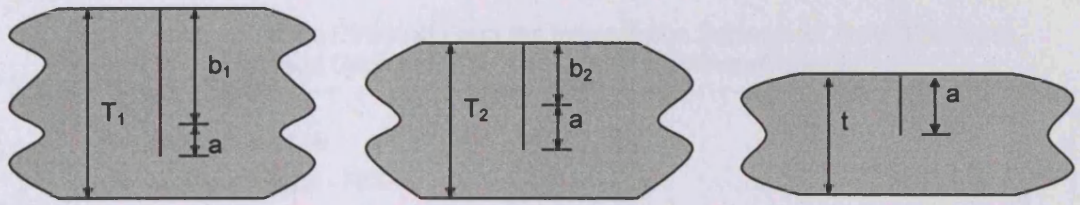

Fig. 6.4 – Base Geometries for Compound Notches of Differing Global Stiffness depicted in Fig. 6.3

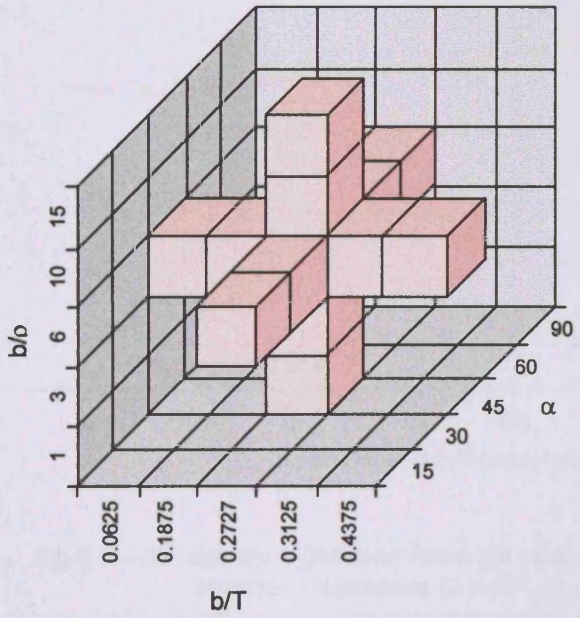

Fig. 6.5
Matrix of Step Notch
Geometeries investigated

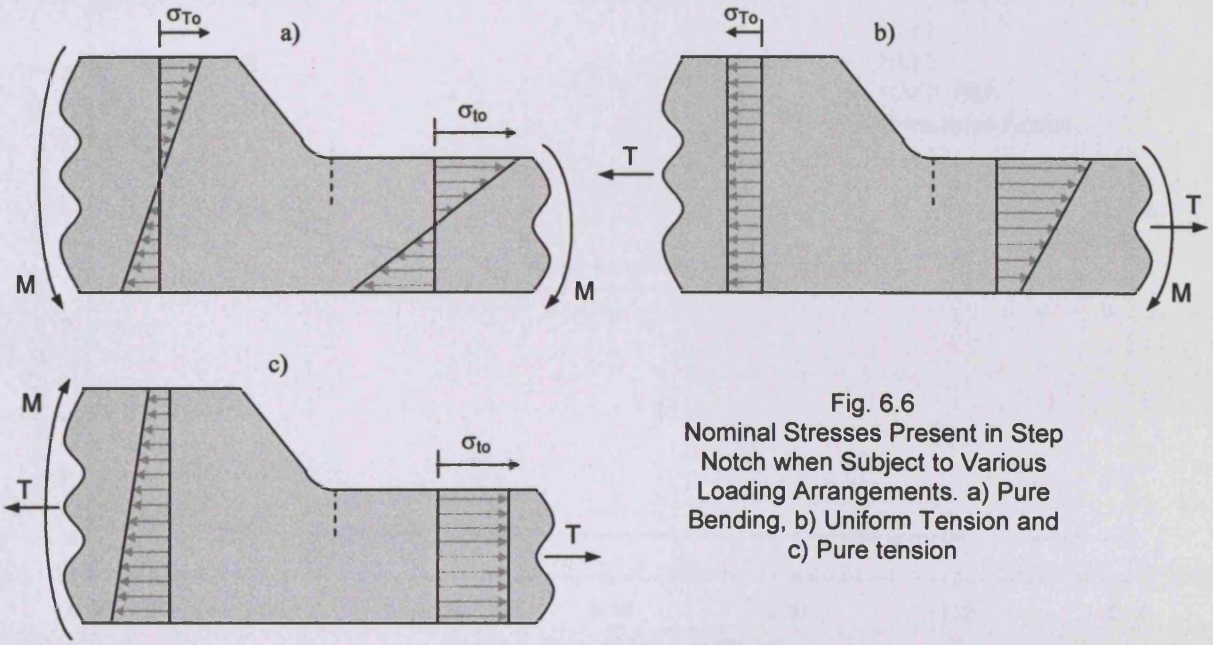

Fig. 6.6
Nominal Stresses Present in Step Notch when Subject to Various Loading Arrangements. a) Pure Bending, b) Uniform Tension and c) Pure tension

Fig.6.7 – SIF Solutions Obtained From the Interpolation Scheme for Finite Thickness, Notched Geometries (α = 45°, b/ρ = 6, Uniform Tension)

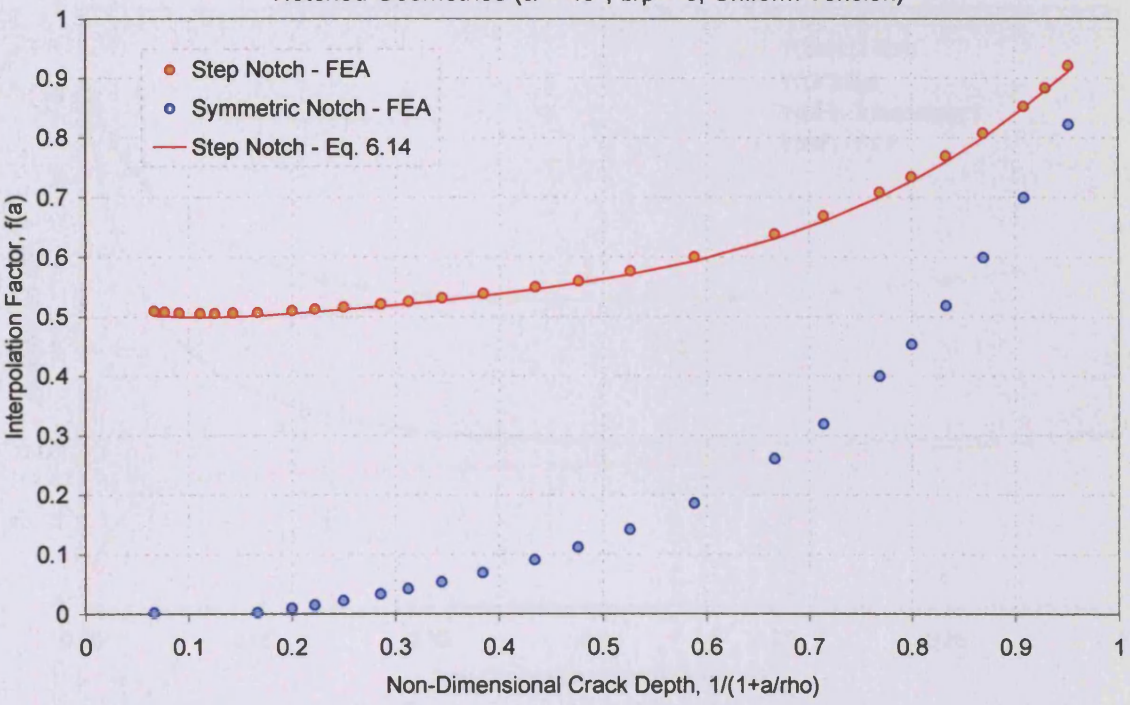

Fig.6.8 – SIF Solutions Obtained From the Interpolation Scheme for Finite Thickness, Notched Geometries (α = 45°, b/ρ = 6, Uniform Tension)

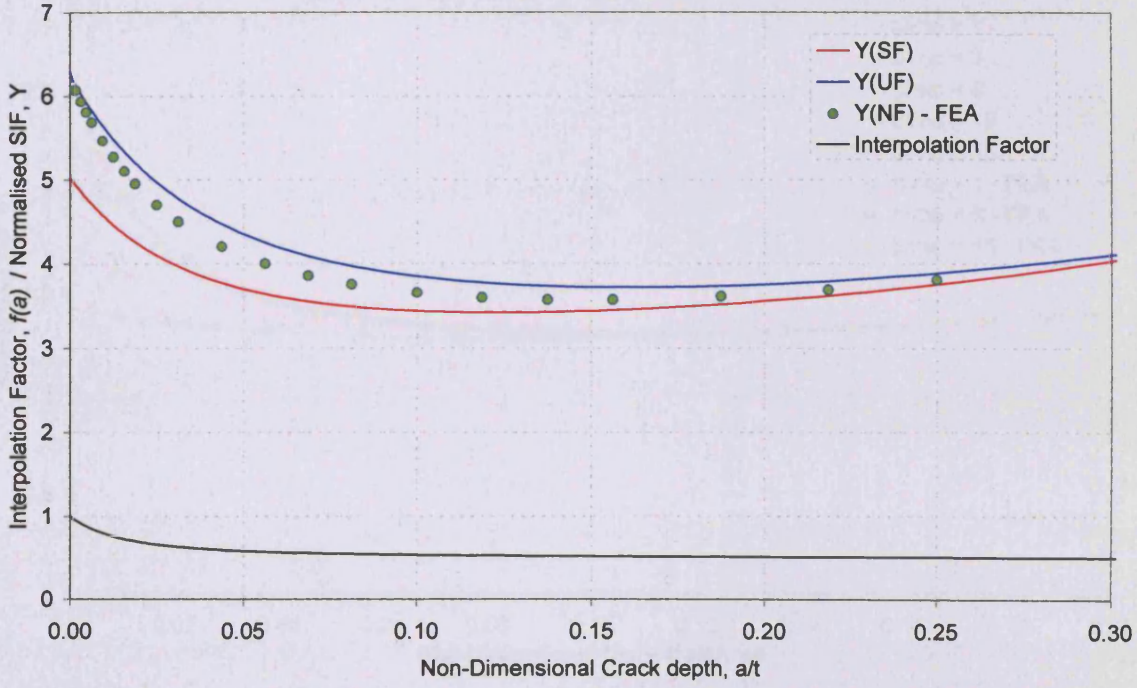

Fig. 6.9 – SIF Solutions Obtained From the Interpolation Scheme for Finite Thickness, Notched Geometries (α = 45°, b/ρ = 6, Uniform Tension)

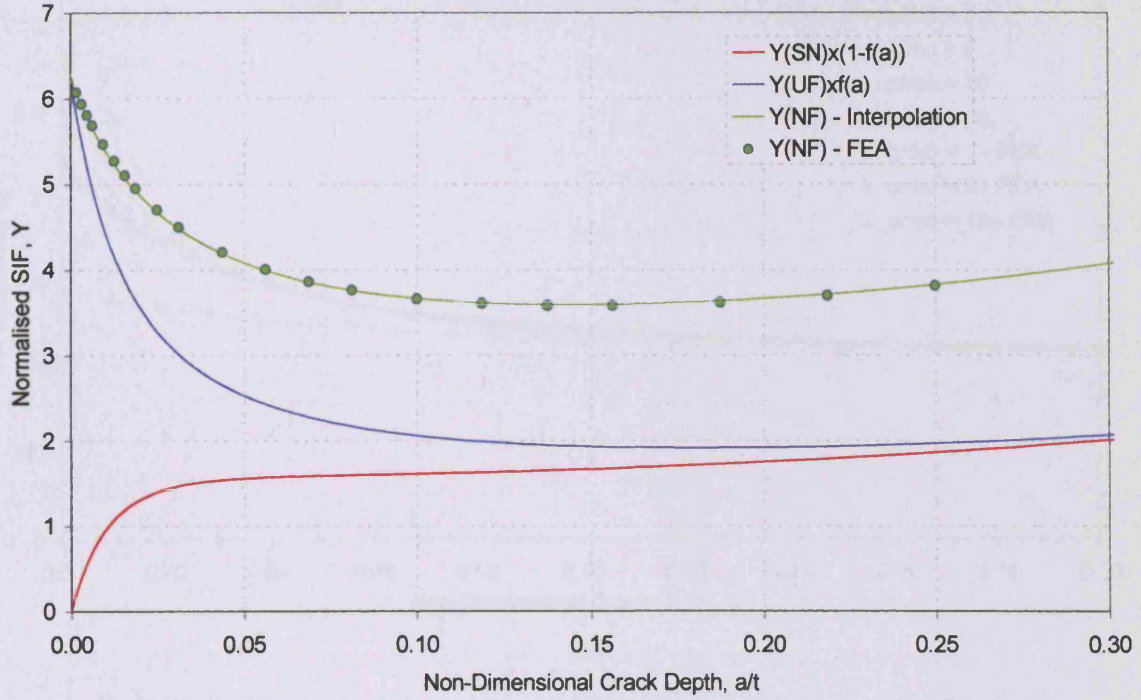

Fig. 6.10 – SIF Solutions Obtained From the Interpolation Scheme for Finite Thickness, Notched Geometries (α = 45°, b/ρ = 6, Pure Tension)

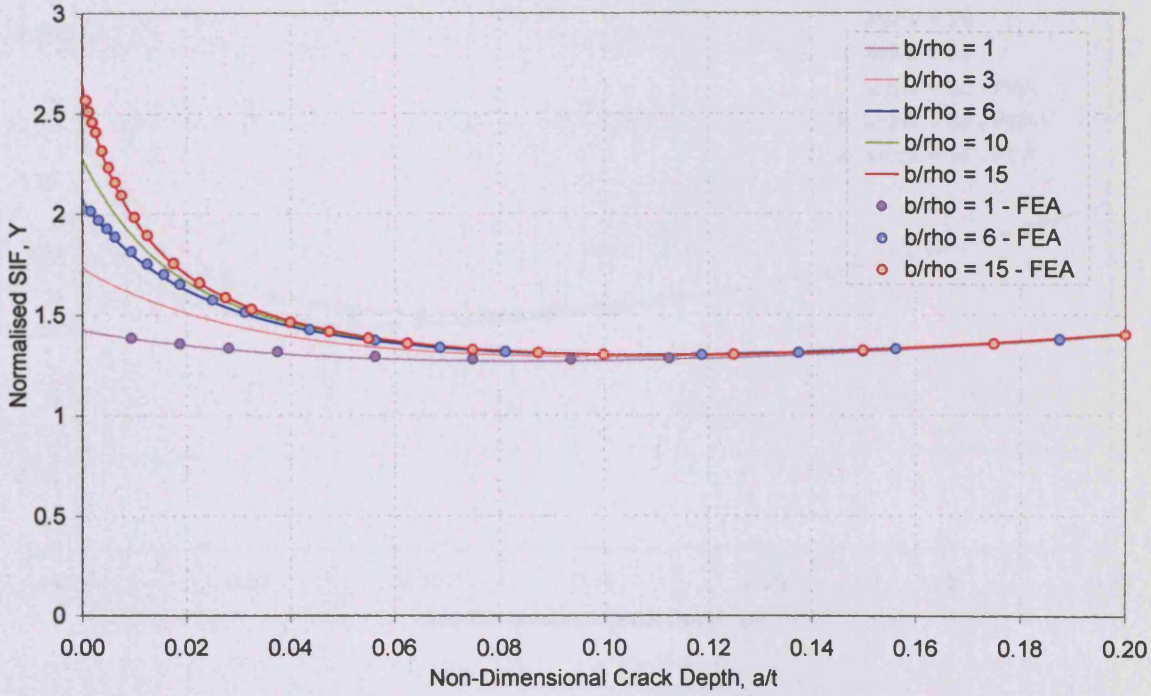

Fig.6.11 – SIF Solutions Obtained From the Interpolation Scheme for Finite Thickness, Notched Geometries (α = 45°, b/T = 0.2727, Pure Bending)

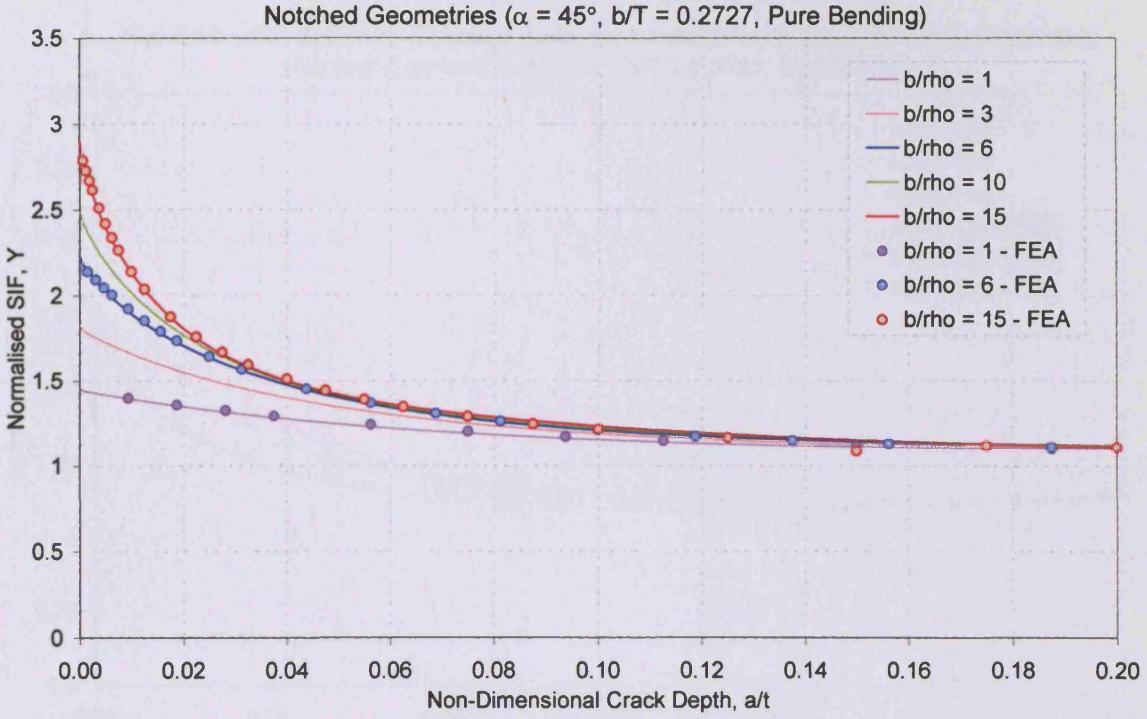

Fig.6.12 – SIF Solutions Obtained From the Interpolation Scheme for Finite Thickness, Notched Geometries (b/ρ = 6, b/T = 0.2727, Pure Tension)

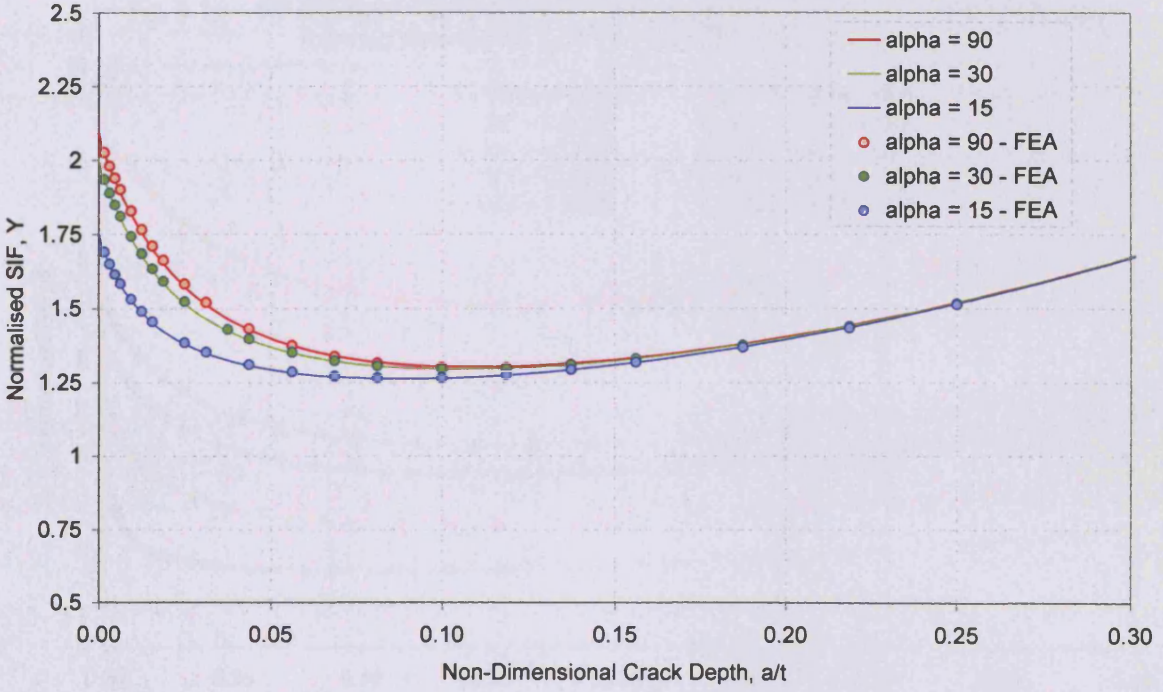

Fig. 6.13 – SIF Solutions Obtained From the Interpolation Scheme for Finite Thickness, Notched Geometries (b/ρ = 6, b/T = 0.2727, Pure Bending)

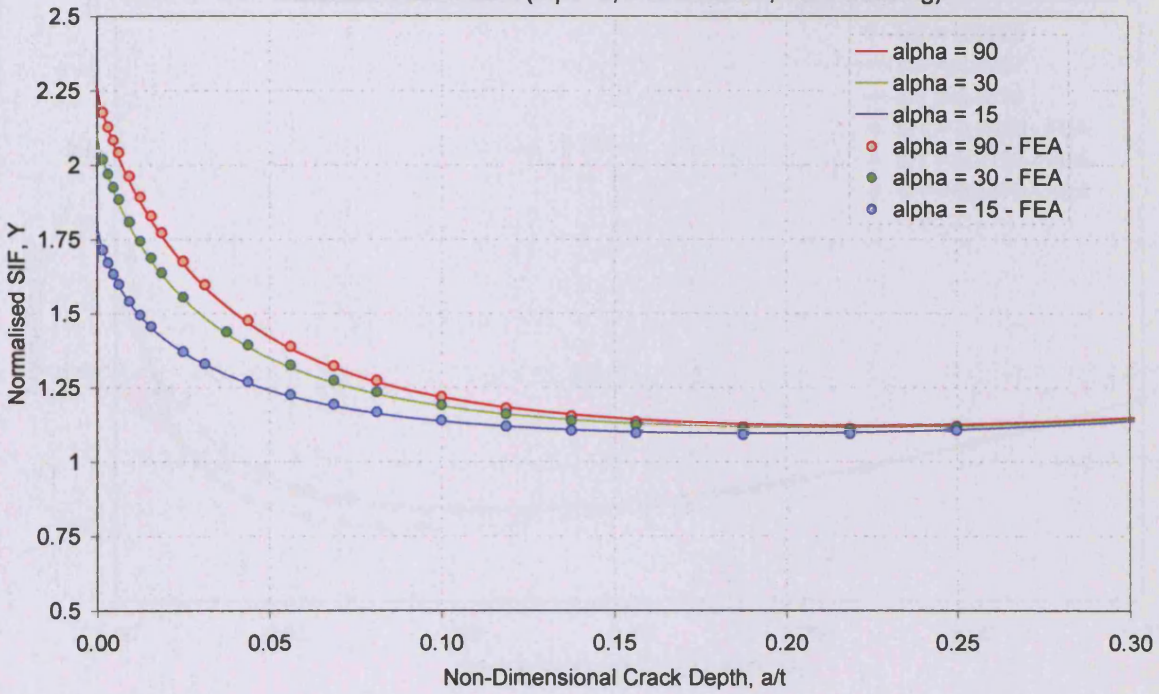

Fig. 6.14 – SIF Solutions Obtained From the Interpolation Scheme for Finite Thickness, Notched Geometries (α = 45°, b/ρ = 6, Uniform Tension)

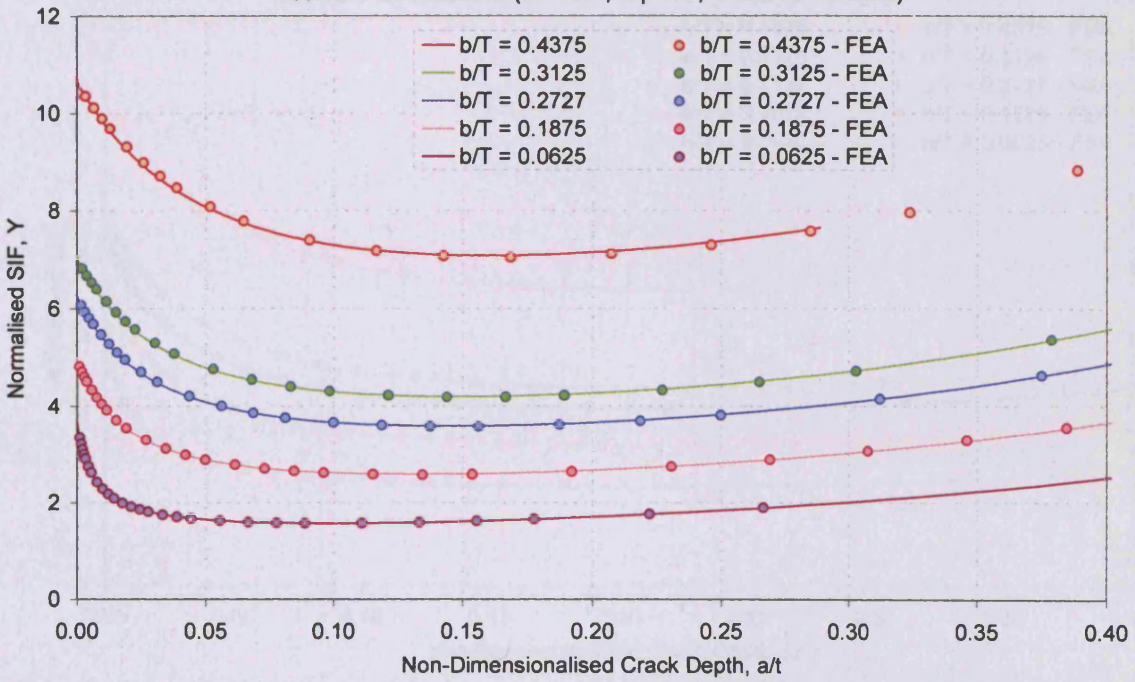

Fig. 6.15 – SIF Solutions Obtained From the Interpolation Scheme for Finite Thickness, Notched Geometries (α = 45°, b/ρ = 6, Pure Tension)

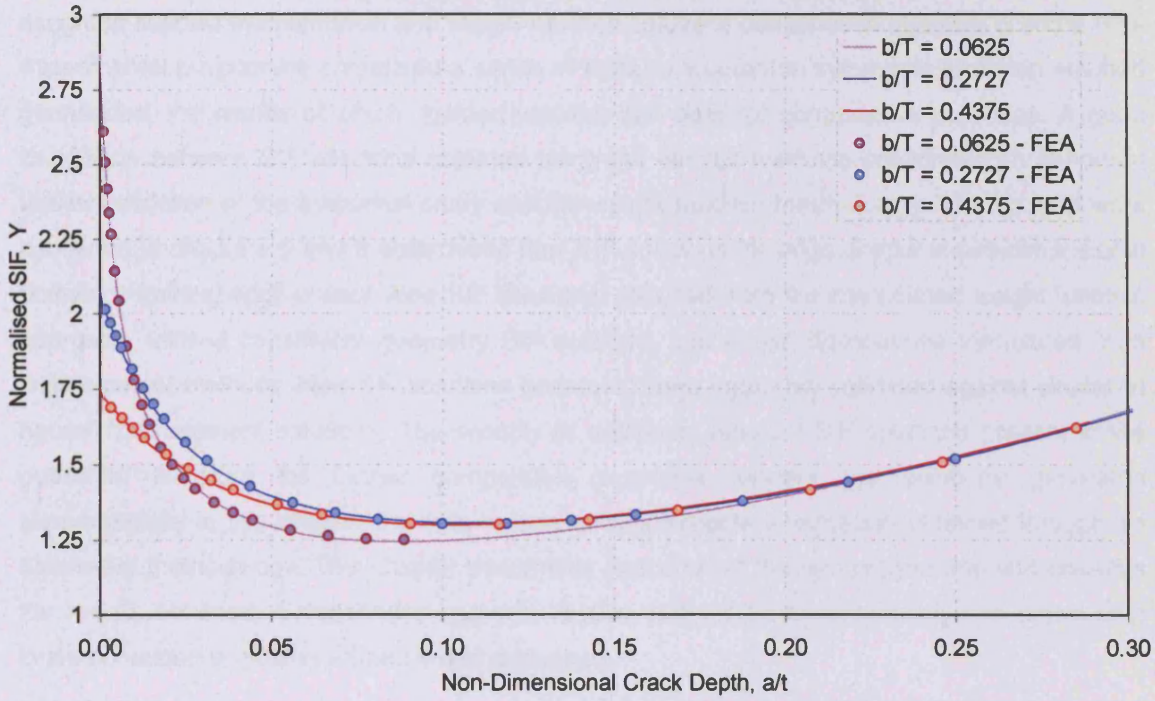

Fig. 6.16 – SIF Solutions Obtained From the Interpolation Scheme for Finite Thickness, Notched Geometries (α = 45°, b/ρ = 6, Pure Bending)

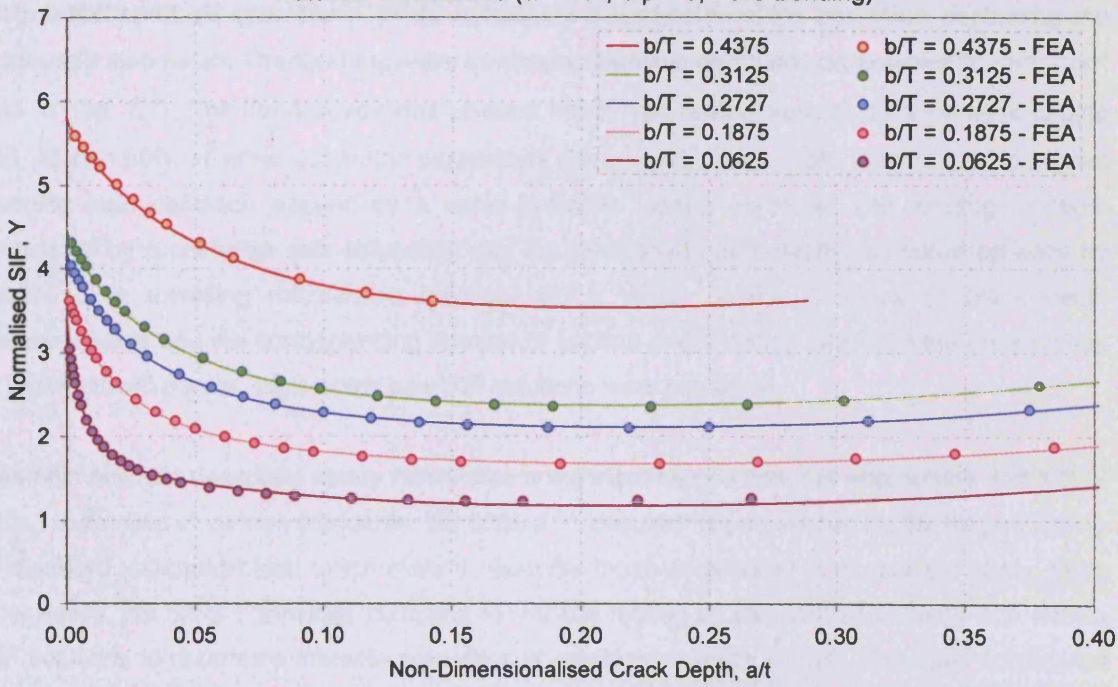

Chapter 7 - Experimental Determination of SIF Solutions

Experimentally derived SIF solutions for the symmetric and step notch geometry types were sought to support the numerical and weight function solutions contained in chapters 5 and 6. The experimental programme comprised a series of tests conducted on symmetric and step notched geometries, the results of which, yielded valuable SIF data for comparative purposes. A good correlation between SIF solutions obtained using the various methods constitutes an important further validation of the numerical study and the weight function methodology. The body of work contained in chapters 5 and 6 determined new SIF solutions for edge cracks in two-dimensional bodies containing edge cracks. New SIF solutions, obtained from the interpolated weight function approach, utilised constituent geometry SIF solutions and stress distributions formulated from finite element methods. New SIF solutions generated were rigorously validated against similar 'in house' finite element solutions. The scarcity of additional relevant SIF solutions present in the published literature for further comparative purposes renders the solutions generated experimentally in this chapter the sole means of supplementary validation obtained through an alternative methodology. This chapter documents execution of the test programme and presents the results obtained. Comparisons between results determined experimentally are drawn with those contained in chapters 5 and 6 and discussed.

7.1 – Introduction

An experimental programme was devised to allow the quantification of SIF solutions through the fatigue testing of six specimens. Three containing a symmetric notch and three containing the equivalent step notch. The term equivalent indicates identical geometric parameters 'T', 'b/T', 'ρ/T' and 'α' (fig. 7.1). The three specimens of each notch type tested were of differing flank angles (30, 45 and 60°); all other geometric parameters were equal. These were subject to a four-point bending load condition applied by a servo-hydraulic testing machine. The loading function, generated by a controller was sinusoidal and the developed crack depth measured optically by means of a travelling microscope mounted on a vernier scale. A series of crack depth measurements and the corresponding number of applied stress cycles permitted the construction of crack growth curves, from which new SIF solutions were extracted.

The brief account described above constitutes a standard fatigue test, the appropriate conduct of which is detailed in various standards. BS 6835-1[7.1] documents procedures for the fatigue testing of standard test specimens, which closely resemble those considered in the current study. More specifically, BS 6835-1 provides guidance for fatigue testing of standard specimens with known SIF solutions to determine material properties characterising crack growth. The tests considered here utilise known material data to calculate unknown SIF solutions. Specimen design,

apparatus, procedure and data manipulation techniques, however remain changed, hence guidance from this source was adhered to on such matters where possible.

7.2 – Specimen Design and Fabrication

This section describes the design of the specimens, based upon guidance given for similar SNEB4 specimens as given in various standards[7.1,7.2]. The standard fatigue test specimen SNEB4 is a single edge cracked strip subject to four point bending and is the standard fatigue specimen which offers the closest approximation to the geometries under investigation in this study. The three limitations on specimen size are categorised as follows by the British Standards Institute[7.1,7.2]

- Absolute Limits:

$$T > 10mm \qquad B \geq 2mm \qquad \text{- (7.1a,b)}$$

- Limits on Specimen Proportions:

$$1 \leq T/B \leq 5 \qquad \text{- (7.2)}$$

- Limits Related to Mechanical Properties:

$$B \geq r_P \qquad a \geq r_P \qquad \frac{a}{T} < \left(1 - \frac{S_P}{T}\right) \qquad \text{- (7.3a,b,c)}$$

where, 'r_P' is the plastic zone size, given by eq. 7.4, and 'S_P', given by eq. 7.5, relates to the crack size at which net section yielding is expected.

$$r_P = \left(\frac{K_{max}}{\sigma_Y}\right)^2 \qquad \text{- (7.4)} \qquad \frac{S_P}{T} = \sqrt{\frac{F_{max} L_2}{0.63 \sigma_f B T^2}} \qquad \text{- (7.5)}$$

In addition to the specimen size requirements detailed above the standards give guidance on the application of loading for the SNEB4 specimen which is reproduced in figs. 7.2 and 7.3.

Further to the specimen design considerations contained in standards, the specimen size is constrained by the test machine dimensions and, to a certain degree, the test-rig components readily available. Also available are off-cuts from cold rolled plates of BS 7191 355D[7.3] (Tabs. 7.1 and 7.2), a high strength offshore steel, measuring 25mm in thickness and 400mm in length. Specimens were manufactured from such off-cuts and therefore specimen overall length was set to 400mm and thickness equal to 25mm. Specimens were designed to be of a size that allowed collection of sufficient SIF data over the range for which the notch has an influence and therefore the dimension, 'T' was made as large as possible within the other geometrical constraints. A notch depth or step height, 'b' of 30mm was selected to leave a minimum section thickness, 't' of

80mm at the position of the crack. With reference to fig. 7.3 the following length dimensions were selected to meet the requirements stated (L = 400mm; $L_1 = L_2$ = 80mm; L_3 = 170mm). A 25mm overhang is left either side of the outermost loading points.

The two notch types investigated were the symmetric and step notches as the numerical and analytical work documented in preceding chapters had shown there to be sufficient variation in SIF solutions between them, which was quantified experimentally. The three flank angles to be investigated were set at 30°, 45° and 60°. A projection of specimen form and definition of geometric parameters is depicted in fig. 7.4. The notch root radius was designed to be representative of those geometries modelled numerically and large enough to ensure that they could be fabricated accurately. The specimens were 'faced off' to remove surface imperfections and therefore improve the surface finish, which allowed the crack to be visible using optical crack detection apparatus. The thickness of the specimens is therefore reduced to 23mm. Further improvement to the surface finish was achieved through the polishing of the specimens to effect a 'mirror-like' finish against which the crack tip was clearly visible through the travelling microscope. Ultimate specimen dimensions selected are as summarised in tab. 7.3. Each specimen is titled in tab. 7.3 according to the notch forms of symmetric and asymmetric (step) types, 'S' and 'A' respectively and by the flank angle in degrees, '30, 45 and 60'. Expressed as non-dimensionalised geometric parameters ('b/ρ = 6' and 'b/T = 0.2727') the specimens are of the same form as those analysed in chapters 5 and 6 permitting direct comparison between results obtained.

It was judged prudent to perform a fatigue test on a plane specimen, titled, 'A' to gain sufficient proficiency in machine operation and test procedure prior to conducting tests on the notched specimens. An additional test specimen was required, which adhered to requirements listed in this and the preceding section. The test specimen was designed to be of comparable size to the notched specimens (23x80x400mm) and was fabricated from BS 7191 355D. In the absence of a notch the crack was initiated from a starter formed from a hacksaw groove approximately 6mm in depth. Successful execution of this test yielded information concerning the material properties of Paris Law exponent and coefficient. Since the SIF solutions for a plane strip in bending are known these properties can be evaluated and compared to those obtained from alternative sources. Availability of accurate material fatigue properties is of considerable importance when considering the quality of results, which were ultimately desired.

7.3 – Specimen Loading

Stress intensity range, 'ΔK' is the driving force governing crack growth, which is characterised empirically by a curve of crack growth rate, 'da/dN' versus stress intensity range, 'ΔK'. The linear

relationship describing the crack growth rate, region II of the familiar sigmoidal portion of the crack growth rate curve, was first suggested by Paris and Erdogan (eq. 7.3), and has gained wide acceptance for describing stable crack growth. Han[7.4] conducted similar crack growth experimentation on compact tension specimens fabricated from the same batch of material, BS 7191 355D, measuring the linear region that exists between approximately '$15\ MPa\ m^{1/2} > \Delta K > 100\ MPa\ m^{1/2}$'. This information was use in conjunction with the SIF data in chapters 5 and 6 to determine an appropriate magnitude of applied loading to ensure the crack initiated and propagated over the desired range (to 35mm in depth) without fracture occurring.

An expression, derived from the engineers' theory of beam bending was employed to relate applied loading to the nominal bending stress, given as eq. 7.6

$$\sigma_{To} = \frac{-6PL_1}{BT^2} \qquad \sigma_{to} = \frac{-6PL_1}{Bt^2} \qquad \text{- (7.6a,b)}$$

Tab. 7.4 summarises maximum and minimum loading, 'F', nominal stress, 'σ_o' and R ratio defined by eq. 7.7 utilised in each test.

$$R = \frac{F_{\min}}{F_{\max}} = \frac{\sigma_{\min}}{\sigma_{\max}} \qquad \text{- (7.7)}$$

Loads were applied to the specimens at the prescribed locations by rollers affixed rigidly to the test machine crossheads. The lower crosshead was mounted upon a pivot to alleviate alignment concerns and provide equal application of loading, therefore ensuring that in sections close to the notch a constant bending moment exists free from any shear loading components. Stresses utilised for the normalisation of results are the extreme fibre stresses present in the larger section, 'σ_{To}'. The loading arrangement described in summarised in fig. 7.5.

7.4 – Test Procedure

A 100kN servo-hydraulic actuator mounted within an Instron frame was used to apply loading to the fatigue test specimens. A Dartec 9600 Digital desk-top control console applied the stated loading to the specimens at a frequency of 1Hz. Each test was carried out in air at room temperature. Crack depth measurements were taken at approximately every quarter of a millimetre of growth using a travelling microscope. A rigid frame was constructed in which the travelling microscope was mounted allowing it to traverse in the vertical plane parallel to the direction of crack growth. A cycle counting function of the controller was employed to monitor the

number of applied stress cycles. Each test was continuous and was executed without significant interruption.

7.5 – Test Results

Fig. 7.6 depicts a number of successfully tested specimens giving a pictorial indication of their size and form. Upon completion of each test the crack surface was inspected to ensure that crack initiation and propagation had developed as desired. Initial tests conducted on the notched specimens showed that cracks initiated at several points and coalesced as crack size increased. Fig. 7.7a shows an example of this phenomenon. Calculation of the most valuable SIF solutions for a short edge crack is impaired by the presence of multiple initiation sites. Specimens for subsequent and repeated tests were scored at the notch root to ensure that the crack initiated from a single site. Fig. 7.7b shows the improved and desired short crack behaviour achieved by the presence of a small groove at the notch root.

Cracks developed in symmetrically notched components propagated via a path in the vertical plane at the notch root, however the crack paths generated in the asymmetric step notched geometries show a curvature. Various crack paths developed in both geometry types are displayed in fig. 7.8. The numerical and weight function analyses conducted in this study have assumed the crack to grow purely in the vertical plane only and therefore crack growth measurements for asymmetric geometries were, as for the symmetric notches, recorded in the vertical plane only.

The crack front was assumed to remain straight and symmetric throughout each test. A slight curvature in the crack front would be expected due to the difference in stress condition at the edges (plane stress) with respect to the mid-crack front point (plane strain). Due to the method of load application, no out of plane loading arises during testing and therefore the crack was assumed to develop symmetrically allowing the measurements taken from one side of the specimen to be both accurate and representative of crack depth.

Calculation of SIF solutions from crack growth data is reliant upon the availability of the crack growth material properties of 'C' and 'm', the Paris Law coefficient and exponent respectively. The law stated below as eq. 7.2 relates crack growth rate to SIF range.

$$\frac{da}{dN} = C\Delta K^m \quad \text{- (7.8)}$$

Han conducted standard compact tension and surface crack growth tests on the same batch of BS7191 355D plate as used for specimen fabrication described in section 7.2. The Paris Law coefficient, 'C' and exponent, 'm' were quantified from experimental measurement of crack growth in compact tension specimens as 3.40×10^{-11} and 2.51 respectively. The crack growth data collected for specimen 'A' may be used in conjunction with a known SIF solution for this geometry in pure bending given by Eq. 7.3 to provide an alternative evaluation of 'C' and 'm'. A crack growth curve, 'a' vs. 'N' constructed from data collected by the testing of specimen 'A' is displayed as fig. 7.9. A smooth curve comprising a large number of observations shows the familiar crack growth form.

$$Y = 1.122 - 1.40\left(\frac{a}{T}\right) + 7.33\left(\frac{a}{T}\right)^2 - 13.08\left(\frac{a}{T}\right)^3 + 14.0\left(\frac{a}{T}\right)^4 \quad \text{- (7.9)}$$

$$\Delta K = \Delta\sigma Y\sqrt{\pi a} \quad \text{- (7.10)}$$

An incremental polynomial method is used to determine the gradient, 'da/dN' of the crack growth curve. All crack growth data collected in this chapter was divided into segments of five sequential data points to which a third order polynomial was fitted. The gradient of the polynomial at the third of the five data points considered is taken as an approximate measurement of 'da/dN' at this point.

Utilisation of eqs. 7.3 and 7.4, the incremental polynomial method and information regarding loading allow an alternative representation of the crack growth data as a plot of 'da/dN' vs. 'ΔK'. Fig. 7.10 shows this representation on logarithmic scales. A fitted line approximates the near-linear correlation shown which is of intercept and gradient equal to 5.04×10^{-8} and 2.39 and equating to Paris Law coefficient and exponent respectively. A comparison of these values is made with those obtained by Han in fig. 7.10.

Fig. 7.11 shows a plot of the crack growth data obtained for the notched specimens. The six curves displayed show data collected from the successful execution of a test for each notch type. Inspection of the figure reveals that the step notch geometries require a greater number of applied stress cycles to reach a given crack size than the symmetrically notched geometries. The total life of each specimen under fatigue loading, comprised a comparatively short initiation period compared to the crack propagation life shown in fig.7.11. The figure illustrates the considerable influence of SIF on the fatigue life of the specimens. Calculation of the SIF solutions from this data using calculated material properties and the processes described above is shown on figs.

7.12 - 7.14 together with the numerical and weight function solutions first presented in chapters 5 and 6.

7.6 – Discussion

Six specimens designed to be representative of those analysed in chapters 5 and 6 were fatigue tested to yield new SIF data to support the analytical and numerical studies. Results attained are presented graphically in figs. 7.12 - 7.14 together with numerical and analytical solutions. Each figure displays results of normalised SIF against non-dimensional crack depth, obtained for a symmetric notch and its step notch equivalent. SIF solutions shown are normalised to the nominal stress present in the thicker section, 'σ_{To}' as given by equation 7.1a. In each case the strong correlation between SIF solutions derived via the three methodologies is clearly evident.

Paris Law coefficient and exponent values determined from test specimen 'A' were used for the calculation of SIF solutions. The values achieved in this study compare well to those obtained by Han[7.4] from crack growth analysis of CT specimens as shown in fig. 7.10.

Experimentation often provides the analyst with valuable appreciation of processes not included in numerical and analytical models. The body of work contained in this thesis has assumed cracks to initiate at the root of the notch and propagate in the vertical plane. This assumption is valid for cracks at symmetric notches under pure mode I opening loading, however when considering cracks at asymmetric notches, which are subject to mixed-mode cracking, validity of the assumption is less certain. Experimental observations verified that cracks in asymmetric notches propagate along a curved path, the curvature of crack path being greatest for short cracks. The curvature of the crack path for asymmetric notches was small, due to the predominantly mode I type loading, to which the crack was subject. The effect of crack path curvature on the SIF data obtained in this series of tests was shown to be negligible and validates the assumption for the loading modes investigated. Cracks subject to mixed-mode loading, for which the mode II component is influential i.e. when subject to a non-symmetric load system, is discussed in chapter 11.

The large number of data points collected for short cracks enabled the SIF detail in this region to be modelled. The significant influence of notch type upon SIF was evident in figs. 7.12 - 7.14 and constitutes a valuable independent assessment of the SIF solution for such geometries for comparative purposes. Short crack data is that which is most valuable, and was sought to capture the notch influence on SIF. Due to the nature of fatigue testing the results are subject to a degree of scatter, however in many instances short crack SIF solutions were successfully captured. SIF solutions obtained are shown to correlate well in terms of both magnitude and shape to those

solutions determined in preceding chapters. The high degree of correlation between solutions was judged sufficient for the validation purposes for which they were intended.

7.7 – Conclusions

New, experimentally determined SIF solutions were sought as a means of supplementary validation of both numerical and weight function approaches applied in chapters 5 and 6. Six specimens were designed to be representative of those analysed analytically and numerically and tested under fatigue loading to yield new SIF solutions. The experimental solutions collected modelled the influence of notch geometry upon the SIF solutions and were shown to compare well to those obtained via other means. Successful execution of the experimental programme yielded new solutions, which were judged to be sufficient for validation of the body of work in chapters 5 and 6. Additional observations, concerning the mixed-mode nature of cracks in asymmetric geometries, were noted as an area of future work.

7.8 – References

[7.1] BS 6835-1:1998, *Method for the Determination of the Rate of Fatigue Crack Growth in Materials – Part 1: Fatigue Crack Growth Rates of above 10^{-8}m per cycle.* British Standards Institute, 1998

[7.2] BS 3518:Part 1:1993, *Methods of Fatigue Testing Part 1. Guide to General Principles.* British Standards Institute

[7.3] BS 7191, *British Standard Specification for weldable structural steels for fixed offshore structures.* British Standards Institute, 1989

[7.4] Han, S., *Fatigue and Fracture Mechanics Analysis of Components Containing Residual Stress Fields.* PhD Thesis (2002), University College London

7.9 – Tables

Tab. 7.1 – Manufacturers Quoted Mechanical Properties of BS 7191 355D Steel Plate

σ_{UTS} (MPa)	σ_Y 0.2% (MPa)	Elongation (%)	Charpy Impact : -20°C		
532	397	31	264	268	266

Tab. 7.2 – Manufacturers Quoted Chemical Composition of BS 7191 355D Steel Plate

C %	Si %	Mn %	S %	P %	V %	Cu %	Al %	Nb %	N %
0.14	0.35	1.49	0.000	0.015	0.002	0.010	0.028	0.035	0.000

Tab. 7.3 – Dimensions of Fatigue Test Specimens

Specimen	T/(mm)	α/(mm)	b/(mm)	ρ/(mm)	L/(mm)	La/(mm)	L_1/(mm)	B/(mm)
A	80	NA	NA	NA	400	NA	90	23
A30	110	30	30	5	400	130.72	90	23
A45	110	45	30	5	400	160	90	23
A60	110	60	30	5	400	176.91	90	23
S30	110	30	30	5	400	130.72	90	23
S45	110	45	30	5	400	160	90	23
S60	110	60	30	5	400	176.91	90	23

Tab. 7.4 – Loading Applied to Specimens

Specimen	$2P_{min}$/(kN)	$2P_{max}$/(kN)	σ_{min}/(MPa)	σ_{max}/(MPa)	Δσ/(MPa)	R
A	6	85	$\sigma_{to} = 11$	$\sigma_{to} = 155$	144	0.07
Notched	5	131	$\sigma_{To} = 5$	$\sigma_{To} = 132$	127	0.04

7.10 – Figures

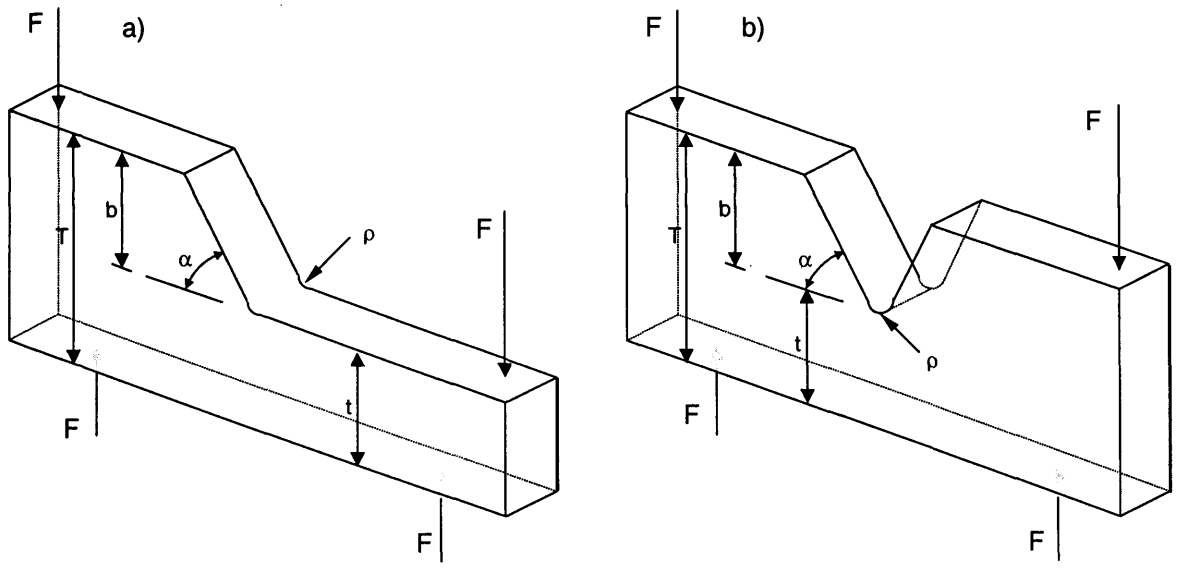

Fig. 7.1 – (a) Step and (b) Symmetric Geometries to be Fatigue Subject to 4 Point Bending. Arrows Indicate Points of Load Application and Magnitude 'F'

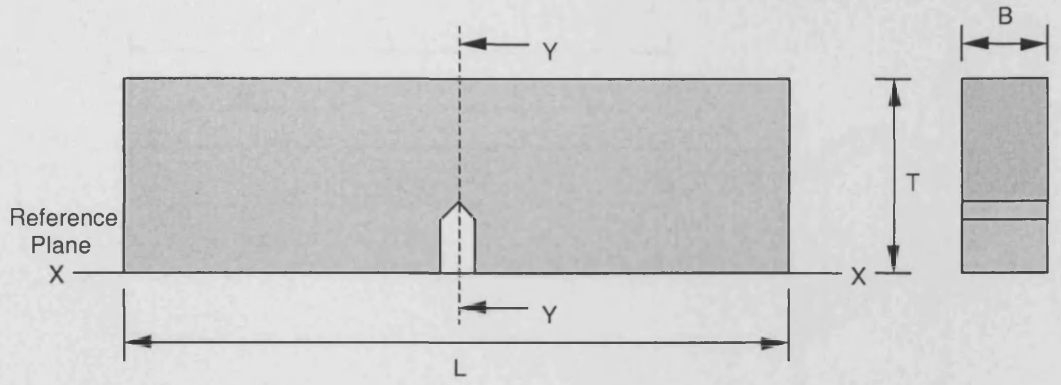

$T \geq 10$

$0.2T \leq B \leq T$

$L \geq (L_1 + L_2 + L_3 + 10)$

Note: The Crack length is measured from the reference plane X-X

All Dimensions are in mm

Fig. 7.2 – SNEB4 Specimen Design Tolerances

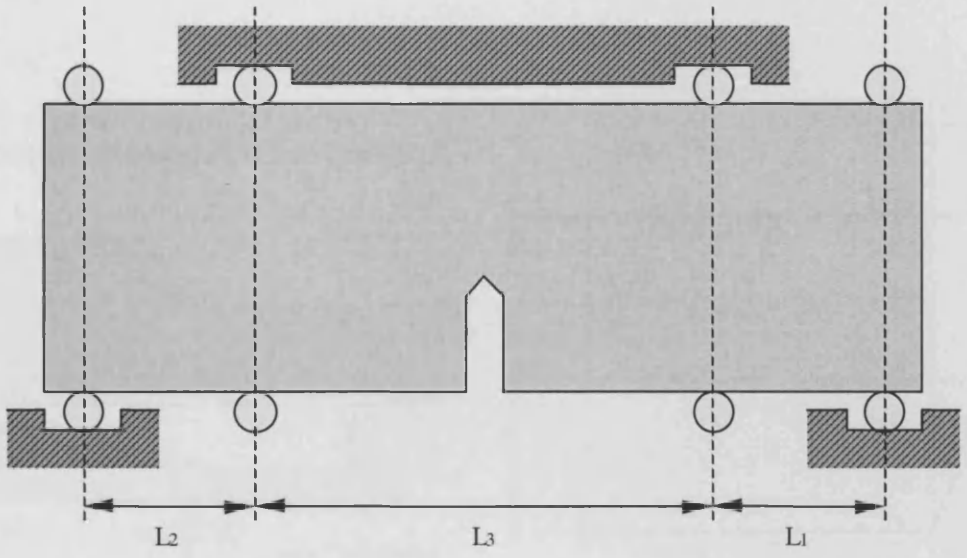

$L_3 \geq 2B$

$L_1, L_2 \geq B$

$L_1 = L_2 \pm 0.01B$

Fig. 7.3 – SNEB4 Specimen Loading Requirements

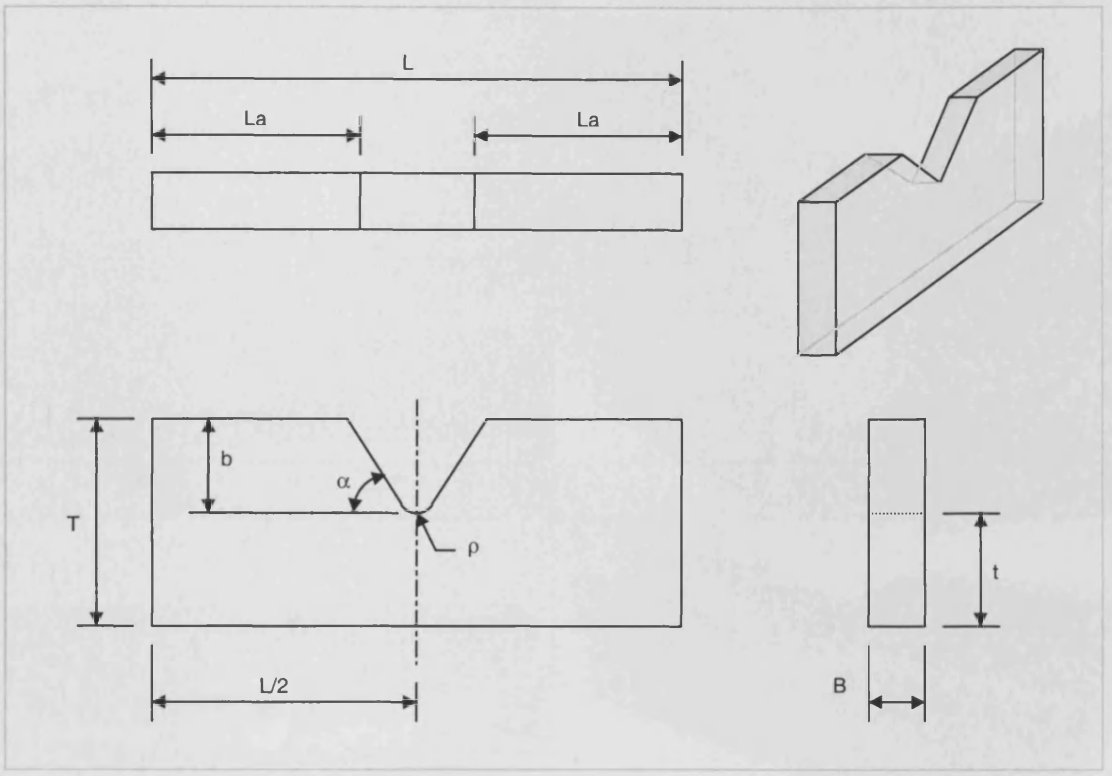

Fig. 7.4 – Specimen Dimensions

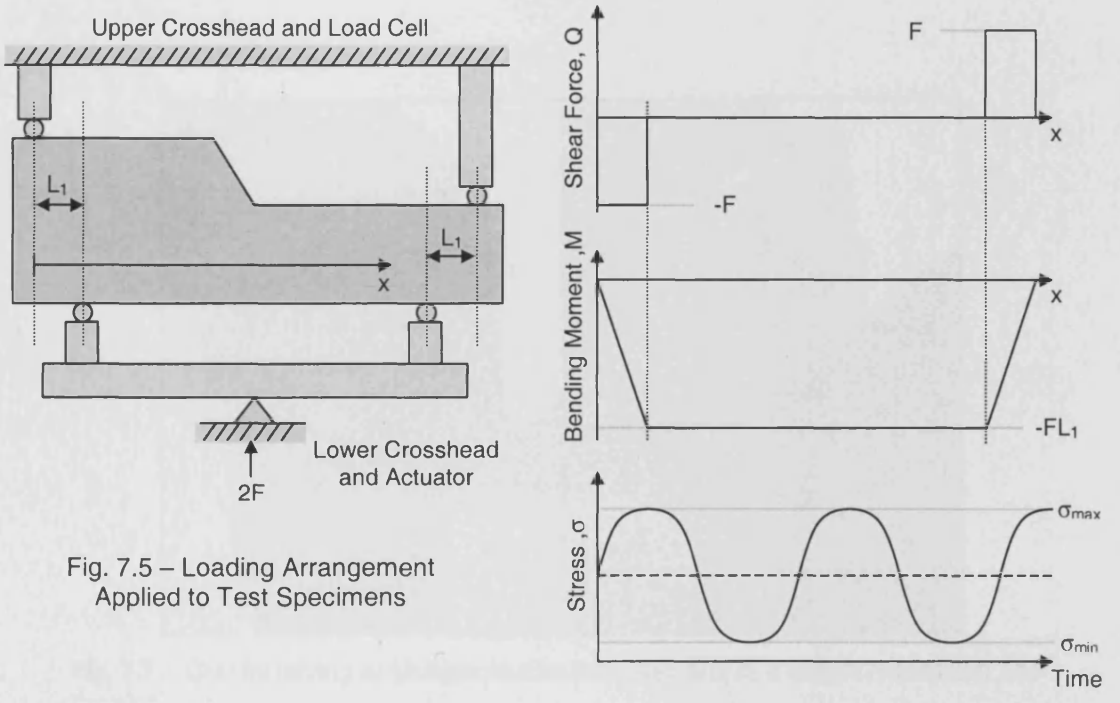

Fig. 7.5 – Loading Arrangement Applied to Test Specimens

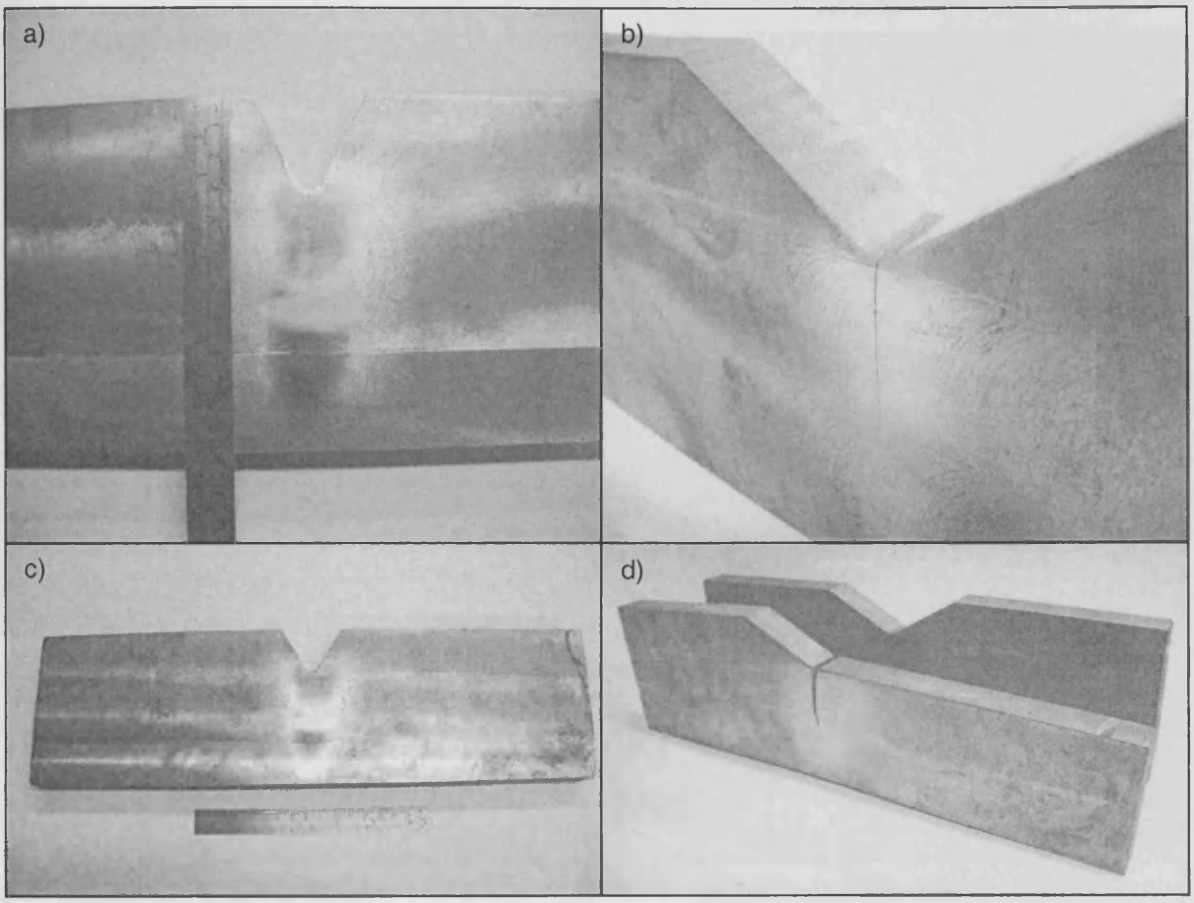

Fig. 7.6 –Tested Specimens

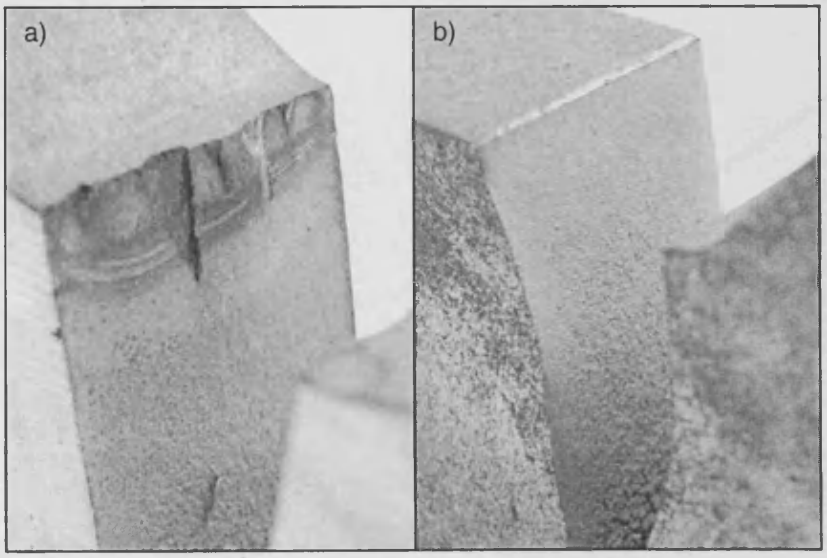

Fig. 7.7 – Cracks having a) Multiple Nucleation Sites and b) a Single Nucleation Site

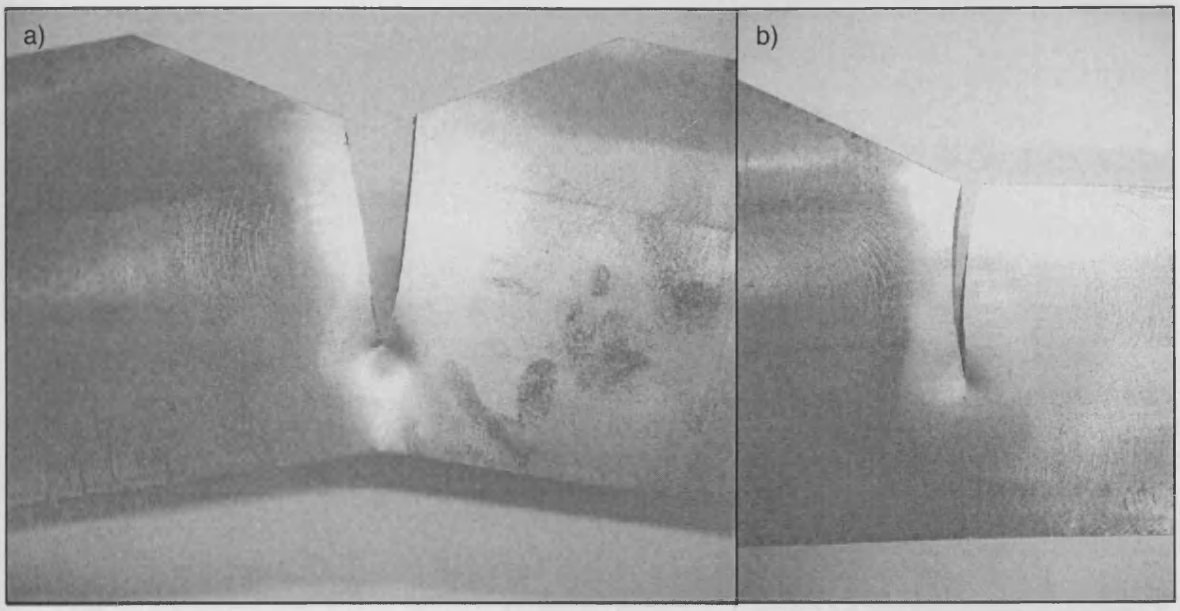

Fig. 7.8 – a) Straight Crack Path, Specimen S30 and b) Curved Crack Path, Specimen A30

Fig. 7.9 – Crack Growth Curve Obtained for Specimen A

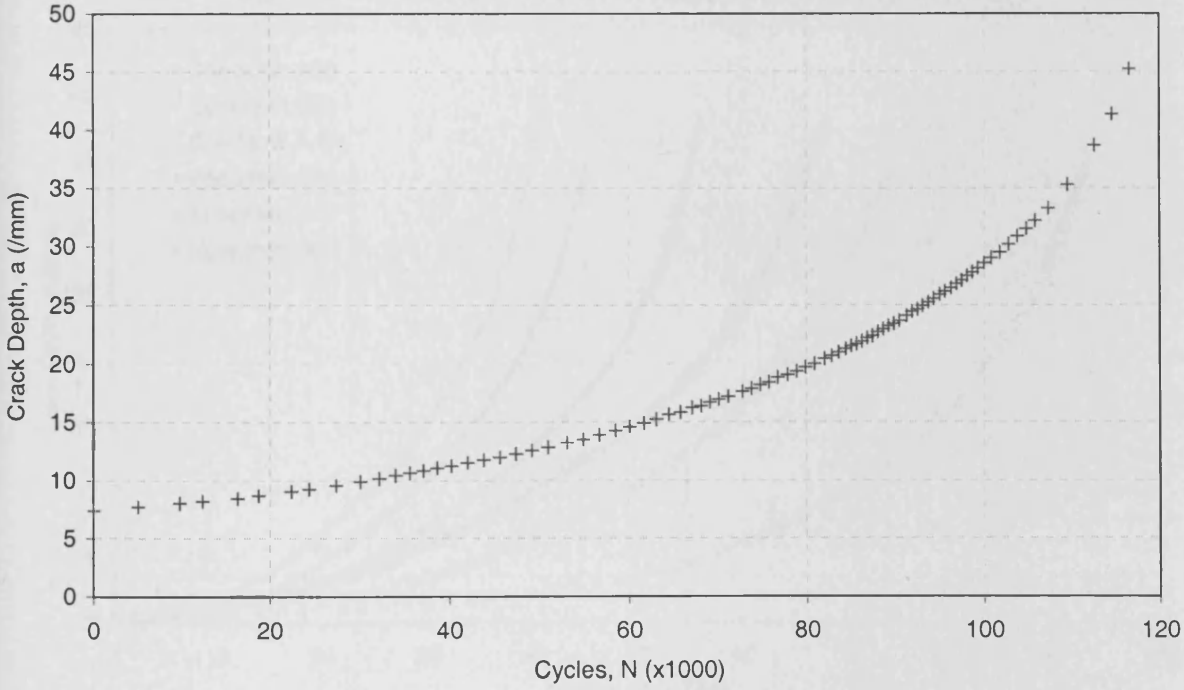

Fig. 7.10 – Crack Growth Rate for Specimen A

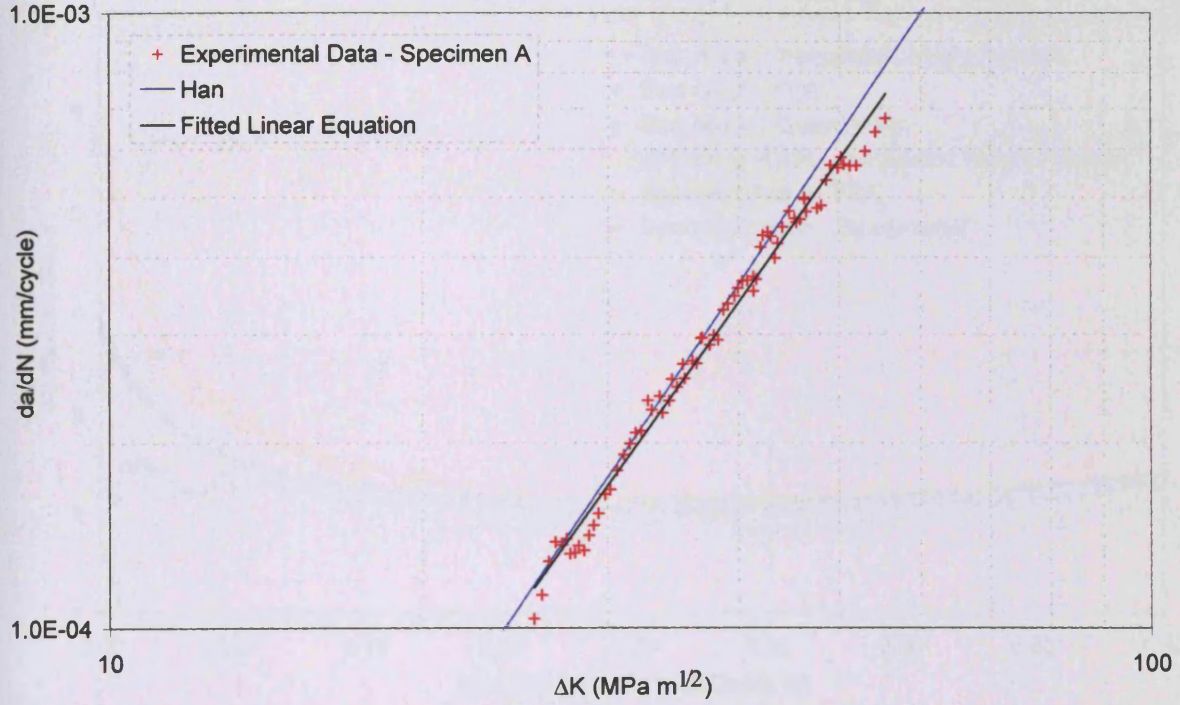

Fig. 7.11 – Crack Growth Curves obtained for the Notched Specimens

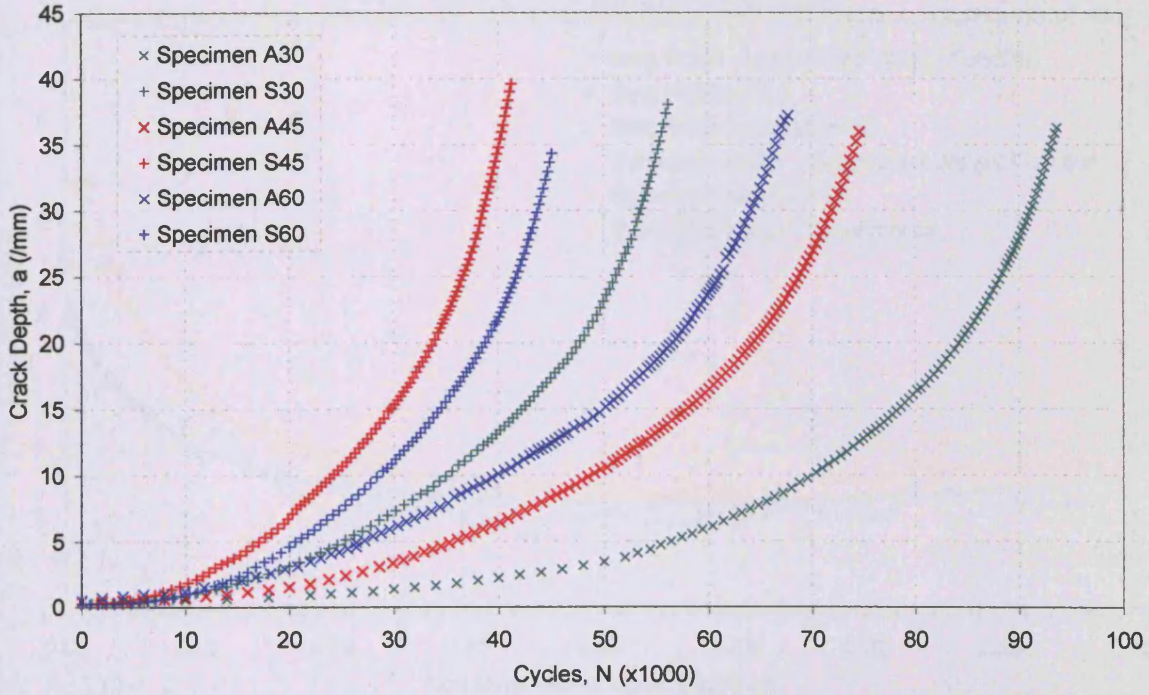

Fig. 7.12 – Comparison of SIF Solutions Determined By Various Means
(α = 30°; b/ρ = 6; b/T = 0.2727; Pure Bending)

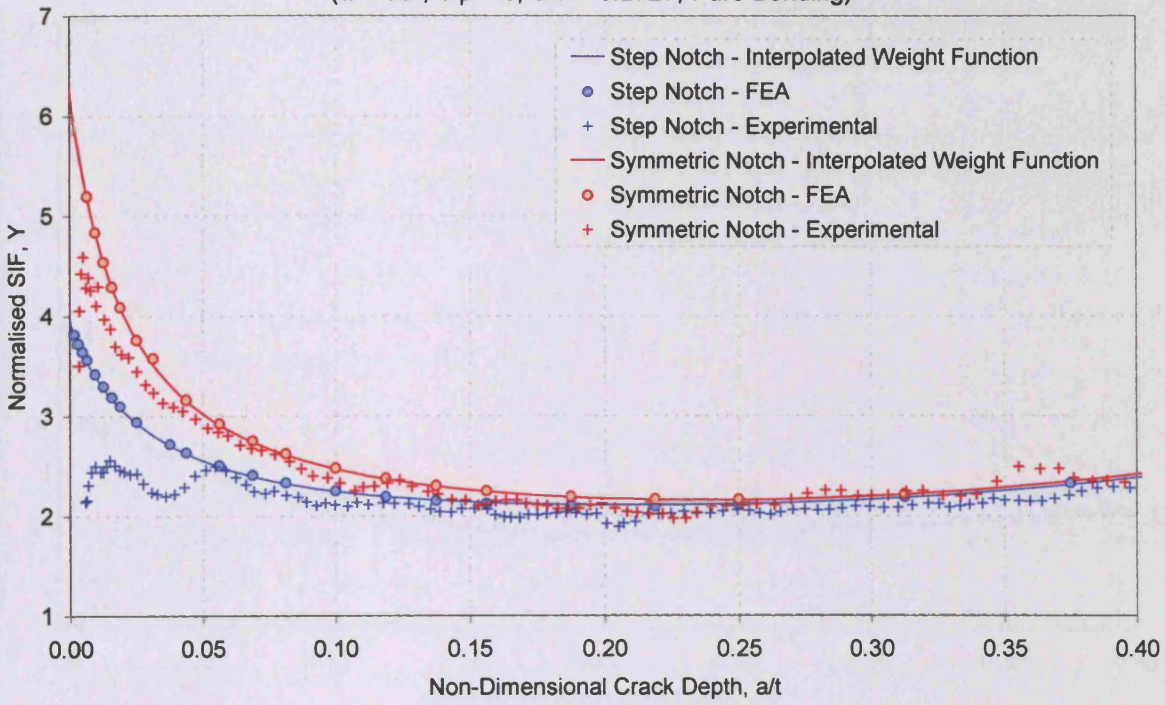

Fig. 7.13 – Comparison of SIF Solutions Determined By Various Means
(α = 45°; b/ρ = 6; b/T = 0.2727; Pure Bending)

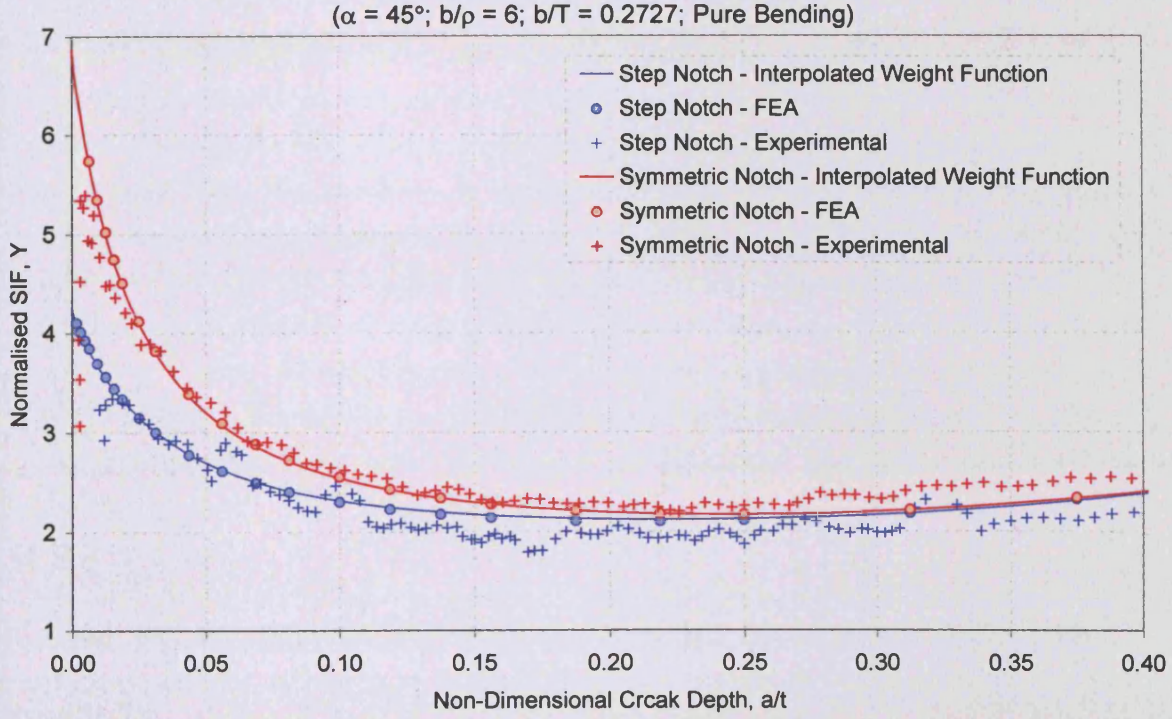

Fig. 7.14 – Comparison of SIF Solutions Determined By Various Means
(α = 60°; b/ρ = 6; b/T = 0.2727; Pure Bending)

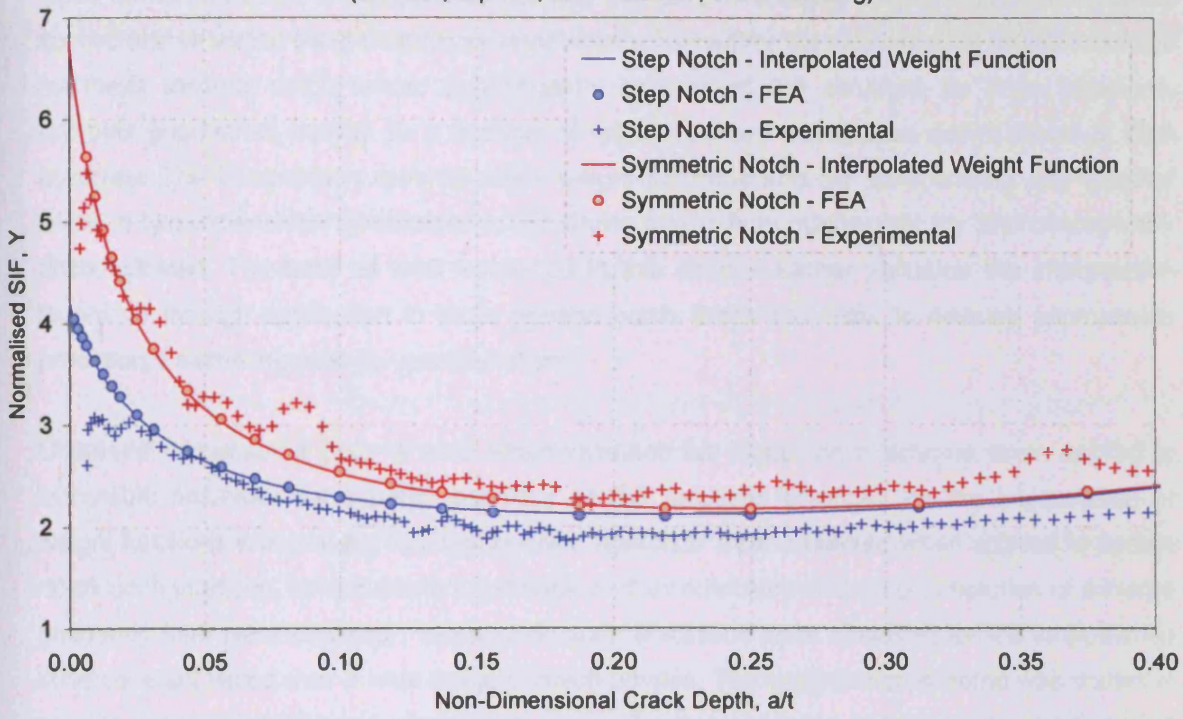

Chapter 8 – Interpolation of Weight Functions for Intrusion/Protrusion Notches

Notch profiles investigated in chapters 5 and 6 were recognised as special cases of more general types termed intrusion and protrusion notches (fig. 8.1). Preceding chapters have successfully applied and validated weight function interpolation schemes for the calculation of weight functions for these external notch forms. Subsequently determined SIF solutions for finite thickness, complex geometries subject to a number of loading modes have been shown to be of high accuracy. The interpolation scheme offers weight functions and SIF solutions for any external notch in two-dimensional geometries in a manner that is both mathematically and conceptually uncomplicated. The body of work contained in this chapter further validates the interpolation technique through application to more general notch forms and aims to develop approximate procedures stemming from its versatile nature.

Chapter 5 comprised a body of work which validated the interpolation scheme when applied to symmetric notches. The superior accuracy of SIF solutions obtained via the interpolation of weight functions with respect to a composition approach were observed when applied to certain notch configurations. Limitations in application of the composition scheme to notches of extreme geometric form were exposed, whereas no such limitations were observed for the interpolation scheme when tested over a wide range of notch profiles. The interpolation scheme was shown to provide a more complete and robust methodology for the calculation of notched geometry weight functions and SIFs.

Chapter 6 sought to apply the interpolation scheme to a similar wide range of step notch forms. Application of a composition approach to this notch form requires significant modification to that applied for symmetric notches, whereas an interpolation approach is universally applicable to all notch types. Observations drawn in preceeding chapters were implemented to realise a methodology of increased economy via usage of constituent geometry solutions for an equivalent symmetric notch. Though not fully investigated, an interpolation scheme for a family of notches termed compound notches was suggested and predicted to apply to asymmetric notches formed from two symmetric notches. The step notch investigated was identified as a compound notch and resulting SIF solutions of high accuracy were simply derived via a methodology requiring only finite thickness crack-line stress distributions and equivalent, constituent symmetric notch geometry solutions.

The interpolation scheme has been shown to provide a universal solution for the calculation of complex, two-dimensional geometry weight functions and SIFs. Constituent geometry solutions are required from which an interpolation factor, characterising the stiffenening influence of the notch upon the crack, is ascertained. Notches embedded in semi-finite geometries have been

shown to be advantageous for this purpose. Interpolation factors are subsequently applied to 'base' geometry weight functions to yield a finite thickness weight function for the notched geometry. Integration of the resulting finite thickness weight function with an arbitary finite thickness, crack-line stress distribution over the crack length generates new SIF solutions. The technique yields weight function and SIF solutions of high accuracy in a manner that is both rapid and robust and that can be readily implemented via a computer-based algorithm. The interpolation scheme, validated against both numerically and experimentally derived SIFs provides a practicable solution to the long-standing problem of calculating complex geometry SIFs identified in chapter 1 and, as an analysis tool, has the potential to provide solutions to a wide range of crack problems.

A 'library' of constituent geometry solutions is envisaged which, though not fully produced in this study, will provide engineers with a close approximation to any notch form adhering to the generic forms available. The not inconsiderable effort required to formulate generic constituent geometry solutions, fit for incorporation into a 'library', is highlighted by fig. 8.2, which displays an illustrative matrix of solutions that such a study would constitute. The number of constituent geometry solutions required to perform a generic study is increased with notch complexity defined by an increased number of geometric parameters. The ability to formulate approximate interpolation factors from the more limited solutions generated in this thesis together with a number of 'auxiliary' solutions is desirable in terms of both the number of constituent geometry solutions required and their ultimate presentation in design standards and codes. A methodology is presented that attempts to isolate the influence of individual geometric notch parameters, upon the crack, expressed as interpolation factors and equations. The methodology is designed to give approximate solutions for both intrusion and protrusion notches in addition to more intricate notch profiles such as embedded notches, representative examples of which are illustrated in fig. 8.3.

This chapter aims to further validate the interpolation scheme by its application to more general notch geometries termed intrusion and protrusion notches. An approximate interpolation methodology is also presented, which isolates the influence of each individual notch geometric parameter upon the weight function, characterised by an interpolation factor. Developed SIF solutions are compared to finite element solutions and discussed.

8.1 – Introduction

Generalised intrusion and protrusion notches are depicted in figs. 8.1a and 8.1b respectively. An additional geometric parameter is introduced for each geometry to describe notch width, 'L_P' and 'L_I' for the protrusion and intrusion notch, respectively. Definition of an interpolation factor and

interpolation equation universally applicable to all externally notched components is reproduced below.

$$m_N^F(a,x) = f(a)m_U^F(a,x) + (1-f(a))m_S^F(a,x) \qquad \text{- (8.1)}$$

$$f(a) = \frac{m_N^S(a,x) - m_S^S(a,x)}{m_U^S(a,x) - m_S^S(a,x)} \qquad \text{- (8.2)}$$

Interpolation factors have, in preceding chapters been determined from an equation of the same form as eq. 8.2, based upon constituent geometry normalised SIFs. The ability to do so is a consequence of the parity of crack-line stress in each constituent geometry. The resulting interpolation factor is therefore independent of crack loading. Utilisation of published constituent notch geometry solutions are unlikely to meet this special loading condition necessitating the use of eq. 8.2 in terms of the weight function. The body of work contained in this chapter develops constituent notched geometry solutions subject to remote boundary loading. The stress raising influence of the notch gives rise to a non-uniform crack-line stress distribution. Other constituent geometry solutions are, however only available for uniform crack loading. The weight function is solely a property of component geometry, and therefore once formulated for each constituent geometry and manipulated as dictated by eq. 8.2 yields an interpolation factor which is a property of notch geometry and independent of loading condition.

A limited, demonstrative study applying the interpolation scheme to intrusion and protrusion notches was undertaken in which the notch width parameter, 'L_P' and 'L_I', was the sole geometric parameter varied. The matrix of fig. 8.2 displays the notches for which new SIF solutions were sought. New SIF solutions for the finite thickness notched geometries were calculated for the commonly sought loading conditions of uniform tension and pure bending for the intrusion notch and pure tension and pure bending for the protrusion notch.

8.2 – An Interpolated Weight Function Solution

Application of an interpolated weight function scheme to intrusion and protrusion notches described in this chapter aims to implement the more generalised form of interpolation equation, for the determination of interpolation factors, using the eq. 8.2. Derivation of constituent geometry SIF solutions subject to remote boundary loading simulates notched geometry SIF solutions commonly contained in published literature. The interpolation factor is a function of crack depth and independent of crack co-ordinate, 'x'.

$$f(a) = \frac{m_N^S(a, x = a/2) - m_S^S(a, x = a/2)}{m_U^S(a, x = a/2) - m_S^S(a, x = a/2)} \quad \text{- (8.3)}$$

SIF and associated crack-line stress distributions are required as reference solutions for the formulation of the semi-finite, notched geometry weight function. Other constituent geometry SIF and crack-line stress solutions for stiffened and unstiffened cracked geometries are well known, firmly established solutions presented and used in preceding chapters of this document.

Once determined, constituent geometry weight functions are applied as dictated by eq. 8.3. A crack co-ordinate, '$x = a/2$' is arbitrarily selected to illustrate the comparable accuracy that may be achieved using this representation of interpolation factor to that calculated from normalised SIFs.

Calculated interpolation factors are applied to base geometry weight functions, as described in preceding chapters, to determine the finite thickness, notched geometry weight function and integrated with finite thickness stress distributions to deduce new SIF solutions. These were validated against finite thickness SIF solutions determined via finite element methods.

8.2.1 – Constituent Geometry Reference SIF Solutions

Finite element methods were employed to determine semi-finite thickness notched geometry SIF solutions subject to remotely applied tension. Discrete data obtained from the FEA is presented in tables 8.1 and 8.2 for protrusion and intrusion notches respectively. The data was fitted to polynomials of the form given by eq. 8.4 to give continuous data required for weight function methodologies. Coefficients, 'M_x' obtained from the curve fitting process are presented in tables 8.3 and 8.4 for a range of protrusion and intrusion notch profiles respectively.

$$Y_I(a) = M_5\lambda^5 + M_4\lambda^4 + M_3\lambda^3 + M_2\lambda^2 + M_1\lambda + M_0 \quad \text{- (8.4)}$$

$$\lambda = \frac{1}{1 + a/\rho} \qquad \text{validity : } 0 < \lambda < 1$$

8.2.2 – Constituent Geometry Reference Stress Distributions

Similar finite element techniques were used to determine the associated geometry crack-line stress distributions. Data produced was normalised to the remote characteristic stress and fitted to an equation of the form of eq. 8.5. Coefficients, 'N_x' are displayed in tables 8.5 and 8.6.

$$\frac{\sigma_{yy}(x)}{\sigma_o} = N_0 + N_1\gamma^1 + N_2\gamma^2 + N_3\gamma^3 + N_4\gamma^4 \qquad \text{- (8.5)}$$

$$\gamma = \frac{1}{1 + x/\rho} \qquad \text{validity : } 0 < \gamma < 1$$

8.2.3 – Finite Thickness Stress Distributions

Stress distributions for the finite thickness, intrusion and protrusion notches investigated are described by an equation of the form of eq. 8.5. Coefficients are presented in tables 8.7 and 8.8.

$$\frac{\sigma_{yy}(x)}{\sigma_o} = P_0 + P_1\gamma^1 + P_2\gamma^2 + P_3\gamma^3 + P_4\gamma^4 \qquad \text{- (8.6)}$$

$$\gamma = \frac{1}{1 + x/\rho} \qquad \text{validity : } 0.5 < \gamma < 1$$

8.3 – An Approximate Interpolated Weight Function Solution

The considerable number of notched constituent geometry solutions required for the formulation of a generic solution has already been stated. Formulation of the required generic solutions in the form of an envisaged 'library' of solutions was not included in the intended scope of work, which sought to demonstrate and validate a weight function methodology meeting the criteria stated in chapters 1 and 2. In the absence of a current 'library' of notched constituent geometries and in light of the flexible nature of the interpolation scheme, an approximate procedure for determining SIF solutions for notched components of the form considered in this study is presented.

The methodology aims to utilise the limited matrix of notched constituent geometry solutions generated in chapter 5, together with a small number of 'auxiliary' solutions, to characterise the stiffening influence of each one of a notches individual geometric parameters upon total notch stiffness expressed in terms of an interpolation factor. Implementation is detailed for initially symmetric notches prior to extension to the more general notch types considered in this chapter.

An interpolation equation is shown in fig. 8.4, which characterises the influence of a sharp V-notch by an interpolation factor (eq. 8.7). The notch considered is defined by a single parameter, 'α' and therefore the resulting interpolation factor, is solely a function of this geometric parameter and is denoted by the subsript, 'α'. Re-arrangement of this expression gives eq. 8.7a.

$$\frac{m_{\alpha}^{S}(a,x)-m_{S}^{S}(a,x)}{m_{U}^{S}(a,x)-m_{S}^{S}(a,x)}=f_{\alpha}(a) \qquad \text{- (8.7)}$$

$$m_{\alpha}^{S}(a,x)=f_{\alpha}(a)m_{U}^{S}(a,x)+(1-f_{\alpha}(a))m_{S}^{S}(a,x) \qquad \text{- (8.7a)}$$

A similar interpolation scheme is displayed in fig. 8.5, which assumes isolation of the geometric influence of the notch root radius, and is represented by eqs. 8.8 and 8.8a.

$$\frac{m_{\alpha,\rho}^{S}(a,x)-m_{\alpha}^{S}(a,x)}{m_{U}^{S}(a,x)-m_{\alpha}^{S}(a,x)}=f_{\rho}(a) \qquad \text{- (8.8)}$$

$$m_{\alpha,\rho}^{S}(a,x)=f_{\rho}(a)m_{U}^{S}(a,x)+(1-f_{\rho}(a))m_{\alpha}^{S}(a,x) \qquad \text{- (8.8a)}$$

An interpolation equation using the stiffened and unstiffened geometry solutions, applied in previous chapters of this study is reproduced below and diagrammatically as fig. 8.6.

$$\frac{m_{\alpha,\rho}^{S}(a,x)-m_{S}^{S}(a,x)}{m_{U}^{S}(a,x)-m_{S}^{S}(a,x)}=f_{\alpha,\rho}(a) \qquad \text{- (8.9)}$$

$$m_{\alpha,\rho}^{S}(a,x)=f_{\alpha,\rho}(a)m_{U}^{S}(a,x)+(1-f_{\alpha,\rho}(a))m_{U}^{S}(a,x) \qquad \text{- (8.9a)}$$

The three interpolation equations presented above (eqs. 8.7a, 8.8a and 8.9a) maybe combined to give an expression for an interpolation factor for a symmetric notch in terms of individual geometric influences.

$$f_{\alpha,\rho}(a)=f_{\rho}(a)(1-f_{\alpha}(a))+f_{\alpha}(a) \qquad \text{- (8.10)}$$

$$\left(1-f_{\alpha,\rho}(a)\right)=\left(1-f_{\rho}(a)\right)\left(1-f_{\alpha}(a)\right) \qquad \text{- (8.11)}$$

An interpolation equation utilising the results given by eqs 8.7 and 8.8 applied to finite thickness geometries is given as eq. 8.12.

$$m_{\alpha,\rho}^{F}(a,x)=\left(f_{\alpha}(a)+f_{\rho}(a)(1-f_{\alpha}(a))\right)m_{U}^{F}(a,x)+\left((1-f_{\rho}(a))(1-f_{\alpha}(a))\right)m_{S}^{F}(a,x) \qquad \text{- (8.12)}$$

The interpolation equation derived and presented above in eq. 8.12 is a more detailed representation of the more simple form of the same equation documented in previous sections of this thesis. Alone, this representation offers no significant advantage over the more basic form.

However, when producing a generic solution, such as those ultimately desired, the possibility exists to exploit this representation of the interpolation equation to reduce the number of constituent geometry solutions required. If the limited study conducted upon symmetric notches detailed in chapter 5, for which notches were completely described by the two geometric parameters of 'b/ρ = 1, 3, 6, 10 and 15' and 'α = 15, 30, 45, 60 and 90' is considered, a complete generic study defining interpolation factors '$f_{\alpha,\rho}(a)$' for each geometric combination requires 'N^2' constituent solutions ($N=5$) using an interpolation expression of the form of eq. 8.1. The same study using eq. 8.12 necessitates only, '$2xN$' constituent geometry solutions.

It is assumed that interpolation equations given by eq. 8.7 and 8.8 and by figs. 8.4 and 8.5 characterise the geometric influence of notch flank angle, '$f_{\alpha}(a)$' and notch root radius, '$f_{\rho}(a)$' only. The possibility exists to calculate these parameters from a relatively small library of constituent geometry solutions and combine them via usage of eq. 8.12 to give solutions for a larger set of constituent geometries. Considering once more the limited parametric study conducted upon symmetric notches and the auxiliary solutions for sharp symmetric notches, described in chapter 5, sufficient information exists to isolate a range of interpolation factors describing '$f_{\alpha}(a)$' and '$f_{\rho}(a)$' permitting as yet unknown interpolation factors, weight functions and SIF solutions to be determined.

A similar procedure to that described above may be applied to an intrusion/protrusion notch. Figs 8.6, 8.7 and 8.8 depict the interpolation schemes considered and introduces the new interpolation factor '$f_L(a)$' characterising notch width.

$$m^F_{\alpha,\rho,L}(a,x) = \left(f_L(a) + f_{\alpha,\rho}(a)(1-f_L(a))\right)m^F_U(a,x) + \left((1-f_L(a))(1-f_{\alpha,\rho}(a))\right)m^F_S(a,x) \quad \text{- (8.13)}$$

For a symmetric notch considered in chapter 5, the interpolation factor describing notch width is equal to zero ('$f_L(a) = 0$') reducing eq 8.13 to the familiar form derived in chapter 4 (eq. 4.13) and applied in chapter 5. A step notch was shown in chapter 4 to comprise an equal characteristic of both stiffened and unstiffened cracks such that '$f_L(a) = 0.5$'. Applying this condition to eq. 8.13 gives an equation equal to that obtained by observation presented in chapter 6 (eq 6.3). Untimately an interpolation equation for the intrusion/protrusion notch in terms of interpolation factors for the individual geometric influences can be deduced as given below.

$$m^F_{\alpha,\rho,L}(a,x) = f_{\alpha,\rho,L}(a)m^F_U(a,x) + (1-f_{\alpha,\rho,L}(a))m^F_S(a,x) \quad \text{- (8.14)}$$

$$f_{\alpha,\rho,L}(a) = f_L(a) + f_\rho(a)(1 - f_L(a)) + f_\alpha(a)(1 - f_\rho(a))(1 - f_L(a)) \quad \text{- (8.14a)}$$

$$(1 - f_{\alpha,\rho,L}(a)) = (1 - f_\alpha(a))(1 - f_\rho(a))(1 - f_L(a)) \quad \text{- (8.14b)}$$

This chapter aims to compare SIF solutions obtained via interpolation methodologies described in this section to isolate individual geometric parameter influences and combine them using eqs. 8.12 and 8.13 and those obtained from the interpolation approach described in section 8.2.

8.4 – Implementation of an Approximate Methodology for Symmetric Notches

Sufficient information exists within the limited study of symmetric notches conducted in chapter 5 to broaden the number of solutions available by completing the matrix of constituent geometry solutions required using the approximate methodology described above. The current 'library' of constituent geometry solutions is expressed as the red elements of the matrix in fig. 8.9a) and certain sharp V-notch solutions are also available 'α = *15, 30 and 45°*. The approximate methodology is utilised in this section to predict the extreme constituent geometry solutions depicted as the green elements of the matrix in fig. 8.9a). New SIF solutions are determined for the finite thickness equivalent geometry as defined by the green elements of the matrix depicted in fig. 8.9b).

The geometric influence of several flank angles, expressed as an interpolation factor determined from eq. 8.7, was obtained form the data contained in tab. 5.3 and is shown in fig. 8.10. Similarly the influence of various notch root radii, expressed as an interpolation factor described by eq. 8.8, are shown in fig. 8.11. The individual geometric influences shown in figs. 8.10 and 8.11 may be combined using eq. 8.12 to give an approximate interpolation factor for any combination of the two parameters. By means of an example the data displayed was used to ascertain an approximate interpolation factor for notches described by the parameters 'b/ρ = *1*, α = *15*' and 'b/ρ = *15*, α = *15*'. These represent extreme notch configurations in the 'library' matrix first presented in chapter 5 and reproduced in fig. 8.9a).

The interpolation factors describing individual geometric parameters were fiited to polynomial expressions of the form shown below. Coefficients 'D_x' and limits of validity, 'ξ' are displayed in table 8.9.

$$f_\rho(a) = D_5\lambda^5 + D_4\lambda^4 + D_3\lambda^3 + D_2\lambda^2 + D_1\lambda + D_0 \quad \text{- (8.15a)}$$

$$f_\alpha(a) = D_5\psi^5 + D_4\psi^4 + D_3\psi^3 + D_2\psi^2 + D_1\psi + D_0 \quad \text{- (8.15b)}$$

$$\lambda = \frac{1}{1 + a/\rho} \qquad \text{validity: } \xi < \lambda < 1$$

$$\psi = \frac{1}{1 + a/b} \qquad \text{validity: } \xi < \psi < 1$$

An interpolation factor describing the stiffening influence of both notch parameters, 'b/ρ' and 'α' by an interpolation factor, '$f_{\rho,\alpha}(a)$' determined from eq. 8.10, for the extreme notches defined in fig. 8.9a, is presented as fig. 8.12. Also plotted on fig. 8.12 is the 'exact' interpolation factor determined from finite element analysis conducted upon the semi-finite notched constituent geometries (tab. 8.10).

Usage of the determined interpolation factor was subsequently applied to the 'base' geometry weight functions to determine a finite thickness weight function for the complex geometry. Integration with the finite thickness crack-line stress distribution gives new SIF solutions. Normalised stress distributions for the notch configurations currently considered are presented in tab. 8.11 in a form compatible with eq. 8.6.

8.5 – Determination of Interpolation factor '$f_L(a)$'

Extension of the approximate methodology to intrusion/protrusion notches requires knowledge of the geometric influence of notch width described by an interpolation factor. Fig. 8.7 provides an expression for the determination of '$f_L(a)$'. However use of a more simplified expression which eliminates the influence of flank angle and root radius is given by fig. 8.13. It introduces new 'auxiliary' geometries which isolate the geometric influence of notch width.

Interpolation factors describing the geometric influence of notch width are determined from analysis of the geometries depicted in fig. 8.14. Both sharp, vertically flanked intrusion and protrusion notches in semi-finite strips are characterised by parameters 'L_P' and 'L_I' and were analysed using the finite element method with uniform loading applied directly to the crack faces as shown. This loading configuration allows direct comparison of obtained SIF solutions with the siffened and unstiffened semi-finite crack solutions to calculate an interpolation factor, '$f_L(a)$'. The only notch variables are notch width, 'L_P' or 'L_I' for protrusion and intrusion notches respectively and notch height or depth, 'b' and can therefore be defined by the single non-dimensional parameter of 'L_I/b' or 'L_P/b'. SIF data, '$Y_N^S(a)$' produced from the finite element study is detailed in tabs. 8.12 and 8.13 and presented graphically in fig. 8.15 alongside the equivalent stiffened and unstiffened SIF solutions. An interpolation factor is formulated via usage of eq. 8.16.

$$f_L(a) = \frac{Y_N^S(a) - Y_S^S(a)}{Y_U^S(a) - Y_S^S(a)} \qquad \text{- (8.16)}$$

Curve fitted expressions for the interpolation factors, '$f_L(a)$' using eq. 8.17 are given in tab. 8.9 and shown graphically as fig. 8.16.

$$f_L(a) = D_5\psi^5 + D_4\psi^4 + D_3\psi^3 + D_2\psi^2 + D_1\psi + D_0 \qquad \text{- (8.17)}$$

$$\psi = \frac{1}{(1 + a/b)} \qquad \text{validity: } \xi < \psi < 1$$

8.6 – Implementation of an Approximate Methodology for Intrusion/Protrusion Notches

Constituent auxiliary solutions, allowing definition of '$f_L(a)$', together with symmetric geometry constituent solutions, allowing definition of '$f_{\rho,\alpha}(a)$', are sufficient for the definition of an interpolation factor, '$f_{L,\rho,\alpha}(a)$', characterising the stiffening influence of an intrusion/protrusion notch via the equations below.

$$f_{L,\alpha,\rho}(a) = f_{\rho,\alpha}(a)(1 - f_L(a)) + f_L(a) \qquad \text{- (8.18)}$$

$$(1 - f_{L,\alpha,\rho}(a)) = (1 - f_{\rho,\alpha}(a))(1 - f_L(a)) \qquad \text{- (8.19)}$$

Also available are 'exact' interpolation factors, for the same geometries, determined through usage of eq. 8.3 and the constituent geometry reference solutions collected. A comparison between values of '$f_{L,\rho,\alpha}(a)$' obtained via the two methodologies is made in fig. 8.17.

8.7 – Discussion

Interpolation factors have been determined for a number of intrusion and protrusion notches. The methodologies applied have differed from those utilised in preceeding chapters. An alternative, more general, form of the interpolation equation expressed in terms of constituent geometry weight functions was applied to give an 'exact' evaluation of the interpolation factor. Use of the weight function, a property of component geometry respects the interpolation factors' sole dependance upon notch geometry. Constituent geometry SIF solutions and stress distributions were calculated and used as reference solutions for weight function formulation. Once determined, interpolation factors were applied to two-dimensional base geometry weight functions as described in preceeding chapters to formulate a weight function for the finite thickness, complex, two-dimensional geometry. The contribution of each base geometry weight function to

the total solution is shown in fig. 8.18. New SIF solutions obtained by integration of the determined weight function with the crack-line stress distribution are displayed in figs. 8.19 - 8.22 for the protrusion notch under pure tension and pure bending and the intrusion notch under uniform tension and pure bending respectively. Also displayed are limiting SIF solutions: the un-notched geometry solution (Brown & Srawley) and the equivalent step notch solution for the protrusion notch and the eqivalent step notch solution and equivalent symmetric notch solution for the intrusion notch. Once more the new SIF solutions obtained through the interpolated weight function methodology are in excellent agreement with those obtained from finite element methods (Appendix A). As observed in preceeding chapters the margin of error between solutions derived via the two methods is negligible and the ease of computation maintained. Though the application of the interpolation technique to intrusion and protrusion notches in this chapter is limited, the results achieved complement the high degree of accuracy achieved in preceeding chapters. The futher validation of the interpolation scheme has been attained and a demonstration of its universal applicability given.

Further to the 'exact' evaluation of new SIF solutions by the direct determination of interpolation factors from constituent geometry solutions, an alternative, approximate methodology was presented. The methodology designed, sought to apply the limited generic study contained in chapter 5, together with a number of auxiliary geometry solutions to formulate approximate interpolation factors for new geometries. The economy to be gained from implementation of such a scheme renders the availablity of interpolation factors for a wider range of geometries from the analysis of relatively few constituent geometries a possibility. If applicable the methodology could permit complete generic studies to be undertaken by the analysis of a greatly reduced number of constituent geometry solutions and potentially permits a large number of new geometry types, such as the embedded notches highlighted in fig. 8.3, to be analysed simply, rapidly and accurately.

Section 8.3 described a methodology using various interpolation schemes to isloate the geometric influence of the rotch root radius and flank angle, each individually expressed as an interpolation factor. Independence of the two geometric influences was assumed and an expression for calculation of an interpolation factor for their combined influence from their individual influences presented. Section 8.4 described application of the appoximate methodology to symmetric notches to calculate interpolation factors for geometric configurations not covered in chapter 5. Interpolation factors for extreme symmetric notch geometry profiles ($b/\rho = 1$, $\alpha = 15°$ & $b/\rho = 1$, $\alpha = 15°$) were calculated and presented against 'exact' results extracted obtained from finite element studies on the relevant constituent geometries.

Comparisons drawn in fig. 8.12 show interpolation factors obtained from the two methodologies to be in good general agreement, however differences between the two indicate that the assumption of independence between the two geometric influences is not wholly valid. A notch root detail defined by the geometrically interacting parameters of radius and flank angle does not allow complete isolation of their geometric influence by the methodology proposed. Variations in the contribution from each base geometry weight function on the total SIF solution, due to the approximate interpolation factor are evident in fig. 8.22. New SIF solutions obtained via usage of interpolation factors calculated from the approximate methodology and finite thickness crack-line stress distributions (tab. 8.11), while marginally degraded, show a good correlation to those obtained from finite element methods (fig. 8.23). The sensitivity of developed SIF solutions on the interpolation factor is an area not covered in this study, however the inherent stability of the interpolation of weight functions methodology appears to be robust with respect to small variations in interpolation factor. The examples given, though encouraging do not constitute a full investigation and validation that is warranted. Limitations of the technique are likely to exist stemming possibly from thickness effects and the base geometry weight functions used. The body of work contained here sought to demonstrate the approximate methodology rather than attempt to identify and quantify where such limitations exist.

Section 8.3 describes application of a similar approximate methodology applied to intrusion and protrusion notches. Once more interpolation factors calculated in chapter 5 were used in conjunction with auxiliary solutions described in section 8.5. Interpolation factors determined via the approximate methodology are compared to those using the methodology described in section 8.2 in fig. 8.17. Approximate interpolation factors again show a good general correlation to the 'exact' interpolation factors determined from analysis of constituent geometries. New SIF solutions obtained from the approximate methodology for the protrusion notch under pure tension are displayed in fig. 8.25. The apparent insensitivity of the ultimate SIF solutions to small variations in interpolation factor are once more evident suggesting that the approximate methodology's economy and new SIF solutions made possible by its implementation may be expoited.

8.8 – Conclusions

This chapter has sought to futher validate the weight function interpolation scheme by application to more generalised intrusion and protrusion notches. An alternative, more general form of expression for the determination of interpolation factor was applied and shown to give new SIF solutions of high accuracy. The versatile nature of this representation of interpolation factor allows its calculation from any consituent geometry SIF solution and associated stress distribution. The

ability to rapidly generate new SIF solutions for complex geometries was, once more demonstrated and implemented by means of a computer algorithm.

The scope of work conducted upon two-dimensional geometries contained in this thesis has successfully developed and validated a weight function methodology for the determination of weight functions and SIF solutions for cracks in complex geometries. Throughout chapters 4 to 8 the interpolation of weight functions has been shown to give new SIF solutions of high accuracy in a manner that is robust and of high stability, rigorously validated against both numerical and experimental solutions. The consistent, good performance of the interpolation scheme was shown to be universally applicable to all notch types investigated with no identified limitations. It may, therefore, be said to provide a 'complete' solution which superceeds the methodologies reviewed in chapter 2, most notably the limited composition of weight functions methodology from which it was developed. SIF solutions for cracks in complex geometries can be simply ascertained from constituent geometry SIF solutions and crack-line stress distributions. It can therefore be said to offer a practicable and readily implementable solution to the long-standing problem of calculating such SIF solutions identified in Chapter 1.

The versatile nature of the interpolation scheme has allowed a number of related interpolation methodologies, of increased economy, to be identified and demonstrated. Though not rigorously examined, results achieved have highlighted the possibility of developing tools allowing the calculation of new SIF solutions for a very large range of external notch types from a relatively small 'library' of constituent geometry solutions. Chapter 11 discusses possibilites arising from these observations and suggests futher applications to internal notches, axi-symmetric notches and multiple crack problems.

8.9 – Tables

Tab. 8.1 – Constituent Geometry Reference SIF Solutions for the Protrusion Notch ($b/\rho = 6$, $\alpha = 90°$, Remotely Applied Tension)

a/ρ	Y_I		
	$L_P/b = 0.25$	$L_P/b = 0.5$	$L_P/b = 1.0$
0.025	1.489	1.716	2.023
0.05	1.454	1.677	1.978
0.075	1.421	1.639	1.934
0.1	1.392	1.604	1.892
0.15	1.342	1.541	1.817
0.2	1.301	1.488	1.751
0.25	1.268	1.443	1.694
0.3	1.242	1.405	1.643
0.4	1.203	1.343	1.560
0.5	1.177	1.296	1.493
0.7	1.147	1.233	1.396
1.1	1.127	1.170	1.284
1.3	1.124	1.155	1.249
1.6	1.122	1.140	1.213
1.9	1.122	1.132	1.188
2.2	-	1.128	1.171
2.5	-	1.125	1.159
3	-	-	1.145
3.5	-	-	1.136
4	-	-	1.131
5	-	-	1.126
6	-	-	1.124

Tab. 8.2 – Constituent Geometry Reference SIF Solutions for the Intrusion Notch ($b/\rho = 6$, $\alpha = 90°$, Remotely Applied Tension)

a/ρ	Y_I	
	$L_P/b = 0.125$	$L_P/b = 0.25$
0.05	4.476	4.122
0.1	4.263	3.924
0.15	4.101	3.775
0.2	3.956	3.640
0.25	3.826	3.520
0.3	3.708	3.412
0.4	3.506	3.228
0.5	3.336	3.076
0.7	3.068	2.840
0.9	2.862	2.666
1.1	2.696	2.530
1.3	2.560	2.420
1.6	2.393	2.289
1.9	2.260	2.183
2.2	2.151	2.096
2.5	2.061	2.021
3	1.941	1.919
3.5	1.848	1.836
4	1.774	1.768
5	1.664	1.663
6	1.586	1.586
8	1.484	1.484
10	1.419	1.419

Tab. 8.3 – SIF Solution Coefficients (eq. 8.4) for the Semi-Finite Protrusion Notch ($b/\rho = 6$, $\alpha = 90°$) Subject to Remotely Applied Tension

L_P/b	M_5	M_4	M_3	M_2	M_1	M_0	R^2
1.0	0.1897	-0.672	0.913	0.6318	-0.1072	1.1215	1.00
0.5	-0.1699	-0.0724	1.2697	-0.4163	0.0296	1.1215	1.00
0.25	-1.457	4.0213	-2.8997	0.8264	-0.0837	1.1215	1.00

Tab. 8.4 – SIF Solution Coefficients (eq. 8.4) for the Semi-Finite Intrusion Notch ($b/\rho = 6$, $\alpha = 90°$) Subject to Remotely Applied Tension

L_I/b	M_5	M_4	M_3	M_2	M_1	M_0	R^2
0.25	-3.3691	8.3799	-5.4837	0.3561	3.3092	1.1215	1.00
0.125	1.0294	-0.7185	-0.3743	0.4533	3.1994	1.1215	1.00

Tab. 8.5 – Stress Distribution Coefficients (eq. 8.5) for the Semi-Finite Protrusion Notch ($b/\rho = 6$, $\alpha = 90°$) Subject to Remotely Applied Tension

L_P/b	N_5	N_4	N_3	N_2	N_1	N_0	R^2
1.0	3.0769	-7.9183	7.384	-1.5685	-0.1077	1.0	1.00
0.5	1.4517	-4.332	5.3898	-2.0323	0.1029	1.0	1.00
0.25	-1.1522	2.9677	-1.4063	-0.0613	0.0020	1.0	1.00

Tab. 8.6 – Stress Distribution Coefficients (eq. 8.5) for the Semi-Finite Intrusion Notch ($b/\rho = 6$, $\alpha = 90°$) Subject to Remotely Applied Tension

L_I/b	N_5	N_4	N_3	N_2	N_1	N_0	R^2
0.25	-9.9799	30.084	-32.335	15.588	-0.1929	1.0	1.00
0.125	-18.188	48.001	-43.79	16.767	0.0236	1.0	1.00

Tab. 8.7 – Stress Distribution Coefficients (eq. 8.6) for the Finite Protrusion Notch ($b/\rho = 6$, $\alpha = 90°$, $b/T = 0.2727$)

L_P/b	Load Case	P_5	P_4	P_3	P_2	P_1	P_0	R^2
1.0	Pure Tension	-5.1722	15.43	-17.12	10.062	2.6101	1.1617	1.00
0.5	Pure Tension	0.4807	-1.3697	1.965	-0.1903	0.3626	1.0351	1.00
0.25	Pure Tension	-0.0465	-0.0543	1.6034	-1.3797	0.2571	0.9859	1.00
1.0	Pure Bending	20.275	-65.168	81.209	-48.066	14.753	-1.163	1.00
0.5	Pure Bending	26.433	-83.48	102.25	-59.645	17.356	-1.3132	1.00
0.25	Pure Bending	23.484	-74.725	93.417	-56.506	17.002	-1.2854	1.00

Tab. 8.8 – Stress Distribution Coefficients (eq. 8.6) for the Finite Intrusion Notch ($b/\rho = 6$, $\alpha = 90°$, $b/T = 0.2727$)

L_I/b	Load Case	P_5	P_4	P_3	P_2	P_1	P_0	R^2
0.25	Unif. Tension	0.9898	-11.392	27.619	-24.422	13.015	-0.0376	1.00
0.125	Unif. Tension	-6.3278	17.092	-13.183	1.4356	6.7038	0.3699	1.00
0.25	Pure Bending	17.789	-63.059	87.872	-58.863	22.114	-1.9909	1.00
0.125	Pure Bending	12.307	-41.769	57.511	-39.757	17.482	-1.6928	1.00

Tab. 8.9 – Curve Fit Coefficients (eqs. 8.15a, 8.15b & 8.17) Describing Geometric Influence of Individual Geometric Parameters as an Interpolation Factor

$f(a)$	α	b/ρ	L_I/b	L_P/b	D_5	D_4	D_3	D_2	D_1	D_0	ξ	R^2
$f_\alpha(a)$	0	0	0	0	0.0	0.0	0.0	0.0	0.0	1.0	0.0	1.00
$f_\alpha(a)$	15	0	0	0	-3.3602	11.614	-16.018	10.441	-2.3594	0.1739	0.16	1.00
$f_\alpha(a)$	30	0	0	0	-0.5099	0.9091	-0.905	1.12125	-0.5806	0.0821	0.30	1.00
$f_\alpha(a)$	45	0	0	0	-2.1387	5.4205	-4.8053	1.8869	-0.3201	0.0168	0.50	1.00
$f_\alpha(a)$	90	0	0	0	0.0	0.0	0.0	0.0	0.0	0.0	0.0	1.00
$f_\rho(a)$	0	1	0	0	8.4042	-23.403	26.274	-12.791	2.7253	-0.207	0.3	1.00
$f_\rho(a)$	0	15	0	0	0.7484	-0.2411	0.3279	0.1318	0.0275	0.0	0.0	1.00
$f_{LI}(a)$	0	0	0	0	0.0	0.0	0.0	0.0	0.0	0.0	0.0	1.00
$f_{LI}(a)$	0	0	0.125	0	9.776	-86.638	199.54	-192.8	84.567	-13.947	0.50	1.00
$f_{LI}(a)$	0	0	0.25	0	50.414	-180.83	247.93	-161.44	50.586	-6.1653	0.40	1.00
$f_{LI}(a)$	0	0	0.5	0	7.0626	-14.997	5.5531	5.956	3.5772	0.5031	0.33	1.00
$f_{LI}(a)$	0	0	1.0	0	-21.485	68.197	-82.304	45.364	10.102	0.7885	0.25	1.00
$f_{LI}(a)$	0	0	2.0	0	4.5793	-17.596	27.223	-21.33	8.5229	-0.8981	0.25	1.00
$f_{LI}(a)$	0	0	∞	0	0.0	0.0	0.0	0.0	0.0	0.5	0.0	1.00
$f_{LP}(a)$	0	0	0	0	0.0	0.0	0.0	0.0	0.0	1.0	0.0	1.00
$f_{LP}(a)$	0	0	0	0.25	107.17	-400.4	586.03	-423.29	151.56	-20.573	0.60	1.00
$f_{LP}(a)$	0	0	0	0.5	1.6555	0.8466	-8.97	8.5237	-2.8793	1.3223	0.40	1.00
$f_{LP}(a)$	0	0	0	1.0	4.9584	-18.919	29.859	-23.577	8.1781	-0.0002	0.33	1.00
$f_{LP}(a)$	0	0	0	2.0	10.623	-33.824	40.492	-21.437	3.7962	0.8495	0.25	1.00
$f_{LP}(a)$	0	0	0	4.0	-6.3422	22.461	31.652	22.428	-8.1464	1.7513	0.25	1.00
$f_{LP}(a)$	0	0	0	∞	0.0	0.0	0.0	0.0	0.0	0.5	0.0	1.00

Tab. 8.10 – SIF Solutions for Cracks at a Symmetric Notch in a Semi-Finite Plane

$\alpha = 30°$, $b/\rho = 1$		$\alpha = 30°$, $b/\rho = 15$	
a/ρ	Y	a/ρ	Y
0.025	1.102	0.1	1.065
0.05	1.087	0.15	1.052
0.075	1.075	0.2	1.043
0.1	1.066	0.25	1.037
0.15	1.052	0.32	1.031
0.2	1.044	0.4	1.027
0.25	1.038	0.5	1.024
0.32	1.033	0.7	1.021
0.4	1.030	0.9	1.019
0.5	1.029	1.1	1.018
0.7	1.028	1.4	1.017
0.9	1.029	1.7	1.017
1.1	1.032	2.2	1.016
1.4	1.036	2.6	1.016
1.7	1.040	3.0	1.016
2.2	1.048	4.0	1.017
2.6	1.054	-	-

Tab. 8.11 – Stress Distribution Coefficients (eq. 8.6) for Finite Symmetric Notches ($\alpha = 15°$, $b/T = 0.2727$, Uniform Tension)

b/ρ	P_5	P_4	P_3	P_2	P_1	P_0	R^2
1	14.14	-37.792	49.23	-36.937	18.507	-2.754	1.00
15	44.282	-113.4	119.18	-61.199	18.998	0.4738	1.00

Tab. 8.12 – SIF Solutions for a Sharp Semi-Finite Intrusion Notch ($b/\rho = 0$, $\alpha = 90°$)

$L_I/b = 4.0$		$L_I/b = 2.0$		$L_I/b = 1.0$		$L_I/b = 0.5$		$L_I/b = 0.25$	
a/b	Y_I	a/b	Y_I	a/b	Y_I	a/b	Y_I	a/b	Y_I
0.450	1.040	0.250	1.028	0.050	1.013	0.025	1.010	0.025	1.009
0.550	1.044	0.350	1.033	0.075	1.015	0.050	1.012	0.050	1.008
0.700	1.049	0.450	1.036	0.100	1.017	0.075	1.013	0.075	1.005
0.850	1.054	0.550	1.039	0.150	1.020	0.100	1.013	0.100	1.000
1.000	1.057	0.700	1.042	0.200	1.022	0.150	1.012	0.125	0.995
1.250	1.062	0.850	1.044	0.250	1.023	0.200	1.010	0.150	0.989
1.500	1.065	1.000	1.045	0.350	1.024	0.250	1.006	0.200	0.979
1.750	1.067	1.200	1.047	0.450	1.024	0.350	0.999	0.250	0.972
2.000	1.069	1.400	1.047	0.500	1.023	0.450	0.994	0.300	0.968
2.150	1.070	1.600	1.048	0.650	1.022	0.550	0.992	0.350	0.966
2.300	1.071	1.800	1.049	0.850	1.020	0.700	0.993	0.450	0.968
2.450	1.071	2.000	1.051	1.000	1.021	0.850	0.997	0.550	0.972
2.600	1.072	2.150	1.052	1.150	1.022	1.000	1.002	0.700	0.981
2.750	1.073	2.300	1.053	1.300	1.024	1.125	1.007	0.850	0.990
2.875	1.073	2.450	1.055	1.450	1.027	1.250	1.012	-	-
3.000	1.074	2.600	1.056	1.650	1.031	1.375	1.017	-	-
-	-	2.750	1.058	1.850	1.035	-	-	-	-
-	-	2.875	1.059	2.000	1.039	-	-	-	-
-	-	3.000	1.061	2.150	1.042	-	-	-	-
-	-	-	-	2.300	1.045	-	-	-	-
-	-	-	-	2.450	1.048	-	-	-	-

Tab. 8.13 – SIF Solutions for a Sharp Semi-Finite Protrusion Notch ($b/\rho = 0$, $\alpha = 90°$)

$L_P/b = 4.0$		$L_P/b = 2.0$		$L_P/b = 1.0$		$L_P/b = 0.5$		$L_P/b = 0.25$	
a/b	Y_I	a/b	Y_I	a/b	Y_I	a/b	Y_I	a/b	Y_I
0.500	1.044	0.200	1.030	0.100	1.027	0.050	1.027	0.025	1.026
0.575	1.048	0.250	1.034	0.150	1.036	0.075	1.035	0.050	1.043
0.650	1.051	0.350	1.042	0.200	1.044	0.100	1.043	0.075	1.057
0.750	1.055	0.450	1.050	0.250	1.051	0.150	1.057	0.100	1.069
0.850	1.059	0.500	1.053	0.350	1.064	0.200	1.069	0.150	1.087
1.000	1.064	0.575	1.058	0.450	1.075	0.250	1.079	0.200	1.100
1.150	1.069	0.650	1.063	0.500	1.080	0.350	1.094	0.250	1.108
1.250	1.072	0.750	1.068	0.575	1.086	0.450	1.105	0.300	1.114
1.400	1.075	0.850	1.074	0.650	1.092	0.500	1.108	0.350	1.117
1.550	1.079	1.000	1.081	0.750	1.098	0.575	1.113	0.450	1.121
1.700	1.082	1.150	1.087	0.850	1.103	0.650	1.116	0.550	1.122
1.850	1.085	1.250	1.091	1.000	1.109	0.750	1.119	0.650	1.120
2.000	1.088	1.400	1.096	1.150	1.114	0.850	1.120	0.750	1.121
2.150	1.091	1.550	1.100	1.300	1.116	1.000	1.122	-	-
2.300	1.093	1.700	1.104	1.450	1.119	1.150	1.120	-	-
2.500	1.096	1.850	1.107	1.650	1.120	1.300	1.120	-	-
2.700	1.099	2.000	1.109	1.850	1.121	1.450	1.121	-	-
2.900	1.101	2.150	1.112	2.000	1.122	-	-	-	-
3.000	1.102	2.300	1.114	-	-	-	-	-	-
-	-	2.500	1.116	-	-	-	-	-	-
-	-	2.700	1.118	-	-	-	-	-	-
-	-	2.900	1.119	-	-	-	-	-	-
-	-	3.000	1.119	-	-	-	-	-	-

8.10 – Figures

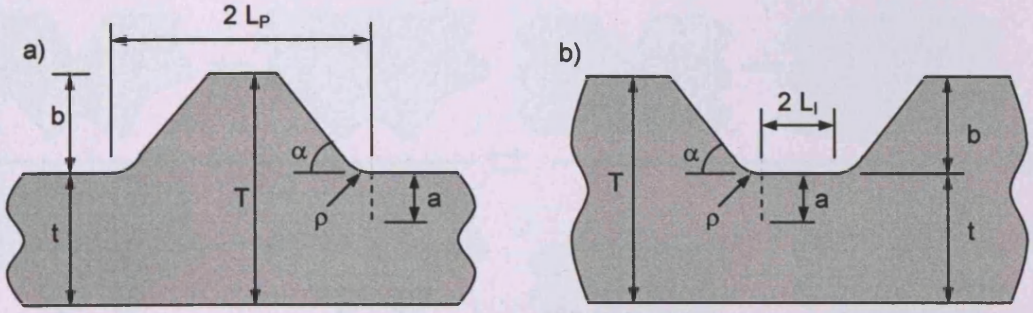

Fig. 8.1 – Geometric Definition of a) Protrusion Notch and b) Intrusion Notch

Fig. 8.2
Matrix of Constituent Notch
Geometries investigated

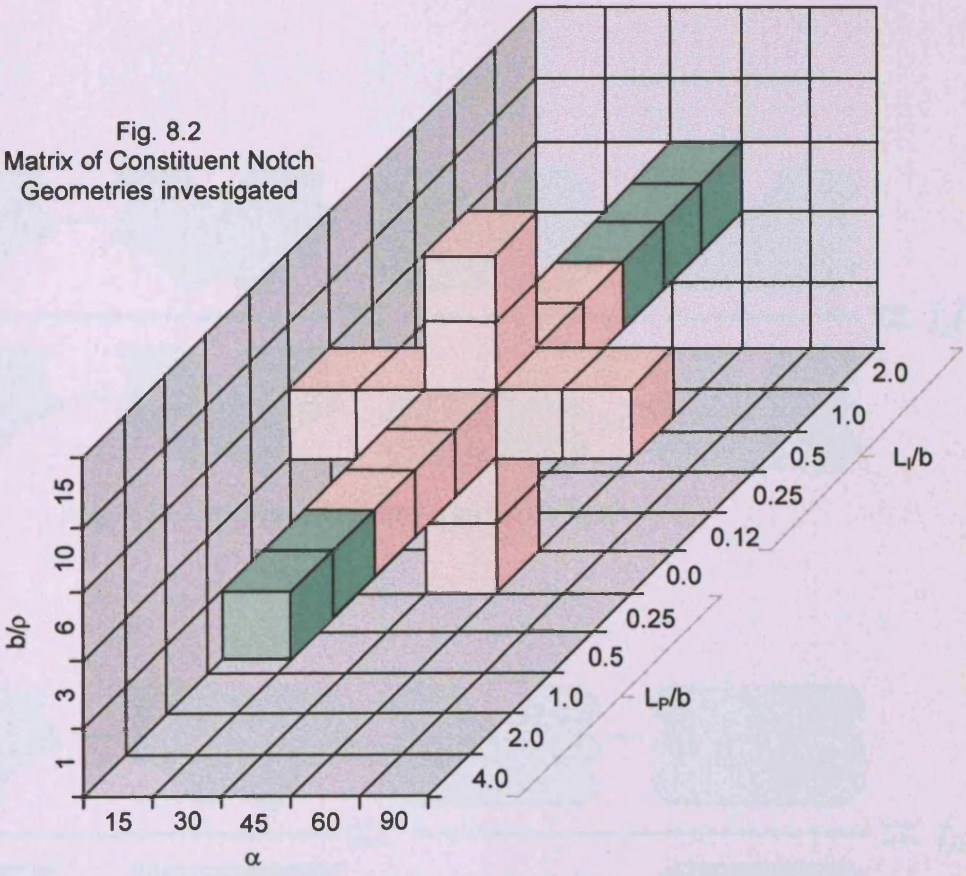

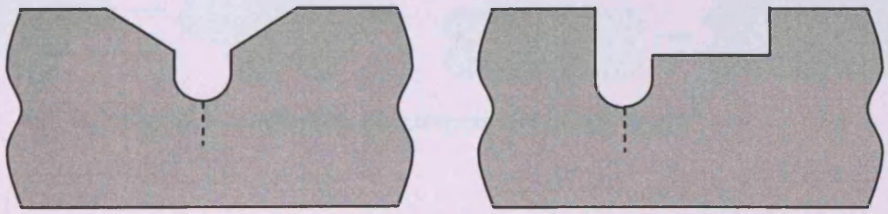

Fig. 8.3 – Examples of Embedded Notch Types

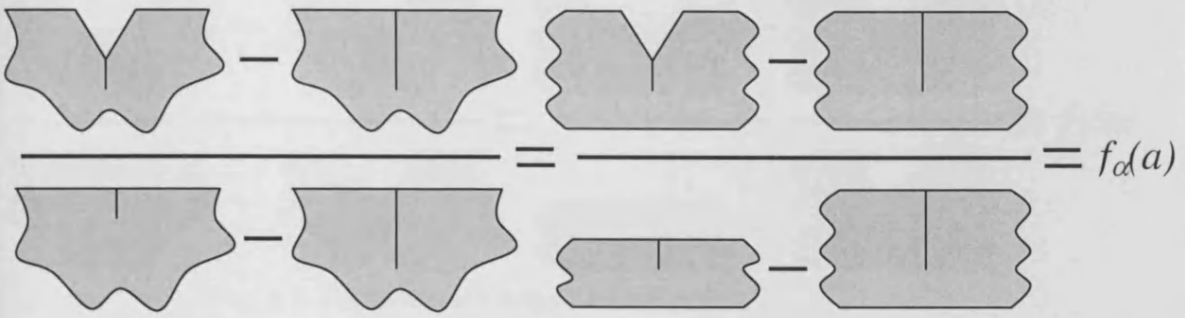

Fig. 8.4 – Definition of Interpolation factor '$f_{\rho}(a)$'

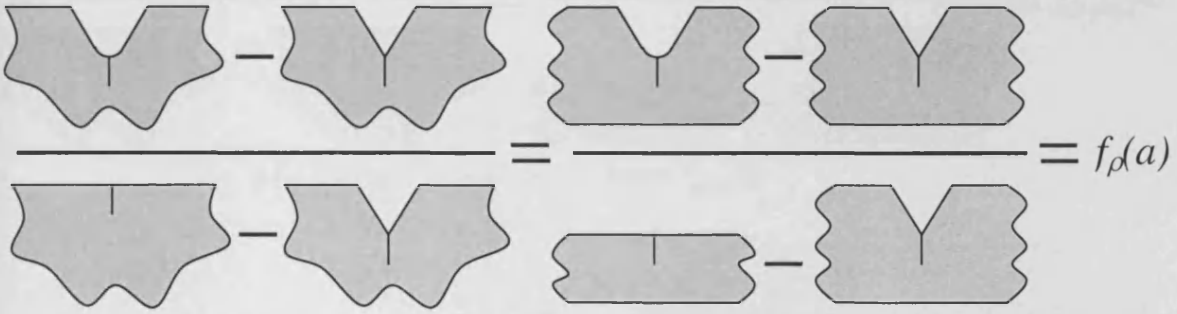

Fig. 8.5 – Definition of Interpolation factor '$f_{\alpha}(a)$'

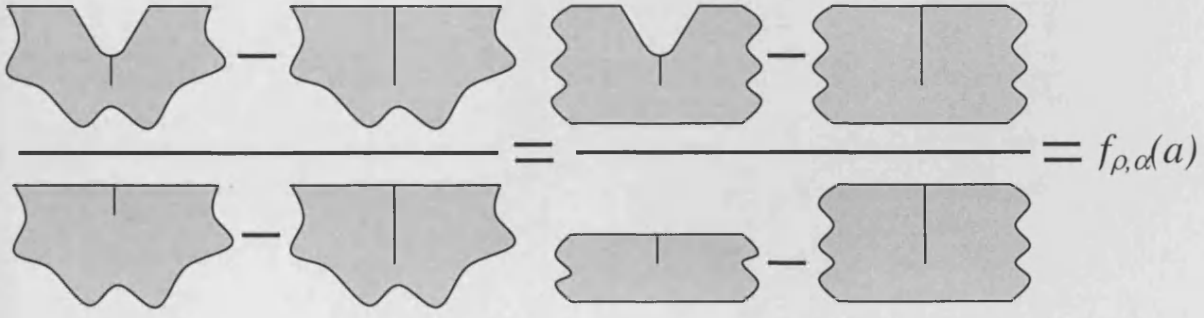

Fig. 8.6 – Definition of Interpolation factor '$f_{\rho,\alpha}(a)$'

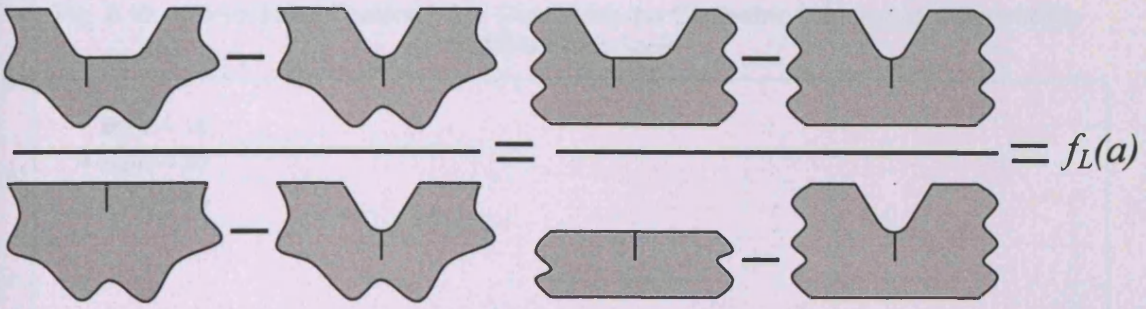

Fig. 8.7 – Definition of Interpolation factor '$f_L(a)$'

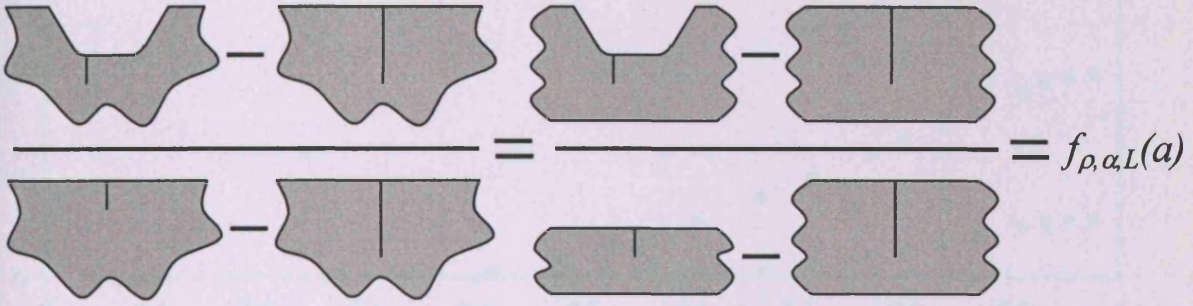

Fig. 8.8 – Definition of Interpolation factor '$f_{\rho,\alpha,L}(a)$'

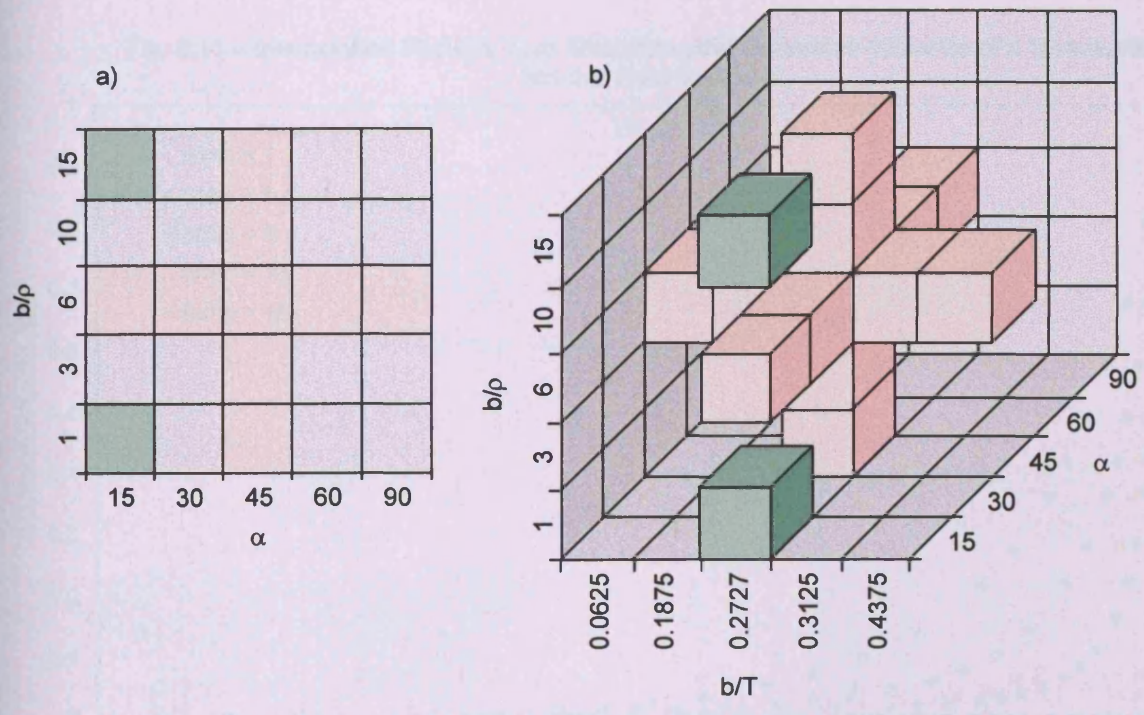

Fig. 8.9 – a) Matrix of Constituent Geometries for Symmetric Notches. b) Matrix of Finite Thickness Solutions Investigated.

Fig. 8.10 – Interpolation Factors, '$f_\alpha(a)$' Describing the Geometric Influence of a Symmetric Notch's Flank Angle

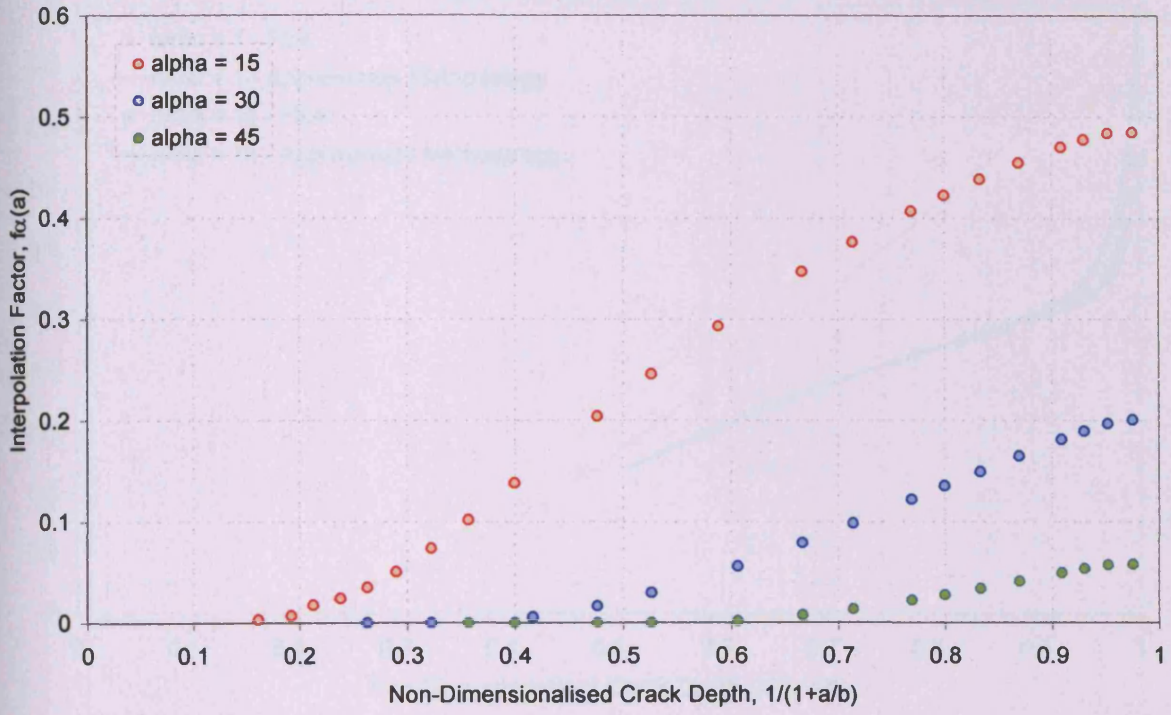

Fig. 8.11 – Interpolation Factors, '$f_\rho(a)$' Describing the Geometric Influence of a Symmetric Notch's Root Radius

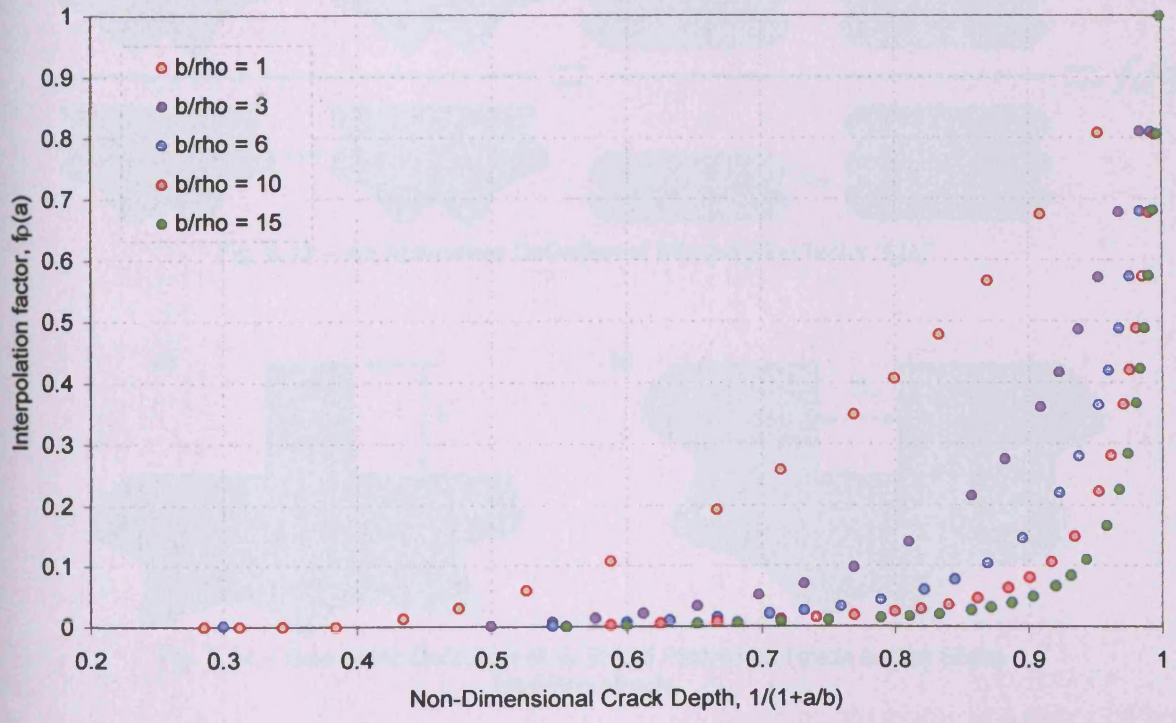

Fig. 8.12 – Comparison of Interpolation Factors Determined by the Approximate Methodology Using Eq. 8.10 and the 'Exact' Methodology Using Data Contained in Tab. 8.10

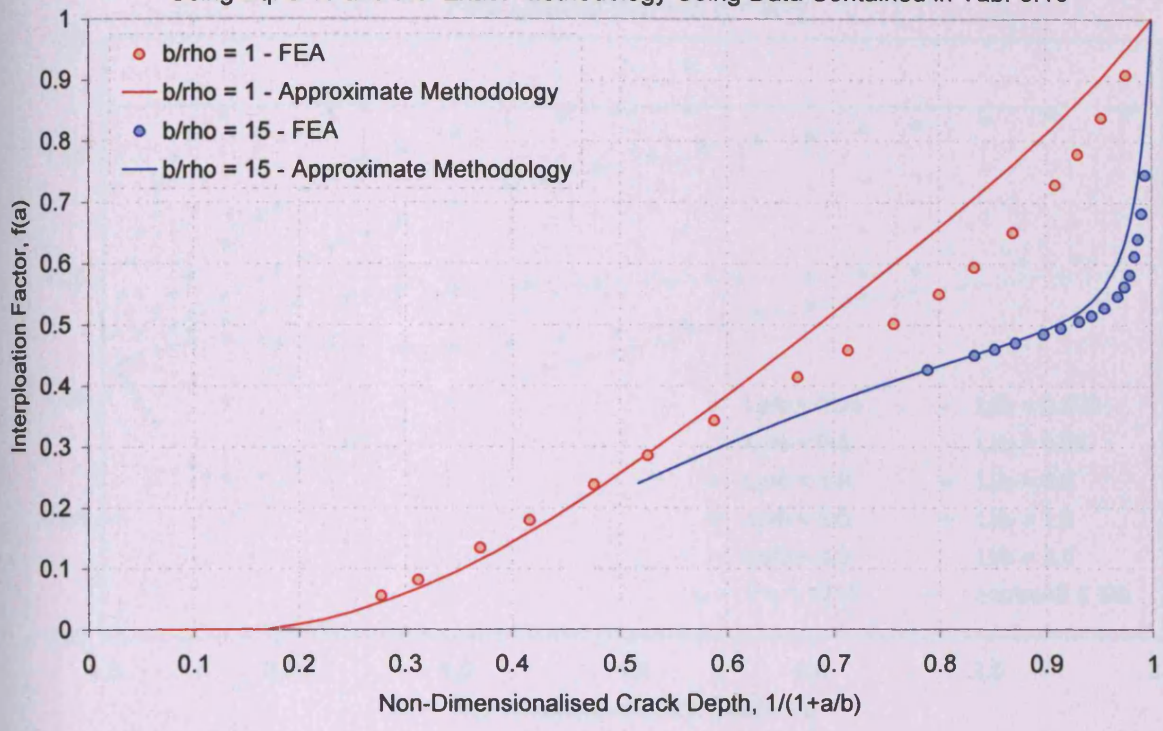

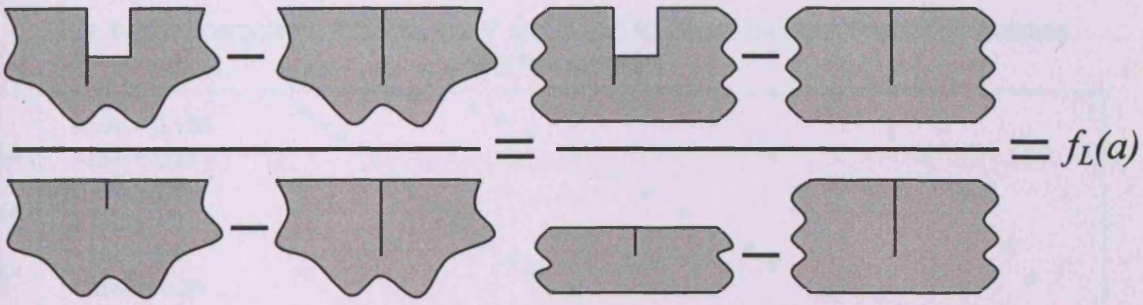

Fig. 8.13 – An Alternative Definition of Interpolation factor '$f_L(a)$'

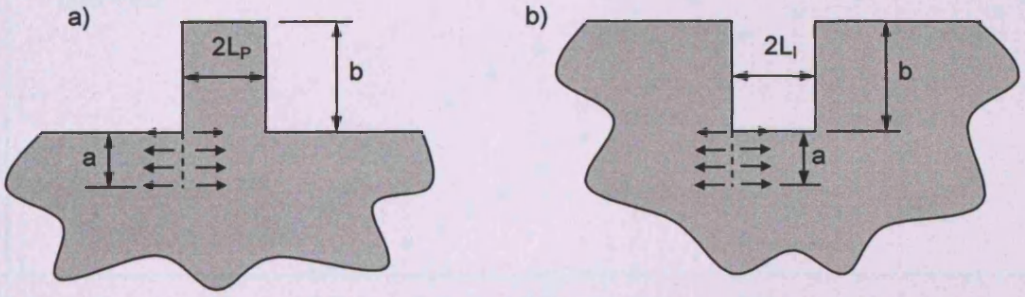

Fig. 8.14 – Geometric Definition of a) Sharp Protrusion Notch and b) Sharp Intrusion Notch

Fig. 8.15 – SIF Solutions for Sharp Intrusion/Protrusion Notches Subject to Uniform Crack Face Loading (b/ρ = 0, α = 90°)

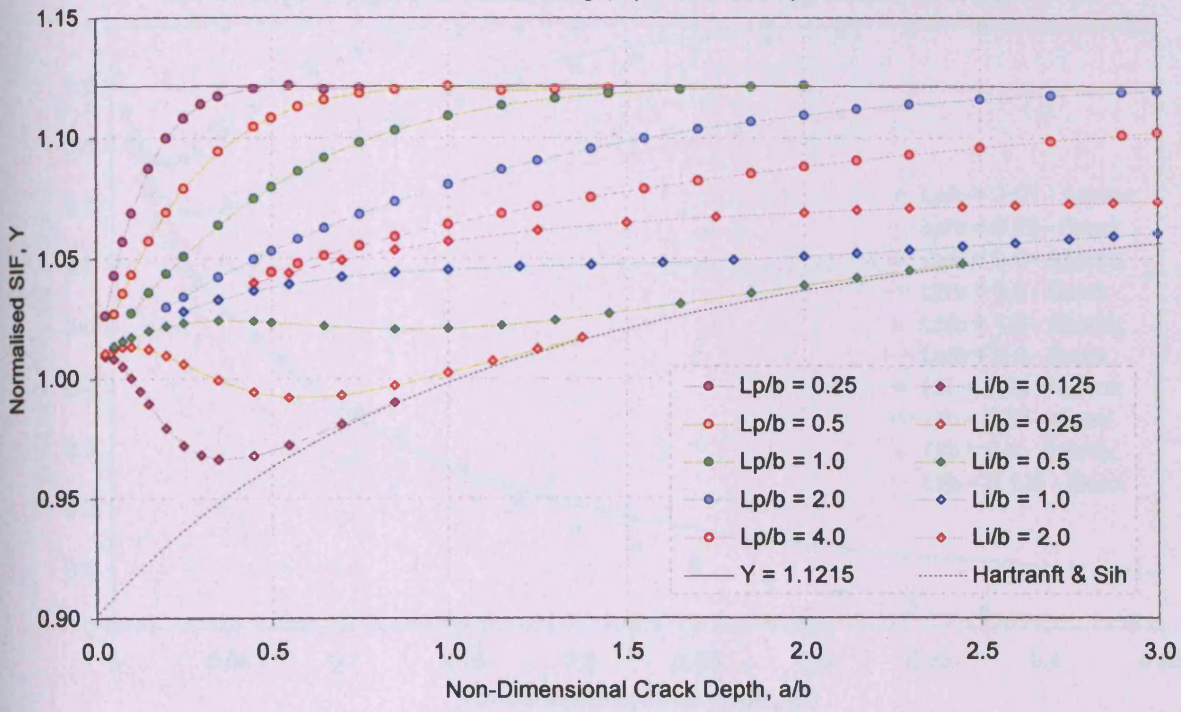

Fig. 8.16 – Interpolation Factors, '$f_{LI}(a)$' and '$f_{LP}(a)$' for Sharp Intrusion/Protrusion Notches (b/ρ = 0, α = 90°)

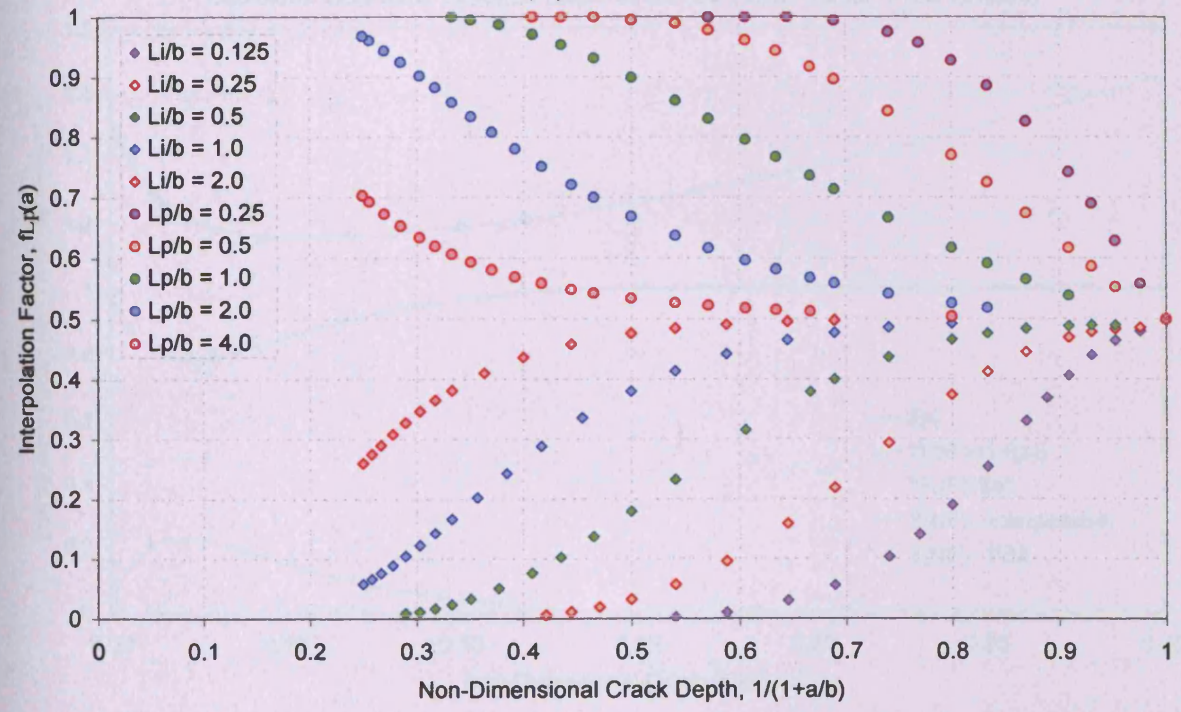

Fig. 8.17 – Comparison of Interpolation Factros Determined by the Approximate Methodology Using Eq. 8.18 and the 'Exact' Methodology Described in Section 8.2

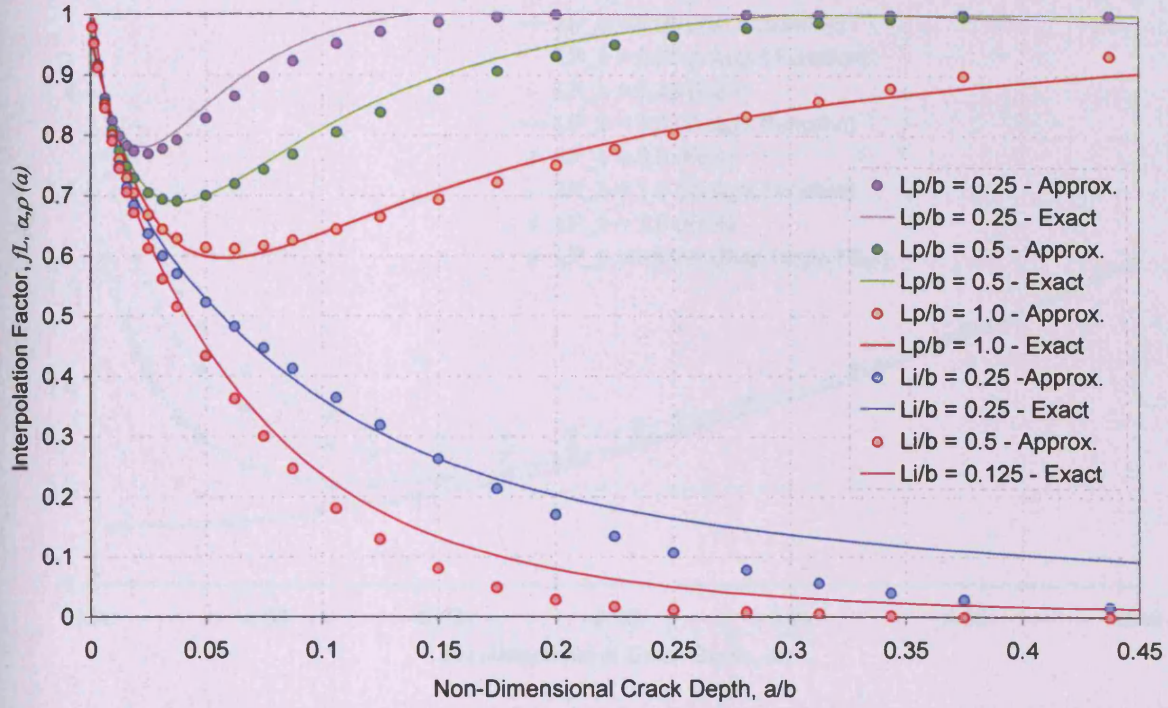

Fig. 8.18 – Influence of the Two Base geometries Upon the Protrusion Notched, Finite Thickness Geomerty Solution (b/ρ = 6, α = 90°, L_P/b = 0.25, Pure tension)

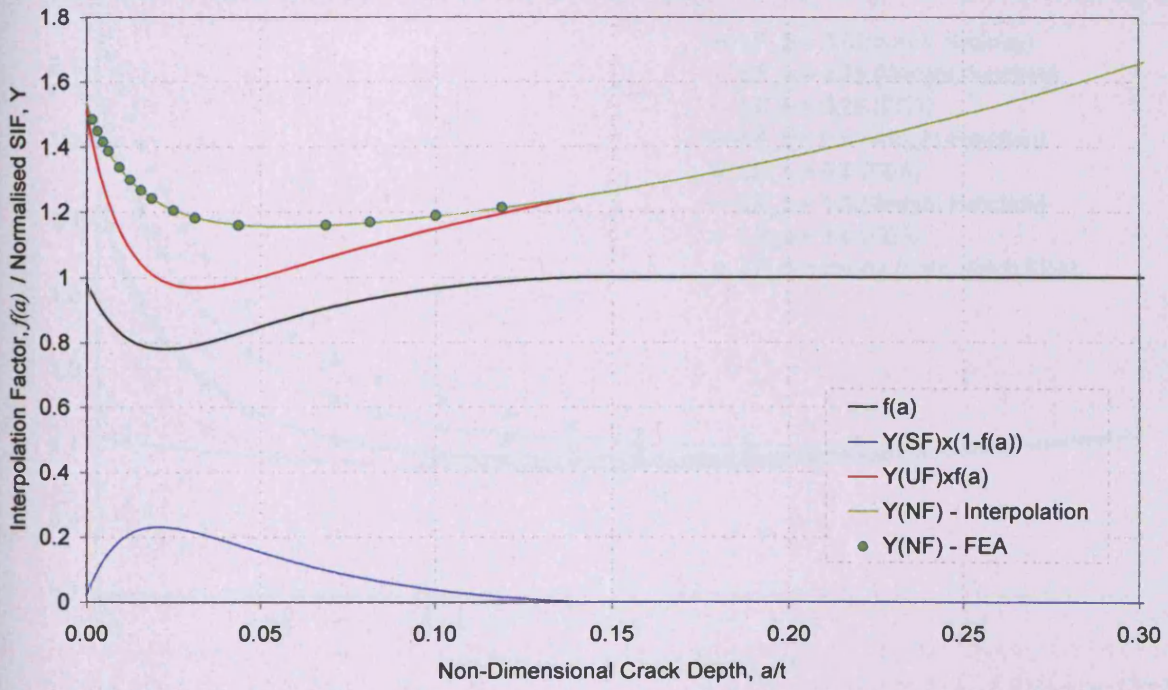

Fig. 8.19 – SIF Solutions Obtained From the Interpolation Scheme for Finite Thickness, Protrusion Notched Geometry (b/T = 0.2727, α = 90°, b/ρ = 6, Pure Tension)

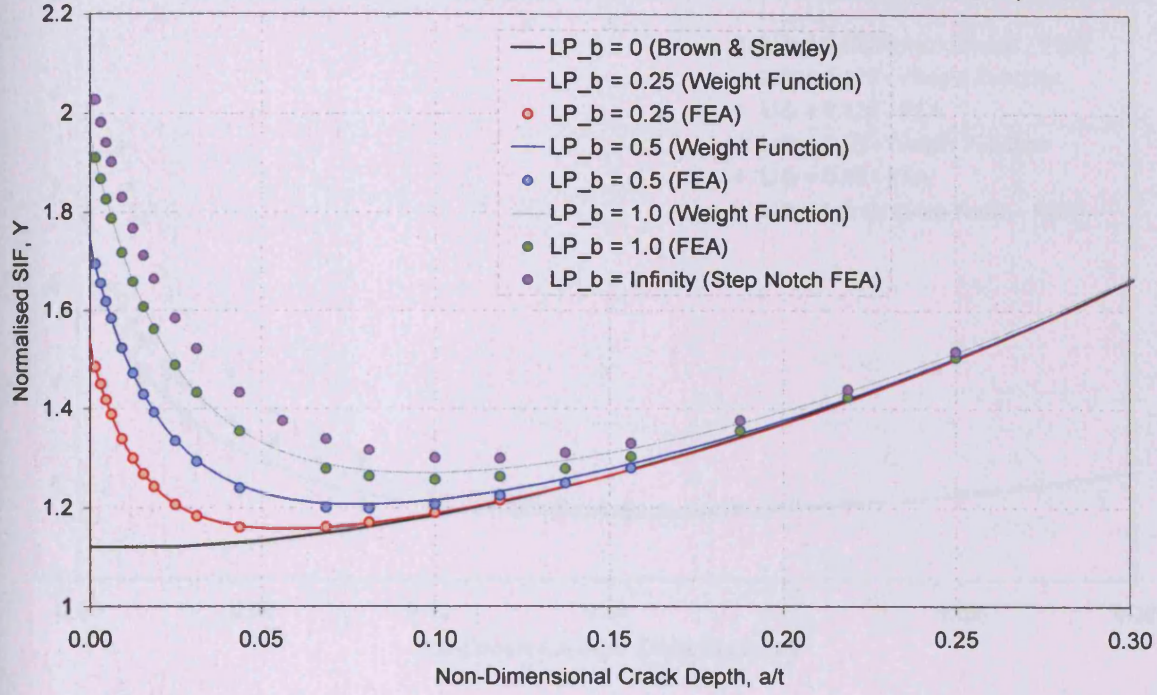

Fig. 8.20 – SIF Solutions Obtained From the Interpolation Scheme for Finite Thickness, Protrusion Notched Geometry (b/T = 0.2727, α = 90°, b/ρ = 6, Pure Bending)

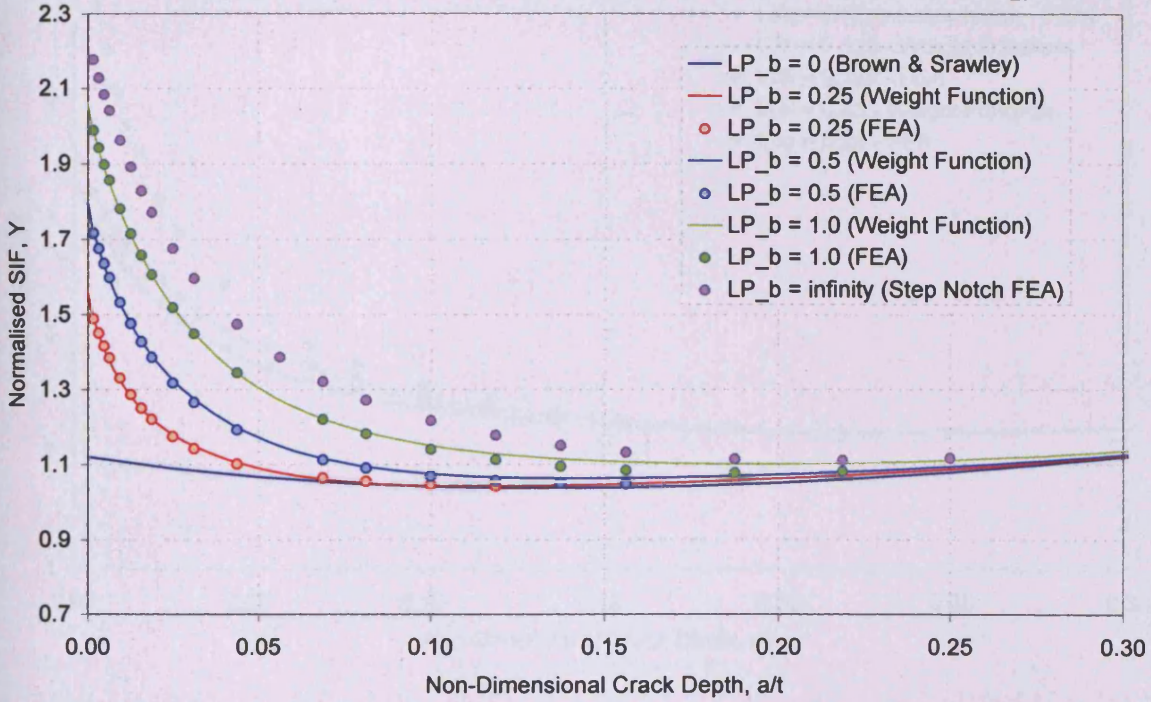

Fig. 8.21 – SIF Solutions Obtained From the Interpolation Scheme for Finite Thickness, Intrusion Notched Geometry (b/T = 0.2727, α = 90°, b/ρ = 6, Uniform Tension)

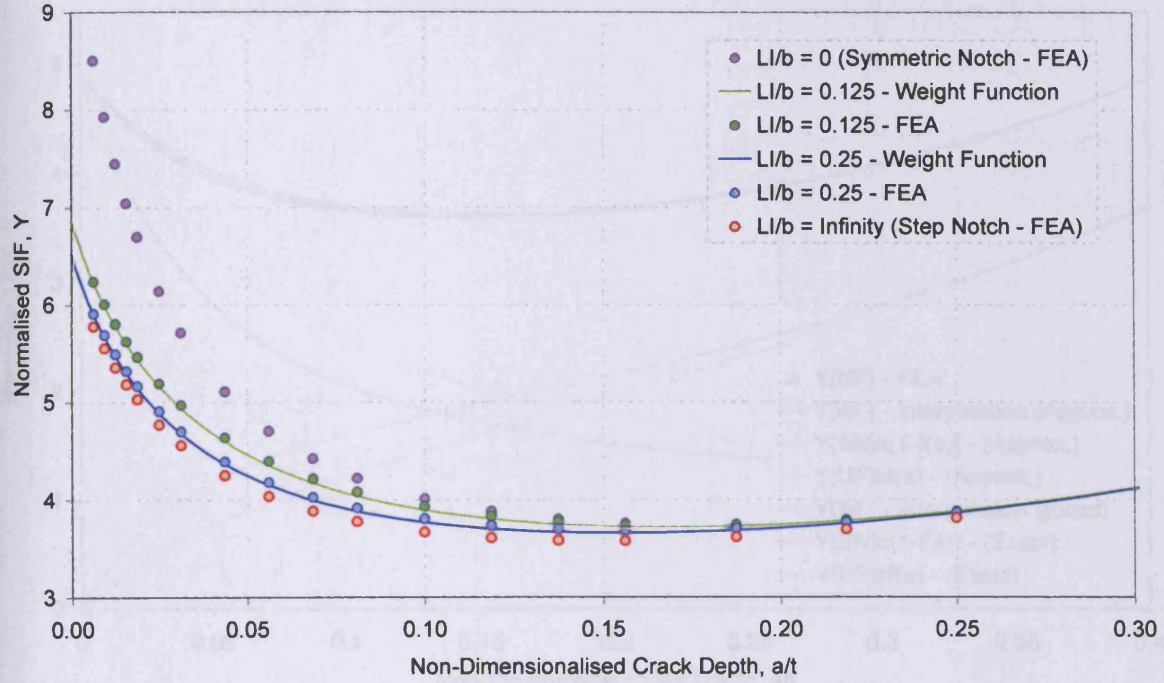

Fig. 8.22 – SIF Solutions Obtained From the Interpolation Scheme for Finite Thickness, Intrusion Notched Geometry (b/T = 0.2727, α = 90°, b/ρ = 6, Pure Bending)

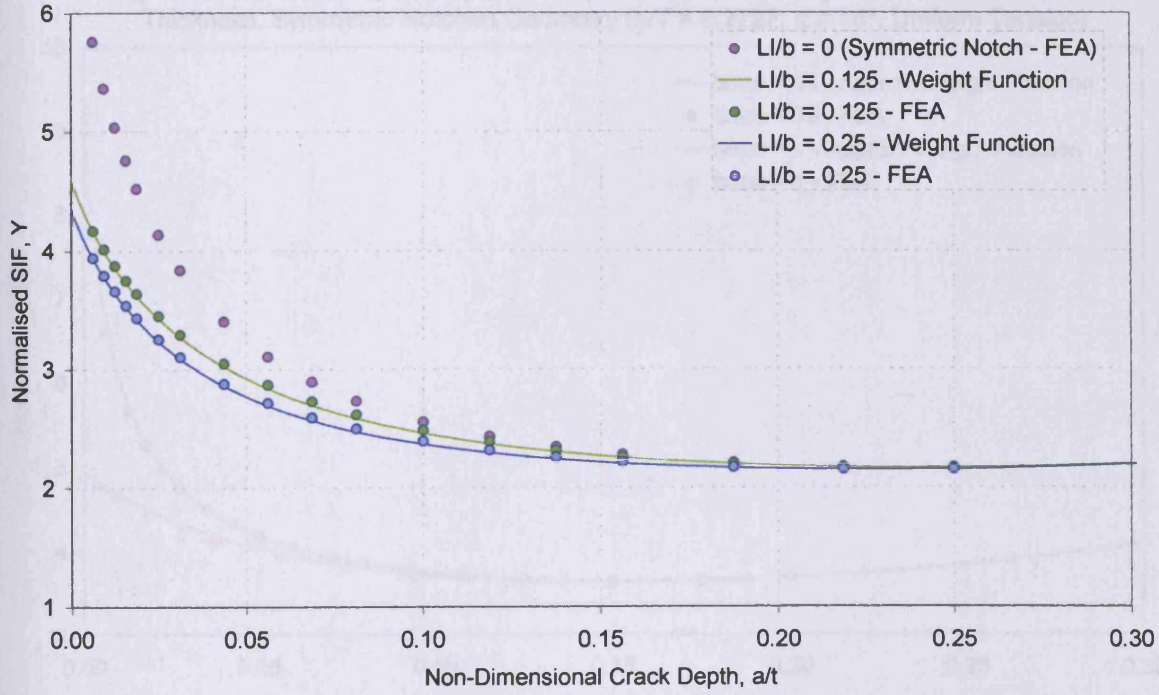

Fig. 8.23 – Contribution to the Total SIF Solution From each Base Geometry Weight Function

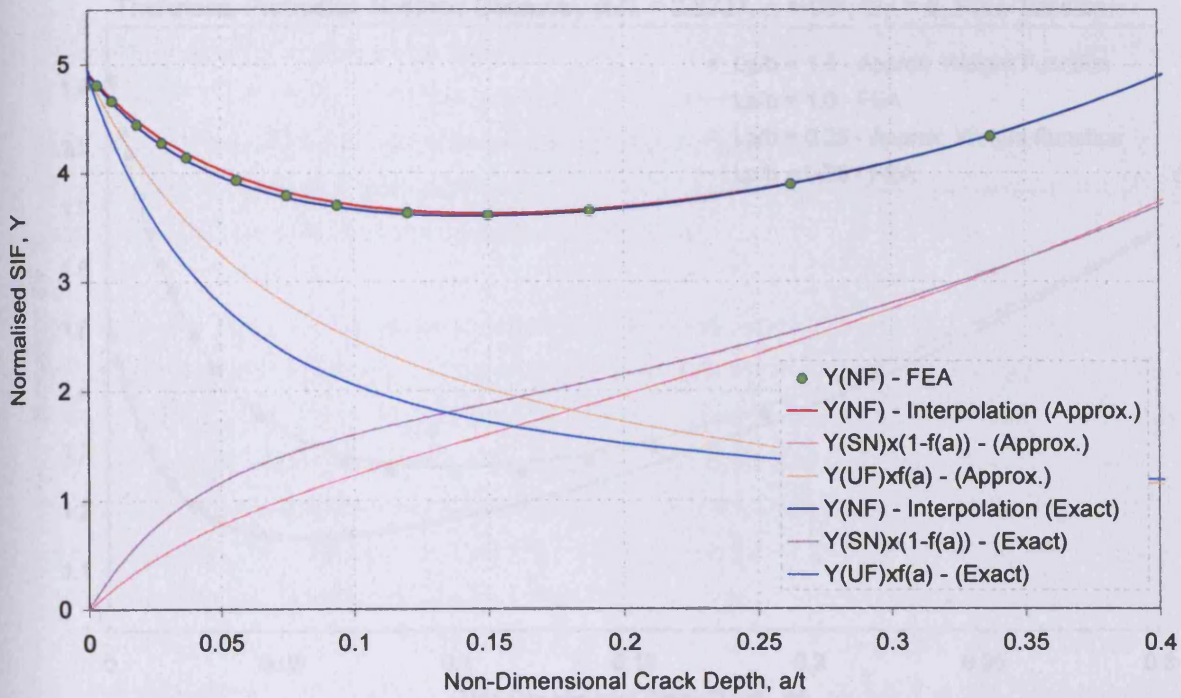

Fig. 8.24 – SIF Solutions Obtained From the Approximate Interpolation Scheme for Finite Thickness, Symmetric Notched Geometry (b/T = 0.2727, α = 15°, Uniform Tension)

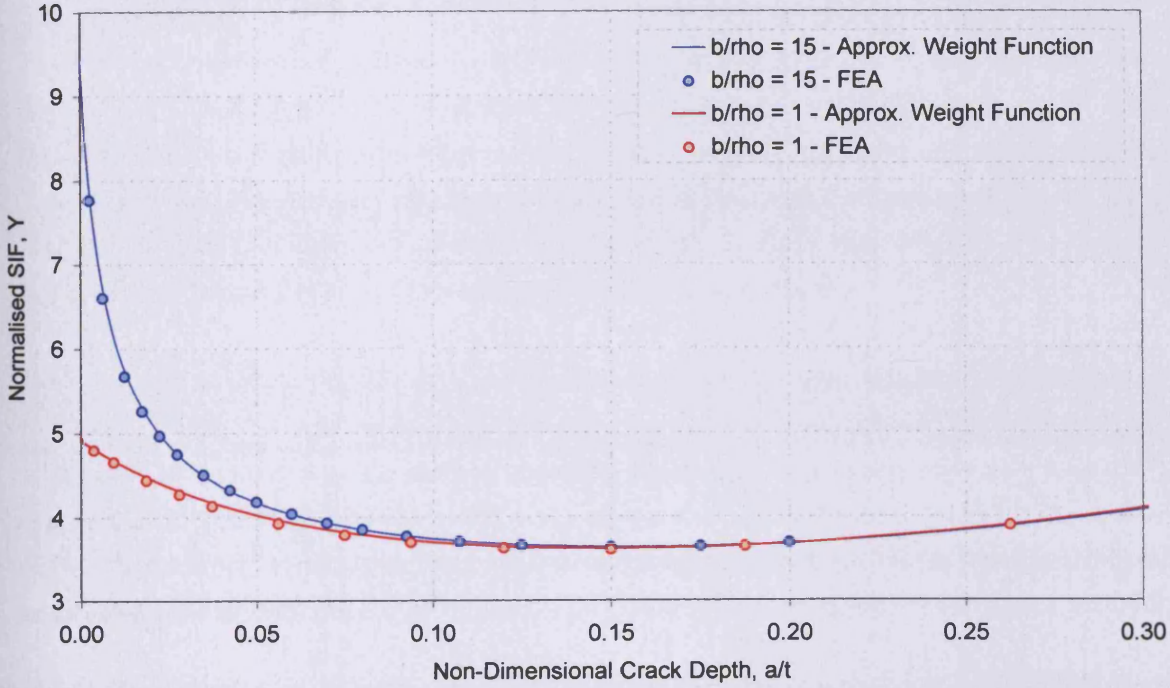

Fig. 8.25 – SIF Solutions Obtained From the Approximate Interpolation Scheme for Finite Thickness, Protrusion Notched Geometry (b/T = 0.2727, α = 90°, b/ρ = 6, Pure Tension)

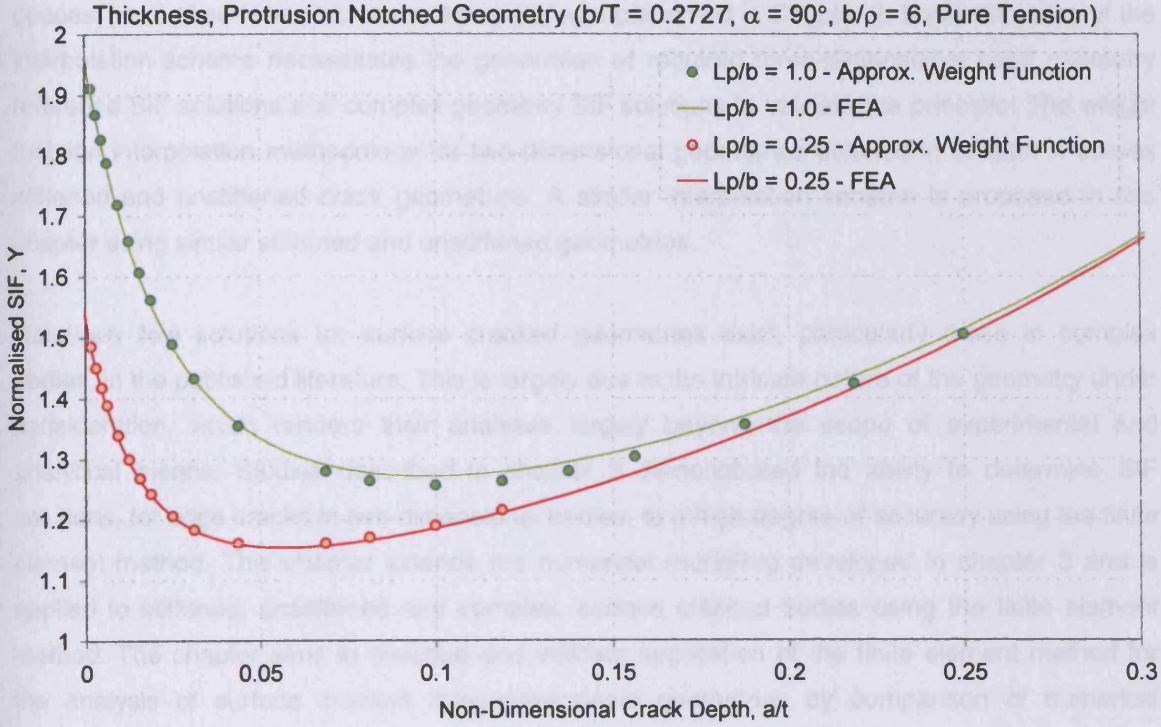

Chapter 9 - Modelling Surface Cracks Using Finite Elements

An extended application of the weight function methodology, to derive new SIF solutions for the deepest point of surface cracks at notch roots, was presented in Chapter 2. Implementation of the interpolation scheme necessitates the generation of required three-dimensional base geometry reference SIF solutions and complex geometry SIF solutions to validate the principle. The weight function interpolation methodology for two-dimensional geometries detailed in chapter 4 utilises stiffened and unstiffened crack geometries. A similar interpolation scheme is proposed in this chapter using similar stiffened and unstiffened geometries.

Relatively few solutions for surface cracked geometries exist, particularly those in complex bodies, in the published literature. This is largely due to the intricate nature of the geometry under consideration, which renders their analyses largely beyond the scope of experimental and analytical means. Studies described in chapter 3 demonstrated the ability to determine SIF solutions, for edge cracks in two-dimensional bodies, to a high degree of accuracy using the finite element method. This chapter extends the numerical modelling developed in chapter 3 and is applied to stiffened, unstiffened and complex, surface cracked bodies using the finite element method. The chapter aims to describe and validate application of the finite element method for the analysis of surface cracked three-dimensional geometries by comparison of numerical solutions obtained to those available in published literature. The geometry used for this purpose is the unstiffened surface cracked flat plate.

9.1 – Introduction

Surface cracks embedded in three-dimensional plates subject to tension and/or bending loads (fig. 9.1), whether notched or un-notched, are assumed to be semi-elliptical in shape. This approximation is supported by a large number of observations made from experimental fatigue crack growth and the analysis of fracture surfaces. Fig. 9.2 depicts a fatigue crack in a flat plate that was subject to a cyclic non-uniform bending stress. A crack has initiated from a starter groove and propagated in a form that closely resembles a semi-ellipse.

Fig. 9.3 shows a surface cracked flat plate in which the crack is positioned centrally in the plate of thickness, 't' width, '$2W$' and length, '$2L$'. The crack size and shape are defined by the semi-ellipse parameters of minor and major axes representing crack depth and crack half-width, 'a' and 'c' respectively. It is commonplace to define crack size and shape in the non-dimensionalised form of 'a/t' and crack aspect ratio 'a/c'. Any position of the crack front is defined by the characteristic angle, 'ϕ' as shown in fig. 9.4.

The surface cracked plate described above constitutes a relatively simple three-dimensional body and is one for which several published solutions are available. The account given in the

remainder of this chapter describes the creation of finite element models of surface cracked flat plates and validation of results obtained by comparison with those in published literature.

9.2 - Mesh Generation

Chapter 3 described the advantages to be gained by creating meshes via a mesh generator program and outlined the principles of its operation. These principles were applied to the creation of the more complex three-dimensional models. The crack front for example is made up of an extrusion of the two-dimensional focused mesh along the path of the crack front. As described in chapter 3 information regarding nodes, elements, loading, boundary conditions, etc. was written to an 'input file' compliant for analysis by the *ABAQUS Standard*[9.2] finite element software.

The geometry presented in fig. 9.3 possesses two planes of symmetry. This property can be exploited to reduce the size of each finite element model and hence increase computational efficiency. Application of symmetrical boundary conditions in the relevant planes allows a quarter model to be representative of the whole geometry. The quarter model is shown diagrammatically in fig. 9.5 with surfaces A and B labelled. With reference to co-ordinate system defined in fig. 9.3 the boundary condition: $U_y = \phi_z = \phi_x = 0$ was applied to surface A and: $U_z = \phi_x = \phi_y = 0$ to surface B. Loading was applied either at the remote boundaries or directly to the crack face as a distributed load over an element face. Twenty node three-dimensional brick elements, 'C3D20' were used throughout the model and were collapsed along one vertex to form elements surrounding the crack tip and along the crack front.

Each model is composed of a cell containing meshing forming the crack detail. The crack cell meshing is automatically generated from the mesh generator program inputs of crack depth, 'a' and crack half-width, 'c'. As shown in fig. 9.6 external faces of the crack cell are composed of a regular arrangement of elements allowing additional element blocks to be simply defined and connected to form the full model.

A plane strain condition is present at most points along the crack front with the exception of the surface point at which a plane stress condition exists. All results presented in this study for points along the crack front are normalised to the plane strain condition. The material response is defined as 'linear elastic' allowing conversion of the J-integral estimates calculated by *ABAQUS/Standard* to a stress intensity factor is given by the equation below.

$$K = \sqrt{JE/\left(1+\upsilon^2\right)} \qquad \text{- 9.1}$$

Non-dimensional SIF solutions are presented normalised as described by eq. 9.2

$$Y = \frac{K}{\sigma_o \sqrt{\pi a}} \quad \text{- 9.2}$$

Figure 9.7a shows a typical mesh produced by the mesh generator program, fig. 9.7b shows the same mesh with boundary conditions applied to surfaces A and B and uniform loading applied to the elements making up the crack face. Fig. 9.7c displays results in the form of the displaced mesh and fig. 9.7d shows a contour plot of stress component, 'σ_{yy}' in the region of the crack. Areas coloured red indicate a high stress magnitude and those coloured blue indicate a low or negative stress magnitude. The crack displayed in fig. 9.7 is subject to loading applied to the crack face, whereas the contour plot depicted in fig. 9.8 shows a similar surface cracked plate subject to a remotely applied tensile loading condition. The possibility exists to derive solutions for surface cracks in plates of any dimension, however as can be seen with reference to figs. 9.7 and 9.8, FE model size is considerably larger than those solved in preceding chapters. In order to produce the numerous solutions required to implement the weight function scheme the models were limited to a single plate size of W/t = 2.75.

9.3 – Surface Cracks in Flat Plates

Validation of the SIF solutions produced by the finite element models was sought by comparing them to those present in published literature. Two of the more salient studies on the geometry under investigation are described below.

Newman and Raju[9.3, 9.4] conducted a finite element study, similar to that presented here, to evaluate SIF solutions for surface cracked plates of infinite width (W/t = ∞) subject to the remote loading conditions of uniform tension and pure bending. Calculated SIF data for a number of points on the crack front were presented as a table of discrete data points and were used in conjunction with results from other sources to formulate a set of empirical equations. The empirical relations are a firmly established set of solutions widely employed on account of their accuracy, broad ranging limits of validity and simplistic form. The equations are valid for tensile and bending load conditions and include a term to account for the influence of finite plate width. These solutions, therefore, represent an important tool for the purposes of validation and verification of the finite element results obtained in this study.

Isida, Noguchi and Yoshida[9.5] produced SIF solutions for surface cracked plates using a body force method quoting an accuracy of less than 1% for the deepest point position. The study analysed plates of infinite width subject to uniform tension and bending loads the results of which are presented in Murakamis' compendium[9.6] as a set of discrete data points.

9.4 – Critique of Results

Numerous finite element models of surface cracks and flat plates were created using the mesh generator and solved by the *ABAQUS/standard* FE software. Three crack shapes of a/c = 1.0, 0.6 and 0.4 were analysed for a range of crack depths from a/t = 0.025 to 0.8 and for a crack shape of a/c = 0.2 crack depths ranging from a/t = 0.025 to 0.5. In total 41 crack configurations were analysed under applied loading of uniform tension and pure bending. The solutions obtained from the finite element method are presented in a tabular form in tabs. 9.1 and 9.2 for uniform tension and pure bending respectively. Graphs, comparing these results to those in the published literature described above, make up figs. 9.9 - 9.13.

Fig. 9.9 shows the variation in stress intensity factor at the deepest point of the crack as a function of crack depth plotted for a range of crack shapes under tensile loading. Also plotted for comparative purposes are the two-dimensional solutions by Brown and Srawley[9.7] alongside those of Newman and Raju and Isida, Noguchi and Yoshida. The stress intensity data collected for each crack shape is lower in magnitude than that of the edge crack solution due to an increased capacity for alternative load paths around the crack, resulting in a comparatively less severe stress condition in the remaining section. For decreasing crack aspect ratio the alternative paths for load redistribution are restricted and therefore the solution tends to that of the edge crack solution.

Fig. 9.9 shows that the data from the three sources display a good general correlation. As crack depth increases the finite element data becomes more conservative with respect to the published solutions, an effect which increases with decreasing crack aspect ratio. The published solutions correspond to a geometry of infinite width and hence contain a greater capacity for load redistribution in the remaining section than the finite width FEA data. This greater capacity is most prevalent at larger crack depths and lower aspect ratios and manifests itself as a decrease in the SIF solution. Conversely, at low crack depths and high aspect ratio the capacity for load redistribution for infinite and finite width models is approximately equal, as finite width effects are negligable. An excellent correlation between the SIF solutions for these crack configurations is achieved.

Fig. 9.10 shows a similar plot of the FE data with the solutions predicted by the empirical relations derived by Newman and Raju. These empirical solutions contain a term for the finite width effect discussed above which is valid for crack sizes of c/W < 0.5. The empirical solutions were calculated for plate width consistent with that of the FE models analysed for the present study. The solutions show an improved correlation over all crack configurations investigated. Newman

and Raju's empirical SIF solutions remain conservative at all times with respect to the FE data, a desirable property for a solution of such broad limits of validity.

Fig. 9.11 shows the variation of SIF as a function of characteristic angle, defining crack front position for various crack shapes of depth equal to '$a/t = 0.2$'. Also shown are those predicted by Newman and Raju's empirical relation. A good correlation between the two solutions is achieved, the Newman and Raju solutions are, once more conservative with respect to those obtained in this study. Fig. 9.7 shows the considerable effect of crack shape upon the SIF solution particularly at the deepest point.

Fig. 9.12 shows the SIF solutions for the deepest point of a surface cracked plate subject to a pure bending load condition against those predicted by the empirical solution of Newman and Raju and those of an edge crack by Brown and Srawley. The solutions again show a good correlation and tend toward the two-dimensional solution with decreasing crack aspect ratio. The empirical solution is conservative with respect to those developed in this study. Fig. 9.13 displays the variation of SIF distribution along the crack front for '$a/t = 0.3$' and subject to pure bending, which again compare well to those predicted by Newman and Raju.

9.5 – A Stiffened Surface Cracked Flat Plate Model

The versatile nature of the mesh generator program allows blocks of elements describing new geometries to be simply added to the existing flat plate model. Chapter 10 defines a geometry described as a stiffened surface crack, required for implementation of the interpolation scheme to surface cracked three-dimensional geometries. It is used in conjunction with the results described above (for an unstiffened surface cracked flate plate) as a base geometry for the interpolation scheme. A pre and post-processed finite element model of a stiffened surface crack model is given in fig. 9.14, which shows additional material added to the validated flat plate model.

As described for the equivalent two-dimensional geometry, the parameter, 'b' or non-dimensionally, 'b/T' denotes the thickness of stiffening material added and was added to the mesh generator program to allow a number of stiffnesses to be investigated. Common to the unstiffened surface cracked flate plate model the stiffened plate geometry is depicted as a quarter model with applied boundary conditions simulating symmetry. Plate size was restricted to be equal to the unstiffened geometry (W/t = 2.75). No suitable SIF solutions are available from published literature with which to compare and validate those obtained from the model. Full presentation and description of the geometry and a discussion of results acquired from the analysis of such models is deferred to chapter 10.

9.6 - Surface Cracks in Notched Bodies

The mesh generator described and utilised in the preceding sections may be used to construct models of notched plates containing a surface crack at the notch root. Simple transformation functions, applied to the nodal co-ordinate data, added to the mesh generator program was used to produce models of more complex geometries. Information pertaining to element description, loading and boundary conditions remain unchanged from the flat plate model. Thus, with relatively little computational effort wide-ranging and valuable SIF data for surface cracks at notches was produced. The surface crack mesh generator was updated to take the notch geometry information of notch depth 'b/T', root radius 'b/ρ' and flank angle 'α' describing the transformation functions, which defines the notch feature.

Limitations however do exist in the depth of crack that can be modelled without causing unacceptable element distortion. Typically the maximum depth of the crack is limited to being less than the notch depth. This allowed a considerable portion of the notch influence to be modelled and was sufficient for the purposes of validation for which they were intended.

An example model of a symmetric V-notch and step notch containing a surface crack is given as figs. 9.15 and 9.16 respectively. Meshing, boundary conditions, model deformations and stress contours are depicted in each. Presentation of results is confined to chapter 10 and appendix A

.

9.7 – Conclusions

A mesh generator for the modelling of surface cracks in flat plates was constructed and used to create numerous meshes of cracks of various size and shape. A wide range of SIF data was collected from execution of these meshes using *ABAQUS/Standard* FE software and compared to published solutions. A good correlation was observed between SIF solutions for both tensile and bending load cases and discrepancy was largely attributed to width effects of the FE models investigated. FE results obtained for all crack configurations investigated compare well to those in published literature. It is concluded, therefore, that the modelling methods and procedures implemented are valid for calculation of SIF solutions for surface cracks.

A modified flat plate model termed a stiffened, surface cracked, flat plate was simply constructed from the validated flat plate model by the addition of stiffening material as shown and described. Results attained from this model are used as a base geometry solution for the interpolation scheme.

The transformation of nodal co-ordinates of the plate models was discussed to create models of more complex three-dimensional geometries. Results from notched three-dimensional geometries

are used to validate the interpolation principle applied to such geometries presented in chapter 10.

9.8 - References

[9.1] Han, S., Fatigue and Fracture Mechanics Analysis of Components Containing Residual Stress Fields, Ph.D. Thesis, University College London, 2002

[9.2] ABAQUS, version 5.7, Hibbet,Karlson and Sorenson Inc., 1997.

[9.3] Raju, I.S. and Newman, J.C., Stress Intensity Factors for a Wide Range of Semi-Elliptical Surface Cracks in Finite-Thickness Plates. *Engineering Fracture Mechanics* Vol. 11, pp 817-829 1979

[9.4] Newman, J.C. and Raju, I.S., An Empirical Stress Intensity Factor Equation for the Surface Crack. *Engineering Fracture Mechanics* Vol. 15, No.1-2, pp.185-192, 1981

[9.5] Isida, M., Noguchi, H. and Yoshida, Y., Tension and Bending of Finite Thickness Plates with a Semi-Elliptical Surface Crack, *Int. J. Frac.*, Vol. 26(1984), pp.157-188

[9.6] Murakami, Y. (editor in Chief) *et al.*, *Stress Intensity Factors Handbook*, Vol. I & II, Pergamon Press, Oxford, 1987. ISBN: 0-08-034809-2

[9.7] Brown Jr., W.F. and Srawley, J.E., Plane Strain Crack Toughness Testing of High Strength Metallic Materials, *ASTM STP 410* (1966), p. 12

9.9 – Tables

Tab. 9.1 – SIF Solutions for a Surface Cracked Flat Plate Subject to remotely Applied Tension

a/c	φ	a/t									
		0.025	0.05	0.1	0.2	0.3	0.4	0.5	0.6	0.7	0.8
	0	0.752	0.752	0.751	0.758	0.773	0.799	0.836	0.881	0.934	0.985
	0.131	0.726	0.726	0.729	0.735	0.751	0.775	0.806	0.846	0.889	0.938
	0.262	0.705	0.706	0.707	0.714	0.727	0.748	0.776	0.810	0.847	0.886
	0.393	0.690	0.691	0.692	0.698	0.711	0.730	0.754	0.784	0.815	0.848
	0.524	0.681	0.681	0.683	0.688	0.700	0.717	0.738	0.763	0.789	0.817
	0.655	0.673	0.673	0.674	0.680	0.691	0.706	0.725	0.747	0.769	0.792
1.0	0.786	0.668	0.668	0.670	0.675	0.686	0.700	0.716	0.735	0.753	0.771
	0.917	0.663	0.663	0.665	0.670	0.679	0.693	0.708	0.723	0.738	0.752
	1.047	0.661	0.662	0.663	0.668	0.677	0.690	0.703	0.716	0.727	0.738
	1.178	0.658	0.658	0.660	0.665	0.674	0.685	0.697	0.709	0.717	0.724
	1.309	0.658	0.658	0.660	0.665	0.673	0.684	0.695	0.705	0.711	0.715
	1.440	0.656	0.656	0.658	0.662	0.671	0.682	0.692	0.701	0.706	0.709
	1.571	0.657	0.658	0.659	0.664	0.672	0.683	0.693	0.701	0.706	0.707
	0	0.739	0.736	0.738	0.753	0.786	0.840	0.917	1.005	1.124	1.264
	0.098	0.715	0.717	0.719	0.733	0.765	0.816	0.887	0.971	1.080	1.207
	0.197	0.704	0.706	0.708	0.721	0.751	0.798	0.864	0.940	1.038	1.152
	0.295	0.704	0.705	0.707	0.720	0.749	0.794	0.855	0.926	1.016	1.119
	0.393	0.710	0.712	0.714	0.726	0.754	0.797	0.855	0.921	1.004	1.098
	0.491	0.721	0.722	0.724	0.737	0.764	0.805	0.859	0.922	0.998	1.083
	0.589	0.735	0.736	0.738	0.750	0.777	0.816	0.868	0.927	0.998	1.074
	0.687	0.749	0.750	0.752	0.765	0.790	0.829	0.879	0.934	0.998	1.067
0.6	0.786	0.764	0.765	0.767	0.780	0.805	0.843	0.891	0.942	1.001	1.062
	0.884	0.778	0.779	0.781	0.793	0.819	0.856	0.902	0.949	1.002	1.055
	0.982	0.792	0.792	0.794	0.807	0.832	0.868	0.913	0.957	1.005	1.049
	1.080	0.803	0.803	0.805	0.817	0.842	0.878	0.921	0.962	1.005	1.041
	1.178	0.813	0.813	0.816	0.828	0.853	0.888	0.930	0.967	1.005	1.035
	1.276	0.820	0.820	0.822	0.835	0.859	0.894	0.935	0.970	1.004	1.028
	1.375	0.826	0.827	0.829	0.841	0.866	0.900	0.940	0.973	1.004	1.022
	1.473	0.829	0.829	0.831	0.844	0.868	0.902	0.942	0.974	1.003	1.019
	1.571	0.831	0.831	0.834	0.846	0.870	0.904	0.943	0.975	1.003	1.017
	0	1.691	1.347	1.108	0.943	0.829	0.752	0.706	0.687	0.683	0.682
	0.098	1.593	1.279	1.060	0.907	0.801	0.730	0.685	0.662	0.659	0.658
	0.197	1.534	1.245	1.041	0.898	0.797	0.728	0.685	0.665	0.662	0.661
	0.295	1.515	1.245	1.052	0.914	0.816	0.748	0.705	0.684	0.681	0.680
	0.393	1.512	1.259	1.073	0.939	0.842	0.774	0.731	0.710	0.707	0.706
	0.491	1.517	1.277	1.101	0.970	0.875	0.807	0.763	0.742	0.738	0.737
	0.589	1.524	1.298	1.128	1.001	0.906	0.838	0.794	0.772	0.768	0.767
	0.687	1.523	1.316	1.156	1.032	0.939	0.870	0.826	0.803	0.799	0.798
0.4	0.786	1.522	1.332	1.180	1.061	0.968	0.899	0.854	0.831	0.827	0.826
	0.884	1.511	1.342	1.201	1.086	0.994	0.926	0.880	0.856	0.853	0.851
	0.982	1.499	1.351	1.219	1.108	1.018	0.950	0.903	0.879	0.875	0.874
	1.080	1.481	1.353	1.232	1.126	1.037	0.969	0.922	0.898	0.894	0.893
	1.178	1.463	1.355	1.244	1.142	1.054	0.986	0.939	0.915	0.911	0.909
	1.276	1.446	1.354	1.251	1.152	1.066	0.998	0.951	0.926	0.922	0.921
	1.375	1.430	1.353	1.257	1.161	1.076	1.009	0.961	0.937	0.932	0.931
	1.473	1.422	1.352	1.259	1.165	1.081	1.013	0.965	0.941	0.937	0.935
	1.571	1.416	1.351	1.261	1.168	1.084	1.016	0.968	0.944	0.940	0.938

a/c	φ	a/t										
		0.025	0.05	0.1	0.15	0.2	0.25	0.3	0.35	0.4	0.45	0.5
	0	0.537	0.538	0.543	0.555	0.574	0.601	0.640	0.693	0.770	0.885	1.094
	0.033	0.528	0.528	0.534	0.545	0.564	0.590	0.628	0.680	0.756	0.868	1.070
	0.066	0.525	0.526	0.531	0.542	0.561	0.587	0.624	0.676	0.750	0.859	1.056
	0.098	0.531	0.531	0.537	0.548	0.567	0.593	0.630	0.681	0.755	0.864	1.059
	0.131	0.541	0.542	0.547	0.559	0.578	0.604	0.642	0.694	0.768	0.878	1.071
	0.164	0.557	0.558	0.564	0.576	0.595	0.622	0.660	0.713	0.788	0.899	1.093
	0.197	0.572	0.573	0.579	0.591	0.610	0.638	0.677	0.731	0.807	0.920	1.115
	0.273	0.623	0.624	0.630	0.643	0.664	0.694	0.735	0.792	0.872	0.989	1.188
	0.349	0.666	0.667	0.674	0.688	0.710	0.742	0.785	0.845	0.928	1.049	1.251
	0.426	0.717	0.718	0.725	0.740	0.763	0.797	0.843	0.906	0.992	1.117	1.320
	0.502	0.758	0.759	0.766	0.782	0.807	0.842	0.890	0.956	1.045	1.173	1.376
	0.578	0.801	0.802	0.810	0.827	0.853	0.890	0.940	1.008	1.100	1.230	1.432
0.2	0.655	0.837	0.839	0.847	0.864	0.891	0.930	0.982	1.052	1.146	1.279	1.479
	0.731	0.873	0.874	0.882	0.901	0.929	0.970	1.024	1.096	3.768	1.326	1.523
	0.807	0.904	0.905	0.913	0.932	0.962	1.004	1.060	1.134	1.231	1.367	1.560
	0.884	0.932	0.933	0.942	0.962	0.993	1.036	1.094	1.170	1.268	1.406	1.593
	0.96	0.957	0.958	0.967	0.987	1.019	1.064	1.123	1.201	1.301	1.440	1.622
	1.036	0.979	0.980	0.990	1.010	1.043	1.089	1.150	1.229	1.330	1.469	1.648
	1.113	0.998	1.000	1.009	1.030	1.064	1.111	1.173	1.254	1.356	1.496	1.673
	1.189	1.014	1.015	1.025	1.046	1.081	1.129	1.192	1.274	1.377	1.517	1.695
	1.266	1.027	1.029	1.039	1.060	1.096	1.145	1.209	1.292	1.395	1.536	1.715
	1.342	1.037	1.038	1.048	1.070	1.106	1.156	1.221	1.305	1.408	1.549	1.728
	1.418	1.045	1.046	1.056	1.079	1.115	1.165	1.231	1.315	1.419	1.560	1.738
	1.495	1.048	1.050	1.060	1.082	1.118	1.170	1.235	1.320	1.424	1.565	1.743
	1.571	1.051	1.052	1.062	1.085	1.121	1.172	1.238	1.323	1.427	1.569	1.745

Tab. 9.2 – SIF Solutions for a Surface Cracked Flat Plate Subject to Remotely Applied Pure Bending

a/c	ϕ	a/t									
		0.025	0.05	0.1	0.2	0.3	0.4	0.5	0.6	0.7	0.8
	0	0.744	0.738	0.729	0.709	0.698	0.693	0.692	0.695	0.696	0.697
	0.131	0.721	0.713	0.698	0.675	0.656	0.642	0.632	0.623	0.614	0.603
	0.262	0.697	0.687	0.669	0.635	0.607	0.583	0.561	0.540	0.518	0.494
	0.393	0.680	0.668	0.646	0.605	0.568	0.534	0.503	0.472	0.439	0.405
	0.524	0.668	0.654	0.627	0.577	0.531	0.487	0.444	0.401	0.356	0.307
	0.655	0.658	0.642	0.612	0.554	0.499	0.447	0.395	0.343	0.289	0.232
1.0	0.786	0.652	0.634	0.599	0.534	0.471	0.409	0.348	0.285	0.218	0.145
	0.917	0.645	0.626	0.588	0.516	0.446	0.378	0.311	0.240	0.168	0.091
	1.047	0.642	0.622	0.581	0.502	0.426	0.351	0.275	0.196	0.113	0.020
	1.178	0.638	0.616	0.573	0.491	0.410	0.331	0.251	0.168	0.081	-0.026
	1.309	0.637	0.614	0.569	0.483	0.398	0.315	0.230	0.141	0.046	-0.053
	1.440	0.634	0.611	0.566	0.478	0.392	0.307	0.220	0.130	0.034	-0.075
	1.571	0.635	0.612	0.566	0.477	0.389	0.303	0.215	0.123	0.024	-0.086
	0	0.728	0.723	0.714	0.705	0.707	0.721	0.743	0.773	0.909	1.085
	0.098	0.711	0.705	0.694	0.678	0.674	0.681	0.696	0.716	0.832	0.982
	0.197	0.697	0.690	0.676	0.655	0.644	0.643	0.648	0.658	0.754	0.877
	0.295	0.696	0.687	0.669	0.641	0.623	0.615	0.611	0.611	0.690	0.789
	0.393	0.700	0.690	0.669	0.634	0.609	0.592	0.579	0.569	0.630	0.704
	0.491	0.709	0.696	0.672	0.629	0.596	0.571	0.549	0.529	0.572	0.623
	0.589	0.721	0.706	0.678	0.628	0.587	0.553	0.522	0.492	0.517	0.544
	0.687	0.733	0.716	0.684	0.627	0.578	0.535	0.496	0.456	0.465	0.469
0.6	0.786	0.746	0.728	0.692	0.627	0.571	0.520	0.471	0.422	0.413	0.392
	0.884	0.758	0.738	0.698	0.627	0.563	0.505	0.448	0.389	0.365	0.322
	0.982	0.770	0.748	0.705	0.627	0.557	0.491	0.426	0.358	0.318	0.250
	1.080	0.779	0.756	0.710	0.626	0.550	0.478	0.407	0.331	0.278	0.191
	1.178	0.788	0.764	0.716	0.626	0.545	0.467	0.389	0.307	0.240	0.128
	1.276	0.794	0.769	0.719	0.626	0.540	0.459	0.376	0.288	0.213	0.089
	1.375	0.800	0.774	0.722	0.626	0.537	0.452	0.365	0.273	0.188	0.044
	1.473	0.802	0.775	0.723	0.625	0.535	0.448	0.360	0.265	0.177	0.030
	1.571	0.804	0.777	0.724	0.625	0.534	0.446	0.357	0.261	0.169	0.015
	0	0.675	0.673	0.667	0.667	0.684	0.715	0.765	0.835	0.931	1.066
	0.098	0.655	0.651	0.643	0.637	0.648	0.673	0.714	0.772	0.853	0.967
	0.197	0.654	0.648	0.637	0.627	0.631	0.648	0.680	0.728	0.795	0.892
	0.295	0.672	0.664	0.650	0.632	0.628	0.639	0.662	0.699	0.753	0.832
	0.393	0.696	0.686	0.668	0.643	0.633	0.636	0.650	0.678	0.719	0.783
	0.491	0.725	0.713	0.690	0.656	0.638	0.632	0.636	0.652	0.679	0.724
	0.589	0.753	0.738	0.712	0.670	0.644	0.629	0.625	0.629	0.643	0.670
	0.687	0.782	0.765	0.733	0.683	0.647	0.623	0.608	0.601	0.600	0.608
0.4	0.786	0.807	0.788	0.753	0.694	0.650	0.618	0.593	0.574	0.559	0.547
	0.884	0.831	0.809	0.769	0.702	0.650	0.609	0.575	0.545	0.515	0.482
	0.982	0.851	0.828	0.784	0.710	0.650	0.601	0.558	0.517	0.471	0.417
	1.080	0.869	0.843	0.796	0.715	0.648	0.592	0.541	0.490	0.431	0.357
	1.178	0.884	0.856	0.806	0.719	0.647	0.585	0.526	0.465	0.393	0.297
	1.276	0.894	0.866	0.813	0.722	0.645	0.578	0.514	0.446	0.364	0.252
	1.375	0.903	0.874	0.819	0.724	0.643	0.572	0.504	0.429	0.338	0.210
	1.473	0.907	0.877	0.822	0.725	0.642	0.570	0.498	0.421	0.326	0.191
	1.571	0.910	0.879	0.824	0.725	0.642	0.568	0.496	0.416	0.318	0.178

a/c	ϕ	a/t										
		0.025	0.05	0.1	0.15	0.2	0.25	0.3	0.35	0.4	0.45	0.5
	0	0.535	0.533	0.532	0.538	0.549	0.565	0.587	0.619	0.665	0.735	0.862
	0.033	0.525	0.523	0.522	0.525	0.535	0.550	0.573	0.604	0.648	0.715	0.837
	0.066	0.522	0.519	0.518	0.521	0.530	0.544	0.566	0.595	0.638	0.703	0.821
	0.098	0.527	0.524	0.522	0.524	0.532	0.546	0.567	0.596	0.637	0.701	0.816
	0.131	0.537	0.534	0.531	0.533	0.540	0.553	0.573	0.602	0.643	0.706	0.820
	0.164	0.553	0.549	0.545	0.546	0.553	0.565	0.584	0.612	0.653	0.716	0.829
	0.197	0.567	0.563	0.558	0.559	0.565	0.577	0.596	0.624	0.664	0.727	0.840
	0.273	0.616	0.610	0.602	0.600	0.604	0.614	0.631	0.657	0.697	0.759	0.869
	0.349	0.658	0.651	0.640	0.636	0.638	0.646	0.662	0.687	0.726	0.787	0.896
	0.426	0.706	0.697	0.682	0.675	0.674	0.679	0.692	0.715	0.752	0.811	0.915
	0.502	0.746	0.735	0.717	0.706	0.702	0.706	0.717	0.738	0.773	0.829	0.930
	0.578	0.787	0.773	0.751	0.737	0.730	0.730	0.738	0.756	0.788	0.841	0.935
0.2	0.655	0.821	0.806	0.780	0.762	0.752	0.750	0.755	0.771	0.800	0.850	0.938
	0.731	0.854	0.837	0.807	0.785	0.772	0.766	0.769	0.782	0.808	0.853	0.935
	0.807	0.883	0.863	0.830	0.805	0.788	0.780	0.780	0.791	0.813	0.855	0.930
	0.884	0.909	0.888	0.851	0.822	0.802	0.791	0.789	0.796	0.816	0.854	0.922
	0.96	0.932	0.909	0.869	0.837	0.814	0.801	0.796	0.801	0.817	0.851	0.914
	1.036	0.952	0.928	0.884	0.849	0.824	0.808	0.800	0.803	0.817	0.847	0.904
	1.113	0.970	0.944	0.897	0.860	0.832	0.814	0.805	0.805	0.816	0.843	0.894
	1.189	0.984	0.957	0.907	0.868	0.838	0.818	0.807	0.805	0.815	0.838	0.885
	1.266	0.997	0.968	0.917	0.875	0.844	0.822	0.809	0.806	0.813	0.834	0.876
	1.342	1.006	0.976	0.923	0.880	0.847	0.824	0.810	0.806	0.812	0.831	0.869
	1.418	1.013	0.982	0.928	0.884	0.850	0.826	0.811	0.806	0.810	0.827	0.864
	1.495	1.016	0.985	0.930	0.885	0.851	0.827	0.812	0.806	0.810	0.826	0.861
	1.571	1.018	0.987	0.932	0.886	0.852	0.827	0.812	0.806	0.809	0.825	0.859

9.10 – Figures

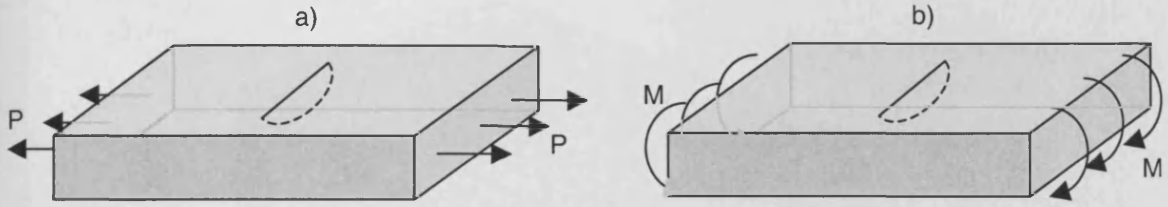

Fig 9.1 – Surface Cracked Flat Plate Subject to a) Tension and b) Pure Bending

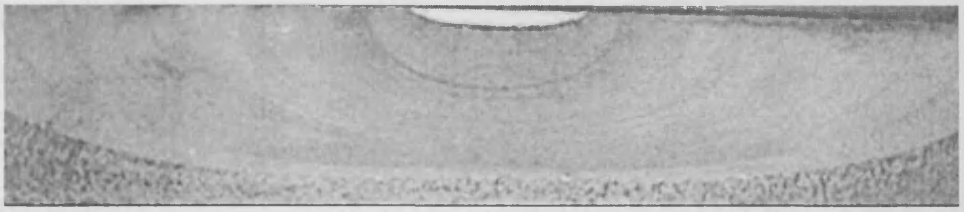

Fig. 9.2 – Semi-Elliptic Fatigue Cracks in an Un-notched Plate Developed Subject to Non-Uniform Bending Loading[9.1]

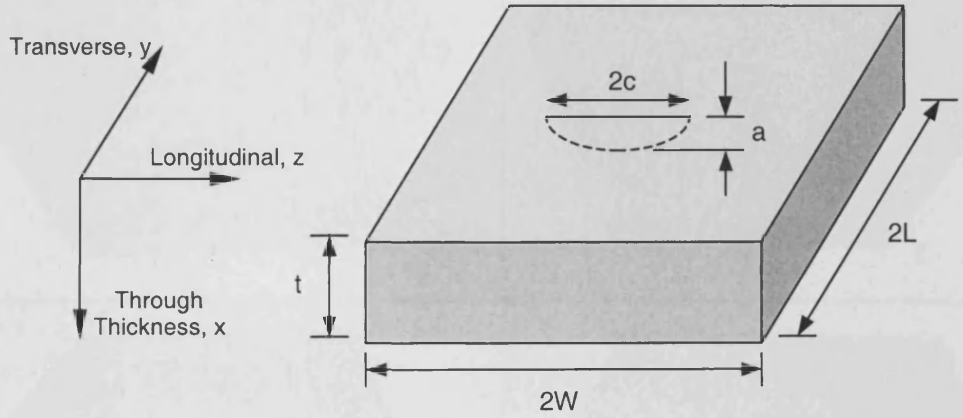

Fig. 9.3 – Definition of Geometric Parameters for the Surface Cracked Plate

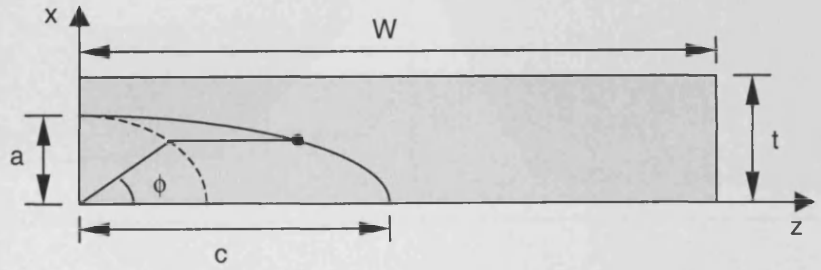

Fig. 9.4 - Definition of Characteristic Angle, ϕ

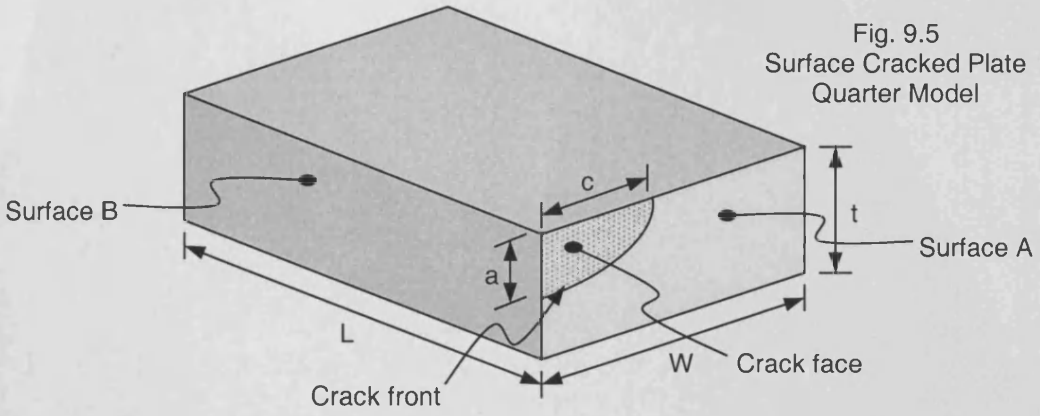

Fig. 9.5
Surface Cracked Plate
Quarter Model

Fig. 9.6 – Meshing Cell Containing Crack Detail (Quarter Model Shown)

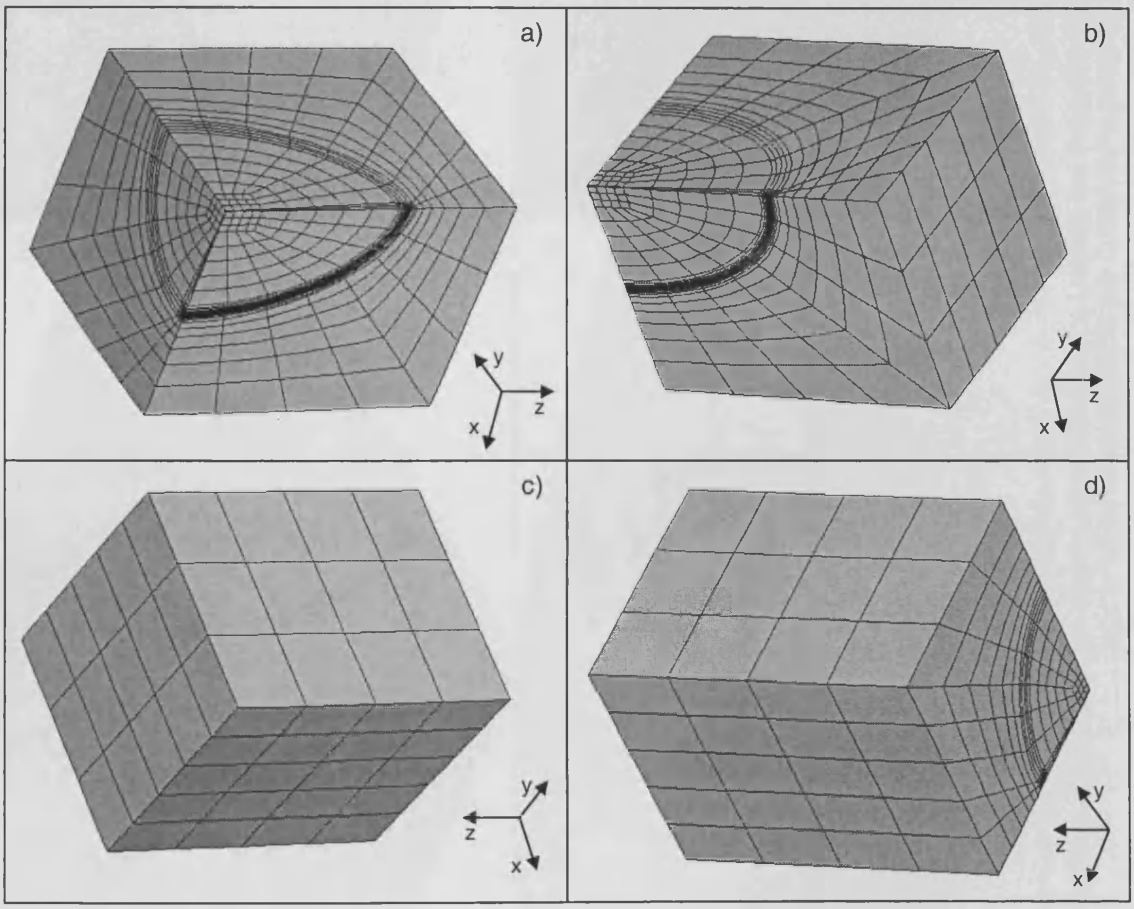

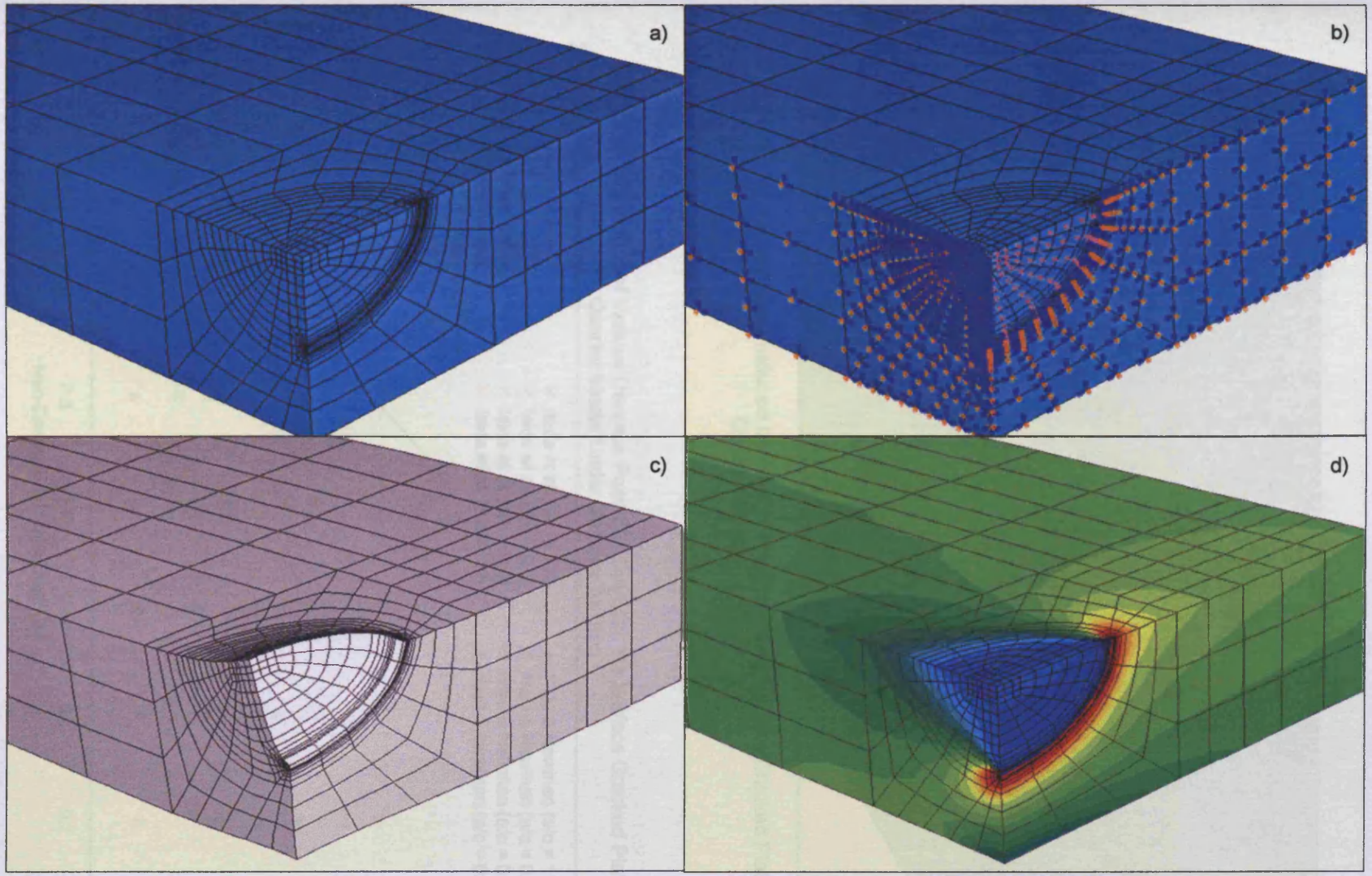

Fig. 9.7 – a) Surface Cracked Plate Quarter Model Meshing, b) Loading and Boundary Conditions Applied c) Displaced Surface Cracked Plate Quarter Model Mesh and d) Stress Contours Produced by Crack Face Loading

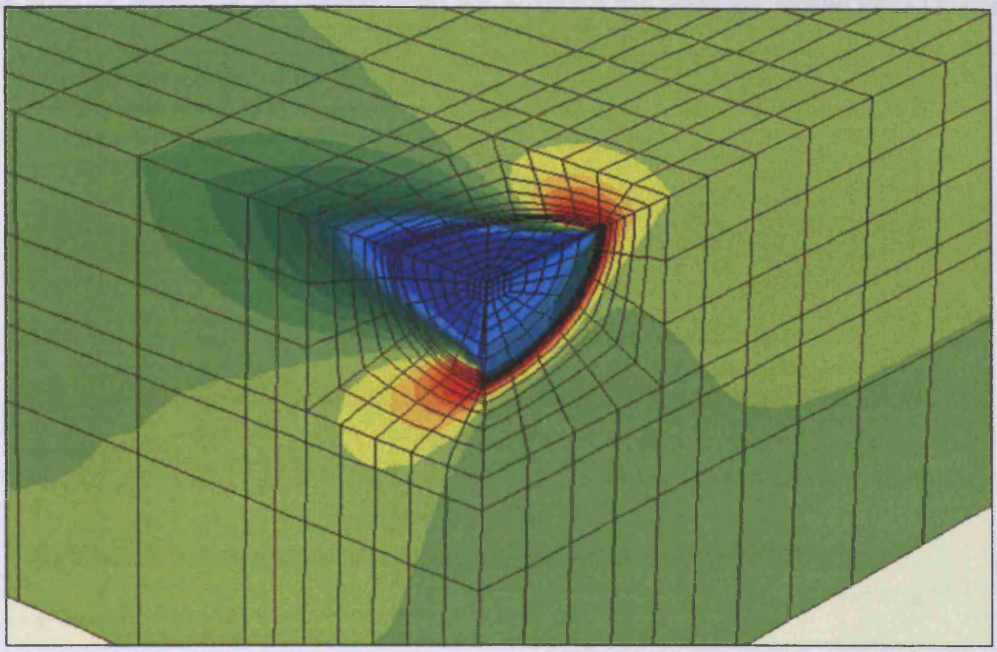

Fig. 9.8 – Stress Contours Produced by Remote Loading on the Surface Cracked Plate Quarter Model

Fig. 9.9 – Comparison of Various Deepest Point SIF Solutions the Surface Cracked Plate Quarter Model Under Uniform Tension

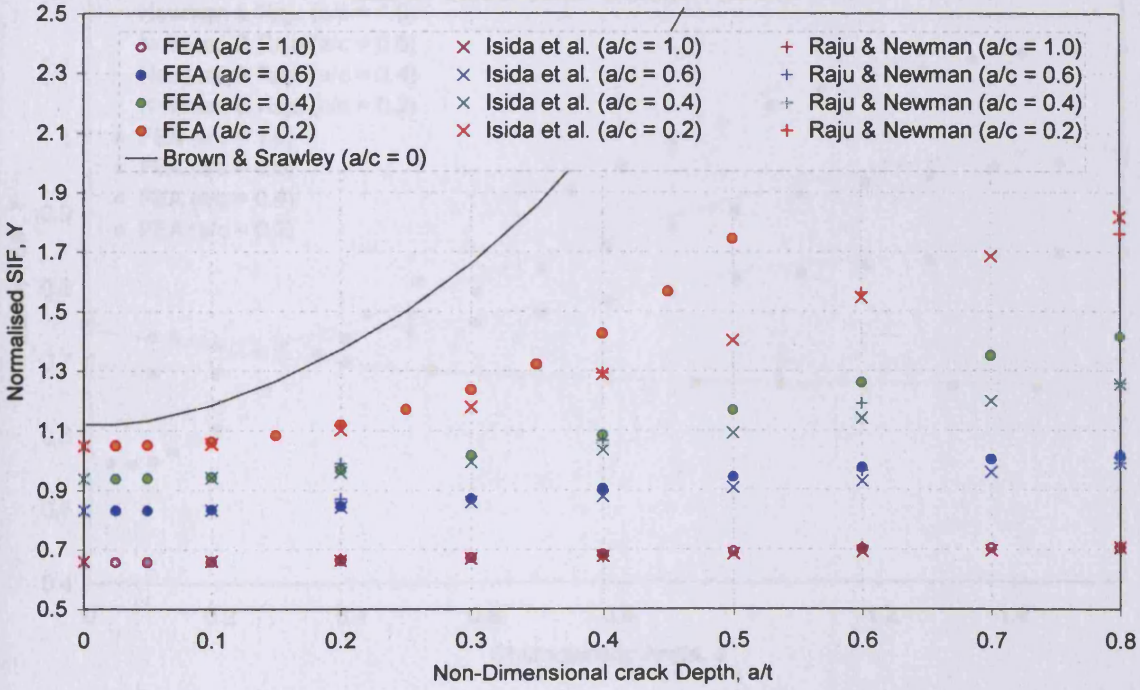

Fig. 9.10 – Comparison of Deepest Point SIF Solutions the Surface Cracked Plate Quarter Model Under Uniform Tension

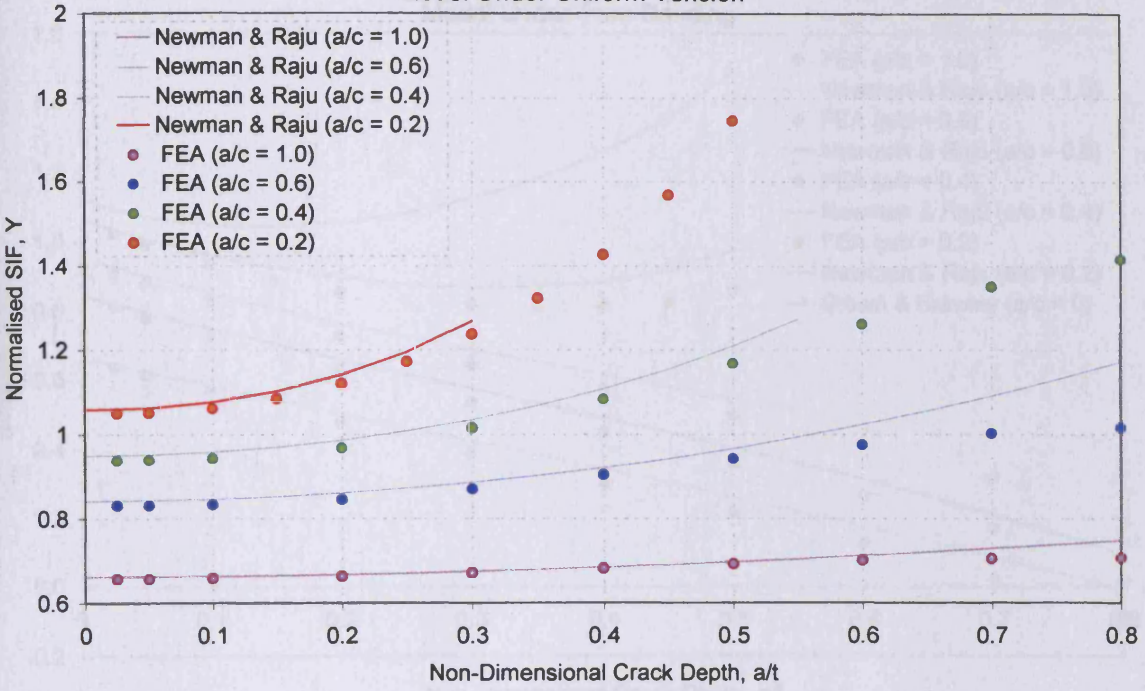

Fig. 9.11 – Comparison of SIF Solutions the Surface Cracked Plate Quarter Model Under Uniform Tension as a Function of Characteristic Angle (a/t = 0.2)

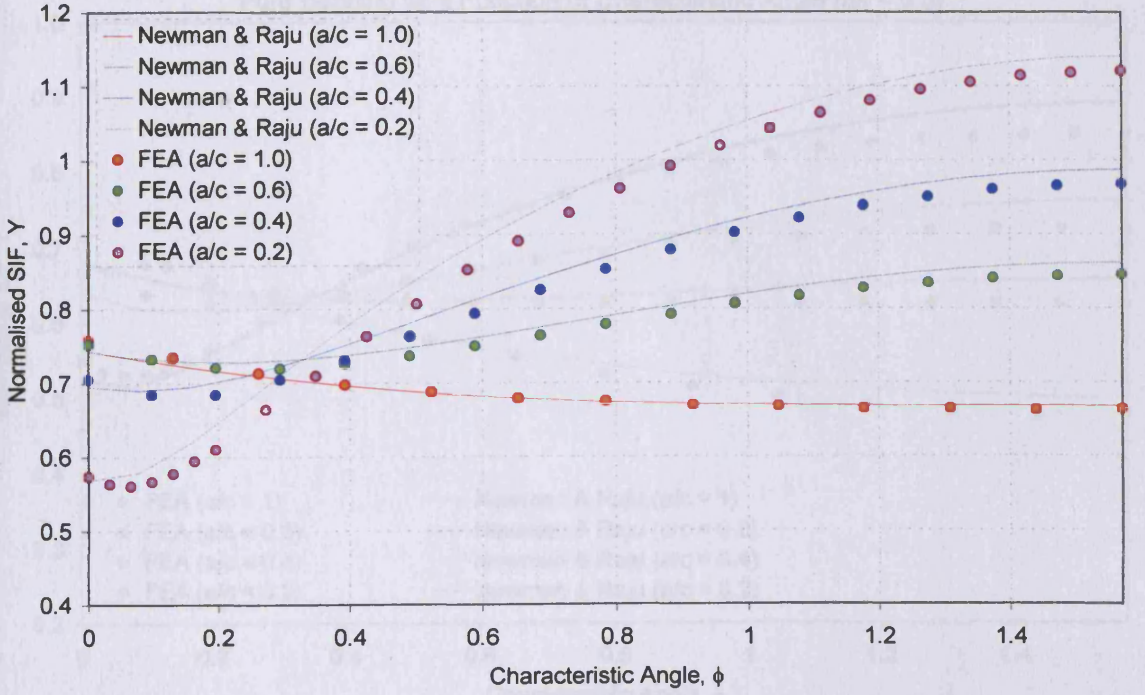

Fig. 9.12 – Comparison of Deepest Point SIF Solutions the Surface Cracked Plate Quarter Model Under Pure Bending

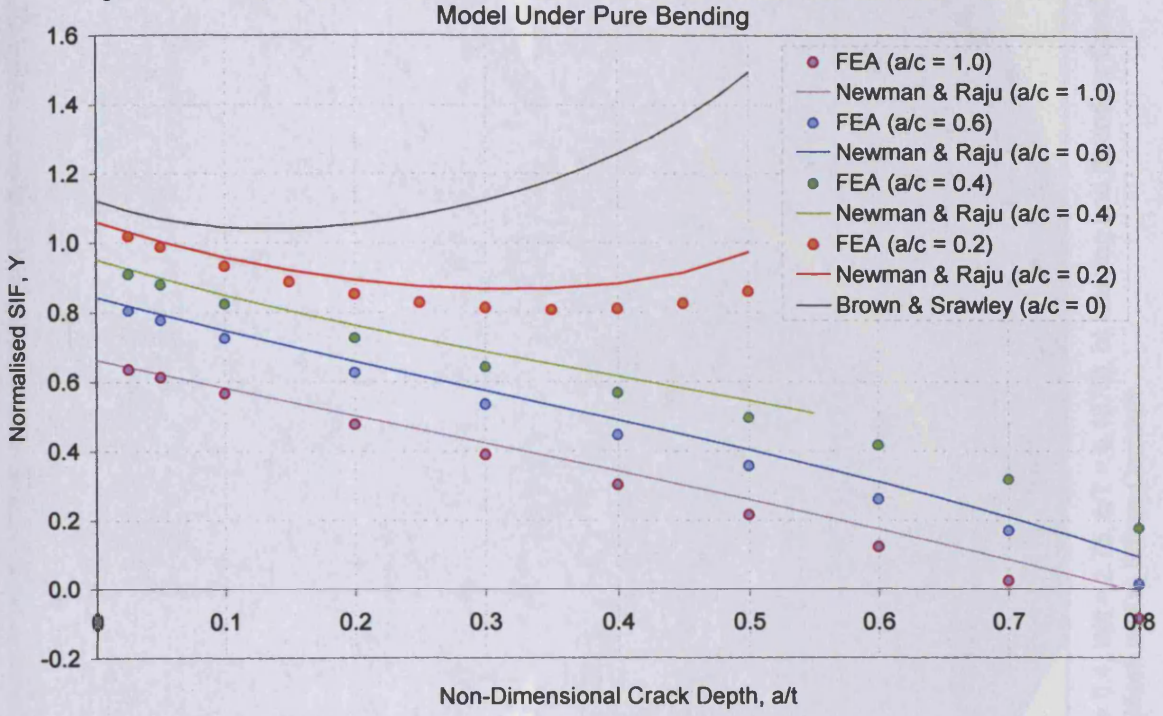

Fig. 9.13 – Comparison of SIF Solutions the Surface Cracked Plate Quarter Model Under Pure Bending as a Function of Characteristic Angle (a/t = 0.3)

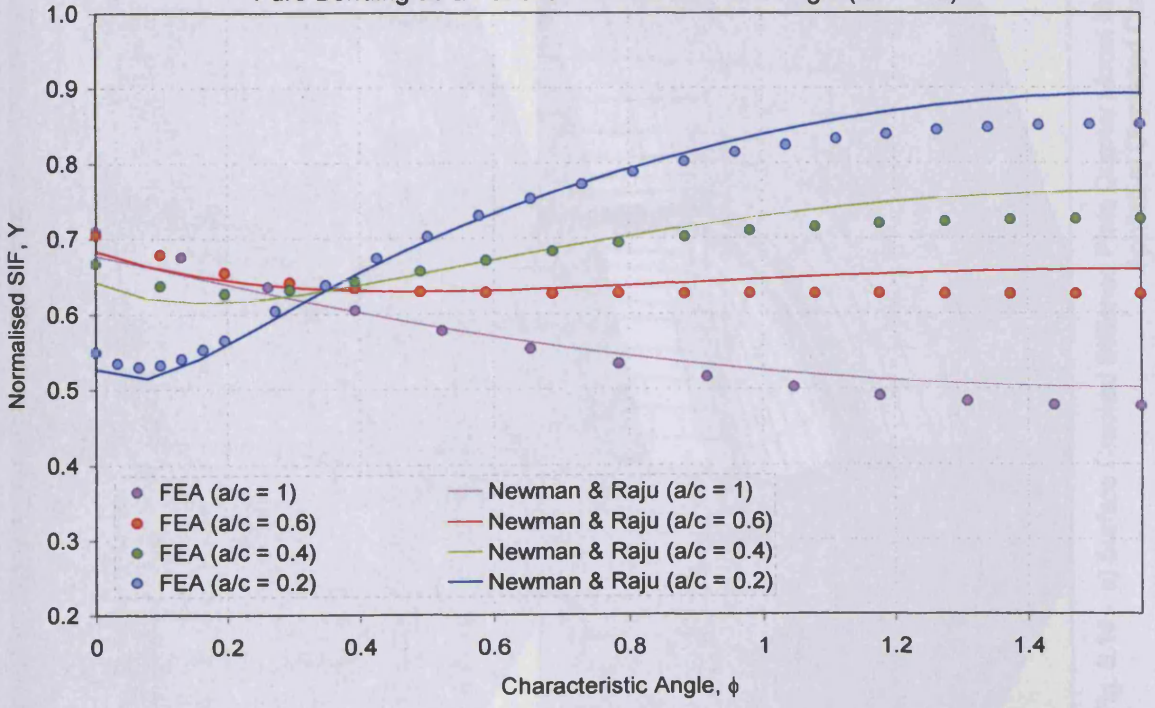

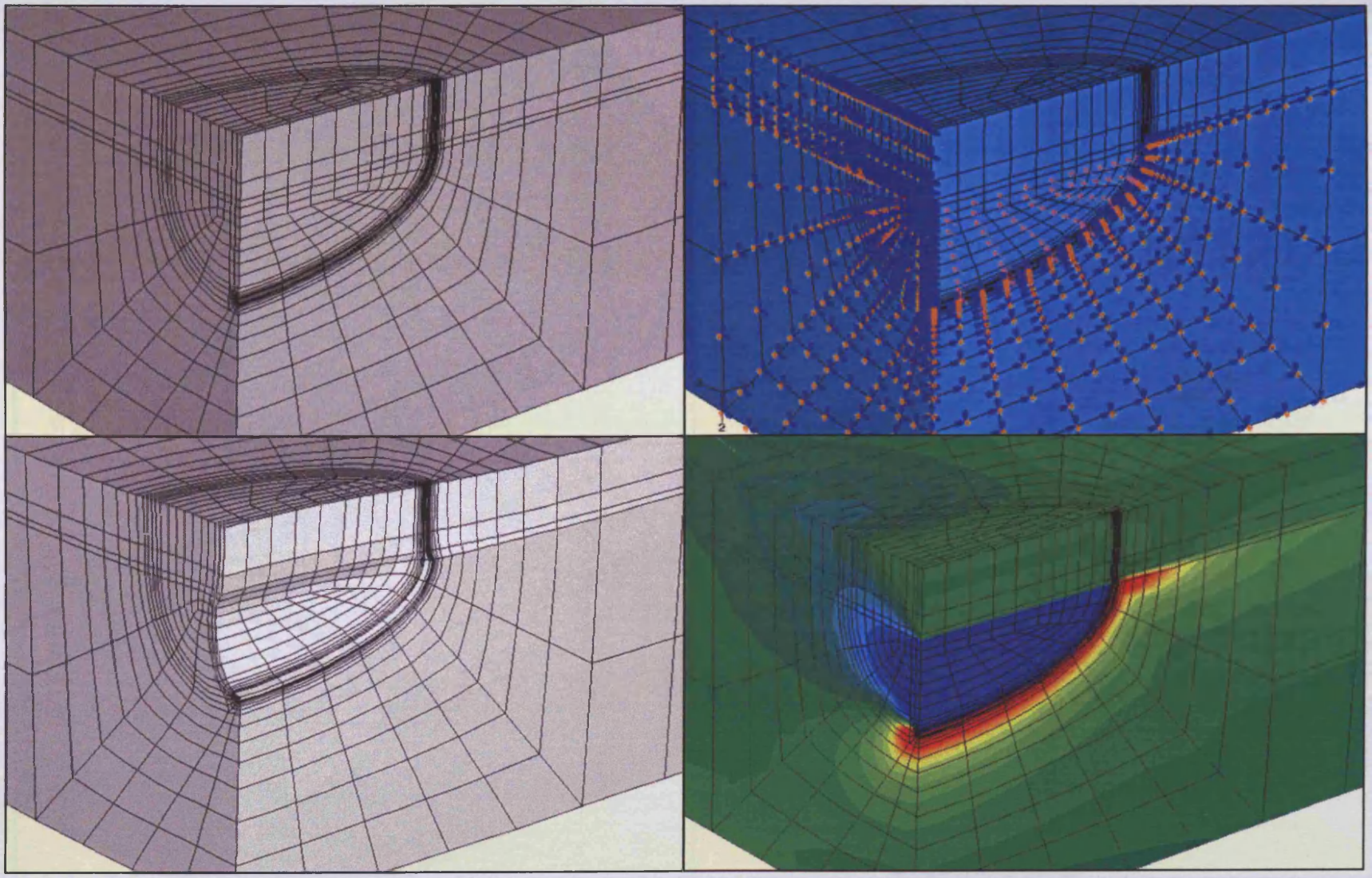

Fig. 9.14 – a) Surface Cracked Stiffened Plate Quarter Model Meshing (a/c = 0.4, W/t = 2.75, b/T = 0.1875), b) Loading and Boundary Conditions Applied c) Displaced Cracked Plate Mesh and d) Stress Contours

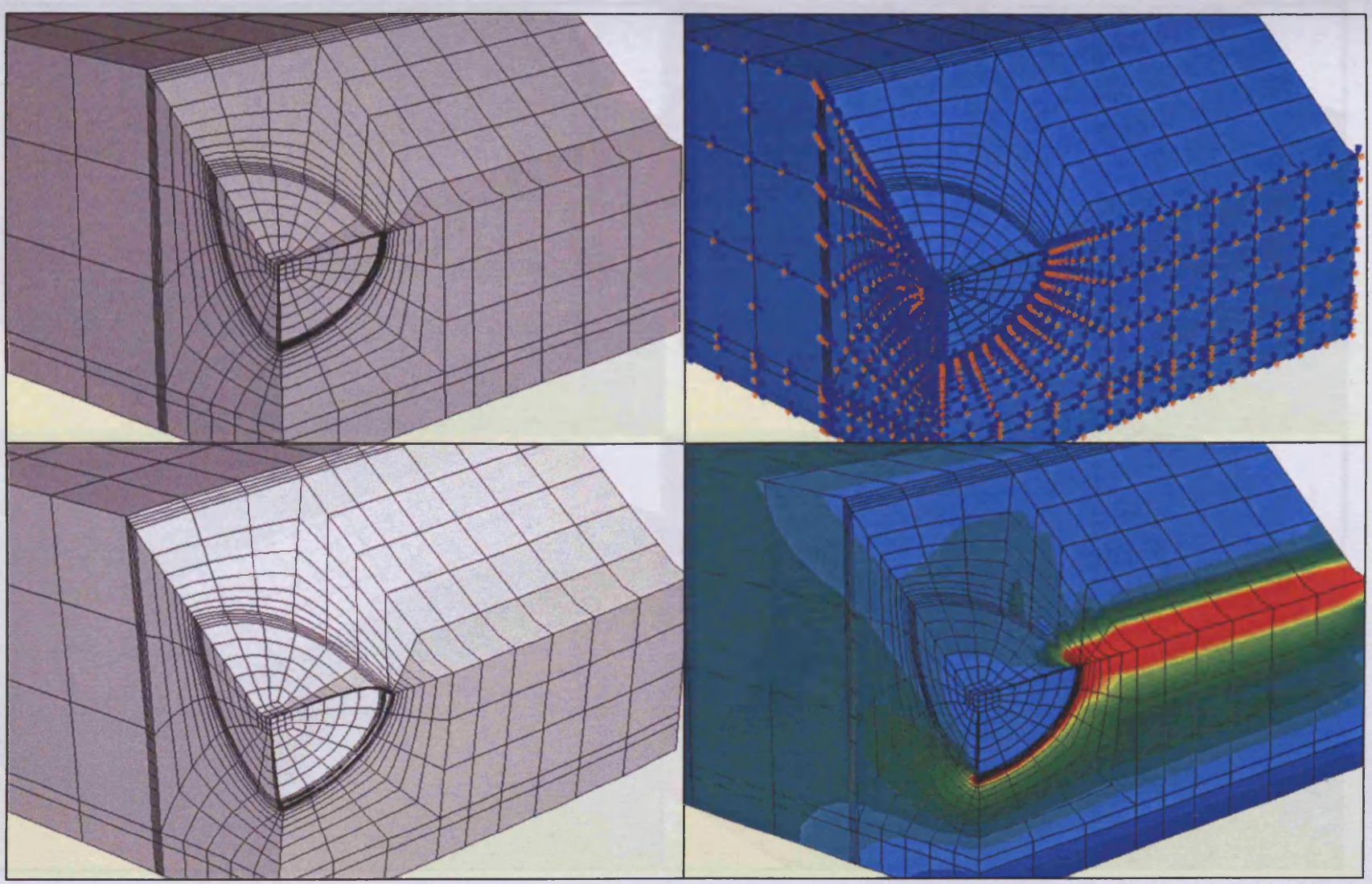

Fig. 9.15 – a) Surface Cracked, Symmetrically Notched, Plate Quarter Model Meshing (a/t = 0.389, a/c = 0.6, W/t = 2.75, b/T = 0.4375, α = 45 Deg, b/ρ = 6, Uniform Tension), b) Loading and Boundary Conditions Applied c) Displaced Mesh and d) Stress Contours

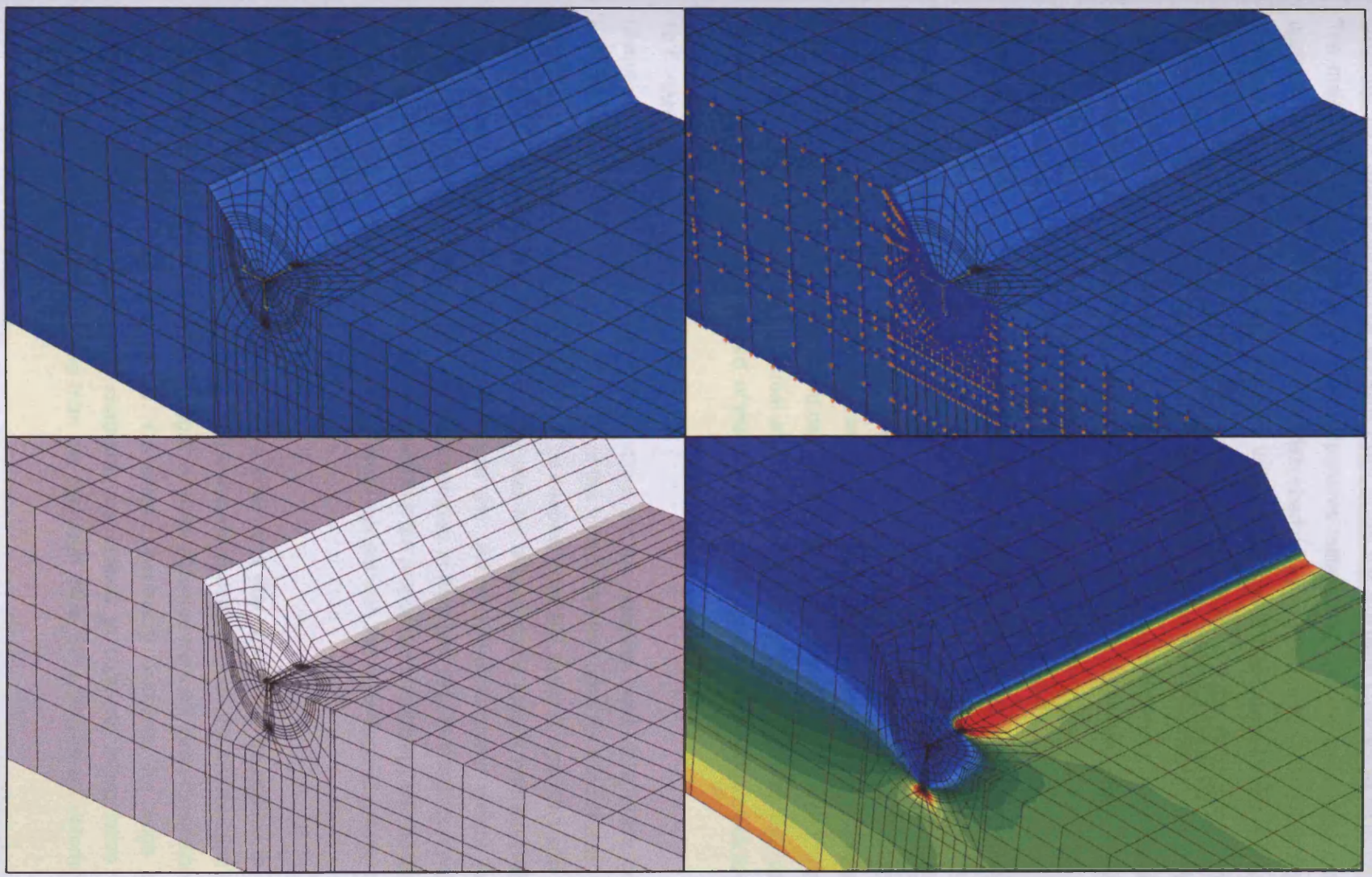

Fig. 9.16 – a) Surface Cracked, Step Notched, Plate Half Model Meshing, b) Loading and Boundary Conditions Applied c) Displaced Mesh and d) Stress Contours

Chapter 10 – Interpolation of Weight Functions for Surface Cracks at Notches

The majority of cracks in engineering components initiate and develop as surface cracks as opposed to edge cracks. Chapters 1 and 2 described a desirable extension to the existing weight function composition scheme, which can be used to estimate SIF solutions for the deepest point of a wide range of surface cracked geometries. A revised weight function methodology termed an interpolation scheme was shown to give superior performance over existing weight function composition techniques when applied to edge cracks in two-dimensional geometries. The interpolation of weight functions scheme was outlined in chapter 4 and successfully implemented in subsequent chapters to yield wide-ranging solutions of high accuracy and stability. This chapter proposes a similar extension to the interpolation scheme, as applied to edge cracks, for the determination of new SIF solutions for the deepest point of surface cracks located at notches.

A weight function solution for a crack situated at notch roots is sought that maintains the stability and accuracy achieved for edge cracks, while retaining the simplicity and flexibility inherent to the interpolation approach. This chapter aims to prove the premise of the weight function interpolation scheme is valid for such geometries and demonstrate the broadening of its applicability to a new class of cracked bodies. The conceptual and mathematical simplicity, and hence the rapidity at which new solutions can be achieved, of the scheme is maintained from the edge crack analysis.

10.1 – Introduction

Chapters 1 and 2 proposed that SIF solutions for the deepest point of a crack could be approximated by means of a weight function of the form commonly used for edge cracks, utilising a procedure outlined by Mattheck *et al*[10.1]. The deepest point SIF (point A, figs. 10.1 and 10.2) is commonly used as the characterising parameter for fatigue crack growth and assessment of structural integrity. This approximation avoids the use of two-dimensional weight functions developed for surface cracks, which are more complex in form and require integration processes to be carried out over the crack area. It is hoped that the proposed methodology can be applied to yield an acceptable approximation to the physical system with the advantage of greatly reduced mathematical complexity.

The interpolation scheme investigated in this chapter is that which may be applied to surface cracks at the root of notched flat plates. The solutions derived through the interpolation of base geometry weight functions are validated against those obtained from full three-dimensional finite element studies on such geometries. Constituent geometry solutions, for edge cracked geometries formulated in preceding chapters, are utilised to calculate interpolation factors, illustrating the economy to be gained from the approach. New SIF solutions are determined via

integration of the calculated complex geometry weight function with the one-dimensional finite thickness stress distributions utilised in preceding chapters.

Suitable base geometry reference solutions are the sole new information required for implementation of the scheme via their substitution into pre-existing interpolation algorithms.

10.2 – Interpolation of Weight Functions for Surface Cracks

Chapters 1 and 2 suggested extension of the pre-existing composition scheme for surface cracks located at notches. A recommended methodology presented in section 1.7 and 2.5 utilises weight functions for two-dimensional constituent geometries describing the geometric influence of the notch composed upon a three-dimensional surface crack geometry. Chapter 4 highlighted the deferred integration of plane geometry weight functions, implemented in Teh's representation of the composition scheme, to affect what was subsequently termed a stiffened geometry weight function. The ability to do so was a consequence of the crack being defined by the single parameter of depth, 'a'. Application of the same principle to surface cracks, defined by both depth, 'a' and half-length, 'c' does not respect consistency of crack shape. Implementation of the interpolation scheme to surface cracked geometries is unhindered by such considerations and simply requires substitution of relevant three-dimensional base geometry weight functions into the existing interpolation equation. Unstiffened and stiffened surface crack geometries are utilised as base geometry solutions and are presented in an interpolation equation in fig. 10.3.

The weight function interpolation scheme presented as fig. 10.3 assumes the stiffening influence of the notch to be equal for both two-dimensional and three-dimensional cases. Thus the two-dimensional constituent geometries are utilised to ascertain an appropriate interpolation factor, '$f(a)$' applied to the three-dimensional base geometry weight functions. This chapter utilises the interpolation scheme depicted in fig. 10.3 together with interpolation factors calculated via constituent geometry weight functions as conducted in chapters 5, 6 and 8. New SIF solutions developed are compared to those obtained by FEA employing models described and presented in chapter 9. The chapter is restricted to notched flat plate bodies, though interpolated weight function results displaying a close correlation to FE data indicates that the interpolation scheme is applicable to a wider range of three-dimensional geometry types. The body of work contained in this chapter is designed to validate the general approach adopted and imply possible further applications to pipe and rod geometries when suitable base geometry reference solutions become available.

10.3 – Three-Dimensional Base Geometry Reference Solutions

With reference to fig. 10.3, two base geometry weight functions are required for implementation of the interpolation scheme: those of the unstiffened and stiffened surface cracked flat plate. A number of solutions for the unstiffened geometry are available as reference solutions in the published literature and were presented in the preceding chapter. Additional solutions for the specific plate size '$W/t = 2.75$' were also produced from the 'in-house' finite element study described in chapter 9. A search of the published literature, however, revealed that no relevant solutions currently exist for the stiffened geometry, detailed in fig. 10.4.

The body of work comprising chapter 9 described and validated modelling practices for the calculation of SIF solutions in three-dimensional geometries using the finite element method. The surface crack mesh generator developed was modified to allow construction of finite element models of a stiffened surface cracked flat plate geometry ($W/t = 2.75$). An example of a model produced is shown in chapter 9, fig. 9.14. Reference SIF solutions for this geometry under uniform crack loading were sought and thus a uniformly distributed load was applied to the element sides which make up the crack face.

Stiffened surface cracked flat plate models of aspect ratios of 1, 0.6, 0.4 and 0.2 for a range of crack depths and 'b/T' values were generated by a mesh generator program modified from that described in chapter 9 and solved using the ABAQUS/Standard FE package. Tabular results of deepest point SIF solutions are given in tabs. 10.1 – 10.4. Selected results are shown graphically in figs. 10.5 and 10.6.

The material added to the plane surface cracked geometry constitutes an additional stiffness, which acts to constrain crack opening. Solutions for stiffened surface cracks are, therefore lower than those of equivalent unstiffened surface cracks as was observed and described for the corresponding two-dimensional case in chapter 4. The presence of the additional material constrains two modes of deformation, each with an associated stiffness which constrain crack opening. Fig 10.7a depicts the deformation of a three-dimensional stiffened edge crack when subject to uniform opening pressure applied to the crack faces. Dashed lines sketched on a quarter-model block show the deformation of material in the vicinity of the crack. The crack face and material in the surrounding region is displaced as a rigid body with respect to the z-direction. A surface crack in the same body under the same loading (fig. 10.7b) gives rise to an additional deformation mode with a corresponding stiffness further restricting crack opening.

Both stiffening influences are present in the solutions presented in fig. 10.5 and cause the stiffened surface crack deepest point SIF solutions to remain below the unstiffened equivalent

solutions. Fig. 10.6 shows solutions with varying additional stiffening material defied by '*b/T*'. At low 'b/T' values the SIF solutions for the stiffened geometry resemble those obtained for the edge crack geometry. The stiffened geometry solution increases in magnitude toward the unstiffened solution with increasing '*a/t*'. Fig. 10.6, however shows that the additional stiffness component is effective for all crack sizes and manifests itself as a constant offset between the two solutions for all '*a/t*' values.

10.4 – Curve Fitting of Reference Solutions

Reference SIF solutions for the base geometry weight functions were fitted to fifth order polynomials of the same form utilised for the two dimensional analysis. New expressions were obtained for both unstiffened and stiffened geometries for the specific plate size of '*W/t = 2.75*' from data displayed in tab 9.1 and tabs 10.1 – 10.3 respectively. Resulting coefficients, 'R_x' of eq. 10.1 are displayed in tabs 10.5 and 10.6.

$$Y = R_5\left(\frac{a}{t}\right)^5 + R_4\left(\frac{a}{t}\right)^4 + R_3\left(\frac{a}{t}\right)^3 + R_2\left(\frac{a}{t}\right)^2 + R_1\left(\frac{a}{t}\right) + R_0 \quad \text{- (10.1)}$$

10.5 – Three-Dimensional Base Geometry Weight Functions

Matteck et al.[10.1] present a weight function methodology to transform a three dimensional surface crack system to that of a two dimensional edge crack. The assumption states that the deepest point SIF of a surface crack loaded by a stress varying in the '*x*' direction only can be calculated from the weight function methodology applied in this study to edge cracks. The study concluded that the applied weight function technique, using the Petroski and Achenbach opening displacement and reference solutions by Newman and Raju, could be used to determine new SIF solutions to within 10% accuracy. Limitations of the Petroski and Achenbach methodology for weight function formulation were described in chapter 1 and coupled with the quoted 5% error associated with Newman and Raju's SIF solutions are obvious sources of error.

To demonstrate the likely accuracy possible using a one-dimensional weight function for the deepest point of surface cracks, the contemporary weight function methodology utilised in this study was applied using fitted data for the surface crack loaded in tension (fig. 10.2a, given in tab. 10.5) as a single reference solution. Once formulated the weight function was utilised to determine deepest point SIF solutions for the cracked plate subject to bending (fig. 10.2b). Solutions for the cracked plate subject to pure bending are displayed as fig. 10.8 against those obtained for the same configuration using in-house FEA (tab. 9.2) for the same plate dimensions.

Also shown are the edge crack solutions for bending using a single uniform tension reference case by Brown and Srawley first described in, and replicated from, chapter 2.

Fig. 10.8 shows that a close correlation is achieved, between weight function and FEA solutions for all crack shapes. The 'drift' between the two sets of solutions with increasing crack depth is of a similar magnitude to that obtained for the edge crack and is a consequence of the usage of a single reference case for weight function formulation, as described in chapter 2.

A single reference load case is available for the stiffened surface crack geometry and, though the results of fig. 10.8 indicate once more the shortcoming of a weight function based upon a single reference load case it is thought satisfactory for the present demonstrative purpose. The interpolated weight function solutions presented in this chapter were obtained from single reference state, base geometry weight functions. Additional reference cases may be simply applied to base geometry weight functions when they become available.

10.6 – An Interpolated Weight Function Solution

The proposed interpolation scheme, shown in fig. 10.3, assumes that a complex geometry weight function is formulated by the interpolation of two relevant base geometry weight functions. Reference solutions for the formulation of base geometry weight functions have been determined and curve fitted to polynomial expressions. An interpolation factor, '$f(a)$' is notch dependent and describes the degree to which the complex geometry weight function acts as either extreme geometry weight function. The influence of the notch is assumed to be a purely two-dimensional effect and therefore, is equal to those determined in preceding chapters of this thesis.

Chapter 5 presented a number of interpolation factors for symmetric notches calculated from the manipulation of semi-finite constituent geometry SIF solutions subject to equal crack loading, eq. 10.2 (that of uniform tension).

$$f(a) = \frac{Y_N^S(a) - Y_S^S(a)}{Y_U^S(a) - Y_S^S(a)} \qquad \text{- (10.2)}$$

Chapter 6 detailed how interpolation factors for symmetric notches could be readily modified to give an interpolation factor for step notches using eq. 10.3.

$$f(a) = \frac{1}{2} + \frac{Y_N^S(a) - Y_S^S(a)}{2\left(Y_U^S(a) - Y_S^S(a)\right)} \qquad \text{- (10.3)}$$

Chapter 8 contained an equally applicable more general approach, for which equivalence of crack loading is not required, through manipulation of constituent geometry weight functions as given by eq. 10.4.

$$f(a) = \frac{m_N^S(a,x) - m_S^S(a,x)}{m_U^S(a,x) - m_S^S(a,x)} \qquad \text{- (10.4)}$$

Constituent geometry reference SIF solutions and associated stress distributions have been detailed in previous chapters together with finite thickness complex geometry stress distributions arising from numerous loading modes. Realisation of a surface crack solution requires substitution of new base geometry reference solutions into existing interpolation algorithms, containing calculation of interpolation factors (eqs 10.2 - 10.4) to calculate new complex geometry weight functions. New SIF solutions are obtained by the integration of the resulting weight function with crack-line stress distributions as defined by eq. 10.5.

$$Y_N^F(a) = \int_0^a \sigma_{yy}^F(x) m(a,x) dx \qquad \text{- (10.5)}$$

This chapter presents a number of new SIF solutions for the deepest point of surface cracks in complex three-dimensional geometries obtained using modified interpolation algorithms used for edge cracks complex in two-dimensional geometries. Where possible, results are presented alongside finite element data, obtained from the 'in-house' analysis of the full, cracked three-dimensional FE models.

10.7 – FE Analysis of Surface Cracked Flat Plates Containing Notches

A full three-dimensional finite element study on a symmetric and step notched flat plate geometry containing a surface crack at the notch root was desired to support and validate the SIF solutions obtained by the weight function methodology. The geometry under consideration is complex in form, however FE models were created by the simple transformation of nodal co-ordinates of the plane flat plate models investigated in chapter 9. All data pertaining to boundary conditions, loading, crack definition, etc, remained unchanged and thus a variety of notched flat plate models were derived with relative ease. Plane flat plate models were validated and example notched models produced by the surface crack mesh generator program were described, in chapter 9. Fig. 9.15 depicts a typical symmetrically notched flat plate model and fig. 9.16 a step notched model used for the calculation of SIF solutions.

The geometric parameters of the notched plates were the same as those investigated for the two-dimensional analyses described in previous chapters. The number of SIF solutions derived is more sparse than that of the two-dimensional analysis due to the size of models created by the mesh generator program. The greatly increased complexity of the models also limits the range of solutions possible. The mesh generator program permits crack configurations for which '$a<b$', and thus for cracks in bodies having a low notch depth the resulting model is prohibitively large to solve economically. Such considerations highlight the shortcomings of the finite element analysis for instances where broad-ranging solutions are required for complex geometries even in circumstances where time, resources and modelling proficiency are available.

The range of solutions obtained, however are judged sufficient for the validatory purposes desired. SIF solutions were obtained for three notch depth values (b/T = *0.1825, 0.2727, 0.4375*), three root radii (b/ρ = *1, 3, 6*) and three flank angles (α = *15, 30, 45*). For each notch geometry, models containing a range of crack sizes and shapes were generated, subject to various loading modes, and solved. Tabulated finite thickness notched flat plate SIF solutions are contained in appendix A.

10.8 – A Weight Function Solution

A weight function solution to the complex crack geometries considered in this chapter is sought by the effective transformation of a three-dimensional problem to that of a two-dimensional problem. Usage of an interpolation factor, '$f(a)$' obtained from the analysis of two-dimensional constituent geometries, with weight functions for surface cracks assumes the influence of the notch to be a purely two-dimensional effect. Comparison of the form of SIF solutions developed for two and three-dimensional base geometry reference solutions indicated that stiffened surface cracks are constrained by additional stiffness not present in two-dimensional geometries. It is proposed that the presence of the notch will have some bearing upon this stiffness mode, however usage of a two-dimensional geometry interpolation factor has no means of accounting for this influence.

This reasoning results in the acceptance that the methodology presented in this chapter does not constitute a 'complete' solution. The impact of the recognised shortcoming of the methodology, outlined above, is unknown, however this chapter aims to demonstrate that it may be applied to give approximate solutions, which are both accurate and readily calculated, and which therefore offer a solution having distinct and appreciable advantages over existing methods.

10.9 – Critique of Results

Results displayed in figs. 10.9 – 10.21 depict a selected number of SIF results for a range of notched flat plate geometries subject to various loading modes. The number of solutions possible, using the interpolation scheme are large and are therefore restricted to show a number of key features. Also presented are FE solutions, where available and plane geometry solutions, where appropriate. The results selected for presentation are, however representative of the form and accuracy of the interpolation scheme and are designed to validate the procedure applied to all notch configurations.

Figs. 10.9 - 10.13 show results obtained from an interpolation algorithm for surface cracks at the root of a number of symmetric notches. SIF solutions for a range of crack aspect ratios under uniform tension and pure bending are displayed in figs. 10.9 and 10.10 together with edge crack solutions and those obtained by finite element means. Results presented display broad features expected: the elevated SIF for short cracks in the region of the notch root and the increasing tendency of the surface crack to show characteristics of an edge crack with decreasing aspect ratio. Both figures display results showing a high degree of correlation, however the weight function methodology gives solutions, which are marginally unconservative with respect to the finite element data. The unconservative nature of the weight function solution is more pronounced for cracks of high aspect ratio. Cracks having low aspect ratio (a/c = 0.4, 0.2) are those which increasingly display characteristics of an edge crack for which the two-dimensional analysis was shown to give excellent performance. Sections 10.5 and 10.8 contained a discussion of the 'incompleteness' of the current methodology, the shortcomings of which, are suspected to be most prevalent for cracks of high aspect ratio and is identified as a possible source of the slight error observed in weight function solutions for such cracks.

The influence of the notch detail upon the SIF solution is shown in greater clarity in figs. 10.11 – 10.13 which each show the variation of a single notch parameter for an otherwise constant geometry and crack configuration. In each case substantial variations in the notch profile due to notch size, notch acuity and flank angle are readily apparent in both weight function and finite element solutions. The more subtle variations between solutions for the differing flank angles and root radii are present in the finite element data are captured by the weight function solution. The three figures serve to demonstrate the flexibility of the interpolation scheme and validate the weight function methodology applied. The accuracy of solutions possible is evident from the results displayed and highlight the economy to be gained from the weight function approach adopted. Though no similar study of the influence of notch profile upon SIF solutions is conducted for other notch types (step, intrusion, etc.), the limited results presented here are judged illustrative of those possible for other notch types.

Figs. 10.14 – 10.16 present SIF solutions from the interpolation scheme for a number of cracks at step notch geometries subject to pure tension and pure bending. Results presented in figs. 10.14 and 10.15 show solutions for a number of crack shapes subject to pure tension and pure bending respectively. Each solution decreases in magnitude to fall below the solution of the equivalent plane plate with increasing crack depth. This characteristic may intuitively appear erroneous, as it suggests that the presence of a notch can increase the fatigue life of a component with respect to that of the plane geometry equivalent. This characteristic however results from the stiffened base geometry reference solution, which was identified as having an additional stiffness resisting crack opening. The same stiffness is present in the notched geometry and is evident in the accompanying finite element solutions, which in all cases correlate well to the weight function solutions. The 'undershoot' observed in both finite element and weight function solutions is present for both loading modes investigated and for all crack aspect ratios greater than zero. The edge crack solution contains no additional constraint and, therefore weight function and finite element solutions converge upon the plane strip solution.

Fig. 10.16 shows variation of the SIF solution for a crack loaded in pure tension at the root of a notch of differing size governed by the depth parameter, 'b/T'. A size effect is present which manifests itself as a change in SCF and hence influences the solution for short crack depths as was observed for edge crack solutions. The solutions presented in fig. 10.15 also show an influence on the magnitude of the 'undershoot' arising from the differing stiffness of the stiffened base geometry utilised in the interpolation scheme.

Fig. 10.17 – 10.21 show results obtained from the interpolation scheme applied to various protrusion and intrusion notches in flat plates. Though no finite element data is available for these configurations, characteristics observed for symmetric and step notched plates, are present in all solutions. Figs. 10.17 and 10.18 show solutions for a protrusion notch containing cracks of various shapes subject to pure tension and pure bending alongside the plane plate solutions. Once more the weight function solutions are shown to fall below those of the plane plate with increasing crack depth due to the additional constraint on crack opening provided by the protrusion. Fig. 10.19 displays solutions for various protrusion lengths governed by the geometric parameter, 'L_P/b' showing a differing magnitude of 'undershoot' with respect to the plane plate solution. As opposed to the solutions shown in fig. 10.15, in which this effect was a consequence of the stiffness of the base geometry solution, the variation in 'undershoot' stems from the interpolation factor, '$f(a)$' acting upon the same base geometry weight functions. Intuitively, the tendency of the solution to fall upon the plane plate solution with decreasing protrusion length would be expected, as it offers a decreasing constraint resisting crack opening, would be expected and is present in the solutions shown.

Figs. 10.20 and 10.21 show SIF solutions for a similar intrusion notch in a flat plate under uniform tension and pure bending respectively. No solutions, other than those of the edge crack equivalent, are available to support the interpolated weight function solutions. The stable and robust nature of the weight function solutions are, as for all notch geometries investigated in the chapter, evident and once more, general features and form of solutions shown are consistent with those expected.

New SIF solutions presented in this chapter are for the deepest points of surface cracks located in complex geometries. A methodology was employed that allowed surface cracks subject to stress, dependent on the 'x' direction only, to be represented by one-dimensional weight functions thus avoiding the need to utilise more complex two-dimensional weight functions. This procedure, as implemented by Mattheck *et al.*, is valid for the deepest point only due to the symmetry of the crack about the '$z = 0$' axis. A more 'complete' solution entails usage and interpolation of full two-dimensional weight functions which potentially allows determination of SIFs at all points on the crack front. While the ability to generate new SIF solutions for the deepest point of surface cracks in complex geometries is useful, a more representative assessment of crack behaviour can be gained from the SIF distribution along the crack front. Chapter 11 introduces aspects of advanced fracture mechanics analyses requiring full description of the crack front SIF distribution.

10.10 – Conclusions

The scope of this chapter has sought to validate a useful extension of the interpolation scheme, as applied to edge cracks at notches, to surface cracks at similar notches in flat plates. The methodology applied utilises weight functions of the form commonly employed for edge cracks to determine SIF solutions for the deepest point of surface cracks. Though the applied methodology contains some recognised shortcomings the results achieved proves the premise that an interpolation scheme is applicable to surface cracks in complex geometries. Results achieved are stable and robust, comparing well to solutions obtained from a full finite element analysis. The interpolation scheme has been demonstrated to give broadly accurate SIF solutions for all notch configurations investigated. A number of solutions were observed to be marginally unconservative with respect to the FE solutions particularly for low aspect ratio cracks. These inaccuracies however should be viewed in the context of the applied methodology, which provides a simple, flexible and powerful tool for the unprecedented rapid calculation of a broad range of SIF solutions.

The presented methodology is currently restricted to the evaluation of only the deepest point SIF. The assumption that one-dimensional weight functions and one-dimensional reference/object stress fields are applicable to the deepest point of a surface crack was employed. The

assumption is not valid, however for points other than the deepest point on the crack front, nor to stress fields that depend on both 'x' and 'y' co-ordinates. A methodology that allows calculation of the weight function at all points on the semi-elliptical crack front is a desirable ultimate objective of application of the interpolation scheme to surface cracks. Such information is essential for a more sophisticated assessment of cracks than those based solely on the deepest point of the crack. Chapter 11 introduces and discusses a number of aspects relating to advanced fracture mechanics analyses and the role to be played by a suitable weight function interpolation scheme. With respect to these ultimate aims, the work contained in this chapter serves as a valuable demonstrator of the interpolation concept applied to surface cracks in complex geometries.

10.11 – References

[10.1] Mattheck, C., Munz, D. and Stamm, H., Stress Intensity Factor for Semi-Elliptical Surface Cracks Loaded by Stress Gradients. *Engineering Fracture Mechanics*, Vol 18, No. 3, pp 633 – 641, 1983

10.12 – Tables

Tab. 10.1 – Deepest Point SIF Solutions for a Stiffened, Surface Cracked Plate (W/t = 2.75, b/T = 0.1875, Uniform Pressure Applied to Crack Faces)

a/t	Y			
	a/c = 1.0	a/c = 0.6	a/c = 0.4	a/c = 0.2
0.025	0.587	0.702	0.766	-
0.050	0.591	0.705	0.771	-
0.100	0.595	0714	0.786	0.880
0.150	-	-	-	0.919
0.200	0.604	0.737	0.827	0.965
0.250	-	-	-	1.019
0.300	0.614	0.764	0.877	1.082
0.350	-	-	-	1.160
0.400	0.625	0.794	0.934	1.256
0.450	-	-	-	1.383
0.500	0.635	0.824	0.999	1.556
0.600	0.646	0.856	-	-
0.700	0.657	0.888	-	-
0.800	0.676	0.925	-	-

Tab. 10.2 – Deepest Point SIF Solutions for a Stiffened Surface Cracked Plate (W/T = 2.75, b/T = 0.2727, Uniform Pressure Applied to Crack Faces)

a/t	Y			
	a/c = 1.0	a/c = 0.6	a/c = 0.4	a/c = 0.2
0.025	0.586	-	-	-
0.030	-	0.702	0.766	-
0.050	0.590	-	-	-
0.060	-	0.704	0.770	-
0.090	-	0.707	0.776	-
0.100	0.592	-	-	0.862
0.120	-	0.711	0.783	-
0.150	-	0.716	0.791	0.894
0.180	-	0.721	0.801	-
0.200	0.599	-	-	0.933
0.210	-	0.727	0.812	-
0.240	-	0.733	0.823	-
0.250	-	-	-	0.983
0.300	0.607	0.746	0.849	1.040
0.350	-	-	-	1.113
0.400	0.616	0.770	0.899	1.205
0.450	-	-	-	1.329
0.500	0.624	0.798	0.957	1.503
0.600	0.634	-	-	-
0.700	0.647	-	-	-
0.800	0.669	-	-	-

Tab. 10.3 – Deepest Point SIF Solutions for a Stiffened, Surface Cracked Plate (W/t = 2.75, b/T = 0.4375, Uniform Pressure Applied to Crack Faces)

a/t	Y			
	a/c = 1.0	a/c = 0.6	a/c = 0.4	a/c = 0.2
0.025	0.585	-	0.761	-
0.030	-	0.697	-	-
0.050	0.589	-	0.766	-
0.060	-	0.702	-	-
0.090	-	0.705	-	-
0.100	0.591	-	0.772	-
0.120	-	0.716	-	-
0.150	-	0.731	-	0.844
0.180	-	0.749	-	-
0.200	0.596	-	0.791	0.874
0.210	-	0.771	-	-
0.240	-	0.798	-	-
0.250	-	-	-	0.914
0.300	0.601	0.831	0.821	0.965
0.350	-	-	-	1.032
0.400	0.607	0.880	0.860	1.120
0.450	-	-	-	1.246
0.500	0.615	-	0.909	1.432
0.600	0.625	-	-	-
0.700	0.639	-	-	-
0.800	0.664	-	-	-

Tab. 10.4 – Deepest Point SIF Solutions for a Stiffened Surface Cracked Plate (W/t = 2.75, a/c = 0.4, Uniform Pressure Applied to Crack Faces)

b/T													
0.0		0.03125		0.0625		0.125		0.1875		0.2727		0.4375	
a/t	Y	a/t	Y	a/t	Y	a/t	Y	a/t	Y	a/t	Y	a/t	Y
0.025	0.938	0.025	0.801	0.025	0.779	0.025	0.769	0.025	0.766	0.03	0.766	0.025	0.761
0.05	0.940	0.05	0.836	0.05	0.801	0.05	0.778	0.05	0.771	0.06	0.770	0.05	0.766
0.1	0.944	0.1	0.876	0.1	0.839	0.1	0.802	0.1	0.786	0.09	0.776	0.1	0.772
0.2	0.968	0.2	0.927	0.2	0.896	0.2	0.853	0.2	0.827	0.12	0.783	0.2	0.791
0.3	1.016	0.3	0.982	0.3	0.955	0.3	0.909	0.3	0.877	0.15	0.791	0.3	0.821
0.4	1.084	0.4	1.050	0.4	1.024	0.4	0.972	0.4	0.934	0.18	0.801	0.4	0.860
0.5	1.168	0.5	1.131	0.5	1.104	0.5	1.043	0.5	0.999	0.21	0.812	0.5	0.909
0.6	1.261	-	-	0.6	1.191	-	-	-	-	0.24	0.823	-	-
0.7	1.351	-	-	0.7	1.279	-	-	-	-	0.3	0.849	-	-
0.8	1.416	-	-	0.8	1.354	-	-	-	-	0.4	0.899	-	-
-	-	-	-	-	-	-	-	-	-	0.5	0.957	-	-

Tab. 10.5 – Curve Fit Coefficients for Deepest Point SIF for a Flat Plate (eq. 10.1)
(W/t = 2.75, Uniform Tension)

a/c	R_5	R_4	R_3	R_2	R_1	R_0
1.0	0.8773	-1.7489	0.9635	-0.0427	0.0165	0.6569
0.6	1.5889	-3.5522	2.033	0.1353	-0.0097	0.8313
0.4	-0.9888	0.3293	0.1299	1.0152	-0.0629	0.9396
0.2	17.878	-13.415	4.7697	1.7407	-0.117	1.0527

Tab. 10.6 – Curve Fit Coefficients for Deepest Point SIF for a Stiffened Flat Plate (eq. 10.1)
(W/t = 2.75, Uniform Pressure Applied to Crack Faces)

b/T	a/c	R_5	R_4	R_3	R_2	R_1	R_0
0.0625	0.4	2.5459	-7.9116	8.2085	-3.2415	1.0993	0.7531
0.1875	0.4	-8.4979	12.714	-7.1888	2.304	0.0586	0.7634
0.2727	1.0	8.7151	-12.312	6.3081	-1.375	0.1886	0.5824
0.2727	0.6	0.824	-0.7362	-0.1343	0.4549	0.0413	0.7002
0.2727	0.4	-1.2657	2.5634	-2.0588	1.2537	0.0337	0.7638
0.2727	0.2	43.218	-40.887	16.162	-1.5512	0.5259	0.8127
0.4375	0.4	9.7106	-13.398	6.7989	-1.059	0.2023	0.7569

10.13 – Figures

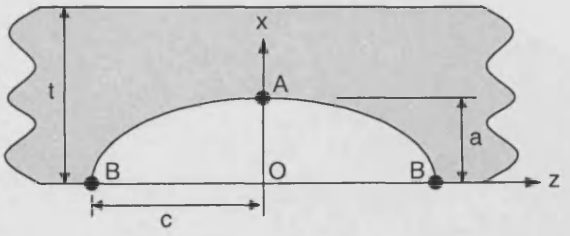

Fig.10.1 – Semi-Elliptical Surface Crack

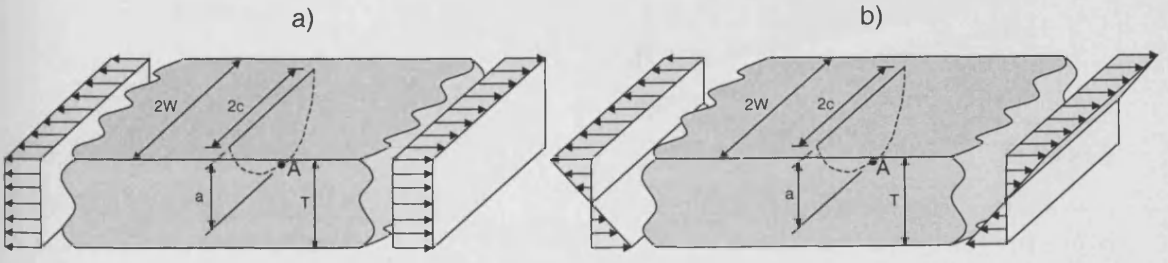

Fig.10.2 – Semi-Elliptical Surface Cracked Plates Under a) Tensile and b) Bending Loading

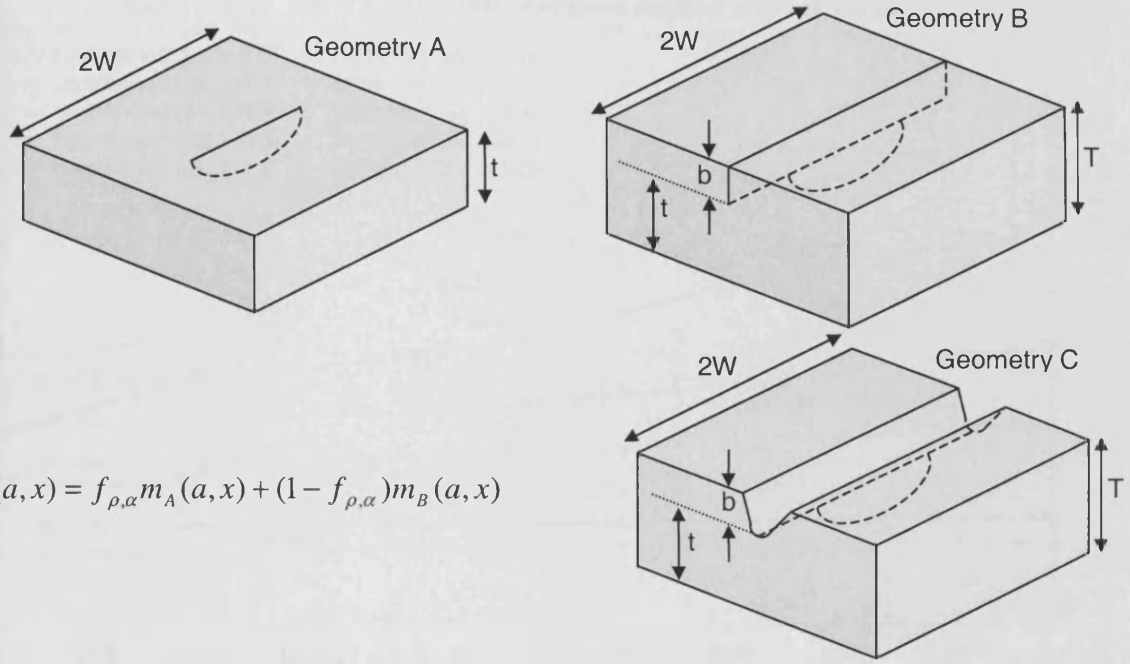

$$m_C(a,x) = f_{\rho,\alpha} m_A(a,x) + (1 - f_{\rho,\alpha}) m_B(a,x)$$

Fig. 10.3 – A Weight Function Solution for a Notched, Surface Cracked Plate Geometry, C, Comprising the Constituent Weight Functions of Geometries, A and B.

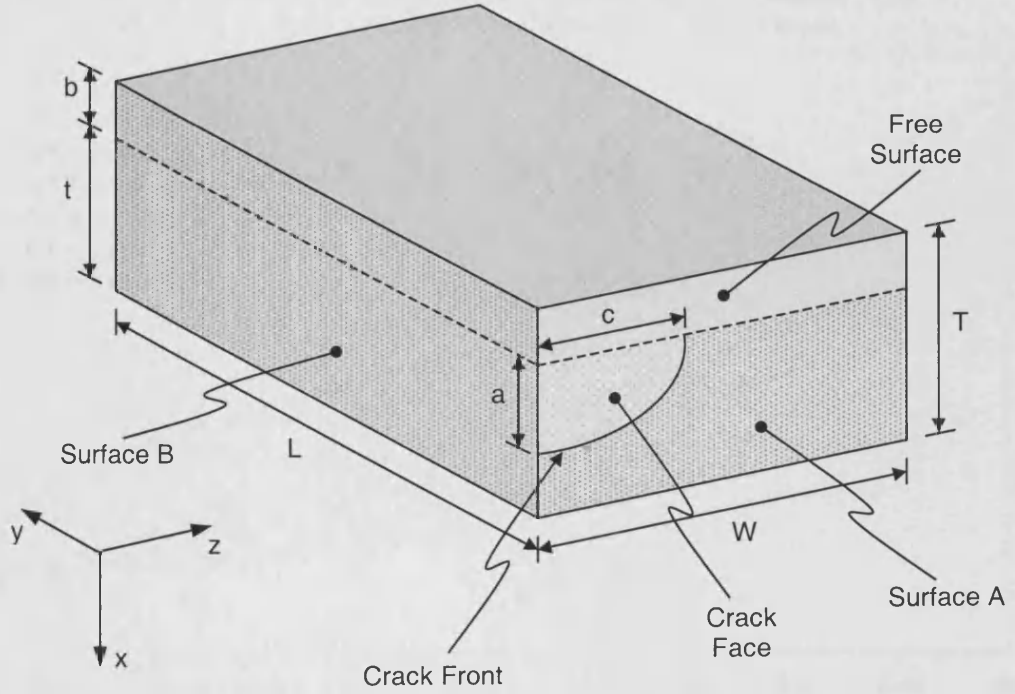

Fig. 10.4 – Definition of Stiffened, Surface Cracked Plate Geometry

Fig. 10.5 – Plot of SIF Solutions for a Stiffened, Surface Cracked Plate
(b/T = 0.2727, W/t = 2.75, Uniform Pressure Applied to Crack Faces)

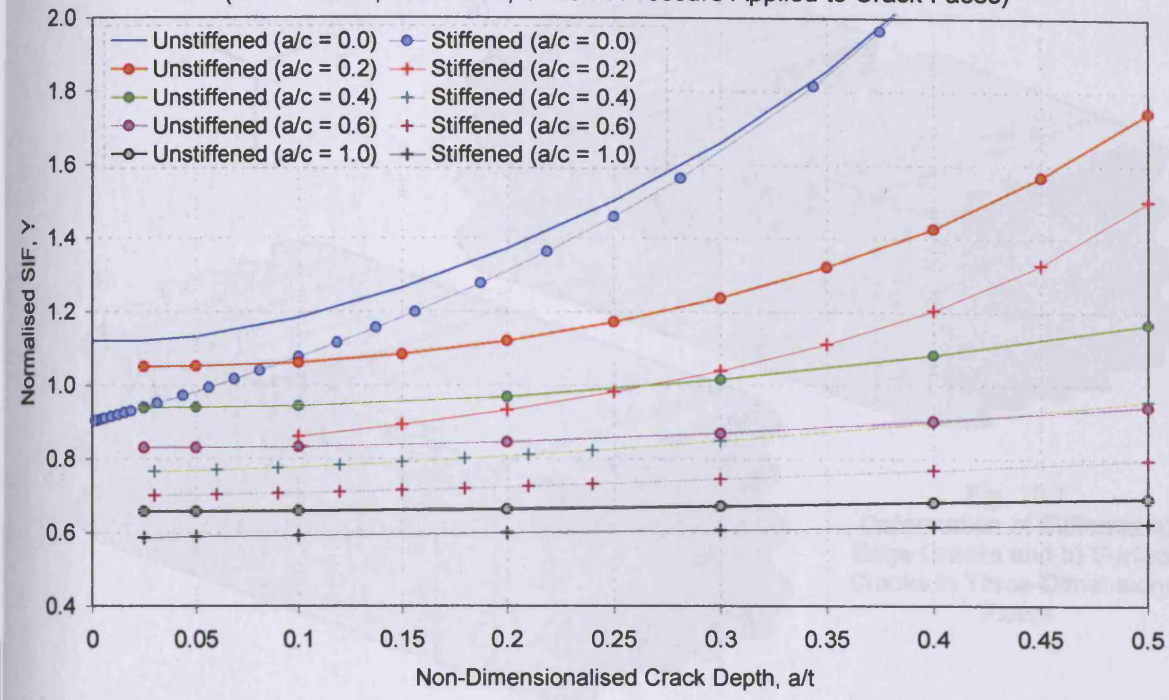

Fig. 10.6 – Deepest Point SIF Solutions for a Stiffened, Surface Cracked Plate
(W/t = 2.75, a/c = 0.4, Uniform Pressure Applied to Crack Faces)

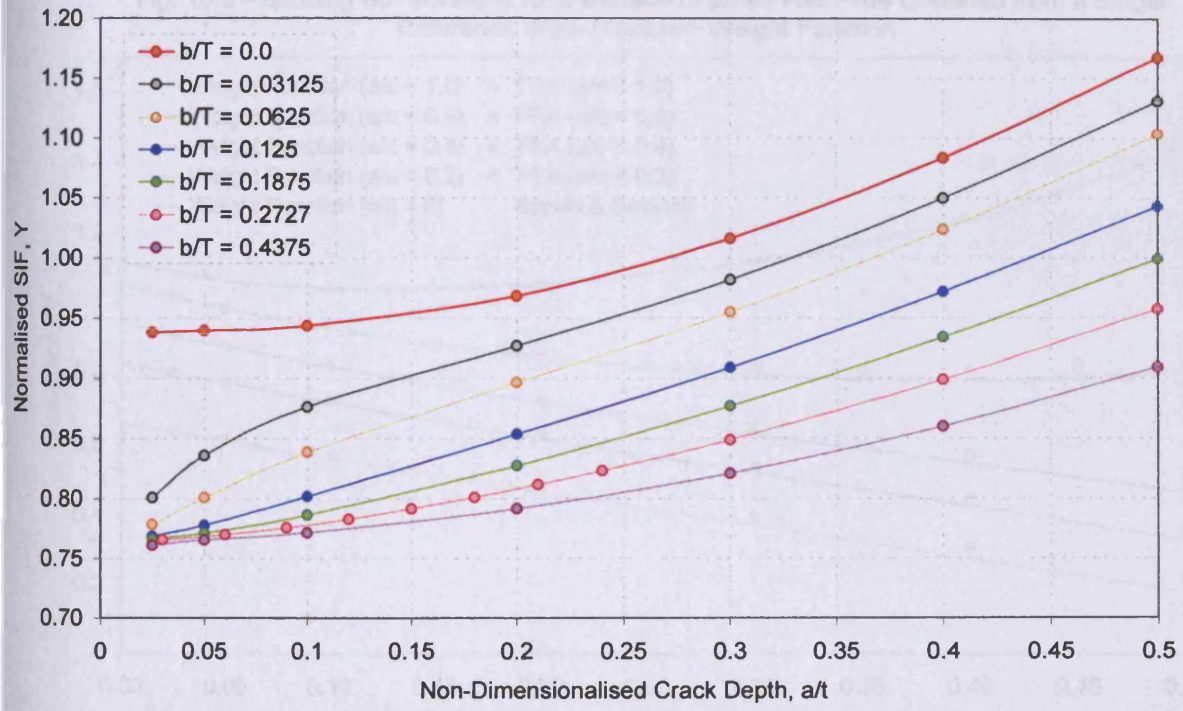

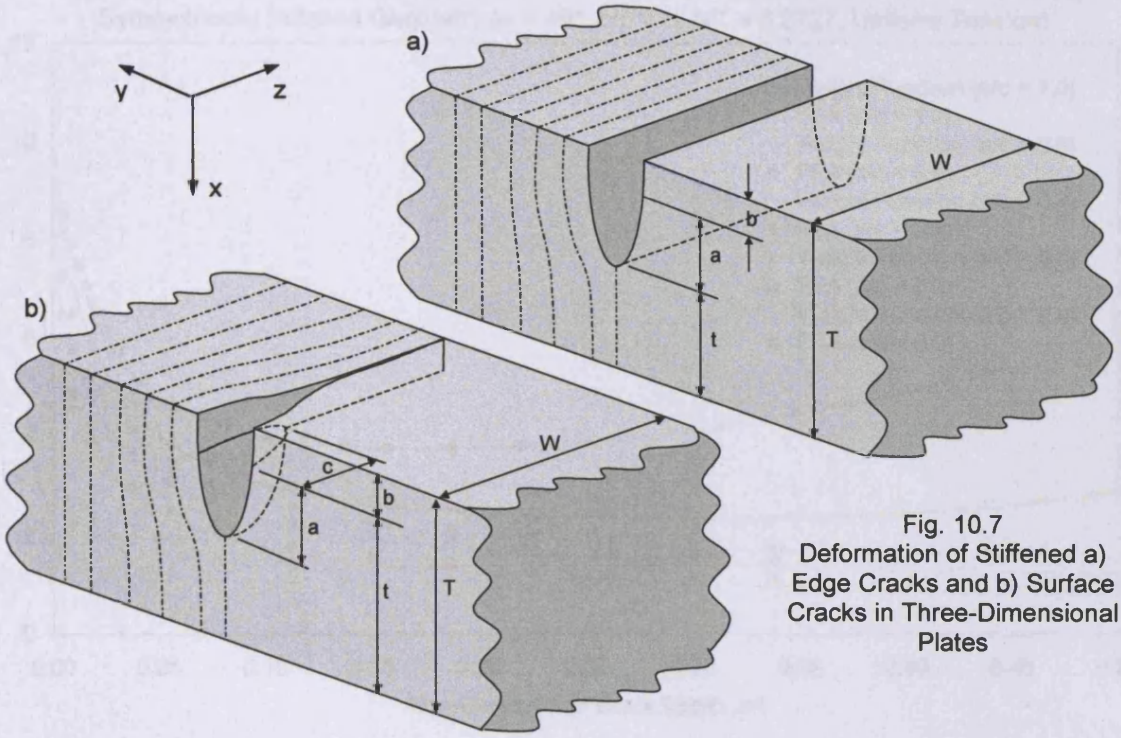

Fig. 10.7
Deformation of Stiffened a) Edge Cracks and b) Surface Cracks in Three-Dimensional Plates

Fig. 10.8 – Bending SIF Solutions for a Surface Cracked Flat Plate Obtained from a Single Reference State (Tension) Weight Function

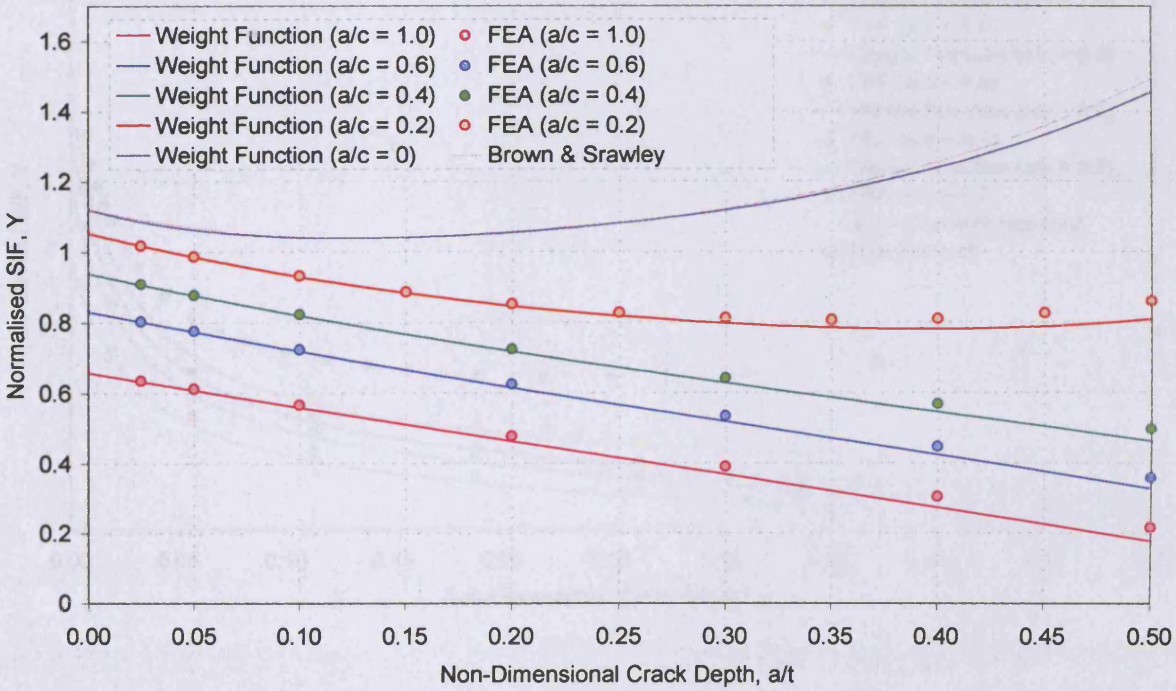

Fig. 10.9 – SIF Solutions Obtained From the Interpolation Scheme for A Finite Thickness, Symmetrically Notched Geometry (α = 45°, b/ρ = 6, b/T = 0.2727, Uniform Tension)

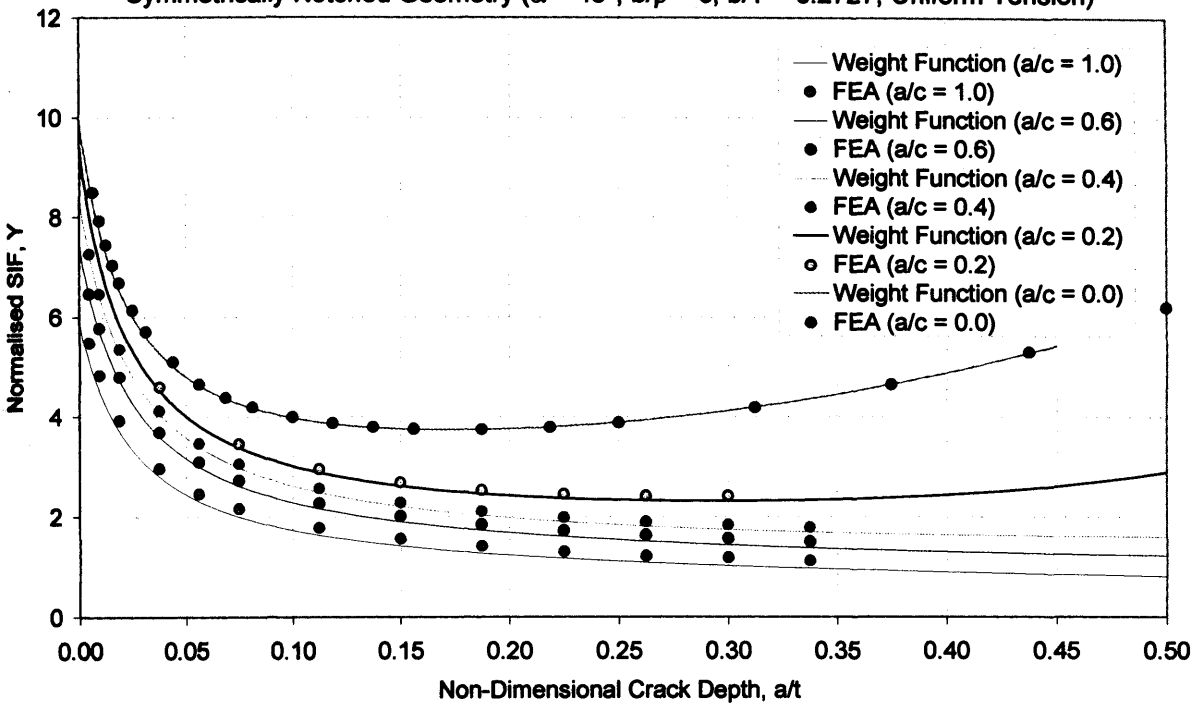

Fig. 10.10 – SIF Solutions Obtained From the Interpolation Scheme for A Finite Thickness, Symmetrically Notched Geometry (α = 45°, b/ρ = 6, b/T = 0.2727, Pure Bending)

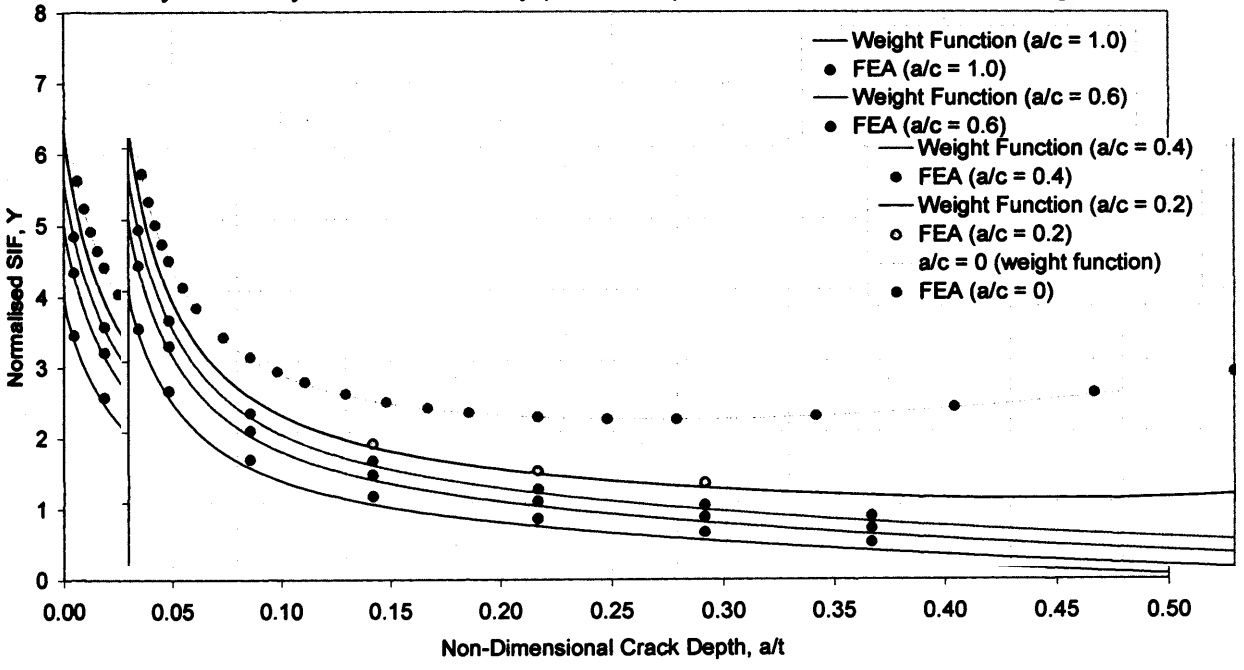

Fig. 10.11 – SIF Solutions Obtained From the Interpolation Scheme for A Finite Thickness, Symmetrically Notched Geometry (α = 45°, b/ρ = 6, a/c = 0.4, Uniform Tension)

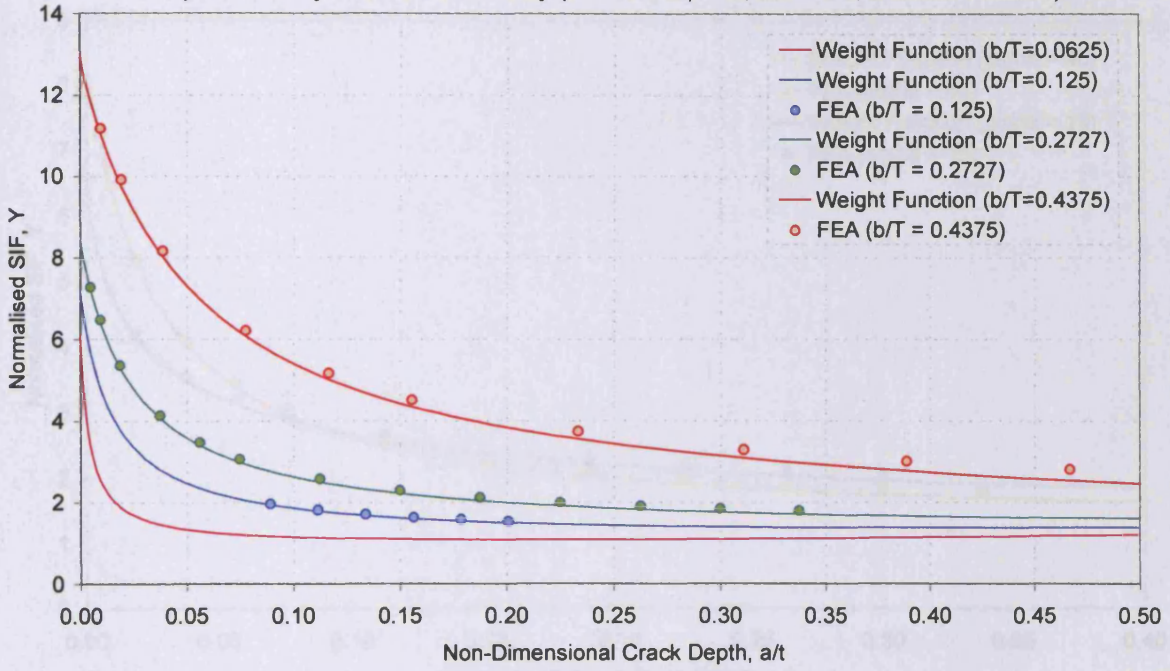

Fig. 10.12 – SIF Solutions Obtained From the Interpolation Scheme for A Finite Thickness, Symmetrically Notched Geometry (α = 45°, b/T = 0.2727, a/c = 0.4, Uniform Tension)

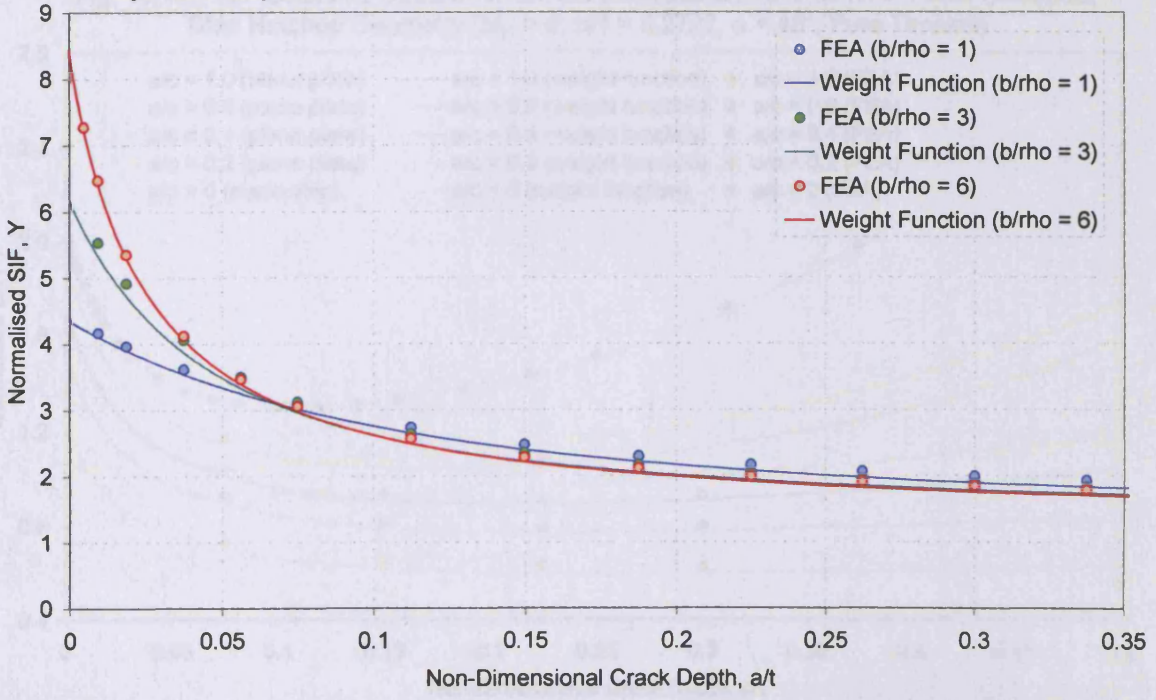

Fig. 10.13 – SIF Solutions Obtained From the Interpolation Scheme for A Finite Thickness, Symmetrically Notched Geometry (b/ρ = 6, b/T = 0.2727, a/c = 0.4, Uniform Tension)

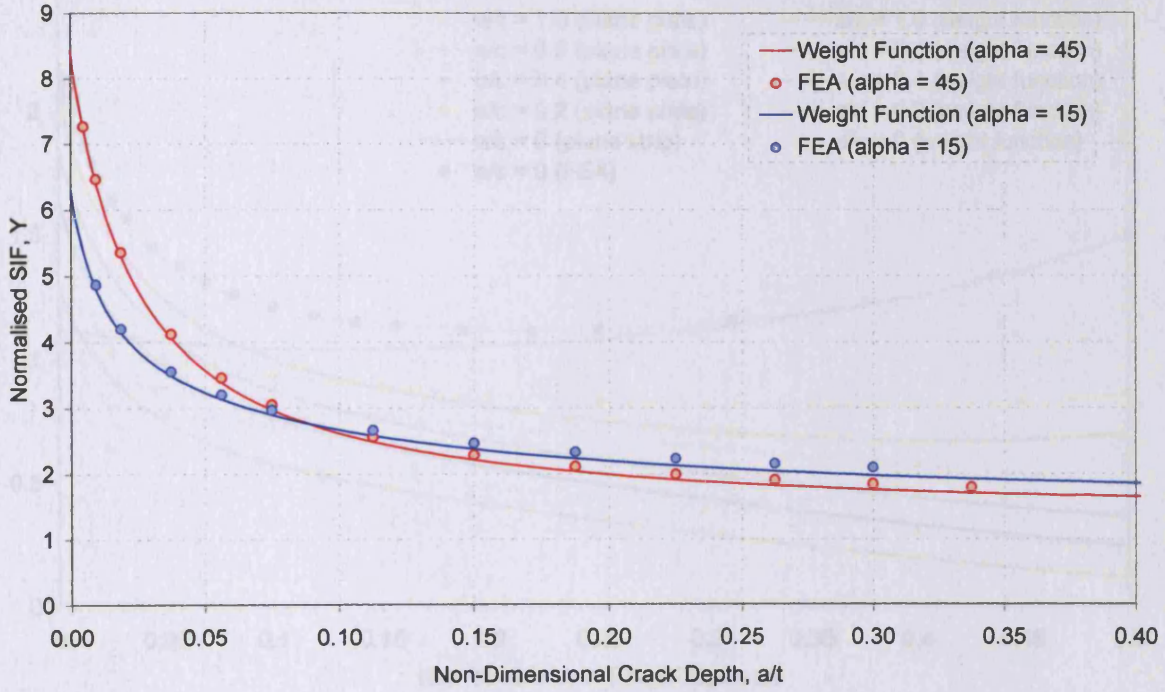

Fig. 10.14 – SIF Solutions Obtained From the Interpolation Scheme for A Finite Thickness, Step Notched Geometry (b/ρ = 6, b/T = 0.2727, α = 45°, Pure Tension)

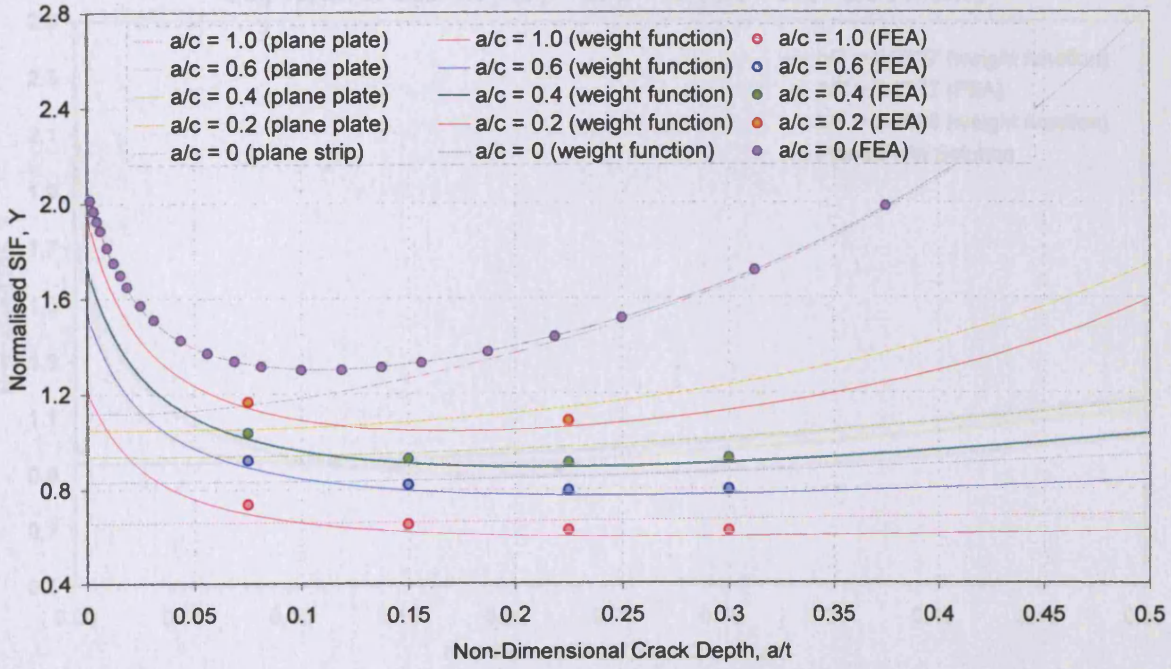

Fig. 10.15 – SIF Solutions Obtained From the Interpolation Scheme for A Finite Thickness, Step Notched Geometry ($b/\rho = 6$, $b/T = 0.2727$, $\alpha = 45°$, Pure Bending)

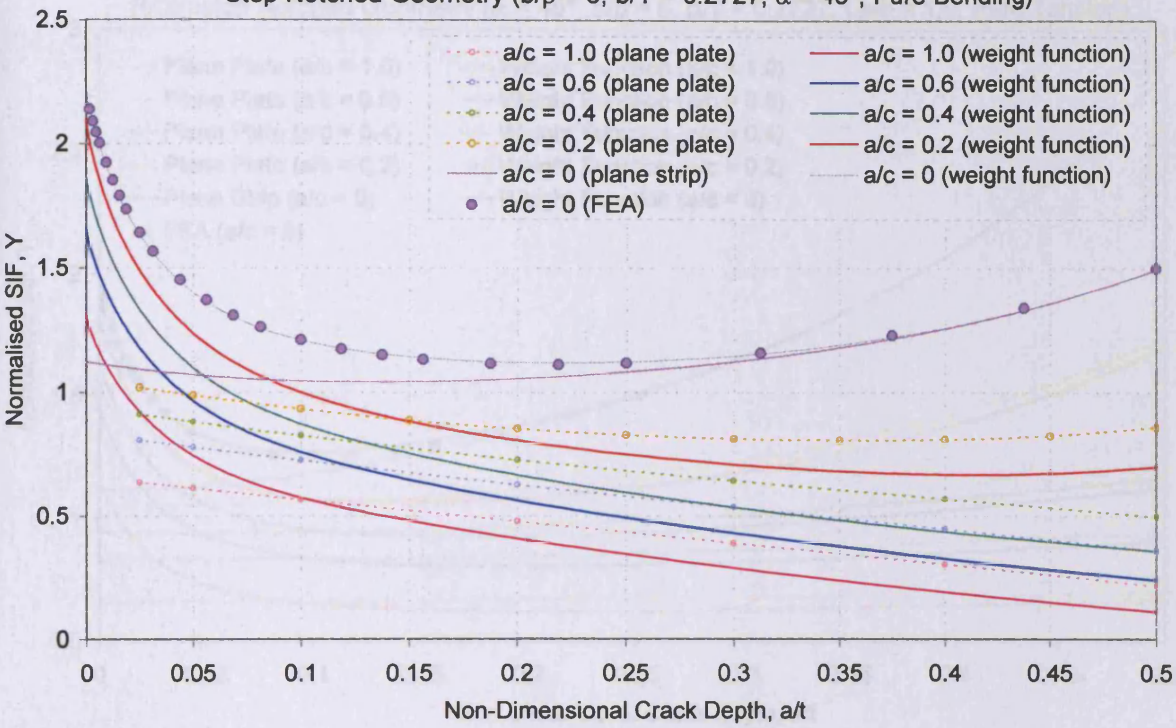

Fig. 10.16 – SIF Solutions Obtained From the Interpolation Scheme for A Finite Thickness, Step Notched Geometry ($b/\rho = 6$, $\alpha = 45°$, $a/c = 0.4$, Pure Tension)

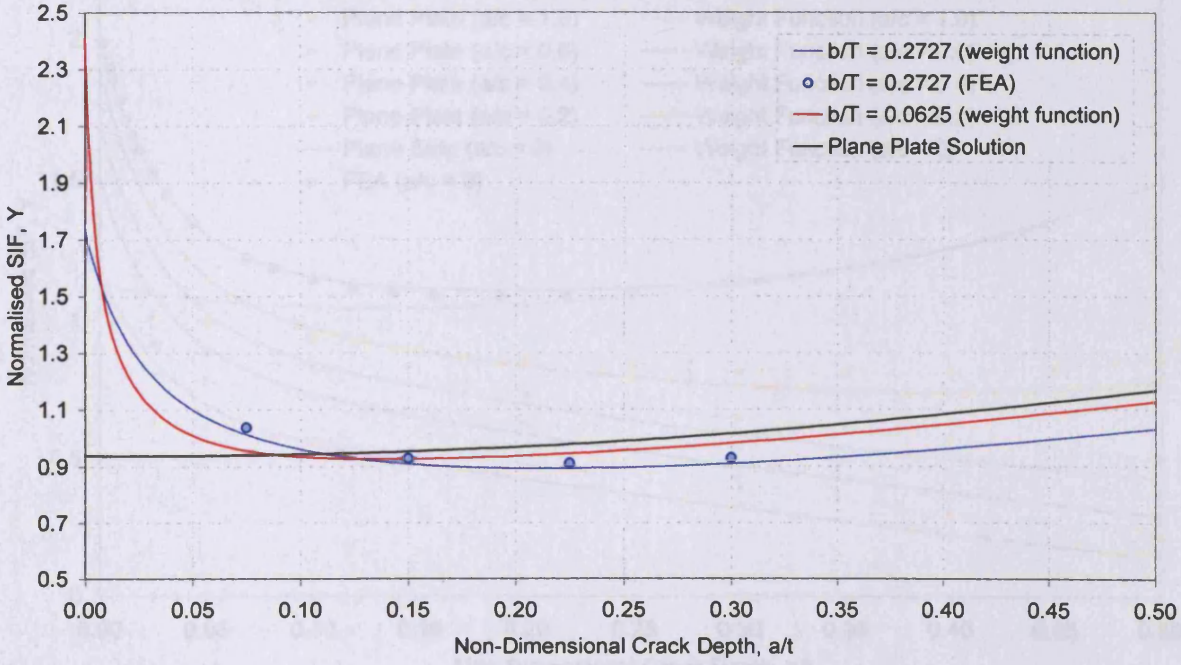

Fig. 10.17 – SIF Solutions Obtained From the Interpolation Scheme for A Finite Thickness, Protrusion Notched Geometry (α = 45°, b/ρ = 6, b/T = 0.2727, Lp/b = 1.0, Pure Tension)

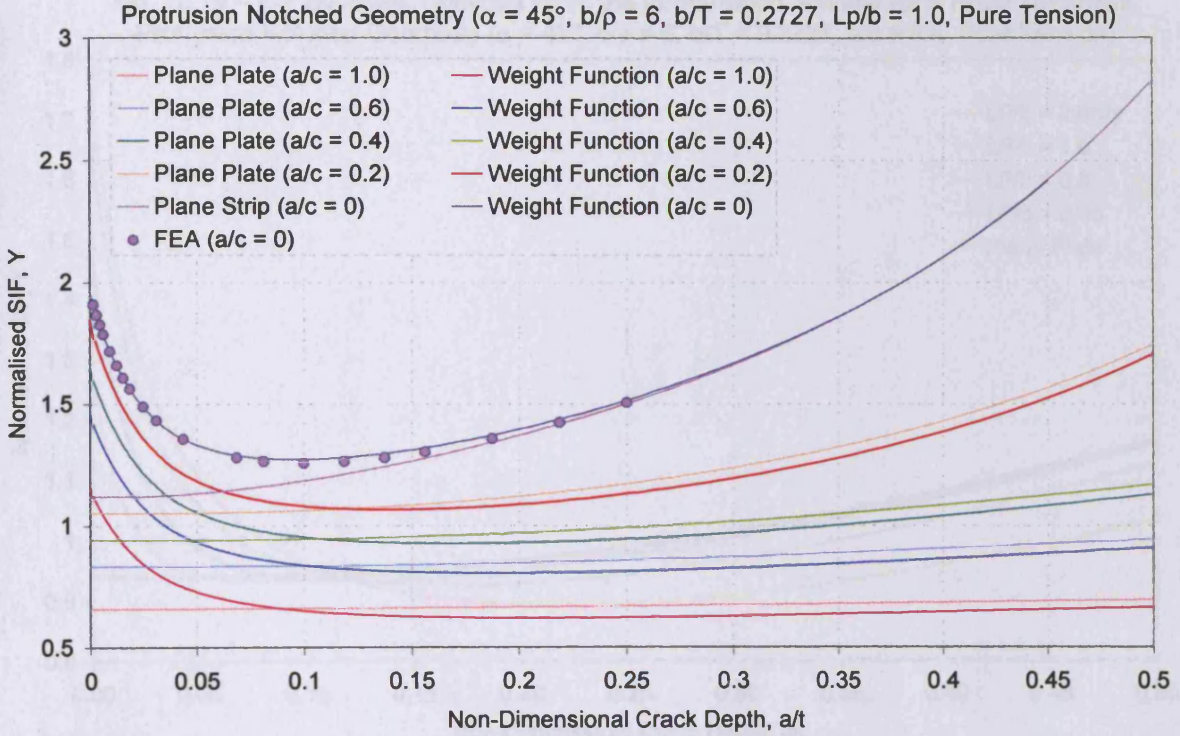

Fig. 10.18 – SIF Solutions Obtained From the Interpolation Scheme for A Finite Thickness, Protrusion Notched Geometry (α = 45°, b/ρ = 6, b/T = 0.2727, Lp/b = 1.0, Pure Bending)

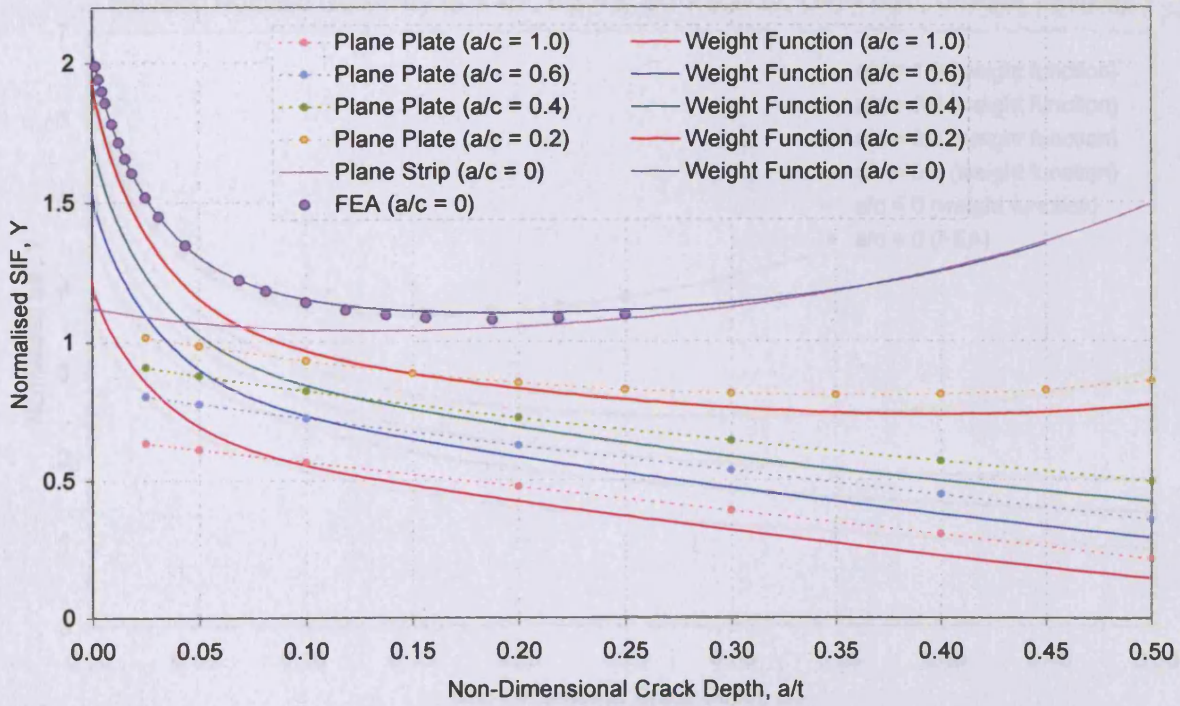

Fig. 10.19 – SIF Solutions Obtained From the Interpolation Scheme for A Finite Thickness, Protrusion Notched Geometry (α = 45°, b/ρ = 6, b/T = 0.2727, a/c = 0.4, Pure Tension)

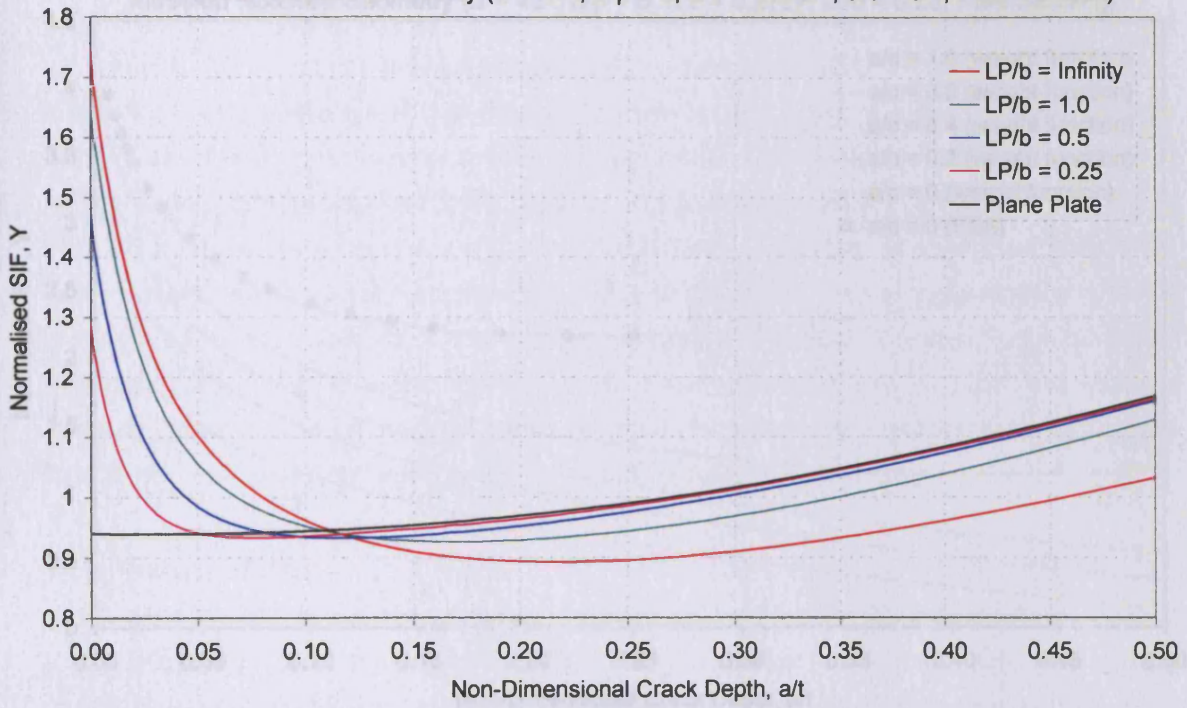

Fig. 10.20 – SIF Solutions Obtained From the Interpolation Scheme for A Finite Thickness, Intrusion Notched Geometry (α = 45°, b/ρ = 6, b/T = 0.2727, LI/b = 0.25, Uniform Tension)

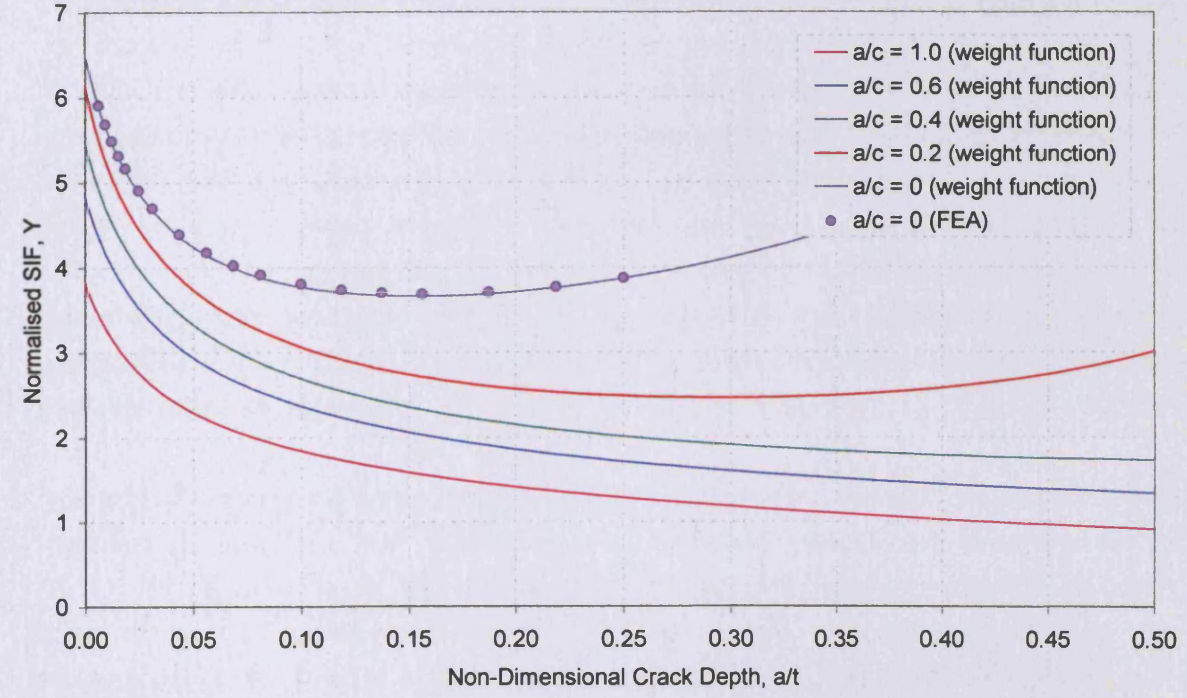

Fig. 10.21 – SIF Solutions Obtained From the Interpolation Scheme for A Finite Thickness, Intrusion Notched Geometry (α = 45°, b/ρ = 6, b/T = 0.2727, LI/b = 0.25, Pure Bending)

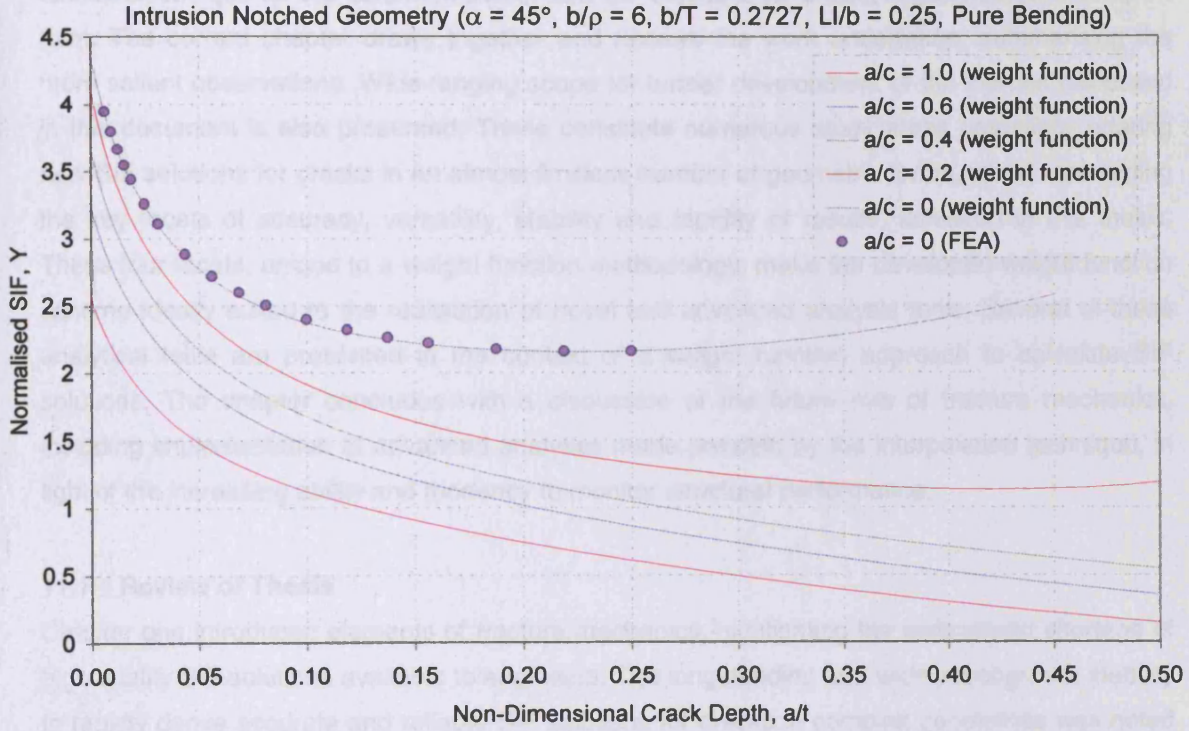

Chapter 11 – Conclusions and Proposals for Future Work

The preceding chapters of this thesis document the formulation and validation of a novel weight function technique for the determination of new SIF solutions for cracks in geometries of complex form. The current chapter draws together and reviews the work undertaken, summarising the more salient observations. Wide-ranging scope for further development of the themes discussed in this document is also presented. These constitute numerous study areas potentially offering new SIF solutions for cracks in an almost limitless number of geometric forms, whilst maintaining the key facets of accuracy, versatility, stability and rapidity of results, achieved in this thesis. These four facets, unique to a weight function methodology, make the developed weight function scheme ideally suited to the realisation of novel and advanced analysis tools. Several of these analytical tools are presented in the context of a weight function approach to calculate SIF solutions. The chapter concludes with a discussion of the future role of fracture mechanics, including implementation of advanced analyses made possible by the interpolation technique, in light of the increasing ability and tendency to monitor structural performance.

11.1 – Review of Thesis

Chapter one introduced elements of fracture mechanics, highlighting the widespread shortage of high quality SIF solutions available to engineers. The longstanding and widely recognised inability to rapidly derive accurate and reliable SIF solutions for cracks in complex geometries was noted as a fundamental limitation in many fatigue and fracture analyses. The weight function was introduced as a potentially powerful and efficient means of calculating new SIF solutions provided suitable reference solutions are available. Calculation of weight functions for complex geometries, has however remained problematic due to cumbersome mathematics, associated with weight function formulation, and the requirement of non-existent reference solutions. This thesis builds upon previous studies in which complex geometry weight functions are 'built' or composed of a number of more simple geometry weight functions, for which reference solutions are either pre-existing or may be simply determined, and formulated using a contemporary approach of enhanced mathematical stability. The critical fact that only the weight function can be used to combine geometric influences upon the SIF, by virtue of its sole dependence on component geometry was recognised as a crucial advancement beyond prior attempts to combine geometric influences upon SIF solutions.

The original scope of the thesis sought to apply the composition of weight functions scheme as defined by Brennan and Teh[11.1] to a number of asymmetric geometries and demonstrate the ability to rapidly develop new, high quality and broad ranging SIF solutions where no such current solutions exist. The composition of weight functions had been successfully applied to a wide range of symmetric external notch types and demonstrated to yield good SIF solutions in all

geometry and loading configurations investigated. Step, protrusion and intrusion notches were identified as being useful constituent geometry solutions having wide ranging applications for the approximation of a number of commonly occurring structural details and engineering components.

Initial investigation revealed that application of the composition of weight functions scheme to asymmetric notches suffered acute limitations. Furthermore, limitations were identified upon application to symmetric notches of extreme geometric form. Recognition of the fact that symmetric and asymmetric geometry types are inter-related, being of a common generic form, indicated that a 'complete' solution universally applicable to all external notch types and all geometric configurations had yet to be realised. Though the work conducted by Teh[11.2] proved the premise that geometric influences upon SIFs could be isolated and combined via the weight function, the precise form of the developed composition scheme was thought to be 'incomplete' resulting in the limitations observed.

A novel weight function methodology termed the interpolation of weight functions was proposed describing a complex geometry weight function as sharing characteristics of extreme planar or 'base' geometry weight functions. The interpolation scheme is closely related to the existing composition scheme, requiring identical constituent geometry weight functions, which are combined to yield an interpolation factor. The interpolation factor operates upon the base geometry weight functions, in essence to describe the extent to which the notch acts as a crack. The interpolation scheme, implemented via a simple computer-based algorithm, was demonstrated to yield excellent SIF solutions correlating well to those obtained by in-house finite element methods and experimental methods for all notch types (symmetric and asymmetric), notch configurations and loading modes investigated. It was shown to satisfy the criteria required without compromising accuracy.

The prospect of extending a similar weight function technique for the analysis of surface cracks situated at notches was identified as a highly desirable objective of the study, broadening application to a wider, more commonly occurring, class of cracks. The interpolation scheme was, once more, recognised as a methodology more suited to this task than the existing composition scheme. A developed methodology entailed the usage of interpolation factors derived from two-dimensional geometry constituent weight functions, representing the geometric influence of the notch, applied to two relevant surface crack base geometry weight functions. The sole new information required was relevant reference solutions for the formulation of base geometry weight functions, which were assumed to be of the form of those more commonly used for edge cracks. The applied methodology therefore, transformed a three-dimensional system to that of a two-

dimensional system and restricted calculation of new SIF solutions to the deepest point of the crack front. The developed methodology is not described as a 'complete' solution, as some limiting approximations exist. SIF solutions, however, obtained through the interpolation scheme were shown to display the excellent performance achieved for edge cracks, which although useful in their own right, demonstrate that the interpolation premise holds and may be used in conjunction with weight functions more representative of surface cracks, to formulate a more 'complete' solution.

11.2 – Conclusions

A novel weight function scheme developed in this document to rapidly and simply determine SIF solutions for complex crack systems has been rigorously validated in this text. The interpolation methodology was designed to provide analysts with a tool for rapid defect assessment permitting SIF solutions not previously possible within required criteria of accuracy, versatility and stability. The findings of the body of work presented here have demonstrated the interpolation approach to be universally applicable to all external notches, without restriction or limitation. The four conducive key facets of SIF solutions, obtained through an interpolation approach, of accuracy, versatility, stability and rapidity are unique to this weight function methodology. Chapters 1 and 2 outlined many of the various existing methods for the calculation of SIF solutions: chapter 1 focusing on those classed as numerical, analytical and experimental and chapter 2 on derivative methodologies which utilise existing SIF solutions, none of which fully satisfy these criteria. The value of the developed weight function methodology is evident in the context of these observations and provides a solution to the longstanding problem of calculation of SIFs, provided that suitable reference solutions are available.

Although the approach described requires a number of reference constituent and base geometry solutions, their number is limited and can be used to formulate an unprecedented, almost limitless number of new SIF solutions. The interpolation procedure calculates a complex geometry weight function, that once formulated, can be used in conjunction with an arbitrary stress field arising from applied, residual or thermally induced stress fields. The body of work presented has validated the interpolation scheme by application of simple loading conditions. Capacity, however exists to exploit this feature to realise new analytical SIF solutions for cracks subject to both applied and residual stress fields, raising tantalising analytical prospects pertaining to controlled failure design to be discussed in section 11.4.3.

Great scope exists for further development of principles developed in this thesis. Some of the many study areas are described in the following sections. Those listed in section 11.3 are confined to two-dimensional geometries, or those modelled as such, some of which constitute the

development of ideas presented in this thesis whereas others identify further application of the interpolation principle to alternative geometry and crack types. Section 11.4 introduces aspects of its application and cites the interpolation scheme as fundamental to the realisation of a number of advanced fracture mechanics analyses concerning surface cracked geometries.

11.3 – Further Interpolation of One-Dimensional Crack Weight Functions

This section outlines potential further extension of the interpolation scheme, applied in this study to edge cracks at externally notched geometries, to new geometry types and loading conditions not considered in this thesis. Each is restricted to the analysis of one-dimensional cracks or those modelled as such which, whilst providing powerful analyses tools in their own right, may also be transferable to the more complex analyses tools described in section 11.4.

11.3.1 – Edge Cracks at Compound Notches

Due to the versatile nature of the weight function scheme developed in this thesis, the possibility exists to combine the geometric influences of two or more notch forms to derive SIF solutions for what were described, in chapter 6, as compound notches. Three examples of such notch forms are reproduced in fig. 11.1. The notches shown are more intricate than those discussed in this thesis but are, however combinations of those considered in this study.

Compound notches, in this context, refer to notches comprising two, or more of the basic notch types analysed in this study. Constituent geometry reference SIF solutions and interpolation factors have been determined for these geometries in this thesis and in Teh's[11.2] existing library, and it is proposed that these may be applied to compound notches. The manner in which solutions are formed via the combination of basic notch interpolation factors is conceptually simple requiring, for the notch depicted in fig. 11.1a a stiffened and unstiffened base geometry weight function. Those notches depicted in fig. 11.1b,c require two stiffened base geometry weight functions (of differing stiffness) and an unstiffened base geometry weight function (fig. 11.2).

The notch depicted in fig. 11.1c closely approximates the profile of a repaired welded joint. A protrusion or step notch can be used to model the profile of welded joints (weld angle and weld root radius). Grinding of the weld toe is a frequently applied practice used to remove flaws or decrease the SCF present at this position. The profile resulting from the grinding process may be approximated by the addition of a semi-circular notch to the protrusion or step. This example of a compound notch acts as an illustrative example of the many useful complex geometry weight function that can be determined via the approaches given in chapter 6 and described below. The weight function solution is given by the expression below.

$$m(a,x)=\left[\frac{1}{2}\left[f_{\rho,\alpha}(a)m_U(a,x)+\left(1-f_{\rho,\alpha}(a)\right)m_{S1}(a,x)\right]+\frac{1}{2}\left[f_{\rho}(a)m_U(a,x)+\left(1-f_{\rho}(a)\right)m_{S2}(a,x)\right]\right] \quad \text{- (11.1)}$$

where: $m_U(a,x)$ is the weight function for the plane unstiffened geometry (fig. 11.2c)

$m_{S1}(a,x)$ is the weight function for the plane stiffened geometry (fig. 11.2a)

$m_{S2}(a,x)$ is the weight function for the plane stiffened geometry (fig. 11.2b)

$f_{\rho,\alpha}(a)$ is the interpolation factor as determined in chapter 5

$f_{\rho}(a)$ is the interpolation factor as determined in chapter 4

The sole new information required is the crack line stress distribution, which is relatively simple to determine, thus demonstrating the computational economy of the interpolation methodology.

Validation of this interpolation methodology is currently limited to the step notches analysed in chapter 6. A short programme of work is envisaged using the existing 'library' of constituent solutions to produce SIF solutions for a broad variety of compound notch types to demonstrate the economy of this technique.

11.3.2 – Edge Cracks at Axi-Symmetric Notches

It is proposed that an additional class of geometries, notched symmetrically about a longitudinal axis, may be solved via an interpolation of weight functions approach. A number of examples of axi-symmetrically notched components is given in fig. 11.3 which may be used to approximate components containing thread forms, shoulders/fillets, welded joints, etc. The existing 'library' of geometric influences presented as interpolation factors is recognised as being applicable to this geometry type, though the precise nature of a suitable interpolation scheme has yet to be formulated. Alternative base geometry weight functions are required in addition to those utilised in this study concerning externally notched components, the form of which are presented in fig. 11.4, in the case shown containing two cracks of equal length. Though the base geometry solutions contain edge cracks, for which the existing methodology for the determination of weight function applies, the interaction between cracks is not accounted for, however the contemporary approach adopted in this study may be simply tailored to suit this crack configuration.

11.3.3 – Cracks at Internal Notches

The study presented in this thesis solely concerns the determination of SIF solutions for edge cracks emanating from the root of externally notched geometries. The applied methodology has been shown to give excellent solutions for all notch configurations investigated. A closely related

weight function scheme is predicted to be applicable to cracks emanating from internally notched components.

In common with edge cracks at external notches, many SIF solutions exist for cracks at internal notches in infinite geometries such as those published by Newman[11.3], for cracks at a circular notch or Nisitani and Isida[11.4] for cracks at elliptical notches. While these solutions are useful for cases where the notch and crack are small compared to plate dimensions, very few satisfactory solutions exist for the finite thickness equivalent. It is proposed that a similar weight function methodology may be applied to give broad ranging solutions of high accuracy using the interpolation approach developed in this study. Various examples of cracks at internal notches are shown in fig. 11.5, which highlight the numerous configurations possible, containing single and multiple cracks, eccentricity, asymmetry and multiple notches. A universal weight function solution, similar to that developed in this study, and applicable to all configurations shown in fig. 11.5, is a desirable objective of the future development of the interpolation scheme.

An interpolation factor '$f_\rho(a)$' may be ascertained from analysis of the notched infinite geometry and the equivalent plane infinite and semi-finite geometries (fig. 11.6a and 11.6b). However as stated for axi-symmetric notches the existing library is thought to contain useful information which can be applied to this geometry type. A weight function for the notched finite thickness geometry would be composed of constituent finite thickness geometries as shown in fig. 11.6c and 11.6d. New SIF solutions are then determined via the integration given below.

$$K_I = \int_0^a \sigma_{yy}^F(x)\left[f_\rho(a)m_U^F(a,x) + \left(1 - f_\rho(a)\right)m_S^F(a,x)\right]dx \qquad \text{- (11.2)}$$

Where: $m_U{}^F(a,x)$ is the equivalent unstiffened plane geometry weight function

$m_S{}^F(a,x)$ is the equivalent stiffened plane geometry weight function

It is thought that the interpolation factor '$f_\rho(a)$' determined via the analysis of constituent geometry SIF solutions will be closely related to that determined in chapter 4 from the semi-finite equivalent geometries. This has yet to be verified, however if proven to be true the possibility exists to derive new SIF solutions for a numerous range of geometry types with greatly reduced computational effort. Base geometry solutions for eccentric internal cracks provided by Terada and Isida[11.5] are useful for analysis of some crack systems shown.

11.3.4 – Surface Cracks in Notched Plates, Pipes, Rods and Shells

Chapter 10 was concerned with the application of the developed weight function method to surface cracks. At present a methodology to determine SIF solutions for the deepest point of such

cracks has been presented and was found to yield new SIF solutions of unprecedented quality whilst maintaining the simplicity and flexibility of the edge crack solution. The same weight function method may be applied to notched plates, pipes, rods and more general shell geometries by utilisation of appropriate base geometry weight functions.

Chapter 10 also contained a description of application of the interpolation technique to give SIF solutions to determine SIF solutions for the deepest point of surface cracks in complex geometries. The existing library of constituent geometries could be used to approximate cracks in welded T-butt joints using stiffened and unstiffened flat plate geometry solutions as base geometry weight functions. Solutions of this form are particularly useful as they allow the inclusion of residual stress effects in SIF calculation. A similar study using thick walled pipes as base geometry weight functions could also be undertaken to approximate the presence of a thread form for the analysis of threaded connections. Both cited applications provide a demonstration of how the adoption of a weight function approach can yield SIF solutions for complex geometries, that have been the subject of much research activity in recent years, and highlight how the interpolation scheme potentially provides a more effective methodology to calculate SIF solutions, than those currently employed.

The potential to extend the applicability of an interpolation scheme to these, and numerous similar, complex engineering geometries is dependent upon the continued development of the library of constituent geometry solutions and also a similar library of planar base geometry solutions. This thesis has not sought to add significantly to the existing library of constituent geometry solutions, though many useful results were presented. The focus was confined to the development and demonstration of a more robust and economic methodology for their implementation. The interpolation scheme requires planar base geometry weight functions, for which suitable reference SIF solutions are a pre-requisite. Two-dimensional geometries are of the form commonly contained in published literature and compendia. Relatively very few, three-dimensional geometry solutions exist, due primarily to the complexity of geometry and crack shape. Most solutions available are determined from FE analyses, however few describe a wide range of geometry and crack forms and comparison between studies is made difficult due to often idiosyncratic description of crack shape.

A programme of work intended to systematically identify, define and describe a library of base geometry reference solutions to be applicable to a wide variety of more commonly occurring structural details and engineering components, is proposed. Fig.11.7 shows complex rod geometries that can be modelled by an interpolation approach to give SIF solutions for cracks at

grooves and fillets in shafts. Fig.11.8 shows required base geometries and fig.11.9 a range of possible crack shape types.

11.3.5 – Cracks Subject to Mixed Mode Loading

The scope of work contained in this thesis is restricted to cracks subject to only, or primarily, mode I loading. Mode I loading is widely acknowledged as the major damaging mode of cracking in the vast majority of engineering structures and components. Application of remote tensile and bending loads to cracks at symmetric notches, results in pure mode I crack opening. The same loading modes applied to asymmetric notches causes a marginal mode II and an additional mode I opening, arising as a result of the presence of shear stress due the geometry's asymmetry about the crack plane. Stress intensity factors for a crack at an asymmetric notch or any crack subject to mixed mode loading can be written as presented by Fett and Munz[11.6] by eq. 11.3. The analyses of asymmetric notch types in this thesis has shown that the induced mode I opening due to the presence of a crack line shear stress, '$K_I^{(2)}$' is negligible when compared to that caused by the direct stress component.

$$K_I = K_I^{(1)} + K_I^{(2)} \qquad \text{- (11.3a)} \qquad\qquad K_{II} = K_{II}^{(1)} + K_{II}^{(2)} \qquad \text{- (11.3b)}$$

The influence of the mode I and II contribution to cracking, for generalised loading systems which have a non-zero nominal shear component is, however less clear. Fig. 11.10 depicts an asymmetric geometry subject to a generalised 3-point bending load condition for which nominal direct and shear stresses are both non-zero. The mode II SIF is analogous to that of the more familiar mode I SIF and may be described accordingly by eq. 11.4.

$$K_{II} = Y_{II}\tau_o\sqrt{\pi a} \qquad \text{- (11.4)}$$

Fett and Munz state that a weight function of the same form, as that used for mode I opening, is applicable to cracks subject to pure mode II opening such that eqs. 11.5 – 11.7 hold. Implementation of the contemporary approach for weight function formulation can be applied to formulate the weight function given by eq. 11.6 provided suitable reference solutions are available. An interpolation approach can be invoked for the formulation of mode II SIFs in complex geometries in the same manner as that conducted in this study for mode I crack opening.

$$K_{II} = \int_0^a \tau(x) h_{II}(x,a)\,dx \qquad \text{- (11.5)} \qquad\qquad h_{II}(x,a) = \frac{E'}{K_{IIr}} \frac{\partial u_r(x,a)}{\partial a} \qquad \text{- (11.6)}$$

$$\frac{\partial u_r(a,x)}{\partial a} = \frac{2\tau}{H}\sqrt{2}\sum_{j=0}^{\infty} c_j \left(1-\frac{a}{x}\right)^{j-1/2} \quad ; \quad c_0 = \frac{F(a/t)}{2} \qquad \text{- (11.7)}$$

The SIF eq. 11.3, for a generalised mixed mode loading condition, can be written in terms of weight functions as given by eq. 11.8. Formulation of each weight function is possible from published SIF solutions and those obtained numerically. An interpolation approach maybe applied to determine 'K_I' and 'K_{II}' for any complex geometry subject to any generalised loading condition.

$$K_I^{(1)} = \int_0^a h_I^{(1)}(x,a)\sigma(x)dx \qquad \text{- (11.8a)} \qquad K_I^{(2)} = \int_0^a h_I^{(2)}(x,a)\tau(x)dx \qquad \text{- (11.8b)}$$

$$K_{II}^{(2)} = \int_0^a h_{II}^{(2)}(x,a)\tau(x)dx \qquad \text{- (11.8c)} \qquad K_{II}^{(1)} = \int_0^a h_{II}^{(1)}(x,a)\sigma(x)dx \qquad \text{- (11.8d)}$$

11.4 – Interpolation Schemes and Advanced Fracture Mechanics Analyses

Future work outlined in section 11.3 constitutes development of the existing interpolation scheme exploiting its versatile nature to broaden applicability to new geometry types. The ability to calculate new SIF solutions in a manner that meets four conducive, key criteria of accuracy, flexibility, stability and rapidity enables realisation of numerous advanced tools for fracture mechanics and defect assessment. Many of the themes presented are not new and have been, in many cases, in existence for a number of years. Though phenomena have been observed experimentally, full benefits provided by engineering optimisation has been hindered by the lack of an analytical framework. This section of future work discusses some of these tools in the context of the newly developed interpolation scheme, placing emphasis on its properties that provide a unique opportunity for their realisation.

11.4.1 – Two-Dimensional Weight Functions

All analyses conducted in this thesis and those considered, thus far, in this chapter have been, or modelled as, edge cracks, defined by the single depth parameter, 'a'. Corresponding weight functions are one-dimensional, again defined by the single parameter, 'a' (though cracks are embedded in a two or three-dimensional geometry). A highly desirable, more representative analysis of surface cracks, defined by parameters, 'a' and 'c' requires a two-dimensional weight function. An appropriate weight function, which varies over the whole crack area, allows calculation of SIFs at all points on the crack front subject to an arbitrary loading arrangement.

The form of two dimensional weight functions is more complex than one-dimensional weight functions, however their determination using an MRS approach is thought possible. Application of the contemporary methodology for weight function formulation may be demonstrated by firstly considering a two-dimensional edge crack as shown in fig. 11.11a. A suggested form of weight function, '$m_H(a,s,e)$' given by Rice[11.7] for a position, 'H' on the crack front, subject to point loading, 'F', may be written in terms of parameters, 's', the minimum distance between the point of load application and the crack front, and 'e', the distance between the point of load application and 'H' (fig.11.11b). The developed weight function can be tested under various combinations of in-plane and out-of-plane loading arrangements and interpolated to give SIF solutions for two-dimensional edge cracks in complex geometries (fig. 11.11c). The precise form of weight functions for this and more general surface cracks is at present unknown, however once ascertained via a limited finite element study, can be calculated by an MRS methodology similar to that utilised in this study.

11.4.2 – RMS SIF

Representative predictions of crack shape evolution are recognised as probably the greatest hindrance to effective defect assessment. Loaded surface cracks characterised by size, 'a/t' and shape, 'a/c' have a stress intensity distribution along the crack front varying significantly with position on the crack front, crack size and shape. Stress intensity distribution along the crack front for a cracked flat plate subject to tensile loading, presented in figs. 9.11 and 9.13, are illustrative of the significant variations with position on the crack front, which may be further augmented by the siting of a crack at a stress raiser or subjecting the crack to a non-uniform stress distribution. Numerous figures in chapters 9 and 10 highlight significant variation with crack size and shape in plane and notched components.

Though closed form solutions for crack front SIFs, covering a wide range of crack sizes and shapes, exist for the simplest surface cracked geometry in a flat plate by Newman and Raju[11.8], no such solutions exist for the more commonly encountered complex geometries, of the form considered in this study. Resulting analysis of crack shape evolution and defect assessment has traditionally based upon deepest point and surface point SIFs for which limited solutions are available: the solutions of Bowness and Lee[11.9] for welded joints provide a good example. Resulting predictions of crack growth are sensitive to these two points, which in the particular case of the surface point may not be either reliable or representative of bulk crack behaviour. More advanced numerical analyses have been applied by Lin and Smith[11.10, 11.11, 11.12] to advance the crack front by a distance based on a calculated local SIF at a number of discrete points on the crack front, however the approach is computationally intensive and is of limited flexibility.

The RMS SIF is designed to overcome the problems associated with methodologies presented above to provide robust and versatile predictions of bulk crack front behaviour. Applied to surface cracks it, in essence, represents an average SIF in two principle directions of crack growth in transverse and longitudinal directions (fig. 11.12). First proposed by Cruse and Besuner[11.13], the RMS SIF is defined by eq. 11.9, which indicates that a continuous SIF distribution along the crack front, defined by the characteristic angle, 'ϕ' is required for the determination of the RMS SIF.

$$K_{RMS(a)} = \sqrt{\frac{1}{\Delta S_A}\int_{\Delta S_A} K^2(\phi)dS_A} \quad \text{- (11.9a)} \qquad K_{RMS(c)} = \sqrt{\frac{1}{\Delta S_C}\int_{\Delta S_C} K^2(\phi)dS_C} \quad \text{- (11.9b)}$$

The RMS approach applied by Mahmoud[11.14], utilising Newman and Raju's SIF solutions, to determine crack growth and shape evolution, produced results that compared well to those obtained experimentally. More widespread usage to complex engineering components is currently acutely limited by the lack of SIF solutions for cracks in such geometries.

A weight function approach given in the preceding section describes a methodology, with which it is envisaged possible, to rapidly generate SIF solutions at all points on a surface crack front. The potential accuracy and versatility offered by a weight function approach can be used in conjunction with an RMS SIF to predict crack growth and shape evolution in cracks situated in complex geomeries and subject to an arbitrary stress field comprising both applied and residual components, and possible material anisotropy. A developed analysis model proposed and described here provides a powerful analysis tool for defect assessment that is either more efficient or more representative than those currently available to assist engineers predictions of remaining component life.

11.4.3 – Controlled Failure Design

The beneficial effects of compressive surface residual stress on the fatigue strength of metallic components, particularly on the increased resistance to fatigue crack initiation are widely appreciated. Acceptance that a fatigue crack will inevitably eventually develop provokes questions concerning the crack growth and shape evolution through the residual stress field. Furthermore, recent experimental evidence by Ngiam and Brennan[11.15] and Knight, Brennan and Dover[11.16] suggests that the judicious use of a non-uniform surface residual stress can be used to control crack propagation along a desired path (e.g. to force the crack to grow deep and short to promote a leak before break failure). It is envisaged that application of a non-uniform residual stress could also be used to promote cracking at known sites leading to the prospect of improved probability of detection (e.g. to promote surface breaking cracks as opposed to subsurface cracks

to produce a component, though weaker in fatigue but more reliably inspected and more responsive to NDT techniques).

A weight function approach developed in this thesis and future work described in this chapter are of significant relevance to the themes described above. Its properties are such that if provides the only viable analytical framework able to effectively incorporate residual stress fields upon SIF solutions, and subsequent fatigue and fracture models. The future work concerning two-dimensional weight functions, their interpolation and a RMS SIF to predict crack shape evolution are of particular consequence to realising an analytical model of the influence of residual stress upon fatigue cracking. The ability to rapidly calculate versatile, high quality SIF solutions, uniquely provided by a weight function approach, is fundamental to realising a fatigue and fracture model of sufficient flexibility that can readily incorporate the numerous variable parameters associated with such an analysis.

11.4.4 – Condition Monitoring and Defect Assessment

Recent years have seen the advent of an increased tendency to monitor structural performance. An ability to determine the response of a structure to influences, such as applied loading or corrosion, provide important information that assist the verification of the design, long term structural integrity assessment and improvement to operating performance of the structure.

There is a growing emergence of organisations dedicated to the integrity management of structures, or assets, offering condition monitoring to increase operational efficiency. Systems monitoring stress and corrosion provide essential data for defect assessment, which currently require expert analysis before meaningful information is passed to operators. Rapid defect assessment of components in service demands broad ranging SIF solutions, which can be readily calculated. The developed weight function methodology described in this thesis is uniquely able to offer the required rapid, versatile and accurate SIF solutions in a manner that is computationally economic. Application of SIF weight function techniques introduces the prospect of integrated systems providing instantaneous and accurate defect assessment providing guidance on remedial action, if required, directly to asset operators.

The prospect of instantaneous defect assessment potentially provide distinct advantages to numerous industries. A notable example is that of the shipping industry, perhaps unique in its position of having yet to embrace the distinct advantages offered by modern fracture mechanics techniques. In addition to economic and operational benefits, the traditionally poor safety record of vessels such as bulk carriers, prone to both ageing and fatigue, may be greatly enhanced. A recent International Maritime Organisation (IMO) requirement to monitor ship hull stress could be

exploited to implement a defect tolerant design methodology. Utilising measured hull stresses and relating these to local stress in the vicinity of a fatigue prone detail would potentially allow in-service monitoring of cracks. Coupled with an appropriate inspection scheme cracks can be managed to ensure that a state of integrity is maintained while the structure remains in service. Crack growth predictions based upon a defect tolerant approach to crack management would greatly assist a ship operator's decision to repair and scheduling of maintenance.

11.5 – Closing Remarks

This thesis contains a description of the development of a novel, weight function interpolation scheme that can be utilised to calculate weight functions and new SIF solutions for cracks in complex geometries. The four, key facets of the technique are rapidity, accuracy, reliability and versatility at which new solutions can be formulated from relatively small libraries of constituent and base geometry solutions. The body of work contained in this thesis has successfully validated and demonstrated the technique applied to edge cracked geometries. It is the author's opinion that great scope exists for further development of the interpolation scheme to broaden applicability to numerous geometry and crack types.

The manner in which new SIF solutions can be calculated using the technique leads to exciting prospect for the realisation of several advanced defect assessment methodologies, which are currently hindered by a lack of required SIF solutions. A weight function methodology is uniquely positioned to make feasible the considerable SIF data required for their implementation. The work contained in this thesis represents a significant advancement towards realising these aims and leads to exciting prospects for future design of defect tolerant components and defect assessment of cracks in structures and geometries of complex shape and/or subject to non-simple stress states.

11.6 – References

[11.1] Brennan, F. P. Teh, L. S., Determination of Crack-Tip Stress Intensity Factors in Complex Geometries by the Composition of Constituent Weight Function Solutions, *Fatigue Fract Engng Mater Struct*, 2003

[11.2] Teh, L.S., *Library of Geometric Influences for Stress Intensity Factor Weight Functions*, Ph.D. Thesis, University College London, 2002

[11.3] Newman Jr, J.C., An Improved Method of Collocation for the Stress Analysis of Cracked Plates with Various Shaped Boundaries, NASA TN D-6376(1971), pp.1-45

[11.4] Nisitani, H. and Isida, M., Simple Procedure for Calculating K_I of a Notch with a Crack of Arbitrary Size and Its Application to Non-propagating Fatigue Crack, *Proc. Joint JSME-SESA Conf. On Experimental Mechanics (1982)*, Part 1, pp.150-155

[11.5] Terada, H. and Isida, M., Analysis of Stress Intensity Factors for Eccentric Cracks, NAL, Technical Report, TR-436, (1975)

[11.6] Fett, T. and Munz, D., *Stress Intensity Factors and Weight Functions*, Computational Mechanics Publications, Southampton, UK, 1997. ISBN: 1-85312-497-4

[11.7] Rice, J.R., Weight Function Theory for Three-Dimensional Elastic Crack Analysis. *Fracture Mechanics – Perspectives and Directions.* ASTM STP 1020, 1987, pp. 29 – 57.

[11.8] Newman, J.C. and Raju, I.S., An Empirical Stress Intensity Factor Equation for the Surface Crack, *Engineering Fracture Mechanics* Vol. 15, No.1-2, pp.185-192, 1981

[11.9] D. Bowness and M.M.K. Lee, Prediction of Weld Toe Magnification Factors for Semi-Elliptical Cracks in T-Butt Joints, *International Journal of Fatigue* 22 (2002) 369 – 387

[11.10] Lin, X.B. and Smith, R.A., Finite Element Modelling of Fatigue Crack Growth of Surface Cracked Plates. Part I: The Numerical Technique. *Engineering Fracture Mechanics*, 63, 1999, pp. 503 – 522.

[11.11] Lin, X.B. and Smith, R.A., Finite Element Modelling of Fatigue Crack Growth of Surface Cracked Plates. Part II: Crack Shape Change. *Engineering Fracture Mechanics*, 63, 1999, pp. 523 – 540.

[11.12] Lin, X.B. and Smith, R.A., Finite Element Modelling of Fatigue Crack Growth of Surface Cracked Plates. Part III: Stress Intensity Factor and Fatigue Crack Growth Life. *Engineering Fracture Mechanics*, 63, 1999, pp. 503 – 522.

[11.13] Cruse, T.A. and Besuner, P.M., Residual Life Prediction for Surface Cracks in Complex Structural Details, *Journal of Aircraft*, Vol. 12, No. 4, pp 369 - 375, April 1975

[11.14] Mahmoud, M.A., Surface Fatigue Crcak Growth Under Combined Tension and Bending Loading, *Engineering Fracture Mechanics*, Vol.36, No. 3, pp 389 – 395, 1990

[11.15] Ngiam, S.S and Brennan, F. P., Experimental Investigation of Crack Shape Evolution in Cold Rolled Components, International Conference on Fatigue Crack Paths, Parma, 18-20 September 2003.

[11.16] Knight, M. J., Brennan, F. P. and Dover, W. D., Controlled Failure Design of Drillstring Threaded Connections, *Fatigue Fract Engng Mater Struct* 26, 1081–1090, 2003.

11.7 – Figures

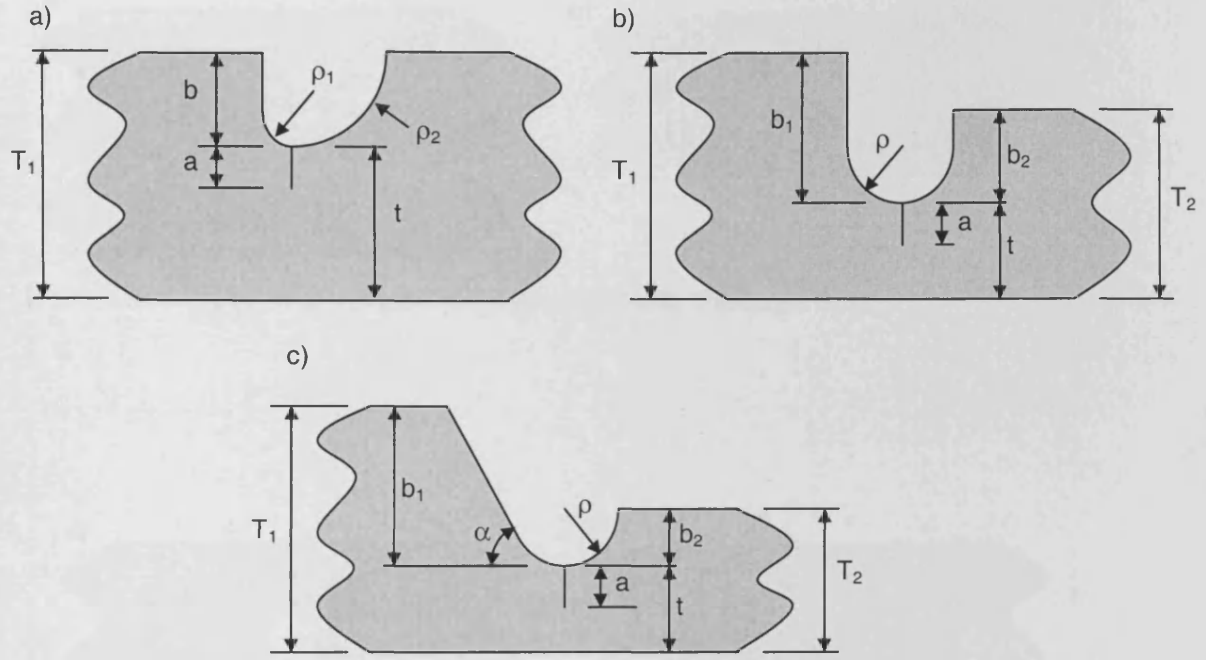

Fig. 11.1 – Compound Notched Geometries Containing Edge Cracks

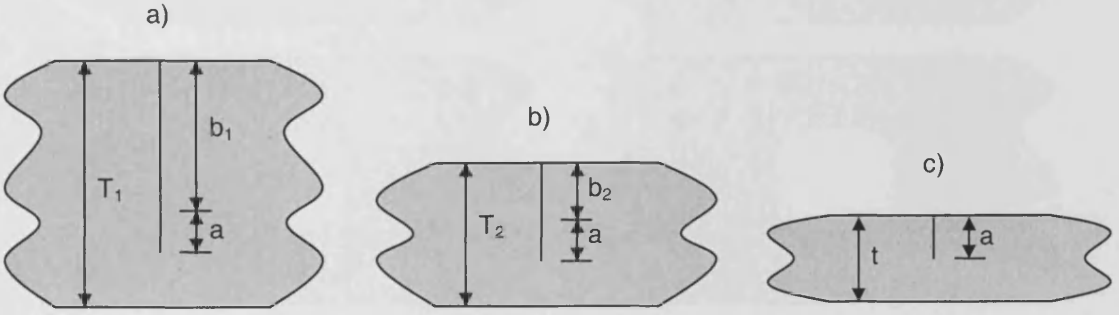

Fig. 11.2 – Constituent Geometries for Compound Notched in Fig. 11.1

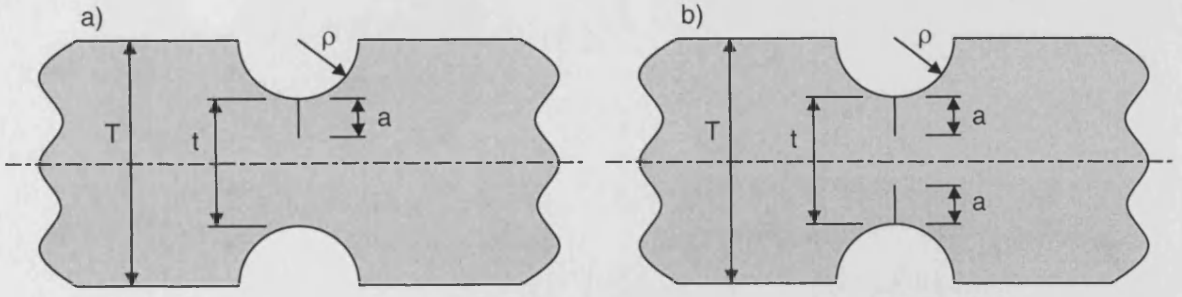

Fig. 11.3 – Edge Cracks in Components Notched about a Longitudinal Axis

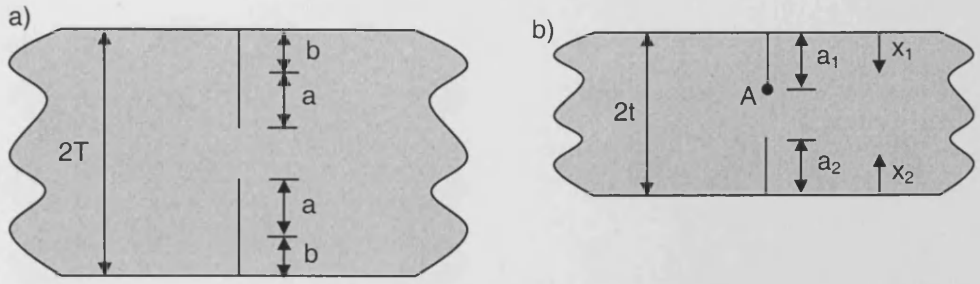

Fig. 11.4 – Double Edge Cracked Finite Thickness Strip

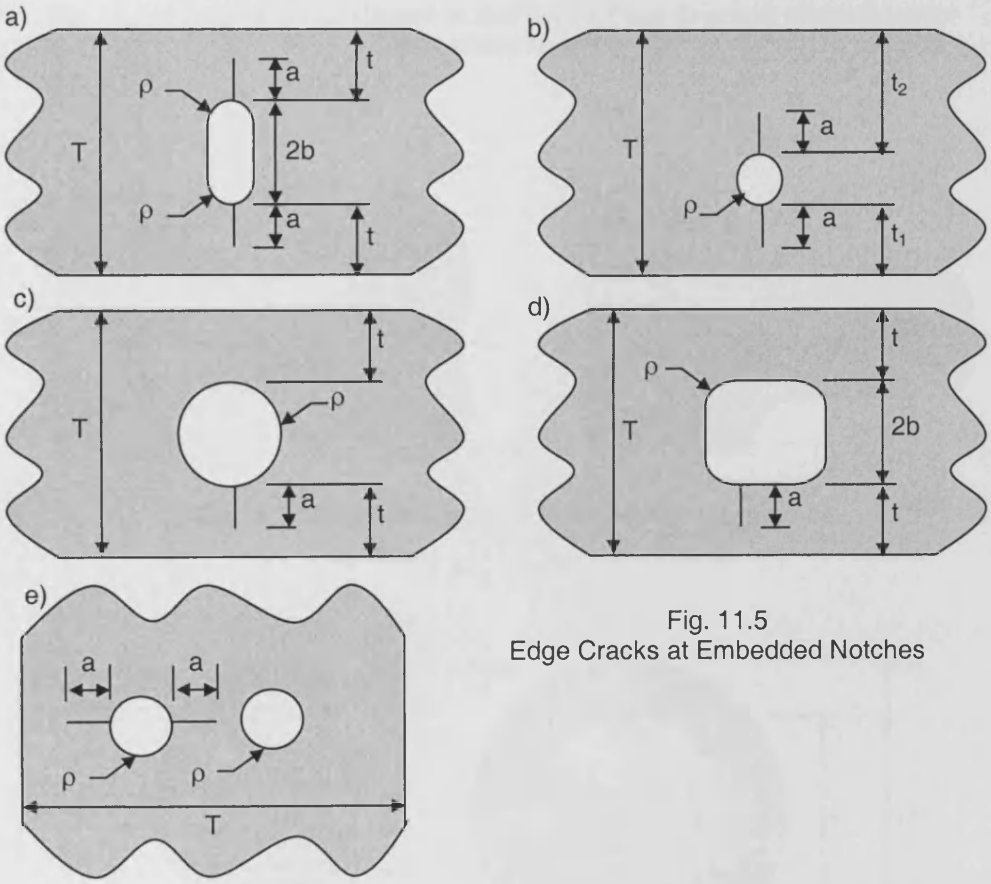

Fig. 11.5
Edge Cracks at Embedded Notches

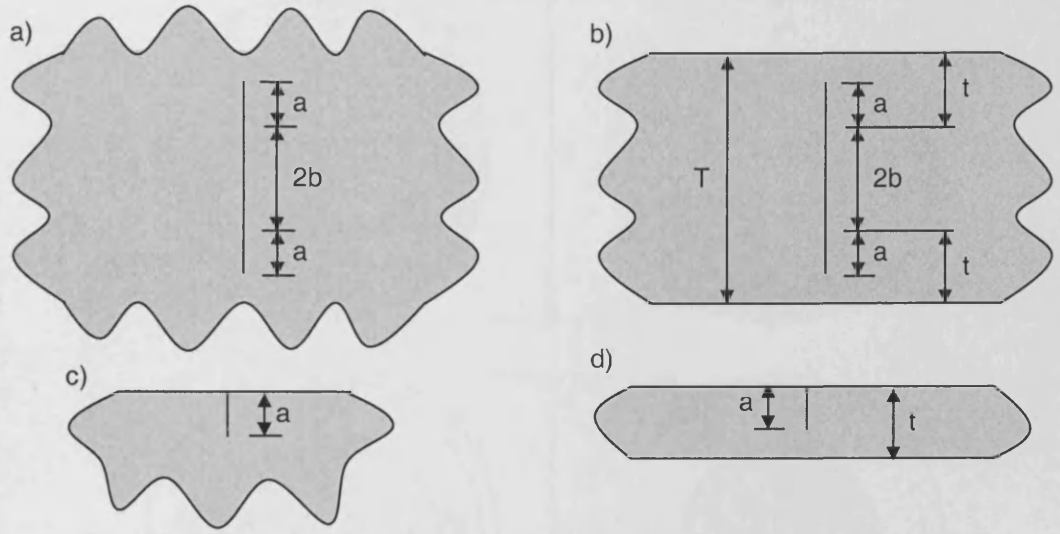

Fig. 11.6 – Cracks in Constituent (a and c) and Base (b and d) Geometries for Embedded Notches

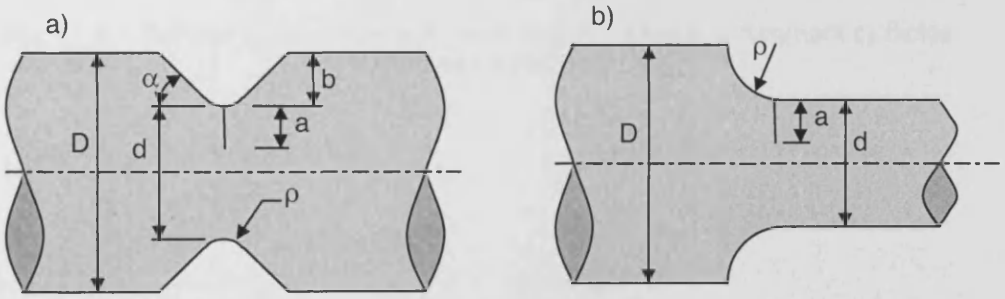

Fig.11.7 – Surface Cracks in Notched Rod Geometries

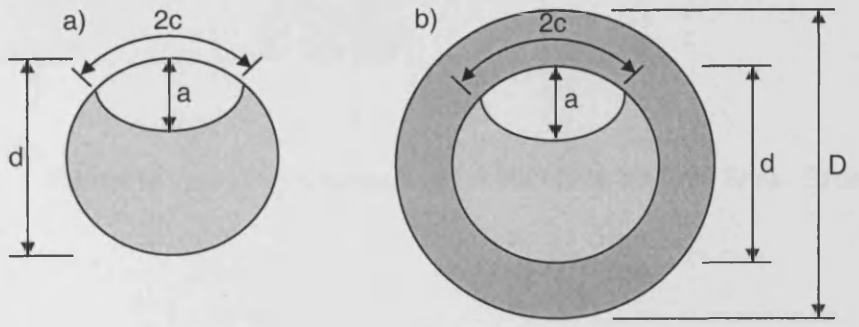

Fig. 11.8 – Surface Cracks in Constituent Rod Geometries a) Unstiffened b) Stiffened

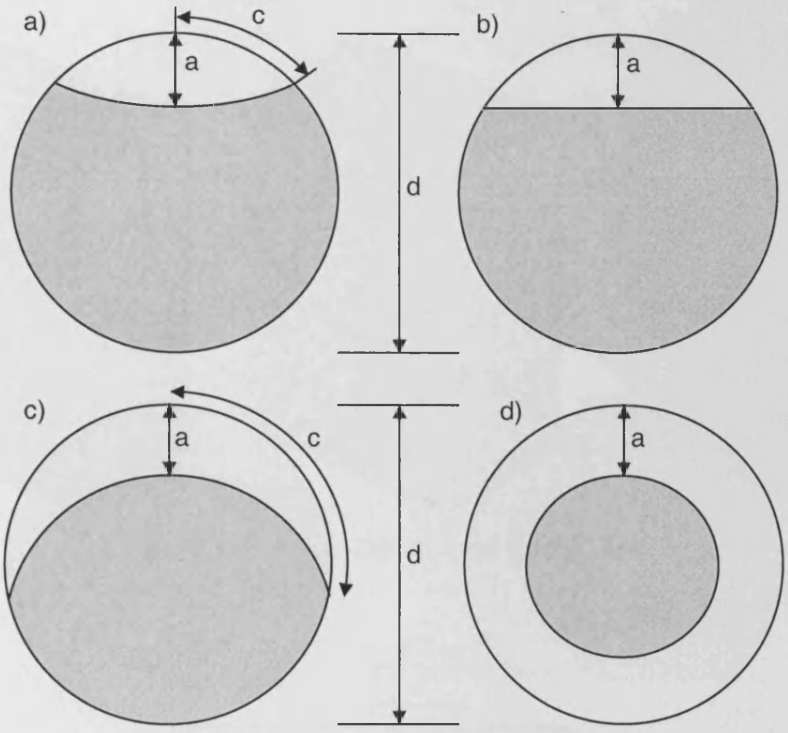

Fig. 11.9 – Surface Crack Shapes in Rods a) Semi-Ellipse b) Segment c) Sickle d) Complete Circumference

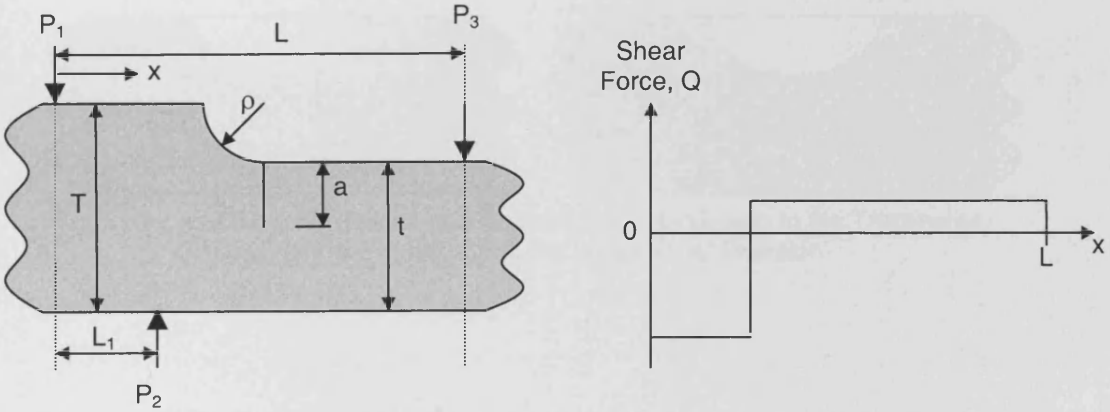

Fig. 11.10 - Loading Arrangement for Non-Zero Nominal Shear Stress

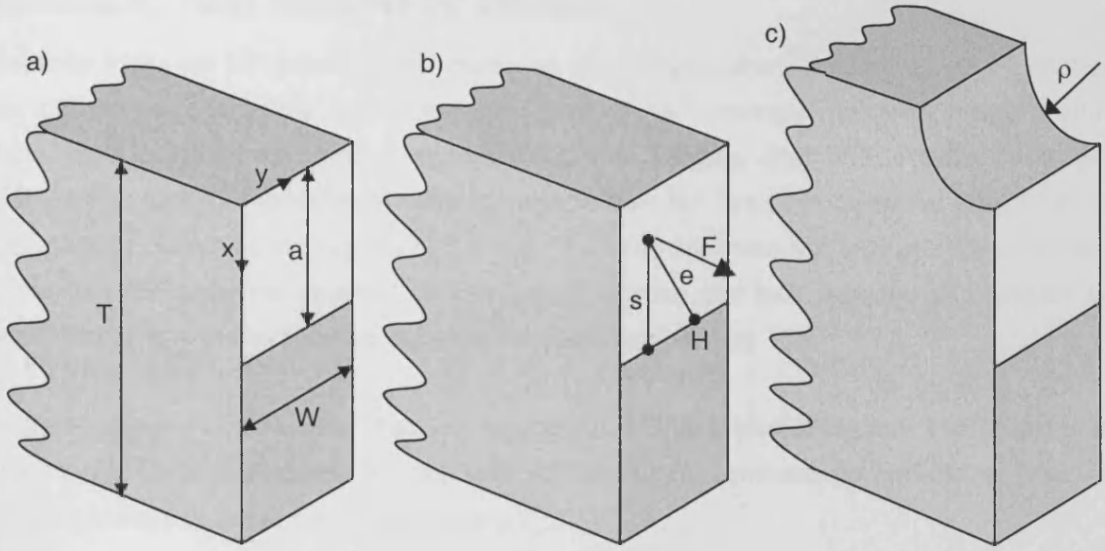

Fig. 11.11 – A Two-Dimensional Edge Crack

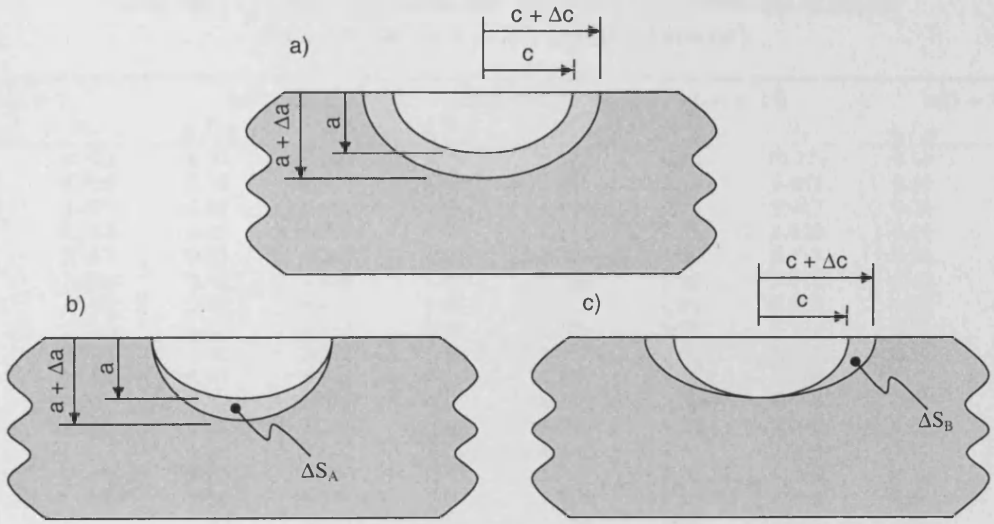

Fig. 11.12 – a) General Growth of a Surface Crack, b) Growth in the Transverse Direction and c) Growth in the Longitudinal Direction

Appendix A – Finite Thickness SIF Solutions

The finite thickness SIF solutions and crack line stress distributions, determined via FE analysis, are too numerous to be included in the main body of this document. The finite thickness stress distributions obtained for uniform tension (UT), pure bending (PB) and in some cases pure tension (PT) loading modes were used to validate new SIF solutions using the weight function methodology presented in chapters 5, 6 and 8. The finite thickness SIF solutions were compared to the new SIF solutions obtained via the weight function and thus provides an important and useful tool for the verification and validation of solutions obtained.

In the interests of conciseness they are reproduced in this separate section. The solutions are divided into three categories A1, A2 and A3 containing solutions for symmetric, step and Intrusion/protrusion notch types respectively.

A1 – Edge Cracks at Symmetric Notches

Tab. A1.1 – Finite Thickness SIF Solutions for Symmetric Notches
(α = 45°, b/T = 0.2727, Uniform Tension)

b/ρ = 1		b/ρ = 3		b/ρ = 6		b/ρ = 10		b/ρ = 15	
a / ρ	Y_I	a / ρ	Y_I	a / ρ	Y_I	a / ρ	Y_I	a / ρ	Y_I
0.05	4.703	0.10	6.344	0.10	8.502	0.10	10.379	0.10	12.373
0.075	4.526	0.15	5.923	0.15	7.927	0.15	9.658	0.15	11.509
0.10	4.377	0.20	5.581	0.20	7.446	0.20	9.057	0.20	10.786
0.15	4.143	0.25	5.299	0.25	7.041	0.25	8.550	0.25	10.175
0.20	3.977	0.30	5.064	0.30	6.695	0.30	8.117	0.30	9.652
0.25	3.859	0.40	4.699	0.40	6.138	0.40	7.418	0.40	8.805
0.30	3.780	0.50	4.434	0.50	5.712	0.50	6.880	0.50	8.149
0.40	3.706	0.70	4.088	0.70	5.106	0.70	6.107	0.70	7.201
0.50	3.716	0.90	3.892	0.90	4.657	0.90	5.580	0.90	6.545
0.70	3.925	1.10	3.788	1.10	4.389	1.10	5.198	1.10	6.065
0.90	4.351	1.30	3.743	1.30	4.196	1.30	4.910	1.30	5.696
1.10	5.015	1.60	3.757	1.60	3.998	1.60	4.590	1.60	5.279
-	-	1.90	3.842	1.90	3.872	1.90	4.360	1.90	4.969
-	-	2.20	3.988	2.20	3.795	2.20	4.189	2.20	4.729
-	-	2.50	4.188	2.50	3.754	2.50	4.060	2.50	4.540
-	-	3.00	4.651	3.00	3.746	3.00	3.911	3.00	4.302
-	-	3.50	5.302	3.50	3.793	3.50	3.818	3.50	4.130
-	-	-	-	4.00	3.885	4.00	3.766	4.00	4.005
-	-	-	-	5.00	4.188	5.00	3.746	5.00	3.845
-	-	-	-	6.00	4.651	6.00	3.808	6.00	3.766
-	-	-	-	7.00	5.303	7.00	3.934	7.00	3.742
-	-	-	-	8.00	6.205	8.00	4.116	8.00	3.759

Tab. A1.2 – Finite Thickness SIF Solutions for Symmetric Notches
(α = 45°, b/T = 0.2727, Pure Bending)

b/ρ = 1		b/ρ = 3		b/ρ = 6		b/ρ = 10		b/ρ = 15	
a / ρ	Y_I	a / ρ	Y_I	a / ρ	Y_I	a / ρ	Y_I	a / ρ	Y_I
0.01	3.314	0.05	4.578	0.10	5.631	0.10	7.023	0.10	8.397
0.025	3.216	0.075	4.392	0.15	5.243	0.15	6.535	0.15	7.812
0.05	3.066	0.10	4.225	0.20	4.919	0.20	6.127	0.20	7.321
0.075	2.941	0.15	3.938	0.25	4.647	0.25	5.782	0.25	6.906
0.10	2.832	0.20	3.703	0.30	4.414	0.30	5.487	0.30	6.550
0.15	2.656	0.25	3.507	0.40	4.040	0.40	5.009	0.40	5.971
0.20	2.523	0.30	3.341	0.50	3.752	0.50	4.639	0.50	5.522
0.25	2.420	0.40	3.080	0.70	3.340	0.70	4.102	0.70	4.869
0.30	2.340	0.50	2.883	0.90	3.059	0.90	3.731	0.90	4.414
0.40	2.233	0.70	2.612	1.10	2.857	1.10	3.459	1.10	4.078
0.50	2.175	0.90	2.439	1.30	2.705	1.30	3.250	1.30	3.818
0.70	2.163	1.10	2.325	1.60	2.538	1.60	3.013	1.60	3.520
0.90	2.256	1.30	2.251	1.90	2.420	1.90	2.837	1.90	3.296
1.10	2.450	1.60	2.188	2.20	2.335	2.20	2.701	2.20	3.119
-	-	1.90	2.168	2.50	2.273	2.50	2.594	2.50	2.977
-	-	2.20	2.180	3.00	2.207	3.00	2.459	3.00	2.793
-	-	3.00	2.342	3.50	2.175	3.50	2.363	3.50	2.654
-	-	3.50	2.541	4.00	2.170	4.00	2.293	4.00	2.547
-	-	-	-	5.00	2.220	5.00	2.208	5.00	2.393
-	-	-	-	6.00	2.342	6.00	2.174	6.00	2.294
-	-	-	-	7.00	2.541	7.00	2.174	7.00	2.231
-	-	-	-	8.00	2.836	8.00	2.204	8.00	2.193

Tab. A1.3 – Finite Thickness SIF Solutions for Symmetric Notches
(b/ρ = 6, b/T = 0.2727, Uniform Tension)

α = 15°		α = 30°		α = 45°		α = 60°		α = 90°	
a / ρ	Y_I	a / ρ	Y_I	a / ρ	Y_I	a / ρ	Y_I	a / ρ	Y_I
0.1	6.209	0.10	7.807	0.10	8.502	0.10	8.491	0.10	8.502
0.15	5.823	0.15	7.269	0.15	7.927	0.15	7.912	0.15	7.927
0.2	5.525	0.20	6.832	0.20	7.446	0.20	7.430	0.20	7.446
0.25	5.289	0.25	6.469	0.25	7.041	0.25	7.025	0.25	7.041
0.32	5.026	0.30	6.166	0.30	6.695	0.30	6.679	0.30	6.695
0.4	4.799	0.40	5.688	0.40	6.138	0.40	6.124	0.40	6.138
0.5	4.579	0.55	5.182	0.50	5.712	0.50	5.699	0.50	5.712
0.7	4.274	0.70	4.830	0.70	5.106	0.70	5.097	0.70	5.106
0.9	4.072	0.90	4.501	0.90	4.657	0.90	4.697	0.90	4.704
1.1	3.930	1.10	4.272	1.10	4.389	1.10	4.418	1.10	4.422
1.3	3.828	1.30	4.106	1.30	4.196	1.30	4.217	1.30	4.219
1.6	3.725	1.60	3.935	1.60	3.998	1.60	4.010	1.60	4.011
1.9	3.665	1.90	3.827	1.90	3.872	1.90	3.880	1.90	3.880
2.2	3.635	2.20	3.763	2.20	3.795	2.20	3.800	2.20	3.800
2.5	3.628	2.50	3.731	2.50	3.754	2.50	3.758	2.50	3.758
3	3.659	3.00	3.731	3.00	3.746	3.00	3.747	3.00	3.747
3.5	3.732	3.50	3.784	3.50	3.793	3.50	3.794	3.50	3.794
4	3.842	4.00	3.880	4.00	3.885	4.00	3.886	4.00	3.886
5	4.167	-	-	5.00	4.188	5.00	4.190	5.00	4.189
6	4.640	-	-	6.00	4.651	6.00	4.652	6.00	4.652
7	5.298	-	-	7.00	5.303	7.00	5.303	7.00	5.303
8	6.204	-	-	8.00	6.205	8.00	6.207	8.00	6.207

Tab. A1.4 – Finite Thickness SIF Solutions for Symmetric Notches
($b/\rho = 6$, $b/T = 0.2727$, Pure Bending)

$\alpha = 15°$		$\alpha = 30°$		$\alpha = 45°$		$\alpha = 60°$		$\alpha = 90°$	
a/ρ	Y_I	a/ρ	Y_I	a/ρ	Y_I	a/ρ	Y_I	a/ρ	Y_I
0.1	4.051	0.10	5.191	0.10	5.631	0.10	5.741	0.10	5.757
0.15	3.796	0.15	4.830	0.15	5.243	0.15	5.349	0.15	5.366
0.2	3.597	0.20	4.535	0.20	4.919	0.20	5.021	0.20	5.039
0.25	3.439	0.25	4.291	0.25	4.647	0.25	4.744	0.25	4.762
0.35	3.200	0.30	4.085	0.30	4.414	0.30	4.507	0.30	4.524
0.4	3.107	0.40	3.758	0.40	4.040	0.40	4.122	0.40	4.138
0.5	2.956	0.50	3.574	0.50	3.752	0.50	3.824	0.50	3.839
0.7	2.740	0.70	3.159	0.70	3.340	0.70	3.394	0.70	3.406
0.9	2.592	0.90	2.922	0.90	3.059	0.90	3.100	0.90	3.109
1.1	2.482	1.10	2.750	1.10	2.857	1.10	2.888	1.10	2.895
1.3	2.399	1.30	2.620	1.30	2.705	1.30	2.728	1.30	2.734
1.6	2.305	1.60	2.476	1.60	2.538	1.60	2.554	1.60	2.558
1.9	2.239	1.90	2.374	1.90	2.420	1.90	2.432	1.90	2.434
2.2	2.191	2.20	2.300	2.20	2.335	2.20	2.343	2.20	2.345
2.5	2.157	2.50	2.246	2.50	2.273	2.50	2.279	2.50	2.280
3	2.125	3.00	2.190	3.00	2.207	3.00	2.211	3.00	2.212
3.5	2.117	3.50	2.164	3.50	2.175	3.50	2.178	3.50	2.179
4	2.127	4.00	2.162	4.00	2.170	4.00	2.172	4.00	2.172
5	2.197	5.00	2.216	5.00	2.220	5.00	2.221	-	-
6	2.330	-	-	6.00	2.342	6.00	2.343	-	-
7	2.536	-	-	7.00	2.541	7.00	2.541	-	-
8	2.835	-	-	8.00	2.836	8.00	2.836	-	-

Tab. A1.5 – Finite Thickness SIF Solutions for Symmetric Notches
($b/\rho = 6$, $\alpha = 45°$, Uniform Tension)

$b/T = 0.0625$		$b/T = 0.1875$		$b/T = 0.2727$		$b/T = 0.3125$		$b/T = 0.4375$	
a/ρ	Y_I	a/ρ	Y_I	a/ρ	Y_I	a/ρ	Y_I	a/ρ	Y_I
0.10	6.033	0.10	7.090	0.10	8.502	0.10	9.157	0.10	12.849
0.15	5.606	0.15	6.596	0.15	7.927	0.15	8.532	0.15	11.998
0.20	5.249	0.20	6.184	0.20	7.446	0.20	8.017	0.20	11.304
0.25	4.947	0.25	5.838	0.25	7.041	0.25	7.585	0.25	10.730
0.30	4.688	0.30	5.542	0.30	6.695	0.30	7.220	0.30	10.250
0.40	4.270	0.40	5.067	0.40	6.138	0.40	6.638	0.40	9.499
0.50	3.947	0.50	4.702	0.50	5.712	0.50	6.198	0.50	8.947
0.70	3.479	0.70	4.181	0.70	5.106	0.70	5.584	0.70	8.214
0.90	3.157	0.90	3.828	0.90	4.657	0.90	5.183	0.90	7.779
1.10	2.921	1.10	3.574	1.10	4.389	1.10	4.910	1.10	7.528
1.30	2.740	1.30	3.385	1.30	4.196	1.30	4.719	1.30	7.401
1.60	2.535	1.60	3.178	1.60	3.998	1.60	4.533	-	-
1.90	2.382	1.90	3.031	1.90	3.872	1.90	4.429	-	-
2.20	2.263	2.20	2.925	2.20	3.795	2.20	4.380	-	-
2.50	2.169	2.50	2.848	2.50	3.754	2.50	4.375	-	-
3.00	2.048	3.00	2.763	3.00	3.746	3.00	4.438	-	-
3.50	1.958	3.50	2.717	3.50	3.793	3.50	4.575	-	-
4.00	1.889	4.00	2.698	4.00	3.885	4.00	4.779	-	-
5.00	1.793	5.00	2.720	5.00	4.188	4.50	5.049	-	-
6.00	1.731	6.00	2.799	6.00	4.651	5.00	5.388	-	-
7.00	1.690	7.00	2.925	7.00	5.303	-	-	-	-
8.00	1.664	8.00	3.095	8.00	6.205	-	-	-	-
10.00	1.639	9.00	3.309	-	-	-	-	-	-
12.00	1.640	10.00	3.572	-	-	-	-	-	-
14.00	1.658	-	-	-	-	-	-	-	-
16.00	1.688	-	-	-	-	-	-	-	-
20.00	1.780	-	-	-	-	-	-	-	-
24.00	1.907	-	-	-	-	-	-	-	-

Tab. A1.6 – Finite Thickness SIF Solutions for Symmetric Notches
($b/\rho = 6$, $\alpha = 45°$, Pure Bending)

b/T = 0.0625		b/T = 0.1875		b/T = 0.2727		b/T = 0.3125		b/T = 0.4375	
a / ρ	Y_I	a / ρ	Y_I	a / ρ	Y_I	a / ρ	Y_I	a / ρ	Y_I
0.10	5.520	0.10	5.394	0.10	5.631	0.10	5.834	0.10	6.981
0.15	5.129	0.15	5.017	0.15	5.243	0.15	5.434	0.15	6.513
0.20	4.802	0.20	4.702	0.20	4.919	0.20	5.102	0.20	6.129
0.25	4.524	0.25	4.436	0.25	4.647	0.25	4.823	0.25	5.809
0.30	4.287	0.30	4.209	0.30	4.414	0.30	4.585	0.30	5.539
0.40	3.903	0.40	3.841	0.40	4.040	0.40	4.203	0.40	5.112
0.50	3.605	0.50	3.557	0.50	3.752	0.50	3.910	0.50	4.790
0.70	3.173	0.70	3.147	0.70	3.340	0.70	3.493	0.70	4.346
0.90	2.873	0.90	2.864	0.90	3.059	0.90	3.211	-	-
1.10	2.653	1.10	2.657	1.10	2.857	1.10	3.011	-	-
1.30	2.483	1.30	2.499	1.30	2.705	1.30	2.862	-	-
1.60	2.289	1.60	2.322	1.60	2.538	1.60	2.703	-	-
1.90	2.100	1.90	2.190	1.90	2.420	1.90	2.595	-	-
2.20	2.029	2.20	2.090	2.20	2.335	2.20	2.522	-	-
2.50	1.937	2.50	2.011	2.50	2.273	2.50	2.474	-	-
3.00	1.817	3.00	1.914	3.00	2.207	3.00	2.436	-	-
3.50	1.726	3.50	1.845	3.50	2.175	3.50	2.438	-	-
4.00	1.654	4.00	1.797	4.00	2.170	4.00	2.473	-	-
5.00	1.549	5.00	1.741	5.00	2.220	4.50	2.538	-	-
6.00	1.475	6.00	1.723	6.00	2.342	5.00	2.632	-	-
7.00	1.421	7.00	1.733	7.00	2.541	-	-	-	-
8.00	1.379	8.00	1.765	8.00	2.836	-	-	-	-
9.00	1.347	9.00	1.819	-	-	-	-	-	-
10.00	1.322	10.00	1.894	-	-	-	-	-	-
12.00	1.287	-	-	-	-	-	-	-	-
16.00	1.254	-	-	-	-	-	-	-	-
20.00	1.252	-	-	-	-	-	-	-	-
24.00	1.271	-	-	-	-	-	-	-	-

A2 – Edge Cracks at Step Notches

Tab. A2.1 – Finite Thickness SIF Solutions for Step Notches
($\alpha = 45°$, $b/T = 0.2727$, Pure Tension)

b/ρ = 1		b/ρ = 3		b/ρ = 6		b/ρ = 10		b/ρ = 15	
a / ρ	Y_I	a / ρ	Y_I	a / ρ	Y_I	a / ρ	Y_I	a / ρ	Y_I
0.025	1.385	0.025	1.706	0.025	2.013	0.025	2.296	0.025	2.567
0.050	1.357	0.050	1.667	0.050	1.969	0.050	2.245	0.050	2.510
0.075	1.335	0.075	1.633	0.075	1.926	0.075	2.198	0.075	2.458
0.100	1.317	0.100	1.601	0.100	1.886	0.100	2.153	0.100	2.408
0.150	1.292	0.150	1.544	0.150	1.814	0.150	2.070	0.150	2.315
0.200	1.280	0.200	1.497	0.200	1.752	0.200	1.997	0.200	2.232
0.250	1.278	0.250	1.458	0.250	1.700	0.250	1.932	0.250	2.158
0.300	1.284	0.300	1.425	0.300	1.650	0.300	1.875	0.300	2.093
0.400	1.318	0.400	1.375	0.400	1.572	0.400	1.779	0.400	1.982
0.500	1.375	0.500	1.341	0.500	1.512	0.500	1.702	0.500	1.892
0.700	1.552	0.700	1.305	0.700	1.426	0.700	1.588	0.700	1.755
0.900	1.814	0.900	1.298	0.900	1.372	0.900	1.508	0.900	1.657
1.000	1.984	1.100	1.311	1.100	1.337	1.100	1.451	1.100	1.584
1.100	2.186	1.300	1.338	1.300	1.316	1.300	1.408	1.300	1.527
1.200	2.426	1.600	1.400	1.600	1.301	1.600	1.363	1.600	1.463
-	-	1.900	1.484	1.900	1.301	1.900	1.334	1.900	1.417
-	-	2.200	1.589	2.200	1.311	2.200	1.315	2.200	1.382
-	-	2.500	1.716	2.500	1.330	2.500	1.304	2.500	1.356
-	-	3.000	1.984	3.000	1.377	3.000	1.299	3.000	1.327
-	-	3.300	2.186	3.500	1.439	3.500	1.307	3.500	1.309
-	-	-	-	4.000	1.517	4.000	1.323	4.000	1.301
-	-	-	-	5.000	1.716	5.000	1.376	5.000	1.303
-	-	-	-	6.000	1.985	6.000	1.453	6.000	1.323
-	-	-	-	7.000	2.342	7.000	1.551	7.000	1.356
-	-	-	-	8.000	2.826	8.000	1.671	8.000	1.400

Tab. A2.2 – Finite Thickness SIF Solutions for Step Notches
(α = 45°, b/T = 0.2727, Pure Bending)

b/ρ = 1		b/ρ = 3		b/ρ = 6		b/ρ = 10		b/ρ = 15	
a / ρ	Y_I	a / ρ	Y_I	a / ρ	Y_I	a / ρ	Y_I	a / ρ	Y_I
0.025	1.398	0.025	1.782	0.025	2.139	0.025	2.466	0.025	2.790
0.050	1.358	0.050	1.738	0.050	2.090	0.050	2.417	0.050	2.730
0.075	1.324	0.075	1.699	0.075	2.045	0.075	2.366	0.075	2.671
0.100	1.293	0.100	1.662	0.100	2.002	0.100	2.317	0.100	2.616
0.150	1.241	0.150	1.595	0.150	1.923	0.150	2.227	0.150	2.513
0.200	1.201	0.200	1.537	0.200	1.852	0.200	2.146	0.200	2.421
0.250	1.170	0.250	1.486	0.250	1.790	0.250	2.073	0.250	2.339
0.300	1.146	0.300	1.442	0.300	1.735	0.300	2.008	0.300	2.266
0.400	1.116	0.400	1.369	0.400	1.641	0.400	1.898	0.400	2.140
0.500	1.103	0.500	1.312	0.500	1.565	0.500	1.808	0.500	2.037
0.700	1.119	0.700	1.230	0.700	1.450	0.700	1.669	0.700	1.877
0.900	1.180	0.900	1.178	0.900	1.368	0.900	1.567	0.900	1.759
1.000	1.228	1.100	1.144	1.100	1.307	1.100	1.489	1.100	1.668
1.100	1.289	1.300	1.123	1.300	1.261	1.300	1.428	1.300	1.595
-	-	1.600	1.110	1.600	1.209	1.600	1.357	1.600	1.510
-	-	1.900	1.113	1.900	1.173	1.900	1.303	1.900	1.443
-	-	2.200	1.129	2.200	1.148	2.200	1.261	2.200	1.390
-	-	2.500	1.156	2.500	1.130	2.500	1.227	2.500	1.347
-	-	3.000	1.229	3.000	1.114	3.000	1.186	3.000	1.290
-	-	3.300	1.290	3.500	1.110	3.500	1.156	3.500	1.247
-	-	-	-	4.000	1.117	4.000	1.136	4.000	1.213
-	-	-	-	5.000	1.157	5.000	1.114	5.000	1.165
-	-	-	-	6.000	1.229	6.000	1.111	6.000	1.090
-	-	-	-	7.000	1.340	7.000	1.123	7.000	1.119
-	-	-	-	8.000	1.499	8.000	1.146	8.000	1.112

Tab. A2.3 – Finite Thickness SIF Solutions for Step Notches
(b/ρ = 6, b/T = 0.2727, Pure Tension)

α = 15°		α = 30°		α = 45°		α = 90°	
a / ρ	Y_I	a / ρ	Y_I	a / ρ	Y_I	a / ρ	Y_I
0.025	1.692	0.025	1.935	0.025	2.013	0.025	2.027
0.05	1.651	0.05	1.890	0.05	1.969	0.05	1.981
0.075	1.616	0.075	1.849	0.075	1.926	0.075	1.940
0.1	1.585	0.1	1.811	0.1	1.886	0.1	1.901
0.15	1.532	0.15	1.743	0.15	1.814	0.15	1.829
0.2	1.490	0.2	1.685	0.2	1.752	0.2	1.766
0.25	1.456	0.25	1.635	0.25	1.700	0.25	1.712
0.4	1.385	0.3	1.592	0.3	1.650	0.3	1.663
0.5	1.353	0.4	1.523	0.4	1.572	0.4	1.584
0.7	1.311	0.6	1.429	0.5	1.512	0.5	1.521
0.9	1.286	0.7	1.397	0.7	1.426	0.7	1.432
1.1	1.272	0.9	1.351	0.9	1.372	0.9	1.375
1.3	1.265	1.1	1.323	1.1	1.337	1.1	1.338
1.6	1.266	1.3	1.306	1.3	1.316	1.3	1.316
1.9	1.276	1.6	1.295	1.6	1.301	1.6	1.300
2.2	1.293	1.9	1.297	1.9	1.301	1.9	1.300
2.5	1.317	2.2	1.309	2.2	1.311	2.2	1.310
3	1.369	2.5	1.329	2.5	1.330	2.5	1.329
3.5	1.434	3	1.376	3	1.377	3	1.376
4	1.513	3.5	1.439	3.5	1.439	3.5	1.439
5	1.715	4	1.517	4	1.517	4	1.516
6	1.984	5	1.716	5	1.716	5	1.716
-	-	-	-	6	1.985	6	1.985
-	-	-	-	7	2.342	7	2.342
-	-	-	-	8	2.826	8	2.825

Tab. A2.4 – Finite Thickness SIF Solutions for Step Notches
(b/ρ = 6, b/T = 0.2727, Pure Bending)

α = 15°		α = 30°		α = 45°		α = 60°		α = 90°	
a / ρ	Y_I	a / ρ	Y_I	a / ρ	Y_I	a / ρ	Y_I	a / ρ	Y_I
0.025	1.713	0.025	2.018	0.025	2.139	0.025	2.172	0.025	2.177
0.05	1.669	0.05	1.969	0.05	2.090	0.05	2.123	0.05	2.128
0.075	1.632	0.075	1.925	0.075	2.045	0.075	2.078	0.075	2.084
0.1	1.598	0.1	1.883	0.1	2.002	0.1	2.035	0.1	2.041
0.15	1.540	0.15	1.808	0.15	1.923	0.15	1.956	0.15	1.962
0.2	1.494	0.2	1.742	0.2	1.852	0.2	1.885	0.2	1.892
0.25	1.455	0.25	1.686	0.25	1.790	0.25	1.822	0.25	1.829
0.4	1.369	0.3	1.636	0.3	1.735	0.3	1.765	0.3	1.772
0.5	1.328	0.4	1.554	0.4	1.641	0.4	1.669	0.4	1.675
0.7	1.267	0.6	1.436	0.5	1.565	0.5	1.590	0.5	1.596
0.9	1.224	0.7	1.392	0.7	1.450	0.7	1.470	0.7	1.475
1.1	1.191	0.9	1.323	0.9	1.368	0.9	1.383	0.9	1.387
1.3	1.165	1.1	1.272	1.1	1.307	1.1	1.319	1.1	1.322
1.6	1.137	1.3	1.232	1.3	1.261	1.3	1.270	1.3	1.272
1.9	1.117	1.6	1.189	1.6	1.209	1.6	1.216	1.6	1.217
2.2	1.103	1.9	1.158	1.9	1.173	1.9	1.177	1.9	1.179
2.5	1.094	2.2	1.136	2.2	1.148	2.2	1.151	2.2	1.151
3	1.089	2.5	1.121	2.5	1.130	2.5	1.132	2.5	1.133
3.5	1.093	3	1.108	3	1.114	3	1.115	3	1.116
4	1.104	3.5	1.107	3.5	1.110	3.5	1.111	3.5	1.112
5	1.150	4	1.115	4	1.117	4	1.118	4	1.118
6	1.226	5	1.155	5	1.157	5	1.157	5	1.157
7	1.338	6	1.229	6	1.229	6	1.230	6	1.230
8	1.498	7	1.339	7	1.340	7	1.340	7	1.340
		8	1.498	8	1.499	8	1.499	8	1.499

Tab. A2.5 – Finite Thickness SIF Solutions for Symmetric Notches
(b/ρ = 6, α = 45°, Pure Tension)

b/T = 0.0625		b/T = 0.1875		b/T = 0.2727		b/T = 0.3125		b/T = 0.4375	
a / ρ	Y_I	a / ρ	Y_I	a / ρ	Y_I	a / ρ	Y_I	a / ρ	Y_I
0.1	2.609	0.025	2.258	0.025	2.013	0.025	1.917	0.025	1.689
0.15	2.507	0.05	2.208	0.05	1.969	0.05	1.874	0.05	1.654
0.2	2.416	0.075	2.161	0.075	1.926	0.075	1.835	0.075	1.620
0.25	2.336	0.1	2.117	0.1	1.886	0.1	1.797	0.1	1.589
0.3	2.264	0.15	2.035	0.15	1.814	0.15	1.730	0.15	1.533
0.4	2.142	0.2	1.963	0.2	1.752	0.2	1.672	0.2	1.486
0.5	2.042	0.25	1.900	0.25	1.700	0.25	1.622	0.25	1.448
0.7	1.890	0.3	1.844	0.3	1.650	0.3	1.579	0.3	1.415
0.9	1.780	0.4	1.750	0.4	1.572	0.4	1.508	0.4	1.367
1.1	1.697	0.5	1.675	0.5	1.512	0.5	1.454	0.5	1.334
1.3	1.632	0.7	1.564	0.7	1.426	0.7	1.381	0.7	1.302
1.6	1.556	0.9	1.487	0.9	1.372	0.9	1.337	0.9	1.299
1.9	1.499	1.1	1.432	1.1	1.337	1.1	1.313	1.1	1.315
2.2	1.454	1.3	1.391	1.3	1.316	1.3	1.301	1.3	1.346
2.5	1.419	1.6	1.349	1.6	1.301	1.6	1.302	1.6	1.414
3	1.373	1.9	1.322	1.9	1.301	1.9	1.317	1.9	1.506
3.5	1.340	2.2	1.305	2.2	1.311	2.2	1.344	2.2	1.621
4	1.315	2.5	1.297	2.5	1.330	2.5	1.380	2.5	1.760
5	1.281	3	1.295	3	1.377	3	1.459	3	2.054
6	1.262	3.5	1.305	3.5	1.439	3.5	1.559	-	-
7	1.252	4	1.324	4	1.517	4	1.682	-	-
8	1.249	5	1.383	5	1.716	-	-	-	-
-	-	6	1.466	6	1.985	-	-	-	-
-	-	7	1.571	7	2.342	-	-	-	-
-	-	8	1.698	8	2.826	-	-	-	-

Tab. A2.6 – Finite Thickness SIF Solutions for Symmetric Notches
($b/\rho = 6$, $\alpha = 45°$, Uniform Tension)

b/T = 0.0625		b/T = 0.1875		b/T = 0.2727		b/T = 0.3125		b/T = 0.4375	
a/ρ	Y_I	a/ρ	Y_I	a/ρ	Y_I	a/ρ	Y_I	a/ρ	Y_I
0.1	3.354	0.025	4.816	0.025	6.072	0.025	6.828	0.025	10.352
0.15	3.223	0.05	4.708	0.05	5.935	0.05	6.673	0.05	10.110
0.2	3.106	0.075	4.609	0.075	5.808	0.075	6.530	0.075	9.890
0.25	3.002	0.1	4.513	0.1	5.688	0.1	6.395	0.1	9.682
0.3	2.909	0.15	4.337	0.15	5.467	0.15	6.147	0.15	9.309
0.4	2.752	0.2	4.182	0.2	5.273	0.2	5.930	0.2	8.988
0.5	2.624	0.25	4.044	0.25	5.102	0.25	5.740	0.25	8.712
0.7	2.428	0.3	3.922	0.3	4.952	0.3	5.573	0.3	8.474
0.9	2.285	0.4	3.715	0.4	4.700	0.4	5.295	0.4	8.089
1.1	2.177	0.5	3.549	0.5	4.499	0.5	5.076	0.5	7.798
1.3	2.092	0.7	3.299	0.7	4.204	0.7	4.758	0.7	7.408
1.6	1.994	0.9	3.122	0.9	4.002	0.9	4.545	0.9	7.186
1.9	1.919	1.1	2.991	1.1	3.860	1.1	4.401	1.1	7.079
2.2	1.860	1.3	2.892	1.3	3.759	1.3	4.303	1.3	7.054
2.5	1.813	1.6	2.784	1.6	3.659	1.6	4.217	1.6	7.127
3	1.753	1.9	2.708	1.9	3.602	1.9	4.182	1.9	7.311
3.5	1.708	2.2	2.655	2.2	3.577	2.2	4.185	2.2	7.594
4	1.674	2.5	2.618	2.5	3.576	2.5	4.218	2.5	7.971
5	1.627	3	2.585	3	3.615	3	4.328	3	8.837
6	1.599	3.5	2.575	3.5	3.696	3.5	4.497	-	-
7	1.582	4	2.584	4	3.813	4	4.726	-	-
8	1.574	5	2.643	5	4.147	5	5.363	-	-
10	1.575	6	2.746	6	4.629	-	-	-	-
12	1.592	7	2.888	-	-	-	-	-	-
14	1.621	8	3.069	-	-	-	-	-	-
16	1.660	9	3.291	-	-	-	-	-	-
20	1.762	10	3.560	-	-	-	-	-	-
24	1.896	-	-	-	-	-	-	-	-

Tab. A2.7 – Finite Thickness SIF Solutions for Symmetric Notches
($b/\rho = 6$, $\alpha = 45°$, Pure Bending)

b/T = 0.0625		b/T = 0.1875		b/T = 0.2727		b/T = 0.3125		b/T = 0.4375	
a/ρ	Y_I	a/ρ	Y_I	a/ρ	Y_I	a/ρ	Y_I	a/ρ	Y_I
0.1	2.677	0.025	2.391	0.025	2.139	0.025	2.037	0.025	1.770
0.15	2.572	0.05	2.337	0.05	2.090	0.05	1.990	0.05	1.728
0.2	2.478	0.075	2.287	0.075	2.045	0.075	1.947	0.075	1.690
0.25	2.394	0.1	2.239	0.1	2.002	0.1	1.906	0.1	1.653
0.3	2.319	0.15	2.151	0.15	1.923	0.15	1.830	0.15	1.587
0.4	2.192	0.2	2.072	0.2	1.852	0.2	1.763	0.2	1.530
0.5	2.087	0.25	2.002	0.25	1.790	0.25	1.704	0.25	1.480
0.7	1.927	0.3	1.939	0.3	1.735	0.3	1.652	0.3	1.436
0.9	1.810	0.4	1.833	0.4	1.641	0.4	1.564	0.4	1.364
1.1	1.720	0.5	1.746	0.5	1.565	0.5	1.493	0.5	1.308
1.3	1.649	0.7	1.613	0.7	1.450	0.7	1.386	0.7	1.228
1.6	1.565	0.9	1.516	0.9	1.368	0.9	1.311	0.9	1.176
1.9	1.500	1.1	1.443	1.1	1.307	1.1	1.257	1.1	1.144
2.2	1.449	1.3	1.385	1.3	1.261	1.3	1.216	-	-
2.5	1.406	1.6	1.319	1.6	1.209	1.6	1.172	-	-
3	1.350	1.9	1.269	1.9	1.173	1.9	1.143	-	-
3.5	1.307	2.2	1.229	2.2	1.148	2.2	1.125	-	-
4	1.272	2.5	1.200	2.5	1.130	2.5	1.115	-	-
5	1.220	3	1.163	3	1.114	3	1.113	-	-
6	1.183	3.5	1.137	3.5	1.110	3.5	1.125	-	-
7	1.156	4	1.120	4	1.117	4	1.149	-	-
8	1.135	5	1.104	5	1.157	5	1.235	-	-
10	1.106	6	1.106	6	1.229	-	-	-	-
12	1.088	7	1.121	7	1.340	-	-	-	-
14	1.079	8	1.149	8	1.499	-	-	-	-
16	1.076	9	1.189	-	-	-	-	-	-
20	1.083	10	1.242	-	-	-	-	-	-
24	1.106	-	-	-	-	-	-	-	-

A3 – Edge Cracks at Intrusion/Protrusion Notches

Tab. A3.1 – Finite Thickness SIF Solutions for Intrusion Notches
($b/\rho = 6$, $\alpha = 45°$, $b/T = 0.2727$,Uniform Tension)

	$L_I/b = 0.125$			$L_I/b = 0.25$	
a/ρ	Y_I (UT)	Y_I (PB)	a/ρ	Y_I (UT)	Y_I (PB)
0.1	6.236	4.170	0.1	5.907	3.943
0.15	6.006	4.016	0.15	5.686	3.795
0.2	5.802	3.878	0.2	5.491	3.662
0.25	5.622	3.754	0.25	5.318	3.543
0.3	5.462	3.643	0.3	5.165	3.437
0.4	5.190	3.453	0.4	4.906	3.255
0.5	4.970	3.297	0.5	4.699	3.107
0.7	4.636	3.053	0.7	4.391	2.881
0.9	4.395	2.872	0.9	4.179	2.718
1.1	4.216	2.731	1.1	4.027	2.595
1.3	4.079	2.618	1.3	3.918	2.500
1.6	3.931	2.487	1.6	3.806	2.394
1.9	3.833	2.389	1.9	3.737	2.316
2.2	3.772	2.316	2.2	3.700	2.259
2.5	3.741	2.261	2.5	3.687	2.217
3	3.740	2.202	3	3.707	2.173
3.5	3.790	2.173	3.5	3.770	2.155
4	3.884	2.169	4	3.872	2.157

Tab. A3.2 – Finite Thickness SIF Solutions for Protrusion Notches
($b/\rho = 6$, $\alpha = 45°$, $b/T = 0.2727$,Pure Tension)

	$L_P/b = 0.25$			$L_P/b = 0.5$			$L_P/b = 1.0$	
a/ρ	Y_I (PT)	Y_I (PB)	a/ρ	Y_I (PT)	Y_I (PB)	a/ρ	Y_I (PT)	Y_I (PB)
0.025	1.486	1.489	0.025	1.694	1.717	0.025	1.910	1.989
0.05	1.450	1.452	0.05	1.654	1.675	0.05	1.866	1.943
0.075	1.418	1.417	0.075	1.617	1.635	0.075	1.825	1.899
0.1	1.388	1.386	0.1	1.583	1.598	0.1	1.787	1.857
0.15	1.339	1.332	0.15	1.522	1.533	0.15	1.717	1.782
0.2	1.300	1.288	0.2	1.471	1.476	0.2	1.658	1.716
0.25	1.268	1.251	0.25	1.428	1.428	0.25	1.606	1.657
0.3	1.243	1.222	0.3	1.392	1.386	0.3	1.561	1.606
0.4	1.206	1.176	0.4	1.335	1.319	0.4	1.488	1.519
0.5	1.183	1.144	0.5	1.293	1.266	0.5	1.432	1.449
0.7	1.161	1.103	0.7	1.240	1.193	0.7	1.355	1.346
1.1	1.160	1.066	1.1	1.200	1.113	1.1	1.279	1.221
1.3	1.170	1.057	1.3	1.198	1.091	1.3	1.263	1.182
1.6	1.190	1.048	1.6	1.206	1.070	1.6	1.256	1.141
1.9	1.215	1.044	1.9	1.225	1.058	1.9	1.263	1.113
-	-	-	2.2	1.250	1.051	2.2	1.279	1.096
-	-	-	2.5	1.280	1.049	2.5	1.303	1.085
-	-	-	-	-	-	3	1.356	1.078
-	-	-	-	-	-	3.5	1.423	1.082
-	-	-	-	-	-	4	1.504	1.095

A4 – Surface Cracks at Symmetrically Notched Flat Plates

Tab. A4.1 – Deepest Point SIF Solutions for Notched, Surface Cracked Plates
(W/t = 2.75, b/T = 0.2727, α = 45°, Uniform Tension)

b/ρ	a/t	a/c = 1.0	a/c = 0.6	a/c = 0.4	a/c = 0.2
	0.009	2.921	3.691	4.162	-
	0.019	2.789	3.517	3.960	-
	0.038	2.559	3.215	3.613	4.021
	0.075	2.200	2.759	3.091	3.459
	0.113	1.939	2.431	2.731	3.083
1	0.150	1.743	2.194	2.475	-
	0.188	1.593	2.017	2.292	2.693
	0.225	1.475	1.877	2.159	2.609
	0.263	1.379	1.776	2.060	2.572
	0.300	1.300	1.691	1.986	2.634
	0.338	1.228	1.615	1.922	-
	0.009	3.921	4.926	5.536	-
	0.019	3.506	4.387	4.914	-
	0.038	2.911	3.629	4.053	4.499
	0.056	2.515	3.131	3.498	-
	0.075	2.233	2.785	3.117	3.508
	0.113	1.865	2.339	2.635	3.012
3	0.150	1.636	2.066	2.347	2.743
	0.188	1.478	1.903	2.161	2.594
	0.225	1.363	1.778	2.034	2.506
	0.263	1.275	1.686	1.945	2.467
	0.300	1.203	1.613	1.880	2.470
	0.338	1.142	1.547	1.825	-
	0.005	5.490	6.470	7.271	-
	0.009	4.831	5.777	6.470	-
	0.019	3.928	4.795	5.354	-
	0.038	2.967	3.689	4.120	4.595
	0.056	2.467	3.091	3.464	-
	0.075	2.164	2.726	3.054	3.455
6	0.113	1.786	2.275	2.567	2.955
	0.150	1.568	2.016	2.286	2.688
	0.188	1.420	1.848	2.109	2.539
	0.225	1.312	1.730	1.989	2.457
	0.263	1.226	1.643	1.905	2.424
	0.300	1.193	1.574	1.844	2.425
	0.338	1.134	1.511	1.791	-

Tab. A4.2 – Deepest Point SIF Solutions for Notched, Surface Cracked Plates
(W/t = 2.75, b/T = 0.2727, α = 45°, Pure Bending)

b/ρ	a/t	a/c = 1.0	a/c = 0.6	a/c = 0.4	a/c = 0.2
	0.005	3.461	4.349	4.851	-
	0.019	2.580	3.215	3.577	-
	0.056	1.614	2.020	2.266	-
6	0.113	1.094	1.395	1.591	1.836
	0.188	0.775	1.019	1.190	1.444
	0.263	0.582	0.799	0.968	1.276
	0.338	0.436	0.635	0.808	-

Tab. A4.3 – Deepest Point SIF Solutions for Notched, Surface Cracked Plates
(W/t = 2.75, b/ρ = 6, α = 45°, Uniform Tension)

b/T	a/t	a/c = 1.0	a/c = 0.6	a/c = 0.4	a/c = 0.2
	0.003	4.289	5.392	-	-
	0.006	3.847	4.817	-	-
	0.011	3.212	4.003	-	-
	0.022	2.484	3.091	-	-
	0.033	2.086	2.601	-	-
	0.045	1.835	2.294	-	-
0.1825	0.067	1.536	1.927	-	-
	0.089	1.362	1.717	1.953	-
	0.112	1.244	1.578	1.804	-
	0.134	1.160	1.480	1.702	-
	0.156	1.097	1.406	1.629	-
	0.179	1.047	1.349	1.574	-
	0.201	0.999	1.294	1.524	-
	0.005	5.490	6.470	7.271	-
	0.009	4.831	5.777	6.470	-
	0.019	3.928	4.795	5.354	-
	0.038	2.967	3.689	4.120	4.595
	0.056	2.467	3.091	3.464	-
	0.075	2.164	2.726	3.054	3.455
0.2727	0.113	1.786	2.275	2.567	2.955
	0.150	1.568	2.016	2.286	2.688
	0.188	1.420	1.848	2.109	2.539
	0.225	1.312	1.730	1.989	2.457
	0.263	1.226	1.643	1.905	2.424
	0.300	1.193	1.574	1.844	2.425
	0.338	1.134	1.511	1.791	-
	0.010	7.977	9.939	11.170	-
	0.019	7.070	8.851	9.915	-
	0.039	5.856	7.303	8.160	-
	0.078	4.438	5.541	6.209	6.960
	0.117	3.642	4.576	5.163	-
	0.156	3.127	3.962	4.509	5.246
0.4375	0.233	2.480	3.214	3.731	4.597
	0.311	2.071	2.755	3.284	4.399
	0.389	1.775	2.435	3.001	4.508
	0.467	1.514	2.188	2.809	4.972
	0.544	1.313	1.979	2.678	-
	0.622	1.127	1.785	2.528	-
	0.700	0.949	1.585	2.411	-

Tab. A4.4 – Deepest Point SIF Solutions for Notched, Surface Cracked Plates
(W/t = 2.75, b/ρ = 6, α = 45°, Pure Bending)

b/T	a/t	a/c = 1.0	a/c = 0.6	a/c = 0.4
	0.005	3.461	4.349	4.851
	0.019	2.580	3.215	3.577
	0.056	1.614	2.020	2.266
0.2727	0.113	1.094	1.395	1.591
	0.188	0.775	1.019	1.190
	0.263	0.582	0.799	0.968
	0.338	0.436	0.635	0.808
	0.010	4.304	5.412	6.093
	0.039	3.166	3.952	4.425
	0.117	1.874	2.282	2.686
0.4375	0.233	1.124	1.490	1.753
	0.389	0.602	0.901	1.173
	0.544	0.227	0.435	0.796
	0.700	-0.111	0.088	0.438

Tab. A4.5 – Deepest Point SIF Solutions for Notched, Surface Cracked Plates (W/t = 2.75, b/ρ = 6, b/T = 0.2727, Uniform Tension)

α	a/t	a/c = 1.0	a/c = 0.6	a/c = 0.4	a/c = 0.2
15°	0.005	3.849	4.850	-	-
	0.009	3.460	4.350	4.870	-
	0.019	2.981	3.749	4.203	-
	0.038	2.506	3.153	3.553	-
	0.056	2.249	2.836	3.202	-
	0.075	2.076	2.625	2.968	-
	0.113	1.846	2.343	2.662	-
	0.150	1.691	2.168	2.465	-
	0.188	1.575	2.038	2.327	-
	0.225	1.483	1.938	2.225	-
	0.263	1.408	-	2.149	-
	0.300	-	-	2.089	-
	0.338	-	-	-	-
30°	0.005	4.847	6.073	-	-
	0.009	4.325	5.414	-	-
	0.019	3.618	4.512	-	-
	0.038	2.841	3.546	-	-
	0.056	2.429	3.035	-	-
	0.075	2.157	2.710	-	-
	0.113	1.828	2.306	-	-
	0.150	1.622	2.062	-	-
	0.188	1.480	1.895	-	-
	0.225	1.374	1.773	-	-
	0.263	1.290	1.680	-	-
	0.300	-	-	-	-
	0.338	-	-	-	-
45°	0.005	5.490	6.470	7.271	-
	0.009	4.831	5.777	6.470	-
	0.019	3.928	4.795	5.354	-
	0.038	2.967	3.689	4.120	4.595
	0.056	2.467	3.091	3.464	-
	0.075	2.164	2.726	3.054	3.455
	0.113	1.786	2.275	2.567	2.955
	0.150	1.568	2.016	2.286	2.688
	0.188	1.420	1.848	2.109	2.539
	0.225	1.312	1.730	1.989	2.457
	0.263	1.226	1.643	1.905	2.424
	0.300	1.193	1.574	1.844	2.425
	0.338	1.134	1.511	1.791	-

A5 – Surface Cracks at Step Notched Flat Plates

Tab. A5.1 – Deepest Point SIF Solutions for Notched, Surface Cracked Plates (W/t = 2.75, b/ρ = 6, b/T = 0.2727, Pure Tension)

a/t	Y			
	a/c = 1.0	a/c = 0.6	a/c = 0.4	a/c = 0.2
0.075	0.736	0.922	1.037	1.167
0.150	0.650	0.819	0.929	
0.225	0.625	0.794	0.911	1.087
0.300	0.622	0.798	0.929	

Appendix B – Flow Diagram Indicating the Interpolation Procedure